

2.12.1.11.11. Case 11 Corner Drop with Thick Shell, Cold Condition and Light Payload

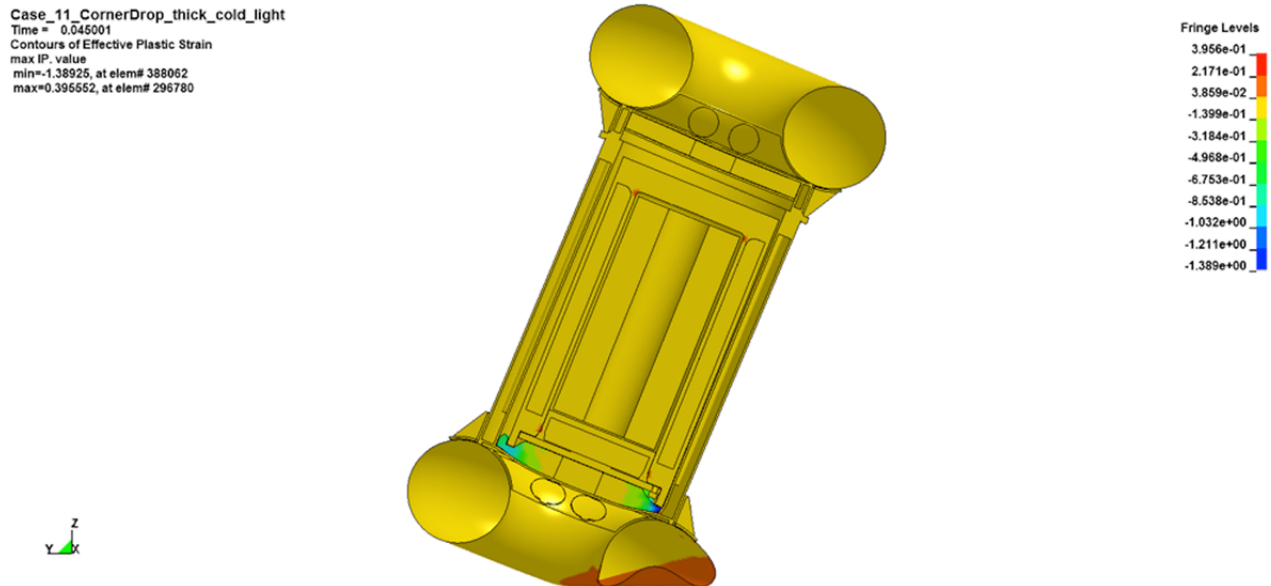


Figure 2.12.1.11-41. Case 11 Deformed Overpack Shape (Effective Plastic Strain)

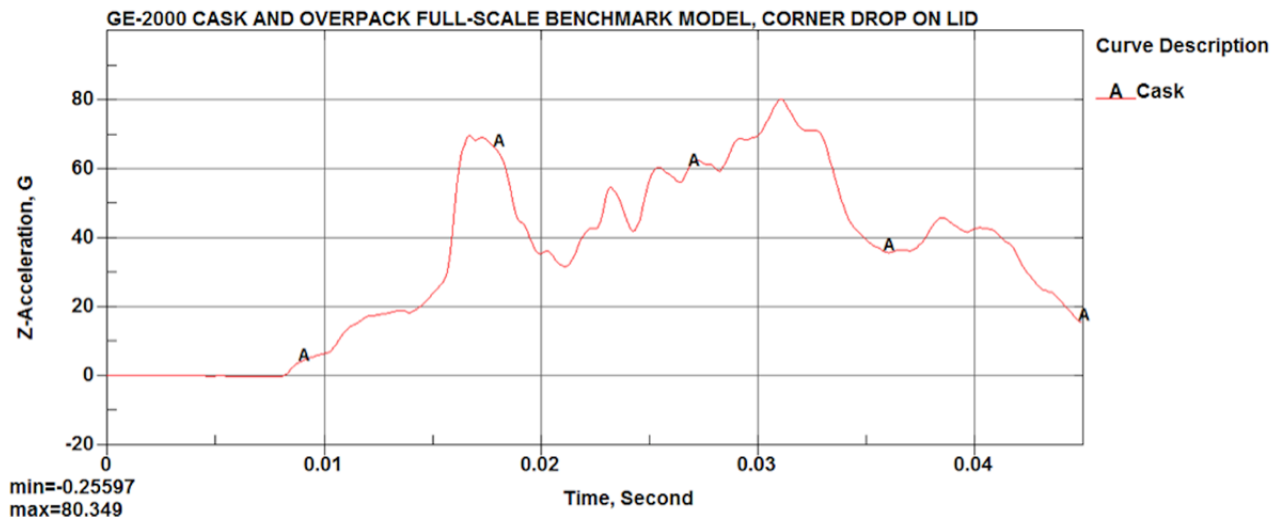


Figure 2.12.1.11-42. Case 11 Payload Acceleration Time History

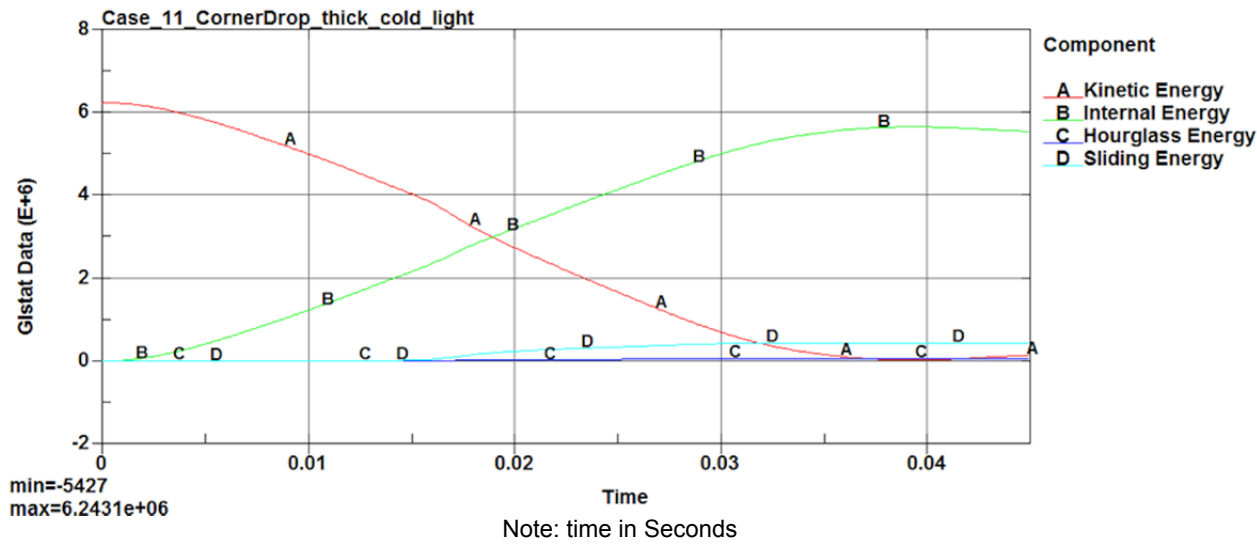


Figure 2.12.1.11-43. Case 11 Impact Energy Plot

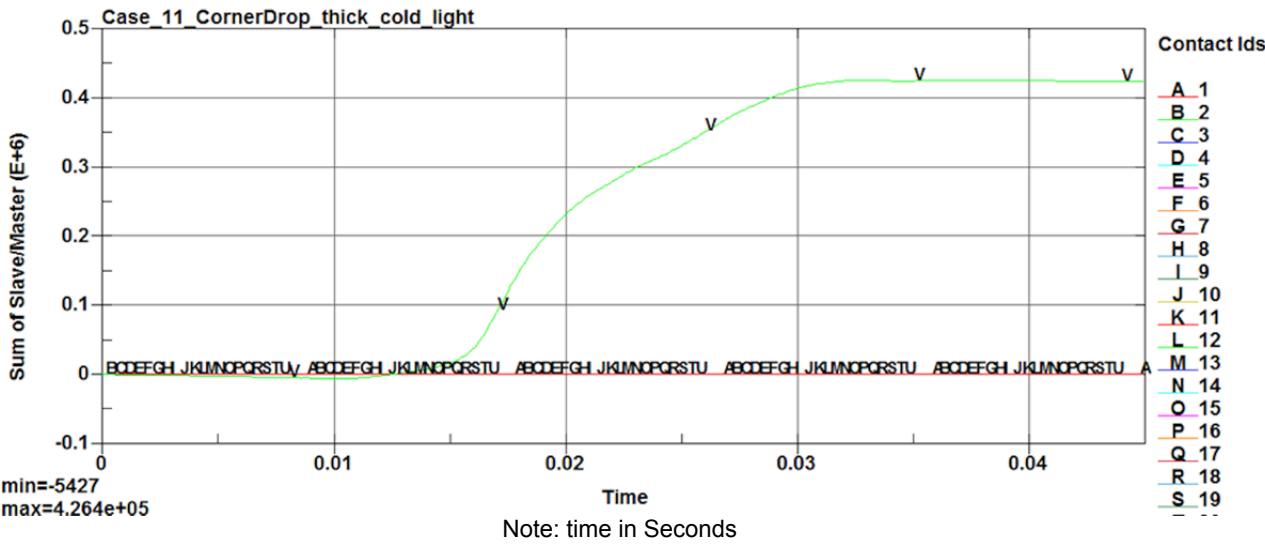


Figure 2.12.1.11-44. Case 11 Interface Sliding Energy Time History

2.12.1.11.12. Case 12 Corner Drop with Thin Shell, Hot Condition and Heavy Payload

Case_12_CornerDrop_thin_hot_heavy
Time = 0.045001
Contours of Effective Plastic Strain
max IP. value
min=-1.59837, at elem# 398060
max=0.470001, at elem# 79087

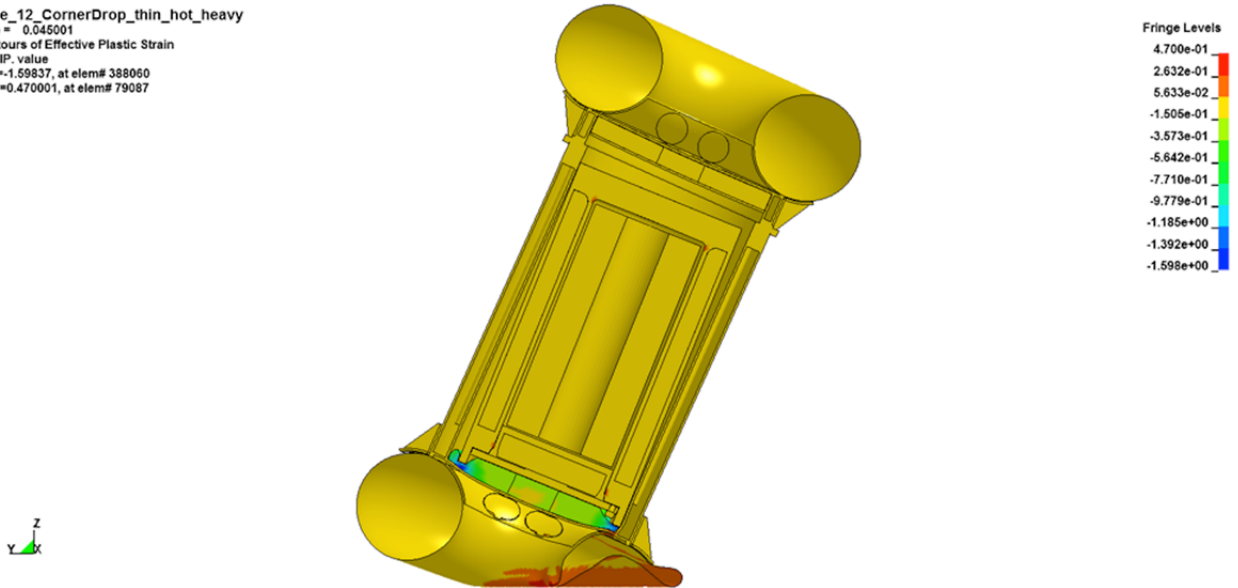


Figure 2.12.1.11-45. Case 12 Deformed Overpack Shape (Effective Plastic Strain)

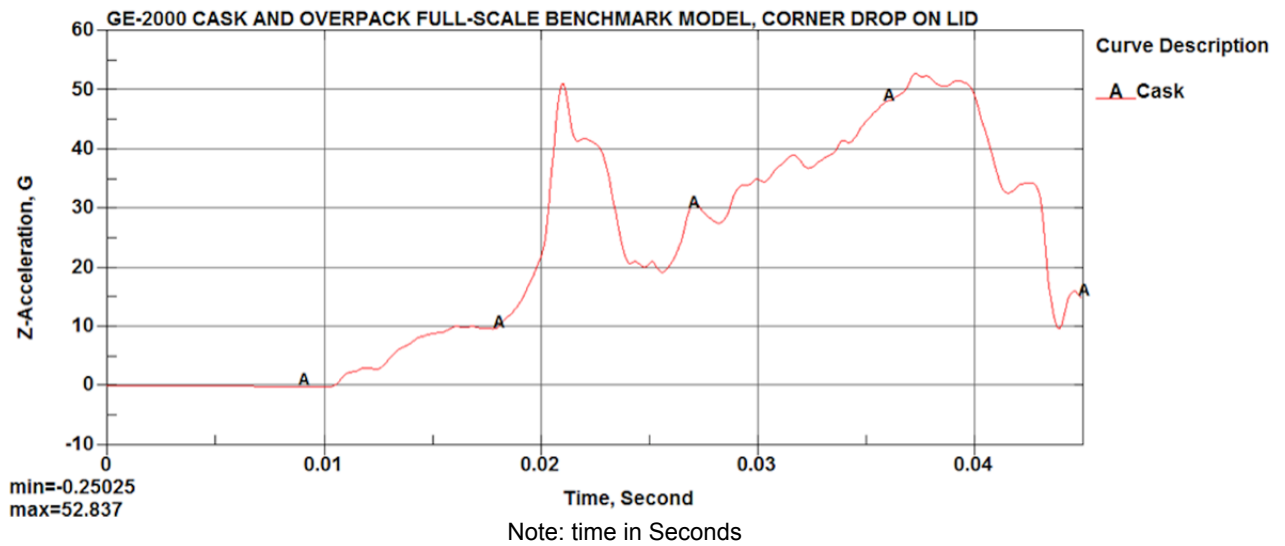


Figure 2.12.1.11-46. Case 12 Payload Acceleration Time History

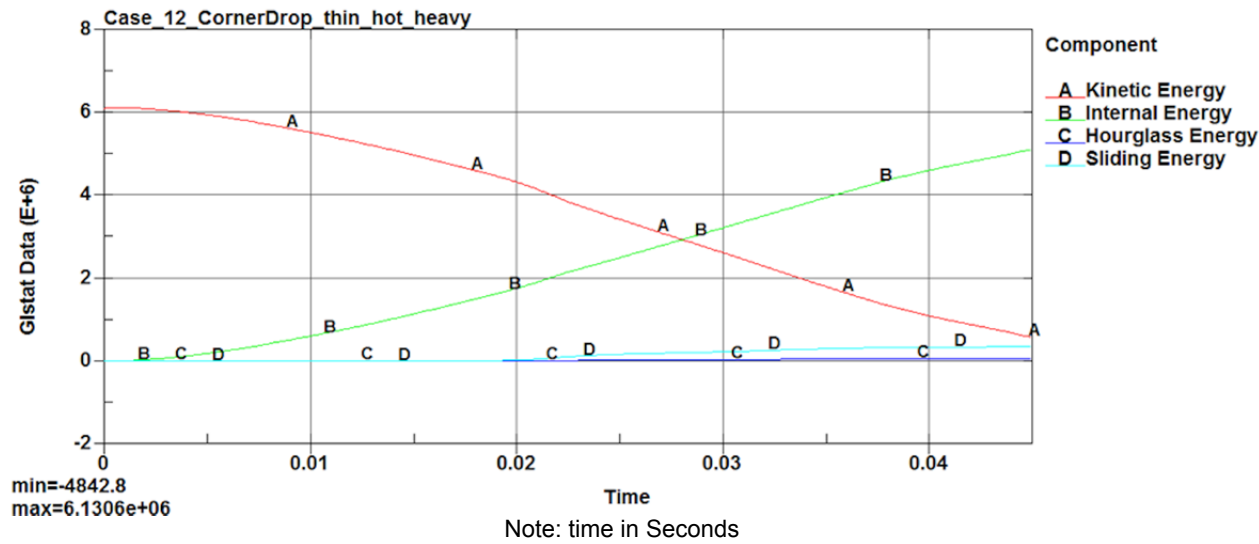


Figure 2.12.1.11-47. Case 12 Impact Energy Plot

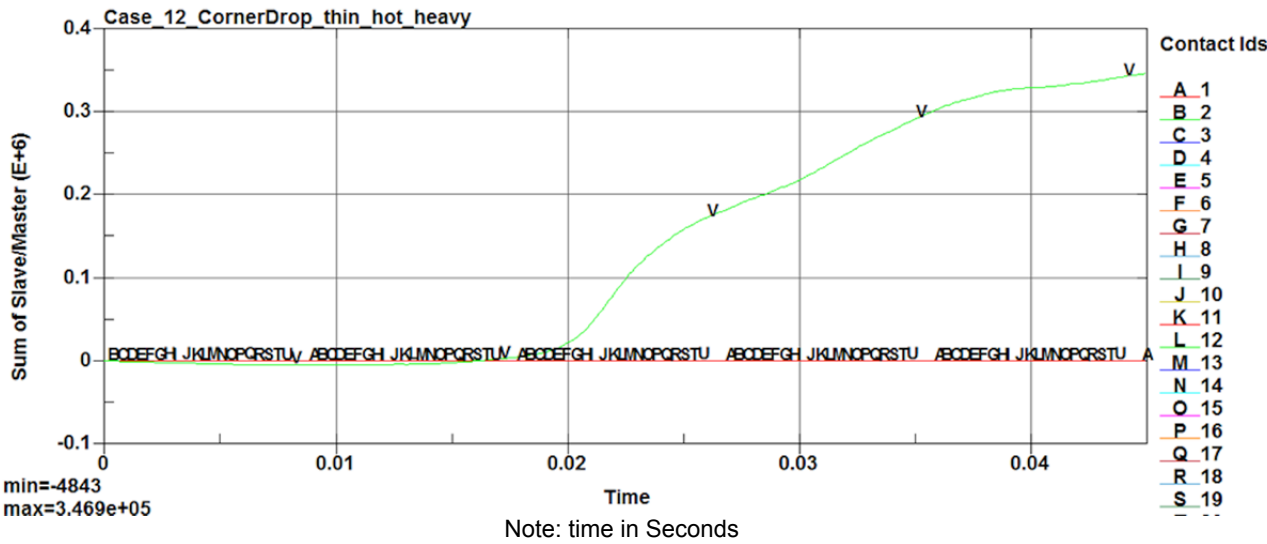


Figure 2.12.1.11-48. Case 12 Interface Sliding Energy Time History

2.12.1.11.13. Case 13 Slapdown Drop (5°), Thick Shell, Ambient Condition and Nominal Payload

Case_13_SlapDown_Thick_ambient_normal
Time = 0.035
Contours of Effective Plastic Strain
max IP. value
min=-0.192596, at elem# 387736
max=0.453218, at elem# 398568

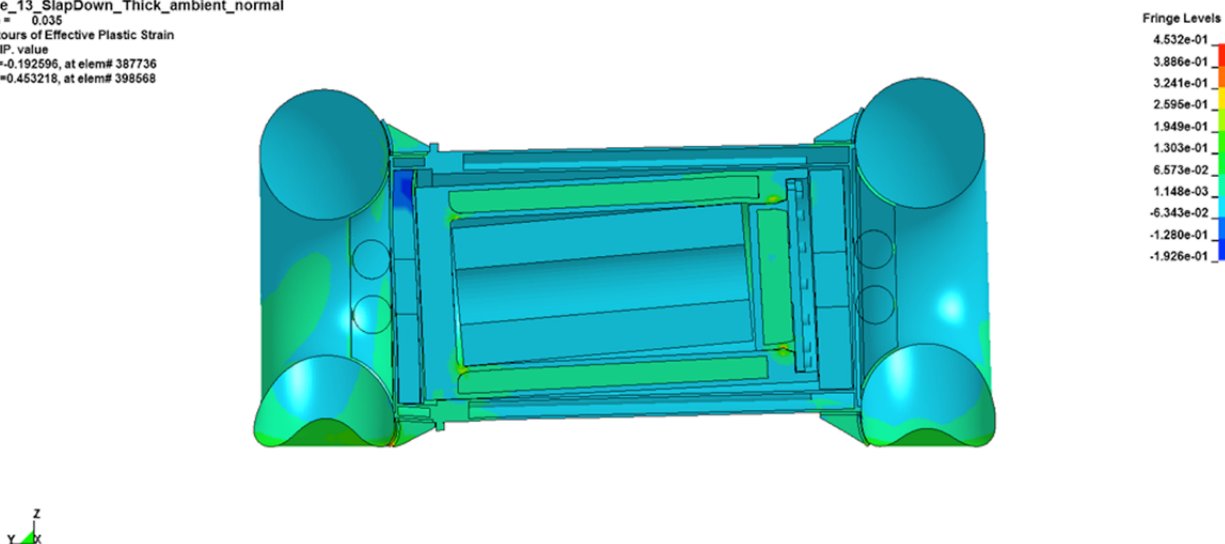


Figure 2.12.1.11-49. Case 13 Deformed Overpack Shape (Effective Plastic Strain)

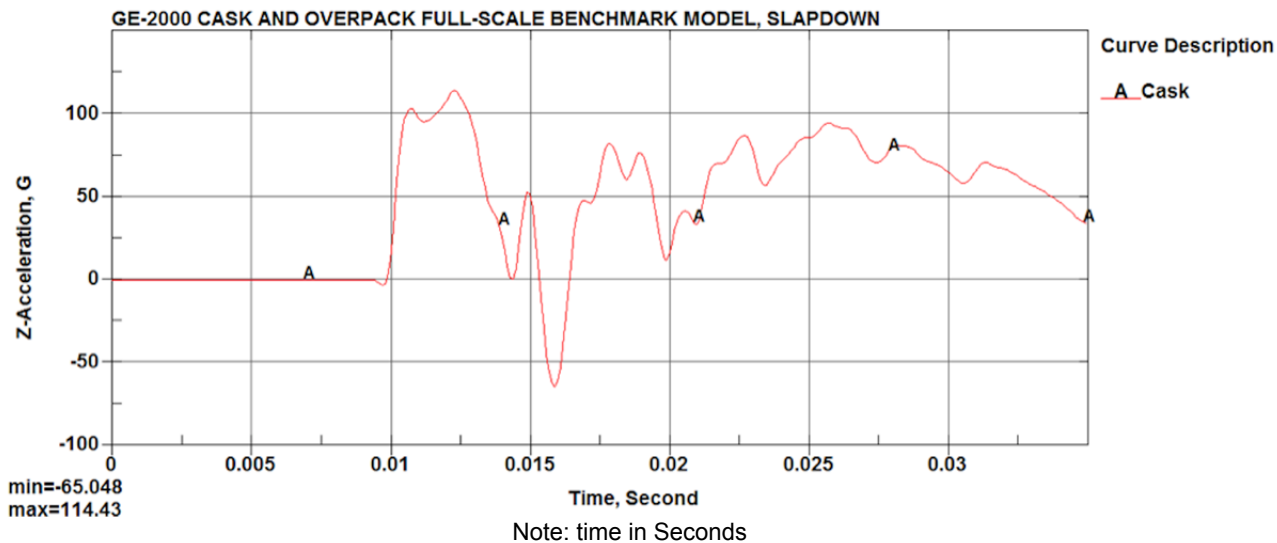


Figure 2.12.1.11-50. Case 13 Payload Acceleration Time History

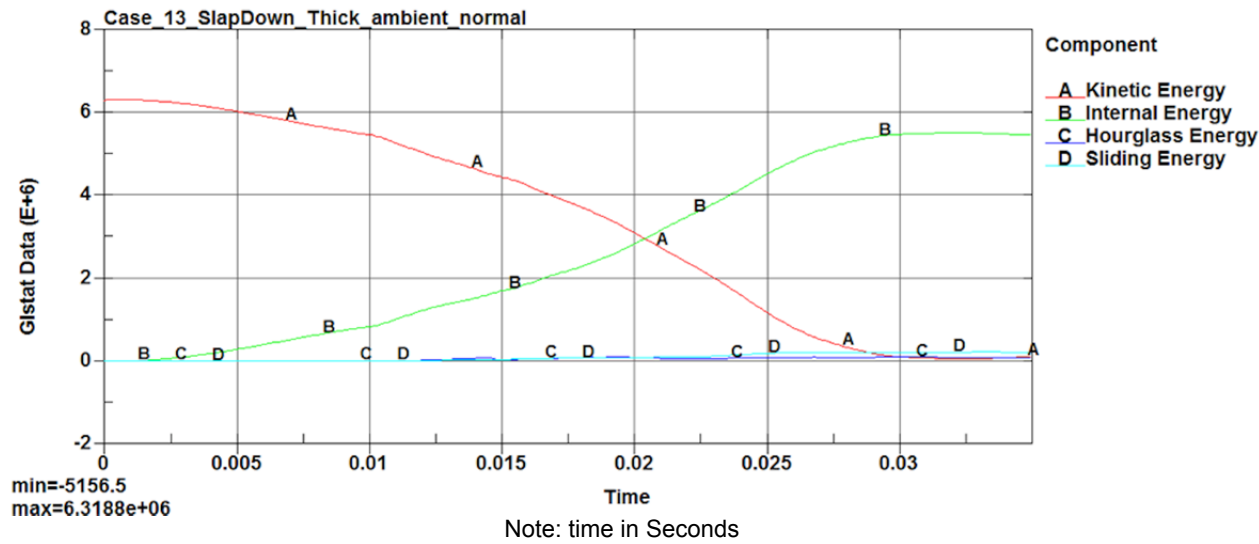


Figure 2.12.1.11-51. Case 13 Impact Energy Plot

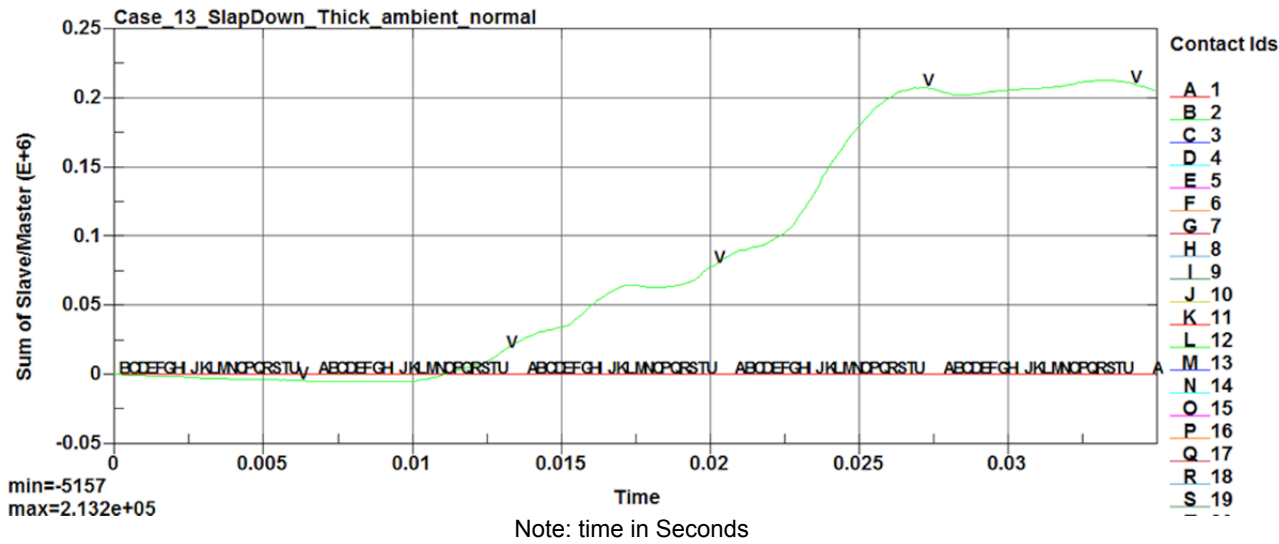


Figure 2.12.1.11-52. Case 13 Interface Sliding Energy Time History

2.12.1.11.14. Case 14 Slapdown Drop (10°), Thick Shell, Ambient Condition and Nominal Payload

Case_14_SlapDown_thick_ambient_normal
Time = 0.05
Contours of Effective Plastic Strain
max IP. value
min=-0.582812, at elem# 387736
max=0.446691, at elem# 777857

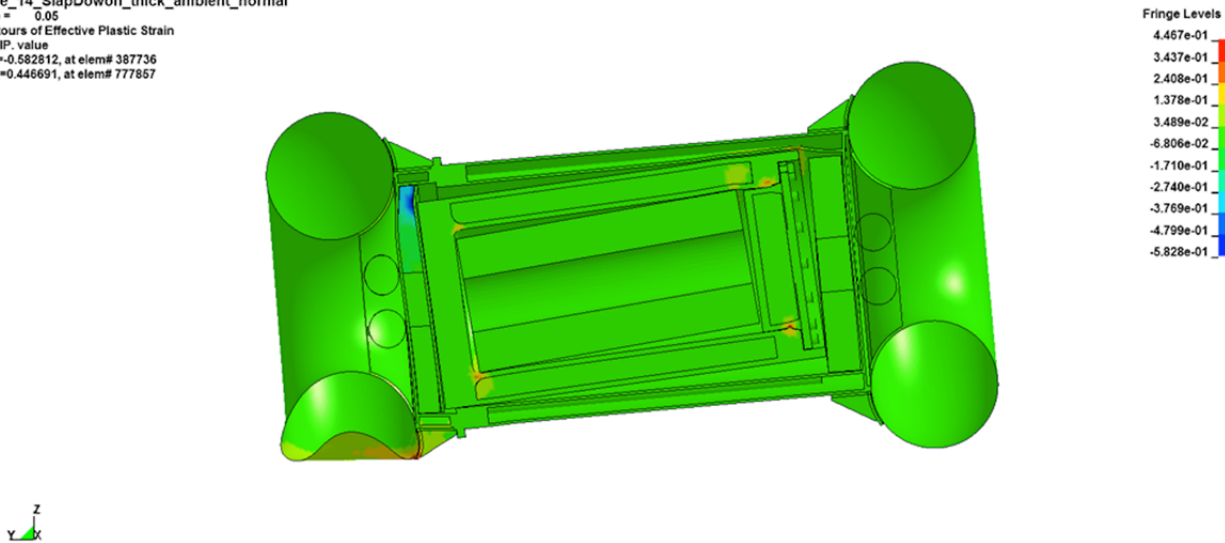


Figure 2.12.1.11-53. Case 14 Deformed Overpack Shape (Effective Plastic Strain)

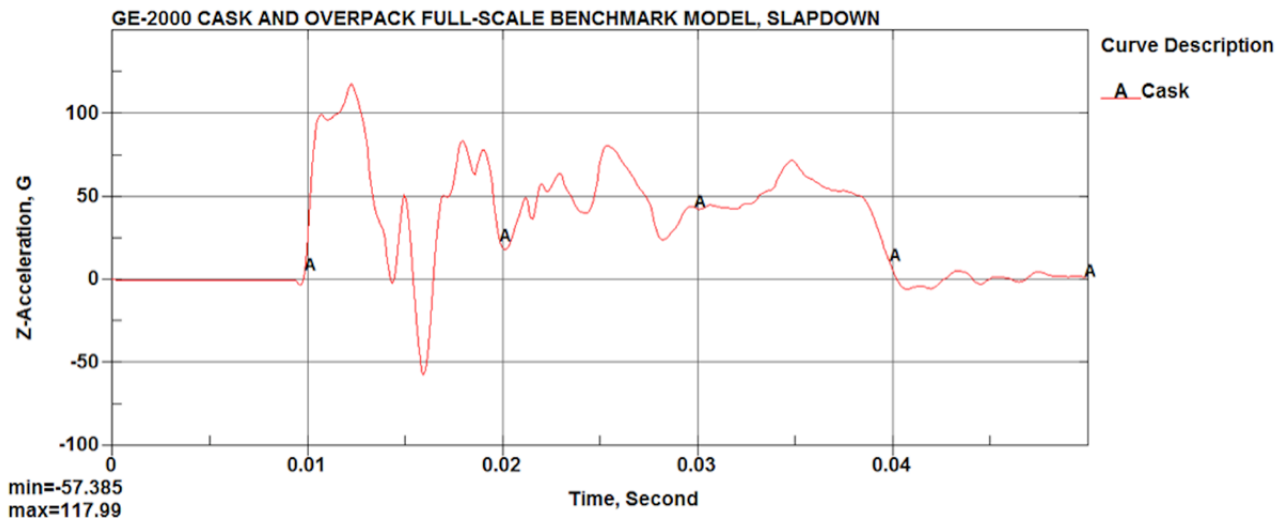


Figure 2.12.1.11-54. Case 14 Payload Acceleration Time History

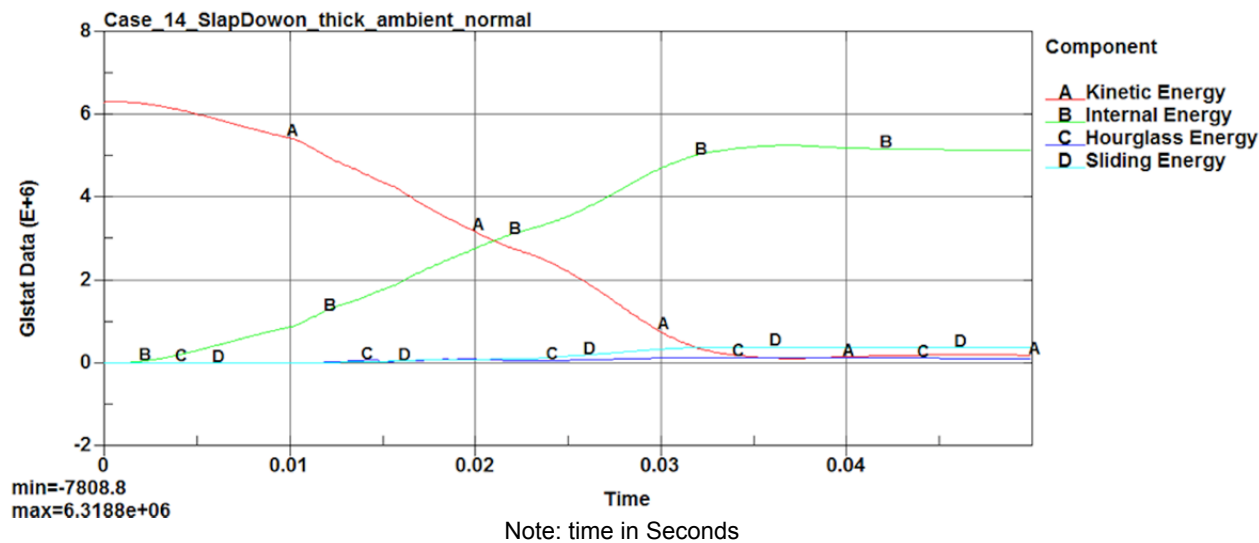


Figure 2.12.1.11-55. Case 14 Impact Energy Plot

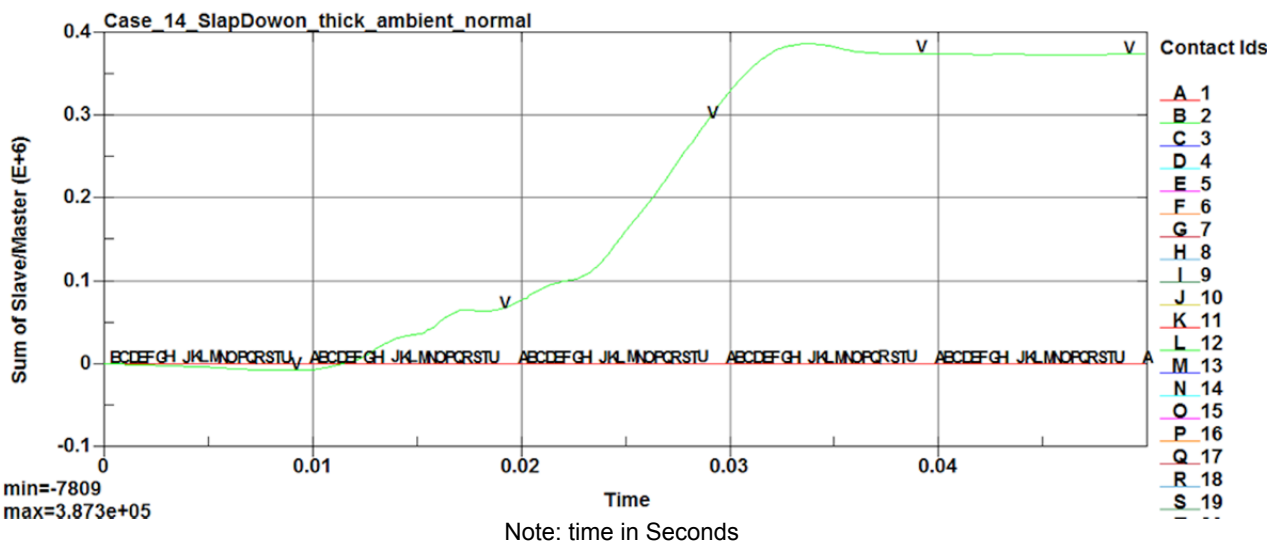


Figure 2.12.1.11-56. Case 14 Interface Sliding Energy Time History

2.12.1.11.15. Results for 30 ft Drop Followed and 40 in Pin Puncture Drop Sequence

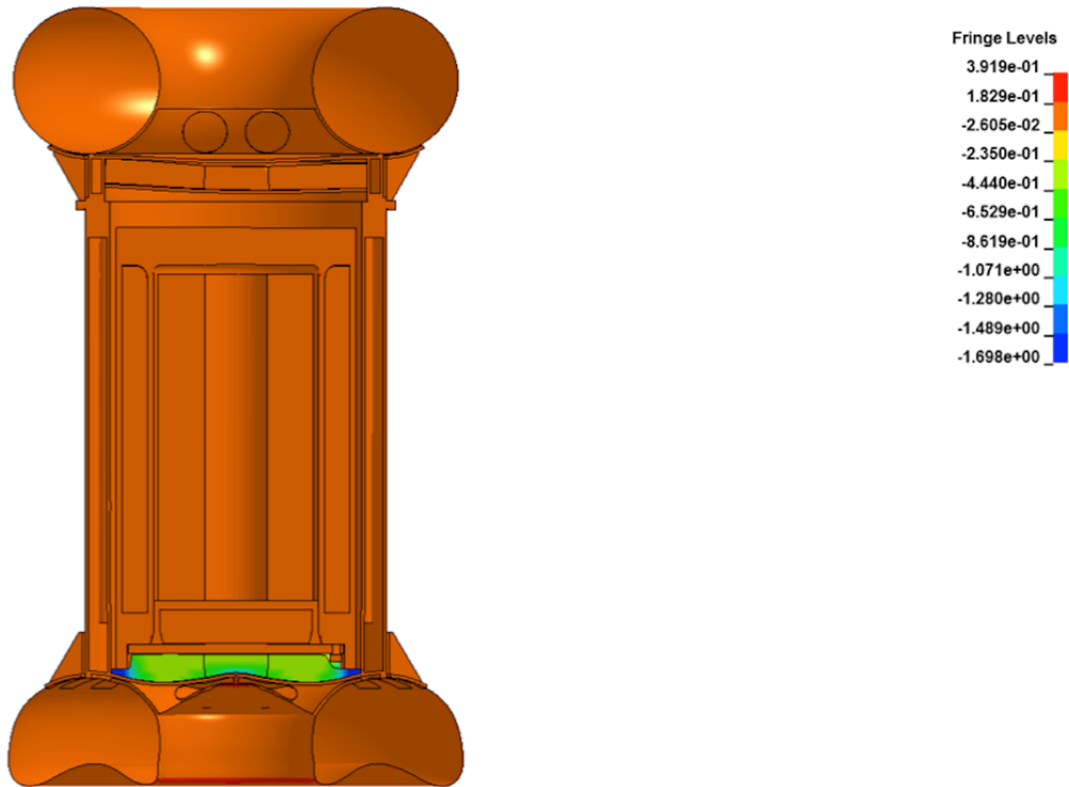


Figure 2.12.1.11-57. Strain Contour of Package after 30 ft End Drop and Pin Puncture Sequence

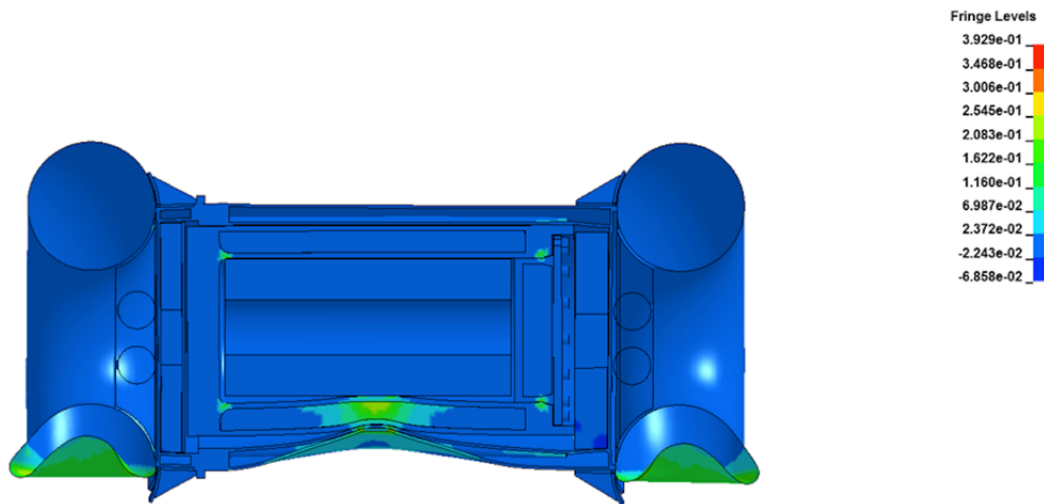


Figure 2.12.1.11-58. Strain Contour of Package after 30 ft Side Drop and Pin Puncture Sequence

2.12.1.12. Summary of Impact Analysis Results

Conservative impact analyses of the Model 2000 cask during the NCT and HAC impact events were performed to evaluate the performance of impact limiter design. This report summarizes the results of structural analyses of the Model 2000 Transport Package during NCT per 10 CFR 71.71 and HAC per 10 CFR 71.73. The summary of results for the bounding drop cases are presented in Table 2.12.1-1.

The worst-case HAC accelerations occur during the cold/thick/light side drop and the hot/thin/heavy bottom end drop. For the bottom end drop, the acceleration trend showed that the accelerations dropped until the honeycomb temperature was increased to 400°F and the honeycomb fully compresses. Because the average temperature of the honeycomb is less than 350°F, the honeycomb has sufficient capacity to protect the package during hot conditions.

The results of the evaluations presented in this section show that the Model 2000 overpack provides sufficient protection of the cask and contents.

2.12.1.12.1. Benchmark Tests

The peak accelerations of the benchmark analysis results from Drop Cases 1 through 3 are compared with the drop test results from Section 2.12.5 in Table 2.12.1-14.

Table 2.12.1-14. Comparison of Benchmark Simulations and Drop Tests Acceleration

| Drop Case No. | Drop Configuration | LS-DYNA Analysis | Drop Test ¹ Measurements | Notes |
|---------------|--------------------|------------------|-------------------------------------|-------------------------------|
| 1 | 30-ft End Drop | 130.0 g | 408/4 = 102 g | Quarter-scale model |
| 2 | 30-ft Side Drop | 157.0 g | Not available | Instrument failure, No result |
| 3 | 30-ft Corner Drop | 70.9 g | 156/4 = 39 g | Quarter-scale model |

Note: 1. Section 2.12.5.

The comparison of 1/4-scale drop test deformation results and the LS-DYNA benchmark simulation is provided in Table 2.12.1-15.

Table 2.12.1-15. Comparison of Benchmark Simulations and Drop Tests Deformations

| Drop Case No. | Drop Configuration | LS-DYNA Analysis | Drop Test ¹ Measurements |
|---------------|--------------------|------------------|-------------------------------------|
| 1 | 30-ft End Drop | 3.5 in | 2.255×4 = 9.0 in |
| 2 | 30-ft Side Drop | 9.4 in | 3.18×4 = 12.7 in |
| 3 | 30-ft Corner Drop | 11.8 in | 5.3×4 = 21.2 in |

Note: 1. Section 2.12.5.

The comparison of measured accelerations and deformations with LS-DYNA analysis results for each drop orientation shows that the LS-DYNA model is stiffer, which results in higher accelerations.

2.12.1.12.2. Shallow Angle Drops—Slap Down

Two shallow angle drop simulations are also performed. The drop configurations include nominal payload at ambient temperature with thick toroidal shell thickness (t=0.76 inches) to

compare with the side-drop test performed for the benchmarking test. The two shallow angles are 5° and 10° slapdown drops that are designated as Drop Cases 13 and 14. The results of shallow angle drops for the 0° (Drop Case 2, side drop), 5° (Drop Case 13) and 10° (Drop Case 14) conclude that the side drop (Drop Case 2) bounds the shallow angle cases with an acceleration of 157 g. Table 2.12.1-16 provides a summary of results for the shallow angle analyses.

Table 2.12.1-16. Comparison of Shallow Angle Drop Analyses

| Drop Case No. | Shallow Angle Drop Angle | Peak Acceleration |
|---------------|--------------------------|-------------------|
| 2 | 0° | 157.0 g |
| 13 | 5° | 115.0 g |
| 14 | 10° | 118.0 g |

2.12.1.12.3. Pin Puncture

Besides the 30-foot drop configurations, two HAC drop configurations (side drop and end drop) are selected to perform the code-required pin puncture test, where the cask is dropped 30-feet and then followed by a drop height of 40 inches onto a rigid pin 6 inches in diameter. Evaluation of the pin puncture results shows that the maximum strain is limited to local area and will not result in the degradation of the containment boundary. As the figures show, the maximum strain is 39%. However review of results show the maximum strain is limited to local deformation of the overpack. The maximum strain in the outer shell of the cask is 31% and limited to the puncture area. Therefore, no gross deformations of the cask are predicted. Additionally, results for the combined 30-foot impact and pin puncture are used as input for the HAC thermal evaluation.

2.12.1.12.4. Containment Integrity

Based on the analyses presented in the calculation, there are no gross structural deformations of the cask body or containment boundary. Therefore, the containment integrity of the cask is maintained.

2.12.2. Lead Slump Calculation

The following sections provide a detailed analysis for lead slump. Section 2.12.2.1 assesses the thermal expansion of the lead at the operating temperature of the lead shielding. Subsequently, in Sections 2.12.2.2 and 2.12.2.3, the shielding capability of the Model 2000 cask is evaluated for the potential of lead slump during a bottom end drop using classic methods to support the shielding analysis assumptions. Further, Sections 2.12.2.4 through 2.12.2.6 assess the thermal contraction of the lead and the lead deformation that results at the NCT extreme cold ambient temperature of -40°F (-40°C).

2.12.2.1. Thermal Expansion of Lead Shielding at Operating Temperature

It is possible that during fabrication an air gap will develop between the lead and the outer steel shell of the cask (Reference 2-24), which could potentially result in a lead slump condition,

meanwhile noting that the lead is inspected during fabrication. However, during NCT the operating temperature of the lead is taken at 500°F (260°C) (see Section 3.3.1.1) to envelope all conditions. The change in the outer radius of the lead shield due to thermal expansion is calculated as follows:

$$r_{\text{final}} = r_0 (1 + \alpha \Delta T) = 18.40 \text{ in (467.4 mm)}$$

where

$$\begin{aligned} r_0 &= 18.25 \text{ in} \\ &= \text{Outside radius of lead shield} \\ \alpha &= 1.90 \times 10^{-5} \text{ in/in/}^\circ\text{F} \\ &= \text{Coefficient of thermal expansion at } 500^\circ\text{F} \\ \Delta T &= 500^\circ\text{F} - 70^\circ\text{F} = 430^\circ\text{F} \\ &= \text{Temperature difference} \end{aligned}$$

NOTE: Coefficient of thermal expansion for lead extrapolated from data provided in Section 2.2.1.

For the outer steel shell the thermal expansion for the inside radius is:

$$r_{\text{final}} = r_i (1 + \alpha \Delta T) = 18.33 \text{ in (465.6 mm)}$$

where

$$\begin{aligned} r_i &= 18.25 \text{ in} \\ &= \text{Inside radius of steel shell} \\ \alpha &= 9.70 \times 10^{-6} \text{ in/in/}^\circ\text{F} \\ &= \text{Coefficient of thermal expansion at } 500^\circ\text{F} \\ \Delta T &= 500^\circ\text{F} - 70^\circ\text{F} = 430^\circ\text{F} \\ &= \text{Temperature difference} \end{aligned}$$

Comparing the final outside radius of the lead shield to the inner radius of the outer shell, the difference is -0.07000 inches (1.800 mm), which indicates that the lead expands more than the steel shell during NCT. Further, this demonstrates the temperature sensitivity of lead and steel at high temperatures. Relative expansion of the lead exceeds the expansion of the steel. Therefore, any existing gap that may have formed during fabrication will close, minimizing the potential for lead slump.

2.12.2.2. Compressive Stress in Lead Slump During Bottom End Drop

The previous section shows that the relative change in thermal expansion does not create a void. However, if the lead shield column did not bond to the mating steel shells during the fabrication process, compressive stress will develop in the column. The maximum stress occurs at the bottom of the column and progressively decreases as the elevation increases. The maximum compressive stress is

$$\sigma_{\text{max}} = \frac{P}{A} = 3,613.6 \text{ psi}$$

where

$$\begin{aligned}
 P &= \text{Total load} \\
 &= W \times G = 1.476 \times 10^6 \text{ lb} \\
 &= \text{Weight of lead shield} \\
 W &= V \times \rho = 9370.2 \text{ lb} \\
 V &= \text{Volume of lead shield} \\
 &= A \times h = 22870.8 \text{ in}^3 \\
 A &= \text{Cross-sectional area of lead shield} \\
 &= \pi(r_o^2 - r_i^2) = 408.4 \text{ in}^2 \\
 r_o &= \text{Outside radius of lead shield} \\
 &= 18.25 \text{ in} \\
 r_i &= \text{Inside radius of lead shield} \\
 &= 14.25 \text{ in} \\
 h &= \text{Height of lead column} \\
 &= 56 \text{ in} \\
 \rho &= \text{Density of lead} \\
 &= 0.4097 \text{ lb/in}^3 \\
 G &= \text{End drop acceleration} \\
 &= 157.5 \text{ g}
 \end{aligned}$$

NOTE: Value for the height of the lead column is rounded up to the nearest integer for conservatism.

Table 2.12.2-1 shows the stresses varying along the length of the lead column. The yield strength at 500°F is 189 psi. However, lead is sensitive to the strain-rate effects of the material. During the end drop, the estimated strain-rate is 12 in/in/sec (see Section 2.12.1). The yield strength varies from 823 psi at 0.002 in/in to 6,279 psi at 0.30 in/in. Therefore, during the end drop if yielding of the lead occurs it is localized to a small region near the bottom of the column.

NOTE: Yield strength of lead shielding at 500°F is extrapolated from data provided in Section 2.2.1.

2.12.2.3. Elastic Deformation During Bottom Impact

The elastic deformation is calculated assuming the cask lead shield column is unsupported by the steel inner and outer shells during an end drop event. The response of the lead shield is determined by multiplying the shield weight by the HAC end drop acceleration of 1,57.5 g. Therefore, an estimate of lead slump during HAC free drop conditions is (Reference 2-19):

$$y_{\max} = \frac{P}{k} = 0.075 \text{ in (1.91 mm)}$$

where

$$\begin{aligned}
 k &= \text{Effective stiffness of the lead shield} \\
 &= \frac{A \times G}{h} = 1.98 \times 10^7 \text{ lb/in} \\
 G &= \text{Bulk modulus of lead} \\
 &= \frac{E}{3(1-2\nu)} = 2.72 \times 10^6 \text{ psi}
 \end{aligned}$$

$$\begin{aligned}
 A &= \text{Cross-sectional area of lead shield} \\
 &= \pi(r_o^2 - r_i^2) = 408.4 \text{ in}^2 \\
 W &= \text{Weight of lead shield} \\
 &= 9370.2 \text{ lb} \\
 P &= \text{Total load} \\
 &= W \times g = 1.476 \times 10^6 \text{ lb} \\
 g &= \text{End drop acceleration} \\
 &= 157.5 \text{ g} \\
 h &= \text{Height of lead column} \\
 &= 56 \text{ in} \\
 E &= 1.63 \times 10^6 \text{ psi} \\
 &= \text{Modulus of elasticity of lead at } 500^\circ\text{F} \\
 \nu &= \text{Poisson's ratio for lead} \\
 &= 0.4
 \end{aligned}$$

The calculation shows that this estimate of lead slump is small for an unsupported lead shield. With the lead fully supported by the inner and outer shells of the cask, the actual lead slump is even smaller.

Table 2.12.2-1. Compressive Stress in Lead Shield

| Column Height from Bottom | Compressive Stress / G (psi) | Compressive Stress (psi) |
|------------------------------|---------------------------------|-----------------------------|
| 55.0 | 0.4 | 64.5 |
| 50.0 | 2.5 | 387.2 |
| 45.0 | 4.5 | 709.8 |
| 40.0 | 6.6 | 1032.4 |
| 35.0 | 8.6 | 1355.1 |
| 30.0 | 10.7 | 1677.7 |
| 25.0 | 12.7 | 2000.4 |
| 20.0 | 14.7 | 2323.0 |

2.12.2.4. Axial Thermal Expansion at NCT Extreme Cold Ambient Temperature

A small gap occurs at the top of the lead column when the cask is exposed to the extreme cold temperature of -40°F (-40°C) per the NRC requirements of 10 CFR 71.71 (c)(2). This is due to changes at the molecular level that cause the materials to contract. This reduction in the height of the lead shield is represented by the following equation:

$$h_{\text{lead}} = h_{0\text{-lead}} (1 + \alpha_{\text{lead}} \Delta T) = 55.904 \text{ in (1420.0 mm)}$$

where

$$\begin{aligned}
 h_{0\text{-lead}} &= \text{Initial lead shield height} \\
 &= 56 \text{ in} \\
 \alpha_{\text{lead}} &= \text{Lead coefficient of thermal expansion at } -40^\circ\text{F} \\
 &= 1.56\text{E}^{-05} \text{ in/in}/^\circ\text{F}
 \end{aligned}$$

$$\begin{aligned}\Delta T &= \text{Temperature difference} \\ &= -40^{\circ}\text{F} - 70^{\circ}\text{F} = -110^{\circ}\text{F}\end{aligned}$$

The same calculation can be made to determine the reduction in the height of the steel shells:

$$h_{\text{steel}} = h_{0\text{-steel}} (1 + \alpha_{\text{steel}} \Delta T) = 55.95 \text{ in (1421.1 mm)}$$

where

$$\begin{aligned}h_{0\text{-steel}} &= \text{Initial steel shell height} \\ &= 56 \text{ in} \\ \alpha_{\text{steel}} &= \text{Steel coefficient of thermal expansion at } -40^{\circ}\text{F} \\ &= 8.09\text{E-}0^6 \text{ in/in/}^{\circ}\text{F} \\ \Delta T &= \text{Temperature difference} \\ &= -40^{\circ}\text{F} - 70^{\circ}\text{F} = -110^{\circ}\text{F}\end{aligned}$$

2.12.2.5. Radial Thermal Expansion at NCT Extreme Cold Ambient Temperature

The radial gaps that occur during exposure to NCT extreme cold conditions can also be calculated in a similar manner by taking the initial radius prior to exposure and then adding the change in radius due to thermal expansion. The outside radius of the lead shield at -40°F is:

$$r_o = r_{0\text{-outer}} (1 + \alpha_{\text{lead}} \Delta T) = 18.22 \text{ in (462.8 mm)}$$

where

$$\begin{aligned}r_{0\text{-outer}} &= \text{Initial outside radius of the lead shield} \\ &= 18.25 \text{ in (463.6 mm)}\end{aligned}$$

Accordingly, the inside radius of the lead shield at -40°F is:

$$r_i = r_{0\text{-inner}} (1 + \alpha_{\text{lead}} \Delta T) = 14.23 \text{ in (361.3 mm)}$$

where

$$\begin{aligned}r_{0\text{-inner}} &= \text{Initial inside radius of the lead shield} \\ &= 14.25 \text{ in (362 mm)}\end{aligned}$$

Now the decrease in radius is evaluated for the steel shells starting with the inside radius of the outer steel shell at -40°F :

$$R_o = R_{0\text{-outer}} (1 + \alpha_{\text{steel}} \Delta T) = 18.23 \text{ in (463.1 mm)}$$

where

$$\begin{aligned}R_{0\text{-outer}} &= \text{Initial inside radius of the outer steel shell} \\ &= 18.25 \text{ in (463.6 mm)}\end{aligned}$$

The decrease in the outside radius of the inner steel shell at -40°F is:

$$R_i = R_{0\text{-inner}} (1 + \alpha_{\text{steel}} \Delta T) = 14.24 \text{ in (361.6 mm)}$$

where

$$\begin{aligned}R_{0\text{-inner}} &= \text{Initial outside radius of the inner steel shell} \\ &= 14.25 \text{ in (362 mm)}\end{aligned}$$

2.12.2.6. Lead Slump Due to Impact After NCT Extreme Cold Ambient Temperature

A small gap occurs during extreme cold exposure due to the contraction of components in relation to each other as determined by the calculations in the previous section. In order to determine the magnitude of lead slump, the reduced height of the lead column based on the net gap is calculated and then the difference between the reduced height of the lead column and the height of the annular region is taken. The volume of the lead column at the extreme cold conditions (-40°F) is:

$$\begin{aligned} V_{f\text{-lead}} &= A_{f\text{-lead}} \times h_{\text{lead}} \\ &= (407.011 \text{ in}^2 \times 55.904 \text{ in}) = 22,753.59 \text{ in}^3 (3.73\text{E}+08 \text{ mm}^3) \end{aligned}$$

where

$$\begin{aligned} A_{f\text{-lead}} &= \pi(r_o^2 - r_i^2) \\ &= \pi[(18.22 \text{ in})^2 - (14.23 \text{ in})^2] = 407.011 \text{ in}^2 (262,587.22 \text{ mm}^2) \end{aligned}$$

The cross sectional area of the annulus between the outer and inner steel shells at -40°F is:

$$\begin{aligned} A_{\text{annulus}} &= \pi(R_o^2 - R_i^2) \\ &= \pi[(18.23 \text{ in})^2 - (14.24 \text{ in})^2] = 407.68 \text{ in}^2 (263,018.83 \text{ mm}^2) \end{aligned}$$

The reduced height of the lead column when taking into account impact after contraction of components is:

$$\begin{aligned} h_{\text{final}} &= \frac{V_f}{A_{\text{annulus}}} \\ &= \frac{22,753.59 \text{ in}^3}{407.68 \text{ in}^2} = 55.81 \text{ in (1417.57 mm)} \end{aligned}$$

Taking the difference between the reduced height of the lead shielding and the height of the annular region, the lead deformation due to impact after NCT extreme cold (-40°F) is:

$$\begin{aligned} h_{\text{slump}} &= h_{\text{steel}} - h_{\text{final}} \\ &= 55.95 \text{ in} - 55.81 \text{ in} = 0.14 \text{ in (3.56 mm)} \end{aligned}$$

2.12.3. Lifting and Tie-Down Analysis

2.12.3.1. Model 2000 Transport Package Lifting Analysis

The purpose and scope of this analysis is to demonstrate the structural integrity of the lifting ears and lid-lifting lug on the Series 2000 shielded shipping casks.

There are two types of ear designs employed during the handling of the Model 2000 cask, standard and auxiliary (see Figure 2.12.3-1). The ear design identified as standard is used for crane and fork truck lifting, and only one pair is required for these operations. The auxiliary ear is used in crane lifting only, and two pairs or four ears are required. The user may combine the different types of ears as follows:

1. 2 Standard/2 Auxiliary

2. 4 Auxiliary
3. 2 Standard

Security-Related Information Figure Withheld Under 10 CFR 2.390.

Figure 2.12.3-1. Structural Locations for Ear Analysis

Both ear designs (Auxiliary and Standard) are attached to the cask outer shell by means of four ASTM A193-B6 1-8 UNC-2-1/2 attaching bolts; only two bolts are shown. Also on this figure, the line of action of the different lifting forces is drawn. The different lifting forces are: Case I, straight up by crane; Case II, angular lift 30° from vertical, also by crane; and Case III, fork truck lift at two different points on the standard ear only. This analysis mainly considers Case II and I. The loading conditions are the following:

- The design rated load, W , shall be 23,630 pounds. This includes the dead weight of the cask (1 body, lid, 2 standard ears, and 2 auxiliary ears) and the cask payload including the liner.
- The two pairs of auxiliary ears (Auxiliary) are to support $3W$ such that the lifting cable does not make an angle of more than +30° measured from the vertical.
- The pair of standard ears (Standard) is to support $3W$.
- These ears are removed from the cask during transport and are shipped separately.

Material properties are based upon 250°F for the outer cask. The 249°F temperature is the maximum temperature under normal conditions for the cask outer surface. Both types of ears, standard and auxiliary, and the cask outer shell are ASTM A240, Type 304 stainless steel. The attaching bolt material is ASTM A193-B6.

The standard ear individual load is obtained by dividing the weight of the cask and content (23,630 lbs.) by 2 (only two standard ears are used), and multiplying the resulting value by 3. The auxiliary ear load is obtained in a similar manner with the weight divided by 4 instead of 2 because 4 ears are used when this design is employed. Case III represents the fork truck loading condition on the standard ear, and it has a magnitude equal to that of Case I for the standard ear. Case III loading is not shown in Figure 2.12.3-2.

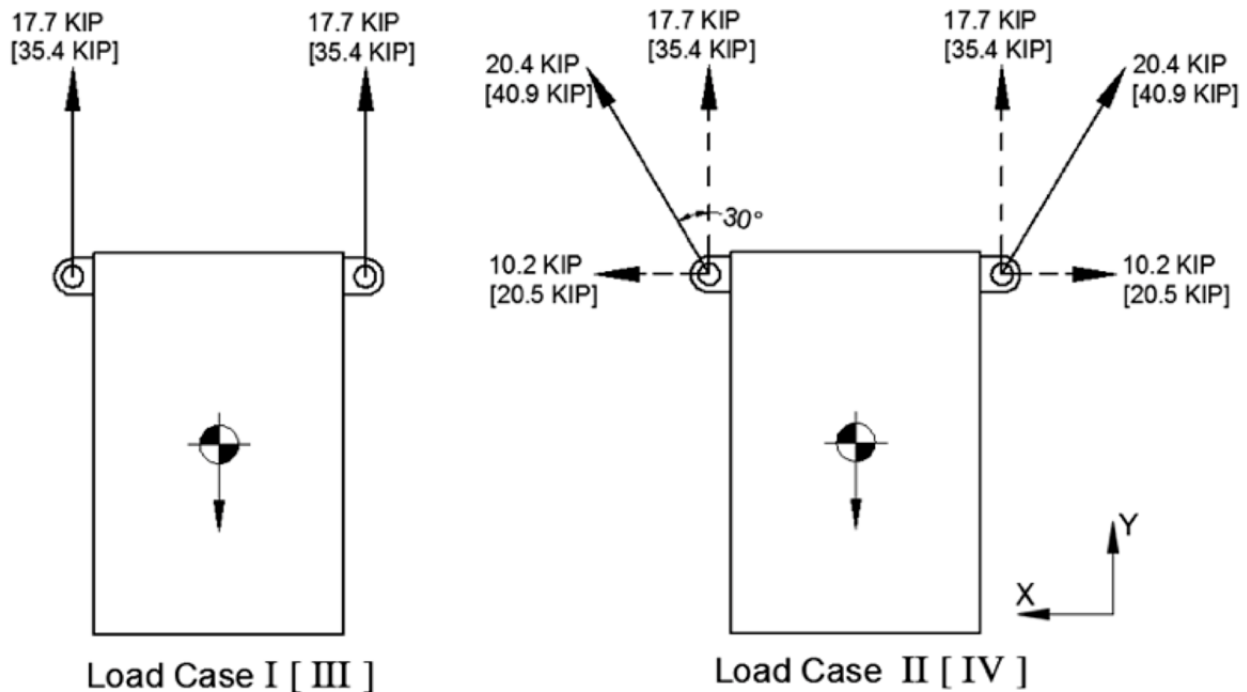


Figure 2.12.3-2. Magnitude and Direction of Loading in Model 2000 Cask

The following modes of failure are investigated for both ear designs:

- Shear tearout of lifting hole
- Tensile failure of ear plate
- Bearing of shackle pin on ear
- Yielding of weld joint
- Yielding of attaching bolt
- Shearing of bolt threads
- Shearing of tapped threads
- Yielding of cask outer shell

• SHEAR TEAR-OUT OF LIFTING HOLE-AUXILIARY AND STANDARD DESIGNS

Auxiliary Ear Design

For Load Case I, the shear tearout stress is computed as follows:

$$\tau = \frac{F}{A} \quad \text{Reference 2-25 page 89.}$$

where

$$F = 17.7 \text{ kip (see Figure 2.12.3-2) and}$$

$$A = \text{cross sectional area along the force line of action}$$

$$= \left(4 - \frac{2.12}{2}\right) \times 1 \quad (\text{see Figure 2.12.3-1}) = 2.94 \text{ in}^2$$

$$\tau = \frac{F}{A} = \frac{17.7}{2.94} = 6.02 \text{ ksi} < 15 \text{ ksi}$$

Standard Ear Design

For Load Case I, the shear tearout stress is:

$$\tau = \frac{F}{A} = \frac{35.4}{\left(5 - \frac{2.12}{2}\right) \times 1} = 8.98 \text{ ksi} < 15 \text{ ksi}$$

• TENSILE FAILURE OF EAR PLATE

Auxiliary Ear Design

In order to compute tensile failure for Load Case II, the internal forces that react to the lifting force are resolved into planes containing the minimum ligament cross-sectional area, as illustrated in Figure 2.12.3-3.

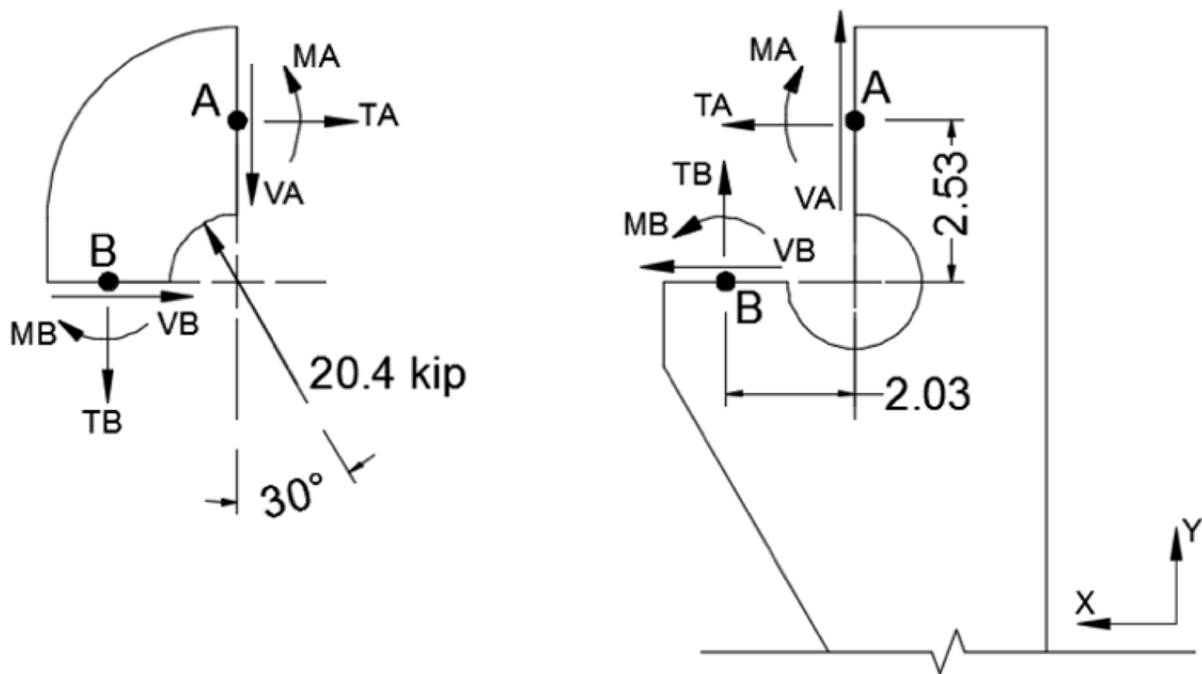


Figure 2.12.3-3. Ear Hole Cross Section

$$\begin{aligned} F_H &= 20.4 (\sin 30^\circ) = 10.2 \text{ kip} \\ F_V &= 20.4 (\cos 30^\circ) = 17.7 \text{ kip} \end{aligned}$$

Equilibrium:

$$\begin{aligned} \text{Eq. I} \quad \sum M_o &= 0 = MA - MB - 2.53 TA + 2.03 TB \\ \text{Eq. II} \quad \sum F_V &= 0 = 17.7 - VA - TB \\ \text{Eq. III} \quad \sum F_H &= 0 = 10.2 - TA - VB \end{aligned}$$

This is a statically indeterminate problem; however, by making some conservative simplifying assumptions, a solution may be obtained without resorting to indeterminate analysis methods. For the evaluation of primary stresses, we may conservatively assume

$MA = MB = 0$. Also, on the basis of relative stiffness, $TA > VB$; consequently, it may be conservatively assumed that $TA = VB$. Therefore, we may write the following:

From Eq. III,

$$TA = VB = \frac{10.2}{2} = 5.1 \text{ kip}$$

From Eq. I,

$$TB = \frac{2.53}{2.03} TA = 6.35 \text{ kip}$$

From Eq. II,

$$VA = 17.7 - TB = 11.35 \text{ kip}$$

The principal stresses will now be calculated at point A.

From Reference 2-25, page 81, the principal stresses are calculated using:

$$\sigma_1, \sigma_2 = \frac{\sigma}{2} \pm \sqrt{\left(\frac{\sigma}{2}\right)^2 + \tau^2}$$

$$\sigma = \frac{TA}{A} = \frac{5.1}{2.94} = 1.735 \text{ ksi}$$

$$\tau = \frac{VA}{A} = \frac{11.35}{2.94} = 3.86 \text{ ksi}$$

$$\sigma_1 = \frac{1.735}{2} + \sqrt{\left(\frac{1.735}{2}\right)^2 + 3.86^2} = 4.82 < 23.7 \text{ ksi}$$

Standard Ear Design

Load Case I or III

Standard ear dimensions and loading are shown in Figure 2.12.3-4. The critical tensile section is at Section X-X, see Figure 2.12.3-4. The exact force distribution cannot be determined without a detailed analysis that would include all of the stiffness characteristics (e.g., a finite element analysis). However, it can be deduced that the limiting load at the critical section (i.e., point “A”) will not exceed $P/2$. Then the tensile stress is:

$$\sigma_T = \frac{P/2}{A} = \frac{35.4/2}{1 \times 1} = 17.7 \text{ ksi} < 23.7 \text{ ksi}$$

Security-Related Information Figure Withheld Under 10 CFR 2.390.

Figure 2.12.3-4. Standard Ear Load Case I or III

- BEARING OF SHACKLE PIN ON EAR

Auxiliary Ear Design

The bearing stress is computed assuming that the force is uniformly distributed over the projected contact area of the pin. This gives a stress:

$$\sigma = \frac{F}{A}$$

Where the projected area for the pin is $A = t \times d$. Here, t is the thickness of the ear plate (1") and d is the pin diameter (2").

$$\sigma = \frac{20.4}{1 \times 2} = 10.2 \text{ ksi} < 23.7 \text{ ksi}$$

Standard Ear Design

Case I

$$\sigma = \frac{35.4}{1 \times 2} = 17.7 \text{ ksi} < 23.7 \text{ ksi}$$

Case III

$$\sigma = \frac{35.4}{1 \times 7.5} = 4.72 \text{ ksi} < 23.7 \text{ ksi}$$

- YIELDING OF WELD JOINTS

Auxiliary Ear Design

Figure 2.12.3-5 shows a free-body diagram of the ear with the lifting force acting through the center of the hole for Load Case I and Case II. The center of gravity of the weld group and of the bottom of the bracket point A is G. The force F_G is the force of the weld group acting on the ear. Because F_G has a different line of action than the lifting force, there is also a moment M .

Load Case I

The moment M produces a bending stress in the welds. The force F_G produces shear throughout the weld. These effects are:

$$M = 17.7 \times 3 = 53.10 \text{ k-in}$$

$$F_G = 17.7 \text{ kip}$$

- WELD GEOMETRY AND CROSS SECTION PROPERTIES

Weld throat area (A_w)

$$A_w = 1.414 (0.375)(6.75 + 2.0 + 2.25) = 5.833 \text{ in}^2$$

Centroid of weld group (G)

$$\bar{Y} = \frac{\sum_1^3 (\bar{Y}_i A_i)}{\sum_1^3 A_i} = \frac{((1.125 \times 2.25 \times 0.375) + (4.75 \times 2 \times 0.375) + (10.625 \times 6.75 \times 0.375))}{(2.25 \times 0.375 + 2 \times 0.375 + 6.75 \times 0.375)} = 7.614$$

in

Unit moment of inertia (I_u):

$$\begin{aligned} I_u &= \sum (I_o + A_i d_i^2) \\ &= 2 \times \left\{ \left(\frac{2.25^3}{12} + 2.25 \times 6.488^2 \right) + \left(\frac{2^3}{12} + 2 \times 2.863^2 \right) + \left(\frac{6.75^3}{12} + 6.75 \times 3.012^2 \right) \right\} \end{aligned}$$

$$= 399.17 \text{ in}^3$$

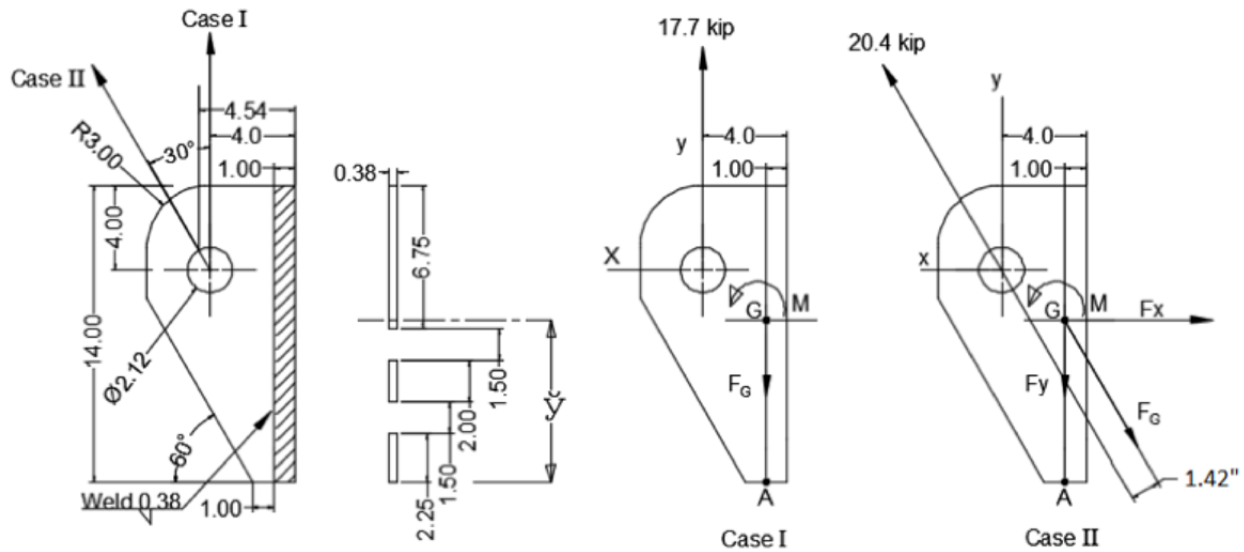


Figure 2.12.3-5. Auxiliary Ear, Case I and Case II Weld Stresses

Then the moment of inertia about an area through G parallel to area Z is:

$$I = 0.707 h I_u = 0.707 (0.375) (399.17) = 105.83 \text{ in}^4$$

For the weld metal the normal stress at point A:

$$\sigma_x = \frac{Mc}{I} = \frac{53.10(7.614)}{105.83} = 3.82 \text{ ksi}$$

The shear stress is:

$$\tau_{xy} = \frac{F}{A} = \frac{17.7}{5.833} = 3.03 \text{ ksi}$$

The resulting Von Mises stress in the weld metal is:

$$\sigma' = \sqrt{\sigma_x^2 + 3\tau_{xy}^2} = \sqrt{3.82^2 + 3(3.03)^2} = 6.5 \text{ ksi} < 75 \text{ ksi}$$

CALCULATION OF STRESS IN THE PARENT METAL:

The area subject to shear is :

$$A = 0.375 (6.75 + 2.0 + 2.25) = 4.125 \text{ in}^2$$

$$\tau_{xy} = \frac{17.7}{4.125} = 4.29 \text{ ksi}$$

The section modulus of the ear at the weld interface is:

$$\frac{I}{C} = \frac{hl_u}{C} = \frac{0.375 \times 0.5 \times 399.17}{7.614} = 9.83 \text{ in}^3$$

Thus, the tensile stress at A in the parent metal is:

$$\sigma_x = \frac{M}{I/C} = \frac{53.10}{9.83} = 5.4 \text{ ksi}$$

$$\sigma' = \sqrt{\sigma_x^2 + 3\tau_{xy}^2} = \sqrt{5.4^2 + 3(4.29)^2} = 9.19 \text{ ksi} < 23.7 \text{ ksi}$$

Load Case II

Figure 2.12.3-5 (Case II) shows a free body diagram of the ear for the Load Case II.

The moment M produces a bending stress in the welds.

The force component Fx produces tension throughout the weld.

The force component Fy produces shear throughout the weld.

These effects are:

$$M = 20.4 (1.42) = 28.97 \text{ k-in.}$$

$$F_x = 10.2 \text{ kip}$$

$$F_y = 17.7 \text{ kip}$$

$$A_w = [(2.25 + 2 + 6.75) \times 0.375 \times 0.707] \times 2 = 5.833 \text{ in}^2$$

At the point A the bending stress and tensile stress due to Fx add. For the weld metal the total normal stress is:

$$\sigma_x = \frac{F_x}{A} + \frac{M_C}{I} = \frac{10.2}{5.83} + \frac{28.97(7.614)}{105.84} = 3.83 \text{ ksi}$$

The shear stress is:

$$\tau_{xy} = \frac{F_y}{A} = \frac{17.7}{5.83} = 3.03 \text{ ksi}$$

Thus, the Von Mises stress in the weld is:

$$\sigma' = \sqrt{\sigma_x^2 + 3\tau_{xy}^2} = \sqrt{3.83^2 + 3(3.03)^2} = 6.51 \text{ ksi} < 23.7 \text{ ksi}$$

The stresses in the parent metal are:

$$A_{pm} = (2.25 + 2 + 6.75) \times 0.375 = 4.125$$

$$\tau_{xy} = \frac{F_y}{A} = \frac{17.7}{4.125} = 4.29 \text{ ksi}$$

$$\sigma_x = \frac{F_x}{A} + \frac{M}{I/C} = \frac{10.2}{4.125} + \frac{28.97}{9.83} = 5.42 \text{ ksi}$$

$$\sigma' = \sqrt{\sigma_x^2 + 3\tau_{xy}^2} = \sqrt{5.42^2 + 3(4.29)^2} = 9.2 \text{ ksi} < 23.7 \text{ ksi}$$

Standard Ear Design

Figure 2.12.3-6 shows a detailed sketch of the standard ear design. It includes dimensions, weld lines identification diagram, and a free body diagram of the ear plate for load conditions Case I and Case II. The investigation of stress on the welds is conducted conservatively by considering only welds A and B are active, in this part the welds are analyzed for both load conditions Case I and Case II. Case III was not analyzed because the resultant force in this case acts along the same line of action as the force in Case I.

Load case I

Figure 2.12.3-6 (Case I) shows a free body diagram of the standard ear for Load Case I.

Centroid of weld group (\bar{Y})

$$\bar{Y} = \frac{\sum_1^2 (\bar{Y}_i A_i)}{\sum_1^2 A_i} = \frac{(2.25 \times 0.375 \times 0.19) + (15.87 \times 0.375 \times 7.935)}{2.25 \times 0.375 + 15.87 \times 0.375} = 6.97 \text{ in}$$

Unit moment of inertia (I_u):

$$\begin{aligned} I_u &= \sum (I_o + A_i d_i^2) \\ &= 2 \times \left\{ \left(\frac{15.87^3}{12} + 15.87 \times (7.935 - 6.97)^2 \right) + (2.25 \times 6.97^2) \right\} \\ &= 914.13 \text{ in}^3 \end{aligned}$$

Then the moment of inertia about an axis through G parallel to axis Z through the weld minimum effective throat is:

$$I = 0.707 h I_u = 0.707 \times (0.375) \times 914.13 = 242.36 \text{ in}^4$$

For the weld metal the normal stress at point A:

$$\sigma_x = \frac{Mc}{I} = \frac{35.4 (5) 6.97}{242.36} = 5.09 \text{ ksi}$$

Security-Related Information Figure Withheld Under 10 CFR 2.390.

Figure 2.12.3-6. Standard Ear, Case I and Case II Weld Stresses

The shear stress is:

$$\tau_{xy} = \frac{F_G}{A} = \frac{35.4}{2(0.707)(2.25 \times 0.375 + 15.87 \times 0.375)} = 3.68 \text{ ksi}$$

The resulting von Mises stress in the weld metal is.

$$\sigma' = \sqrt{\sigma_x^2 + 3\tau_{xy}^2} = \sqrt{5.09^2 + 3(3.68)^2} = 8.16 \text{ ksi} < 23.7 \text{ ksi}$$

CALCULATION OF STRESS IN THE PARENT METAL:

The area subject to shear is:

$$A = 2 \times (0.375) \times (2.25 + 15.87) = 13.59 \text{ in}^2$$

Thus, the shear stress on the parent metal is:

$$\tau_{xy} = \frac{F_G}{A} = \frac{35.4}{13.77} = 2.6 \text{ ksi} < 13.7 \text{ ksi}$$

The section modulus of the ear plate at the weld interface is:

$$\frac{I}{C} = \frac{0.38 \times 914.33}{6.97} = 49.85 \text{ in}^3$$

Thus, the tensile stress at A in the parent metal is:

$$\sigma_x = \frac{35.4 (5)}{49.85} = 3.6 \text{ ksi}$$

$$\sigma' = \sqrt{\sigma_x^2 + 3\tau_{xy}^2} = \sqrt{3.6^2 + 3(2.6)^2} = 5.77 \text{ ksi} < 23.7 \text{ ksi}$$

Load Case II

Figure 2.12.3-6 (Case II) shows a free body diagram of the standard ear for Load Case II.

$$A = 2(0.707)(0.375)(2.25 + 15.87) = 9.61 \text{ in}^2$$

$$M = 40.9(0.31) = 12.68 \text{ k-in}$$

$$F_x = 20.5 \text{ kip}$$

$$F_y = 35.4 \text{ kip}$$

At the point B the bending stress and the tensile due to F_x add. For the weld metal the total normal stress is:

$$\sigma_x = \frac{F_x}{A} + \frac{Mc}{I} = \frac{20.5}{9.61} + \frac{12.68(16.25-6.97)}{242.36} = 2.62 \text{ ksi}$$

The shear stress is:

$$\tau_{xy} = \frac{F_y}{A} = \frac{35.4}{9.61} = 3.68 \text{ ksi}$$

Thus, the von Mises stress in the weld is:

$$\sigma' = \sqrt{\sigma_x^2 + 3\tau_{xy}^2} = \sqrt{2.62^2 + 3(3.68)^2} = 6.9 \text{ ksi} < 23.7 \text{ ksi}$$

The stresses in the parent metal are:

$$A = 2 \times (0.375) \times (2.25 + 15.87) = 13.59 \text{ in}^2$$

$$\tau_{xy} = \frac{35.4}{13.59} = 2.6 \text{ ksi}$$

$$\sigma_x = \frac{20.5}{13.59} + \frac{12.68}{49.85} = 1.77 \text{ ksi}$$

$$\sigma' = \sqrt{1.77^2 + 3(2.6)^2} = 4.85 \text{ ksi} < 23.7 \text{ ksi}$$

- YIELDING OF ATTACHING BOLT AND SHEARING OF BOLT AND TAPPED THREAD

Bolt Loading Auxiliary Ear Design

For the auxiliary ear design, the external bolt force produced by the lifting condition is:

Load Case I

The moment applied to the bolts is:

$$M = 17.7(4.00) = 70.8 \text{ k-in}$$

The tensile stress σ_{tb} at the bottom of contact area due to the applied moment is:

$$\sigma_{tb} = \frac{Md/2}{I} = \frac{Md/2}{bd^3/12} = \frac{6M}{bd^2}$$

Where b and d are the base and height dimensions of the contact area. The tensile load on the bolt is the area A_{tb} of each fastener times σ_{tb} .

$$F_T = \frac{6M}{bd^2} A_{tb}$$

Where A_{tb} for the bottom row bolt is:

$$A_{tb} = 3.00 \times (2.5 + 1.75) = 12.75 \text{ in}^2$$

$$F_T = \frac{6(70.8)}{6.0 \times 9.5^2} \times 12.75 = 10.00 \text{ kip}$$

Load Case II

The moment for this Load Case is reduced by the action of the horizontal component as follows:

$$M = 17.7 \times (4.54) - 10.2 \times (0.92 + 0.50 + 3.50 + 1.75) = 12.32 \text{ k-in. see}$$

Figure 2.12.3-1.

The tensile load on the bolt is:

$$F_T = \frac{6M}{bd^2} \times A_{tb} + \frac{F_H}{4} = \frac{6(12.32)(12.75)}{6.0(9.5)^2} + \frac{10.2}{4} = 1.74 + 2.55 = 4.29 \text{ kip}$$

Bolt Loading, Standard Ear Design

Load Case I and Case III (Slot Lift)

The moment applied to the bolt is:

$$M = 35.4(6.00) = 212.4 \text{ k-in}$$

$$A_{tb} = 3.00(3 + 1.75) = 14.25 \text{ in}^2$$

The tensile load F_t per bolt at the bottom row of bolts due to the applied moment is:

$$F_t = \frac{6MA_{tb}}{bd^2} = \frac{6(212.4)(14.25)}{6.0(10.0)^2} = 30.27 \text{ kip}$$

Load Case II

The moment for Load Case II is:

$$M = 35.4 (6.54) - 20.5 (0.92 + 7.75 + 3.50 + 1.75) = -53.84 \text{ k-in}$$

The tensile load F_t per bolt at the top row of bolts is:

$$A_{tb} = 3.00(3.5 + 1.75) = 15.75 \text{ in}^2$$

$$F_t = \frac{6(53.84)(15.75)}{6.0(10.0)^2} + \frac{20.5}{4} = 13.61 \text{ kip}$$

Load Case III ear base lift is not considered because the moment area is less than that of Load Case I and the load acts on the same directions as Load Case I.

Table 2.12.3-1 presents a summary of bolt loading for each of the ear designs (auxiliary and standard). Because the standard design under Load Case I, straight lift, imposes the largest tensile load on the bolt than in the other conditions, this load value (30.27 kip) is used in the analysis of the bolt.

Table 2.12.3-1. Bolt Loading Per Ear Design and Load Case

| Ear Design | Bolt Loading (kip) | | | Yield Strength (ksi) | Shear Strength (ksi) |
|------------|--------------------|-------|-----------------|----------------------|----------------------|
| | Load Case | | | | |
| | I | II | III (Slot Lift) | | |
| Auxiliary | 10 | 4.29 | N/A | 85 | 51 |
| Standard | 30.27 | 13.61 | 30.27 | 85 | 51 |

Bolt Analysis

Bolt and thread section properties use in the analyses for both internal and external threads are evaluated for a standard 1-8 UNC x 2-1/2 in bolt as follows.

Tensile stress area (A_t) for high strength bolt with $\sigma_{tb} > 100\text{ksi}$, as provided in *Machineries Handbook*, Reference 2-26, Page 1490 is:

$$A_t = \pi \left(\frac{E_{smin}}{2} - \frac{0.16238}{n} \right)^2$$

where:

$$E_{smin} = \text{Minimum pitch diameter} = 0.9188 \text{ inches}$$

$$n = \text{Number of threads per inch} = 8$$

$$A_t = \pi \left(\frac{0.9188}{2} - \frac{0.16238}{8} \right)^2 = 0.61 \text{ in}^2$$

Shear area of the external (A_s) and the internal (A_n) threads, Machineries Handbook, Reference 2-26, Page 1491.

$$A_s = \pi n L_e K_{n_{\max}} \left[\frac{1}{2n} + 0.57735 (E_{s_{\min}} - K_{n_{\max}}) \right]$$

where:

$$\begin{aligned} n &= 8 \\ L_e &= \text{Length of engagement} = 1.680 \text{ inches} \\ K_{n_{\max}} &= \text{Maximum minor diameter of internal thread} = 0.8795 \text{ inches} \\ A_s &= \pi (8)(1.680)(0.8795) \left[\frac{1}{2(8)} + 0.57735 (0.9188 - 0.8795) \right] = 3.164 \text{ in}^2 \\ A_n &= \pi n L_e D_{s_{\min}} \left[\frac{1}{2n} + 0.57735 (D_{s_{\min}} - E_{n_{\max}}) \right] \end{aligned}$$

where:

$$\begin{aligned} D_{s_{\min}} &= \text{Minimum major diameter of external thread} = 0.9848 \text{ inches} \\ E_{n_{\max}} &= \text{Maximum pitch diameter of internal thread} = 0.9242 \text{ inches} \\ A_n &= \pi (8)(1.680)(0.9848) \left[\frac{1}{2(8)} + 0.57735 (0.9848 - 0.9242) \right] = 4.05 \text{ in}^2 \end{aligned}$$

Bolt Preload

J.E. Shigley and L.D. Mitchell (Reference 2-27) suggest the preload (F_i) on the bolt should be between 60% and 90% of the proof load. The proof load is equal to 85% of the yield strength (S_y) multiplied by the tensile stress area (A_t). Therefore, using 80% of the load, the preload value is:

$$F_i = 0.80(0.85 S_y A_t) = 0.8(0.85) \times 85(0.6057) = 35.01 \text{ kip}$$

The tightening torque for a lubricated bolt is:

$$T = k F_i d$$

Where:

$$\begin{aligned} T &= \text{torque} \\ k &= \text{torque coefficient} = 0.2 \\ d &= \text{bolt nominal diameter} \\ T &= 0.2(35030)(1/12) \cong 600 \text{ ft lb} \end{aligned}$$

Stresses produced by preload:

Bolt tension

$$\sigma = \frac{F_i}{A_t} = \frac{35.03}{0.606} = 57.80 \text{ ksi}$$

Bolt thread stripping

$$\tau = \frac{F_i}{A_s} = \frac{35.03}{3.164} = 11.07 \text{ ksi}$$

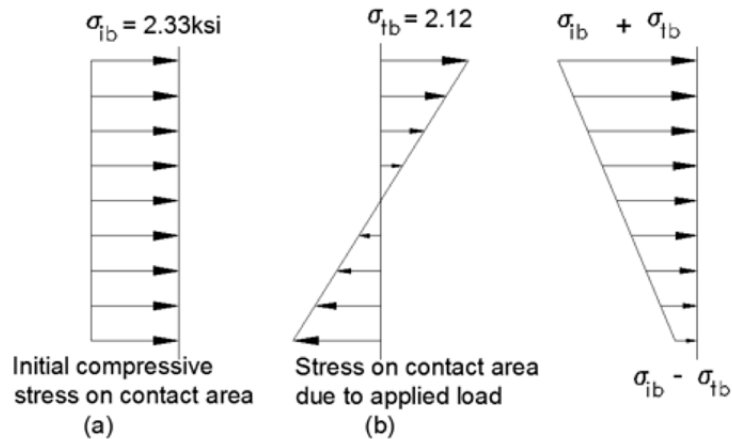
Tapped thread stripping

$$\tau = \frac{F_i}{A_n} = \frac{35.03}{4.054} = 8.64 \text{ ksi}$$

Bearing stress between cask and ear

$$\sigma_{ib} = \frac{(\# \text{ of bolt})(F_i)}{\text{Contact Area}} = \frac{4(35.03)}{6.0(10.0)} = 2.33 \text{ ksi}$$

The initial bearing pressure, σ_{ib} , previously calculated, is assumed to be uniform over the contact area. The bearing pressure should not be exceeded by tensile stress, σ_{tb} .



$$\sigma_{tb} = \frac{6M}{bd^2} = \frac{6(212.4)}{6(10.0)^2} = 2.12 \text{ ksi}$$

$$\sigma_{ib} > \sigma_{tb}$$

The moment M (212.4 k-in) is produced by Load Case I or III on the standard ear design attaching bolt as previously calculated.

The nominal tensile stress, σ_t , in the bottom row bolts is:

$$\sigma_t = \frac{F_t}{A_t}$$

As previously calculated the tensile load for Load Case I is 30.27 kip per bolt.

$$\sigma_t = \frac{30.27}{0.606} = 49.95 \text{ ksi} < 85 \text{ ksi}$$

and the direct-shear component is:

$$\tau = \frac{35.4}{4(0.606)} = 14.6 \text{ ksi} < 51 \text{ ksi}$$

The interaction equation for the strength of a connection with bolts in combined shear and tension may be approximated by the elliptical relationship:

$$\left(\frac{\sigma_t}{\sigma_y}\right)^2 + \left(\frac{\tau}{0.6\sigma_y}\right)^2 \leq 1.0$$

$$\left(\frac{49.95}{85.0}\right)^2 + \left(\frac{14.60}{0.6(85)}\right)^2 \leq 1.0$$

$$0.43 \leq 1.0$$

Therefore, the selected bolts are adequate to carry the lifting load criteria.

For the shearing of the bolt threads due to tensile load F_t .

$$\tau = \frac{F_t}{A_s} = \frac{30.27}{3.164} = 9.57 \text{ ksi} < 51.0 \text{ ksi}$$

For the shearing of the tapped threads due to tensile load F_t .

$$\tau = \frac{F_t}{A_n} = \frac{30.27}{4.054} = 7.47 \text{ ksi} < 51.0 \text{ ksi}$$

Bolt Fatigue Analysis

Bolt and Load Data:

1-8 UNC-2A, ASTM A193-B6

| | |
|-------------------------|-----------------------------|
| Yield Strength: | 85 ksi (minimum) |
| Operating Temperature: | 250°F |
| Modulus of Elasticity: | 28.1 (10 ⁶) psi |
| Maximum Tensile Stress: | 57.8 ksi (Preload) |
| Maximum Shear Stress: | 14.6 ksi |

(Shear neglects the reducing effect of friction between ear and cask body.)

The maximum cycle of stress is due to a combination of the preload stress, 57.80 ksi, and the shear stress (14.6 ksi) due to lifting. These give a maximum principal stress of:

$$\sigma_{\max} = \frac{57.80}{2} + \sqrt{\left(\frac{57.8}{2}\right)^2 + 14.6^2} = 61.28 \text{ ksi}$$

From ASME Section III NB 3232.3, the fatigue strength reduction factor to be used is 4.0. Because the fatigue curve (ASME Section III, Figure I-9.4 (Reference 2-28)) is based on modulus of elasticity of 30(10⁶) psi and the bolt has a modulus of elasticity of 28.1(10⁶) psi, the stress range is given by:

$$S = (61.28 \text{ ksi}) \times 4(30(10^6)/28.1(10^6)) = 261.7 \text{ ksi}$$

To select the correct fatigue curve, the stress intensity value, S_m , of 26.5 ksi is used at 250°F. Calculating the alternating stress:

$$S_a = \frac{1}{2} S = \frac{1}{2} (261.7) = 130.85 \text{ ksi}$$

Using the fatigue curve for a maximum nominal stress $\leq 2.7 S_m$ the fatigue limit is $\cong 600$ cycles as provided in Figure 2.12.3-7. Assuming an average of four ear lifts per usage and 12 usages per year, this gives a bolt life of:

$$\frac{600}{\left(12 \frac{\text{usages}}{\text{year}}\right) \left(4 \frac{\text{cyc.}}{\text{usage}}\right)} = 12.5 \text{ yrs.}$$

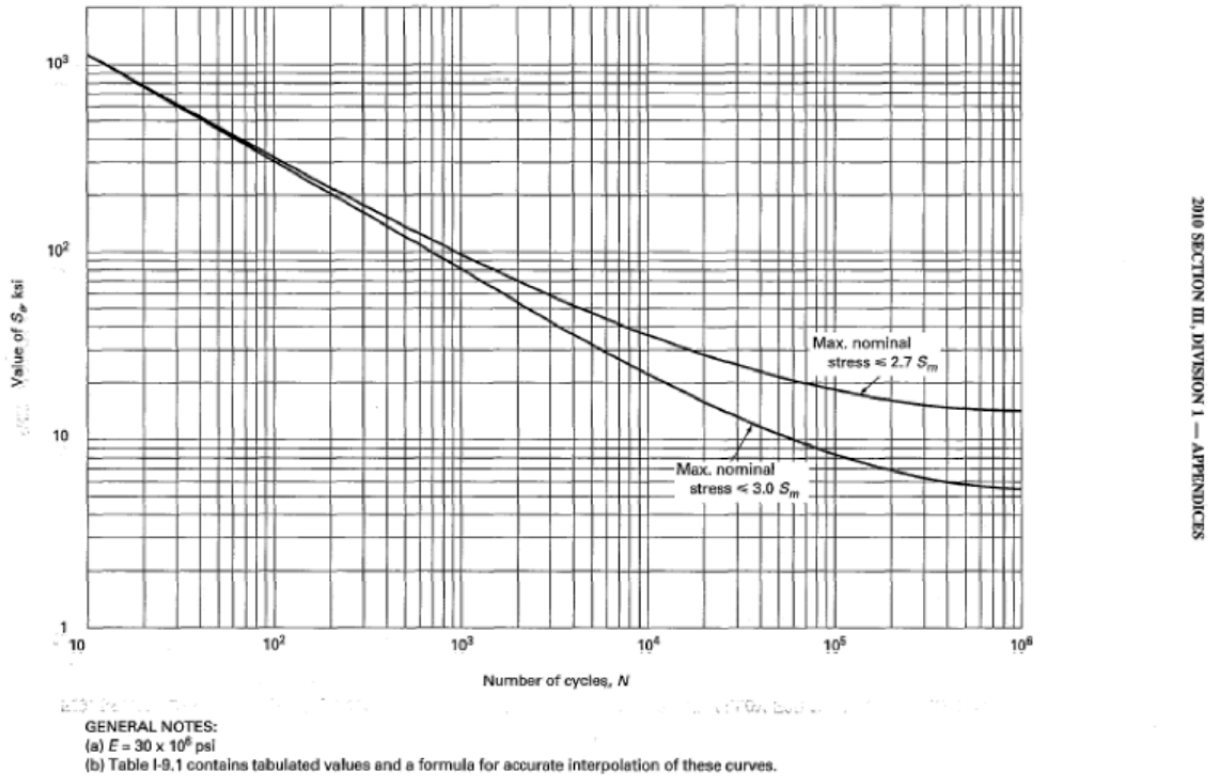


Figure 2.12.3-7. Design Fatigue Curves For High Strength Steel Bolting Above 700°F
(from Reference 2-18)

- YIELDING OF CASK OUTER SHELL**

The lifting ears are mounted to the outer shell of the cask on a mounting plate embedded to the cask. The mounting plate is embedded about 1.75 inches into the cask through the outer shell and the lead shield. However 1 inch thickness of the outer shell and the maximum vertical load of 35.4 kip (standard ear) are conservatively considered for yielding due to the lifting load.

$$\sigma_c = \frac{F_c}{A} = \frac{35.4}{7.5} = 4.72 \text{ ksi}$$

where Area (A) = thickness of shell x width of mounting plate = 1 x 7.5 = 7.5 in²

$$\tau = \frac{F}{A_s} = \frac{35.4}{12.5} = 2.83 \text{ ksi}$$

where the shear area (A) = 2 x (6.25 x 1) = 12.5 in²

$$\sigma_b = \frac{Mc}{I} = \frac{247.8 \times 3.125}{152.59} = 5.07 \text{ ksi}$$

where M = 35.4 x 7 = 247.8 k-in,

$$c = 6.25/2 = 3.125 \text{ in}$$

$$I = \frac{bh^3}{12} = \frac{7.5 \times 6.25^3}{12} = 152.59 \text{ in}^4$$

$$\sigma' = \sqrt{(4.72 + 5.07)^2 + 3 \times (2.83)^2} = 10.95 \text{ ksi}$$

- EXCESSIVE LOAD FAILURE

The lifting devices must be designed such that their failure under excessive load would not impair the ability of the package to meet other requirements of 10 CFR 71. In this section a margin of safety (MS) is determined for each of the lifting system components based on the results presented in Table 2.12.3-2.

Table 2.12.3-2. Summary of Ear Analysis for Model 2000

| Condition | Stress Level (ksi) | | Allowable (ksi) Based on Yield | MS(y) Aux./Std. | Allowable Based on Su | MS(U) Aux./Std. |
|-------------------------------|--------------------|----------|--------------------------------|-----------------|-----------------------|-----------------|
| | Auxiliary | Standard | | | | |
| Shear tearout of lift hole | 6.02 | 8.98 | 14 | 1.33/0.56 | 26.18 | 3.35/1.92 |
| Tensile failure of ear plate | 4.82 | 17.7 | 23.7 | 3.92/0.34 | 68.6 | 13.23/2.88 |
| Bearing of shackle pin on ear | 10.2 | 17.7 | 23.7 | 1.32/0.34 | 68.6 | 5.73/2.88 |
| Yielding of weld joint | 9.2 | 8.16 | 23.7 | 1.58/1.9 | 68.6 | 6.46/7.41 |
| Yielding of attaching bolt | --- | 57.8 | 85 | 0.47 | 110 | 0.90 |
| Shearing of bolt thread | --- | 11.07 | 51 | 3.61 | --- | --- |
| Shearing of tapped thread | --- | 8.64 | 14 | 0.62 | 26.18 | 2.03 |
| Yielding of cask outer shell | --- | 10.95 | 23.7 | 1.16 | 68.6 | 5.26 |

Note:

Bolt and bolt thread stress levels are documented in Table 2.12.3-2 for standard ear because maximum bolt loading is documented during slot lift (Case III) of the standard ear (see Table 2.12.3-1).

The margins of safety MS (y) with respect to yield is calculated as follows:

$$MS(yield) = \frac{\text{Allowable based on yield strength}}{\text{Stress level}} - 1$$

The ear and cask shell material is ASTM 240 type 304 stainless steel. The margins of safety with respect to ultimate failure M(U)are:

For shear tear-out of lifting hole

$$\text{Shear Strengths} = \frac{\sigma_{ult}}{2(1+\mu)} = \frac{68.6}{2(1.31)} = 26.18 \text{ ksi}$$

$$\tau = 8.98 \text{ ksi (Standard Ear, Load Case I)}$$

$$MS(U) = \frac{26.18}{8.98} - 1 = 1.92$$

For tensile failure of ear plate

$$\sigma_T = 17.7 \text{ ksi (Standard Ear, Load Case III)}$$

$$MS(U) = \frac{68.6}{17.7} - 1 = 2.88$$

For yielding of weld joints

$$\sigma' = 9.2 \text{ ksi (Auxiliary Ear, Load Case II)}$$

$$MS(U) = \frac{68.6}{9.2} - 1 = 6.46$$

For bolts

$$P_{ult} = 110 \times 0.606 = 66.66 \text{ kip}$$

$$F_t = 57.8(0.606) = 35 \text{ kip}$$

$$MS(U) = \frac{66.66}{35.0} - 1 = 0.904$$

For yielding of cask outer shell

$$\sigma' = 10.95 \text{ ksi}$$

$$MS(U) = \frac{68.6}{10.95} - 1 = 5.26$$

A review of the above margin of safety indicates that, under excessive loading, the ear attaching bolts will fail before the ear plates, ear welds or cask shell. Failure of the bolts assures that the ability of the package to meet any other regulatory requirements is not impaired.

- MODEL 2000 LID LIFTING LUG ANALYSIS

The lifting lug is covered during transport. It is shown by analysis that this lifting device complies with requirements of 10 CFR 71.45(a). The lifting lug is able to support three times the weight of the lid without yielding.

The weakest part of the lifting lug is the fillet weld, which attaches the stainless steel loop to the cask lid. Using the maximum shear stress theory the weld is determined to have a factor of safety of 1.76 when analyzed for lifting 3 times the weight of the lid.

The lifting lug is analyzed by considering the rigid frame shown in Figure 2.12.3-8. The analytical model has the same height and distance between the supports as the lifting lug.

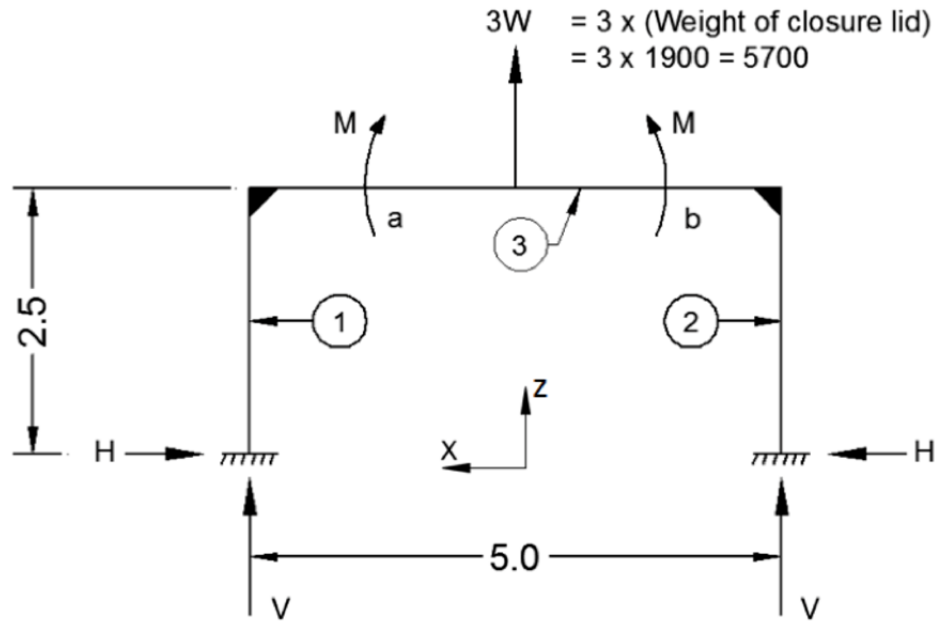


Figure 2.12.3-8. Analytical Model of Lifting Lug

The statistically indeterminate forces and moments are obtained by solving the following set of equations from Reference 2-29.

$$\frac{-1/3HL^3_1}{I_1} + \frac{1/2M_1L^2_1}{I_1} = \frac{1/3HL^3_2}{I_2} - \frac{1/2M_2L^2_2}{I_2}$$

$$\frac{-1/2HL^2_1}{I_1} + \frac{M_1L_1}{I_1} = \frac{-1/3M_1L_3}{I_3} + \frac{1/6W(bL_3 - \frac{b^3}{L_3})}{I_3} - \frac{1/6M_2L_3}{I_3}$$

$$\frac{-1/2HL^2_2}{I_2} + \frac{M_2L_2}{I_2} = \frac{1/3M_2L_3}{I_3} + \frac{1/6M_1L_3}{I_3} - \frac{1/6W[2bL_3 + (\frac{b^3}{L_3}) - 3b^2]}{I_3}$$

And by symmetry:

$$M_1 = M_2 = M$$

$$H_1 = H_2 = H$$

$$V_1 = V_2 = V = 2,850 \text{ lb.}$$

Also,

$$L_1 = L_2 = 2.5$$

$$L_3 = 5.0$$

$$I_1 = I_2 = I_3$$

$$a = b = 2.5$$

Using substitution and solving the above equations simultaneously gives:

$$\begin{aligned} V &= 2,850 \text{ lb} \\ H &= 2,671 \text{ lb} \\ M &= 4,452 \text{ lb-in} \end{aligned}$$

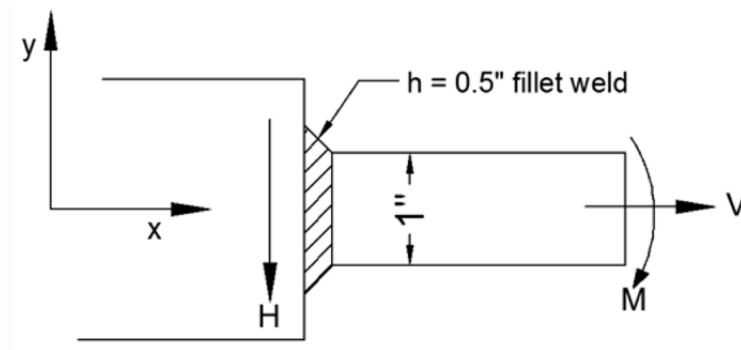


Figure 2.12.3-9. Loading on the Weld Area

The loading in the weld area is shown in Figure 2.12.3-9. The moment M produces a bending stress, σ_m , in the weld. This stress is assumed to act normal to the throat area (see Reference 2-27, P. 427).

The unit moment of inertia of the welds is from Reference 2-27, P. 429, given by:

$$I_u = \pi r^3$$

But the moment of inertia based on the weld throat is:

$$I = 0.707h\pi r^3$$

The normal stress in the weld is therefore given by:

$$\sigma = \frac{MC}{I} = \frac{MC}{0.707h\pi r^3}$$

The maximum stress occurs at the outer fibers where:

$$C = r$$

$$Z = 2\pi r$$

The maximum stress is therefore given by:

$$\sigma_m = \pm \frac{M}{0.707h\pi r^2}$$

From Reference 2-27, Equation (9.3), p. 417, the stress in the weld due to the force V is given by:

$$\tau_v = \frac{V}{0.707hZ}$$

Similarly, from Reference 2-27, Equation (a), p. 427, the stress in the weld due to the force H is given by:

$$\tau_H = \frac{H}{0.707hZ}$$

Figure 2.12.3-10 shows the stresses acting on the weld at the point where the bending moment is a maximum.

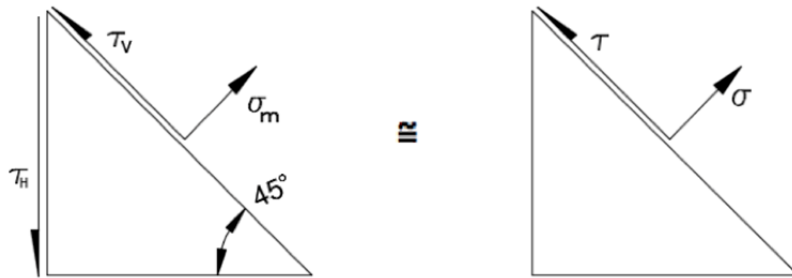


Figure 2.12.3-10. Stresses Acting on the Weld

$$\sigma = \sigma_m = \frac{4452}{0.707 \times 0.5 \times \pi \times (0.5)^2} = 16,035.3 \text{ psi}$$

$$\begin{aligned} \tau &= \tau_v - \tau_h \cos 45^\circ \\ &= \frac{2,850}{0.707 \times 0.5 \times 2 \pi \times 0.5} - \frac{2,671}{0.707 \times 0.5 \times 2 \pi \times 0.5} \times 0.707 \\ \tau &= 2,566 - 1,700 = 866 \text{ psi} \end{aligned}$$

From Reference 2-27, p.31, the principal stresses are found using:

$$\begin{aligned} \sigma_1, \sigma_2 &= \frac{\sigma}{2} \pm \sqrt{\left(\frac{\sigma}{2}\right)^2 + \tau^2} \\ \tau_{\max} &= \pm \sqrt{\left(\frac{\sigma}{2}\right)^2 + \tau^2} \end{aligned}$$

Substituting for σ and τ yields

$$\begin{aligned} \sigma_1, \sigma_2 &= \frac{16,035.3}{2} \pm \sqrt{\left(\frac{16,035.3}{2}\right)^2 + 866^2} \\ &= 8,017.7 \pm 8064.3 \\ \sigma_1 &= 16,082 \text{ psi} \\ \sigma_2 &= -46.6 \text{ psi} \\ \tau_{\max} &= \pm 8064.3 \text{ psi} \end{aligned}$$

The maximum shear stress is applied to determine the likelihood of failure or safety.

$$\text{Allowable} = \tau_{\text{allowable}} = 0.6 S_y$$

Where S_y denotes the yield strength.

The yield strength of stainless steel Type 304 is 23.7 ksi.

Substituting into equation (32)

$$\text{Allowable Stress} = 0.6 \times 23.7 = 14.22 \text{ ksi}$$

$$\tau_{\max} = 8.06 \text{ ksi} \leq 14.22 \text{ ksi}$$

Therefore, the factor of safety is given by

$$\text{FS} = \frac{14.22}{8.06} = 1.76 \text{ (this is for lifting 3W)}$$

2.12.3.2. Tie-Down Analysis

The purpose and scope of this analysis is to demonstrate the structural integrity of the tie-down rib. The Model 2000 Transport Package is shipped normally by truck. Figure 2.12.3-11 shows the overall plan for tying the package to the vehicle. Eight wire ropes or chains tie the package to the vehicle: four connect to the upper tie-down ribs of the overpack, and the other four connect to the overpack base tie-down ribs. In addition, the base of the package is wedged to the truck bed to prevent sliding. Evaluation of the tie-down loading on the tie-down rib adjacent area consisted of the following:

- 1) Identification of the maximum tie-down member tension force due to loading.
- 2) Evaluation of the effect of the above force on the tie-down rib.

Classical hand calculation is used to identify the maximum tie-down member tension forces due to the combined loads. The results of this analysis were added to establish the maximum load. Table 2.12.3-3 gives a summary of each rope tie-down tension load for each force component and the total force. The maximum tie-down wire tension force is estimated to be 148.62 kips. This maximum load is then applied to the tie-down rib to determine the structural integrity of the tie-down rib by analyzing the following modes of failure:

- Shear tear-out of tie-down rib hole
- Bearing of shackle pin on ear
- Yielding of weld joints and parent metal

Security-Related Information Figure Withheld Under 10 CFR 2.390.

Figure 2.12.3-11. Tie-Down of Transport Package to Vehicle

- TIE-DOWN MEMBER TENSION FORCES

The package (wt. = 33,550 lb) is subject to accelerations of 10g longitudinal, 5g transverse, and 2g vertical (up) Per IAEA's "Package stowage and retention" regulations. These accelerations result in the following forces acting on the C.G. of the cask:

$$F_{\text{long}} = 33,550(10) = 335,500 \text{ lbf}$$

$$F_{\text{trans}} = 33,550(5) = 167,750 \text{ lbf}$$

$$F_{\text{vert}} = 33,550(2) = 67,100 \text{ lbf}$$

In this calculation, each load is independently applied to the package and the tensile load on members for each case is calculated. The tensile loads are then added to calculate the maximum tension load on members.

10g Longitudinal

Because the base of the package is chocked, the 10g acceleration will cause it to rotate about point "o" counterclockwise (-x direction). This rotation will cause Ropes 1, 2, 3 and 4 to go slack and tension Ropes 5, 6, 7 and 8. From Figure 2.12.3-12.

$$F_7 = F_8$$

$$F_5 = F_6$$

The component forces for these ropes are:

$$\begin{aligned} F_{5y} &= F_{6y} = F_6 \cos 23.2^\circ \cos 32.7^\circ = 0.774 F_6 \\ F_{5z} &= F_{6z} = F_6 \sin 23.2^\circ = 0.394 F_6 \\ F_{7y} &= F_{8y} = F_8 \cos 46.3^\circ \cos 18.69^\circ = 0.654 F_8 \\ F_{7z} &= F_{8z} = F_8 \sin 46.3^\circ = 0.723 F_8 \end{aligned}$$

The reaction forces from chocking and friction (R_F) and bearing on the package base (R_B) are:

$$\begin{aligned} R_F &= F_{5y} + F_{6y} + F_{7y} + F_{8y} - W_a \\ R_B &= F_{5z} + F_{6z} + F_{7z} + F_{8z} + W_g \quad (\text{assuming } F_1 = F_2 = F_3 = F_4 = 0) \end{aligned}$$

The center of gravity is 63.60 inches.

$$\begin{aligned} \Sigma M_{ox} &= 0 = -W_a 63.60 + W_g 24.25 - R_B 24.25 + (F_{5y} + F_{6y}) 25.5 + (F_{7y} + F_{8y}) \\ &\quad 105.0 + (F_{5z} + F_{6z} + F_{7z} + F_{8z}) 46.25 \\ \Sigma M_{ox} &= -W_a 63.60 + W_g 24.25 - (F_{5z} + F_{6z} + F_{7z} + F_{8z} + W_g) 24.25 + \dots \\ &\quad \dots (F_{5y} + F_{6y}) 25.5 + (F_{7y} + F_{8y}) 105.0 + (F_{5z} + F_{6z} + F_{7z} + F_{8z}) 46.25 \\ &= -W_a 63.60 - [2 \times 0.394 F_6 + 2 \times 0.723 F_8] 24.25 + 2 \times 0.774 F_6 (25.5) + \dots \\ &\quad \dots 2 \times 0.654 F_8 (105.0) + [2 \times 0.394 F_6 + 2 \times 0.723 F_8] 46.25 \\ &= -W_a 63.60 - 19.1 F_6 - 35.1 F_8 + 39.5 F_6 + 137.3 F_8 + 36.4 F_6 + 66.9 F_8 \\ &= -W_a 63.60 + (-19.1 + 39.5 + 36.4) F_6 + (-35.1 + 137.3 + 66.9) F_8 \\ &= -(63.60) W_a + (56.8) F_6 + (169.1) F_8 \\ \Rightarrow 2.134 (10^7) &= (56.8) F_6 + (169.1) F_8 \end{aligned}$$

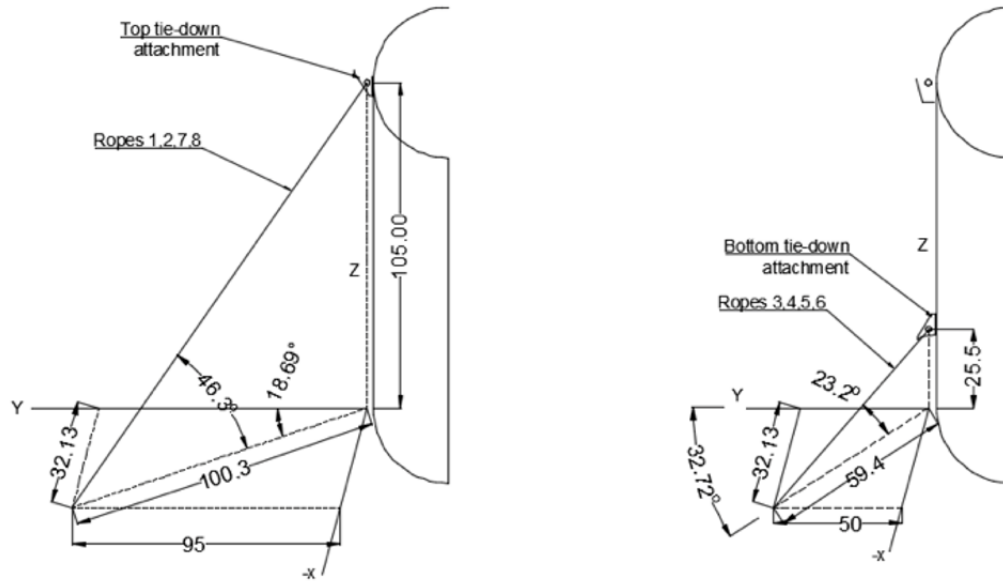


Figure 2.12.3-12. Tie-Down Wire Ropes

This cannot be solved for F6 and F8 so an additional equation relating F6 and F8 is required. By making certain assumptions, this equation can be obtained from consideration of the force and deflection (or extension) characteristics of the different length wire ropes. Figure 2.12.3-13 shows the extension of the ropes at small angle rotation. Assuming the ropes initially have no tension, the ratio of loads due to stretching of the ropes is:

$$\frac{F_7}{F_5} = \frac{\frac{\delta_7 EA}{L_7}}{\frac{\delta_5 EA}{L_5}}$$

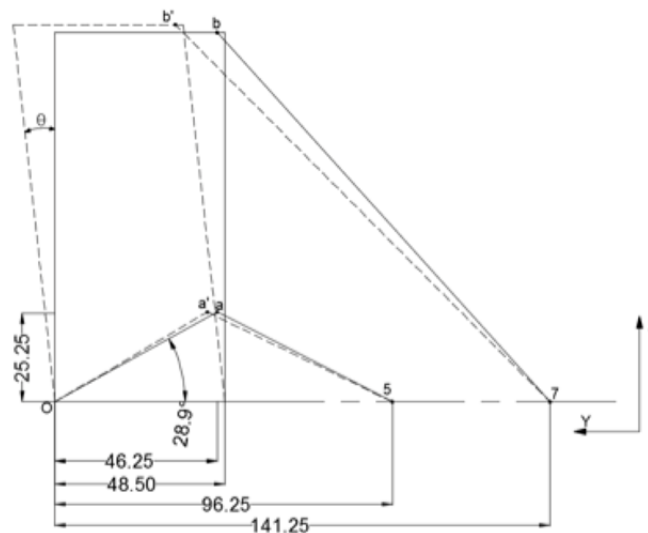


Figure 2.12.3-13. Wire Rope Extension at Small Angle (θ) Rotation

Because both ropes are of the same size and material,

$$\frac{F_7}{F_5} = \frac{\delta_7 L_5}{\delta_5 L_7}$$

For a rotation of θ° about point “O”, line 5 would be extended as follows

$$\delta_5 Z L_{5f} - L_{5i}$$

L_{5f} is the final length of rope 5 as shown in Figure 2.12.3-14.

$$L_{5i} = \sqrt{59.4^2 + 25.5^2} = 64.6 \text{ in}$$

$$\overline{oa'} = \overline{oa} = \sqrt{46.25^2 + 25.5^2} = 52.8 \text{ in}$$

Change in “a” in y direction is:

$$\overline{aa'_y} = 52.8[\cos 28.9^\circ - \cos(28.9 + \theta)]$$

Change in “a” in z direction is:

$$\overline{aa'_z}$$

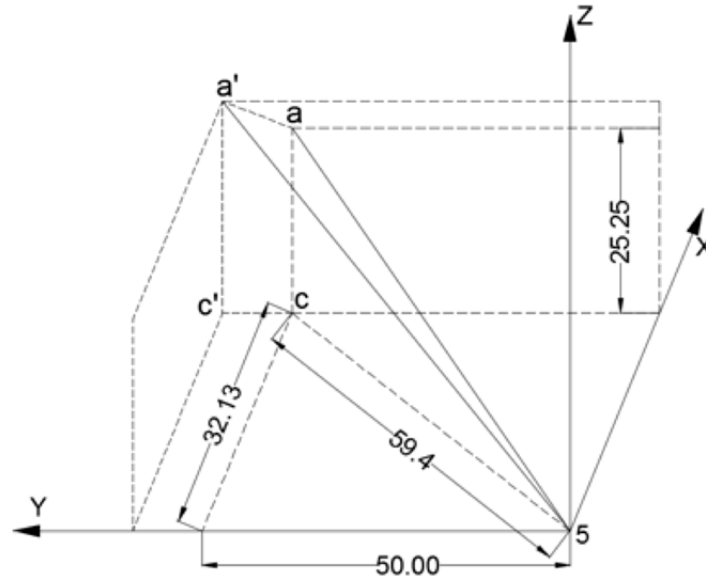


Figure 2.12.3-14. Final Length of Rope 5

$$L_{5f} = \sqrt{(25.5 + 52.8[\sin(28.9^\circ + \theta) - \sin 28.9^\circ])^2 + \dots + (32.13^2 + (50.0 + 52.8[\cos 28.9^\circ - \cos(28.9^\circ + \theta)])^2)}$$

To evaluate the effect of small rotations, L_{5f} will be evaluated for $\theta = 0.1^\circ$, $\theta = 1^\circ$ and $\theta = 10^\circ$.

$$\begin{aligned} L_{5f_{.1^\circ}} &= \sqrt{\frac{(25.5 + 52.8[\sin(29.0^\circ) - \sin 28.9^\circ])^2 + \dots}{32.13^2 + (50.0 + 52.8[\cos 28.9^\circ - \cos(29.0^\circ)])^2}} \\ &= \sqrt{654.4 + 3,536.8} = 64.7 \text{ in} \end{aligned}$$

$$\begin{aligned} L_{5f_{1^\circ}} &= \sqrt{\frac{(25.5 + 52.8[\sin(29.9^\circ) - \sin 28.9^\circ])^2 + \dots}{32.13^2 + (50.0 + 52.8[\cos 28.9^\circ - \cos(29.9^\circ)])^2}} \\ &= \sqrt{691.8 + 3,577.8} = 65.3 \text{ in} \end{aligned}$$

$$\begin{aligned} L_{5f_{10^\circ}} &= \sqrt{\frac{(25.5 + 52.8[\sin(38.9^\circ) - \sin 28.9^\circ])^2 + \dots}{32.13^2 + (50.0 + 52.8[\cos 28.9^\circ - \cos(38.9^\circ)])^2}} \\ &= \sqrt{1,098.2 + 4,072.0} = 71.9 \text{ in} \end{aligned}$$

A similar evaluation for line 7 yields:

$$L_{7i} = \sqrt{100.3^2 + 105^2} = 145.2 \text{ in}$$

$$\overline{ob} = \overline{ob'} = \sqrt{46.25^2 + 105^2} = 114.7 \text{ in}$$

Change in “b” in y direction is:

$$\overline{bb'_y} = 114.7[\cos 66.2^\circ - \cos(66.2 + \theta)]$$

Change in “b” in z direction is:

$$\begin{aligned} \overline{bb'_y} &= 114.7 [\sin(66.2 + \theta) - \sin 66.2] \\ L_{7f} &= \sqrt{\frac{(105 + 114.7[\sin(66.2 + \theta) - \sin 66.2])^2 + \dots}{32.13^2 + (95 + 114.7[\cos 66.2 - \cos(66.2 + \theta)])^2}} \end{aligned}$$

Evaluation at $\theta = 0.1^\circ$, $\theta = 1^\circ$ and $\theta = 10^\circ$ gives:

$$\begin{aligned} L_{7f_{.1^\circ}} &= \sqrt{\frac{(105 + 114.7[\sin 66.3 - \sin 66.2])^2 + \dots}{32.13^2 + (95 + 114.7[\cos 66.2 - \cos 66.3])^2}} \\ &= \sqrt{11041.9 + 10,092.2} = 145.4 \text{ in} \end{aligned}$$

$$L_{7f_{1^\circ}} = \sqrt{11,191.9 + 10,410.1} = 147.0 \text{ in}$$

$$L_{7f_{10^\circ}} = \sqrt{12,419.6 + 14,011.7} = 162.6 \text{ in}$$

Calculation of the ratio $\frac{L_f}{L_i}$ for each rope at each rotation value yields:

| θ | Lf/Li | |
|----------|--------|--------|
| | Rope 5 | Rope 7 |
| 0.1° | 1.002 | 1.001 |
| 1° | 1.011 | 1.012 |
| 10° | 1.113 | 1.120 |

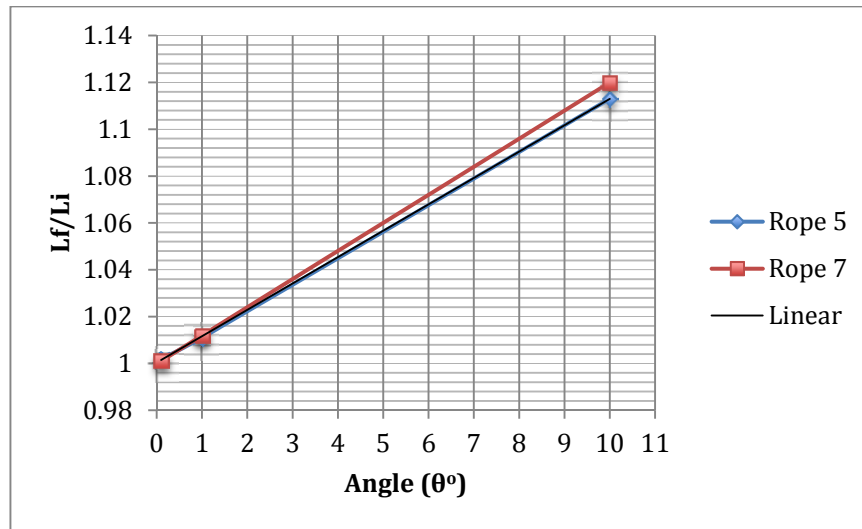


Figure 2.12.3-15. Final to Initial Rope Length Ratio per Small Angle Rotation

The fact that the ratios are the same for each rope and liner indicates that their derivation is correct. Their similarity and linearity would be expected from rigid body rotation.

Back to the relation between F_6 and F_8 (or F_5 and F_7), the ratio of loads due to stretching are for $\delta = 0.1^\circ$:

$$\begin{aligned}\frac{F_7}{F_5} &= \frac{\delta_7 L_5}{\delta_5 L_7} \\ \frac{F_7}{F_5} &= \frac{0.2 * 64.6}{0.1 * 145.2} = 0.8898...^{**} \\ L_5 &= 64.6 \\ L_7 &= 145.2 \\ \delta_5 &= L_{5f} - L_{5i} \\ &= 64.7 - 64.6 = 0.1 \\ \delta_7 &= 145.4 - 145.2 = 0.2\end{aligned}$$

For $\theta = 10^\circ$

$$\frac{F_7}{F_5} = \frac{17.4}{7.3} = 1.061$$

Because the ropes cannot stretch 7.3 or 17.4 inches, this just shows that the ratio of forces in the ropes is fairly close at the two extremes. For the purpose of analysis, the value of 0.8898 will be used as this represents a more realistic elongation of the ropes.

$$F_7 = F_8 = 0.8898 F_5 = 0.8898 F_6$$

NEDO-33866 Revision 0
Non-Proprietary Information – Class I (Public)

$$F_6 56.8 + (0.8898 F_6) \times 169.1 = 2.134 (10^7)$$

$$\begin{aligned} F_5 &= F_6 = 102,960.00 \\ F_7 &= F_8 = 0.8898 F_6 = 91,614.00 \\ RF &= F_{5y} + F_{6y} + F_{7y} + F_{8y} - W_a \\ &= 0.774F_5 + 0.774F_6 + 0.654F_7 + 0.654F_8 - 335,500 = -56,287 \text{ lb} \end{aligned}$$

5g Transverse

This time the 5g acceleration will cause the package to rotate at a point 90° clockwise from point “o”. This will cause ropes 2, 4, 6 and 8 to go slack, and tension ropes 1, 3, 5 and 7. From symmetry the following assumptions can be made with reference to 2.12.3-11.

$$\begin{aligned} F_1 &= F_7 \\ F_3 &= F_5 \end{aligned}$$

The component forces for these ropes are:

$$\begin{aligned} F_{3x} &= F_{5x} = F_5 \cos 23.2^\circ \sin 32.7^\circ &= 0.497 F_3 \\ F_{3z} &= F_{5z} = F_5 \sin 23.2^\circ &= 0.394 F_3 \\ F_{1x} &= F_{7x} = F_7 \cos 46.3^\circ \sin 18.69^\circ &= 0.221 F_1 \\ F_{1z} &= F_{7z} = F_7 \sin 46.3^\circ &= 0.723 F_1 \end{aligned}$$

The reaction forces from chocking and friction (RF) and bearing on the package base (RB) are:

$$RF = F_{5x} + F_{3x} + F_{7x} + F_{1x} - W_a$$

$$RB = F_{5z} + F_{3z} + F_{7z} + F_{1z} + W_g$$

RB is calculated assuming $F_2 = F_4 = F_6 = F_8 = 0$

$$\begin{aligned} \Sigma M_{ox} &= 0 = -W_a 63.60 + W_g 24.25 - RB 24.25 + (F_{5x} + F_{3x})25.5 + (F_{7x} + F_{1x}) \\ &\quad 105.0 + (F_{5z} + F_{3z} + F_{7z} + F_{1z}) 40.12 \end{aligned}$$

$$\begin{aligned} \Sigma M_{ox} &= -W_a 63.60 + W_g 24.25 - (F_{5z} + F_{3z} + F_{7z} + F_{1z} + W_g)24.25 + \dots \\ &\quad \dots (F_{5x} + F_{3x})25.5 + (F_{7x} + F_{1x})105.0 + (F_{5z} + F_{3z} + F_{7z} + F_{1z})40.12 \\ &= -W_a 63.60 - [2 \times 0.394F_3 + 2 \times 0.723F_1]24.25 + 2 \times 0.497F_3(25.5) + \dots \\ &\quad \dots 2 \times 0.221F_1(105.0) + [2 \times 0.394F_3 + 2 \times 0.723F_1]40.12 \\ &= -W_a 63.60 - 19.1F_3 - 35.1F_1 + 25.3F_3 + 46.41F_1 + 31.6F_3 + 58F_1 \\ &= -W_a 63.60 + (-19.1 + 25.3 + 31.6) F_3 + (-35.1 + 46.41 + 58) F_1 \\ &= - (63.60) W_a + (37.8)F_3 + (69.31)F_1 \\ &\Rightarrow 1.063 (10^7) = (37.8)F_3 + (69.3)F_1^* \end{aligned}$$

From equation** F_5 and F_7 are related as:

$$\begin{aligned} F_7 &= 0.8898F_5 \\ &= 0.8898F_3 = F_1 \\ &\Rightarrow 1.063 (10^7) = (37.8)F_3 + (69.3)(0.8898F_3)^* \\ F_3 &= 106,874 \end{aligned}$$

NEDO-33866 Revision 0
Non-Proprietary Information – Class I (Public)

$$\begin{aligned} F_5 &= 106,874 \\ F_1 &= 95,096 \\ F_7 &= 95,096 \end{aligned}$$

$$\begin{aligned} \text{From above: } RF &= F_{5x} + F_{3x} + F_{7x} + F_{1x} - W_a \\ &= 0.497F_5 + 0.497F_3 + 0.221F_7 + 0.221F_1 - 167,100 = -18,835 \text{ lb} \end{aligned}$$

2g Vertical

During the 2g vertical load all 8 members are expected to experience tension, and all vertical components of the members will react. From symmetry the following assumptions can be made with reference to Figure 2.12.3-12.

Assumption from symmetry: For the 2g vertical load, all ropes at the bottom (3,4,5,6) experience equal load and all ropes on top (1,2,7,8) experience equal load.

$$\begin{aligned} F_{5Z} &= F_{4Z} = F_{3Z} = F_{6Z} = \sin(23.2)F_3 = 0.394 F_3 \\ F_{7Z} &= F_{2Z} = F_{1Z} = F_{8Z} = \sin(46.3)F_1 = 0.723 F_1 \end{aligned}$$

Where Fz is the vertical component of the forces on the ropes.

$$\begin{aligned} \Sigma F_z &= 0 = (F_{5Z} + F_{4Z} + F_{3Z} + F_{6Z}) + (F_{7Z} + F_{2Z} + F_{1Z} + F_{8Z}) + W_g - W_a = 0 \\ &= 4 F_{5Z} + 4 F_{7Z} + W_g - W_a = 0 \\ &= 4 \times 0.394 F_3 + 4 \times 0.723 F_1 + W_g - 2W_g = 0 \\ &= 1.576F_3 + 2.892F_1 - W_g = 0 \\ &= 1.576F_3 + 2.892F_1 = 33,500 \end{aligned}$$

$$\text{From above, } F_1 = 0.8898F_3.$$

$$\text{Hence } \Rightarrow \frac{1.576}{0.8898} F_1 + 2.892F_1 = 33,500$$

$$\begin{aligned} &\Rightarrow 1.771F_1 + 2.892F_1 = 33,500 \\ &= 4.663F_1 = 33,500 \end{aligned}$$

$$\Rightarrow F_1 = 7183.93 = F_2 = F_7 = F_8$$

$$\Rightarrow F_3 = 8073.65 = F_4 = F_5 = F_6$$

Table 2.12.3-3. Tie-Down Ropes Tension Forces

| Rope No. | 10W Long. (lb) | 5W Transv. (lb) | 2W Vert.(lb) | Total (lbf) |
|----------|----------------|-----------------|--------------|------------------------------|
| 1 | --- | 95,096 | 7,184 | 95,367 |
| 2 | --- | --- | 7,184 | 7,184 |
| 3 | --- | 106,874 | 8,074 | 107,179 |
| 4 | --- | --- | 8,074 | 8,074 |
| 5 | 102,960 | 106,874 | 8,074 | 148,620^{max} |
| 6 | 102,960 | --- | 8,074 | 103,276 |
| 7 | 91,614 | 95,096 | 7,184 | 132,242 |
| 8 | 91,614 | --- | 7,184 | 91,895 |
| Friction | 56,287 | 18,835 | --- | --- |

As documented in Table 2.12.3-3, the maximum cable tension force is 148.62 kip. This load value is used in subsequent tie-down analysis of the rib.

- TIE-DOWN RIB ANALYSIS

The tie-down ribs are triangular plate two inches thick supported at the short side by a 5 inch x 6.5 inch pad that is 0.5 inch thick. This plate is rolled to conform with the toroidal shell contour. The vertical edge of the tie-down rib is welded to a stiffening ring. The tie-down rib, pad and stiffening ring are fabricated from ASTM A240, Type [[]] material. The toroidal shell material is ASTM A403, Type 304 stainless steel; and the overpack outer shell, where the stiffening ring attaches, is fabricated from ASTM A240, SS304.

The maximum temperature, 249°F, of the overpack bottom toroidal shell, where the tie-down ribs will be attached, is used as a reference.

Several modes of failure are investigated for the components of the tie-down rib system. These modes of failure are:

- Shear tearout of tie-down rib hole
- Bearing of shackle pin on ear
- Yielding of weld joints and parent metal

- SHEAR TEAROUT OF TIE-DOWN RIB HOLE

Figure 2.12.3-16 shows a sketch of the tie-down rib with the rope tension force line of action and lines of failure in shear.

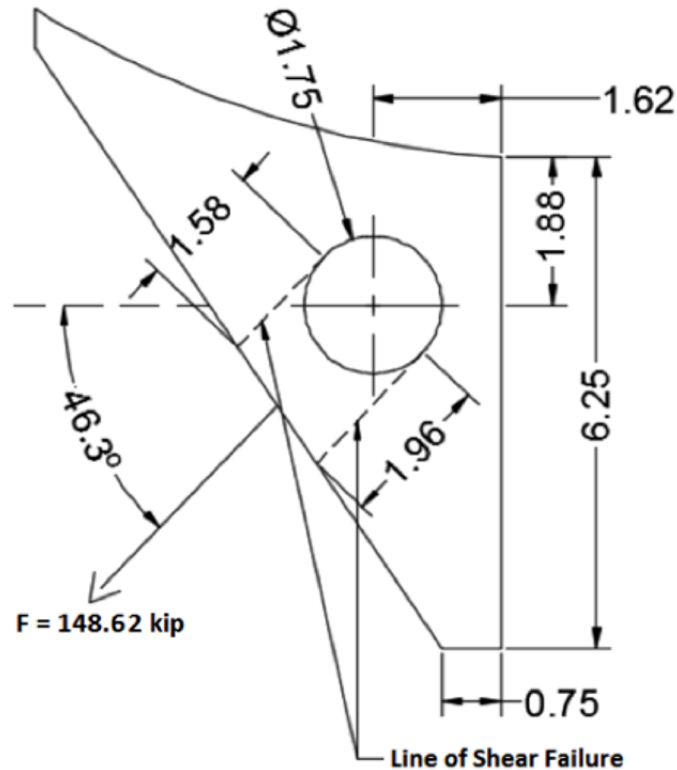


Figure 2.12.3-16. Tie-Down Rib Hole Loading

$$\tau = \frac{F}{A}$$

where $A = 2 \times (1.58 + 1.96) = 7.08 \text{ in}^2$

$$\tau = \frac{148.62}{7.08} = 20.99 \text{ ksi} < 27.12 \text{ ksi}$$

- BEARING OF SHACKLE PIN ON EAR

The bearing stress is computed assuming that the force is uniformly distributed over the projected contact area of the pin's 1.75-inch diameter. This gives for the stress:

$$\sigma = \frac{F}{A} = \frac{148.62}{2.0 \times 1.75} = 42.3 \text{ ksi}$$

$$\sigma = 42.5 \text{ ksi} < 45.2 \text{ ksi}$$

- YIELDING OF WELD JOINTS AND PARENT METAL

Figure 2.12.3-17 shows the approximate weld pattern for the top tie-down rib.

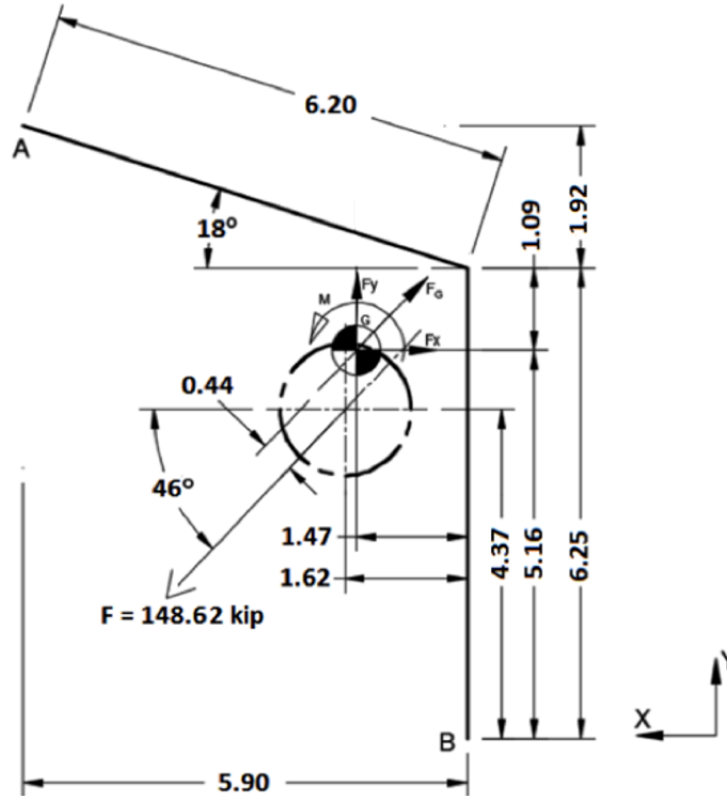


Figure 2.12.3-17. Weld Pattern of Top Tie Down Rib

Using the line load method (actual weld is ½ inch fillet 2 sides):

$$L = 6.2 + 6.25 = 12.45 \text{ inches}$$

$$\bar{X} = \frac{\sum \bar{X}_i L_i}{\sum L_i} = \frac{6.2 \times \left(\frac{6.2 \cos(18^\circ)}{2} \right)}{12.45} = \frac{6.2 \times 2.95}{12.45} = 1.47 \text{ in}$$

$$\bar{Y} = \frac{\sum \bar{Y}_i L_i}{\sum L_i} = \frac{6.25 \times (6.25/2) + 6.2 \times \left(6.25 + \left(\frac{6.2 \sin(18^\circ)}{2} \right) \right)}{12.45} = 5.16 \text{ in}$$

$$I_x = \sum (I_o + Ad^2)$$

$$= \frac{6.25^3}{12} + 6.25 (5.16 - (6.25/2))^2 + \frac{6.2^3 \sin^2 18^\circ}{12} + \dots$$

$$\dots 6.2(6.25 + \left(\frac{6.2 \sin(18^\circ)}{2} \right) - 5.16)^2$$

$$= 74.13 \text{ in}^4/\text{in}$$

$$I_y = \frac{6.2^3 \cos^2(18^\circ)}{12} + 6.2(2.95 - 1.47)^2 + 6.25 (1.47)^2$$

$$= 45 \text{ in}^4/\text{in}$$

$$\therefore I_Z = I_X + I_Y = 119.14 \text{ in}^4/\text{in}$$

There are two welds:

$$\begin{aligned}\therefore I_Z &= 119.14 \times 2 = 238.28 \text{ in}^4/\text{in} \\ \therefore M_Z &= F \times r = 148.62 \times 0.44 = 65.39 \text{ k-in.}\end{aligned}$$

$$F_X = F \cos \theta = 148.62 \cos 46^\circ = 103.24 \text{ kip}$$

$$F_Y = F \sin \theta = 148.62 \sin 46^\circ = 106.91 \text{ kip}$$

\therefore @ Point A:

$$P_X = \frac{F_X}{L} + \frac{M_{ZY}}{I} = \frac{103.24}{2(12.45)} + \frac{(65.39)(6.25+1.92-5.16)}{(238.28)} = 4.97 \text{ k/in}$$

$$P_Y = \frac{F_Y}{L} + \frac{M_{ZX}}{I} = \frac{106.91}{(24.9)} + \frac{(65.39)(6.2 \cos(18)-1.47)}{(238.28)} = 5.51 \text{ k/in}$$

$$P_Z = 0$$

Total line load:

$$P_T = \sqrt{P_X^2 + P_Y^2 + P_Z^2} = 7.42 \text{ k/in.}$$

Shear stress in the effective throat area of the weld is:

$$S_v = \frac{7.42}{0.707t} = \frac{7.42}{0.707 \times 0.5} = 20.99 \text{ ksi} < 27.12 \text{ ksi (allowable base metal)}$$

Shear stress on the weld leg

$$S_t = \frac{7.42}{0.5} = 14.84 \text{ ksi}$$

\therefore @ Point B:

$$P_X = \frac{103.24}{24.9} + \frac{(65.39)(5.16)}{(238.28)} = 5.56 \text{ kip}$$

$$P_Y = \frac{106.9}{(24.9)} + \frac{(65.39)(1.47)}{(238.28)} = 4.7 \text{ k/in}$$

$$P_T = \sqrt{(5.56^2 + 4.7^2 + 0)} = 7.28 \text{ k/in}$$

$$S_v = \frac{7.28}{0.3535} = 20.59 \text{ ksi} < 27.12 \text{ ksi}$$

Shear stress on leg of weld:

$$S_t = \frac{7.28}{0.5} = 14.56 \text{ ksi} < 27.12 \text{ ksi}$$

The following analysis checks weld failure mode of weld attaching tie-down rib and gusset to overpack, refer to Figure 2.12.3-18.

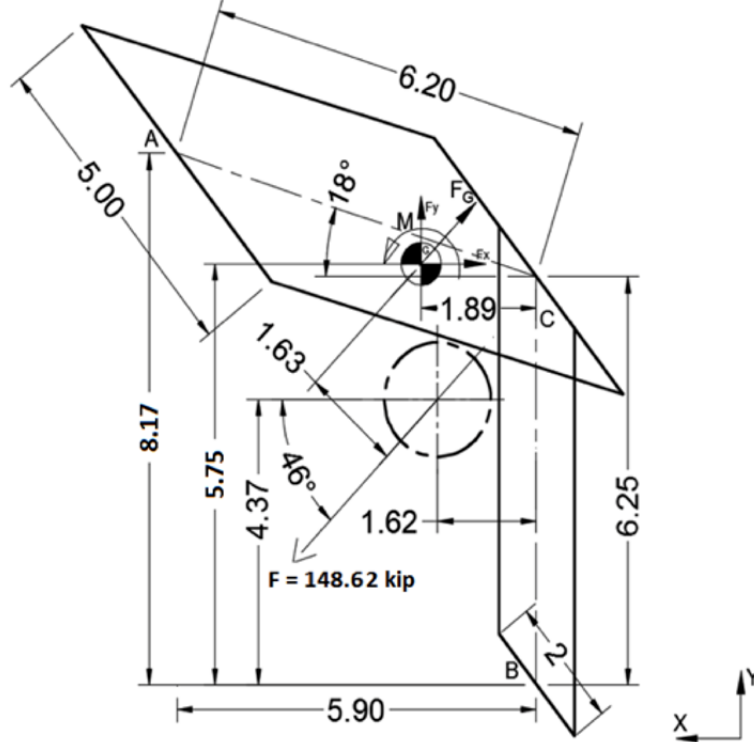


Figure 2.12.3-18. Weld Geometry of Tie-Down Rib and Gusset to Overpack

$$L = 5 + (6.2) \times 2 + 5 + 6.25 \times 2 = 34.9 \text{ inches}$$

$$\bar{X} = \frac{\sum \bar{X}_i L_i}{\sum L_i} = \frac{5 \times 6.2 \cos(18) + 12.4 \times \left(\frac{6.2 \cos(18)}{2}\right)}{34.9} = 1.89 \text{ in}$$

$$\bar{Y} = \frac{\sum \bar{Y}_i L_i}{\sum L_i} = \frac{5 \times (6.25 + 6.2 \sin(18)) + 12.4 \times \left(6.25 + \left(\frac{6.2 \sin(18)}{2}\right)\right) + 5 \times (6.25) + 12.5 \times \left(\frac{6.25}{2}\right)}{34.9} = 5.75 \text{ in}$$

$$\begin{aligned} I_z &= (5) \left[(6.2 \cos(18) - 1.89)^2 + (6.2 \sin(18) + 6.25 - 5.75)^2 \right] \\ &\quad + (12.4) \left[\left(\frac{6.2 \cos(18)}{2} - 1.89\right)^2 + \left(6.25 + \frac{6.2 \sin(18)}{2} - 5.75\right)^2 \right] \\ &\quad + (5) \left[(6.25 - 5.75)^2 + 1.89^2 \right] + (12.5) \left[1.89^2 + \left(\frac{6.25}{2} + (6.25 - 5.75)\right)^2 \right] + \frac{6.2^3}{12} + \frac{6.25^3}{12} \\ &= 339.77 \text{ in}^3 \end{aligned}$$

$$MZ = 148.62 \times 1.15 = 170.91 \text{ k-in.}$$

∴ @ Point A:

$$P_x = \frac{103.24}{34.9} + \frac{(170.89)(8.17 - 5.75)}{339.77} = 4.18 \frac{k}{in}$$

NEDO-33866 Revision 0
Non-Proprietary Information – Class I (Public)

$$P_Y = \frac{106.91}{34.9} + \frac{(170.55)(5.9-1.89)}{339.77} = 5.08 \frac{k}{in}$$

$$P_Z = 0$$

∴ Total line load:

$$P_T = \sqrt{4.18^2 + 5.08^2} = 6.58 \frac{k}{in}$$

Shear stress in the effective throat area of the weld is:

$$S_V = \frac{6.58}{0.707t} = \frac{6.58}{0.707 \times 0.5} = 18.60 \text{ ksi} < 27.12 \text{ ksi (allowable base metal)}$$

For a ½ inch fillet, shear stress in the weld leg is:

$$S_V = \frac{6.58}{(0.5)} = 13.15 \text{ ksi} < 27.12 \text{ ksi}$$

∴ @ Point B:

$$P_X = \frac{103.24}{34.9} + \frac{(170.91)(5.75)}{339.77} = 5.85 \frac{k}{in}$$

$$P_Y = \frac{106.91}{34.9} + \frac{(170.91)(1.89)}{339.77} = 4.02 \frac{k}{in}$$

$$P_Z = 0$$

∴ Total line load:

$$P_T = \sqrt{5.83^2 + 4.00^2} = 7.09 \frac{k}{in}$$

Shear stress in the effective throat area of the weld is:

$$S_V = \frac{7.09}{0.707t} = 20.07 \text{ ksi} < 27.12 \text{ ksi}$$

For a ½ inch fillet, maximum shear stress on the weld is:

$$S_V = \frac{7.09}{(0.5)} = 14.19 \text{ ksi} < 27.12 \text{ ksi}$$

The lower allowable stress for welds made to the A240 material is not a problem because of the direction of the applied load. The weld takes the load in tension. At Point C:

$$P_X = \frac{103.24}{34.9} + \frac{170.91(-0.5)}{339.77} = 2.71 \frac{k}{in}$$

$$P_Y = \frac{106.9}{34.9} + \frac{170.91(1.89)}{339.77} = 4.01 \frac{k}{in}$$

Forces acting in tension against the A240 are:

$$P_T = P_X \sin \theta + P_Y \cos \theta$$

$$= 2.71 \times \sin 18^\circ + 4.01 \times \cos 18^\circ = 4.65 \frac{k}{in}$$

$$S_t = \frac{4.65}{0.5} = 9.31 \text{ ksi} < 23.7 \text{ ksi}$$

• EXCESSIVE LOAD FAILURE

The tie-down system must be designed such that its failure under excessive load would not impair the ability of the package to meet the requirements of 10 CFR 71. The tie-down system is attached to the overpack structure; the cask (containment vessel) resides within the overpack without attachment to its inner surface. Therefore, failure of the tie-down will not affect the performance of the cask. The results are presented in Table 2.12.3-4.

Table 2.12.3-4. Tie-Down System Stress Analysis Results

| Condition | Stress Level (ksi) | Allowable based on Yield Strength (ksi) | MS (y) | Allowable based on Ultimate Strength (ksi) | MS (U) |
|-------------------------|--------------------|-----------------------------------------|--------|--------------------------------------------|--------|
| Shear tear-out of hole | 20.99 | 0.6*45.2 = 27.12 | 0.29 | 36.95 | 0.76 |
| Bearing of shackle pin | 42.46 | 45.2 | 0.06 | 96.80 | 1.28 |
| Yielding of weld joints | 20.99 | 0.6*45.2 = 27.12 | 0.29 | 36.95 | 0.76 |

The tie-down rib and pin materials are type [[]] stainless steel.

The margins of safety (MS (y)) with respect to yield is calculated as follows:

$$MS \text{ (yield)} = \frac{\text{Allowable based on yield strength}}{\text{Stress level}} - 1$$

The margins of safety with respect to ultimate failure are:

Shear Strength:

$$\frac{\sigma_{ult}}{2(1+\mu)} = \frac{96.8}{2(1.31)} = 36.95 \text{ ksi}$$

Shear tear-out of tie-down rib hole

$$MS = \frac{36.95}{20.99} - 1 = 0.76$$

Bearing of shackle pin

$$MS = \frac{96.8}{42.46} - 1 = 1.28$$

Yielding of weld joints

$$MS = \frac{36.95}{20.99} - 1 = 0.76$$

2.12.4. Cask Closure Bolt Evaluation

2.12.4.1. Cask Lid Bolt Torque Calculation

This section documents the cask lid bolt torque calculation. The torque is calculated using the following equation:

$$T = K \times D \times P \quad \text{Reference 2-14, Page 19}$$

where

$$K = \text{Torque friction coefficient}$$

$$= 0.15 \text{ (Reference 2-30)}$$

$$D = \text{Nominal bolt diameter (in)}$$

$$\begin{aligned} &= 1.25 \text{ in} \\ P &= \text{Clamp force (lb)} \end{aligned}$$

The bolt clamp force is defined as the sum of the non-prying tensile bolt force due to temperature, non-prying tensile bolt force due to pressure, axial load for gasket seating, and axial load for gasket operation for this calculation. The non-prying tensile bolt force due to temperature and non-prying tensile bolt force due to pressure can be easily calculated utilizing the parameters and formulas specified in NUREG-6007 (Reference 2-15). The axial load for gasket varies depending on the gasket material used and gasket width, which is the focus of this evaluation. The formulas for the axial loads for gasket seating and gasket operation are given in Equation (1) and Equation (2), respectively (Reference 2-15, Table 4.2, page 13).

$$F_a = \frac{\pi D_{lg} b y}{N_b} \quad (1)$$

where

$$\begin{aligned} D_{lg} &= \text{Closure lid diameter at the location of the gasket load} \\ &= 29.25 \text{ in} \\ b &= \text{Effective gasket surface seating width (in)} \\ y &= \text{Minimum design seating stress (psi)} \\ N_b &= \text{Total number of closure bolts} \\ &= 15 \\ F_a &= \frac{2 \pi D_{lg} b m (P_{li} - P_{lo})}{N_b} \quad (2) \\ m &= \text{Gasket factor for operating conditions} \\ P_{li} &= \text{Pressure inside the closure lid (psi)} \\ &= 30 \text{ psi} \\ P_{lo} &= \text{Pressure outside the closure lid (psi)} \\ &= 15 \text{ psi} \end{aligned}$$

Equations (1) and (2) use two experimentally determined constants, which are the gasket factor, m , and the minimum design seating stress, y . The gasket factor is taken into consideration for the axial load for gasket operation and is defined as the ratio of the required minimum gasket pressure to the pressure contained by the gasketed joint. Additionally, the seating stress is applied for the axial load for gasket seating and is defined as the minimum design seating stress of the gasket. Both of these constants are determined per Table E-1210-1 of the ASME B&PVC Section III Division 1 Appendices (Reference 2-18, page 222).

Further, equation (1) and equation (2) both utilize the parameter b , which is the effective gasket or joint contact surface seating width. The effective gasket seating width is determined by first calculating the basic gasket seating width (b_o) per Table E-1210-2 of the ASME B&PVC Section III Division 1 Appendices (Reference 2-18). From Table E-1210-2, face sketch is used for the evaluation due to the fact that this sketch is the closest to the actual geometry as

Figure B-1 depicts. It can be seen that b_o is a function of the variable w for face sketch, which is based upon the contact width between the flange facing and the gasket. Following, the effective gasket seating width is determined based off of the following criteria (Reference 2-18, page 223):

$$\begin{aligned} b &= b_o, \text{ when } b_o \leq \frac{1}{4} \text{ in} \\ b &= C_b \sqrt{b_o}, \text{ when } b_o > \frac{1}{4} \text{ in} \end{aligned}$$

where

$$\begin{aligned} C_b &= \text{effective width factor} \\ &= 0.5 \text{ for U.S Customary calculations} \\ &= 2.5 \text{ for SI calculations} \end{aligned}$$

Once the effective gasket seating width is determined, both axial loads for gasket seating and gasket operation can be calculated by use of Equation (1) and Equation (2). For the calculations of this document, the parameters presented above are determined for soft aluminum, soft steel, and stainless steel. Furthermore, the seal detail drawing shown in Figure 2.12.4-1 is used to establish the contact width between the flange facing and the gasket (w) and is shown to be 0.872 inches ($0.218 \text{ inches} \times 4$).

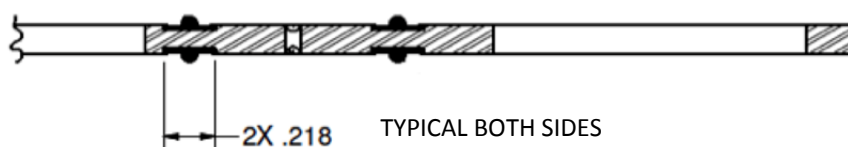


Figure 2.12.4-1. Seal with Contact Width Dimension

The gasket factor, minimum design seating stress, basic gasket seating width (b_o), and effective gasket width (b) are tabulated in Table 2.12.4-1 for each gasket material.

Table 2.12.4-1. Input Parameters

| Material | Gasket Factor, m | Gasket Seating Stress, y (psi) | Basic Gasket Seating Width, b_o (in) | Effective Gasket Seating Width, b (in) |
|-----------------|--------------------|----------------------------------|----------------------------------------|------------------------------------------|
| Aluminum | 4.00 | 8800 | .109 | .109 |
| Carbon Steel | 5.50 | 18000 | .109 | .109 |
| Stainless Steel | 6.50 | 26000 | .109 | .109 |

The calculation for the basic gasket seating width (b_o) and effective gasket seating width (b) is determined by use of face sketch per Table E-1210-2. Therefore, the effective gasket width is:

$$b_o = \frac{w}{8} = \frac{.872 \text{ in}}{8} = .109 \text{ in}$$

Because b_o is less than $\frac{1}{4}$ in, b_o is equal to b .

With all parameters calculated, the axial loads due to gasket seating and gasket operation can be calculated and the required bolt torque determined accordingly. Table 2.12.4-2 is a summary of the calculation for the stainless steel gasket retainer:

Table 2.12.4-2. Bolting Calculation

[[

]]

Table 2.12.4-3 summarizes the magnitude of each of the loads and the resulting bolt clamp force.

Table 2.12.4-3. Clamp Force Loads

| Material | Axial Load Due to Pressure (lb) | Axial Load Due to Temperature (lb) | Axial Load For Gasket Seating (lb) | Axial Load For Gasket Operation (lb) | Bolt Clamp Force, P (lb) |
|-----------------|----------------------------------------------------|-------------------------------------------------------|-------------------------------------------------------|---------------------------------------------------------|-----------------------------------------|
| Aluminum | 671.96 | 10856.79 | 5876.16 | 80.13 | 17485.04 |
| Carbon Steel | 671.96 | 10856.79 | 12019.42 | 110.18 | 23658.35 |
| Stainless Steel | 671.96 | 10856.79 | 17361.38 | 130.21 | 29020.35 |

Now that the required clamp force has been determined for each of the selected gasket materials, the required torque is calculated. The new torque values for each material type is shown in Table 2.12.4-4.

Table 2.12.4-4. Required Bolt Torque

| Material | Torque (lb-in) | Torque (lb-ft) |
|-----------------|-------------------|--------------------------------|
| Aluminum | 3278 | $273 + 10\% = 300$ |
| Carbon Steel | 4435 | $370 + 10\% = 407$ |
| Stainless Steel | 5441 | $453 + 10\% = 499 \approx 500$ |

The sections below provide a detailed analysis of the forces and moments that are subjected to the bolted joint of the Model 2000 cask during normal and accident conditions.

2.12.4.2. Lid Bolt Evaluation

2.12.4.2.1. Required Length of Engagement

For this analysis, a 1¼-7 UNC-2A external thread with a 1¼-7 UNC-2B internal thread is considered at an operating temperature of 150°F. The external thread material is ASTM A-540, Grade B22, Class 3 and the internal thread material is ASME SA-182, F304. Table 2.12.4-5 lists the required parameters needed for the analysis.

Table 2.12.4-5. Lid Bolt Evaluation Input Parameters

| Parameter | Variable | Input | Units |
|----------------------------------------------|-------------|--------|-------|
| Tensile Strength of External Thread at 150°F | S_{u1} | 145* | ksi |
| Tensile Strength of Internal Thread at 150°F | S_{u2} | 73 | ksi |
| Minimum Pitch Diameter (External Thread) | $E_{s,min}$ | 1.1476 | in |
| Minimum Major Diameter (External Thread) | $D_{s,min}$ | 1.2314 | in |
| Maximum Pitch Diameter (Internal thread 2B) | $E_{n,max}$ | 1.1668 | in |
| Maximum Major Diameter (Internal thread 2B) | $K_{n,max}$ | 1.123 | in |
| Threads Per Inch | n | 7 | in |
| Bolt Pre-Load | P | 82.8 | kip |

References:

Reference 2-30 Minimum Pitch Diameter: Table 3, Page 1827

Reference 2-30 Minimum Major Diameter: Table 3, Page 1827

Reference 2-30 Maximum Pitch Diameter (2B): Table 3, Page 1827

Reference 2-30 Maximum Minor Diameter (2B): Table 3, Page 1827

Based on these given inputs, it must be determined if the bolt will fail before the threads of either the internal or external fixtures or vice versa. To do this, the required length of engagement must be calculated and checked against the actual geometry. The length of engagement (L_e) is calculated as follows (Reference 2-30, Page 1536),

$$L_e = \frac{2A_t}{\pi(K_{n,max})(\frac{1}{2} + .57735n[E_{s,min} - K_{n,max}])}$$

Where,

$$A_t = \text{Screw thread tensile stress area}$$

and A_t is given by the equation,

$$A_t = \pi \left[\frac{E_{s,min}}{2} - \frac{0.16238}{n} \right]^2$$

The length of engagement (L_e) is for mating external and internal threads of the same strength. If the materials of the internal and external threads do not have the same strength, the relative strength (J) must be calculated to determine if the internal thread could strip before the bolt breaks. The relative strength is calculated as follows,

$$J = \frac{A_s \times S_{ut \text{ of external thread material}}}{A_n \times S_{ut \text{ of internal thread material}}}$$

where

$$A_s = \text{Shear area of external threads}$$

$$A_n = \text{Shear area of internal threads}$$

Also, the shear area of the external and internal threads are given by,

$$A_s = \pi n L_e K_{n,max} \left[\frac{1}{2n} + .57735(E_{s,min} - K_{n,max}) \right]$$

and,

$$A_n = \pi n L_e D_{s, \min} \left[\frac{1}{2n} + .57735(D_{s,min} - E_{n,max}) \right]$$

where

$$n = \text{number of threads per inch}$$

If the relative strength is calculated to be less than or equal to 1, then the length of engagement (L_e) is sufficient to prevent stripping of the internal thread. If the relative strength is calculated to be greater than 1, then the required length of engagement is calculated by taking the product of the J factor and the length of engagement as given is:

$$Q = J L_e$$

where

$$Q = \text{Required length of engagement}$$

Once the required length of engagement is calculated, this value is checked against the actual geometry to determine if the internal threads will strip before the bolt breaks or vice versa. Table 2.12.4-6 presents the results.

Table 2.12.4-6. Calculation of Required Length of Engagement at 150°F

| Parameter | Variable | Result | Units |
|------------------------------------------------|----------|--------|-----------------|
| Tensile stress area of bolt | A_t | 0.952 | in ² |
| Effective length | L_e | 0.901 | in |
| Shear area of internal threads | A_n | 2.652 | in ² |
| Shear area of external threads | A_s | 1.905 | in ² |
| Relative strength of external/internal threads | J | 1.427 | -- |
| Required length of engagement if $J > 1$ | Q | 1.285 | in |

Looking at the actual geometry, the engagement = 3.00 inches (lid bolt length) – 1.625 inches (flange + seal) = 1.375 inches. At 150°F, the required length of engagement is less than the engagement of the geometry. Therefore, a thread engagement of 1.375 inches will ensure that the threads of either the internal or external fixture will not strip before the bolt fails for a Class 2A bolt in 2B threads.

2.12.4.2.2. Applied Load Analysis

The maximum load on the bolt to break the threaded portion is determined by taking the product of the ultimate tensile strength of the external thread and the bolt thread tensile stress area (Reference 2-30).

$$\begin{aligned}
 P_{\max} &= S_u A_t \\
 &= (145 \text{ ksi})(.952 \text{ in}^2) \\
 P_{\max} &= 138 \text{ kip}
 \end{aligned}$$

Now that the maximum load has been calculated, the minimum thread engagement, L_e , based on the applied pre-load is:

$$\begin{aligned}
 P &= \sigma A_n \\
 &= \text{bolt pre-load} \\
 &= 82.8 \text{ kip} \\
 &= \text{Tensile strength of internal thread} \\
 A_n &= \text{Internal thread shear area (Class 2A + 2B)}
 \end{aligned}$$

From Reference 2-30:

$$P = \sigma \times \pi \times n \times L_e \times D_{s,\min} \times [1/2n + .57735(D_{s,\min} - E_{n,\max})]$$

Solving for the effective length:

$$L_e = P / (\sigma \times \pi \times n \times D_{s,\min} \times [1/2n + .57735(D_{s,\min} - E_{n,\max})])$$

Solving, the minimum thread engagement is 0.3852 inches at an operating temperature of 150°F. accordingly, calculating the product of the effective length and the number of threads per inch, the minimum thread engagement to prevent internal 2B thread stripping is approximately three threads.

2.12.4.2.3. Bolt Stress Analysis

The cask lid of the Model 2000 cask is fastened to the cask flange by way of 15 uniformly spaced ASTM A540, Grade B-22, Class 3 socket head screws. Table 2.12.4-7 provides the input parameters that are to be used in the analysis at an operating temperature of 500°F.

Table 2.12.4-7. Model 2000 Stress Analysis Design Input Parameter

| Parameter | Variable | Input | Units |
|-----------------------------------------------------------------------------------------|----------|-----------|-----------------|
| Number of Bolts | N_b | 15 | -- |
| Lid Diameter at Bolt Circle | D_{lb} | 32.25 | in |
| Lid Diameter at Gasket | D_{lg} | 29.25 | in |
| Nominal Bolt Diameter | D_b | 1.25 | in |
| Lid Diameter at Inner Edge | D_{li} | 28 | in |
| Lid Diameter at Outer Edge | D_{lo} | 34.75 | in |
| Thickness of Lid | t_l | 1.75 | in |
| Thickness of Lid Flange | t_{lf} | 1.5 | in |
| Thickness of Cask Wall | t_c | 6 | in |
| Bolt Engagement Length | BEL | 1.625 | in |
| Bolt Moment of Inertia/Cir | XIB | 0.018 | in ³ |
| Young's Modulus For Lid | E_l | 25900000 | psi |
| Young's Modulus For Cask | E_c | 25900000 | psi |
| Young's Modulus For Bolt | E_b | 27400000* | psi |
| Poisson's Ratio For Lid | N_{ul} | 0.31 | -- |
| Poisson's Ration For Cask | N_{uc} | 0.31 | -- |
| Lid Thermal Expansion Coefficient | a_l | 9.70E-06 | 1/°F |
| Bolt Thermal Expansion Coefficient | a_b | 7.30E-06* | 1/°F |
| Weight of Cask Contents | W_C | 5450 | lb |
| Weight of Cask Lid | W_l | 1900 | lb |
| Dynamic Load Factor | DLF | 1 | -- |
| Preload Torque | Q | 6000 | lb-in |
| Nut Factor For Preload Torque | K_a | 0.15 | -- |
| Gasket Seating Width | G_b | 0.109 | in |
| Gasket Seating Stress | G_v | 26000 | psi |
| Gasket Factor | G_m | 6.5 | -- |
| Wall Thermal Expansion Coefficient | a_c | 9.70E-06 | 1/°F |
| Basic Allowable Stress Limit | S_m | 7.71E+04 | psi |
| Minimum Yield Strength | S_y | 115700 | psi |
| Minimum Ultimate Strength | S_u | 145000 | psi |
| Maximum rigid body impact acceleration (g) | a_i | 25** | -- |
| Impact angle between the cask axis and the target surface | x_i | 90° | -- |
| Maximum axial vibration acceleration (g) at the cask support | ava | 2 | -- |
| Maximum transverse vibration acceleration (g) at the cask support | avt | 5 | -- |
| Vibration transmissibility of acceleration between the cask support and the closure lid | VTR | 1 | -- |

References:

Reference 2-31 Gasket Seating Width: Table E-1210-2
Reference 2-31 Gasket Seating Stress: Table E-1210-1
Reference 2-31 Gasket Factor: Table E-1210-1
Reference 2-15 Basic Allowable Stress Limit: Table 6.1, Page 28
Reference 2-1 Maximum Axial Vibration Acceleration (g) at the Cask Support
Reference 2-1 Maximum Transverse Vibration Acceleration (g) at the Cask Support
Reference 2-15 Vibration transmissibility of acceleration between the cask support and the closure lid

Notes:

* Grade B21 bolt properties used because temperature dependent values could not be found for Grade B22.
** Section 2.12.1, Figure 2.12.1.11-30 presents the justification for the reduced impact acceleration during the HAC end drop.

NUREG/CR-6007 (Reference 2-15) is used to accurately verify whether or not the closure bolts can effectively hold up to the various loads in both normal conditions of transport and hypothetical accident conditions. This includes forces and moments due to pressure, temperature, vibration, impact, preload, gasket, puncture, and prying. Also, NUREG/CR-6007 gives procedures for combining loads and stress limits that must be met. Loads include the axial force (F_a), shear force (F_s), fixed-edge closure-lid force (F_t), fixed edge closure lid moment (M_t), and also torsional moments (M_t) that are created by the torque wrench in the preload and gasket seating operations. All of which are elaborated on in the following sections.

2.12.4.2.4. Forces/Moments Generated By Preload

Found in Table 4.1 in NUREG/CR-6007, are the bolts loads due to use of a torque wrench. The non-prying axial bolt force per bolt is given by the equation,

$$F_a = Q / (K_q \times D_b)$$

The torsional bolt force per bolt is defined by the formula,

$$M_t = 0.5 Q$$

2.12.4.2.5. Forces/Moments Generated By Gasket Loads

Per Table 4.2 in NUREG/CR-6007, are the formulas for calculating the forces and moments generated by gasket loads by utilization of a torque wrench. The axial force produced by the gasket seating operation is evaluated by use of the following equation,

$$F_a = \frac{\pi \times D_{lg} \times G_b \times G_y}{N_b}$$

and the torsional bolt moment due to the seating operation is,

$$M_t = \frac{0.5 \times \pi \times K_q \times D_b \times D_{lg} \times G_b \times G_y}{N_b}$$

Also, The non-prying tensile bolt force per bolt produced by the operating gasket seating is determined by,

$$F_a = \frac{2 \times \pi \times D_{lg} \times G_b \times G_m (P_{li} - P_{lo})}{N_b}$$

2.12.4.2.6. Forces/Moments Generated By Pressure Loads

Table 4.3 in NUREG/CR-6007 is applied to determine the moments and forces that are generated due to the pressure difference between the inside and outside of the cask. The associated equation for the axial force due to pressure loads is,

$$F_a = \frac{\pi \times D_{lg}^2 \times (P_{li} - P_{lo})}{4 \times N_b}$$

where

$$\begin{aligned} P_{li} &= \text{Pressure inside the closure lid} \\ &= 30 \text{ psi} \\ P_{lo} &= \text{Pressure outside the closure lid} \\ &= 15 \text{ psi} \end{aligned}$$

The shear bolt force per bolt is then,

$$F_s = \frac{\pi \times E_t \times t_t \times (P_{li} - P_{lo}) \times D_{lb}^2}{2 \times N_b \times E_c \times t_c \times (1 - N_{ul})}$$

where

$$\begin{aligned} P_{ci} &= \text{Pressure inside the cask wall} \\ &= 30 \text{ psi} \\ P_{co} &= \text{Pressure outside the cask wall} \\ &= 15 \text{ psi} \end{aligned}$$

The fixed-edge closure-lid force generated by internal pressure is,

$$F_f = \frac{D_{lb}(P_{li} - P_{lo})}{4}$$

and the fixed-edge moment is,

$$M_f = \frac{D_{lb}^2(P_{li} - P_{lo})}{32}$$

2.12.4.2.7. Forces/Moments Generated By Temperature Loads

Table 4.4 of NUREG/CR-6007 gives the formulas for bolt forces/moments generated by thermal expansion difference between the closure lid, bolt, and wall. The axial force due to a temperature difference between the closure bolt and lid is:

$$F_a = \frac{1}{4} \times \pi \times D_b^2 \times E_b \times (\alpha_l \times T_l - \alpha_b \times T_b)$$

where

$$\begin{aligned} T_l &= \text{Temperature change of the closure lid} \\ &= 117.5^\circ\text{F} \\ T_b &= \text{Temperature change of the closure bolt} \\ &= 111.9^\circ\text{F} \end{aligned}$$

The shear force acting on each bolt is given by,

$$F_s = \frac{\pi \times E_l \times t_l \times D_{lb} \times (\alpha_l \times T_l - \alpha_c \times T_c)}{N_B \times (1 - N_{ul})}$$

where,

$$\begin{aligned} T_c &= \text{Temperature change of the cask wall} \\ &= 118^\circ\text{F} \end{aligned}$$

Fixed-edge force and fixed-edge moment due to temperature difference between the inner and outer surface of the closure lid is determined by use of the following equations.

$$\begin{aligned} F_f &= 0 \text{ lb/bolt} \\ M_f &= \frac{E_l \times a_l \times t_l^2 \times (T_{lo} - T_{li})}{12 \times (1 - \nu_{ul})} \end{aligned}$$

where,

$$\begin{aligned} T_{lo} &= \text{Temperature change of the outer surface of the closure lid} \\ &= 118.1^\circ\text{F} \\ T_{li} &= \text{Temperature change of the inner surface of the closure lid} \\ &= 116.8^\circ\text{F} \end{aligned}$$

2.12.4.2.8. Forces/Moments Generated By Impact Loads

For this evaluation, the loads created by impact are analyzed for a cask with a protected closure lid and are found via Table 4.5 in NUREG/CR-6007. As follows, the non-prying tensile bolt force per bolt due to impact is:

$$F_a = \frac{1.34 \times \sin(\alpha) \times DLF \times a_l \times (W_l - W_c)}{N_b}$$

Further, the shear bolt force per bolt is evaluated using,

$$F_s = \frac{\cos(\alpha) \times a_l \times W_l}{N_b}$$

Accordingly the fixed-edge force and fixed-edge moment are defined by,

$$F_f = \frac{1.34 \times \sin(\alpha) \times DLF \times a_l \times (W_l - W_c)}{\pi \times D_{lb}}$$

and,

$$M_f = \frac{1.34 \times \sin(\alpha) \times DLF \times a_l \times (W_l - W_c)}{8\pi}$$

2.12.4.2.9. Forces/Moments Generated By Vibration Loads

Looking at Table 4.8 in NUREG/CR-6007, the loads that are generated due to vibration are outlined. The tensile bolt force per bolt due to vibration is:

$$F_a = \frac{VTR \times a_{va} \times W_l}{N_b}$$

The shear bolt force per bolt is calculated by use of the equation,

$$F_s = \frac{VTR \times a_{vt} \times W_l}{N_b}$$

The fixed-edge force and fixed edge moment are:

$$F_f = \frac{VTR \times a_{va} \times W_l}{\pi \times D_{lb}}$$

and,

$$M_f = \frac{VTR \times \text{ava} \times W_l}{8\pi}$$

2.12.4.2.10. Prying Action Forces Generated by Applied Loads

Table 2.1 of NUREG/CR-6007 lays out the analysis to evaluate the axial bolt force per bolt caused by prying action of the lid is:

$$F_{ap} = \left(\frac{\pi D_{lb}}{N_b} \right) \left[\frac{\frac{2 \times M_f}{D_{lo} - D_{lb}} - C1(B - F_f) - C2(B - P)}{C1 + C2} \right]$$

where

$$\begin{aligned} C1 &= 1 \\ C2 &= \left(\frac{8}{3(D_{lo} - D_{lb})^2} \right) \left(\frac{E_l \times t_l^3}{1 - N_{ul}} + \frac{(D_{lo} - D_{li}) E_{lf} \times t_{lf}^3}{D_{lb}} \right) \left(\frac{L_b}{N_b D_b^2 E_b} \right) \\ L_b &= \text{Bolt length between the top and bottom surfaces of the closure lid at the bolt circle} \\ &= 1.5 \text{ in} \\ B &= F_f \text{ if } F_f > P, \text{ otherwise } B = P \end{aligned}$$

It should be noted that the fixed-edge force and fixed-edge moment are inputs from Table 4.2, 4.3 and 4.8 for NCT and Table 4.2, 4.3 and 4.5 for HAC.

2.12.4.2.11. Bending Bolt Moment Generated by Applied Loads

Located in Table 2.2 of NUREG/CR-6007 is the formula for calculating the bending bolt moment per bolt caused by the rotation or bending of the closure lid and is:

$$M_{bb} = \left(\frac{\pi D_{lb}}{N_b} \right) \left(\frac{K_b}{K_b + K_l} \right) M_f$$

where

$$\begin{aligned} K_b &= \left(\frac{N_b}{L_b} \right) \left(\frac{E_b}{D_{lb}} \right) \left(\frac{D_b^4}{64} \right) \\ K_l &= \frac{E_l t_l^3}{3 \left[(1 - N_{ul}^2) + (1 - N_{ul})^2 \left(\frac{D_{lb}}{D_{lo}} \right) \right] D_{lb}} \end{aligned}$$

Once again, it should be noted that the fixed-edge force and fixed-edge moment are inputs from Table 4.2, 4.3 and 4.8 for NCT and Table 4.2, 4.3 and 4.5 for HAC.

2.12.4.2.12. Calculation of Total Loads and Bolt Stresses

In order to accurately combine tensile bolt forces, Table 4.9 of NUREG/CR-6007 is applied. To calculate the total non-prying axial load, the axial bolt force from Tables 4.3-4.8 is summed. The same process is used to determine the total fixed-edge force and fixed-edge moment. Further, the bolt stresses can be formulated from Table 5.1 of NUREG/CR-6007. Calculating the average bolt direct stress caused by the tensile bolt force is:

$$S_{ba} = 1.2732 F_a / D^2$$

and the average bolt shear stress is formulated as,

$$S_{bs} = 1.2732 F_s / D^2$$

The maximum bending stress and maximum shear stress are represented as,

$$S_{bb} = 10.186 M_{bb} / D^3$$

$$S_{bt} = 5.093 M_t / D^3$$

Where F_a , F_s , M_{bb} , and M_t all represent total values of the tensile bolt force, shear bolt force, bending bolt moment, and torsional bolt moment respectively.

2.12.4.2.13. Limits on Bolt Stresses

Table 6.1 of NUREG/CR-6007 gives the acceptance criteria for normal conditions of transport. The acceptance criteria state that the average stress must be less than the allowable stress in tension. For shear, the average stress must be less than 60 percent of the allowable stress. In addition, the sum of the squares of the stress ratio for average tensile stress and stress ratio for average shear stress must be less than one. Further, the maximum stress intensity must be less than 1.35 times the allowable stress for bolts having a minimum tensile strength greater than 100 ksi and 1.5 times for bolts having a minimum tensile strength less than 100 ksi.

Looking at Table 6.3 for HAC, the average stress in tension must be less than the smaller of $0.7S_u$ or S_y at temperature. The average stress in shear must be less than the smaller of $0.42S_u$ or $0.6S_y$ at temperature. Furthermore, the sum of the squares of the stress ratio for average tensile stress and stress ratio for average shear stress must be less than one.

2.12.4.2.14. Analytical Results

Forces and Moments

The forces and moments that the Model 2000 Transport Package closure lid, wall, and bolt are subjected to during normal conditions of transport and hypothetical accident conditions are shown in Table 2.12.4-8 and Table 2.12.4-9, respectively.

Table 2.12.4-8. Forces/Moments Results (NCT)

| Load Condition | Forces/Moments | Variable | Magnitude | Units |
|----------------|----------------------------------------|----------|-----------|-------|
| PRESSURE | Non-Prying Tensile Bolt Force | F_a | 671.96 | lb |
| | Shear Bolt Force Per Bolt | F_s | 690.58 | lb |
| | Fixed-Edge Closure-Lid Force | F_f | 120.94 | lb |
| | Fixed-Edge Closure-Lid Moment | M_f | 487.53 | lb-in |
| TEMPERATURE | Non-Prying Tensile Bolt Force | F_a | 10856.79 | lb |
| | Shear Bolt Force Per Bolt | F_s | -2151.88 | lb |
| | Fixed-Edge Closure-Lid Force | F_f | 0 | lb |
| | Fixed-Edge Closure-Lid Moment | M_f | 120.80 | lb-in |
| VIBRATION | Non-Prying Tensile Bolt Force | F_a | 253.33 | lb |
| | Shear Bolt Force Per Bolt | F_s | 633.33 | lb |
| | Fixed-Edge Closure-Lid Force | F_f | 37.51 | lb |
| | Fixed-Edge Closure-Lid Moment | M_f | 151.2 | lb-in |
| PRELOAD | Non-Prying Tensile Bolt Force Per Bolt | F_a | 32000 | lb |
| | Torsional Bolt Moment Per Bolt | M_t | 3000 | lb-in |
| GASKET | Axial Load For Gasket Seating | F_a | 17361.38 | lb |
| | Axial Load For Gasket Operation | F_a | 130.21 | lb |
| | Torque Due to Gasket | M_t | 1627.63 | lb-in |
| PRYING | Axial Load Due to Prying | F_a | -25628.50 | lb |
| | Bending Moment Due to Prying | M_{bb} | 173.84 | lb-in |

Table 2.12.4-9. Forces/Moments Results (HAC)

| Load Condition | Forces/Moments | Variable | Magnitude | Units |
|----------------|----------------------------------------|----------|-----------|-------|
| PRESSURE | Non-Prying Tensile Bolt Force | F_a | 671.96 | lb |
| | Shear Bolt Force Per Bolt | F_s | 690.58 | lb |
| | Fixed-Edge Closure-Lid Force | F_f | 120.94 | lb |
| | Fixed-Edge Closure-Lid Moment | M_f | 487.53 | lb-in |
| TEMPERATURE | Non-Prying Tensile Bolt Force | F_a | 10856.79 | lb |
| | Shear Bolt Force Per Bolt | F_s | -2151.88 | lb |
| | Fixed-Edge Closure-Lid Force | F_f | 0 | lb |
| | Fixed-Edge Closure-Lid Moment | M_f | 120.80 | lb-in |
| IMPACT | Non-Prying Tensile Bolt Force | F_a | 16415.00 | lb |
| | Shear Bolt Force Per Bolt | F_s | 0 | lb |
| | Fixed-Edge Closure-Lid Force | F_f | 2430.26 | lb |
| | Fixed-Edge Closure-Lid Moment | M_f | 9796.98 | lb-in |
| PRELOAD | Non-Prying Tensile Bolt Force Per Bolt | F_a | 32000 | lb |
| | Torsional Bolt Moment Per Bolt | M_t | 3000 | lb-in |
| GASKET | Axial Load For Gasket Seating | F_a | 17361.38 | lb |
| | Axial Load For Gasket Operation | F_a | 130.21 | lb |
| | Torque Due to Gasket | M_t | 1627.63 | lb-in |
| PRYING | Axial Load Due to Prying | F_a | 12115.39 | lb |
| | Bending Moment Due to Prying | M_{bb} | 2381.63 | lb-in |

2.12.4.2.15. Total Loads and Bolt Stresses Results

Now that all of the forces and moments have been calculated for both NCT and HAC, the loads can be combined appropriately to determine the total loads. Additionally, the bolt stresses can be calculated from the total loads. The results are displayed below for NCT and HAC in Table 2.12.4-10 and Table 2.12.4-11 respectively.

Table 2.12.4-10. Total Loads/Bolt Stresses (NCT)

| Total Loads/ Bolt Stresses | Variable | Magnitude | Units |
|-----------------------------|----------|-----------|-------|
| Total Bolt Axial Load | F_a | 6371.50 | lb |
| Total Bolt Shear Load | F_s | -827.97 | lb |
| Total Bolt Bending Moment | M_b | 759.52 | lb-in |
| Total Bolt Torsional Moment | M_t | 3000 | lb-in |
| Average Bolt Direct Stress | S_{ba} | 6574.39 | psi |
| Average Bolt Shear Stress | S_{bs} | -854.33 | psi |
| Maximum Bending Stress | S_{bb} | 5644.44 | psi |
| Maximum Shear Intensity | S_{bi} | 23939.14 | psi |
| Total Bolt Shear Stress | S_{bt} | 11147.32 | psi |

Table 2.12.4-11. Total Loads/Bolt Stresses (HAC)

| Total Loads/ Bolt Stresses | Variable | Magnitude | Units |
|-----------------------------|----------|-----------|-------|
| Total Bolt Axial Load | F_a | 89420.53 | lb |
| Total Bolt Shear Load | F_s | -1461.30 | lb |
| Total Bolt Bending Moment | M_b | 12786.94 | lb-in |
| Total Bolt Torsional Moment | M_t | 3000 | lb-in |
| Average Bolt Direct Stress | S_{ba} | 92267.96 | psi |
| Average Bolt Shear Stress | S_{bs} | -1507.83 | psi |
| Maximum Bending Stress | S_{bb} | 95026.74 | psi |
| Total Bolt Shear Stress | S_{bt} | 11147.32 | psi |

2.12.4.2.16. Limits on Bolt Stresses Results

Accordingly, the code evaluation is conducted using the information given in the previous subsection and the appropriate tables from NUREG/CR-6007 for both NCT and HAC. Per Table 6.1 of NUREG/CR-6007, the limits for NCT are evaluated as,

$$\begin{aligned}\Sigma_{\beta\alpha} &< \Sigma_{\mu} \\ 6574.39 \text{ } \pi\sigma_1 &< 77,130 \text{ } \pi\sigma_1\end{aligned}$$

and,

$$\begin{aligned}\Sigma_{\beta\sigma} &< 0.6\Sigma_{\mu} \\ -854.33 \pi\sigma_1 &< 46278 \pi\sigma_1\end{aligned}$$

also,

$$\begin{aligned}R_t^2 + R_s^2 &< 1 \\ (0.0852)^2 + (-0.0185)^2 &< 1\end{aligned}$$

where,

$$\begin{aligned}R_t &= \text{Stress ratio for average tensile stress} \\ R_s &= \text{Stress ratio for average shear stress}\end{aligned}$$

Per Table 6.3 of NUREG/CR-6007, the limits for HAC are evaluated as,

$$\begin{aligned}S_{ba} &< 0.7S_u \\ 92267.96 \text{ psi} &< 101500 \text{ psi}\end{aligned}$$

and,

$$\begin{aligned}S_{bs} &< 0.42S_u \\ -1507.83 \text{ psi} &< 60900 \text{ psi}\end{aligned}$$

also,

$$\begin{aligned}R_t^2 + R_s^2 &< 1 \\ (0.91)^2 + (-0.02)^2 &< 1\end{aligned}$$

2.12.4.2.17. Fatigue Analysis

The fatigue analysis considers vibration and operating stresses, which come from the NCT bolt stress. Included in the operating stress are the pressure, preload, gasket load, and temperature stresses. Therefore, the loads are:

$$\begin{aligned}S_{\text{Operating}} &= 49617.7 \text{ psi} \\ S_{\text{Vibration}} &= 206 \text{ psi}\end{aligned}$$

Using ASME Code, Section III, NB-3232.3 (Reference 2-32, page 91), the alternating stresses can be found by the equation below,

$$\begin{aligned}S_{a\text{-Operating}} &= RF \times S_{\text{Operating}} \left(\frac{E_{dc}}{E_a} \right)^U \\ S_{a\text{-Vibration}} &= RF \times S_{\text{Vibration}} \left(\frac{E_{dc}}{E_a} \right)^U\end{aligned}$$

where

$$\begin{aligned}RF &= \text{Fatigue Strength Reduction Factor (Reference 2-32)} \\ E_{dc} &= \text{Modulus of Elasticity on Design Fatigue Curve} \\ &\quad \text{(Reference 2-18, Figure I-9.4, page 12)} \\ E_a &= \text{Modulus of Elasticity used in the Analysis} \\ U &= \text{Cumulative Usage Factor} \\ U &= 1 \text{ (Reference 2-32)}\end{aligned}$$

Applying ASME Section III, Figure I-9.4, the fatigue limit for maximum nominal stress $\leq 2.7 S_m$ for the loads of this analysis are,

$$N_{a-Operating} = 192 \text{ Cycles}$$

$$N_{a-Vibration} = 10^{11} \text{ Cycles}$$

The above values are accurately calculated by interpolating the tabular data given in ASME Section III, Table I-9.0 (Reference 2-18, page 2). Assuming 10^7 cycles for vibration load and 190 transports:

$$N_{Operating} = 190 \text{ Cycles}$$

The accumulative usage is then,

$$R = \left(\frac{N_{Operating}}{N_{a-Operating}} \right) + \left(\frac{N_{Vibration}}{N_{a-Vibration}} \right)$$

Shown in Table 2.12.4-12 are the results from the analysis.

Table 2.12.4-12. Fatigue Analysis Results

| Parameter | Variable | Value | Units |
|----------------------------------------|-------------------|----------|-------|
| Vibration Stress | $S_{vibration}$ | 206 | psi |
| Operating Stress | $S_{operating}$ | 49617.7 | psi |
| Fatigue Strength Reduction Factor | RF | 4 | -- |
| Cumulative Usage Factor | U | 1 | -- |
| E given on design curve | E_{dc} | 30000000 | psi |
| E used in analysis | E_a | 25900000 | psi |
| Ratio of Modulus of Elasticity | E_{ratio} | 1.16 | -- |
| Alternating Stress due to Vibration | $S_{a-Vibration}$ | 954 | psi |
| Alternating Stress due to Operating | $S_{a-Operating}$ | 230000 | psi |
| Number of Alt. Cycles due to Vibration | $N_{a-Vibration}$ | 1E+12 | -- |
| Number of Alt. Cycles due to Operating | $N_{a-Operating}$ | 192 | -- |
| Number of Cycles for Vibration Load | $N_{Vibration}$ | 1.00E+08 | -- |
| Number of Cycles for Operating Load | $N_{Operating}$ | 190 | -- |
| Accumulative Usage | R | 0.99 | -- |

Because the accumulative usage is less than one, it is acceptable to have up to 190 transports before all bolts are replaced. After 190 transports, all bolts must be replaced.

2.12.5. Model 2000 Scale Model Drop Test Report

Model 2000 Drop Test Report No. 87-08-01 is provided in the following pages.



560 San Antonio Road Suite 101 Palo Alto, California 94306 (415) 494-7351

**30-FT. FREE DROP TESTS OF A
QUARTER-SCALE MODEL 2000
TRANSPORT PACKAGE**

Submitted To:

**GENERAL ELECTRIC COMPANY
VALLECITOS NUCLEAR CENTER,
PLEASANTON, CA**

**Report No. 87-08-01
August 1987**



This report describes a series of 30-foot, free drop tests performed on a 1/4-scale model of a General Electric Model 2000 Transport Package. The work was performed for General Electric Vallecitos Nuclear Center under Purchase Order No. 205-87C338.

Prepared by: David A. Kienholz
David A. Kienholz, Ph.D.
Principal Engineer

Bradley R. Allen
Bradley R. Allen
Engineer



CONTENTS i

Contents

| | |
|----------------------------------------------------------|-----------|
| 1. Introduction and Summary | 1 |
| 2. Objectives | 1 |
| 3. Test Article | 2 |
| 3.1 Scaling Relations | 6 |
| 4. Instrumentation | 8 |
| 4.1 Acceleration Measurements | 8 |
| 4.2 Force Distribution Measurements | 11 |
| 4.3 Photography | 13 |
| 4.4 Deformation Measurements | 15 |
| 5. Procedure | 16 |
| 6. Results | 19 |
| 6.1 Head-On Drop | 19 |
| 6.1.1 Acceleration Data and High-Speed Photography | 19 |
| 6.1.2 Pressure- Sensing Film | 24 |
| 6.1.3 Cask and Overpack Deformation Measurements | 26 |
| 6.2 Side Drop | 28 |
| 6.2.1 Acceleration Data and High-Speed Photography | 28 |
| 6.2.2 Pressure-Sensing Film | 35 |
| 6.2.3 Cask and Overpack Deformation Measurements | 35 |
| 6.3 CG-Over-Corner Drop | 35 |
| 6.3.1 Acceleration Data and High-Speed Photography | 35 |
| 6.3.2 Pressure- Sensing Film | 42 |
| 6.3.3 Cask and Overpack Deformation Measurements | 42 |
| 7. Summary and Conclusions | 44 |

List of Figures

| | | |
|----|----------------------------------------------------------------------------------------------------------|----|
| 1 | Quarter-scale model of Model 2000 Transport Package showing accelerometer locations for drop tests | 2 |
| 2 | Model 2000 Transport Package details | 3 |
| 3 | Overpack weldments..... | 4 |
| 4 | Assembled package | 5 |
| 5 | Accelerometers mounted inside the cask..... | 9 |
| 6 | Accelerometers mounted outside the overpack..... | 10 |
| 7 | Accelerometer signal processing | 11 |
| 8 | Apparatus for testing response speed of pressure sensing film | 12 |
| 9 | Pressure-sensing film being applied to cask..... | 14 |
| 10 | Measurement of toroid profile..... | 15 |
| 11 | Drop test orientations..... | 16 |
| 12 | Package rigged for side drop | 17 |
| 13 | Head-on drop, vertical acceleration | 20 |
| 14 | Head-on drop, frames taken at 2.12 millisecond intervals | 21 |
| 15 | Overplot of cask and overpack acceleration, head-on drop..... | 22 |
| 16 | Toroid deformation caused by head-on drop..... | 23 |
| 17 | Time integral of cask vertical acceleration, head-on drop | 24 |
| 18 | Pressure-sensing film from head-on drop..... | 25 |
| 19 | Gage numbering for inspection of overpack top toroid..... | 26 |
| 20 | Side drop, vertical acceleration | 30 |
| 21 | Side drop, frames taken at 2.13 millisecond intervals | 31 |
| 22 | Overpack weldments separating after impact, side drop..... | 32 |
| 23 | Package after side drop | 33 |
| 24 | Time integral of cask vertical acceleration prior to cable fault, drop | 34 |
| 25 | Pressure-sensing film from side drop..... | 36 |
| 26 | Rigging for CG-over-corner drop..... | 37 |
| 27 | CG-over-corner drop vertical acceleration..... | 38 |
| 28 | CG-over-corner drop, frames taken at 2.16 millisecond intervals..... | 39 |
| 29 | Deformation of overpack produced by CG-over-corner drop..... | 40 |
| 30 | Time integral of cask vertical acceleration, CG-over-corner drop..... | 41 |
| 31 | Pressure-sensing film from CG-over-corner drop | 43 |

1. INTRODUCTION AND SUMMARY

The General Electric Company Vallecitos Nuclear Center (GEVNC) designs and tests containers for shipping radioactive materials. These shielded containers must meet stringent safety requirements, including a 30-foot free drop onto a hard, unyielding horizontal surface. The package must withstand this drop without functional damage to the inner cask containing the radioactive payload.

CSA Engineering, Inc., was retained to perform a series of drop tests of 1/4-scale replicas of the Model 2000 transport package. Performed at the GEVNC facility on June 10, 11, and 14, 1987, the design and execution of the tests are governed by GE procurement specification 22A9367 (Rev. 2), dated June 8, 1987. This report documents the objectives, methods, results and conclusions of the tests.

Drop tests from three orientations were performed with no measurable deformation or other damage to the inner cask. Head-on and CG-over-corner drops were successfully completed with no unexpected results. Complete data on acceleration and internal load distribution were obtained for use in design verification.

An unexpected failure of the overpack bolted joint occurred when the cask was dropped on its side. The causes of the failure and requalification of the joint will be covered in a separate report.² The structural failure also caused the loss of some acceleration data. Nonetheless, a valid trace was obtained for the most important part of the impact event, including the portion during which plastic deformation of the overpack occurred and, probably, including the point of maximum vertical cask acceleration.

Subject to the above uncertainty in the side drop test, the maximum vertical accelerations recorded by sensors inside the cask for the head-on, side, and CG-over-corner drops were 408, 185, and 156 G's respectively.

2. OBJECTIVES

The objectives of the tests were to determine, for each of three drop orientations:

1. The damage, if any, suffered by the inner cask.
2. The vertical acceleration of the cask at impact.
3. The force distribution at impact between the inner cask and the outer protective overpack.

² Pomares, R. J., to be published

3. TEST ARTICLE

Figures 1 and 2 show the transport package in cross section with dimensions given for the 1/4-scale model. Figures 3 and 4 show the actual test article. The package is composed of two major assemblies: the inner cask and the outer protective overpack. The cask provides containment and radiation shielding for the payload. The overpack provides mechanical and thermal protection for the cask.

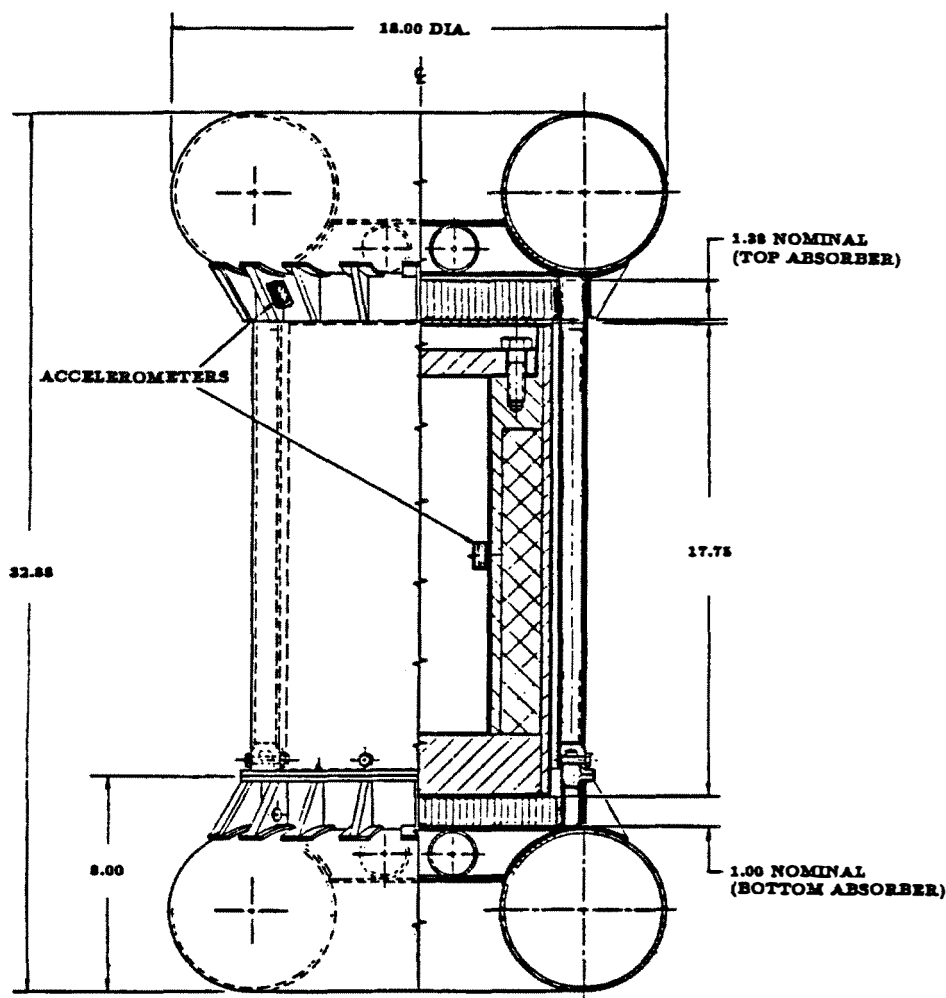
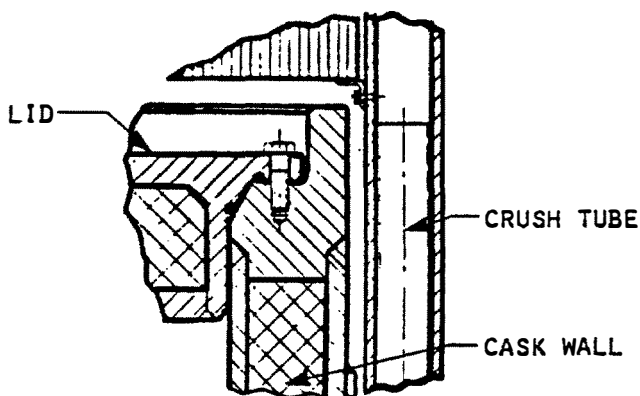
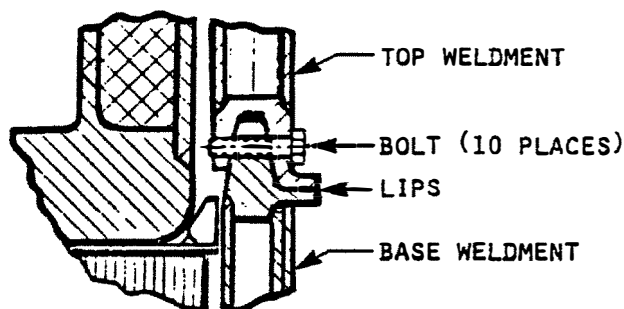


Figure 1. Quarter-scale model of Model 2000 Transport Package showing accelerometer locations for drop tests

The cask is essentially a thick-walled cylinder with a raised rim around the lid seal to protect this critical area. Of particular interest for this test are the impact-limiting features of the overpack. Constructed entirely of 304 stainless steel, it is composed of a double-walled cylindrical shell with identical toroidal shell "bumpers" at either end. Regardless of drop orientation, the initial impact will be taken by one of the toroids. They are designed to plastically deform and buckle inward at a specific load level and thus limit the acceleration of the cask. The cylindrical walls of the overpack are separated by tubular members running parallel to the cask axis. These are likewise designed to crush at a known load. Honeycomb "cushions" are provided between either end of the cask and the overpack for further impact limiting under axial acceleration.



Lid Detail



Joint Detail

Figure 2. Model 2000 Transport Package details

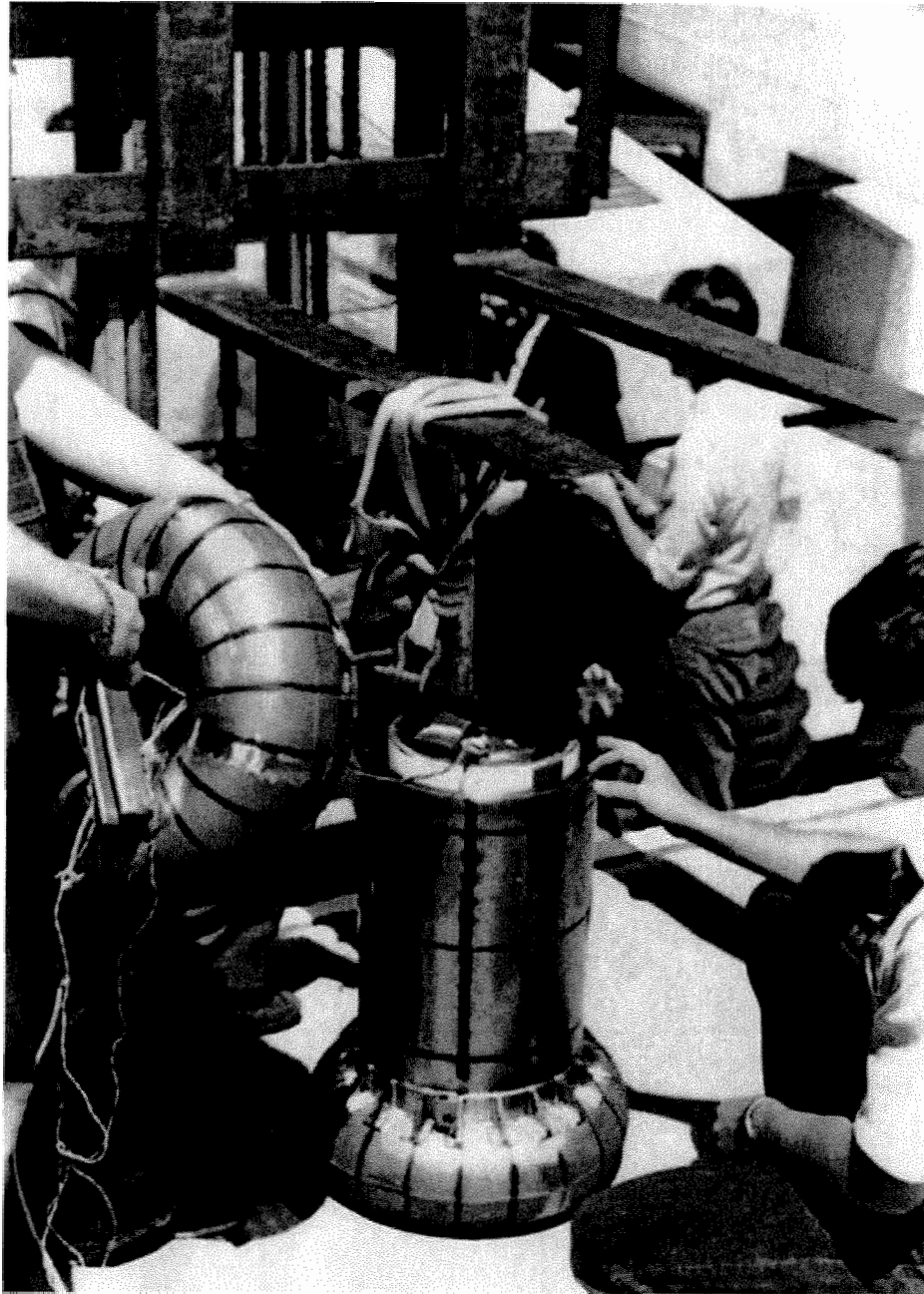


Figure 3. Overpack weldments

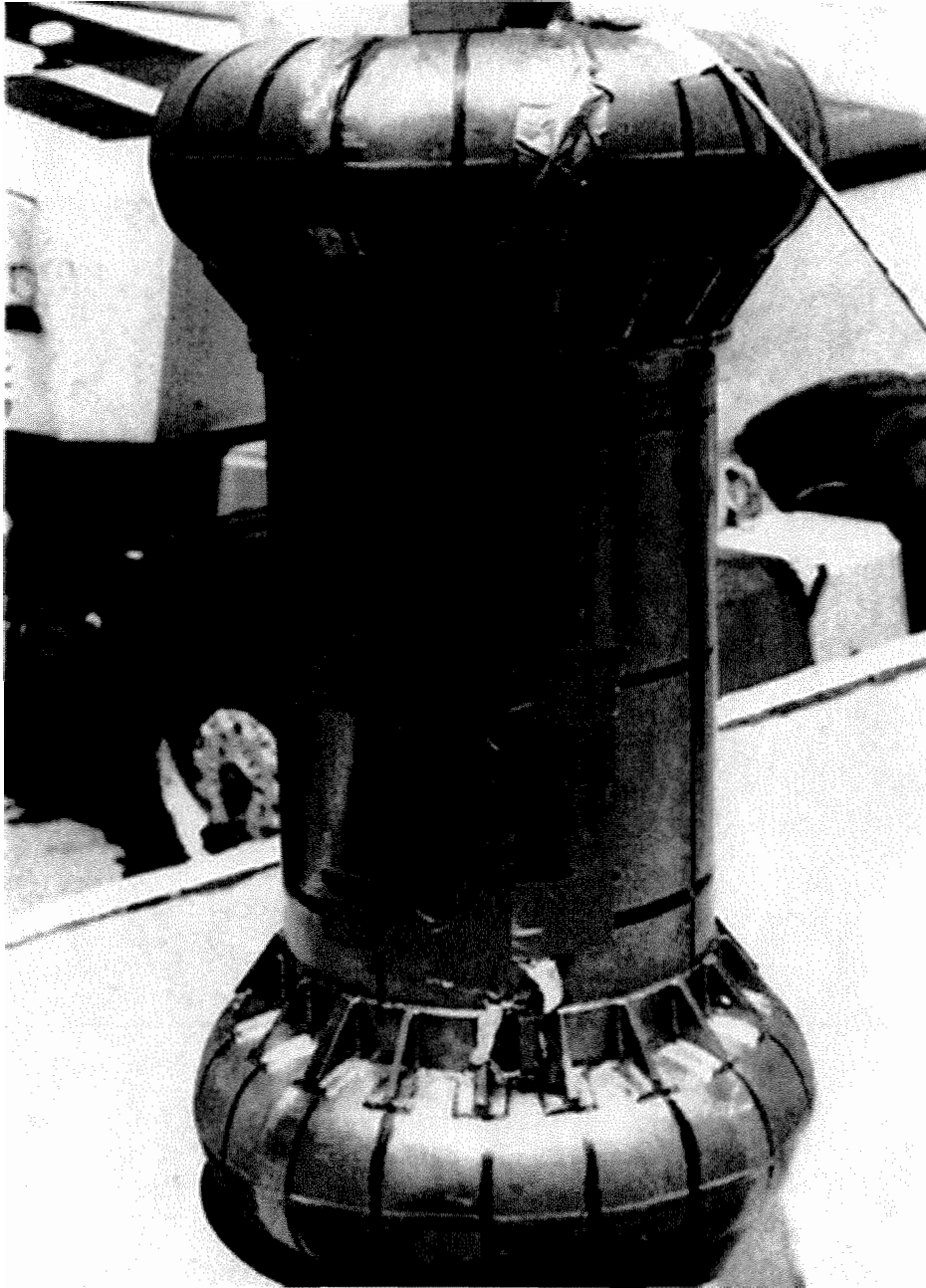


Figure 4 . Assembled package

The overpack is fabricated as two weldments bolted together at a lip joint running circumferentially around the cylinder just inboard of one toroid (see Figures 1 through 4). The smaller weldment is called the base and the larger is called the top. During normal assembly the cask is positioned, lid upwards, on the base and the top is lowered over it. The two weldments are joined at the lip seal by ten bolts, 1/4-inch in diameter for the scale model, inserted radially through the lips as shown in Figure 2.

The payload inside the cask was simulated by blocks of heavy metal, one attached to the lid and one to the floor. Weights of the package components are shown in Table 1.

Table 1: GE Model 2000 Transport Package
Component Weights (lbm)

| | Full-scale Prototype | 1/4-Scale Model |
|----------------|-------------------------|--------------------|
| Overpack | 9,822 | 154 |
| Cask | 17,647 | 276 |
| Payload (max.) | <u>5,450</u> | <u>85</u> |
| Total | 32,919 | 515 |

One scale model cask and two scale model overpacks were fabricated for the tests. Two complete overpacks were required to insure that the initial impact in each of the three required drops occurred on an undeformed area.

3.1 Scaling Relations

The test article is a near-replica constructed at 1/4-scale. Table 2 shows the classical replica scaling relations for a model constructed of the same material as the full-scale prototype.

The scaling ratios of primary interest here are those for velocity, acceleration, and stress. Velocity scales independent of length. The drop height for the scale model is therefore the same as for a full-scale prototype in order to produce the correct impact velocity. Acceleration scales as $1/\lambda$. A measured value of a_{model} in the current model test therefore corresponds to $a_{model}/4$ for the prototype. Neglecting strain rate effects, stress scales independent of length. Yielding or rupture of material in the model therefore implies a similar result for the prototype.

3.1 Scaling Relations

7

Table 2: Scaling Relations

Assumptions

- Monolithic structure
- Same material for model and prototype
- Length ratio (model/prototype) = λ

| Quantity | Model/Prototype Ratio | |
|----------------|--------------------------|----------------------------|
| | as function of λ | value for $\lambda = 0.25$ |
| Length | λ | 0.25 |
| Mass or weight | λ^3 | 0.0156 |
| Time | λ | 0.25 |
| Frequency | $1/\lambda$ | 4.00 |
| Displacement | λ | 0.25 |
| Velocity | 1 | 1.00 |
| Acceleration | $1/\lambda$ | 4.00 |
| Force | λ^2 | 0.0625 |
| Moment | λ^3 | 0.0156 |
| Stress | 1 | 1.00 |
| Strain | 1 | 1.00 |
| Stiffness | λ | 0.25 |

4. Instrumentation

Several diverse types of instrumentation were utilized to sense and record the impact phenomena. These included:

1. Accelerometers with signals recorded on analog magnetic tape
2. Pressure-sensing film
3. High-speed film and videotape photography
4. Micrometers and dial gauge arrays

Details on each are given in this section.

4.1 Acceleration Measurements

Seven accelerometers were mounted on the package: four inside the cask and three on the outside of the overpack. Locations are shown in Figure 1. All were piezoelectric, integrated amplifier (voltage mode) devices with a time constant of 0.5 seconds or greater. A triaxial array mounted inside the cask sensed in the axial, radial, and tangential directions. An additional uniaxial sensor was mounted inside the cask sensing in a direction 29 degrees off the cask axis. Denoted as the cask oblique sensor, its purpose was to measure vertical acceleration of the cask during the CG-over-corner drop. All sensors inside the cask were miniature, general purpose accelerometers with a maximum usable range of 1000 G's. Figure 5 shows the transducers on their mounting block bonded to the inner surface of the cask.

The triaxial array outside the overpack was composed of three sensors mounted in a special machined block to sense in the axial, radial, and tangential directions. These miniature shock accelerometers have a usable range of 10,000 G's. The arrangement is shown in Figure 6.

An eighth accelerometer was mounted on the steel drop pad, several feet away from the impact point. Its output signal was to be used for a timing trigger during data processing. However it was found that using one of the package sensor signals with a small pre-trigger delay was both more reliable and more convenient. The pad accelerometer data was therefore not used.

A schematic of the accelerometer signal chain is shown in Figure 7. Signals were recorded on an instrumentation FM tape recorder for later replay and analysis. The most important signals (vertical acceleration of the cask and overpack) were recorded on two tape channels apiece with different gain settings to optimize the signal/noise ratio. One channel of each pair was ranged to

4.1 Acceleration Measurements

9

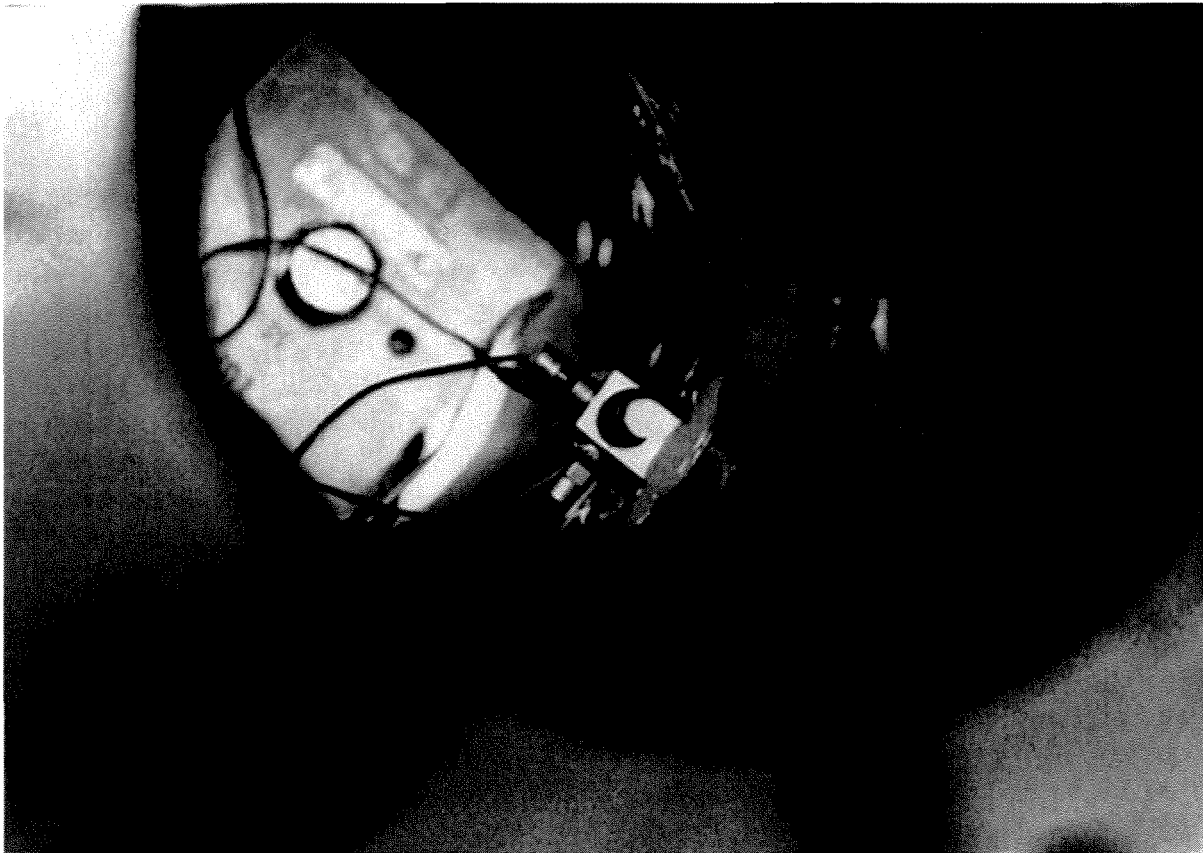


Figure 5. Accelerometers mounted inside the cask

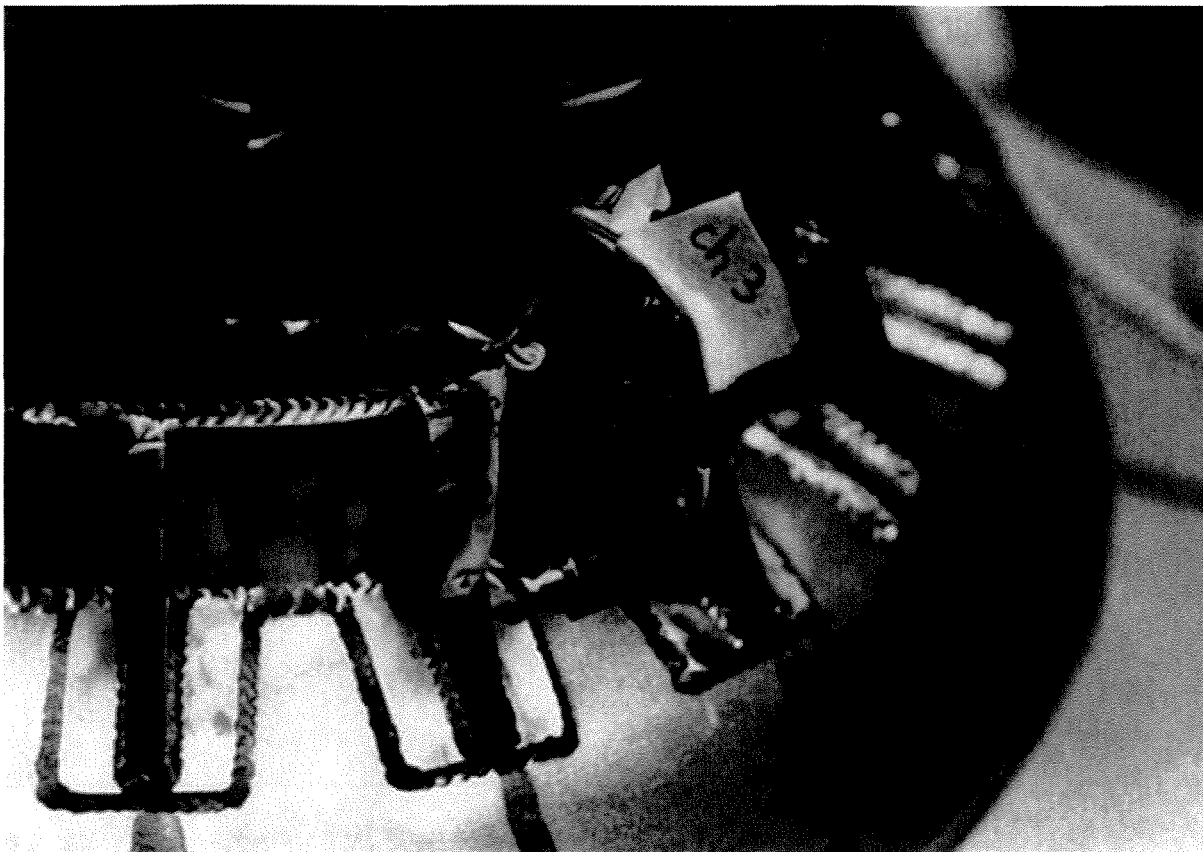


Figure 6. Accelerometers mounted outside the overpack

4.2 Force Distribution Measurements

11

accommodate a signal level about 3 dB above the anticipated maximum and the other was set to provide about 9 dB of headroom. On playback, the channel from each pair whose signal came closest to full-scale without exceeding it was used for analysis.

The digital signal analyzer (Figure 7) provided analog-to-digital data conversion with a maximum sampling frequency of 102.4 kHz per channel. This was effectively increased even further for certain data records by replaying the tape at a speed lower than used for recording. Data was either displayed immediately on the real time display or passed via a DMA link to the main computer for further processing.

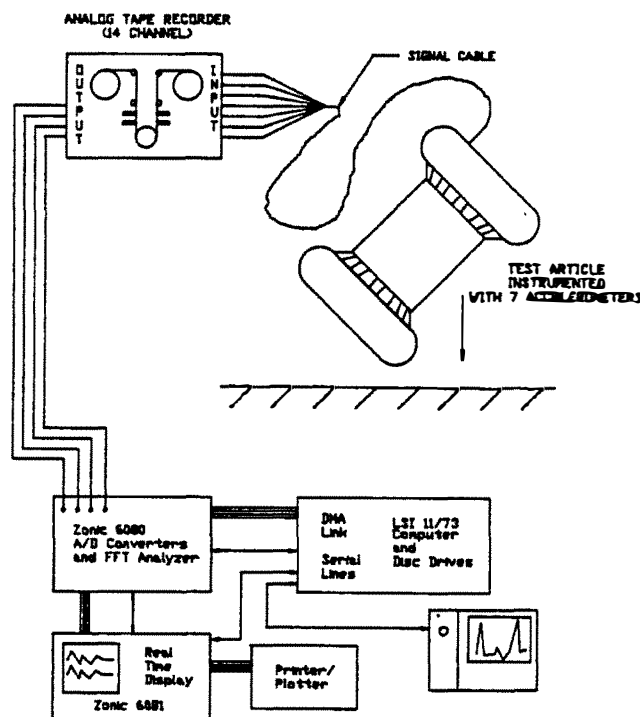


Figure 7. Accelerometer signal processing

4.2 Force Distribution Measurements

The distribution of force between the cask and overpack was determined by means of a pressure-sensing film on the cask exterior surface. The film undergoes a permanent color change from white to red when subjected to pressure. The color change is gradual with increasing pressure, allowing the approximate maximum pressure at any location to be determined by comparing

the exposed film to a calibrated color chart. More accurate reading is possible using a special densitometer. While somewhat subjective, the simpler comparison method was considered adequate for the present purpose.

The film provided a convenient method for determining the load distribution on the cask. It is available in several grades, each designed for a specific pressure range. The grade used for the drop test progresses from white to pink to red as the applied pressure is increased from 1000 to 3500 psi. Higher pressures have no effect, with the film simply retaining its maximum redness.

The film is normally used for static pressure measurements such as checking the flatness of mating surfaces of pipe flanges, cylinder heads, etc. Its manufacturer could not supply data on the time required for color change under sudden, impact loads. Therefore, a simple laboratory test was performed to assess its speed of response. Figure 8 shows the apparatus. Film specimens exposed at 2000 psi for a few hundred microseconds were compared to specimens exposed to the same pressure for two minutes. The specimens showed equal shades of red. It was concluded that the color change was effectively instantaneous.

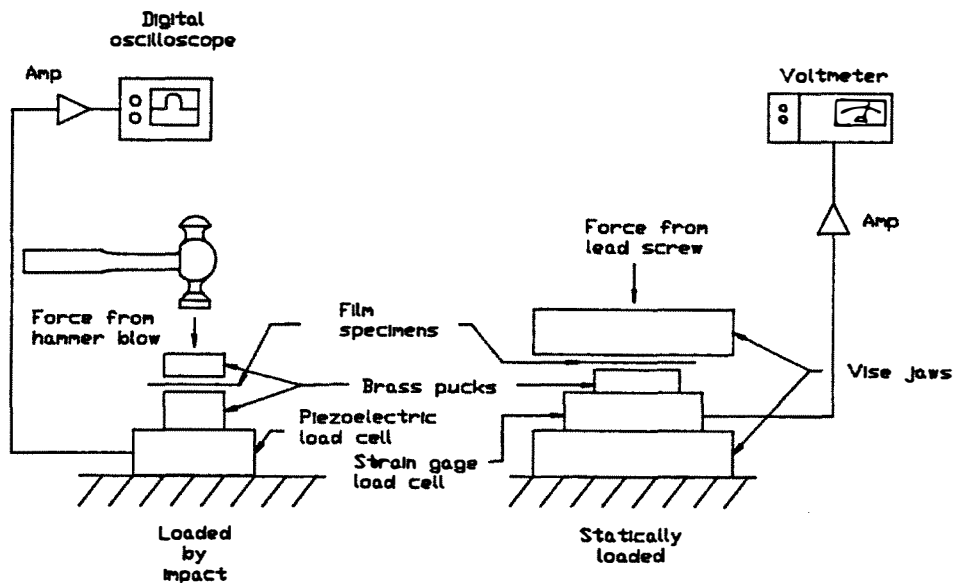


Figure 8. Apparatus for testing response speed of pressure sensing film

4.3 Photography

13

The film is composed of two separate layers, each resembling glossy paper with a total thickness is 0.008 inches. Under pressure, chemicals in the two layers react causing one layer to change color. It provides the pressure signature and the other layer is discarded.

Pieces were cut to fit the surfaces of the cask and held in place with adhesive tape as shown in Figure 9. A machined cover plate was located on the lid end of the cask to distribute the load over the entire surface of the circular honeycomb cushion. The film was placed between the cushion and the cover plate. Following each drop, the film was removed and the colored layer was annotated to become part of the permanent test record. Photographs in a later section show exposed film from each drop.

4.3 Photography

High-speed films were taken of each drop using two identical cameras viewing the scene from angles 90 degrees apart. Rated speed for the cameras was 500 frames/second.

A length scale and a time scale were located in the field of view of each camera, just behind the impact point. These scales, used in film interpretation, are shown later in photographs. Length scales were simply long rulers, graduated in inches and placed vertically in the field of view of each camera. Each time scale resembled a large clock with only one hand. The hand rotated clockwise at a measured speed of 3577 RPM. The time scales allowed accurate determination of frame rates, necessary for correlating the films with acceleration traces. Frame rates for the head-on, side, and CG-over-corner drop were 471.7, 469.5, and 463.0 frames/second respectively for the camera which produced the frames shown in this report.

A standard commercial videotape camera was also used to record the tests. By providing instant replay, it allowed the orientation of the package at impact to be verified immediately following each drop. Videotape was also used to document much of the test preparation.

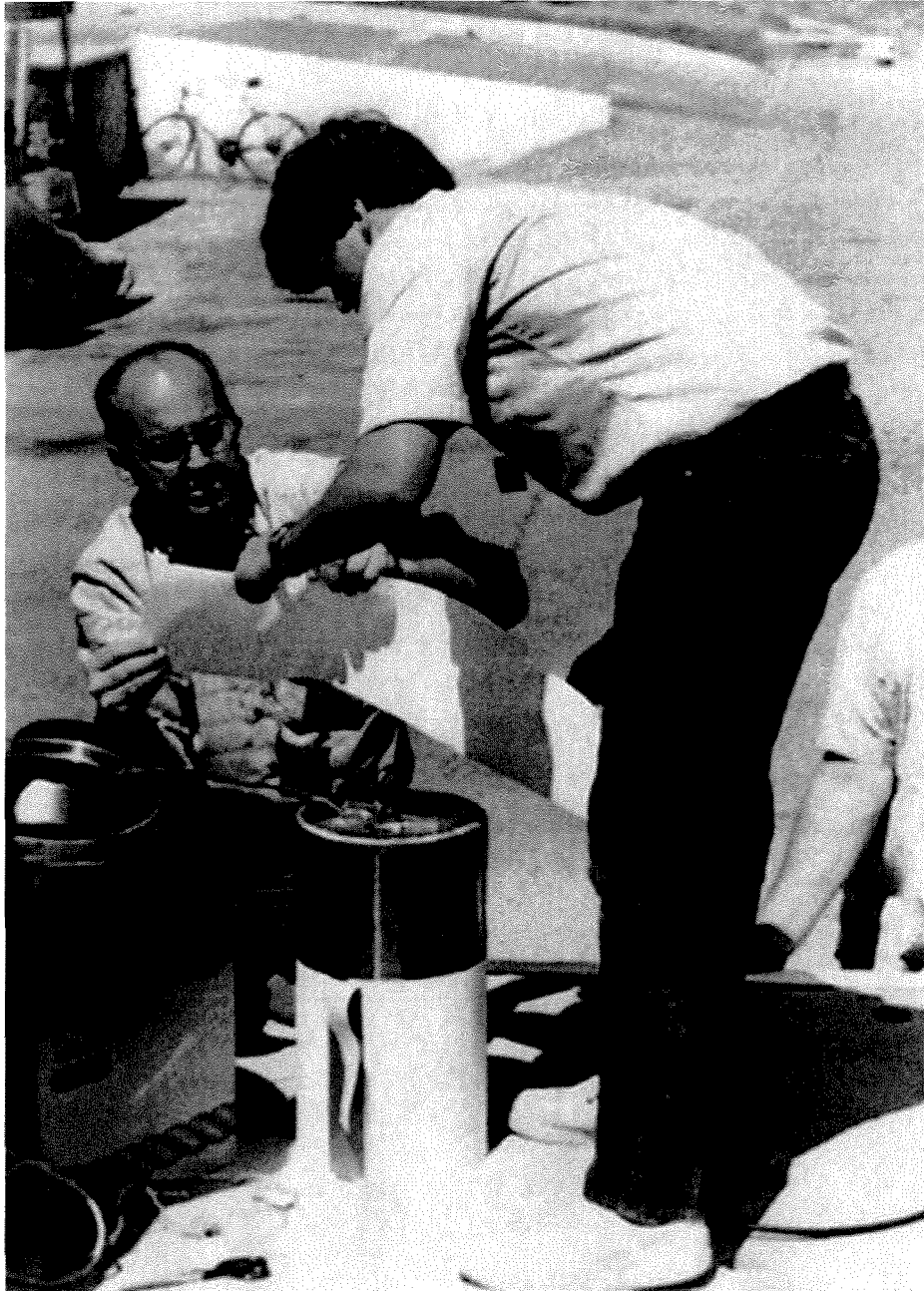


Figure 9. Pressure-sensing film being applied to cask

4.4 Deformation Measurements

Micrometer measurements of the cask diameter were made at several axial locations before and after each drop to check for plastic deformation.

Since the top of one overpack was used for two drops (side and CG-over-corner), it was necessary to carefully record the damage due to the first to insure that the effects of the two were determined separately. The fixturing for these measurements, performed before and after each drop, is shown in Figure 10. The cask was mounted between centers in a large lathe and an array of dial gages was used to determine the deformation of the toroids at a number of relocatable positions. Plaster molds were also made of the deformed sections of the toroids.

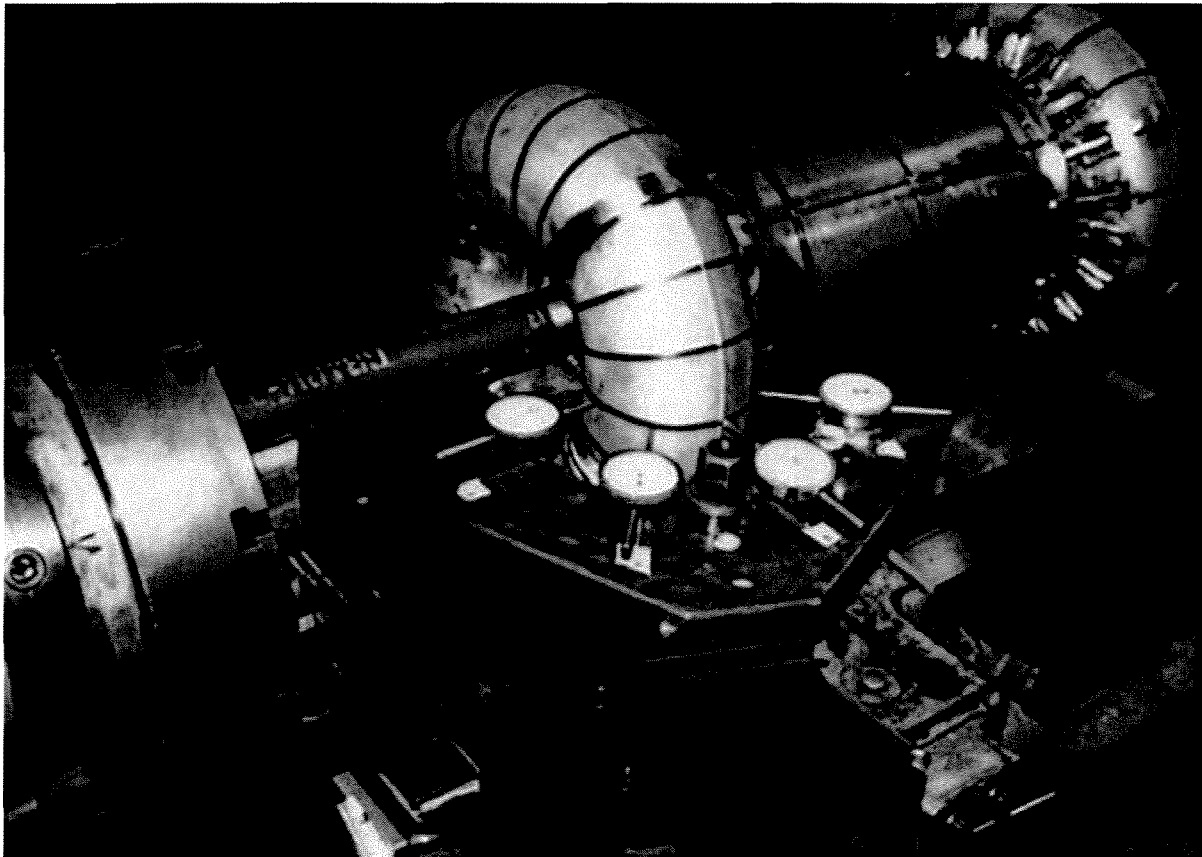


Figure 10. Measurement of toroid profile

5. PROCEDURE

Drop tests were performed for three different orientations of the cask. Depicted graphically in Figure 11, they are denoted in the order of performance as the head-on drop, the side drop, and the CG-over-corner drop. In the head-on and CG-over-corner drops, the cask lid and top of the overpack were oriented downwards to produce the worst-case load on the seal area of the cask.

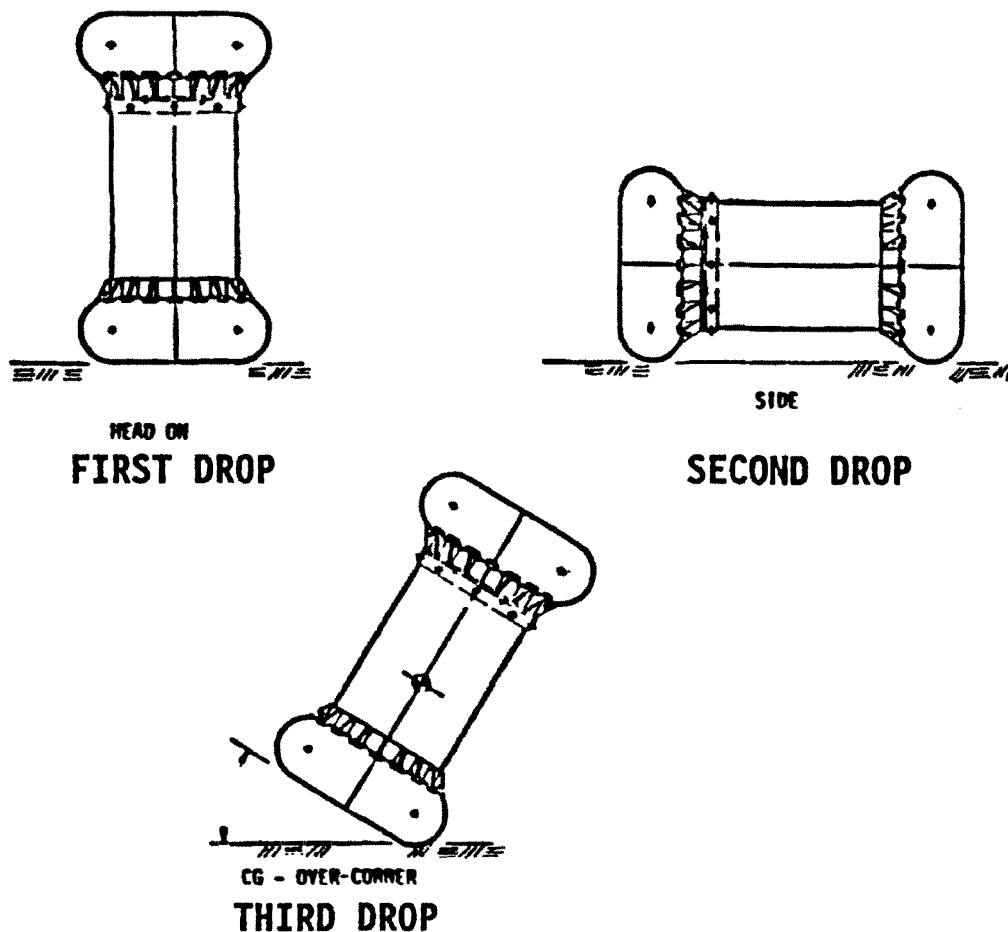


Figure 11. Drop test orientations

One cask and two complete overpack assemblies were fabricated. Overpack No. 1 was used for the head-on drop and No. 2 was used for the side drop. The CG-over-corner drop used the base of overpack No. 1 (still undamaged) and the top of overpack No. 2 with the package oriented such that the impact on the top occurred at an undamaged section.

Following the pre-drop dimensional inspection of the cask and overpack, the pressure sensing film was installed. The lateral sides and/or the lid end of the cask were covered, depending on the drop orientation. A cover plate was used between the lid end of the cask and the honeycomb cushion to distribute the load.

The cask and overpack were assembled, taking care to insure that the instrumentation cable was properly routed. The package was rigged for hoisting from the crane using an electromagnet and safety line. A magnet grip plate was secured to the overpack by a welded bracket which could be adjusted to obtain the correct orientation. Figure 12 shows the package rigged for the side drop. Special rigging was used for the CG-over-corner drop to balance the package over the contact point.

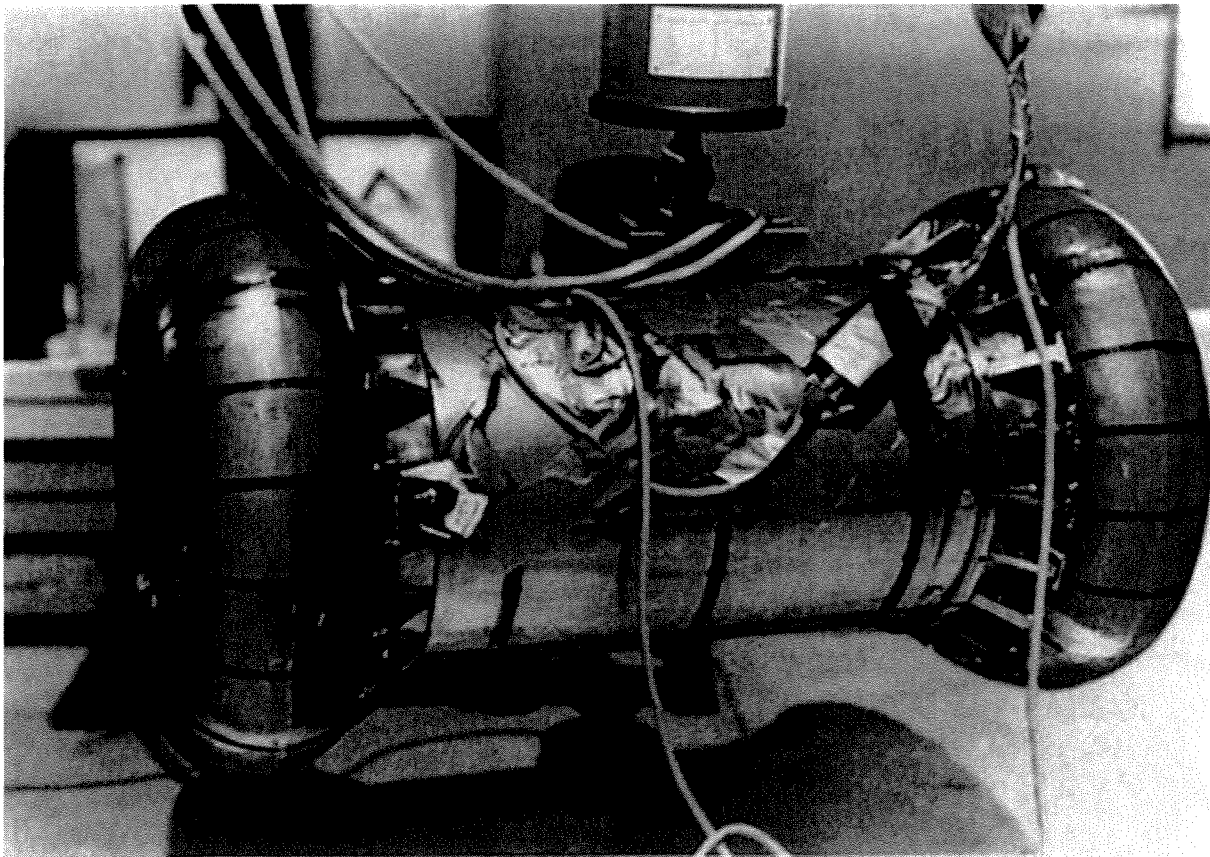


Figure 12. Package rigged for side drop

The package was hoisted by a mobile crane and the drop height was verified by a light, graduated chain hanging from the crane. The instrumentation cable was carefully routed and supported to prevent any interference with the free fall. The chain and safety line were removed just before the drop.

After a final check of all equipment, the tape recorder was started and voice-logged. The cameras were started and, after a one-second pause to allow them to reach speed, the polarity of the DC voltage to the electromagnet was reversed to release the package. Filming continued until the package came to rest.

Post-drop procedure included the following.

1. Data tapes were replayed to check signal ranging.
2. Pressure-sensing film was removed, inspected, annotated, and stored.
3. The cask and overpack were measured to determine the extent of plastic deformation.
4. Videotapes were replayed to check the package orientation at impact.

Detailed check lists were kept with each item initialed by the responsible individual after it was performed. These will become part of the final Product Quality Record.

6. RESULTS

Results of the drop tests are given in this section, organized by drop orientation.

6.1 Head-On Drop

6.1.1 Acceleration Data and High-Speed Photography

Figures 13 and 14 illustrates the impact event. The traces show the time history of vertical acceleration as measured by the axial accelerometers on the overpack and cask. The photographs are from the high-speed film, taken at a rate of 471.7 frames/second (2.12 milliseconds/frame). They are numbered in order of increasing time with zero being the frame closest to initial impact. The numbered vertical lines on the plot indicate the corresponding frame. The small markers along the bottom of each plot are spaced at 2.00 millisecond intervals.

Polarity of the vertical acceleration signal is not necessarily consistent between tests having different drop orientations. The sensors were simply installed in the most convenient way that provided correct alignment. Polarity was not considered important since the sense of the net velocity change, and thus the rigid-body component of acceleration at impact, was obviously known in advance.

Interpretation of the data from the head-on drop is straightforward. The acceleration seen by each sensor is composed of two parts. Low frequency components are present, corresponding to the rigid-body deceleration that produces the net change in velocity. A large number of high frequency components (ringing) are also produced by the resonant response of the vibration modes of the package. The low frequency portion, corresponding to a smoothed version of the trace, is of primary interest since it indicates the portion of the loading relevant to the package design.

Figure 15 shows the vertical acceleration of the cask and overpack plotted on the same scale. Peak acceleration of the cask is 408 G's, much lower than the 4853 G level experienced at the overpack sensor. The impact limiters greatly reduce the acceleration experienced by the cask.

Figure 16 shows the top toroid following the head-on drop. It has buckled inwards in an almost perfect axisymmetric pattern. The package rebounded almost straight up with negligible rotation and came to rest on the impact surface. These facts indicate that the accelerating force was essentially symmetric around the cask axis. The high-speed film showed a maximum rebound height at the overpack CG of 7.6 inches. The 408 G acceleration of the cask was the highest level seen in any of the three drops. This was as expected since the head-on drop distributed the crushing load over the largest portion of the toroid surface, thus producing the highest total force.

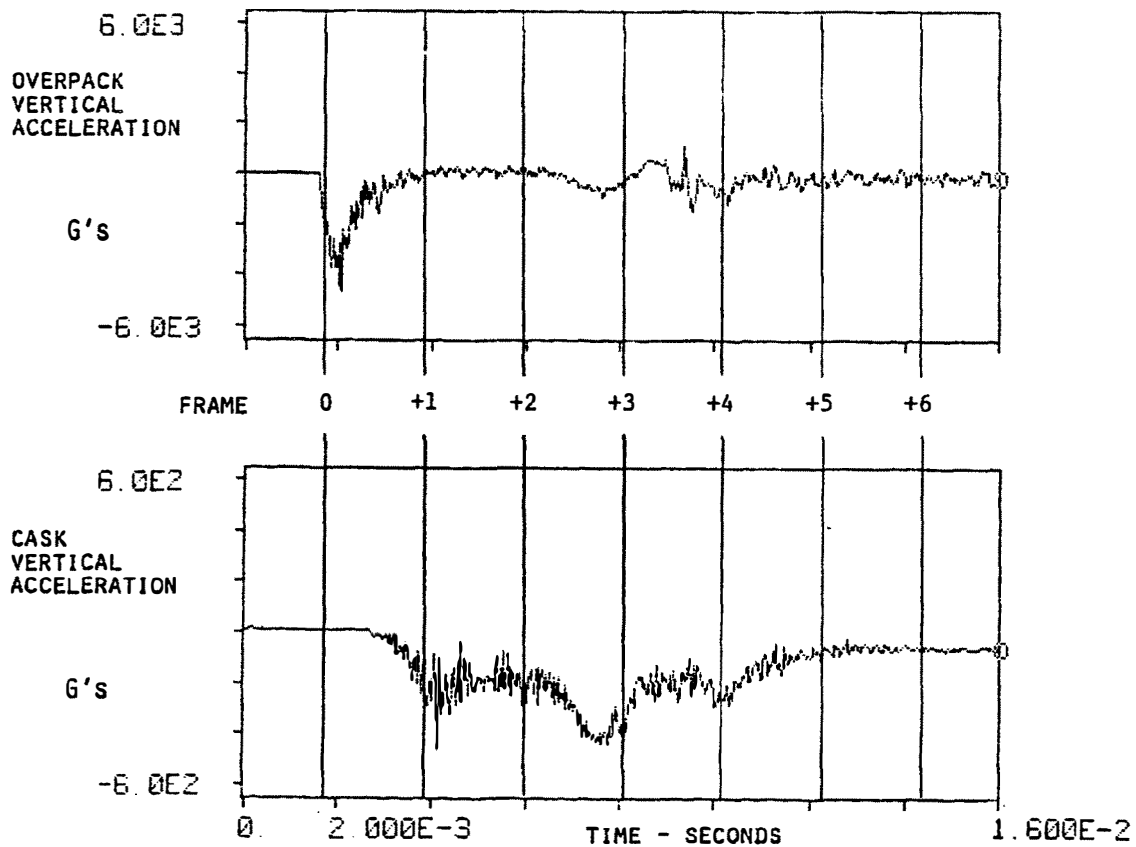


Figure 13. Head-on drop, vertical acceleration

6.1 Head-On Drop

21

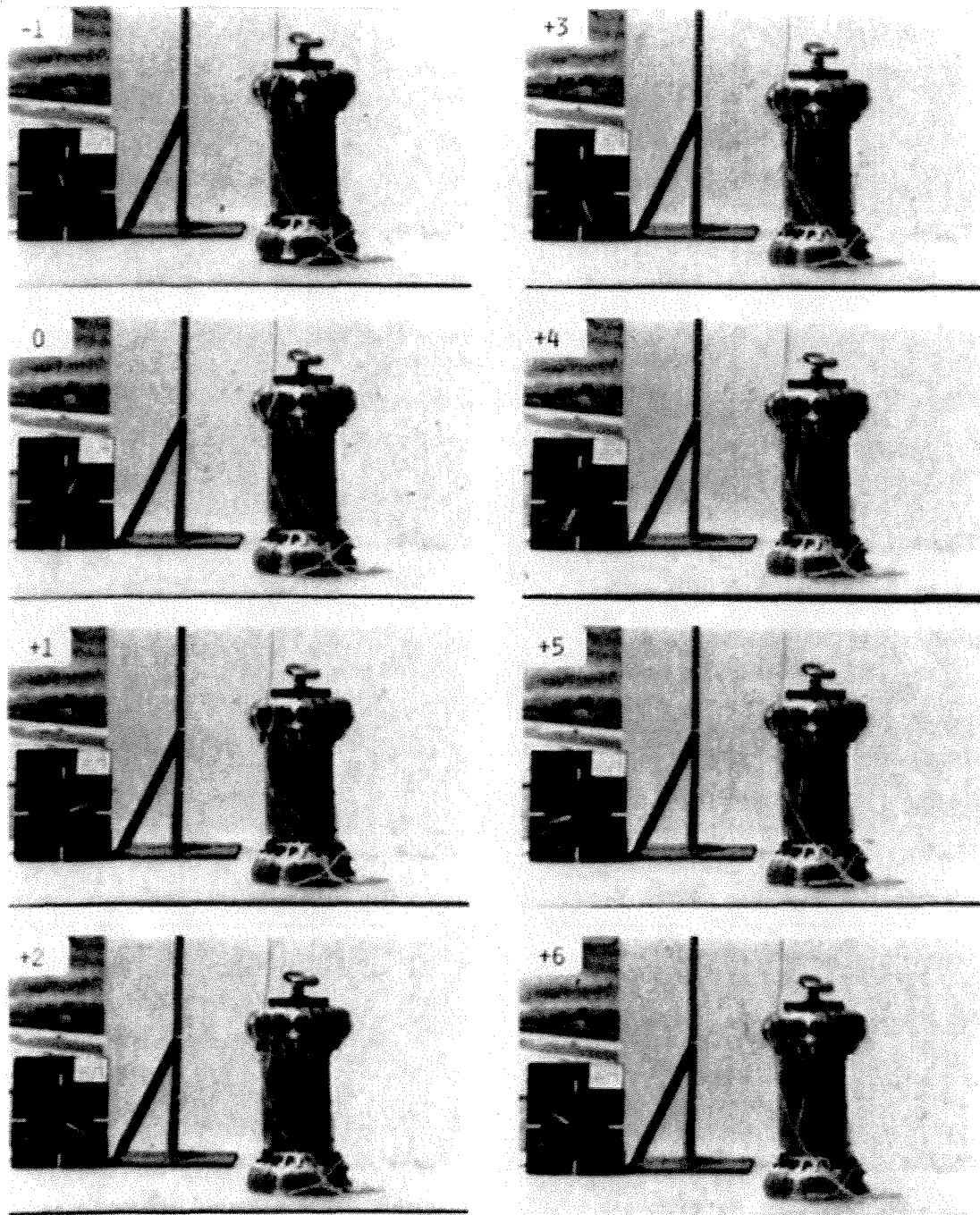


Figure 14. Head-on drop, frames taken at 2.12 millisecond intervals

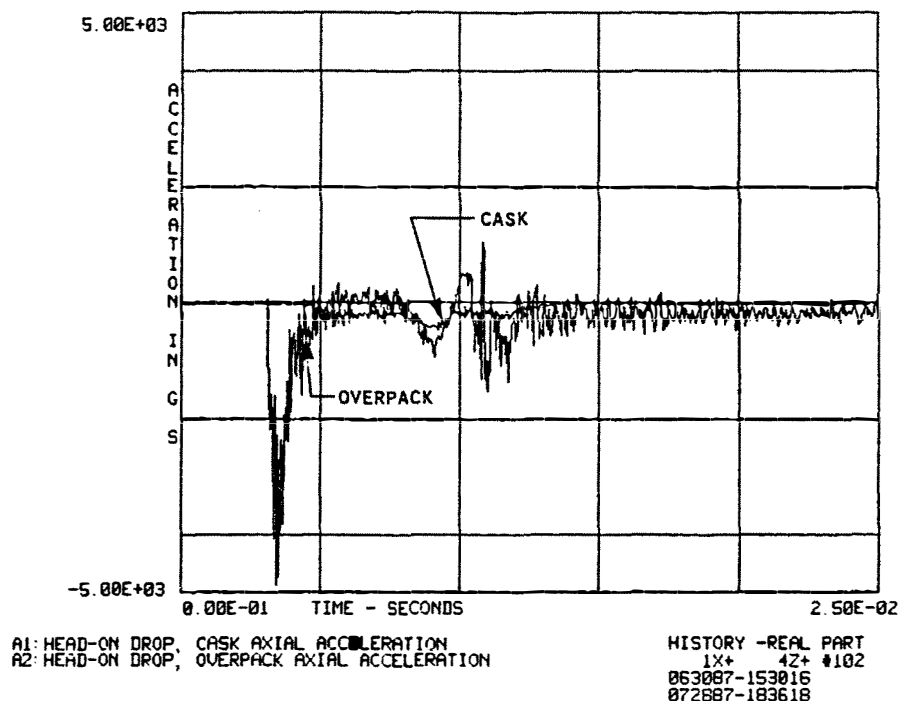


Figure 15. Overplot of cask and overpack acceleration, head-on drop

A smoothed version of the cask acceleration trace shows three distinct peaks. In Figure 13, these occur just after frame 1, just before frame 3, and just after frame 4. It is believed, based on analysis of the data from all three drops, that the first two peaks are typical of the nonlinear force-deflection characteristics of the toroid at large deformations. The momentary reduction in acceleration after the first peak probably occurs when the convex surface of the toroid is pushed through to present a concave surface over the impact area. The second, larger peak occurs as the crushing continues and this concave surface, now stiffer, is enlarged.

Figure 17 shows the time integral of the cask acceleration, computed as a forward sum over the digitized time history of Figure 15. The difference between initial and final values of the integral indicates the net velocity change. This calculation provides a check on the accuracy of the acceleration signal chain. The indicated velocity change must equal or exceed the initial impact velocity of 527 inches/second. The value of 645 inches/second indicated in Figure 17 is consistent with the observed rebound height.

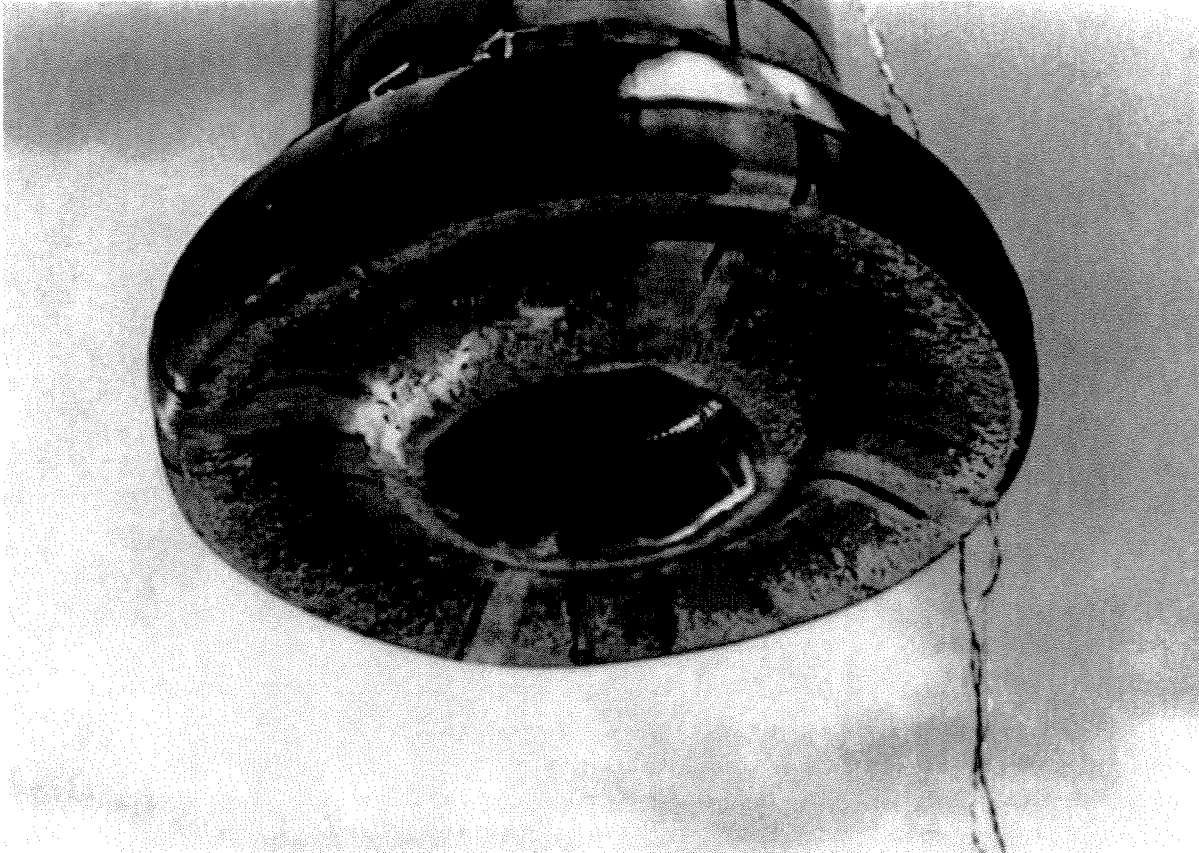


Figure 16. Toroid deformation caused by head-on drop

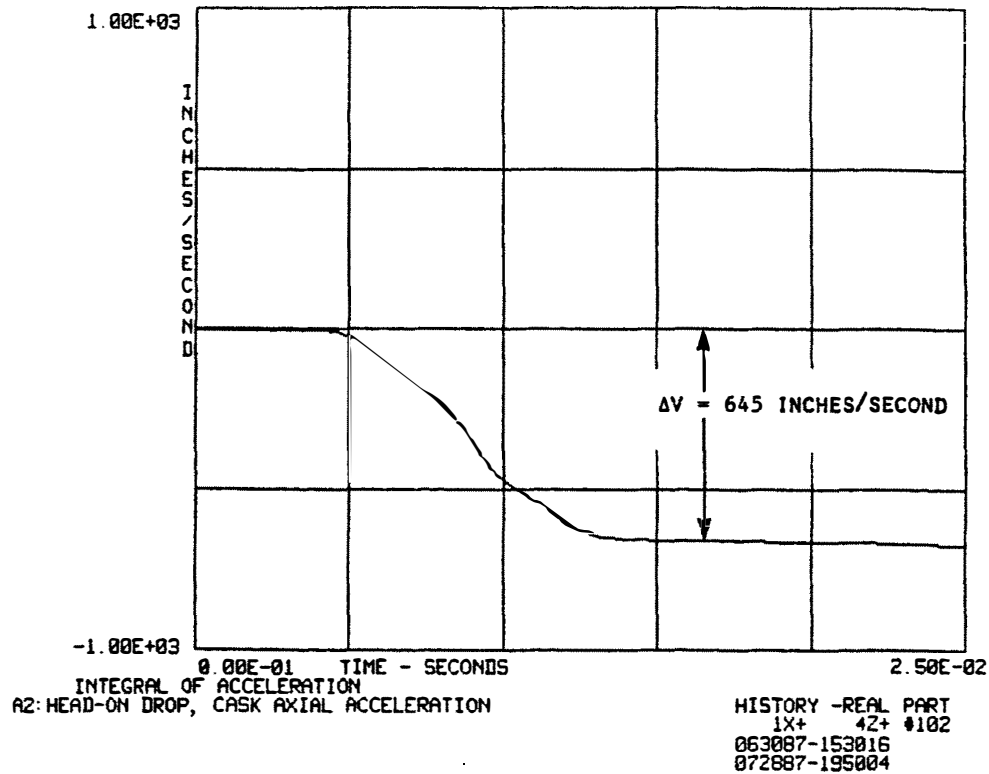


Figure 17. Time integral of cask vertical acceleration, head-on drop

6.1.2 Pressure-Sensing Film

Figure 18 shows the pressure sensing film after the head-on drop. The large rectangular piece, removed from the lateral sides of the cask, shows that significant pressure was applied in only a few small areas. The circular piece, removed from the cover plate on the lid end of the cask, shows an essentially axisymmetric pressure distribution. Most of the load was taken by a one-inch-wide band around the edge where the raised lip bears against the cover plate. This could occur only after the honeycomb cushion bottomed; until that point the cover plate and cushion would serve to distribute the load evenly. The film color near the rim indicates a peak pressure in excess of 3500 psi, consistent with the measured acceleration and weight of the cask.

The film color in the circular area inside the band is not quite uniform. Circular striations are visible, caused by tooling marks on the plate. This is not a defect of the film. It simply indicates the difficulty of producing a truly uniform pressure over the contact area between two hard surfaces.

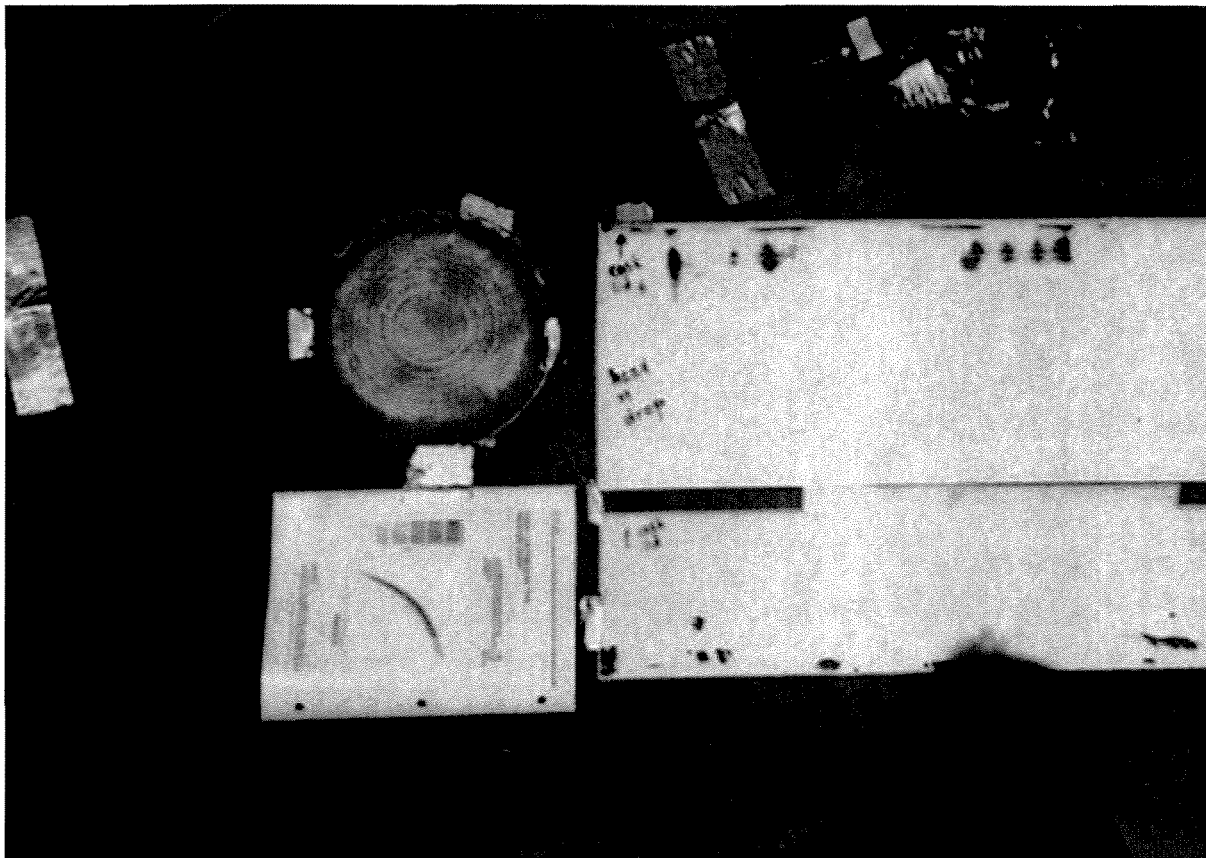


Figure 18. Pressure-sensing film from head-on drop

6.1.3 Cask and Overpack Deformation Measurements

Micrometer measurements were made of the cask diameter at a number of axial and azimuthal stations before and after the head-on drop. No change was found; no measurable plastic deformation of the cask had occurred.

Table 3 shows measurements of the deformed top toroid using the apparatus of Figure 10. Numbering of the dial gages is shown in Figure 19. Measurements of the toroid indicated that damage to it was localized to the impact area and was essentially axisymmetric.

The entire set of measurements made before and after the head-on drop is quite extensive and is documented in General Electric Inspection Report No. 6431, dated June 11, 1987. Data given here is excerpted from that report.

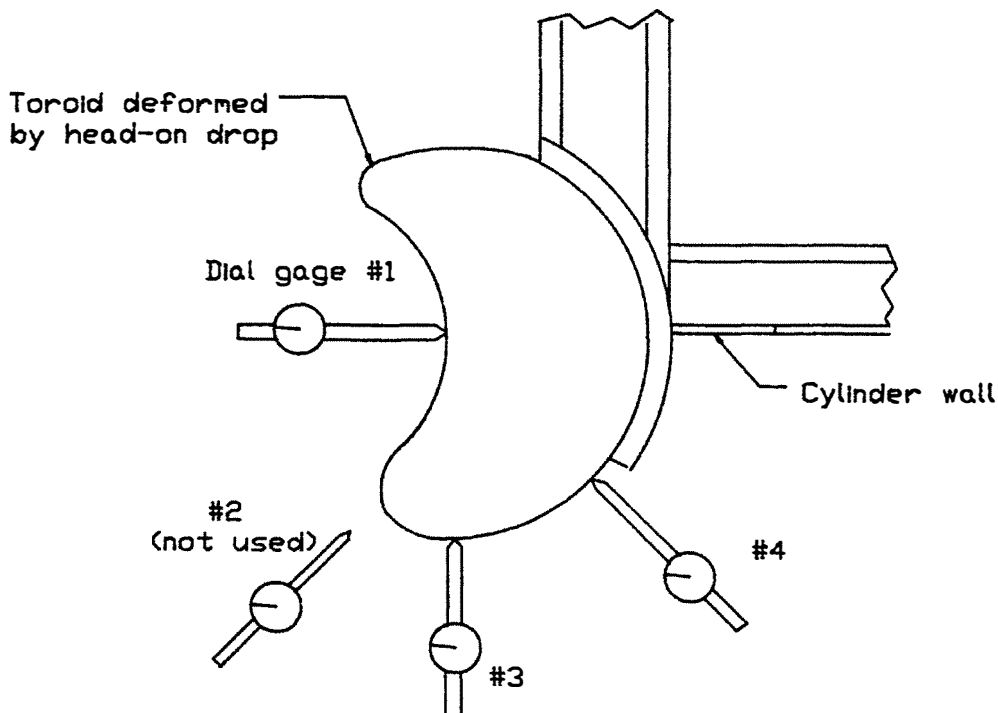


Figure 19. Gage numbering for inspection of overpack top toroid

6.1 Head-On Drop

27

Table 3. Deformation of top toroid due to head-on drop

| Gauge Azimuth (Degrees) | 1 | 2* | 3 | 4 |
|----------------------------|-------|----|--------|--------|
| 0 | 2.115 | | -0.033 | -0.001 |
| 90 | 2.009 | | -0.018 | 0.007 |
| 180 | 2.393 | | -0.063 | -0.020 |
| 270 | 2.501 | | -0.063 | 0.002 |

*not used - deformation pattern did not produce meaningful readings
(see Figure 19)

All reading in inches, positive values indicate inward deformation

6.2 Side Drop

An unexpected failure of the overpack occurred during the side drop. The bolted joint between the overpack top and base failed completely, shearing off all ten bolts and allowing the base to separate from the package. The cable carrying signals from the sensors inside the cask (routed through a hole in the overpack base) was broken almost instantaneously. As the two weldments separated, the cable connector was also pulled apart, causing loss of signal from the remaining accelerometers outside the overpack.

The causes of the overpack joint failure as well as its requalification will be discussed in a separate report.² The remainder of this subsection presents the data from the side drop test. The data suggests that, in spite of the failure, the acceleration record extends through the instant at which the peak value occurred.

6.2.1 Acceleration Data and High-Speed Photography

Figure 20 shows the time history of vertical acceleration as measured by the radial accelerometer inside the cask and the tangential accelerometer on the overpack. The photographs in Figure 21, taken at intervals of 2.13 milliseconds, show the critical time period between initial impact and loss of signal.

The high-speed films revealed that the package rotated slightly as it fell to strike the pad, top end first, with its axis inclined 10 degrees from the horizontal. This was probably caused either by a slight swinging of the package at the instant of release or a failure of the magnet to release uniformly over its entire surface. Implications of the contact angle for a side drop are considered in a separate report.³

Figures 20 and 21 contain much valuable information in spite of the fact that the instrumentation cable from the cask sensors was destroyed 11 milliseconds after the initial impact. Indicated on Figure 20 is the time interval during which crushing of the top toroid occurred. Following the initial impact at frame 0, the acceleration pattern shows a double peak, believed to be characteristic of the snap-through behavior of the toroid. The toroid on the overpack base strikes approximately 8 milliseconds later, after the crushing of the top toroid is complete. The second impact causes the vertical acceleration to again rise rapidly. The bolts break about 2 milliseconds later, releasing the base weldment which rotates outward and is propelled away from the package. Figure 22 shows a still photograph taken just after impact, with the base weldment in midair. Figure 23 shows the aftermath of the side drop.

²Ibid.

³Ibid.

6.2 Side Drop

29

Based on the acceleration traces and the high-speed films, the signal cable is believed to have faulted 11 milliseconds after impact, between frames +5 and +6 of the film. This coincides approximately with the point in time when the joint flange of the overpack top struck the pad. The signal went low, indicating the cable had shorted. It later went high when the conductors parted completely. There is no certain way of determining the last instant at which the acceleration signal is accurate. The point indicated on Figure 20 is based on inspection of the signal itself and the high-speed film.

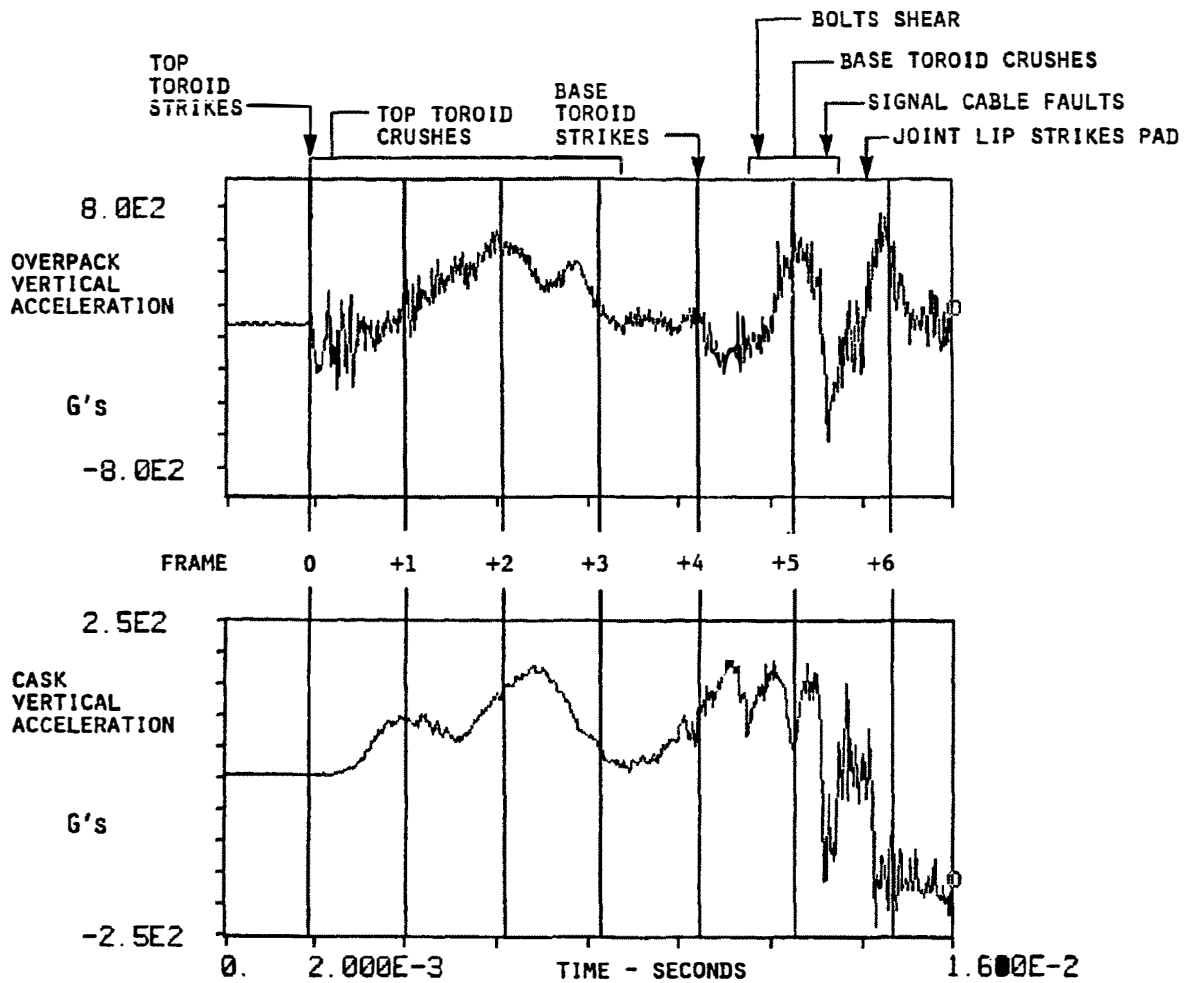


Figure 20. Side drop, vertical acceleration

6.2 Side Drop

31

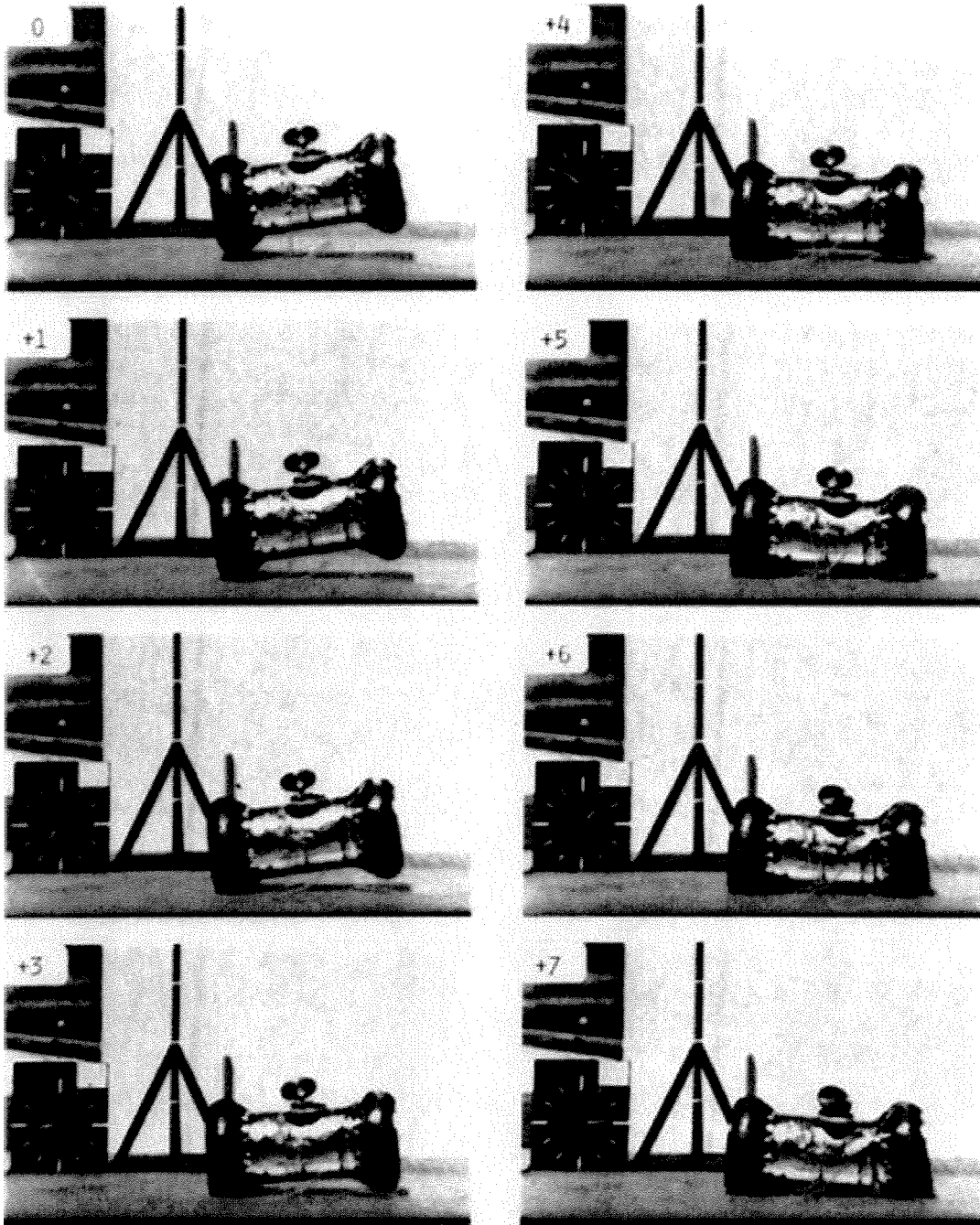


Figure 21. Side drop, frames taken at 2.13 millisecond intervals

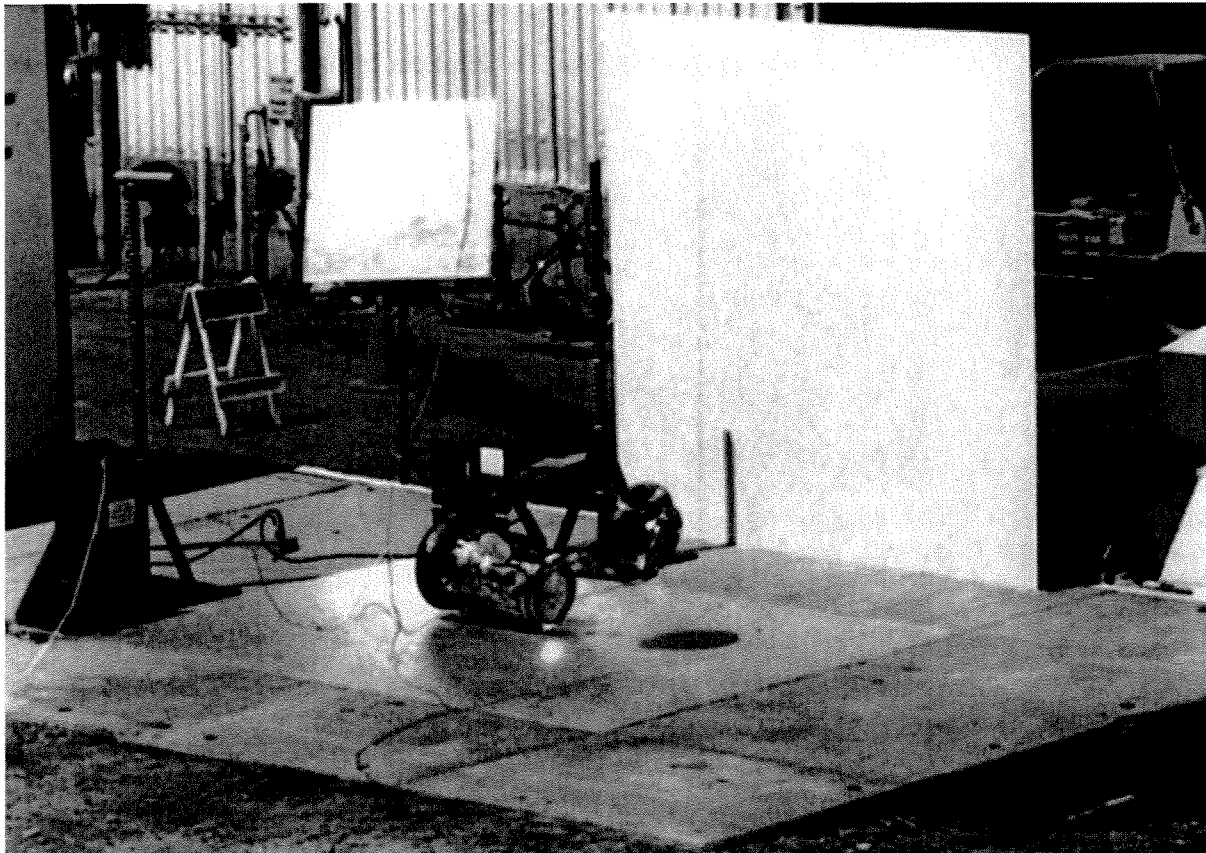


Figure 22. Overpack weldments separating after impact, side drop

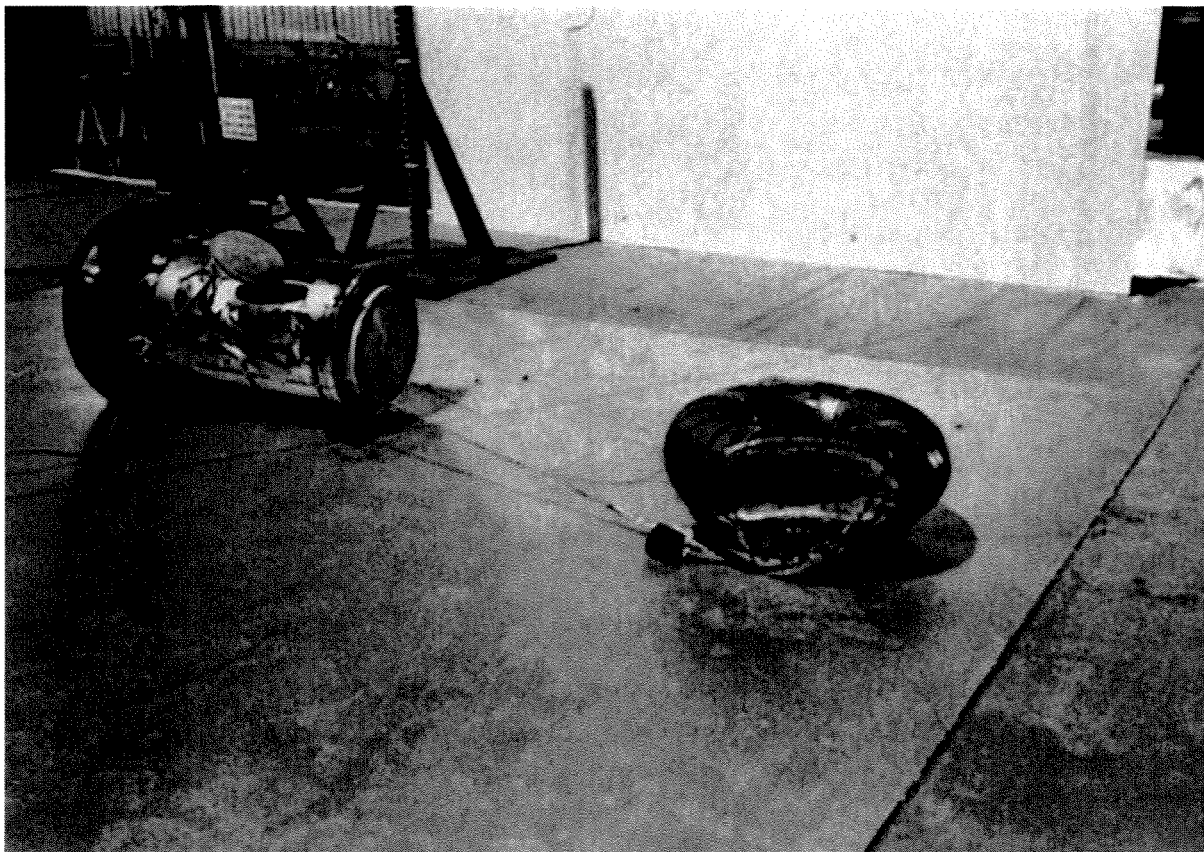


Figure 23. Package after side drop

It may be shown, however, that the important part of the impact event occurred prior to the indicated loss-of-signal point. Figure 24 shows the calculation of the net change in the cask vertical velocity between initial impact and the cable fault. The trace was zeroed from the fault point through the end of the record prior to integration. The result indicates that the cask had not come completely to rest when the signal was lost. The net velocity change up to that point was 379 inches/second. Since the impact velocity was 527 inches/second, the remaining velocity change was $527 - 379 = 148$ inches/second. This corresponds to a free drop from 28 inches, an event unlikely to damage even an unprotected cask. Stated another way, since kinetic energy is proportional to velocity squared, the percent of the initial energy remaining when the signal was lost was only $(148/527)^2 \times 100 = 7.9\%$ of the initial value. In effect, the impact event was essentially over before the signal was lost.

Likewise, since the toroids were extensively deformed by the side drop (Figure 23) and this deformation could only have occurred while the sensing channel was still intact, the observed maximum acceleration of 185 G's is a reasonable estimate of the maximum that would have occurred if the bolted joint had not failed.

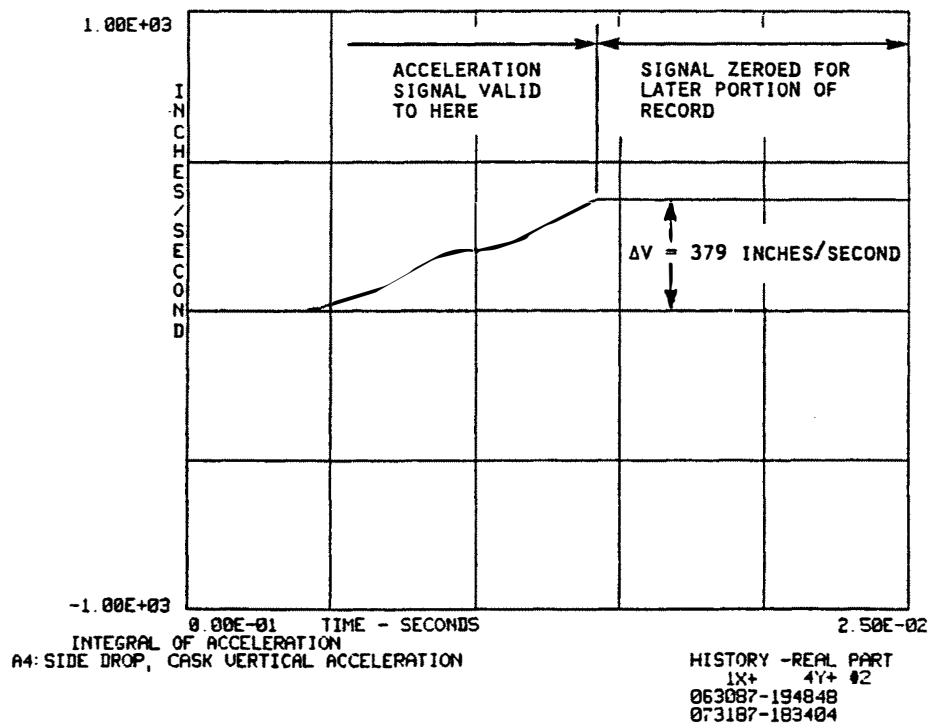


Figure 24. Time integral of cask vertical acceleration prior to cable fault, side drop

6.2.2 Pressure- Sensing Film

Figure 25 shows the pressure-sensing film after the side drop. The film was applied only to the lateral sides of the cask. It shows that the load tended to concentrate towards the ends of the cask, except for two narrow lines parallel to the cask axis. These localized areas of high pressure were caused by the crush tubes between the double walls of the overpack cylinder.

6.2.3 Cask and Overpack Deformation Measurements

Micrometer measurements were made of the cask diameter at a number of axial and azimuthal stations before and after the side drop. No change was found; no measurable plastic deformation of the cask had occurred.

Extensive measurements of the overpack before and after the side drop are given in General Electric Inspection Report No. 6430, dated June 12, 1987. The radial indentation of the top toroid (which struck the ground first) was found to be 3.18 inches in depth. Damage to the base toroid was slightly greater.

6.3 CG-Over-Corner Drop

For the final drop, the cask was oriented as shown in Figure 26. The orientation, with the cask axis 22 degrees off the vertical, positioned the package center-of-gravity directly over the impact point on the top toroid. This was verified by balancing the cask on the contact point. The angle proved to be slightly different from the calculated value of 29 degrees used in the design of the mounting block for the cask oblique accelerometer. The resulting 7 degree misalignment of the sensing axis was not considered significant since it reduced the acceleration signal by less than 1%.

The drop was performed without incident to conclude the test series.

6.3.1 Acceleration Data and High-Speed Photography

Figures 27 and 28 illustrate the impact event. The lower trace in Figure 27 shows the time history of cask acceleration in the vertical direction as sensed by the cask oblique accelerometer. The upper trace is from the overpack axial accelerometer and gives the vertical acceleration attenuated by about 7% due to the 22 degree misalignment of the sensor axis from vertical. The photographs in Figure 27 were taken at intervals of 2.16 milliseconds.

Upon striking the pad, the package rebounded in a direction roughly parallel to its axis while rotating counterclockwise (as seen in the view of Figure 28) in

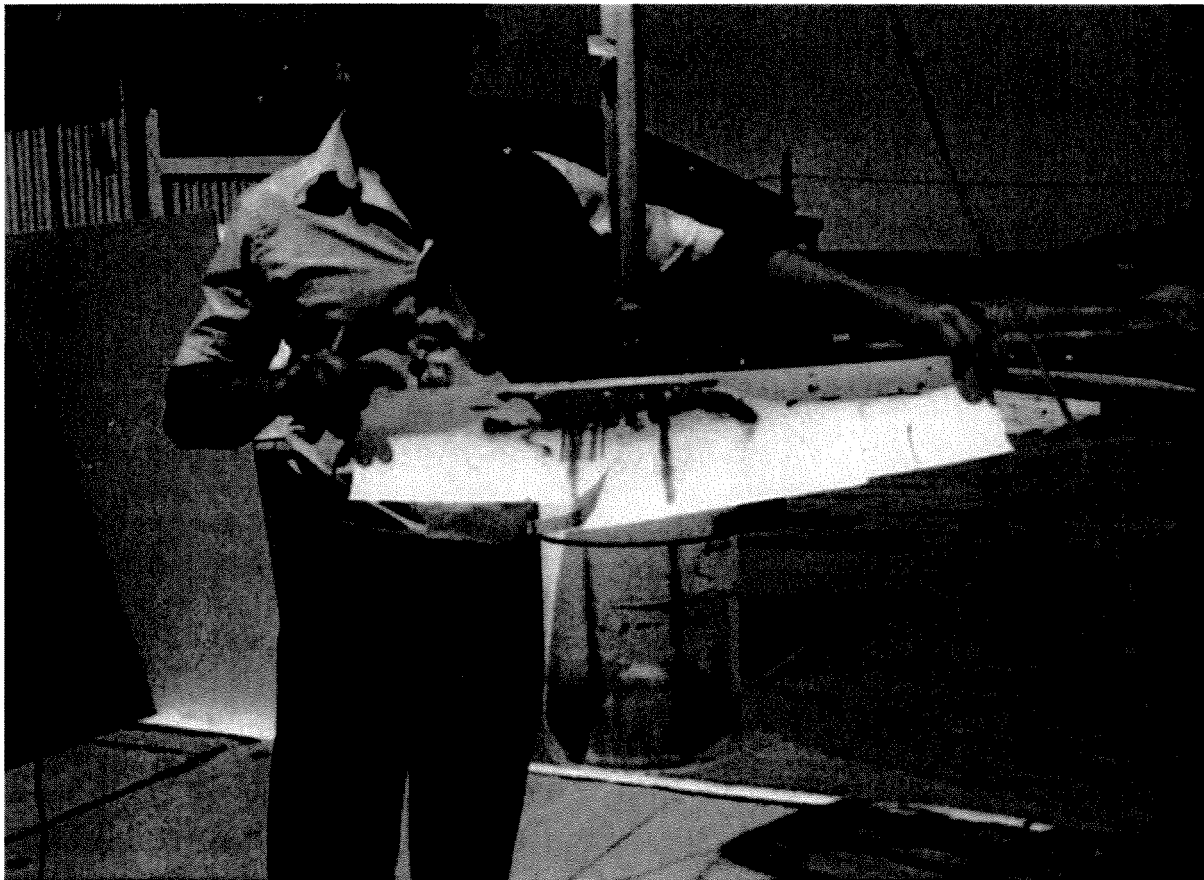


Figure 25. Pressure-sensing film from side drop

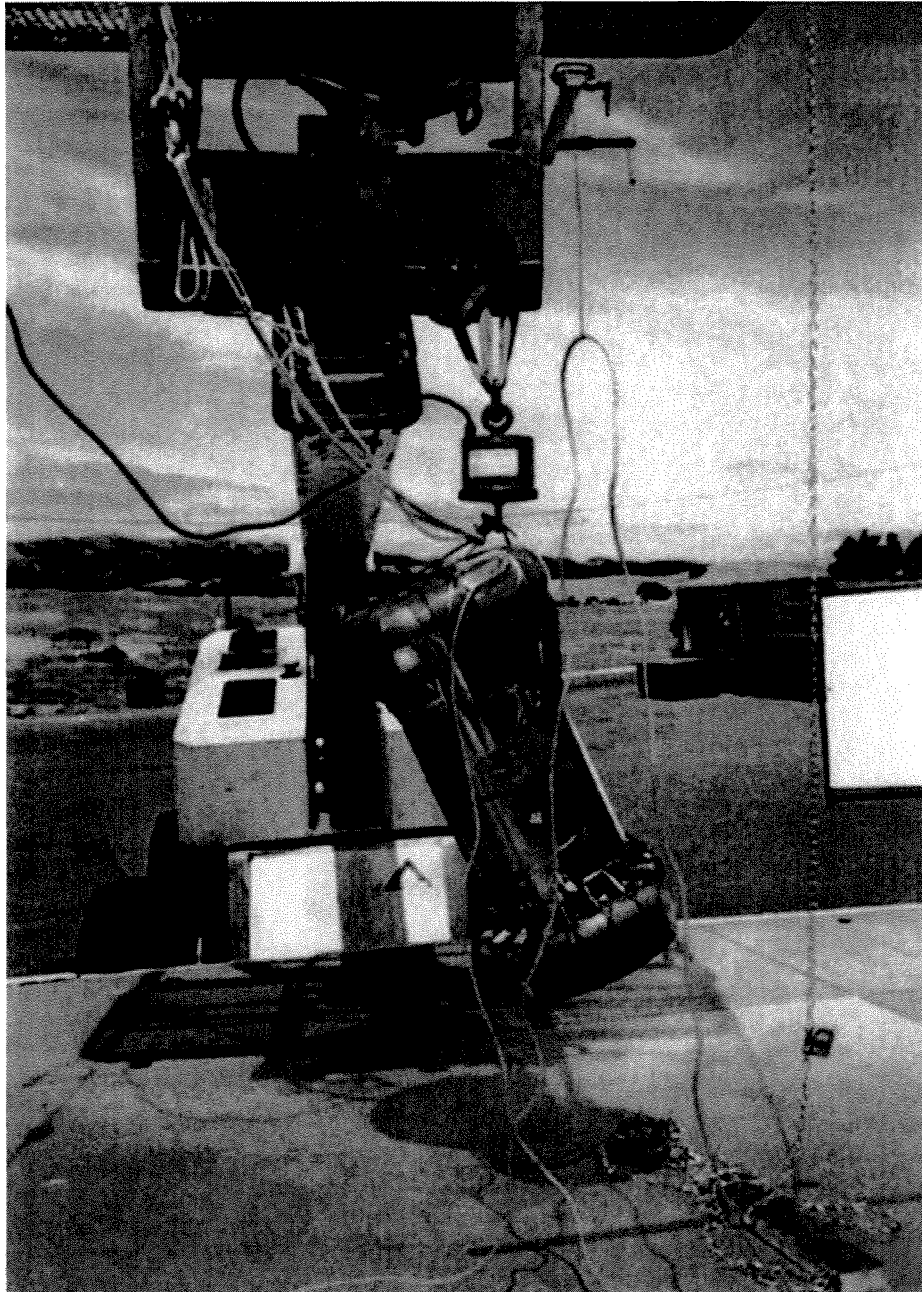


Figure 26. Rigging for CG-over-corner drop

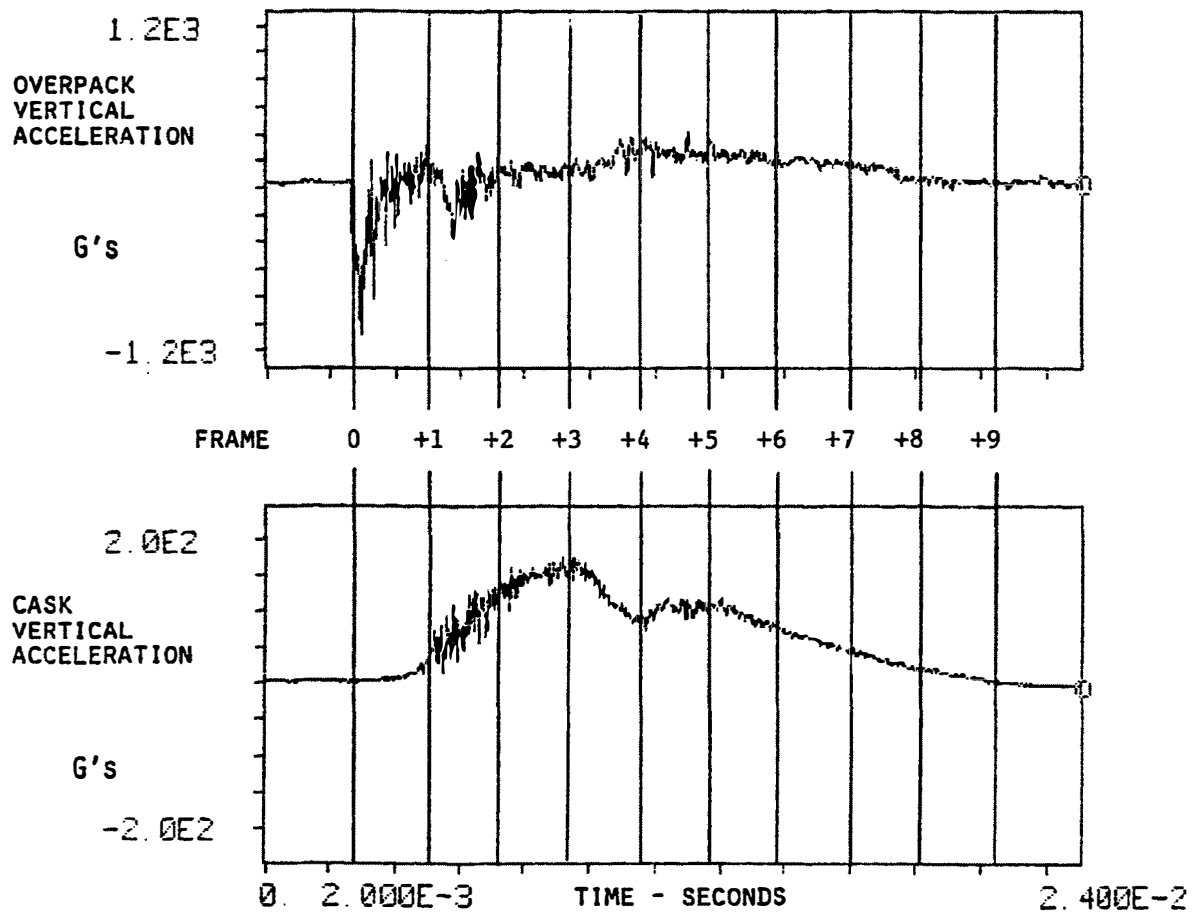


Figure 27. CG-over-corner drop, vertical acceleration

6.3 CG-Over-Corner Drop

39

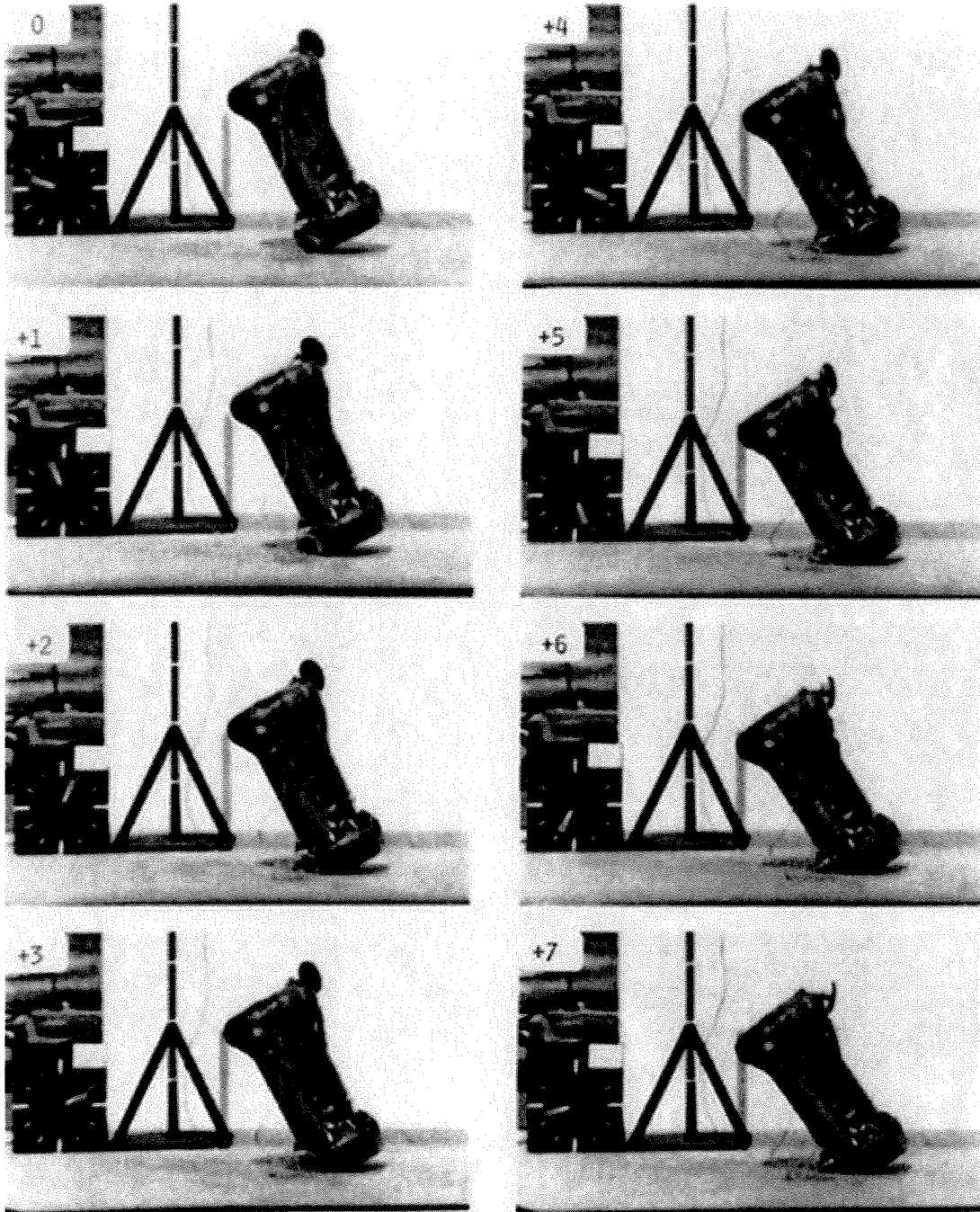


Figure 28. CG-over-corner drop, frames taken at 2.16 millisecond intervals

midair through about 250 degrees before coming to rest. The maximum rebound height and rotational velocity, determined from the high-speed films, were 4.7 inches and 15.1 radians/second. The rotational velocity produced by the impact does not mean that the CG was not aligned over the impact point. Rather, it simply implies that the deformation pattern of the toroid produced a force whose resultant did not pass through the CG. Figure 29 shows the deformation of the top toroid.

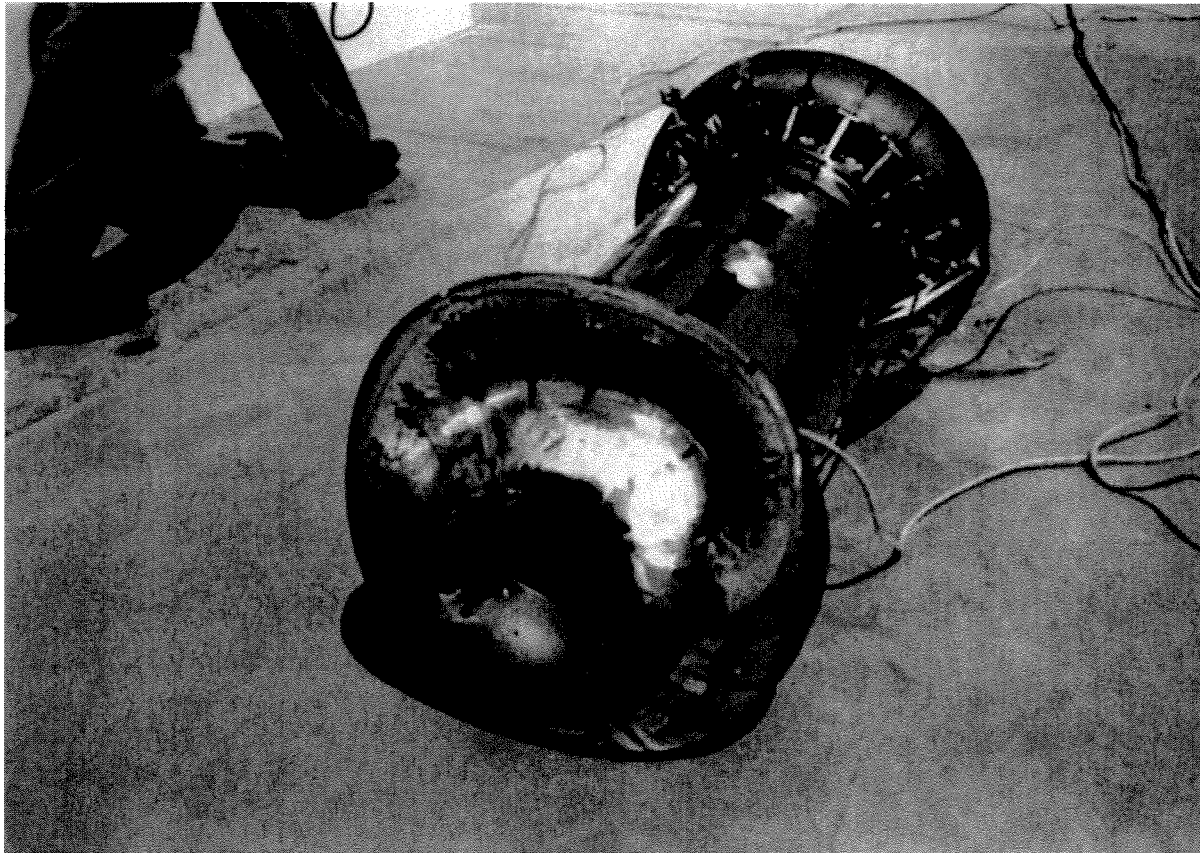


Figure 29. Deformation of overpack produced by CG-over-corner drop

6.3 CG-Over-Corner Drop

41

The cask acceleration transient, lasting about 18 milliseconds, was substantially longer than for either the head-on or side drop. This is related to the fact that a toroid struck on a corner produces a softer "cushion" than when struck head-on or from the side. The greater compliance produces a longer acceleration transient with a lower peak value; maximum cask acceleration was the lowest of the three tests at 156 G's. The transient showed the characteristic double peak.

Determination of the net velocity change was straightforward and is shown in Figure 30. The value of 548 inches/second, slightly greater than the impact velocity, is reasonable based on the small value of the rebound height.

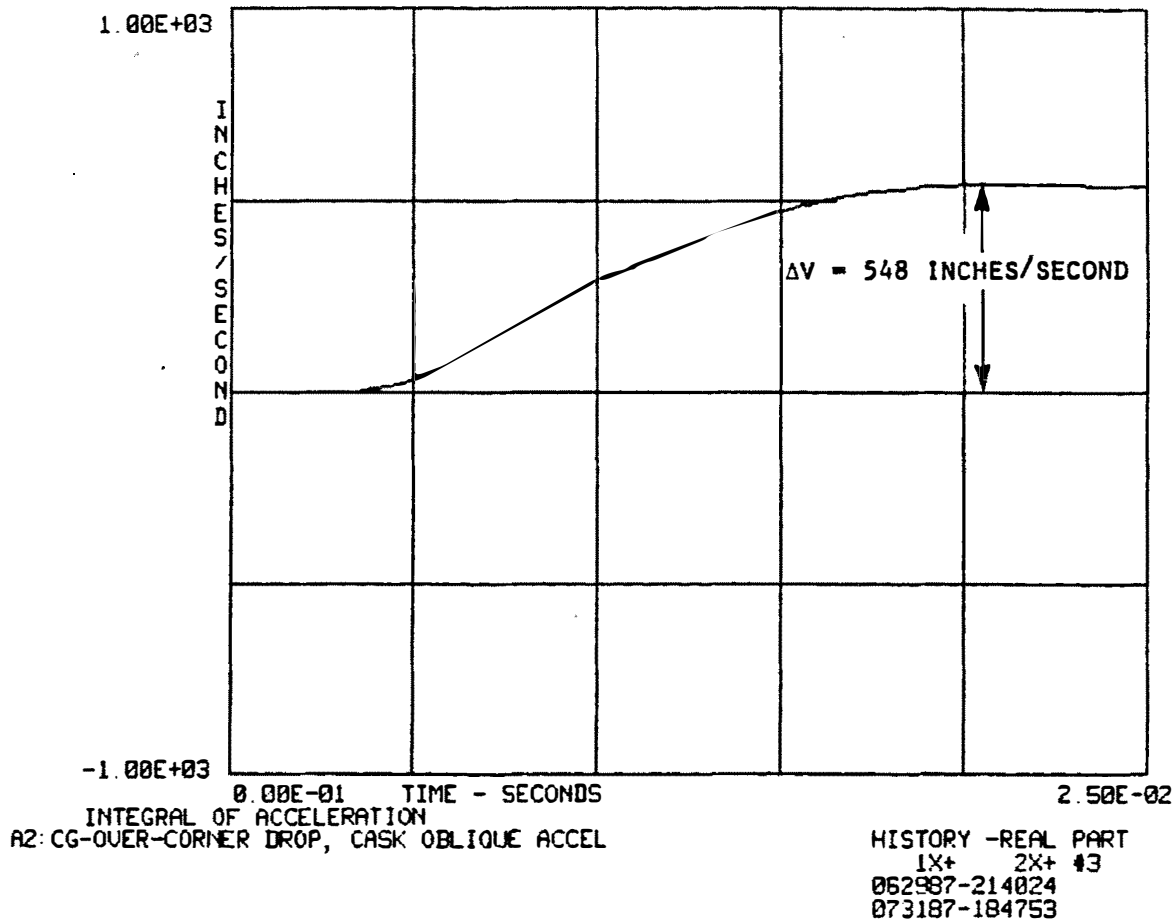


Figure 30. Time integral of cask vertical acceleration, CG-over-corner drop

6.3.2 Pressure-Sensing Film

Figure 31 shows the pressure sensitive film, still on the cask, following the CG-over-corner drop. The pressure over the end cover plate was fairly uniform, consistent with the fact that the honeycomb cushion did not bottom. Pressure on the lateral sides of the cask was confined to circumferential bands near the ends, particularly the lid end which was oriented downwards at impact. The pressure band extends essentially all the way around the cask although the highest pressure was seen on the downward side, as would be expected. Loading of the other side probably occurred on the second impact.

6.3.3 Cask and Overpack Deformation Measurements

Micrometer measurements were made of the cask diameter at a number of axial and azimuthal stations before and after the side drop. No change was found; no measurable plastic deformation of the cask had occurred.

Extensive measurements of the overpack before and after the CG-over-corner drop are given in General Electric Inspection Report No. 6432, dated June 18, 1987. Deformation, as shown in Figure 29, was significant, but was confined to the region around the impact. Maximum depth of the indenting, measured parallel to the package axis along a minor diameter of the toroid, was approximately 5.3 inches.



Figure 31. Pressure-sensing film from CG-over-corner drop

7. Summary and Conclusions

Drop tests in three orientations were performed with no measurable deformation or other damage to the cask. The head-on and CG-over-corner drops were successfully completed with no unexpected results. Complete acceleration and internal load distribution data were obtained for use in design verification.

An unexpected failure of the overpack bolted joint occurred during the side drop. The causes of the failure and the requalification of the joint will be covered in a separate report. The structural failure also caused the loss of some acceleration data. Nonetheless, a valid trace was obtained for the most important part of the impact event, including the portion during which plastic deformation of the overpack occurred and, probably containing the point of maximum acceleration.

Subject to the above uncertainty in the side drop test, the maximum vertical accelerations recorded by the sensors inside the cask for the head-on, side, and CG-over-corner drops were 408, 185, and 156 G's respectively.

2.12.6. Fabrication Stresses

The following sections provide a detailed evaluation of the stresses that occur during the fabrication process of lead pour and also service at extreme cold temperatures between the inner stainless steel shell, lead shell, and outer stainless steel shell of the Model 2000 cask body.

2.12.6.1. Fabrication Stresses Due to Lead Pour

During the fabrication process, liquid lead is poured into the annulus between the inner and outer stainless steel shells of the Model 2000 cask at a temperature of ~620°F with the ambient temperature at ~70°F. Before coming into contact with the liquid lead, the stainless steel shells are at the ambient temperature. Once the liquid lead comes into contact with the stainless steel shells, the temperature difference between the two materials increases the energy in the stainless steel causing the material to expand. The dimensions of the inner and outer shells at 70°F are as follows in Table 2.12.6-1.

Table 2.12.6-1. Dimensions of Stainless Steel Shells

| Parameter | Variable | Input | Units |
|-------------------------------|----------|-------|-------|
| Outer Diameter of Inner Shell | d_o | 28.5 | in |
| Inner Diameter of Inner Shell | d_i | 26.5 | in |
| Mean Radius Inner Shell | R_i | 13.75 | in |
| Outer Diameter of Outer Shell | D_o | 38.5 | in |
| Inner Diameter of Outer Shell | D_i | 36.5 | in |
| Mean Radius Outer Shell | R_o | 18.75 | in |
| Thickness of Inner Shell | t_i | 1 | in |
| Thickness of Outer Shell | t_o | 1 | in |

2.12.6.1.1. Thermal Expansion of Stainless Steel Shells

When the inner and outer shells are subjected to the lead temperature of 620°F, the mean radius and thickness of each shell increases and is calculated with the following equations:

$$R' = R (1 + \alpha \Delta T)$$

where

$$R = \text{Mean Radius of Shell}$$

$$\alpha = \text{Coefficient of Thermal Expansion For } 304 \text{ Stainless Steel at } 620^\circ\text{F} \text{ (} 9.92\text{E-}06 \text{ in/in/}^\circ\text{F)}$$

$$\Delta T = \text{Temperature difference (} 620^\circ\text{F} - 70^\circ\text{F} = 550^\circ\text{F)}$$

and

$$t' = t (1 + \alpha \Delta T)$$

where

$$t = \text{Thickness of Shell}$$

Using the above equations, the shell growth of the inner shell is:

$$\begin{aligned} R_i' &= 13.75[1 + 9.92\text{E-}06 \times 550] \\ &= 13.825 \text{ in} \\ t_i' &= 1[1 + 9.92\text{E-}06 \times 550] \\ &= 1.005 \text{ in} \end{aligned}$$

Further, the shell growth of the outer shell is:

$$\begin{aligned} R_o' &= 18.75[1 + 9.92\text{E-}06 \times 550] \\ &= 18.852 \text{ in} \\ t_o' &= 1[1 + 9.92\text{E-}06 \times 550] \\ &= 1.005 \text{ in} \end{aligned}$$

Accordingly, the dimensions at 620°F for the inner and outer radius of each shell can be calculated using the equations below. For the inner stainless steel shell:

$$\begin{aligned} r_{ii}' &= r_{ii}(1 + \alpha \Delta T) \\ &= 13.25[1 + 9.92\text{E-}06 \times 550] \\ &= 13.322 \text{ in} \end{aligned}$$

where

$$\begin{aligned} r_{ii}' &= \text{Inside radius of inner shell at 620°F} \\ r_{ii} &= \text{Inside radius of inner shell at 70°F} \end{aligned}$$

and

$$\begin{aligned} r_{oi}' &= r_{oi}(1 + \alpha \Delta T) \\ &= 14.25[1 + 9.92\text{E-}06 \times 550] \\ &= 14.328 \text{ in} \end{aligned}$$

where

$$\begin{aligned} r_{oi}' &= \text{Outside radius of inner shell at 620°F} \\ r_{oi} &= \text{Outside radius of inner shell at 70°F} \end{aligned}$$

For the outer stainless steel shell:

$$\begin{aligned} r_{io}' &= r_{io}(1 + \alpha \Delta T) \\ &= 18.251[1 + 9.92\text{E-}06 \times 550] \\ &= 18.350 \text{ in} \end{aligned}$$

where

$$\begin{aligned} r_{io}' &= \text{Inside radius of outer shell at 620°F} \\ r_{io} &= \text{Inside radius of outer shell at 70°F} \end{aligned}$$

and

$$\begin{aligned} r_{oo}' &= r_{oo}(1 + \alpha\Delta T) \\ &= 19.25[1 + 9.92E-06 \times 550] \\ &= 19.355 \text{ in} \end{aligned}$$

where

$$\begin{aligned} r_{oo}' &= \text{Outside radius of outer shell at } 620^{\circ}\text{F} \\ r_{oo} &= \text{Outside radius of outer shell at } 70^{\circ}\text{F} \end{aligned}$$

2.12.6.1.2. Hydrostatic Pressure

In order to determine the stresses that develop in the stainless steel shells, the static pressure that develops due to the column of lead is first calculated as follows,

$$q = \rho_{\text{lead}} \times h_{\text{lead}}$$

where

$$\begin{aligned} q &= \text{Static Pressure} \\ \rho_{\text{lead}} &= \text{Density of lead (0.4097 lbf/in}^3\text{)} \\ h_{\text{lead}} &= \text{Height of lead column (56 in)} \end{aligned}$$

NOTE: Value for the density of lead is interpolated to just below the melting point (620°F). The solid lead value is conservative because the density for liquid lead at 620°F is less and would result in a lower hydrostatic pressure and therefore lower membrane stresses.

Therefore the hydrostatic pressure is:

$$\begin{aligned} q &= 0.4097 \times 56 \\ q &= 22.943 \text{ psi} \end{aligned}$$

This hydrostatic pressure increases the outer shell radius and decreases the inner shell radius as is determined with the following equations. Decrease in inner shell mean radius due to static (Reference 2-19, Table 13.8, Page 608):

$$\begin{aligned} \Delta R_i' &= \frac{-q \times (R_i')^2}{E \times t_i'} \\ &= \frac{-22.943 \times (13.825)^2}{25.2E06 \times 1.005} \\ &= -0.000173 \text{ in} \end{aligned}$$

where

$$\begin{aligned} E &= \text{Modulus of Elasticity} \\ &\text{of 304 Stainless Steel at } 620^{\circ}\text{F (25.2E06 psi)} \end{aligned}$$

Increase in outer shell mean radius due to static pressure (Reference 2-19, Table 13.8, Page 608):

$$\begin{aligned} \Delta R_o' &= \frac{q \times (R_o')^2}{E \times t_i'} \\ &= \frac{22.943 \times (18.852)^2}{25.2E06 \times 1.005} \\ &= 0.000322 \text{ in} \end{aligned}$$

2.12.6.1.3. Membrane Stresses

he lead column creates a radial pressure on the inner and outer shells. The stresses due to the maximum external pressure on the inner shell are (Reference 2-19, Table 13.8, Page 608):

$$\sigma_1 = 0 \text{ psi}$$

where

$$\sigma_1 = \text{Meridional Stress}$$

$$\begin{aligned}\sigma_2 &= \frac{-q \times r'_{oi}}{t'_i} \\ &= \frac{-22.943 \times 14.328}{1.005} \\ &= -326.941 \text{ psi}\end{aligned}$$

where

$$\sigma_2 = \text{Hoop Stress}$$

$$\sigma_3 = -22.943 \text{ psi}$$

where

$$\sigma_3 = \text{Radial Stress}$$

It should be noticed that the sign for the hoop stress and radial stress is negative. This is because the direction of the static pressure is acting inward instead of outward. The stresses due to the maximum internal pressure on the outer shell are (Reference 2-19, Table 13.8, Page 608) :

$$\begin{aligned}\sigma_1 &= 0 \text{ psi} \\ \sigma_2 &= \frac{q \times r'_{io}}{t'_o} \\ &= \frac{22.943 \times 18.350}{1.005} \\ &= 418.713 \text{ psi} \\ \sigma_3 &= 22.943 \text{ psi}\end{aligned}$$

The allowable stress is the yield stress for the stainless steel, which is equal to 18,240 psi at 620°F. Comparing this allowable stress with the meridional, hoop and radial stresses for the inner and outer shells shows that they are all below the allowable stress and thus acceptable.

2.12.6.1.4. Buckling

Additional analysis is performed to see if the inner shell will buckle due to the external pressure (Reference 2-33, Equation 188, Page 220):

$$\begin{aligned}P_{cr} &= \frac{(h/R'_i) \times \sigma_{y.p.}}{1 + 4(\sigma_{y.p.}/E) \times (R'^2_i/h^2)} \\ &= \frac{(1.005/13.825) \times 18240}{1 + 4(18240/25.2E06) \times (13.825^2/1.005^2)} \\ &= 857.28 \text{ psi}\end{aligned}$$

where

$$\begin{aligned} E &= \text{Modulus of Elasticity} \\ &\text{of 304 Stainless Steel at 620°F (25.2E06 psi)} \\ P_c &= \text{Critical Pressure} \\ h &= \text{Thickness of Wall of } [[\quad]] \\ \sigma_{y.p.} &= \text{Yield Point in Compression at 620°F} \end{aligned}$$

As the analysis shows, the critical pressure is larger than the pressure on the inner shell. Therefore, the liquid lead has a negligible effect on the inner and outer stainless steel shells.

2.12.6.2. Stresses Due to Lead Solidification and Lead Shrinkage

For this analysis, the dimensions of the unloaded solid lead shell are used as a reference point for interference fits. To do this, the loads due to the hydrostatic pressure are removed. The dimension of the inner and outer shells at 620°F are given in Table 2.12.6-2.

Table 2.12.6-2. Dimensions of Inner and Outer Shell at 620°F

| Input Parameter | Variable | Input | Units |
|--------------------------------------|-----------|--------|-------|
| Inner Radius of Inner Shell at 620°F | r_{ii}' | 13.322 | in |
| Outer Radius of Inner Shell at 620°F | r_{oi}' | 14.328 | in |
| Inner Radius of Outer Shell at 620°F | r_{io}' | 18.350 | in |
| Outer Radius of Outer Shell at 620°F | r_{oo}' | 19.355 | in |

The dimensions given in Table 2.12.6-2 are used to obtain the loaded lead dimensions of the lead shell. The inside radius of the lead shell is set equal to the outside radius of the inner steel shell and the outer radius of the lead shell is set equal to the inside radius of the outer steel shell as follows:

$$R_{i\text{-lead}} = 14.328 \text{ in}$$

$$R_{o\text{-lead}} = 18.350 \text{ in}$$

2.12.6.2.1. Unloaded Lead Dimensions

To obtain the unloaded lead dimensions, a negative load is applied to the loaded dimensions. To do this, the internal and external pressures that are acting on the lead shell are first determined. For the internal pressure acting on the inner surface of the lead shell, the change in the outer radius of the lead (Δa) is (Reference 2-19, Table 13.5, Page 696):

$$\begin{aligned} \Delta a &= \frac{qab^2(2-\nu)}{E(a^2-b^2)} \\ &= \frac{22.943 \times 18.350 \times 14.328^2(2-0.4)}{1.49E06 \times (18.350^2 - 14.328^2)} \\ &= 0.000706 \text{ in} \end{aligned}$$

where

$$a = \text{Outside Radius of Lead Shell}$$

NEDO-33866 Revision 0
Non-Proprietary Information – Class I (Public)

| | | |
|-------|---|-------------------------------------------------------|
| b | = | Inside Radius of Lead Shell |
| ν | = | Poisson's Ratio for lead at 620°F (0.4) |
| E | = | Modulus of Elasticity for Lead at 620°F (1.49E06 psi) |

NOTE: Value for poisson's ratio and modulus of elasticity are that of solid lead at just below the melting point of 620°F.

The change in the inside radius of the lead (Δb) is (Reference 2-19, Table 13.5, Page 696):

$$\begin{aligned}\Delta b &= qb \frac{a^2(1+\nu)+b^2(1-2\nu)}{E(a^2-b^2)} \\ &= 22.943 \times 14.328 \frac{18.350^2(1+0.4)+14.328^2(1-2 \times 0.4)}{1.49E06 \times (18.350^2 - 14.328^2)} \\ &= 0.000860 \text{ in}\end{aligned}$$

For the external pressure acting on the outer surface of the lead shell, the change in outer radius of the lead is:

$$\begin{aligned}\Delta a &= -qa \frac{a^2(1-2\nu)+b^2(1+\nu)}{E(a^2-b^2)} \\ &= -22.943 \times 18.350 \frac{18.350^2(1-2 \times 0.4)+14.328^2(1+0.4)}{1.49E06 \times (18.350^2 - 14.328^2)} \\ &= -0.000763 \text{ in}\end{aligned}$$

The change in the inside radius of the lead due to the external pressure is:

$$\begin{aligned}\Delta b &= \frac{-qba^2(2-\nu)}{E(a^2-b^2)} \\ &= \frac{-22.943 \times 14.328 \times 18.350^2(2-0.4)}{1.49E06 \times (18.350^2 - 14.328^2)} \\ &= -0.000904 \text{ in}\end{aligned}$$

Now that the loaded dimensions have been determined, the unloaded dimensions are determined by removing the loads. Removing the internal pressure first:

$$\begin{aligned}\Delta a &= -0.000706 \text{ in} \\ \Delta b &= -0.000860 \text{ in}\end{aligned}$$

Followed by removing the external pressure:

$$\begin{aligned}\Delta a &= 0.000763 \text{ in} \\ \Delta b &= 0.000904 \text{ in}\end{aligned}$$

Therefore the total change in the outer and inner radius of the lead with no load is:

$$\begin{aligned}\Delta a_{\text{total}} &= 0.000763 - 0.000706 \\ &= 0.000057 \text{ in} \\ \Delta b_{\text{total}} &= 0.000904 - 0.000860 \\ &= 0.000044 \text{ in}\end{aligned}$$

The dimensions of the lead at 620°F with no load is:

$$\begin{aligned} R_{i\text{-lead}} &= 14.3277480 + 0.000044 \\ &= 14.327792 \text{ in} \\ R_{o\text{-lead}} &= 18.3495720 + 0.000057 \\ &= 18.3496285 \text{ in} \end{aligned}$$

The results show that the difference between the loaded and unloaded dimensions is negligible. Using the unloaded dimensions, a check for interference is completed.

2.12.6.2.2. Interference

At 70°F, stresses will accumulate between the lead and the inner stainless steel shell due to shrinkage of the materials as they cool down from the lead pour. To determine these stresses, the lead dimensions are calculated at 70°F. It is known that at 620°F the lead outer radius is 18.35 inches. Therefore, the equation shown below is used to determine the outer radius of the lead at 70°F.

$$\begin{aligned} R_{o70} &= \frac{R_{o620}}{(1+\alpha\Delta T)} \\ &= \frac{18.350}{1+24.6E-06 \times 550} \\ &= 18.105 \text{ in} \end{aligned}$$

where

$$\begin{aligned} R_{o620} &= \text{Outer Radius of Lead at 620°F} \\ R_{o70} &= \text{Outer Radius of Lead at 70°F} \\ \alpha &= \text{Coefficient of Thermal Expansion} \\ &\quad \text{for Lead at 620°F (24.6E-06 in/in/°F)} \end{aligned}$$

Accordingly, the inner radius of the lead shell at 620°F is 14.328 in and

$$\begin{aligned} R_{i70} &= \frac{R_{i620}}{1+\alpha\Delta T} \\ &= \frac{14.358}{1+24.6E-06 \times 550} \\ &= 14.137 \text{ in} \end{aligned}$$

The no-load dimensions at 70°F for all shells are displayed in Table 2.12.6-3.

Table 2.12.6-3. Dimensions of Shells at 70°F

| Parameter | | Variable | Input | Units |
|-----------|----------------------------------|-----------|--------|-------|
| 1 | Inner Radius Inner Shell at 70°F | r_{ii} | 13.25 | in |
| 2 | Outer Radius Inner Shell at 70°F | r_{oi} | 14.25 | in |
| 3 | Inner Radius Outer Shell at 70°F | r_{io} | 18.25 | in |
| 4 | Outer Radius Outer Shell at 70°F | r_{oo} | 19.25 | in |
| 5 | Inner Radius of Lead at 70°F | R_{i70} | 14.137 | in |
| 6 | Outer Radius of Lead at 70°F | R_{o70} | 18.105 | in |

The air gap between the outer shell and lead is 18.25 inches – 18.105 inches = 0.145 inches. Additionally, the interference between the inner shell and the lead is:

$$\delta = 14.25 \text{ in} - 14.137 \text{ in} = 0.113 \text{ in}$$

2.12.6.2.3. Interference Contact Pressure

Because there is interference between the inner shell and the lead, an interference contact pressure p arises between the two shells and is calculated with the following press fit equation (Reference 2-34, Equation 3-56, Page 110):

$$\delta = \frac{b_L p \left(\frac{C^2 + b_L^2}{C^2 - b_L^2} + \nu_L \right)}{E_L} + \frac{b_s p \left(\frac{b_s^2 + a^2}{b_s^2 - a^2} - \nu_s \right)}{E_s}$$

solving,

$$p = \frac{\delta}{\frac{b_L \left(\frac{C^2 + b_L^2}{C^2 - b_L^2} + \nu_L \right)}{E_L} + \frac{b_s \left(\frac{b_s^2 + a^2}{b_s^2 - a^2} - \nu_s \right)}{E_s}}$$

where

| | | |
|----------|---|--------------------------------------------------------|
| δ | = | Interference between contact surfaces |
| b_L | = | Inner radius of lead shell |
| C | = | Outer radius of lead shell |
| ν_L | = | Poisson's Ratio for lead at 70°F (0.4) |
| E_L | = | Modulus of Elasticity for lead at 70°F (2.42E06) |
| b_s | = | Outer radius of inner shell |
| ν_s | = | Poisson's Ratio for 304 stainless steel at 70°F (0.31) |
| a | = | Inner radius of inner shell |
| E_s | = | Modulus of Elasticity for 304 stainless steel at 70°F |

Substituting values:

$$p = \frac{0.113}{\frac{14.137 \left(\frac{18.105^2 + 14.137^2}{18.105^2 - 14.137^2} + 0.4 \right)}{2.42E06} + \frac{14.25 \left(\frac{14.25^2 + 13.25^2}{14.25^2 - 13.25^2} - 0.31 \right)}{2.83E07}}$$

$$= 3417.512 \text{ psi}$$

An interface pressure of this magnitude will cause the lead to yield.

2.12.6.2.4. Internal and External Loads on Lead Shell and Inner Shell

To determine a more accurate interface pressure, the maximum pressure is set equal to the pressure that corresponds to the hoop stress at which the lead yields.

Loads at 70°F

The yield strength of lead at 70°F is 620 psi and is set to the hoop stress to obtain the maximum pressure. For a thick-walled shell (Reference 2-19, Table 13.5, Page 696):

$$\begin{aligned}
 p &= \frac{\sigma_2(c^2 - b_L^2)}{c^2 + b_L^2} \\
 &= \frac{620(18.105^2 - 14.137^2)}{18.105^2 + 14.137^2} \\
 p &= 150.338 \text{ psi}
 \end{aligned}$$

This pressure will translate to the inner shell causing a hoop stress of (Reference 2-19, Table 13.5, Page 696):

$$\begin{aligned}
 \sigma_2 &= -\frac{p(b_s^2 + a^2)}{b_s^2 - a^2} \\
 &= -\frac{150.338(14.25^2 + 13.25^2)}{14.25^2 - 13.25^2} \\
 &= -2069.882 \text{ psi}
 \end{aligned}$$

It should be noted that any relaxation due to creep can be conservatively neglected.

Loads at -20°F

Now consider the HAC temperature of -20°F for the worst hoop stress on the inner shell. The coefficient of thermal expansion for the lead and stainless steel at the HAC -20°F temperature is:

$$\begin{aligned}
 \alpha_{ss-20} &= 8.17\text{E-}06 \text{ (in/in/°F)} \\
 \alpha_{L-20} &= 1.57\text{E-}05 \text{ (in/in/°F)}
 \end{aligned}$$

Then the steel and lead shell dimensions at -20°F are as follows

$$\begin{aligned}
 a &= 13.25[1 + 8.17\text{E-}06 \times -90] &= 13.240 \text{ in} \\
 b_s &= 14.25[1 + 8.17\text{E-}06 \times -90] &= 14.240 \text{ in} \\
 b_L &= 14.1365[1 + 1.57\text{E-}05 \times -90] &= 14.117 \text{ in} \\
 C &= 18.105[1 + 1.57\text{E-}05 \times -90] &= 18.079 \text{ in}
 \end{aligned}$$

This gives an interference of 0.123 in between the inner shell and the lead at -20°F. This interference will cause the lead to yield. Once again, to achieve a more accurate interface pressure, set the maximum pressure to be equal to the pressure that corresponds to the hoop stress at which the lead yields. The yield strength of lead at -20°F is 763 psi, which gives an interface pressure of (Reference 2-19, Table 13.5, Page 696):

$$\begin{aligned}
 p &= \frac{\sigma_2(c^2 - b_L^2)}{c^2 + b_L^2} \\
 &= \frac{763(18.079^2 - 14.117^2)}{18.079^2 + 14.117^2} \\
 &= 185.013 \text{ psi}
 \end{aligned}$$

This pressure will translate to the inner shell causing a hoop stress of (Reference 2-19, Table 13.5, Page 696):

$$\sigma_2 = -\frac{p(b_s^2 + a^2)}{b_s^2 - a^2}$$

$$= -\frac{185.013(14.24^2 + 13.24^2)}{14.24^2 - 13.24^2}$$

$$= -2547.290 \text{ psi}$$

Loads at -40°F

Now consider the normal conditions of transport extreme cold temperature of -40°F for the worst hoop stress on the inner steel shell. The coefficient of thermal expansion for the lead and stainless steel at the HAC -40°F temperature is:

$$\alpha_{ss-40} = 8.09\text{E-}06 \text{ (in/in/°F)}$$

$$\alpha_{L-40} = 1.56\text{E-}05 \text{ (in/in/°F)}$$

Calculating the lead and steel shell dimensions at -40°F, the following results:

$$\begin{aligned} a &= 13.25[1 + 8.09\text{E-}06 \times -110] &= 13.238 \text{ in} \\ b_s &= 14.25[1 + 8.09\text{E-}06 \times -110] &= 14.237 \text{ in} \\ b_L &= 14.1365[1 + 1.56\text{E-}05 \times -110] &= 14.112 \text{ in} \\ C &= 18.105[1 + 1.56\text{E-}05 \times -110] &= 18.074 \text{ in} \end{aligned}$$

This results in an interference fit of 0.125 in between the inner shell and lead. Accordingly, the yield strength of lead at -40°F is 795 psi, which is set to the hoop stress to obtain maximum pressure as follows (Reference 2-19, Table 13.5, Page 696):

$$\begin{aligned} p &= \frac{\sigma_2(C^2 - b_L^2)}{C^2 + b_L^2} \\ &= \frac{795(18.074^2 - 14.112^2)}{18.074^2 + 14.112^2} \\ &= 192.77 \text{ psi} \end{aligned}$$

Calculating the hoop stress in the inner shell (Reference 2-19, Table 13.5, Page 696):

$$\begin{aligned} \sigma_2 &= -\frac{p(b_s^2 + a^2)}{b_s^2 - a^2} \\ &= \frac{192.77(14.237^2 + 13.238^2)}{14.237^2 - 13.238^2} \\ &= -2654.123 \text{ psi} \end{aligned}$$

2.12.6.2.5. Axial Stresses and Strains

The previous calculations only deal with hoop stresses. Axial shrinkage of the lead will cause axial stresses to develop in the inner stainless steel and lead shells.

Cooling From 620°F to -20°F

Axial stresses and strains will occur in the inner shell from cooling down from 620°F to -20°F. The axial strain that results between the lead and stainless steel from the cooling to the extreme cold temperature of -20°F is:

$$\begin{aligned} \Sigma_{\text{strain}} &= (\alpha_{L620} - \alpha_{ss620}) \Delta T + (\alpha_{L-20} - \alpha_{ss-20}) \Delta T \\ &= (24.6\text{E-}06 - 9.92\text{E-}06)(550) + (15.7\text{E-}06 - 8.18\text{E-}06)(-90) \end{aligned}$$

$$= 0.0074$$

$$= 0.74\%$$

As a result of this tensile strain, the lead will yield. The yield strength for lead at -20°F is 763 psi, which will produce an effective force of:

$$\begin{aligned} P_{axial} &= S_y A \\ &= 763(\pi)(18.079^2 - 14.117^2) \\ &= 305,805 \text{ lb} \end{aligned}$$

The same force can develop a compressive axial stress in the inner steel shell from equilibrium as follows:

$$\begin{aligned} \sigma &= -\frac{P_{axial}}{A} \\ &= -\frac{305,805}{\pi(14.240^2 - 13.240^2)} \\ &= -3544.88 \text{ psi} \end{aligned}$$

Cooling From 620°F to -40°F

The axial strain that results between the lead and stainless steel from the cooling to the extreme cold temperature of -40°F is:

$$\begin{aligned} \Sigma_{strain} &= (\alpha_{L620} - \alpha_{SS620}) \Delta T + (\alpha_{L-40} - \alpha_{SS-40}) \Delta T \\ &= (24.6E-06 - 9.92E-06)(550) + (15.6E-06 - 8.09E-06)(-110) \\ &= 0.00725 \\ &= 0.725\% \end{aligned}$$

Once again, as a result of this tensile strain, the lead will yield. The yield strength for lead at -40°F is 795 psi, which will produce an effective force of

$$\begin{aligned} P_{axial} &= S_y A \\ &= 795(\pi)(18.074^2 - 14.112^2) \\ &= 318,437 \text{ lb} \end{aligned}$$

From equilibrium, the same force can develop a compressive axial stress in the inner steel shell as calculated below:

$$\begin{aligned} \sigma &= -\frac{P_{axial}}{A} \\ &= -\frac{318,437}{\pi(14.237^2 - 13.238^2)} \\ &= -3692.45 \text{ psi} \end{aligned}$$

2.12.6.3. Summary of Results

The stresses on the inner shell of the Model 2000 cask produce an axial stress of -3692.45 psi and a hoop stress of -2654.12 psi when at the low temperature of -40°F. In the case of the -20°F low temperature, an axial stress of -3544.88 psi and a hoop stress of -2547.29 psi is produced on the inner shell.

In the 620°F case, a hoop stress of -326.94 psi is produced on the inner shell and a hoop stress of 418.71 psi is produced on the outer shell. Table 2.12.6-4 below is a summary of stresses that occur in the inner and outer stainless steel shells due to lead pouring, solidification, and shrinkage.

Table 2.12.6-4. Summary of Stresses Due to Lead Pouring, Solidification, and Shrinkage

| Temperature (°F) | Inner Shell Stress (psi) | | | Outer Shell Stress (psi) | | | Lead Yield Stress (psi) |
|---------------------|-----------------------------|------------|------------|-----------------------------|------------|------------|----------------------------|
| | σ_1 | σ_2 | σ_3 | σ_1 | σ_2 | σ_3 | S_y |
| 620 | 0 | -326.94 | -22.94 | 0 | 418.71 | 22.94 | Liquid |
| 70 | 0 | -2069.88 | -150.34 | 0 | 0 | 0 | 620 |
| -20 | -3544.88 | -2547.29 | -185.01 | 0 | 0 | 0 | 763 |
| -40 | -3692.45 | -2654.12 | -192.29 | 0 | 0 | 0 | 795 |

The results of the analysis indicate that the Model 2000 cask meets the general requirements of 10 CFR 71.43 and also the requirements of the standard review plan NUREG-1609.

2.13 References

- 2-1 U.S. NRC, 10 CFR 71, "Packaging and Transportation of Radioactive Material," Washington D.C., 2016.
- 2-2 U.S. NRC, "Regulatory Guide 7.8, Load Combinations for the Structural Analysis of Shipping Casks for Radioactive Material," March 1989.
- 2-3 ASME, "Boiler & Pressure Vessel Code, Section III—Subsection NF, Supports," 2010.
- 2-4 U.S. NRC, "Regulatory Guide 7.11, Fracture Toughness Criteria of Base Material for Ferritic Steel Shipping Cask Containment Vessels with a Maximum Wall Thickness of 4 Inches (0.1 m)," 7.11, June 1991.
- 2-5 U.S. NRC, "Fabrication Criteria for Shipping Containers," NUREG/CR-3854, 1985.
- 2-6 U.S. NRC, "Classification of Transportation Packaging and Dry Spent Fuel Storage System Components According to Importance to Safety," NUREG/CR-6407, February 1996.
- 2-7 ASME, "Boiler & Pressure Vessel Code (BPVC), Section II, Part D, Properties Materials," 2010.
- 2-8 American Society for Metals (ASM), "Metals Handbook Tenth Edition, Volume 2, Properties and Selection: Nonferrous Alloys and Special Purpose Materials, Uranium and Uranium Alloys," Metals Park, OH, 1990.
- 2-9 Battelle Columbus Laboratories, "The Mechanical Properties of Depleted Uranium - 2 w/o Molybdenum Alloy," BMI-2032, 1979.
- 2-10 Henry J. Rack and Gerald A. Knorovsky, "An Assessment of Stress-Strain Data Suitable for Finite-Element Elastic-Plastic Analysis of Shipping Containers," Sandia Laboratories, NUREG/CR-0481, 1978.
- 2-11 W. Hoffman, *Lead and Lead Alloys*, English Translation of the Second Revised German Edition ed. New York: Springer-Verlag, 1970.
- 2-12 Thomas E. Tietz, "Determination of the Mechanical Properties of a High Purity Lead and a 0.058 % Copper-Lead Alloy," Stanford Research Institute, WADC 57-695, 1958.
- 2-13 Eugene A. Avallone, Theodore Baumeister III, and Ali M. Sadegh, "Marks' Standard Handbook for Mechanical Engineers," Eleventh Edition, 2007.
- 2-14 Parker-Hannifin Corporation, "Gask-O-Seal and Integral Seal Design Handbook," 2010.
- 2-15 G. C. Mok, L. E. Fischer, and S. T. Hsu, "Stress Analysis of Closure Bolts for Shipping Casks," LLNL, NUREG/CR-6007, 1993.
- 2-16 ANSYS®, "Mechanical, Revision 14.0," November 2011.
- 2-17 U.S. NRC, "Regulatory Guide 7.6, Stress Allowables for the Design of Shipping Cask Containment Vessels," February 1977.

- 2-18 ASME, "Boiler and Pressure Vessel Code (BPVC), Section III, Division 1 - Appendices," 2010.
- 2-19 Warren C. Young, *"Roark's Formulas for Stress & Strain,"* Seventh Edition ed. New York: McGraw Hill, 2002.
- 2-20 Livermore Software Technology Corporation, *"LS-DYNA, A Program for Nonlinear Dynamic Analysis of Structure in Three Dimensions,"* Version 971, Ed. Livermore, CA, 03/23/2011.
- 2-21 ASME, "Boiler and Pressure Vessel Code (BPVC), Section VIII, Division 2, Alternative Rules, Annex 3.D – Strength Parameters," New York, 2008.
- 2-22 R. K. Blandford and D. K. Morton, *Impact Tensile Testing of Stainless Steels at Various Temperatures, INL/EXT-08-14082.* Idaho Falls, Idaho 83415: Idaho National Laboratory, March 2008.
- 2-23 Hexcel Corporation, *HexWeb Honeycomb Energy Absorption System - Design Data.* Southbury, CT, March 2005.
- 2-24 Oak Ridge National Laboratory, "A Guide to the Design of Shipping Casks for the Transportation of Radioactive Material, ORNL-TM-681," Oak Ridge, TN, April 1965.
- 2-25 Richard G. Budynas and J. Keith Nisbett, *Shigley's Mechanical Engineering Design*, 9th ed., 2011.
- 2-26 E. Oberg, F. D. Jones, H. L. Horton, and H. H. Ryffel, *Machineries Handbook*, 26th ed., Christopher J. McCauley, Ed. New York, United States: Industrial Press INC., 2000.
- 2-27 J. E. Shigley and L. Mitchell, *Mechanical Engineering Design*, 4th ed. New York, United States: McGraw-Hill, 1965.
- 2-28 ASME, "Rules for Construction of Nuclear Facility Components," in *2010 ASME Boiler and Pressure Vessel Code, Section VIII, Division 1*, ASME, Ed. New York, United States: The American Society of Mechanical Engineers, 2010.
- 2-29 R.J. Roark, *Formulas for Stress and Strain*, 4th ed. New York, United States: McGraw-Hill INC., 1965.
- 2-30 Erik Oberg and Franklin D. Jones, *Machinery's Handbook*, 29th ed. New York: Industrial press, 2012.
- 2-31 American Society of Mechanical Engineers (ASME), "Rules for Construction of Nuclear Facility Components," Article E-1000, Section III, Division I, Appendices, 2010.
- 2-32 American Society of Mechanical Engineers (ASME), "Article NB-3000," Section III, Division I, 1998.
- 2-33 Stephen P. Timoshenko, *Strength of Materials*, 2nd ed. New York: Van Nostrand, 1948.
- 2-34 Richard G. Budynas and J. Keith Nisbett, *Shigley's Mechanical Engineering Design*, 8th ed. Boston: McGraw-Hill, 2008.

3 THERMAL EVALUATION

This section presents the thermal evaluation of the Model 2000 Transport Package and High Performance Insert (HPI) in two configurations: Configuration 1, with a contents thermal loading of 1500 W and Configuration 2, with a contents thermal loading of 3000 W, both under Normal Conditions of Transport (NCT) and Hypothetical Accident Conditions (HAC) as prescribed by 10 CFR 71 (Reference 3-1). The Configuration 2 results are presented in Sections 3.3 and 3.4, and the Configuration 1 results are presented in Section 3.5.1.

Specifically, the following requirements of 10 CFR 71 are addressed:

- 1) General standards for all packages, 10 CFR 71.43(g)

A package must be designed, constructed, and prepared for transport so that in still air at 100°F and in the shade, no accessible surface of a package would have a temperature exceeding 122°F in a nonexclusive use shipment, or 185°F in an exclusive use shipment.

- 2) Normal Conditions of Transport—heat, 10 CFR 71.71(c)(1)

Evaluation of the package design for exposure to an ambient temperature in still air and insolation according to Table 3-1.

Table 3-1. Insolation Data per 10 CFR 71.71

| Form and Location of Surface | Total Insolation for a 12-Hour Period (g cal/cm ²) |
|--------------------------------------------|----------------------------------------------------------------|
| Flat surfaces transported horizontally; | |
| Base | None |
| Other surface | 800 |
| Flat surfaces not transported horizontally | 200 |
| Curved surfaces | 400 |

- 3) Hypothetical Accident Conditions—thermal, 10 CFR 71.73(c)(4)

Exposure of the package fully engulfed in a hydrocarbon fuel/air fire of sufficient extent, and in sufficiently quiescent ambient conditions, to provide an average emissivity coefficient of at least 0.9, with an average flame temperature of at least 1475°F for a period of 30 minutes, or any other thermal test that provides the equivalent total heat input to the package and which provides a time averaged environmental temperature of 1475°F.

For purposes of calculation, the surface absorptivity coefficient must be either that value which the package may be expected to possess if exposed to the fire specified or 0.8, whichever is greater; and the convective coefficient must be that value which may be demonstrated to exist if the package were exposed to the fire specified. Artificial cooling may not be applied after cessation of external heat input, and any combustion of materials of construction, must be allowed to proceed until it terminates naturally.

§71.73(b) With respect to the initial test conditions, the ambient air temperature before and after the test must remain constant at that value between -20°F and 100°F which is most unfavorable for the feature under consideration.

To demonstrate that the Model 2000 Transport Package, shown in Figure 3-1, meets these requirements, a three-dimensional finite element model of the package was developed and analyzed using the general-purpose finite element analysis (FEA) code ANSYS, Release 14.0 (Reference 3-2). Multiple ANSYS thermal calculations were performed simulating NCT and HAC using the finite element representation of the Model 2000 Transport Package with HPI.

Security-Related Information Figure Withheld Under 10 CFR 2.390.

**Figure 3-1. Model 2000 Transport Package
(High Performance Insert and Material Basket Not Shown)**

3.1 Description of Thermal Design

3.1.1. Design Features

The Model 2000 Transport Package, described in Section 1.2, is designed with a thermally passive system. The cask is enclosed in an overpack that serves as a fire shield. The overpack is designed to reduce heat flow from the fire environment into the cask structure by the use of enclosed air spaces. It is composed of two concentric cylindrical SS304 shells approximately 83 inches long with an OD of 48.5 inches and an ID of 40.5 inches. The shells are separated radially by eight equally spaced [] along the length of the shells, and horizontally by two [] sections to provide closed air spaces. A 24-inch diameter toroidal shell is attached at both ends of the outer shell with a circular plate enclosing the inner regions of the torus. The internal shell is also closed at each end by a circular plate. All materials are SS304. The vertical tubes have a 3-inch OD and are 0.25 inches thick. The horizontal [] sections have a 7.25-inch OD and are 0.375 inches thick. Attached at both ends of the overpack inner surface are aluminum honeycomb pads.

The cask is designed with lead shielding on three sides and a 6-inch thick stainless steel forging at the base that functions as a heat sink that allows the heat to flow through the bottom of the package. When the cask is placed in the overpack during assembly, air gaps of 1.0-inch radially and 1.0-inch at the top separate the cask from the overpack inner surfaces.

The cask lid seal design, which includes an [] and metal retainer component are based on the two previously defined content decay heat configurations. The cask lid seal for Configuration 1 is a [] retainer with four Parker Compound No. [] rings. The cask lid seal for Configuration 2 is a [] retainer with four Parker Compound No. [] rings. The cask lid is secured to the cask body by fifteen (15) 1¼-inch diameter socket head screws.

The HPI is described in Section 1.2.2.1.

3.1.2. Content's Decay Heat

The derivations of the decay heats for the different content configurations of the Model 2000 Transport Package are presented in Chapter 5. The decay heat for irradiated fuels is based on the source term calculations discussed in Section 5.5.1. The decay heat for irradiated hardware and by-product, and cobalt-60 isotope rod contents is determined using watt-per-Curie conversion factors, listed in Section 5.5.4 and the radionuclide inventory of the contents. Configuration 1 is evaluated to support 1500 W decay heat and Configuration 2 at 3000 W decay heat.

3.1.3. Summary Tables of Temperatures

Thermal design criteria are specified for regions throughout the cask, cask cavity, and the outside overpack wall. The Configuration 2 cask lid seal and port O-ring is limited to the temperature listed in Table 3.1.3-1, and this serves as the thermal criteria for the region associated with the seal area. The maximum allowable internal pressure is 30 psia, which corresponds to air of 100% humidity heated to 600°F at constant volume.

Table 3.1.3-1 presents the maximum design temperatures of the components or materials that affect structural integrity, containment, and shielding under both NCT and HAC for Configuration 2. Where available, temperature limits for the Model 2000 Transport Package components are obtained from manufacturers' literature. Otherwise, component temperature limits are defined as the melting temperature of the material of construction.

Table 3.1.3-1. Temperature Limits

| Component or Material | Temperature Limit (°F) |
|-----------------------------------------|-------------------------|
| Stainless Steel Components | 2546 |
| Lead Shielding ^a | 622 |
| Depleted Uranium Shielding ^a | 2071 |
| Aluminum Honeycomb ^b | 350 |
| Cask Lid Seal | 5 to 508 ^c |
| Cask Ports | -40 to 612 ^c |
| Accessible Surfaces Of Package | < 185 ^d |

Notes:

- a. Temperature limit is melting temperature (Reference 3-3).
- b. Maximum operating temperature (Reference 3-4).
- c. Seal acceptance testing, Reference (Reference 3-5).
- d. Exclusive use requirement per 10 CFR 71.43(g).

3.1.3.1. NCT Temperature Summary

Per the requirements of 10 CFR 71.71(c)(1) (Reference 3-1), Configuration 2 is evaluated for NCT. Specifically, a steady-state thermal analysis is performed simulating exposure of the package to a 100°F ambient temperature in still air and insolation as specified in Table 3-1. The results of the analysis are presented in Section 3.3. The temperatures of several key package components are summarized and compared with their allowable temperatures in Table 3.1.3-2.

Table 3.1.3-2. NCT Temperature Summary and Comparison with Allowable Temperatures

| Item | NCT Temperatures (°F) | Allowable Temperature (°F) |
|----------------------------------|------------------------------------|----------------------------|
| Material Basket | 1,001 (max) | 2,546 |
| HPI Shielding (Depleted Uranium) | 601 (max) | 2,071 |
| Cask Lid Seal | 432 (max) | 508 |
| Cask Shielding (Lead) | 449 (max) | 622 |
| Honeycomb Impact Limiters | 359 (max) ^a / 334 (avg) | 350 |
| Cask Drain Port (Bottom) | 370 | 612 |
| Cask Test Port (Top) | 426 | |
| Cask Vent Port (Lid) | 442 | |
| Overpack Outer Surface | 215 | 185 ^b |

Notes:

- a. The maximum honeycomb impact limiter temperature of 359°F exceeds the allowable temperature of 350°F. However, this maximum temperature occurs in a very limited area of the impact limiter and is based on steady-state boundary conditions for the hot case, which ignores the removal of solar insolation during the night cycle. The

majority of the impact limiter temperatures are below 350°F. Therefore, the average temperature of 334°F is appropriate to compare to the allowable temperature.

- b. Limit specified in 10 CFR 71.43(g), which requires the addition of a personnel barrier to satisfy this requirement. Refer to Section 7.1.4, Preparation for Transport.

The Model 2000 Transport Package components remain below their allowable temperatures for NCT with insolation. Therefore, when exposed to NCT with insolation, Configuration 2 maintains containment of the contents, as neither the shielding nor the impact limiting materials exceed temperatures that would adversely affect their performance.

3.1.3.2. HAC Temperature Summary

When exposed to the HAC fire prescribed in the regulations, Configuration 2 must maintain containment of its contents and maintain its shielding capabilities. The results of the HAC thermal evaluation are presented in Section 3.4. As shown in Table 3.1.3-3, the maximum temperatures of the different package components are below the allowable temperatures. Therefore, the HAC fire does not adversely affect the package's ability to provide containment and shielding for its contents. Note, that the maximum average fill gas temperatures in the HPI and cask are 740°F and 571°F, respectively. The maximum average combined fill gas temperature (HPI + cask) is 585°F.

Table 3.1.3-3. HAC Maximum Temperature Summary and Comparison with Allowable Temperatures

| Item | HAC Maximum Temperature (°F) | Allowable Temperature (°F) |
|-----------------------------------------------------------|------------------------------|----------------------------|
| Material Basket | 1,045 | 2,546 |
| HPI Shielding (Side) | 670 | 2,071 |
| HPI Shielding (Top) | 599 | 2,071 |
| HPI Shielding (Bottom) | 618 | 2,071 |
| Cask Lid Seal | 508 | 508 |
| Cask Shielding (Side) | 570 | 622 |
| Cask Shielding (Top) | 529 | 622 |
| Cask Shell (Puncture Location) | 782 | - |
| Cask Shell (Opposite side to Puncture Location) | 512 | - |
| Overpack Outer Shell (Puncture Location) | 1,103 | - |
| Overpack Outer Shell (Opposite Side to Puncture Location) | 1,337 | - |
| Cask Drain Port (bottom) | 612 ^a | 612 |
| Cask Test Port (top) | 608 ^a | 612 |
| Cask Vent Port (lid) | 520 | 612 |
| HPI Fill Gas (Average) | 740 | - |
| Cask Fill Gas (Average) | 571 | - |
| Combined HPI and Cask Fill Gas (Average) | 585 | - |

Note:

- a. Temperatures for Drain Port and Test Port exceed 600°F for 21 minutes and 11 minutes, respectively. Seal acceptance testing conditions for cask lid seal and port containment components are specified in Reference 3-5.

3.1.4. Summary Tables of Maximum Pressures

Table 3.1.4-1 shows the maximum normal operating pressure and the maximum pressure under hypothetical accident conditions.

Table 3.1.4-1. Maximum Pressures

| Component or Material | Reference | Pressure (psia) |
|------------------------------------|---------------|-----------------|
| Maximum Design Internal Pressure | Section 2.4.3 | 30.0 |
| Maximum Normal Operating Pressure | Section 3.3.2 | 26.8 |
| Maximum Average Pressure under HAC | Section 3.4.3 | 29.0 |

3.2 Material Properties and Component Specifications

3.2.1. Material Properties

The thermal properties of the materials of construction used in the analyses for the thermal evaluation are presented in Table 3.2.1-1. When available from the open literature, temperature-dependent properties are used in the analyses. Additionally, the thermal properties of the HPI and cask fill gas (helium) and overpack gas (air) are presented in Table 3.2.1-2 (Reference 3-3).

Table 3.2.1-1. Thermal Properties of Solid Regions in the Model 2000 Finite Element Thermal Model

| Material | Temperature (°F) | Density (lbm/in ³) | Thermal Conductivity (Btu/h-in-°F) | Specific Heat (Btu/lbm-°F) | Emissivity |
|---------------------------------------|------------------|--------------------------------|------------------------------------|------------------------------|------------|
| AISI 304 Stainless Steel ^a | -100 | --- | 0.607 | 0.096 | --- |
| | 80 | 0.285 | 0.717 | 0.114 | 0.22 |
| | 260 | --- | 0.799 | 0.123 | 0.22 |
| | 620 | --- | 0.953 | 0.133 | 0.24 |
| | 980 | --- | 1.088 | 0.139 | 0.28 |
| | 1340 | --- | 1.223 | 0.146 | 0.35 |
| | 1700 | --- | 1.348 | 0.153 | --- |
| | 2240 | --- | 1.526 | 0.163 | --- |
| Lead ^a | -100 | --- | 1.767 | 0.030 | --- |
| | 80 | 0.410 | 1.700 | 0.031 | --- |
| | 260 | --- | 1.637 | 0.032 | --- |
| | 620 | --- | 1.512 | 0.034 | --- |
| Depleted Uranium ^a | -100 | --- | 1.209 | 0.026 | --- |
| | 80 | 0.689 | 1.329 | 0.028 | --- |
| | 260 | --- | 1.425 | 0.030 | --- |
| | 620 | --- | 1.637 | 0.035 | --- |
| | 980 | --- | 1.858 | 0.042 | --- |
| | 1340 | --- | 2.114 | 0.043 | --- |
| | 1700 | --- | 2.359 | 0.038 | --- |
| AISI 316 Stainless Steel ^a | 80 | 0.298 | 0.645 | 0.112 | 0.22 |
| | 260 | --- | 0.732 | 0.120 | 0.22 |
| | 620 | --- | 0.881 | 0.131 | 0.24 |
| | 980 | --- | 1.026 | 0.138 | 0.28 |
| | 1340 | --- | 1.165 | 0.144 | 0.35 |
| [[]] Steel ^b | --- | Same as AISI 304 or AISI 316 | Same as AISI 304 or AISI 316 | Same as AISI 304 or AISI 316 | 0.44 |
| Aluminum Honeycomb ^c | -100 | --- | 0.465 | --- | --- |
| | 0 | --- | 0.608 | --- | --- |
| | 75 | 0.0046 | 0.715 | 0.208 | 0.20 |
| | 100 | --- | 0.751 | --- | --- |
| | 200 | --- | 0.894 | --- | --- |
| | 300 | --- | 1.073 | --- | --- |

Notes:

- a. Reference 3-3, Table A.1 (density, thermal conductivity, and specific heat) and Table A.11 (emissivity).
- b. Reference 3-6.
- c. Density and thermal conductivity – Reference 3-4. Specific heat of Aluminum 2024-T6– Reference 3-3, Table A.1. Emissivity of heavily oxidized aluminum– Reference 3-7, Appendix D.

Table 3.2.1-2. Thermal Properties of Gaseous Regions in the Finite Element Thermal Model

| Material | Temperature (°F) | Density (lbm/in ³) | Thermal Conductivity (Btu/h-in-°F) | Specific Heat (Btu/lbm-°F) | Emissivity |
|----------|------------------|--------------------------------|------------------------------------|----------------------------|------------|
| Helium | -64 | --- | 5.93E-3 | --- | --- |
| | -28 | --- | 6.26E-3 | --- | --- |
| | 8 | --- | 6.60E-3 | --- | --- |
| | 44 | --- | 6.98E-3 | --- | --- |
| | 80 | 5.871E-6 | 7.32E-3 | 1.24 | --- |
| | 170 | --- | 8.19E-3 | --- | --- |
| | 260 | --- | 9.00E-3 | --- | --- |
| | 350 | --- | 9.82E-3 | --- | --- |
| | 440 | --- | 1.06E-2 | --- | --- |
| | 620 | --- | 1.21E-2 | --- | --- |
| | 710 | --- | 1.27E-2 | --- | --- |
| | 800 | --- | 1.34E-2 | --- | --- |
| | 890 | --- | 1.40E-2 | --- | --- |
| | 980 | --- | 1.46E-2 | --- | --- |
| | 1160 | --- | 1.59E-2 | --- | --- |
| | 1340 | --- | 1.70E-2 | --- | --- |
| Air | -100 | --- | 8.72E-4 | 0.241 | --- |
| | -10 | --- | 1.07E-3 | 0.240 | --- |
| | 80 | 4.196E-5 | 1.27E-3 | 0.241 | --- |
| | 170 | --- | 1.44E-3 | 0.241 | --- |
| | 260 | --- | 1.63E-3 | 0.242 | --- |
| | 350 | --- | 1.80E-3 | 0.244 | --- |
| | 440 | --- | 1.96E-3 | 0.246 | --- |
| | 530 | --- | 2.11E-3 | 0.248 | --- |
| | 620 | --- | 2.26E-3 | 0.251 | --- |
| | 710 | --- | 2.39E-3 | 0.254 | --- |
| | 800 | --- | 2.52E-3 | 0.257 | --- |
| | 890 | --- | 2.64E-3 | 0.260 | --- |
| | 980 | --- | 2.76E-3 | 0.263 | --- |
| | 1070 | --- | 2.87E-3 | 0.263 | --- |
| | 1160 | --- | 2.99E-3 | 0.268 | --- |
| | 1250 | --- | 3.10E-3 | 0.270 | --- |
| | 1340 | --- | 3.21E-3 | 0.273 | --- |
| | 1520 | --- | 3.44E-3 | 0.277 | --- |
| | 1700 | --- | 3.67E-3 | 0.281 | --- |

3.2.2. Component Specifications

The Model 2000 Transport Package component materials are primarily stainless steel, lead, and aluminum. The maximum allowable temperatures of these materials are given in Table 3.1.3-1. The temperatures resulting from normal and accident thermal conditions fall within these temperatures.

The only component material that is temperature sensitive is the [[]] material in the cask lid seal and port plug O-rings. For Configuration 2, the material used is a high temperature [[]] that offers the highest operating temperature range of any [[]] material (Reference 3-8). Part of the Configuration 2 cask lid seal design includes a stainless steel [[]]; temperatures resulting from normal and accident thermal conditions fall within the material limits.

3.3 Thermal Evaluation under Normal Conditions of Transport

The thermal performance of Configuration 2 is analyzed for NCT (with and without insolation) by performing steady-state heat transfer analyses on a finite element representation of the package. Specifically, the general-purpose finite element code ANSYS, Release 14.0 (Reference 3-2), is used to model and analyze the Model 2000 Transport Package with a content heat load of 3000 W for NCT. Several ANSYS macros are created in order to build the model, apply boundary conditions, and perform the steady-state analyses.

Assumptions made for this evaluation are:

- The Model 2000 Transport Package is assumed to be in an upright (vertical) orientation during NCT.
- The cask and HPI are backfilled with Helium at 70°F and 14.7 psia.
- Natural convection within the package cavities is neglected.
- The contents of the HPI are assumed to generate a maximum of 3000 W that is uniformly distributed among the [[]] material basket [[]].
- During NCT, the package is assumed to have an emissivity consistent with the material of construction at temperature.

As mentioned above, for the NCT analysis, a steady-state thermal analysis was performed simulating exposure of the package to a 100°F ambient temperature in still air and insolation as specified in Table 3-1. The results of the analysis are presented below. The temperatures of the key package components are summarized and compared with their allowable temperatures in Table 3.1.3-2.

NCT sensitivity studies were also performed to evaluate the thermal performance of the package using boundary conditions applied as both steady state and as constant boundary conditions solved as a transient. Because the solutions are radiation-dominated, the transient solution results in better convergence and slightly higher temperatures. To achieve steady-state conditions with the transient solver, a simulated time of 2000 hours was used. The 2000-hour duration of the transient analyses is sufficiently long enough for the temperatures within the package to reach

steady-state values, that is, the temperature of a node within the package model doesn't change from one time step to the next.

Model Description

The general-purpose finite element code ANSYS, Release 14.0 (Reference 3-2), is used to model and analyze the Model 2000 Transport Package with a content heat load of 3000 W for NCT. Several ANSYS macros are created in order to build the model, apply boundary conditions, and perform the steady-state analyses.

The model, shown in Figure 3.3-1 through Figure 3.3-3, represents a half-symmetry of the package. A half-symmetry model is used so that damage from the HAC drop/puncture test may be incorporated using the same model.

In the model, the decay heat of the contents, applied as a heat flux to the material basket [[]], is transferred through the solid and gaseous regions via conduction heat transfer, across gaseous regions separating solids via thermal radiation, and then rejected to the surroundings via natural convection and thermal radiation. Heat transfer via convection within the package is not considered. In addition to the decay heat of the contents, other heat sources—insolation (heat flux) and/or fire (convection/thermal radiation)—are also included as boundary conditions where appropriate.

To simulate this heat flow, a finite element model of the Model 2000 Transport Package with HPI is generated with the ANSYS Parametric Design Language (APDL) using a combination of SOLID70, CONTA173, TARGE170, LINK34, SURF152, and SURF252 elements. Each of the element types used to model the Model 2000 Transport Package and the modes of heat transfer modeled by the various element types are discussed in the following paragraphs.

The SOLID70 elements are three-dimensional (3D), 8-node, single degree-of-freedom (DOF) thermal solid elements and are used to model heat flow through the solid and gaseous regions of the package via conduction heat transfer.

The CONTA173/TARGE170 pairs are 3D, 4-node, surface-to-surface contact elements that are overlaid onto area faces of the SOLID70 elements and are used to model heat flow across interfaces between contacting components or across interfaces between dissimilar meshes. The LINK34 elements are uniaxial elements with the ability to convect heat between 2 nodes; however, because thermal contact conductance has the same units as the convection heat transfer coefficient, the LINK34 elements are used to model heat flow between contacting components that either have a line-of-contact or are physically separated in the model and, therefore, do not lend themselves to the use of the CONTA173/TARGE170 pairs.

The SURF152 3D thermal surface effect elements are overlaid onto area faces of the SOLID70 elements and are used to apply heat flux (fuel material basket [[]] internal surfaces) and convection (overpack external surfaces) boundary conditions. For NCT, insolation (heat flux) is applied directly to area faces of the SOLID70 elements; SURF152 elements are not used to apply this heat load.

Finally, radiation exchange between solid surfaces separated by gaseous regions is modeled using the radiosity solver in conjunction with SURF252 elements. SURF252 are 3D, 4-node, radiosity surface elements that are overlaid onto area faces of the SOLID70 elements that have a radiosity boundary condition using the RSUF command, and then expanded into full 360° in order to properly calculate radiation view factors for models that only model a portion of the actual item due to symmetry.

[[

]]

**Figure 3.3-1. Finite Element Model of the Model 2000 Transport Package
(Configuration 2)**

[[

]]

Figure 3.3-2. Finite Element Model of the Model 2000 Transport Package - Air and Helium Not Shown (Configuration 2)

[[

]]

**Figure 3.3-3. Finite Element Model of the Model 2000 Transport Package - Exploded View
(Configuration 2)**

Thermal Contact Resistance/Conductance

To simulate welded joints (e.g., the cask cavity shell welded to the cask bottom), the nodes of each mating component are merged at the weld joint. This allows heat to flow across these welded interfaces. However, for all other component interfaces, each component in the finite element model is independent and does not share nodes with its neighboring component(s). Therefore, in order to allow heat to flow through the model, each component is connected to its neighboring component using CONTA173/TARGE170 thermal contact/target elements. For components that have only a line of contact (e.g., Hertzian contact), or if the elements of contacting components are not physically modeled as being in contact, LINK34 convection 2-node elements are used to model the contact resistance.

Thermal contact resistance, R_{tc} , between mating parts results in a temperature drop across the interface between these parts (see Figure 3.3-4). Note that the surface roughness is exaggerated in the figure. The existence of a finite contact resistance is due primarily to the surface roughness of the mating parts. Other factors that affect the contact resistance are the mating materials, interfacial fluid/gas, and pressure. Theoretical methods to calculate this resistance have been developed; however, empirically derived resistances have provided better correlation with actual measured temperature drops across contact interfaces (Reference 3-3).

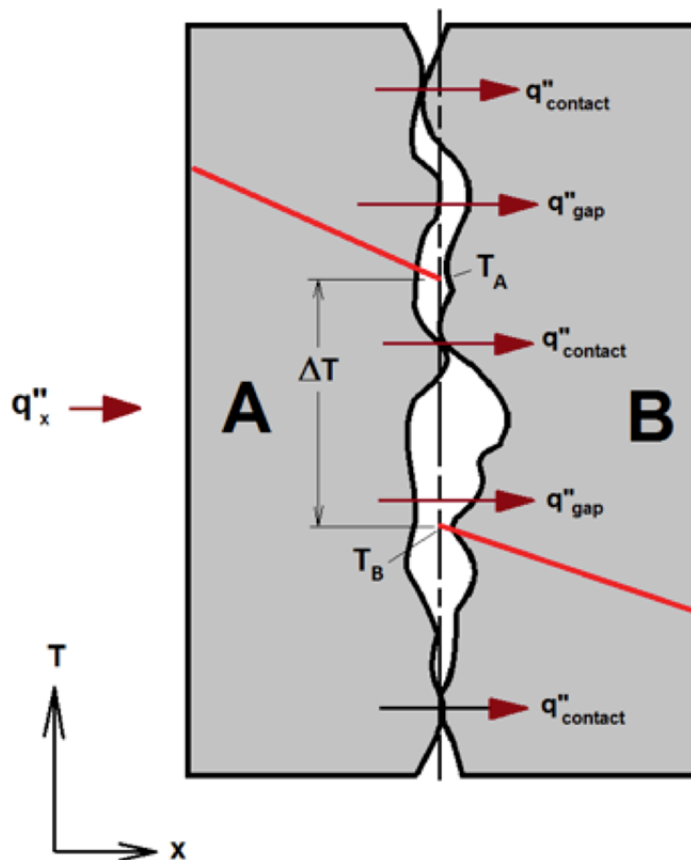


Figure 3.3-4. Heat Transfer Through the Contact Plane Between Two Solid Surfaces

The thermal resistance effect shown in Figure 3.3-4 is described by the following equation from Reference 3-3, Equation 3.20, for a unit area of interface:

$$R''_{tc} = \frac{T_A - T_B}{q''_x}$$

where R''_{tc} = thermal resistance per unit area,
 T_A = temperature of material A,
 T_B = temperature of material B, and
 q''_x = heat flux.

Thermal contact is modeled in ANSYS by specifying the thermal contact conductance (TCC) of the interface either as a real constant (for the CONTA173/TARGE170 pairs) or as a material property (LINK34). The TCC is defined as the reciprocal of the thermal contact resistance; therefore, a high TCC value implies low thermal contact resistance, and a low TCC value implies high thermal contact resistance.

While the LINK34 is a 2-node convection element, the natural convection coefficient has the same units as that of thermal contact conductance. Therefore, the LINK34 element can be used to simulate thermal contact between two nodes by substituting the TCC value for the convection coefficient.

Experimentally determined TCC values for various mating materials, surface finishes, interfacial gases, and interface pressures are shown in Table 3.3-1.

Because there are a large number of thermal contact interfaces to manage in the Model 2000 Transport Package thermal model, and because exact conditions (such as surface finish and pressure) at the interfaces are unknown, a subjective approach is taken when assigning TCC values to these interfaces in the FEA model. To this end, five contact resistance levels ranging from low to high resistance are established with an assigned TCC value based on the typical values obtained from the open literature as presented in Table 3.3-1. The five TCC values used in the analyses presented in this report are presented in Table 3.3-2. Then, each thermal contact interface in the model is assigned one of these five resistance levels (see Table 3.3-3 and Figure 3.3-5). The approach to assigning the five contact resistance levels is:

- The interfaces (when dissimilar meshes exist) between elements representing fill gases and their adjacent solid meshes are assigned “Low” resistance levels.
- Interfaces between bolted junctures are assigned “Low” or “Low/Moderate” resistance levels.
- Interfaces between shielding materials and the shells that contain them are assigned “Low/Moderate” resistance levels.
- Interfaces between loosely fitted components (e.g., the cask lid cylindrical sides and the cask top flange) are assigned “High” resistance levels.

- Interfaces between heavy objects and the component on which they rest are assigned “Low/Moderate”, “Moderate”, or “Moderate/High” resistance levels depending on how heavy the object is and how much the component on which they rest may flex under the weight.

During normal transport, Configuration 2 is in an upright orientation with the material basket bottom contacting the HPI bottom [[]], the HPI bottom [[]] contacting the cask bottom, and the cask bottom contacting the cask support plate of the overpack. Because the inner surface of the cask bottom is dished to allow for water drainage, the entire surface of the HPI bottom [[]] will not be in contact with the cask bottom. Additionally, in order to maintain well-shaped elements, the outer, bottom corner of the HPI is modeled with a small offset from the cask bottom. Therefore, LINK34 elements are used to model a line of contact between the outer edge of the HPI bottom [[]] and cask bottom. The LINK34 elements are assigned a thermal conductance value of 15.0 Btu/h-in²-°F, and the contact area is modeled as a 2.5-inch wide annular band with an outer diameter equivalent to the outer diameter of the HPI bottom [[]].

Table 3.3-1. Typical Thermal Contact Conductance Values from Open Literature

| Material (Both Surfaces) | Surface Roughness (μ in) | Interfacial Gas | Pressure (psi) | TCC (Btu/h-in ² -°F) | Source |
|-----------------------------|--------------------------------|--------------------|-------------------|------------------------------------|-----------------------------|
| Stainless Steel | Not Specified | Vacuum | 14.5 | 0.5 – 2.0 | Reference 3-3 Table 3.1 |
| Stainless Steel | Not Specified | Vacuum | 1450 | 3.1 – 17.5 | Reference 3-3 Table 3.1 |
| Stainless Steel | Normal Finish | Air | 14.7 – 1470 | 2.1 – 4.5 | Reference 3-9 Table 2.3 |
| 416 Stainless Steel | 30 | Air | 100 | 13.9 | Reference 3-10 Table 1.2 |
| 416 Stainless Steel | 100 | Air | 44 – 368 | 4.6 | Reference 3-9 Table 2.3 |
| 304 Stainless Steel | 45 | Air | 588 – 1029 | 2.3 | Reference 3-9 Table 2.3 |
| Carbon Steel | 1000 | Air | 100 – 300 | 0.6 – 0.8 | Reference 3-10 Table 1.2 |
| Carbon Steel | 63 | Air | 100 – 300 | 3.5 – 4.6 | Reference 3-10 Table 1.2 |
| Aluminum | Not Specified | Vacuum | 14.5 | 2.4 – 8.2 | Reference 3-3 Table 3.1 |
| Aluminum | Not Specified | Vacuum | 1450 | 30.6 – 61.2 | Reference 3-3 Table 3.1 |
| Aluminum | 397 | Air | 14500 | 4.4 | Reference 3-3 Table 3.1 |

Table 3.3-1. Typical Thermal Contact Conductance Values from Open Literature

| Material (Both Surfaces) | Surface Roughness (μ in) | Interfacial Gas | Pressure (psi) | TCC (Btu/h-in ² -°F) | Source |
|-----------------------------|-------------------------------------|--------------------|-------------------|------------------------------------|-----------------------------|
| Aluminum | 397 | Helium | 14500 | 11.6 | Reference 3-3 Table 3.1 |
| Aluminum | Normal Finish | Air | 14.7 – 1470 | 2.7 – 14.7 | Reference 3-9 Table 2.3 |
| Aluminum | Rough | Vacuum | Low | 0.2 | Reference 3-9 Table 2.3 |
| Aluminum | 120 | Air | 100 – 300 | 6.3 – 11.5 | Reference 3-10 Table 1.2 |
| Aluminum | 65 | Air | 100 – 300 | 9.0 – 14.6 | Reference 3-10 Table 1.2 |
| Aluminum | 100 | Air | 176 – 368 | 13.9 | Reference 3-9 Table 2.3 |
| Aluminum | 10 | Air | 176 – 368 | 69.4 | Reference 3-9 Table 2.3 |

Table 3.3-2. TCC Values Used in the Thermal Analyses

| Thermal Contact Resistance ID | Thermal Contact Resistance Level | TCC (Btu/h-in ² -°F) |
|----------------------------------|-------------------------------------|------------------------------------|
| 1 ^a | Low (Perfect Contact) | 1000 |
| 2 | Low/Moderate | 15 |
| 3 | Moderate | 5 |
| 4 | Moderate/High | 1 |
| 5 | High | 0.5 |

Note:

- a. Thermal contact resistance ID #1 is used to connect dissimilar meshes in which perfect contact is desired.

Table 3.3-3. Thermal Contact Resistance Levels Assigned to the Modeled Contact Elements

| Contact ID (Real Constant) | Surface 1 (CONTA173) | Surface 2 (TARGE170) | Thermal Contact Resistance ID (See Table 3.3-2) |
|-------------------------------------------|-----------------------------------------------|--------------------------------------|----------------------------------------------------------------|
| 101 | Cask Shield (Side) | Cask Bottom | 2 |
| 102 | Cask Shield (Side) | Cask Shell | 2 |
| 103 | Cask Shield (Side) | Cask Cavity Shell | 2 |
| 104 | Cask Shield (Side) | Cask Top | 2 |
| 105 | Cask Bottom | Cask Shell | 4 |
| 106 | Cask Top | Cask Shell | 4 |
| 107 | Cask Top | Cask Cavity Shell | 4 |
| 108 | Cask Shield (Lid) | Cask Lid | 2 |
| 109 | Cask Lid (At Bolted Interface) | Cask Top | 2 |
| 110 | Cask Lid (Cylindrical Sides) | Cask Top | 5 |
| 112 | Cask Fill Gas | Cask Bottom | 1 |
| 113 | Cask Fill Gas | Cask Cavity Shell | 1 |
| 114 | Cask Fill Gas | Cask Lid | 1 |
| 115 | Overpack Toroidal Stiffener (Bottom) | Overpack Toroidal Shell (Bottom) | 4 |
| 116 | Overpack Gusset Base (Bottom) | Overpack Toroidal Shell (Bottom) | 2 |
| 117 | Overpack Gusset (Bottom) | Overpack Stiffening Ring (Bottom) | 2 |
| 118 | Overpack Gusset & Stiffening Ring (Bottom) | Overpack Bolting Ring (Bottom) | 2 |
| 119 | Overpack Stiffening Ring (Bottom) | Overpack Outer Shell | 4 |
| 120 | Overpack Bolting Ring (Bottom) | Overpack Outer Shell | 4 |
| 121 | Overpack Bolting Ring (Bottom) | Overpack Inner Shell | 4 |
| 122 | Overpack [[]] (Bottom) | Overpack Bottom End Plate | 5 |
| 123 | Overpack [[]] (Bottom) | Overpack Bottom Plate | 2 |
| 124 | Honeycomb Impact Limiter (Bottom) | Overpack Bottom Plate | 5 |
| 125 | Honeycomb Impact Limiter (Bottom) | Overpack Inner Shell | 5 |
| 126 | Honeycomb Impact Limiter (Bottom) | Overpack Cask Support Plate | 5 |
| 127 | Overpack Gas | Overpack Cask Support Plate | 1 |

Table 3.3-3. Thermal Contact Resistance Levels Assigned to the Modeled Contact Elements

| Contact ID (Real Constant) | Surface 1 (CONTA173) | Surface 2 (TARGE170) | Thermal Contact Resistance ID (See Table 3.3-2) |
|-------------------------------|-----------------------------------|-----------------------------------|-------------------------------------------------------|
| 128 | Overpack Gas | Overpack Inner Shell | 1 |
| 129 | Overpack Gas | Overpack Bolting Ring (Bottom) | 1 |
| 130 | Overpack Bolting Ring (Bottom) | Overpack Bolting Ring (Top) | 4 |
| 131 | Cask Bottom Or Cask Top* | Overpack Cask Support Plate OR | 3 |
| 132 | Overpack Bolting Ring (Top) | Overpack Outer Shell | 4 |
| 133 | Overpack Bolting Ring (Top) | Overpack Inner Shell | 4 |
| 134 | Overpack [[]] (Between Shells) | Overpack | 4 |
| 135 - 139 | ---Not Used--- | | |
| 140 | Overpack Stiffening Ring (Top) | Overpack Outer Shell | 4 |
| 141 | Overpack Gusset (Top) | Overpack Stiffening Ring (Top) | 2 |
| 142 | Overpack Gusset Base (Top) | Overpack Toroidal Shell (Top) | 2 |
| 143 | Overpack Toroidal Stiffener (Top) | Overpack Toroidal Shell (Top) | 4 |
| 144 | Honeycomb Impact Limiter (Top) | Overpack Top Plate | 5 |
| 145 | Honeycomb Impact Limiter (Top) | Overpack Inner Shell (Top) | 5 |
| 146 | Overpack [[]] (Top) | Overpack Top Plate | 2 |
| 147 | Overpack [[]] (Top) | Overpack End Plate (Top) | 5 |
| 148 | Overpack Gas | Overpack Bolt Ring (Top) | 1 |
| 149 | Overpack Gas | Overpack Inner Shell (Top) | 1 |
| 150 | Overpack Gas | Honeycomb Impact Limiter (Top) | 1 |
| 151 | Cask Fill Gas | HPI Top Lid | 1 |
| 152 | Cask Fill Gas | HPI Bottom Lid | 1 |
| 153 | Cask Fill Gas | HPI Horizontal Plate | 1 |
| 154 | ---Not Used--- | | |
| 155 | [[]] | [[]] | 5 |
| 156 | [[]] | [[]] | 2 |
| 157 | [[]] | [[]] | 2 |
| 158 | [[]] | [[]] | 3 |
| 159 | [[]] | [[]] | 3 |
| 160 | [[]] | [[]] | 2 |

Table 3.3-3. Thermal Contact Resistance Levels Assigned to the Modeled Contact Elements

| Contact ID (Real Constant) | Surface 1 (CONTA173) | Surface 2 (TARGE170) | Thermal Contact Resistance ID (See Table 3.3-2) |
|----------------------------------|-------------------------|-------------------------|-------------------------------------------------------|
| 161 | [[]] | [[]] | 2 |
| 162 | [[]] | [[]] | 2 |
| 163 | [[]] | [[]] | 2 |
| 164 | [[]] | [[]] | 3 |
| 165 | [[]] | [[]] | 2 |
| 166 | [[]] | [[]] | 2 |
| 167 | [[]] | [[]] | 2 |
| 168 | HPI Fill Gas | [[]] | 1 |
| 169 | HPI Fill Gas | [[]] | 1 |
| 170 | HPI Fill Gas | [[]] | 1 |
| 171 | ---Not Used--- | | |
| 172* | Material Basket [[]] | [[]] | 3 |
| 173* | [[]] | Cask Lid Or Cask Bottom | 2 |

Note: * Used only if the material basket, HPI, and/or cask are not centered axially in the cavities (NCT).

[[

]]

Figure 3.3-5. Thermal Contact Pair Locations in the Finite Element Model

Boundary Conditions

The following boundary conditions are applied to the model to simulate NCT (steady-state analysis with the package modeled in an upright orientation):

- 1) Natural convection from the package external surfaces to the 100°F environment
- 2) Thermal radiation (emissivity, ϵ , of package surfaces approximately 0.22 (see Table 3.2.1-1))
- 3) Solar heat flux per 10 CFR 71.71 (additional case is run without solar heat flux to address the requirements of 10 CFR 71.43(g))
- 4) Heat flux to material basket [[]] to simulate the content heat generation.

Natural Convection and Thermal Radiation to the Environment

Heat is rejected from the model via natural convection and thermal radiation boundary conditions. In order to simplify the application of boundary conditions, a single convection boundary condition is applied to each external surface of the package that has a convection coefficient (h), combining natural convection (h_c) based on the geometry of that surface and thermal radiation (h_r) based on the emissivity of that surface. This combined, temperature-dependent convection coefficient ($h_c + h_r$) is defined for each external surface and stored in an ANSYS material property definition.

The natural convection coefficient is calculated using the following from Reference 3-3, Equation 9.24:

$$h_c = \frac{Nu \times k}{L}$$

where, Nu = Nusselt number,

k = thermal conductivity of air at the film temperature, and

L = characteristic length of the surface.

The Nusselt number (Nu) is a function of surface geometry and the Rayleigh number (Ra). The Rayleigh number is, in turn, a function of surface geometry, temperature, and properties of the surrounding air and is calculated using the following equation from Reference 3-3, Equation 9.25:

$$Ra = \frac{g \beta (T_s - T_\infty) L^3}{\nu \alpha}$$

where, g = gravitational constant (386.1 in/s²),

β = $1/(T_f + 459.67)$,

T_f = film temperature = $(T_s + T_\infty)/2$,

T_s = surface temperature,

T_∞ = ambient temperature,

L = characteristic length,

ν = air kinematic viscosity at T_f , and
 α = air thermal diffusivity at T_f .

Horizontal Cylinder—natural convection to environment

The characteristic length, L , of a horizontal cylinder is its diameter, D . The Nusselt number for a horizontal cylinder for a wide range of Rayleigh numbers is calculated using the following equation (Reference 3-3, Equation 9.34):

$$Nu = \left\{ 0.60 + \frac{0.387 Ra^{1/6}}{[1 + (0.559/Pr)^{9/16}]^{8/27}} \right\}^2 (Ra \leq 10^{12})$$

where, Ra = Rayleigh number, and

Pr = Prandtl number.

Horizontal Plate—natural convection environment

The characteristic length, L , of a horizontal plate is the ratio of its surface area to its perimeter (for circular plates, this is equal to $D/4$, where D = the plate diameter). The Nusselt number for the upper surface of a heated horizontal plate is calculated using one of the following equations (Reference 3-3, Equations 9.30 and 9.31):

$$Nu = 0.54 Ra^{1/4} \quad (10^4 \leq Ra \leq 10^7)$$

$$Nu = 0.54 Ra^{1/3} \quad (10^4 \leq Ra \leq 10^7)$$

The Nusselt number for the lower surface of a heated horizontal plate is calculated using the following equation (Reference 3-3, Equation 9.32):

$$Nu = 0.27 Ra^{1/4}$$

Vertical Flat Plate—natural convection to environment

The characteristic length, L , of a flat plate is its length. The Nusselt number for a vertical plate over the entire range of Rayleigh numbers (laminar and turbulent) is calculated using the following equation (Reference 3-3, Equation 9.26):

$$Nu = \left\{ 0.825 + \frac{0.387 Ra^{1/6}}{[1 + (0.492/Pr)^{9/16}]^{8/27}} \right\}^2$$

For laminar flow (i.e., $Ra < 10^9$), the Nusselt number for a vertical flat plate is calculated with slightly better accuracy using the following equation (Reference 3-3, Equation 9.27):

$$Nu = 0.68 + \frac{0.670 Ra^{1/4}}{[1 + (0.492/Pr)^{9/16}]^{4/9}}$$

The thermophysical properties of air used in the calculation of the natural convection coefficients are presented in Table 3.3-4.

**Table 3.3-4. Thermophysical Properties of Dry Air
(from Reference 3-3)**

| Temperature (°F) | Density (lbm/in ³) | Thermal Conductivity (Btu/h-in-°F) | Specific Heat (Btu/lbm-°F) | Viscosity (in ² /h) | Thermal Diffusivity (in ² /h) | Prandtl Number |
|---------------------|-----------------------------------|------------------------------------------|-------------------------------|-----------------------------------|------------------------------------------------|-------------------|
| -10 | 5.039E-5 | 1.074E-3 | 2.403E-1 | 6.384E+1 | 8.872E+1 | 0.720 |
| 80 | 4.196E-5 | 1.266E-3 | 2.405E-1 | 8.867E+1 | 1.255E+2 | 0.707 |
| 170 | 3.595E-5 | 1.445E-3 | 2.410E-1 | 1.167E+2 | 1.668E+2 | 0.700 |
| 260 | 3.147E-5 | 1.628E-3 | 2.422E-1 | 1.474E+2 | 2.137E+2 | 0.690 |
| 350 | 2.796E-5 | 1.796E-3 | 2.439E-1 | 1.807E+2 | 2.634E+2 | 0.686 |
| 440 | 2.516E-5 | 1.960E-3 | 2.460E-1 | 2.164E+2 | 3.164E+2 | 0.684 |
| 530 | 2.286E-5 | 2.114E-3 | 2.484E-1 | 2.543E+2 | 3.722E+2 | 0.683 |
| 620 | 2.097E-5 | 2.258E-3 | 2.510E-1 | 2.940E+2 | 4.291E+2 | 0.685 |
| 710 | 1.935E-5 | 2.393E-3 | 2.539E-1 | 3.360E+2 | 4.871E+2 | 0.690 |
| 800 | 1.797E-5 | 2.523E-3 | 2.568E-1 | 3.800E+2 | 5.468E+2 | 0.695 |
| 890 | 1.677E-5 | 2.644E-3 | 2.596E-1 | 4.261E+2 | 6.082E+2 | 0.702 |
| 980 | 1.573E-5 | 2.759E-3 | 2.625E-1 | 4.739E+2 | 6.696E+2 | 0.709 |
| 1070 | 1.480E-5 | 2.870E-3 | 2.651E-1 | 5.234E+2 | 7.310E+2 | 0.716 |
| 1160 | 1.397E-5 | 2.985E-3 | 2.678E-1 | 5.742E+2 | 7.979E+2 | 0.720 |
| 1250 | 1.324E-5 | 3.096E-3 | 2.702E-1 | 6.261E+2 | 8.649E+2 | 0.723 |
| 1340 | 1.258E-5 | 3.212E-3 | 2.725E-1 | 6.802E+2 | 9.374E+2 | 0.726 |
| 1520 | 1.144E-5 | 3.443E-3 | 2.768E-1 | 7.912E+2 | 1.088E+3 | 0.728 |

Forced Convection Correlations

During the HAC 30-minute fire, heat is transferred from the environment to the model via forced convection and thermal radiation boundary conditions. Again, in order to simplify the application of boundary conditions, a single convection boundary condition is applied to each external surface of the package that has a convection coefficient (h) combining forced convection (h_c) based on the geometry of that surface and thermal radiation (h_r) based on the emissivity of that surface. This combined temperature-dependent convection coefficient ($h_c + h_r$) is defined for each external surface and stored in an ANSYS material property definition.

The forced convection coefficient is calculated using the following equation (Reference 3-3, Equation 6.5.7):

$$h_c = \frac{Nu \times k}{L}$$

where, Nu = Nusselt number,
 k = thermal conductivity of air at the film temperature, and
 L = characteristic length of the surface.

The Nusselt number (Nu) is a function the Reynolds number (Re) and the Prandtl number. The Reynolds number is, in turn, a function of surface geometry, temperature, flow velocity, and properties (density and viscosity) of the surrounding air, which is calculated using the following equation (Reference 3-3, Equation 6.45):

$$Re = \frac{VL}{\nu}$$

where, V = air free-stream velocity,
 L = characteristic length,
 ν = air dynamic viscosity at T_f ,
 T_f = film temperature = $(T_s + T_\infty)/2$,
 T_s = surface temperature, and
 T_∞ = ambient temperature.

Cylinder in Cross Flow—forced convection from environment to package

The characteristic length, L , of a cylinder is its diameter, D . The Nusselt number for a cylinder in cross flow is calculated using the following equation (Reference 3-3, Equation 7.55b):

$$Nu = C Re_D^m Pr^{1/3}$$

where, Re_D = Reynolds number, and
 Pr = Prandtl number.

The constants ‘C’ and ‘m’ in the previous equation are functions of the Reynolds number (Re_D) and are listed in Table 3.3-5.

Table 3.3-5. Constants 'C' and 'm' for the Nusselt Number Calculation of a Cylinder in Cross Flow (from Reference 3-3, Table 7.2)

| Re_D | C | m |
|-----------------------|----------|----------|
| 0.4 – 4 | 0.989 | 0.330 |
| 4 – 40 | 0.911 | 0.385 |
| 40 – 4,000 | 0.683 | 0.466 |
| 4,000 – 40,000 | 0.193 | 0.618 |
| 40,000 – 400,000 | 0.027 | 0.805 |

For mixed parallel flow (laminar and turbulent), the Nusselt number for a flat plate is calculated using the following equation (Reference 3-3, Equation 7.44):

$$Nu = 0.037 Re_L^{4/5} Pr^{1/3} (5 \times 10^5 < Re_L \leq 10^8)$$

where, Re_L = Reynolds number.

For mixed parallel flow (laminar and turbulent), the Nusselt number for a flat plate is calculated using the following equation (Reference 3-3, Equation 7.44):

$$Nu = 0.037 Re_L^{4/5} Pr^{1/3} (5 \times 10^5 < Re_L \leq 10^8)$$

Thermal Radiation to Environment

As previously discussed, the convection boundary conditions applied to the model are a combination of both natural convection and thermal radiation coefficients. The thermal radiation coefficient (hr) is calculated by linearizing the radiation. Assuming a view factor of 1.0 with the surroundings, the heat transfer rate by thermal radiation, Q_{rad} , from a surface can be described as follows:

$$Q_{rad} = \epsilon \sigma A (T_s^4 - T_\infty^4)$$

where, ϵ = emissivity,

σ = Stefan-Boltzmann constant (1.19 E -11 Btu/h-in²-°F),

A = surface area,

T_s = surface temperature (R), and

T_∞ = temperature of surroundings (R).

Due to the temperatures being raised to the 4th power in the previous equation, the heat transfer rate is nonlinear. Instead, treating the thermal radiation as a convection boundary condition and substituting hr (radiation coefficient) for hc (convection coefficient) yields the linear equation:

$$Q_{rad} = hr A (T_s - T_\infty)$$

Setting the two equations for Qrad equal to each other yields the following equation:

$$hr A(T_s - T_\infty) = \varepsilon \sigma A (T_s^4 - T_\infty^4)$$

Solving for the thermal radiation coefficient (hr) yields:

$$hr = \varepsilon \sigma (T_s^2 + T_\infty^2)(T_s + T_\infty)$$

Normal Conditions Convection Coefficients

During normal transport, the Model 2000 Transport Package is transported in an upright orientation as depicted in Figure 1.2-3. For the purpose of calculating natural convection coefficients, the overpack top and bottom toroidal shells are approximated as horizontal cylinders ($L = D = 24$ inches), the overpack top cover is approximated as a heated flat plate facing up ($L = D/4 = 48$ inches/ $4 = 12$ inches), the overpack bottom end plate is approximated as a heat flat plate facing down ($L = D/4 = 24$ inches/ $4 = 6$ inches), and the cylindrical sides of the overpack are approximated as a vertical plate ($L = 83.5$ inches). The convection boundary conditions for NCT are shown on a cross-section of the model in Figure 3.3-6. The calculated natural convection coefficients (hc) and radiation coefficient (hr) for NCT (in shade and with insolation) are presented graphically in Figure 3.3-7.

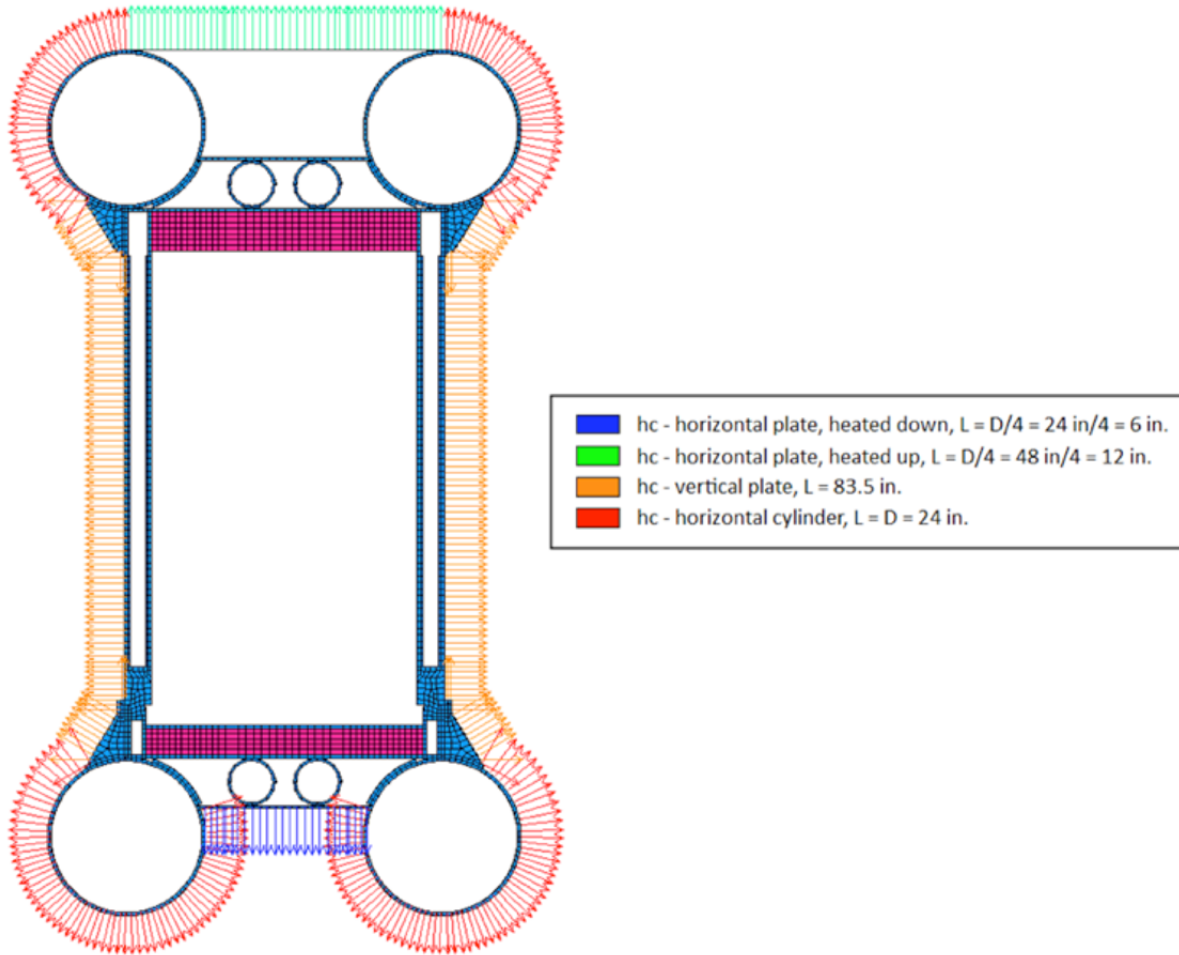


Figure 3.3-6. Natural Convection Boundary Conditions for NCT

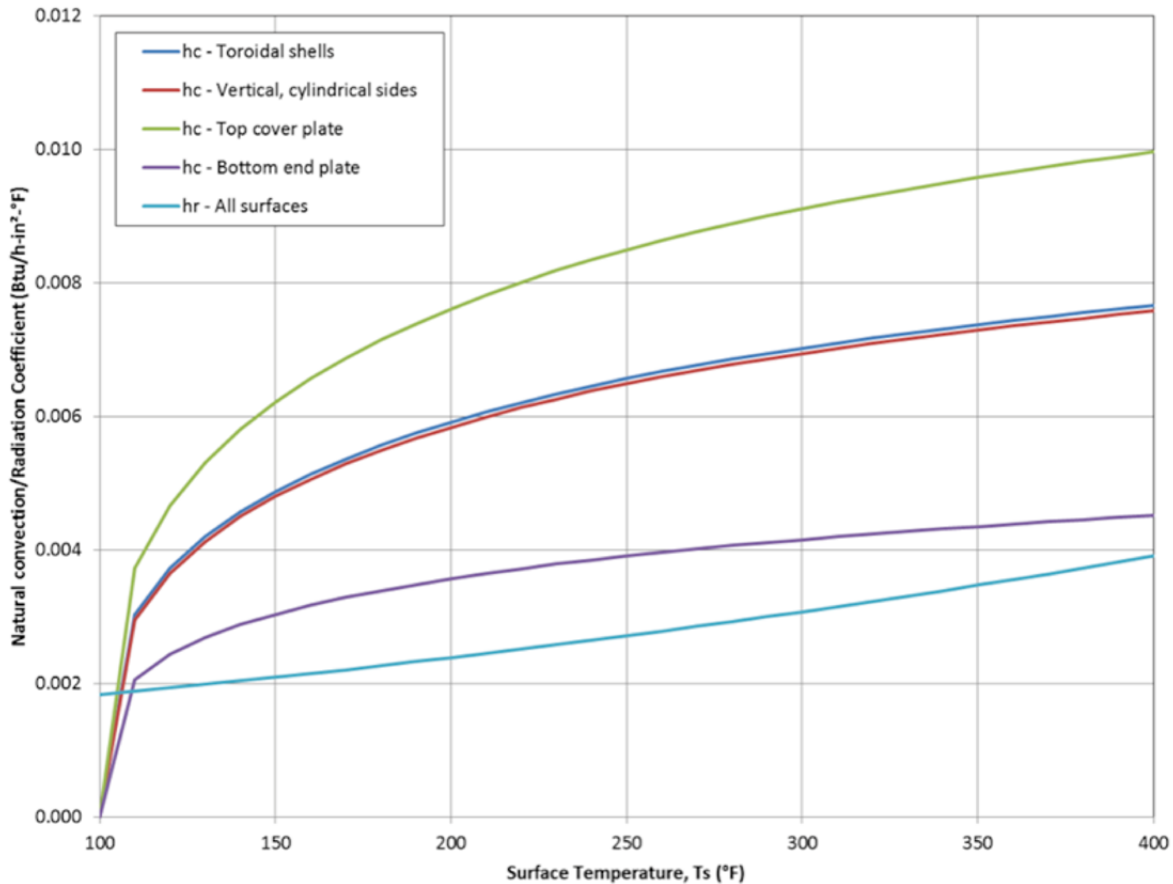


Figure 3.3-7. Natural Convection and Thermal Radiation Coefficients for NCT

(Note data for NCT in shade and with insolation)

Heat Generation by Contents

In order to utilize the 3000 W decay heat limit of Configuration 2, the HPI material basket must be used. The contents are not specifically modeled in the analyses. Rather, the 3000 W of decay heat is included as a heat flux applied to the material basket [[]] contained within the HPI.

As described in Section 1.2.2.2, the material basket has nineteen locations that are formed by twenty [[]] and [[]]. The center position does not have a full-length [[]], but instead two 2.0-inch long [[]], one fastened at either end, form the center area. In the thermal model, the 3000 W of decay heat is assumed to be evenly distributed among the nineteen [[]]; therefore, each [[]] has approximately 157.9 W applied to its inner surface as a uniformly distributed heat flux over its length ([[]] inches). For the center area, the heat load is applied to the inner surface of the two shorter [[]] and to the external surfaces of the surrounding pipes where they would contact the center [[]] if one existed. This results in a lower heat flux at the center due to the larger area.

SURF152 elements are overlaid onto the SOLID70 thermal solid elements of the material basket [[]], and the heat flux is calculated based on the area of these elements. The actual area of the

SURF152 elements (obtained using the *GET command in ANSYS) is used to calculate the applied heat flux rather than using the area calculated from the dimensions of the [[]].

The heat flux, q''_{gen} , applied to the [[]] that surround the center [[]] is:

$$q''_{gen} = \frac{[[]] \times Q_{[[]}}{A_{SURF152}} = \frac{[[]] \times 157.9 W \left(\frac{3.4123 Btu/h}{W} \right)}{2 \times 2021.89204 in^2} = 2.398 \frac{Btu}{h-in^2}$$

where, $A_{SURF152}$ = the area of the SURF152 elements overlaid on the inner surface of the [[]] (note: multiplied by 2 to account for the half-symmetry of the model).

Similarly, the heat flux applied to the center [[]] and outer surfaces of the [[]] around the center region is:

$$q''_{gen} = \frac{Q_{[[]}}{A_{SURF152}} = \frac{157.9 W \left(\frac{3.4123 Btu/h}{W} \right)}{2 \times 229.78484 in^2} = 1.172 \frac{Btu}{h-in^2}$$

where, $A_{SURF152}$ = the area of the SURF152 elements overlaid on the inner surface of the center [[]] plus the outer surfaces of the [[]] surrounding the center [[]] (note: multiplied by 2 to account for the half-symmetry of the model).

The actual heat flux applied to the material basket [[]] is shown in Figure 3.3-8.

[[

]]

Figure 3.3-8. Contents Heat Flux Applied to Material Basket [[]]

3.3.1. Heat and Cold

3.3.1.1. Hot Case

3.3.1.1.1. NCT Solar Heat Flux (Insolation)

Per the requirements of the regulations for NCT, the Model 2000 Transport Package is exposed to an ambient temperature of 100°F and insolation according to Table 3-1. The solar heat fluxes specified to Table 3-1 are per 12-hour period. This 12-hour period represents a 12-hour long “day” in a 24-hour day/night cycle. Because the solar heat flux is constant, the insolation value should be time averaged over 24 hours in order to maintain the proper total heat flux to the package over the full day/night cycle. Therefore, to simulate a day-night cycle, these heat fluxes are time-averaged over a 24-hour period as follows:

Flat surfaces (other than transported horizontally base)

$$q'' = \frac{800 \text{ cal/cm}^2}{24 \text{ h}} \left(\frac{4.1868 \text{ J}}{\text{cal}} \right) \left(\frac{100 \text{ cm}}{\text{m}} \right)^2 \left(\frac{1 \text{ h}}{3600 \text{ s}} \right) \left(\frac{1 \text{ W}}{1 \text{ J/s}} \right) \left(\frac{0.3171 \frac{\text{Btu}}{\text{h-ft}^2}}{1 \text{ W/m}^2} \right) \left(\frac{1 \text{ ft}^2}{144 \text{ in}^2} \right)$$

$$= 0.854 \frac{Btu}{h \cdot in^2}$$

Curved surfaces

$$q'' = \frac{400 \text{ cal/cm}^2}{24 \text{ h}} \left(\frac{4.1868 \text{ J}}{\text{cal}} \right) \left(\frac{100 \text{ cm}}{\text{m}} \right)^2 \left(\frac{1 \text{ h}}{3600 \text{ s}} \right) \left(\frac{1 \text{ W}}{1 \text{ J/s}} \right) \left(\frac{0.3171 \frac{Btu}{h \cdot ft^2}}{1 \text{ W/m}^2} \right) \left(\frac{1 \text{ ft}^2}{144 \text{ in}^2} \right)$$

$$= 0.427 \frac{Btu}{h \cdot in^2}$$

Flat surfaces not transported horizontally

$$q'' = \frac{200 \text{ cal/cm}^2}{24 \text{ h}} \left(\frac{4.1868 \text{ J}}{\text{cal}} \right) \left(\frac{100 \text{ cm}}{\text{m}} \right)^2 \left(\frac{1 \text{ h}}{3600 \text{ s}} \right) \left(\frac{1 \text{ W}}{1 \text{ J/s}} \right) \left(\frac{0.3171 \frac{Btu}{h \cdot ft^2}}{1 \text{ W/m}^2} \right) \left(\frac{1 \text{ ft}^2}{144 \text{ in}^2} \right)$$

$$= 0.214 \frac{Btu}{h \cdot in^2}$$

During normal transport, the Model 2000 Transport Package is oriented in an upright position. As such, for the case with insolation, a heat flux of 0.854 Btu/h-in² is applied to the top cover plate, and a heat flux of 0.427 Btu/h-in² is applied to the toroidal shells and overpack sides as shown in Figure 3.3.1-1.

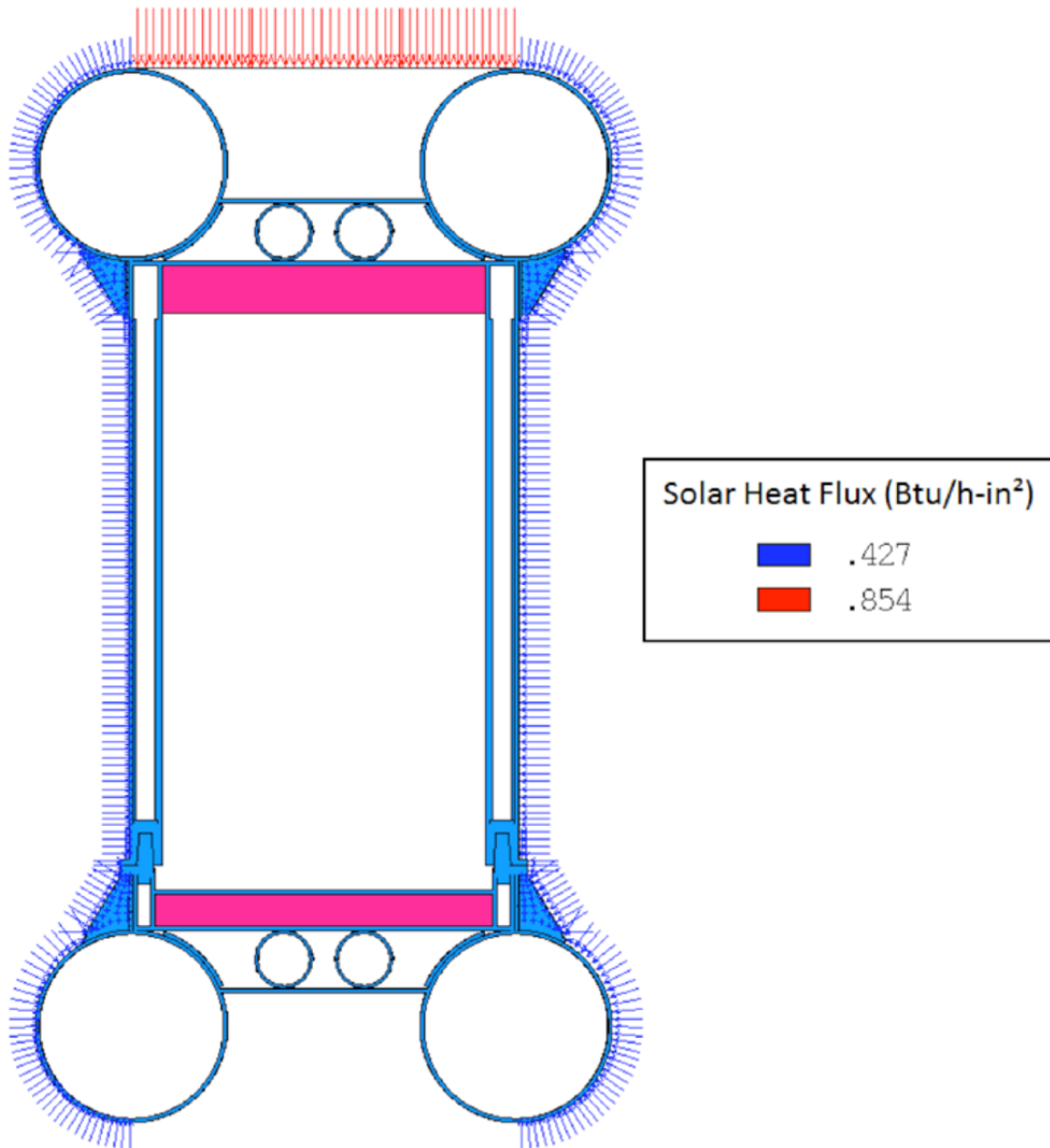


Figure 3.3.1-1. Solar Heat Flux Boundary Conditions for NCT

3.3.1.1.2. Detailed NCT Results

The results of the steady-state thermal analyses are presented in tabular format in Table 3.3.1-1 and graphically (temperature contours) in Figure 3.3.1-2. The Configuration 2 thermal analysis demonstrates that the Model 2000 Transport Package components remain below their allowable temperatures for NCT with insolation. There is no change in material conditions that would affect structural, shielding, or impact-limiting performance. Further, the package will maintain containment of the contents.

Table 3.3.1-1. Temperature Results, NCT (in Shade and with Insolation)

| Component | 100°F Ambient Temperature, in Shade, (°F) | | | 100°F Ambient Temperature, with Insolation (°F) | | |
|--------------------------------------------|-------------------------------------------|-----|-----|-------------------------------------------------|-----|-----|
| | Max | Min | Avg | Max | Min | Avg |
| Material Basket | 989 | 465 | 801 | 1,001 | 490 | 815 |
| HPI | 581 | 360 | --- | 604 | 388 | --- |
| HPI shielding (top) | 517 | 506 | 513 | 539 | 529 | 535 |
| HPI shielding (sides) | 581 | 435 | 544 | 601 | 460 | 565 |
| HPI shielding (bottom) | 477 | 427 | 451 | 501 | 452 | 475 |
| Cask (bottom, shells, top, lid) | 430 | 309 | --- | 455 | 338 | --- |
| Cask shielding (lid) | 424 | 408 | 414 | 449 | 433 | 440 |
| Cask shielding (sides) | 405 | 341 | 385 | 431 | 370 | 412 |
| Cask lid seal | 406 | 383 | --- | 432 | 409 | --- |
| Cask drain port (bottom) | 342 | 309 | --- | 370 | 338 | --- |
| Cask test port (top) | 400 | 383 | --- | 426 | 409 | --- |
| Cask vent port (lid) | 416 | 410 | --- | 442 | 435 | --- |
| Overpack base | 335 | 159 | --- | 364 | 184 | --- |
| Overpack cover | 272 | 108 | --- | 308 | 174 | --- |
| Overpack toroidal shell (top) | 159 | 110 | 125 | 207 | 165 | 179 |
| Overpack toroidal shell (bottom) | 215 | 114 | 139 | 249 | 136 | 176 |
| Overpack honeycomb impact limiter (top) | 220 | 205 | 215 | 263 | 249 | 258 |
| Overpack honeycomb impact limiter (bottom) | 330 | 275 | 304 | 359 | 305 | 334 |
| HPI fill gas | 971 | 460 | 672 | 983 | 485 | 689 |
| Cask fill gas | 574 | 346 | 462 | 594 | 374 | 486 |
| HPI and Cask fill gas, combined | 971 | 346 | 481 | 983 | 374 | 505 |

[[

]]

Figure 3.3.1-2. Steady-State Temperature Distribution—NCT (Configuration 2)

3.3.1.1.3. Maximum Surface Temperature Results

Configuration 2 is also evaluated to the requirements of 10 CFR 71.43(g) (Reference 3-1), which requires that no accessible surface of the package exceed 185°F in an exclusive use shipment when exposed to a 100°F ambient temperature in still air and shade. As shown in Figure 3.3.1-3, the overpack in the region of the bolting ring exceeds the allowable temperature of 185°F. Therefore, a personnel barrier not part of the packaging will be used to block access to this region when readied for transport.

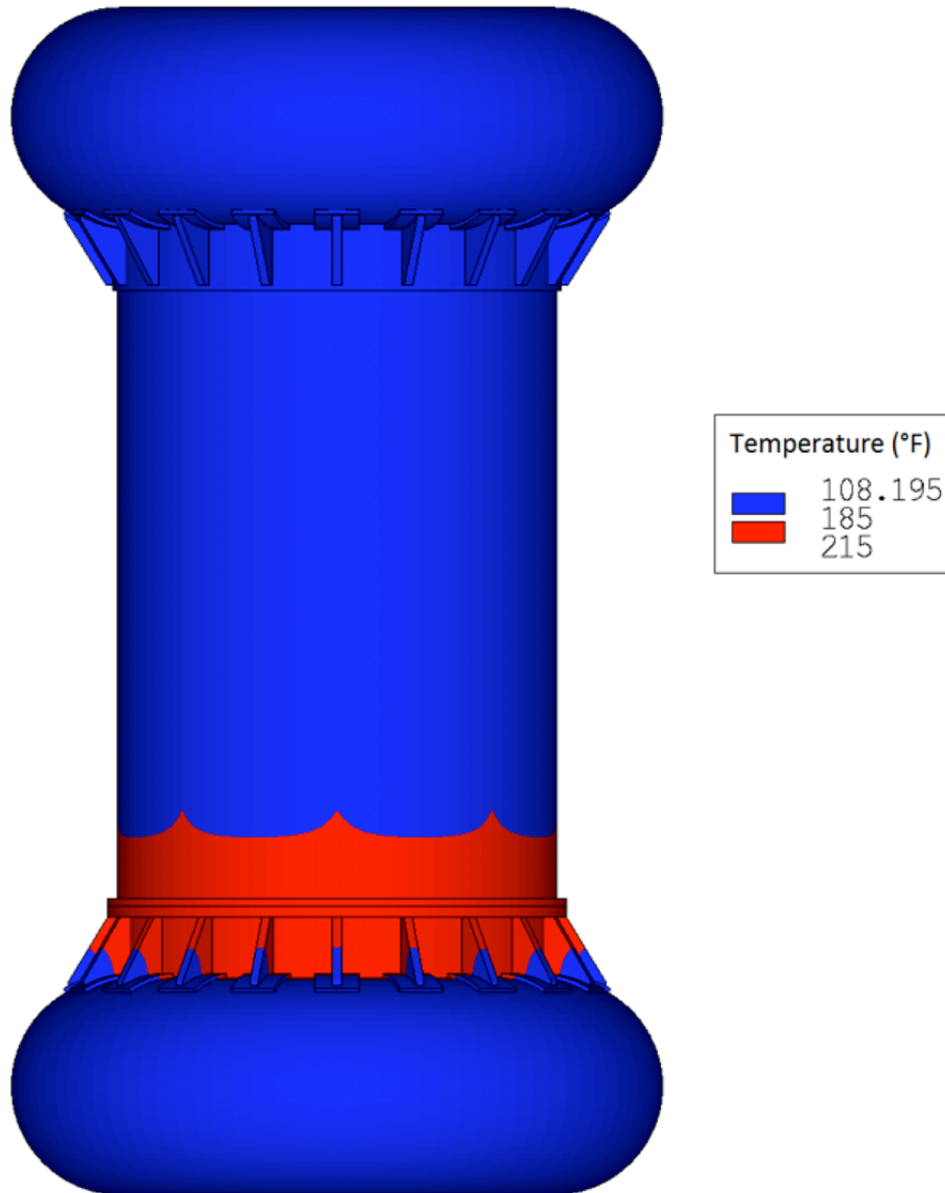


Figure 3.3.1-3. Overpack Steady-State Temperatures, 100°F Ambient Temperature (Configuration 2)

(Note: Assumes ambient temperature in shade)

3.3.1.1.4. NCT Thermal Contact Resistance Sensitivity Study

The presented thermal analyses have thermal contact resistance modeled between contacting components that have a mixture of low (perfect contact) to high resistance levels as discussed above. In order to assess the effect that using the mixed thermal resistance levels have on package temperatures, the analyses for NCT (with insulation) is repeated with all of the thermal resistance levels set to “low” (i.e., perfect contact). The results of this analysis is compared with the results from Table 3.3.1-1, and presented in Table 3.3.1-2.

Table 3.3.1-2. Comparison of Mixed and Perfect Thermal Contact for NCT with Insolation

| Item | 100°F Ambient temperature, with insolation, mixed thermal contact resistance ¹ (°F) | | | 100°F Ambient temperature, with insolation, perfect contact (°F) | | |
|--------------------------------------------|------------------------------------------------------------------------------------------------|-----|-----|------------------------------------------------------------------|-----|-----|
| | Max | Min | Avg | Max | Min | Avg |
| Material Basket | 1,001 | 490 | 815 | 998 | 482 | 811 |
| HPI | 604 | 388 | --- | 598 | 379 | --- |
| HPI shielding (top) | 539 | 529 | 535 | 534 | 523 | 530 |
| HPI shielding (sides) | 601 | 460 | 565 | 596 | 452 | 559 |
| HPI shielding (bottom) | 501 | 452 | 475 | 494 | 444 | 468 |
| Cask (bottom, shells, top, lid) | 455 | 338 | --- | 450 | 327 | --- |
| Cask shielding (lid) | 449 | 433 | 440 | 443 | 428 | 434 |
| Cask shielding (sides) | 431 | 370 | 412 | 426 | 361 | 407 |
| Cask lid seal | 432 | 409 | --- | 428 | 405 | --- |
| Cask drain port (bottom) | 370 | 338 | --- | 362 | 327 | --- |
| Cask test port (top) | 426 | 409 | --- | 422 | 405 | --- |
| Cask vent port (lid) | 442 | 435 | --- | 436 | 430 | --- |
| Overpack base | 364 | 184 | --- | 356 | 184 | --- |
| Overpack cover | 308 | 174 | --- | 305 | 174 | --- |
| Overpack toroidal shell (top) | 207 | 165 | 179 | 206 | 165 | 179 |
| Overpack toroidal shell (bottom) | 249 | 136 | 176 | 250 | 136 | 177 |
| Overpack honeycomb impact limiter (top) | 263 | 249 | 258 | 259 | 243 | 254 |
| Overpack honeycomb impact limiter (bottom) | 359 | 305 | 334 | 355 | 298 | 329 |
| HPI fill gas | 983 | 485 | 689 | 979 | 477 | 684 |
| Cask fill gas | 594 | 374 | 486 | 589 | 366 | 480 |
| HPI and Cask fill gas, combined | 983 | 374 | 505 | 979 | 366 | 499 |

Note:

1. In general, the package temperatures are lower when modeling the thermal contact as perfect as opposed to the mixed thermal contact levels. This is because the mixed thermal contact resistances impede the flow of the heat generated by the contents from getting out of the package where it is rejected to the surroundings.

3.3.1.2. Cold Case

For the cold case, the thermal model is modified to calculate package temperatures for exposure to an ambient temperature of -40°F in the shade. Various content heat loads are considered, and the results are presented in Table 3.3.1-3. The cask lid seal and cask ports maintain temperatures above their minimum allowable temperatures presented in Table 3.1.3-1. It can be noted in this table that the minimum temperature at the cask lid seal and port O-rings is 21°F with an internal wattage of only 500 W.

Table 3.3.1-3. Model 2000 Transport Package Temperatures for Exposure to -40°F in Shade

| Item | Temperature (°F) | | | | | | | | | | | |
|---------------------------------|-------------------------------|-----|-----|---------------------------------|-----|-----|---------------------------------|-----|-----|---------------------------------|-----|-----|
| | Q _{contents} = 500 W | | | Q _{contents} = 1,000 W | | | Q _{contents} = 2,000 W | | | Q _{contents} = 3,000 W | | |
| | Max | Min | Avg | Max | Min | Avg | Max | Min | Avg | Max | Min | Avg |
| Material Basket | 259 | 66 | 195 | 460 | 150 | 357 | 745 | 283 | 588 | 954 | 387 | 756 |
| HPI | 104 | 36 | --- | 216 | 96 | --- | 391 | 193 | --- | 523 | 269 | --- |
| HPI shielding (top) | 84 | 81 | 83 | 182 | 176 | 179 | 334 | 325 | 331 | 451 | 439 | 446 |
| HPI shielding (sides) | 103 | 59 | 91 | 214 | 136 | 194 | 388 | 259 | 355 | 520 | 355 | 478 |
| HPI shielding (bottom) | 69 | 57 | 63 | 155 | 132 | 143 | 291 | 252 | 271 | 400 | 346 | 372 |
| Cask (bottom, shells, top, lid) | 55 | 21 | --- | 132 | 69 | --- | 256 | 147 | --- | 354 | 209 | --- |
| Cask shielding (lid) | 54 | 51 | 52 | 129 | 123 | 126 | 251 | 239 | 244 | 347 | 330 | 337 |
| Cask shielding (sides) | 49 | 31 | 42 | 120 | 87 | 108 | 235 | 177 | 215 | 325 | 249 | 300 |
| Cask lid seal | 50 | 45 | --- | 122 | 113 | --- | 237 | 221 | --- | 328 | 304 | --- |
| Cask drain port (bottom) | 31 | 21 | --- | 88 | 69 | --- | 178 | 147 | --- | 250 | 209 | --- |
| Cask test port (top) | 48 | 45 | --- | 119 | 113 | --- | 232 | 221 | --- | 321 | 304 | --- |
| Cask vent port (lid) | 52 | 51 | --- | 127 | 124 | --- | 246 | 241 | --- | 339 | 332 | --- |
| Overpack base | 30 | -22 | --- | 84 | -9 | --- | 171 | 11 | --- | 240 | 27 | --- |
| Overpack cover | -2 | -38 | --- | 32 | -37 | --- | 96 | -36 | --- | 155 | -34 | --- |
| Overpack toroid (top) | -28 | -37 | -34 | -17 | -36 | -30 | 4 | -34 | -22 | 24 | -32 | -14 |
| Overpack toroid (bottom) | -6 | -36 | -28 | 19 | -34 | -21 | 60 | -31 | -8 | 94 | -29 | 2 |
| Overpack honeycomb (top) | -16 | -19 | -17 | 7 | 0 | 4 | 50 | 38 | 46 | 93 | 75 | 87 |
| Overpack honeycomb (bottom) | 29 | 10 | 20 | 82 | 49 | 67 | 167 | 113 | 143 | 235 | 165 | 204 |
| HPI fill gas | 255 | 65 | 147 | 453 | 148 | 281 | 732 | 279 | 476 | 935 | 382 | 619 |
| Cask fill gas | 101 | 32 | 66 | 212 | 89 | 150 | 383 | 180 | 283 | 513 | 253 | 387 |
| HPI + Cask fill gas, combined | 255 | 32 | 74 | 453 | 89 | 162 | 732 | 180 | 301 | 935 | 253 | 408 |

3.3.2. Maximum Normal Operating Pressure

3.3.2.1. NCT Pressure Evaluation

During NCT, the average temperature of the cask fill gas (including the gas within the HPI) is 505°F. Using the ideal gas law, the cask internal pressure from gas expansion is:

$$\frac{P_1}{T_1} = \frac{P_2}{T_2}$$

$$P_2 = 14.7 \text{ psia} \times \left(\frac{505+460}{70+460} \right) = 26.8 \text{ psia} < 30 \text{ psia}$$

where,

$$\begin{aligned} P_1 &= 14.7 \text{ psia} && \text{initial fill gas pressure,} \\ T_1 &= 70^\circ\text{F} && \text{initial fill gas temperature, and} \\ T_2 &= 505^\circ\text{F} && \text{average gas volume temperature during NCT.} \end{aligned}$$

The cask internal pressure during NCT is less than the design pressure of 30 psia. Therefore, no further evaluation is required.

3.4 Thermal Evaluation under Hypothetical Accident Conditions

The thermal performance of Configuration 2 is analyzed for HAC by performing a transient heat transfer analysis on a finite element representation of the package. The model represents the Model 2000 Transport Package with damage consistent with a 30-foot side drop and 40-inch drop onto a 6-inch pin. Again, the general-purpose finite element code ANSYS, Release 14.0, is used to analyze the Model 2000 Transport Package with a content heat load of 3000 W for HAC. Several ANSYS macros are created in order to build the model, modify nodal locations to simulate damage, apply boundary conditions, and perform the transient analysis. Many of the macros used to evaluate the package for NCT are used to evaluate it for HAC.

Assumptions made for this evaluation are:

- The package is assumed to be in a horizontal orientation during the HAC fire because the package is modeled with damage consistent with a side drop.
- The cask and HPI are backfilled with Helium at 70°F and 14.7 psia.
- Natural convection within the package cavities is neglected.
- The contents of the HPI are assumed to generate a maximum of 3000 W that is uniformly distributed among the [[]] material basket [[]] and is consistent with the isotope rod design where the Co-60 source is uniformly distributed along the length of each rod [[]].
- For HAC, the package is assumed to be exposed to the NCT prior to and following the 30-minute fire.
- During pre-fire/post-fire HAC, the package is assumed to have an emissivity consistent with the material of construction at temperature. However, during the HAC fire, the

package is assumed to have an emissivity value of 0.9. Post-fire, the package is assumed to have an emissivity value of 0.8.

Boundary Conditions

The following boundary conditions are applied to the model to simulate HAC (with the package modeled in a horizontal orientation):

Pre-fire (steady-state analysis)

- Heat flux to material basket $[\dot{q}]$ to simulate the content heat generation
- Natural convection from the package external surfaces to the 100°F environment
- Thermal radiation (emissivity, ϵ , of package surfaces approximately 0.22 (see Table 3.2.1-1))
- Solar heat flux per 10 CFR 71.71

Thirty minute fire (transient analysis)

- Heat flux to material basket $[\dot{q}]$ to simulate the content heat generation
- Forced convection from the 1475°F environment to the package external surfaces
- Thermal radiation exchange between the fire and the package surfaces ($\epsilon = 0.9$)

Post-fire cool-down (transient analysis)

- Heat flux to material basket $[\dot{q}]$ to simulate the content heat generation
- Natural convection from the package external surfaces to the 100°F environment
- Thermal radiation ($\epsilon = 0.8$, which is consistent with a heavily oxidized steel surface)
- Solar heat flux per 10 CFR 71.71

3.4.1. Initial Conditions

When evaluating the package for the HAC 30-minute fire, the package must include damage from a 30-foot drop onto an unyielding surface and a 40-inch drop onto a 6-inch diameter pin (Reference 3-1). The structural evaluation of the Model 2000 Transport Package considers several drop orientations for HAC; however the side-drop orientation is chosen as the worst-case from a thermal standpoint. The reason for this is due primarily to the damage to the overpack side from the 40-inch drop onto the 6-inch diameter pin. The drop onto the pin causes the overpack outer and inner shells to come in contact—thus, creating a path for the heat from the fire to more easily reach the cask (and cask shielding). Although the damage from the drop onto the pin is not modeled in the deformed geometry (Figure 3.4.1-1), its effect is included by using LINK34 elements to model the contact of the two shells.

[[

]]

**Figure 3.4.1-1. Three-Dimensional Finite Element Model of the Model 2000
(Half Symmetry)**

(Note: damage consistent with that sustained from a 30-foot drop and 40-inch drop onto a 6-inch pin—elements representing air and helium not shown for clarity.)

3.4.1.1. Additional Thermal Contact for the Hypothetical Accident Condition

Because the Model 2000 Transport Package is assumed to be in a horizontal orientation during the HAC fire and cool-down, additional thermal contact modeling is required. The components are not physically shifted to be in contact (e.g., the sides of the cask shell contacting the overpack inner shell). Therefore, the CONTA173/TARGE170 pairs will not be appropriate to use to model the thermal contact that will be present when the package is oriented horizontally. To model the contact present when the package is on its side, LINK34 convection elements are incorporated into the model. Although these are convection elements, they can be used to model thermal contact because the thermal contact conductance has the same units as the convection coefficient used by these elements.

When oriented on its side, the contact between the material basket [[]], and HPI inner [[]], between the HPI [[]] and cask cavity shell, and between the cask shell and overpack [[]] are modeled with a “Low/Moderate” thermal contact resistance (thermal contact conductance of 15.0 Btu/h-in²-°F) and 2° of contact as shown in Figure 3.4.1-2. Additionally, the puncture damage is simulated by adding LINK34 elements (20° contact area) between the overpack inner and outer shells as shown in Figure 3.4.1-2. The “Low/Moderate” thermal contact resistance is chosen for these contact elements in order to maximize the heat from the contents and the HAC fire into the cask shield at the puncture location.

3.4.1.2. Hypothetical Accident Conditions Convection Coefficients

For HAC, the Model 2000 is modeled with damage simulating a side drop from 30 feet onto an unyielding surface followed by a drop from 40 inches onto a 6-inch diameter pin. The HAC thermal analysis simulates exposure of the model to a 30-minute fire following this side drop/puncture; therefore, the package is assumed to be on its side when exposed to the fire. For the purpose of calculating natural convection (pre-fire and post-fire) and forced convection (fire)

coefficients, the overpack sides are approximated as a horizontal cylinder ($L = D = 48.5$ inches), the overpack toroidal shells are approximated as horizontal cylinders ($L = D = 24$ inches), and the overpack top and bottom end plates are approximated as vertical flat plates ($L = D = 24$ inches). The convection boundary conditions for HAC are shown on a cross-section of the model in Figure 3.4.1-3. The calculated natural and forced convection coefficients (h_c) and radiation coefficients for HAC (pre-fire, fire, and post-fire cool-down) are presented graphically in Figure 3.4.1-4.

[[

]]

Figure 3.4.1-2. LINK34 Incorporated to Simulate HAC Side Contact and Puncture Damage

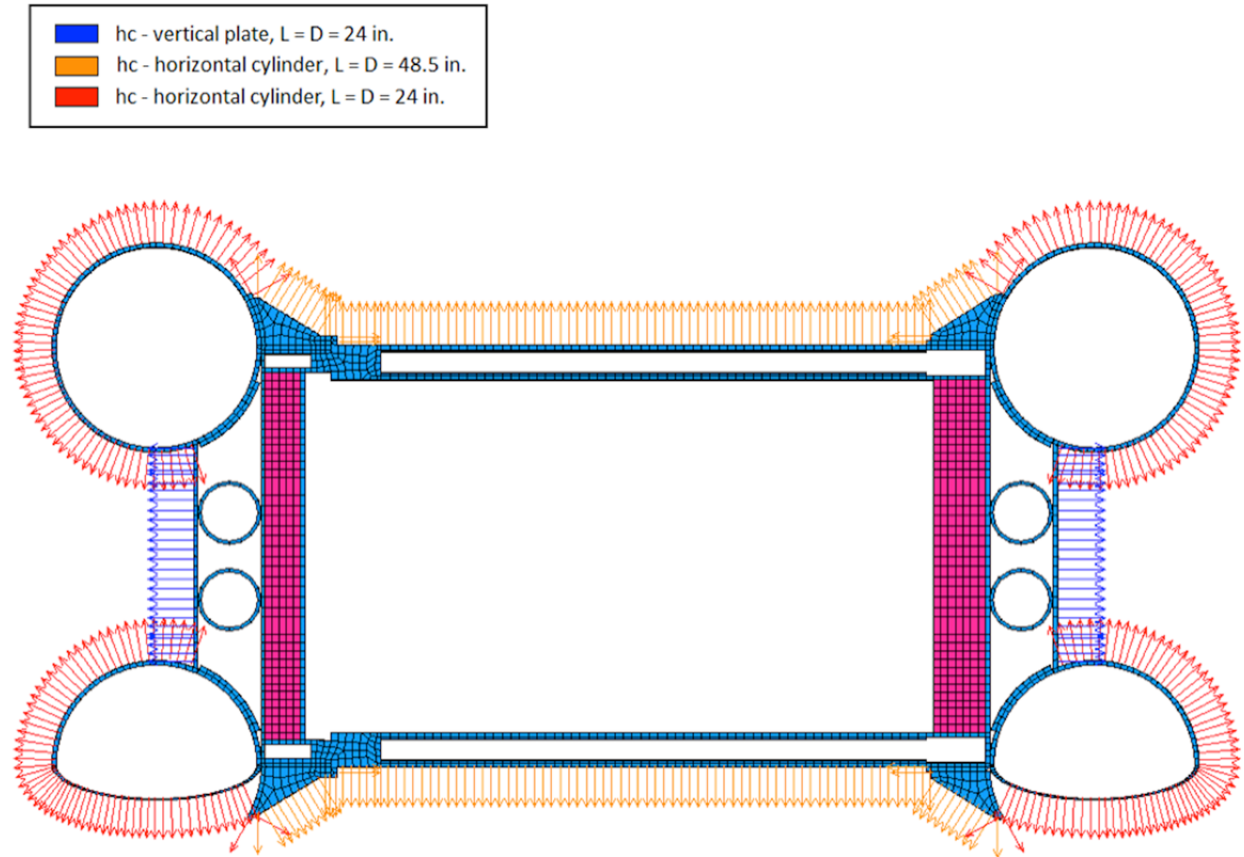


Figure 3.4.1-3. Natural Convection Boundary Conditions for HAC

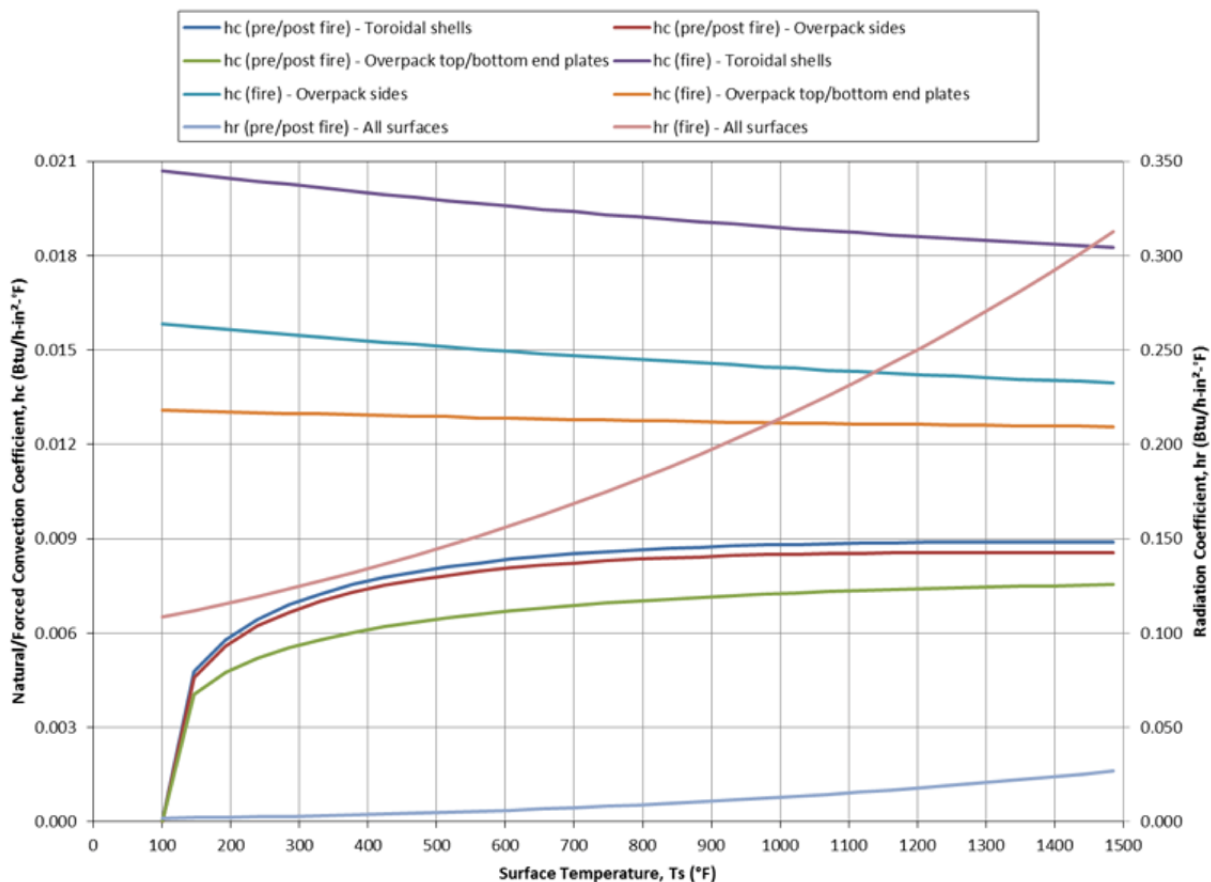


Figure 3.4.1-4. Natural/Forced Convection and Thermal Radiation Coefficients for HAC

(Note: Coefficients are for HAC Pre-Fire, Fire, and Post-Fire)

3.4.2. Fire Test Conditions

3.4.2.1. HAC Solar Heat Flux (Insolation)

Previous versions of 10 CFR 71.73 (i.e., prior to ~1997), stated that insolation need not be considered before, during, or after the 30-minute hypothetical accident fire. However, the current regulations do not specifically address whether insolation should be included prior to, during, or after the HAC fire. The HAC thermal analysis presented in this report does not include insolation during the HAC fire; however, insolation is applied to the package surfaces during steady-state conditions prior to the fire and during the transient post-fire cool-down. Because the side drop and side puncture damage is simulated for the HAC thermal evaluation, the Model 2000 Transport Package is assumed to be in a horizontal orientation. Therefore, prior to the fire and during the post-fire cool-down, a heat flux of 0.427 Btu/h-in² is applied to the toroidal shells and overpack sides, and a heat flux of 0.214 Btu/h-in² is applied to the overpack top and bottom end plates as shown in Figure 3.4.2-1.

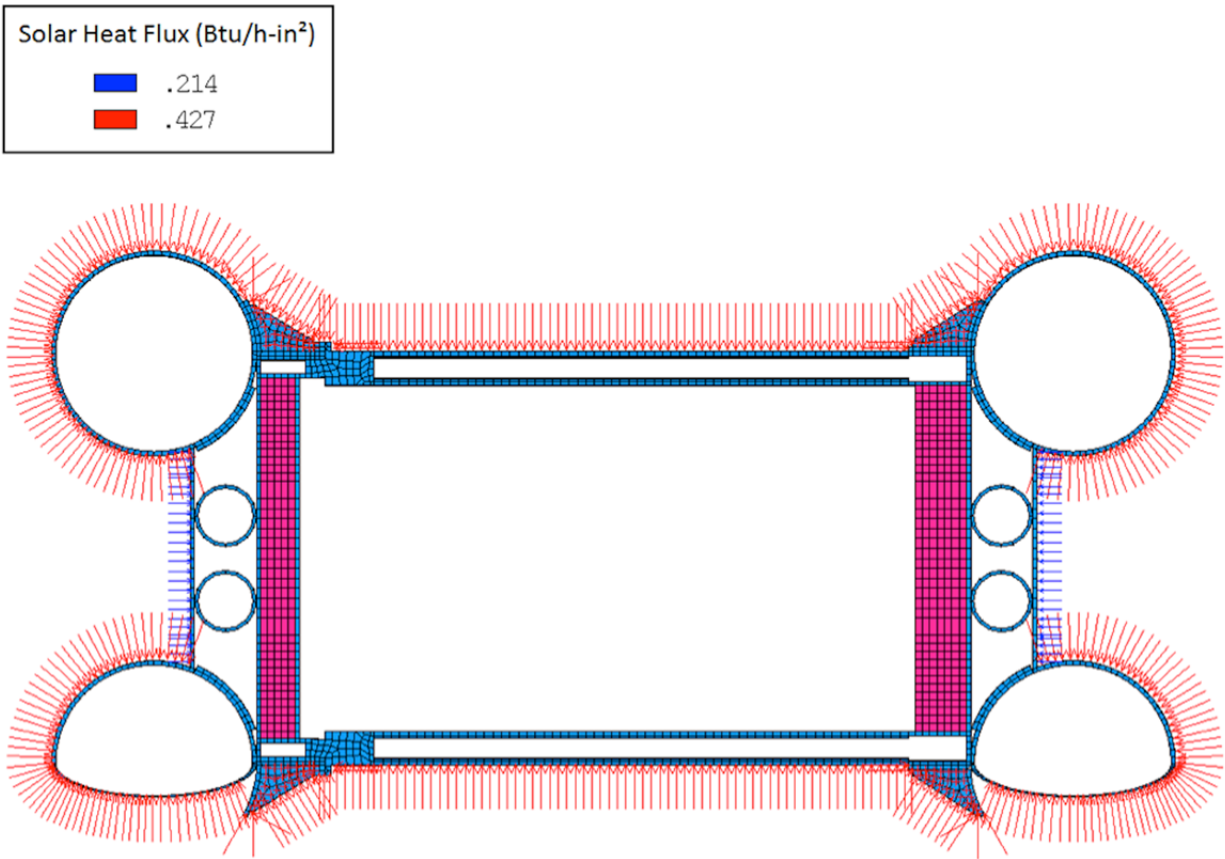


Figure 3.4.2-1. Solar Heat Flux Boundary Conditions for HAC (Post-Fire Cool-Down)

3.4.3. Maximum Temperatures and Pressure

When exposed to the HAC fire prescribed in 10 CFR 71.73(c)(4) (Reference 3-1), Configuration 2 must maintain containment of its contents and maintain its shielding capabilities. The results of the HAC thermal evaluation are presented in Table 3.4.3-1. Comparing with Table 3.1.3-1, it can be seen that the maximum temperatures of the different components are below the allowable temperatures. Therefore, the HAC fire will not adversely affect the package's ability to provide containment and shielding for its contents.

3.4.3.1. HAC Temperature Results

A transient thermal analysis was performed on the model. This transient analysis simulates exposure of the Model 2000 Transport Package to a 30-minute hypothetical accident fire followed by a 36-hour cool-down period in which the package is exposed to a 100°F ambient temperature and insolation (solar heat flux). The 36-hour cool-down period is of sufficient length to allow the package temperatures to reach their peak values. The results of the transient HAC thermal analysis are presented in Table 3.4.3-1.

Table 3.4.3-1. Temperature Results, Hypothetical Accident Conditions (Configuration 2)

| Item | Peak Temperature (°F) | Time at Which Peak Temperature Occurs (Hours) |
|----------------------------------------------------------|-----------------------|-----------------------------------------------|
| Material Basket | 1045 | 13.0 |
| HPI shielding (side) | 670 | 11.0 |
| HPI shielding (top) | 599 | 9.0 |
| HPI shielding (bottom) | 618 | 11.0 |
| Cask lid seal | 508 | 6.2 |
| Cask shielding (side) | 570 | 0.6 |
| Cask shielding (top) | 529 | 7.1 |
| Cask shell, puncture location | 782 | 0.5 |
| Cask shell, opposite side to puncture location | 512 | 4.0 |
| Overpack outer shell, puncture location | 1,103 | 0.5 |
| Overpack outer shell, opposite side to puncture location | 1,337 | 0.5 |
| Cask drain port (bottom) | 612 ^a | 0.8 |
| Cask test port (top) | 608 ^b | 0.6 |
| Cask vent port (lid) | 520 | 7.1 |
| HPI fill gas (average) | 740 | 11.0 |
| Cask fill gas (average) | 571 | 7.1 |
| HPI and Cask fill gas, combined (average) | 585 | 8.0 |

Notes: a. The cask bottom port exceeds 600°F for approximately 0.34 hours during the HAC transient analysis.
b. The cask top port exceeds 600°F for approximately 0.17 hours during the HAC transient analysis.

Additionally, temperature-history plots of several package components are presented in Figure 3.4.3-1 through Figure 3.4.3-4 (Note: the steady-state starting temperatures are shown between time = -5 and 0 hours in these figures). As shown in these figures, the cool-down period of 36 hours is sufficient to allow all package temperatures to achieve their peak values. Finally, the temperature contours of the Model 2000 Transport Package with HPI for hypothetical accident conditions are shown in Figure 3.4.3-5.

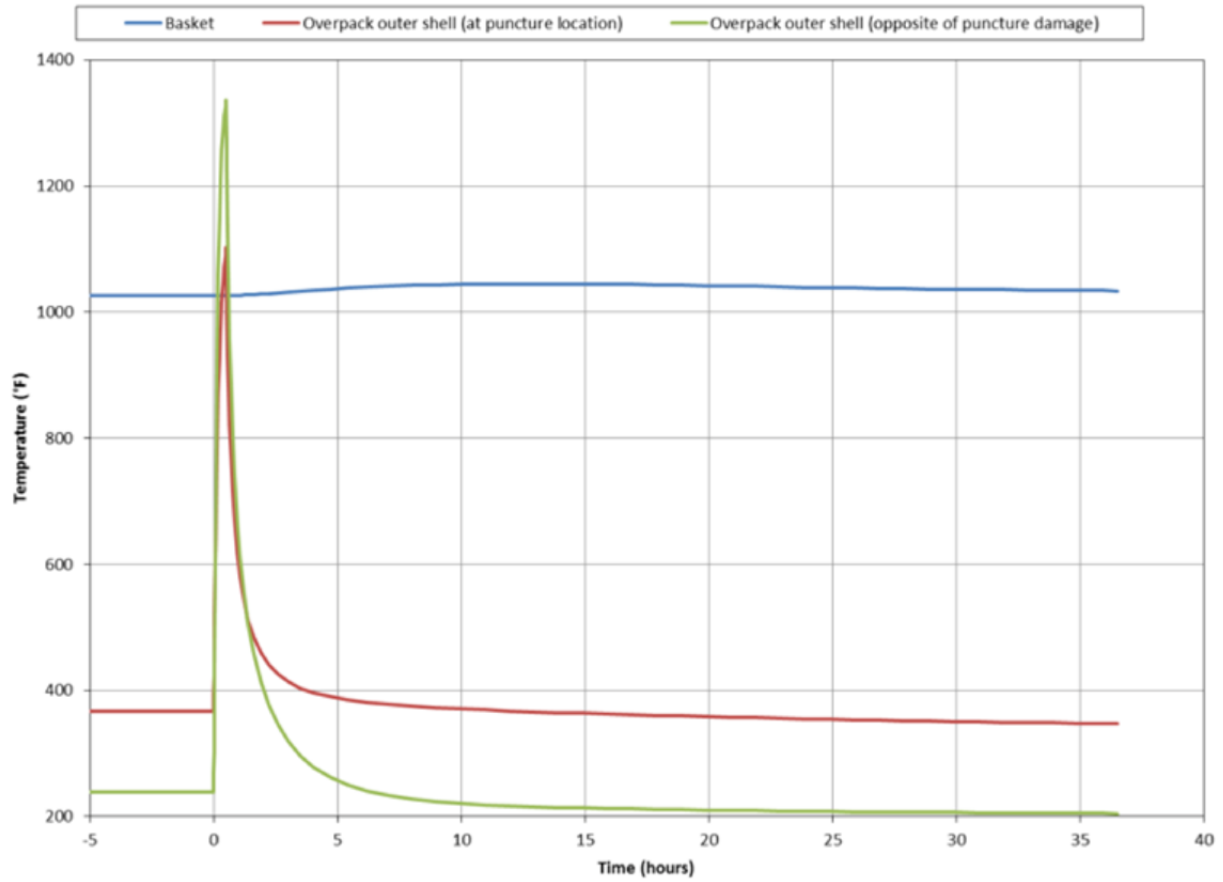


Figure 3.4.3-1. Temperature-History of the Material Basket and Overpack for HAC (Configuration 2)

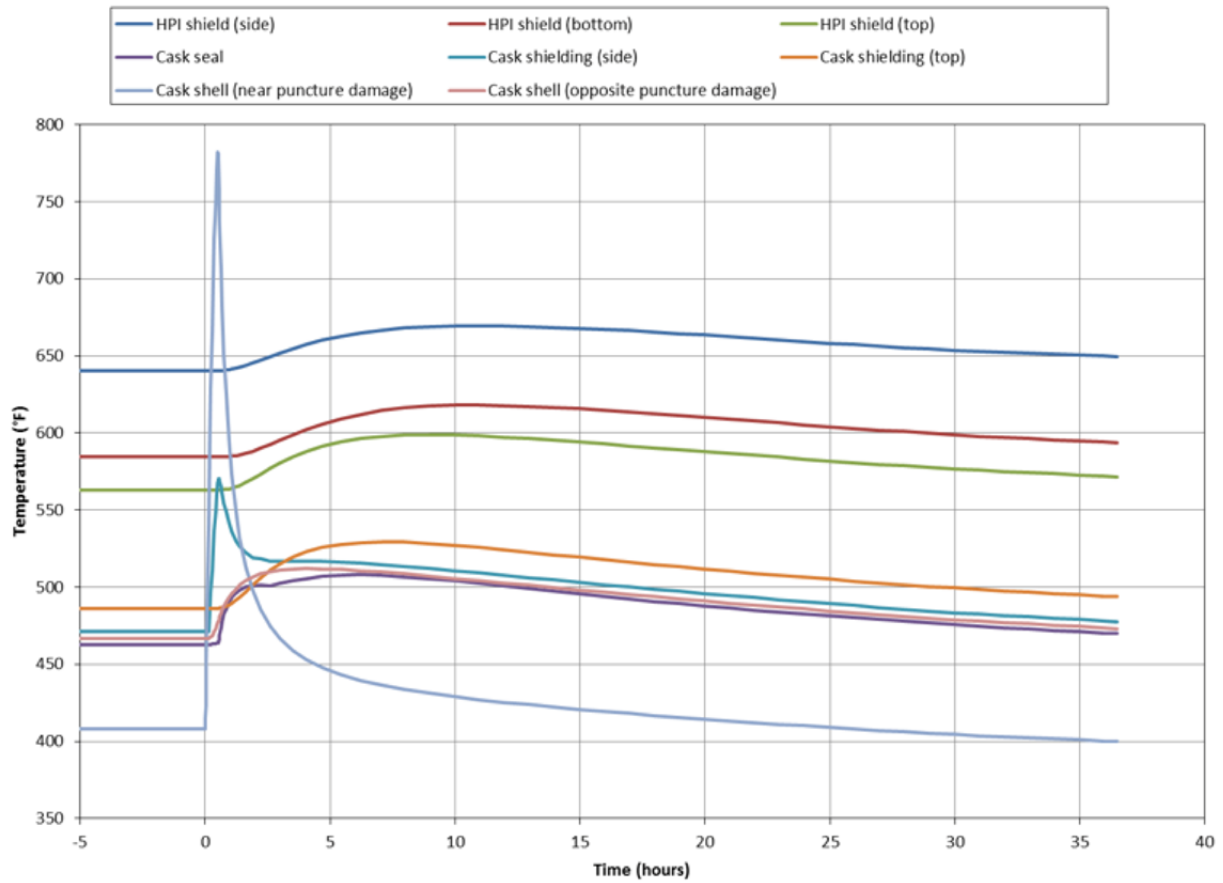


Figure 3.4.3-2. Temperature-History of the HPI and Cask for HAC (Configuration 2)

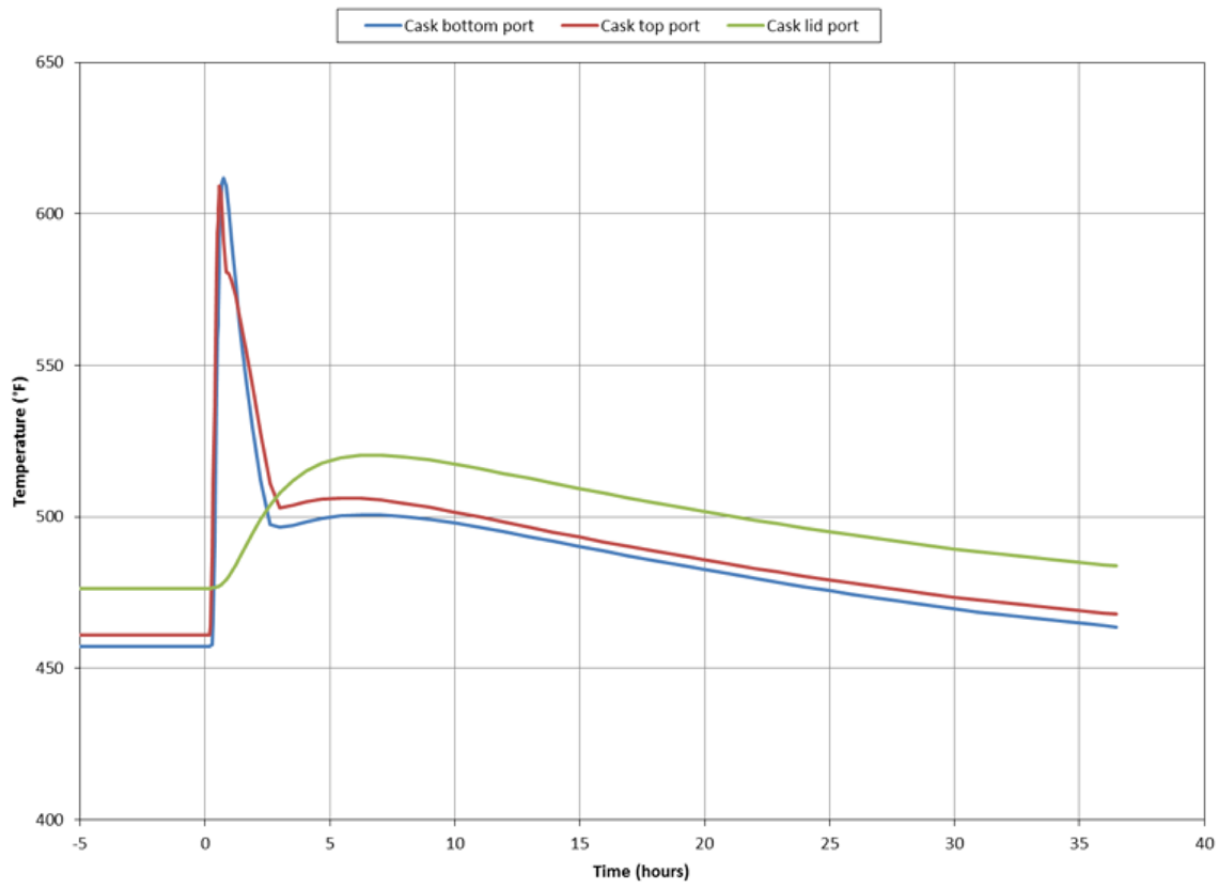


Figure 3.4.3-3. Temperature-History of the Cask Ports for HAC (Configuration 2)

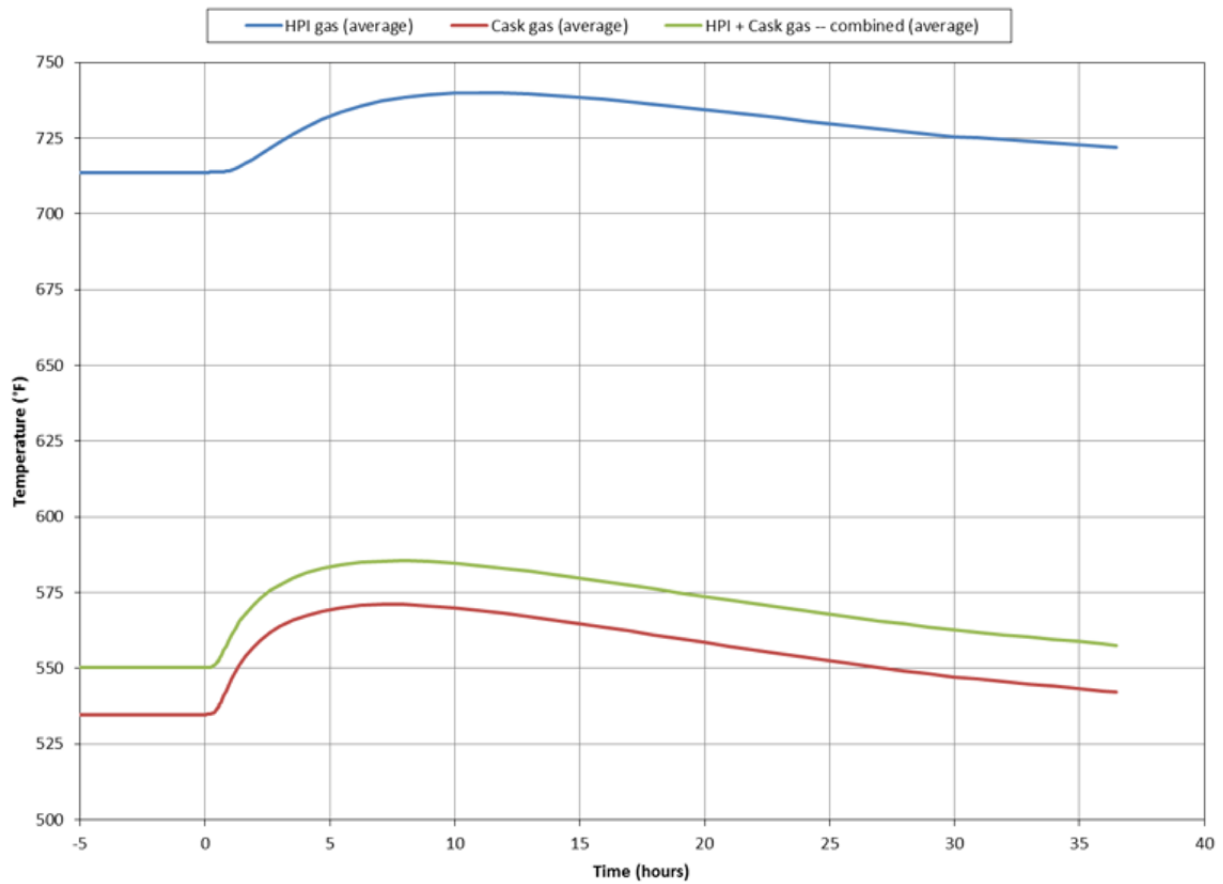


Figure 3.4.3-4. Temperature-History of the HPI and Cask Fill Gases (Configuration 2)
(Note: Volumetric Average Temperature)

[[

]]

**Figure 3.4.3-5. Temperature Contours During HAC 30-Minute Fire and Cool-Down
(Configuration 2)**

HAC Thermal Contact Resistance Sensitivity Study

Similar to the NCT thermal conductivity resistance sensitivity study, to assess the effect that using the mixed thermal resistance levels have on package temperatures, the analyses for HAC is repeated with all of the thermal resistance levels set to “low” (i.e., perfect contact). The results of this analysis is compared with the results from Table 3.4.3-1, and presented in Table 3.4.3-2.

**Table 3.4.3-2. Comparison of Mixed and Perfect Thermal Contact for HAC
(Configuration 2)**

| Item | Peak temperature (°F) | |
|----------------------------------------------------------|----------------------------------|-------------------------|
| | Mixed Thermal Contact Resistance | Perfect Thermal Contact |
| Material basket | 1,045 | 1,043 |
| HPI shielding (side) | 670 | 668 |
| HPI shielding (top) | 599 | 596 |
| HPI shielding (bottom) | 618 | 617 |
| Cask lid seal | 508 | 506 |
| Cask shielding (side) | 570 | 576 |
| Cask shielding (top) | 529 | 527 |
| Cask shell, puncture location | 782 | 795 |
| Cask shell, opposite side to puncture location | 512 | 511 |
| Cask drain port (bottom) | 612 ^a | 655 ^c |
| Cask test port (top) | 609 ^b | 613 ^d |
| Cask vent port (lid) | 520 | 518 |
| Overpack outer shell, puncture location | 1,103 | 1,094 |
| Overpack outer shell, opposite side to puncture location | 1,337 | 1,336 |
| HPI fill gas (average) | 740 | 738 |
| Cask fill gas (average) | 571 | 569 |
| HPI and cask fill gases, combined (average) | 585 | 584 |

- Notes:
- a. The cask bottom port exceeds 600°F for approximately 0.34 hours during the HAC transient analysis.
 - b. The cask top port exceeds 600°F for approximately 0.17 hours during the HAC transient analysis.
 - c. The cask bottom port exceeds 600°F for approximately 0.69 hours during the HAC transient analysis.
 - d. The cask top port exceeds 600°F for approximately 0.20 hours during the HAC transient analysis.

The same conclusion that was made for NCT thermal contact resistance can be made for HAC in that, in general, the package temperatures are lower when modeling the thermal contact as perfect as opposed to the mixed thermal contact levels. However, the cask drain port (bottom) and the cask test port (top) have peak temperatures that are higher when modeling the thermal contact as perfect. This is due to their proximity to the modeled puncture damage, which allows the heat from the fire to more readily enter the package.

It should be noted that the significant increase in the maximum temperature at the bottom port (drain port) for the perfect contact case is due to the perfect contact between the bottom [[]] of the HPI and the bottom of the cask cavity. This perfect contact causes a significant increase in the heat driven out the bottom of the cask from the internal heat load. However, it should be

considered that perfect contact between the HPI bottom [[]] and the bottom of the cask is an unrealistic scenario. For drainage purposes, there is a slight dish in the bottom of the Model 2000 cask cavity that will provide a significant separation between the HPI bottom [[]] and the bottom of the cask. This separation, shown in Figure 3.4.3-6, will cause the temperature for the cask drain port (bottom) to be more accurately calculated with mixed thermal resistance.

[[

]]

Figure 3.4.3-6. Gap Between HPI Bottom [[]] and Cask Cavity Bottom (INCH)

3.4.3.2. HAC Maximum Pressure Calculation

During HAC, the average temperature of the cask fill gas (including the gas within the HPI) peaks at 585°F 11 hours after the end of the 30-minute fire. Using the ideal gas law, the cask internal pressure from gas expansion is:

$$\frac{P_1}{T_1} = \frac{P_2}{T_2}$$

$$P_2 = 14.7 \text{ psia} \times \left(\frac{585+460}{70+460} \right) = 29.0 \text{ psia} < 30 \text{ psia}$$

where,

$$\begin{aligned} P_1 &= 14.7 \text{ psia} && \text{initial fill gas pressure,} \\ T_1 &= 70^\circ\text{F} && \text{initial fill gas temperature, and} \\ T_2 &= 585^\circ\text{F} && \text{average gas volume temperature during HAC.} \end{aligned}$$

The cask internal pressure during HAC is less than the design pressure of 30 psia. Therefore, no further evaluation is required.

3.4.4. Maximum Thermal Stresses

Section 2.7.4.3 discusses thermal stresses.

3.4.5. Accident Conditions for Fissile Material Packages for Air Transport

The Model 2000 Transport Package will not be transported by air.

3.5 Appendix

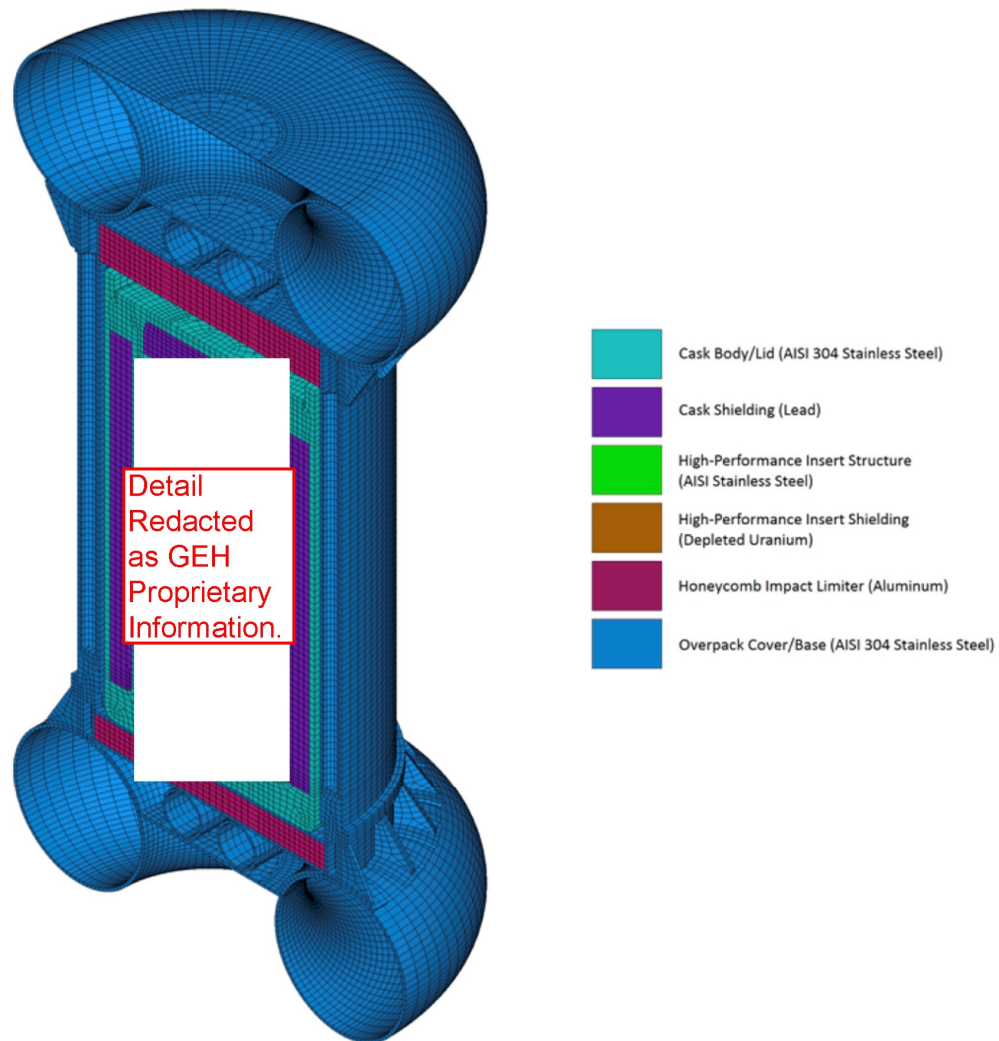
3.5.1. Configuration 1 – Model 2000 Transport Package with HPI and No Material Basket

This section evaluates the Model 2000 Transport Package with the HPI and no material basket in Configuration 1, 1500 W, for both NCT and HAC using a subset of the finite element model described in the main text of this document. The evaluation presented in this section concludes that the temperatures and pressures generated in the Model 2000 Transport Package by 1500 W of decay heat results in package temperatures and pressures which are bounded by Configuration 2, 3000 W.

3.5.1.1. Thermal Model with HPI and No Material Basket 1500 Watt Decay Heat

The model (see Figure 3.5.1-1) consists of the Overpack (with trapped air), cask, HPI, and cask fill gas. The contents are assumed to generate 1500 W of heat that is uniformly distributed on the internal surfaces of the HPI.

[[



]]

Figure 3.5.1-1. 3D FEA Model of the Model 2000 Transport Package with HPI and No Material Basket (Half Symmetry) - Elements Representing Air and Helium Not Shown for Clarity (Configuration 1)

$$q''_{\text{gen}} = \frac{Q}{A_{\text{SURF152}}} = \frac{1500 \text{ W} \left(\frac{3.4123 \text{ Btu/h}}{\text{W}} \right)}{2 \times 816.846194 \text{ in}^2} = 3.133 \frac{\text{Btu}}{\text{h-in}^2}$$

where

A_{SURF152} = the area of the SURF152 elements overlaid on the inner surface of the HPI (multiplied by 2 to account for the half-symmetry of the model).

The package is exposed to NCT and HAC using boundary conditions as described in the main text of this document. Additionally, the package is modeled with damage consistent with a side drop for HAC as described in the main text of this document. For HAC, the package is assumed to be exposed to a 100°F ambient temperature with insolation prior to and following the 1,475°F

fire, and is assumed to be exposed to a -20°F ambient temperature in shade prior to and following the 1,475°F fire.

3.5.1.2. NCT Temperature Results

The NCT thermal analysis results are presented in Table 3.5.1-1 (NCT, 100°F ambient temperature) and Table 3.5.1-2 (NCT cold conditions, -40°F and -20°F ambient temperatures). Table 3.5.1-3 provides a comparison of the component temperature and allowable. As the table shows, the cask lid seal and port temperatures are within the allowable limits for the [[]] seal material and port testing as specified in Chapter 4. Additionally, the steady-state temperature contours for NCT (100°F ambient temperature) are shown in Figure 3.5.1-2. As evident from Figure 3.5.1-3, no accessible surface of the package is greater than or equal to 185°F (maximum is less than 175°F) when exposed to a 100°F ambient temperature in shade.

**Table 3.5.1-1. Model 2000 Transport Package with HPI (No Material Basket)
Temperature Results, NCT (100°F Ambient Temperature in Shade and with Insolation),
Configuration 1**

| Item | 100°F Ambient Temperature, in Shade (°F) | | | 100°F Ambient Temperature, with Insolation (°F) | | |
|--------------------------------------------|------------------------------------------|-----|-----|-------------------------------------------------|-----|-----|
| | Max | Min | Avg | Max | Min | Avg |
| HPI | 390 | 254 | --- | 420 | 289 | --- |
| HPI shielding (top) | 356 | 346 | 352 | 388 | 378 | 383 |
| HPI shielding (sides) | 389 | 300 | 367 | 419 | 334 | 398 |
| HPI shielding (bottom) | 313 | 294 | 306 | 346 | 328 | 340 |
| Cask (bottom, shells, top, lid) | 296 | 223 | --- | 331 | 261 | --- |
| Cask shielding (lid) | 292 | 283 | 287 | 327 | 318 | 322 |
| Cask shielding (sides) | 280 | 242 | 267 | 316 | 279 | 303 |
| Cask lid seal | 282 | 269 | --- | 317 | 305 | --- |
| Cask drain port (bottom) | 243 | 223 | --- | 279 | 261 | --- |
| Cask test port (top) | 278 | 269 | --- | 314 | 305 | --- |
| Cask vent port (lid) | 288 | 284 | --- | 323 | 319 | --- |
| Overpack base | 239 | 136 | --- | 275 | 158 | --- |
| Overpack cover | 193 | 105 | --- | 237 | 171 | --- |
| Overpack toroidal shell (top) | 131 | 106 | 114 | 185 | 163 | 171 |
| Overpack toroidal shell (bottom) | 168 | 109 | 124 | 212 | 130 | 164 |
| Overpack honeycomb impact limiter (top) | 163 | 155 | 161 | 213 | 205 | 210 |
| Overpack honeycomb impact limiter (bottom) | 236 | 202 | 220 | 272 | 241 | 258 |
| Cask fill gas | 385 | 245 | 316 | 415 | 281 | 349 |

**Table 3.5.1-2. Model 2000 Transport Package with HPI (No Material Basket)
Temperature Results, -40°F & -20°F Ambient Temperatures in Shade, Configuration 1**

| Item | -40°F Ambient Temperature, in Shade (°F) | | | -20°F Ambient Temperature, in Shade (°F) | | |
|--------------------------------------------|---------------------------------------------|-----|-----|---------------------------------------------|-----|-----|
| | Max | Min | Avg | Max | Min | Avg |
| HPI | 305 | 147 | --- | 317 | 162 | --- |
| HPI shielding (top) | 268 | 258 | 263 | 280 | 270 | 276 |
| HPI shielding (sides) | 304 | 201 | 279 | 316 | 215 | 291 |
| HPI shielding (bottom) | 216 | 195 | 208 | 230 | 209 | 222 |
| Cask (bottom, shells, top, lid) | 199 | 110 | --- | 213 | 126 | --- |
| Cask shielding (lid) | 195 | 185 | 189 | 208 | 199 | 203 |
| Cask shielding (sides) | 182 | 134 | 164 | 195 | 150 | 179 |
| Cask lid seal | 183 | 171 | --- | 197 | 184 | --- |
| Cask drain port (bottom) | 135 | 110 | --- | 150 | 126 | --- |
| Cask test port (top) | 179 | 171 | --- | 193 | 184 | --- |
| Cask vent port (lid) | 190 | 187 | --- | 204 | 200 | --- |
| Overpack base | 130 | 1 | --- | 145 | 21 | --- |
| Overpack cover | 64 | -36 | --- | 83 | -16 | --- |
| Overpack toroidal shell (top) | -7 | -35 | -26 | 13 | -15 | -6 |
| Overpack toroidal shell (bottom) | 41 | -33 | -14 | 59 | -12 | 6 |
| Overpack honeycomb impact limiter (top) | 29 | 19 | 25 | 48 | 39 | 45 |
| Overpack honeycomb impact limiter (bottom) | 127 | 82 | 107 | 142 | 100 | 123 |
| Cask fill gas | 301 | 137 | 221 | 312 | 152 | 234 |

Table 3.5.1-3. NCT Temperature Summary and Comparison with Allowable Temperatures (Configuration 1)

| Item | NCT Temperatures (°F) | Allowable Temperature (°F) |
|----------------------------------|-----------------------|----------------------------|
| HPI Shielding (Depleted Uranium) | 419 (max) | 2071 |
| Cask lid seal | 317 (max) | 400 ^b |
| Cask Shielding (Lead) | 327 (max) | 622 |
| Honeycomb Impact Limiters | 272 | 350 |
| Cask Drain Port (Bottom) | 279 | 612 ^a |
| Cask Test Port (Top) | 314 | |
| Cask Vent Port (Lid) | 323 | |
| Overpack Outer Surface | 175 | 185 |

Notes: See Table 3.1.3-1 for allowable temperature referencing;

^a Temperature limit applies to the port plug containment boundary

^b See Section 4

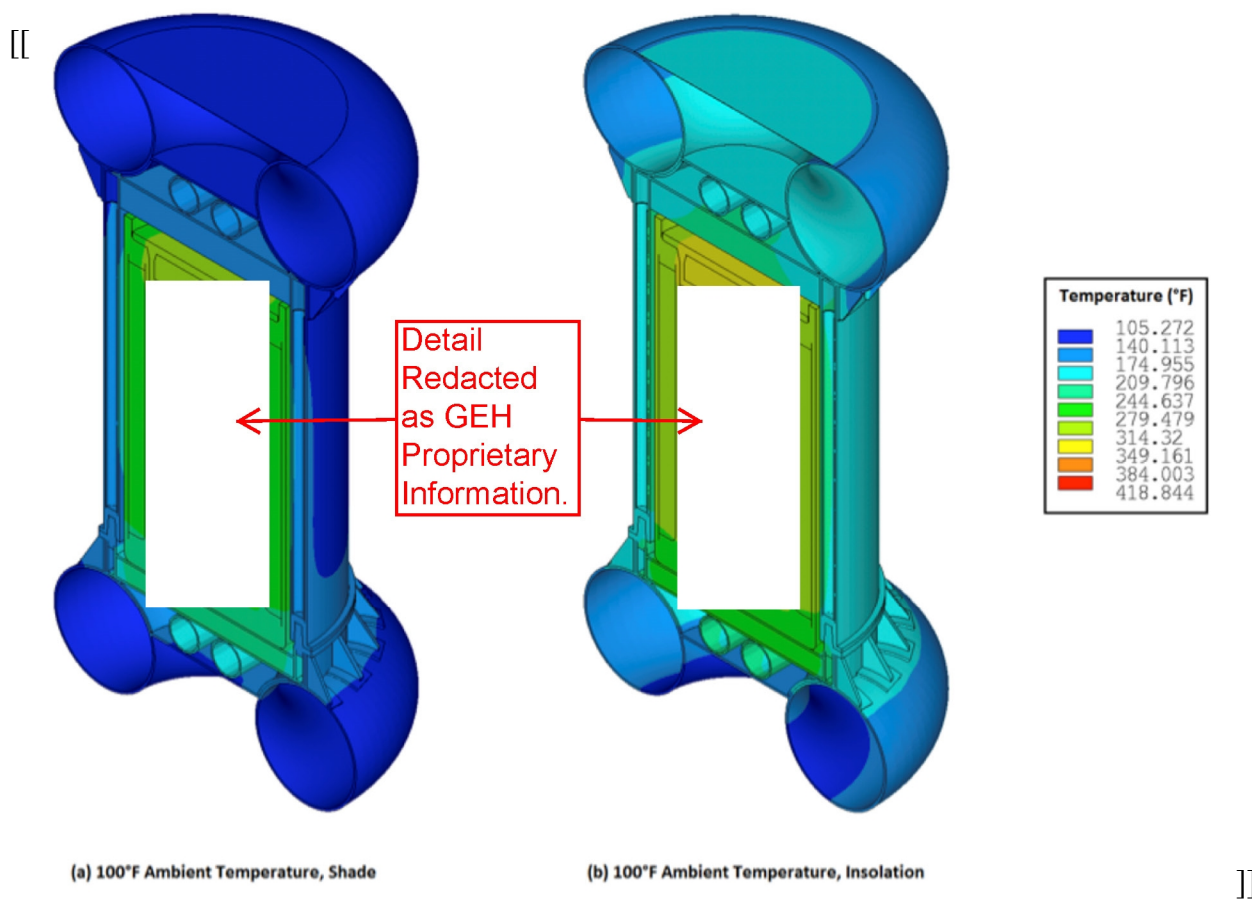


Figure 3.5.1-2. Package Temperature Contours for NCT with 100°F Ambient Temperature in Shade and with Insolation, Configuration 1

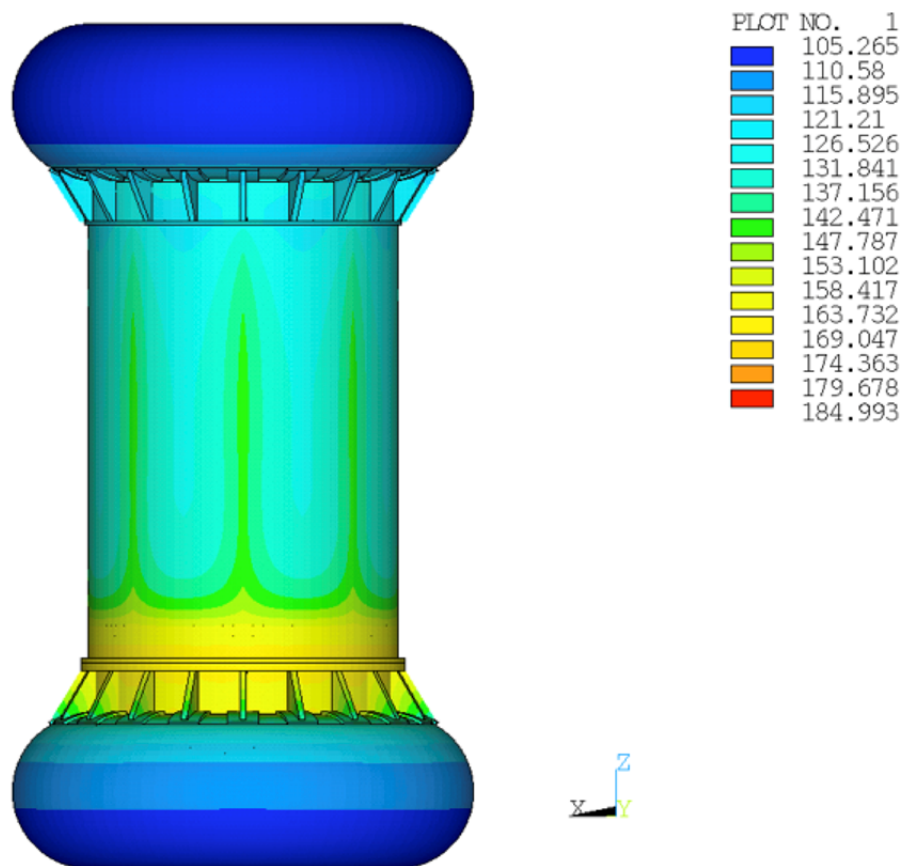


Figure 3.5.1-3. Package Exterior Surface Temperature Contours for NCT with 100°F Ambient Temperature in Shade, Configuration 1

3.5.1.3. HAC Temperature Results

The HAC thermal analysis results are presented in Table 3.5.1-4. The table presents the temperature results for both hot and cold pre/post fire conditions. Table 3.5.1-5 provides a comparison of the component temperature and allowable. As the table shows, the cask lid seal and port temperatures are within the allowable limits for the [[]] seal material as specified in Chapter 4.

**Table 3.5.1-4. Model 2000 Transport Package with HPI (No Material Basket)
Temperature Results, HAC, Configuration 1**

| Item | Fire with 100°F and Insolation Pre/Post Fire | | Fire with -20°F and Shade Pre/Post Fire | |
|----------------------------------------------------------|----------------------------------------------|-----------------------------------------|-----------------------------------------|-----------------------------------------|
| | Peak Temp. (°F) | Time at Which Peak Temp. Occurs (hours) | Peak Temp. (°F) | Time at Which Peak Temp. Occurs (hours) |
| HPI shielding (side) | 482 | 12.3 | 389 | 16.5 |
| HPI shielding (top) | 439 | 10.3 | 338 | 13.5 |
| HPI shielding (bottom) | 446 | 12.3 | 348 | 15.5 |
| Cask lid seal | 389 | 2.2 | 275 | 10.5 |
| Cask shielding (side) | 456 | 0.6 | 344 | 0.6 |
| Cask shielding (top) | 396 | 8.3 | 287 | 10.5 |
| Cask shell, puncture location | 704 | 0.5 | 621 | 0.5 |
| Cask shell, opposite side to puncture location | 385 | 5.6 | 273 | 8.5 |
| Overpack outer shell, puncture location | 1,063 | 0.5 | 1,017 | 0.5 |
| Overpack outer shell, opposite side to puncture location | 1,330 | 0.5 | 1,314 | 0.5 |
| Cask drain port (bottom) | 537 | 0.8 | 435 | 0.8 |
| Cask test port (top) | 515 | 0.6 | 406 | 0.6 |
| Cask vent port (lid) | 392 | 8.3 | 283 | 10.5 |
| Cask fill gas (average) | 421 | 9.3 | 319 | 12.5 |

Table 3.5.1-5. HAC Temperature Summary and Comparison with Allowable Temperatures, Configuration 1

| Item | HAC Temperatures (°F) | Allowable Temperature (°F) |
|----------------------------------|-----------------------|----------------------------|
| HPI Shielding (Depleted Uranium) | 482 (max) | 2071 |
| Cask lid seal | 389 (max) | 400 ([]) ^b |
| Cask Shielding (Lead) | 456 (max) | 622 |
| Cask Drain Port (Bottom) | 537 | 612 ^a |
| Cask Test Port (Top) | 515 | |
| Cask Vent Port (Lid) | 392 | |

Notes: See Table 3.1.3-1 for allowable temperature referencing;

^a Temperature limit applies to the port plug containment boundary

^b See Section 4

3.5.1.4. Thermal Contact Resistance Study

The thermal contact resistance levels in this model are modified to simulate perfect contact, and the NCT (100°F ambient with insolation) and HAC (100°F ambient with insolation during pre-fire and post-fire) analyses are performed and compared with those that include mixed thermal contact resistances. The results of these studies are presented in Table 3.5.1-6 (NCT) and Table 3.5.1-7 (HAC). As shown in Table 3.5.1-6, the simulation with perfect thermal contact results in component temperatures being lower than their mixed thermal contact counterparts.

The simulation for HAC with perfect thermal contact results in most component temperatures being lower than their mixed thermal contact counterparts while other component temperatures are higher for the case with perfect thermal contact. The item exhibiting the greatest sensitivity in the HAC study is the cask drain port (increased temperature of 50°F). However, as discussed in Section 3.4.3.1, there is a slight dish in the bottom of the Model 2000 cask cavity that will provide a significant separation between the HPI bottom [[]] and the bottom of the cask. This separation, shown in Figure 3.4.3-6, will cause the temperature for the cask drain port (bottom) to be more accurately calculated with mixed thermal resistance. Therefore, a maximum temperature of 537°F is predicted for the drain port.

Table 3.5.1-6. Model 2000 Transport Package with HPI (No Material Basket) Temperature Results, 100°F Ambient Temperature with Insolation, NCT, Configuration 1—Thermal Contact Resistance Study

| Item | Mixed Contact Resistances (°F) | | | Perfect Contact (°F) | | |
|--------------------------------------------|--------------------------------|-----|-----|----------------------|-----|-----|
| | Max | Min | Avg | Max | Min | Avg |
| HPI | 420 | 289 | --- | 415 | 283 | --- |
| HPI shielding (top) | 388 | 378 | 383 | 384 | 374 | 379 |
| HPI shielding (sides) | 419 | 334 | 398 | 414 | 327 | 393 |
| HPI shielding (bottom) | 346 | 328 | 340 | 341 | 322 | 334 |
| Cask (bottom, shells, top, lid) | 331 | 261 | --- | 326 | 253 | --- |
| Cask shielding (lid) | 327 | 318 | 322 | 322 | 314 | 317 |
| Cask shielding (sides) | 316 | 279 | 303 | 312 | 272 | 298 |
| Cask lid seal | 317 | 305 | --- | 313 | 301 | --- |
| Cask drain port (bottom) | 279 | 261 | --- | 273 | 253 | --- |
| Cask test port (top) | 314 | 305 | --- | 310 | 301 | --- |
| Cask vent port (lid) | 323 | 319 | --- | 318 | 315 | --- |
| Overpack base | 275 | 158 | --- | 269 | 157 | --- |
| Overpack cover | 237 | 171 | --- | 235 | 170 | --- |
| Overpack toroidal shell (top) | 185 | 163 | 171 | 184 | 162 | 170 |
| Overpack toroidal shell (bottom) | 212 | 130 | 164 | 208 | 130 | 164 |
| Overpack honeycomb impact limiter (top) | 213 | 205 | 210 | 210 | 202 | 207 |
| Overpack honeycomb impact limiter (bottom) | 272 | 241 | 258 | 268 | 236 | 254 |
| Cask fill gas | 415 | 281 | 349 | 411 | 275 | 344 |

**Table 3.5.1-7. Model 2000 Transport Package with HPI (No Material Basket)
Temperature Results, 100°F Ambient with Insolation During Pre- and Post-Fire, HAC,
Configuration 1—Thermal Contact Resistance Study**

| Item | Mixed Contact Resistances | | Perfect Contact | |
|------------------------------------------------------|---------------------------|-----------------------------------------|-----------------|-----------------------------------------|
| | Peak Temp. (°F) | Time at Which Peak Temp. Occurs (hours) | Peak Temp. (°F) | Time at Which Peak Temp. Occurs (hours) |
| HPI shielding (side) | 482 | 12.3 | 480 | 12.2 |
| HPI shielding (top) | 439 | 10.3 | 438 | 10.2 |
| HPI shielding (bottom) | 446 | 12.3 | 446 | 12.2 |
| Cask lid seal | 389 | 2.2 | 389 | 2.2 |
| Cask shielding (side) | 456 | 0.6 | 463 | 0.2 |
| Cask shielding (top) | 396 | 8.3 | 395 | 8.2 |
| Cask shell, puncture location | 704 | 0.5 | 718 | 0.5 |
| Cask shell, opposite side to puncture location | 385 | 5.6 | 384 | 5.5 |
| Overpack outer shell, puncture location | 1,063 | 0.5 | 1,054 | 0.5 |
| Overpack outer shell, opposite side to puncture loc. | 1,330 | 0.5 | 1,330 | 0.5 |
| Cask drain port (bottom) | 537 | 0.8 | 587 | 0.7 |
| Cask test port (top) | 515 | 0.6 | 519 | 0.9 |
| Cask vent port (lid) | 392 | 8.3 | 390 | 7.2 |
| Cask fill gas (average) | 421 | 9.3 | 420 | 9.2 |

3.6 References

- 3-1 US. NRC, "Title 10, Part 71—Packaging and Transportation of Radioactive Material," 10 CFR 71, November 2014.
- 3-2 ANSYS®, "Mechanical, Revision 14.0," November 2011.
- 3-3 Incropera, Frank P., and DeWitt, David P., "Fundamentals of Heat and Mass Transfer," Fifth Edition, John Wiley & Sons, Inc., New York, 2002.
- 3-4 Hexcel Corporation, "HexWeb Honeycomb Energy Absorption System - Design Data," Southbury, CT, March 2005.
- 3-5 GE Hitachi Nuclear Energy, "Model 2000 Cask Containment Boundary Testing," Test Specification 003N1962, Revision 0 (2015), or latest revision.
- 3-6 Editors H.K Hammond III and H.L Mason, "Precision Measurement and Calibration, Selected NBS Papers on Radiometry and Photometry," Editors H.K Hammond III and H.L Mason, Ed.: National Bureau of Standards (NBS), 1971, Volume 7.
- 3-7 Robert Siegel and John R. Howell, "Thermal Radiation Heat Transfer, Second Edition," Hemisphere Publishing Corporation, New York, 1981.
- 3-8 Parker Hannifin Corporation. (2014) Parker O-Ring Handbook, 50th Anniversary Edition.
- 3-9 Lienhard IV, John H., and Lienhard V, John H., "A Heat Transfer Textbook," Fourth Edition, Phlogiston Press, Cambridge, Massachusetts, 1981.
- 3-10 Guyer, Eric C., Editor, "Handbook of Applied Thermal Design," McGraw-Hill, New York, 1989.

4 CONTAINMENT

This section demonstrates the ability of the Model 2000 Transport Package to meet the containment requirements of 10 CFR 71 (Reference 4-1). The containment system for the Model 2000 Transport Package consists of the cask alone. The other components (e.g., overpack, high performance insert (HPI)) are not part of the containment system. The entire primary containment boundary, including containment welds and base metals (as shown in Figure 4.1.3-1), are leakage rate tested for fabrication, maintenance, and periodically as defined in Chapter 8.

4.1 Description of Containment System

The cask design has been evaluated to support 1500 W (Configuration 1) and 3000 W (Configuration 2) decay heat. The cask features two seal and O-ring design options for use at various decay heat ranges. See Sections 4.1.3.2 and 4.1.3.3 for more specific information regarding the seal options.

4.1.1. Containment Vessel

Figure 1.2-1 shows the containment vessel (cask) for the Model 2000 Transport Package. The containment boundary for the cask is shown in Figure 4.1.3-1. The cask is constructed of a steel-clad lead cylinder with a stainless steel forging at each end. The cask lid is placed within the upper forging to protect the seal area during the accident conditions. Refer to Section 2.2 for information regarding the materials of construction of the cask.

4.1.2. Closure

The cask lid connects to the cask body by fifteen 1.25-inch diameter ASTM A540, Grade B22 or ASME SA540 socket head screws, which compress the cask lid seal. The screws are equally spaced on a 32.25-inch diameter bolt circle. Each screw is tightened to 500 ft-lb of torque, as shown in Section 2.12.4. The cask lid closure evaluation is presented in Section 2.4.3. The stress analysis of these screws is given in Section 2.12.4. These analyses show that positive closure is maintained during all conditions.

4.1.3. Containment Penetrations

The Model 2000 cask has three penetrations or ports. One port, located two inches from the bottom of the cask, serves as a drain for the cask cavity. This port is made by a series of offset ½-inch drilled holes through the 6-inch thick steel forging. The second penetration is located approximately in the center of the cask lid. It is made of 3/8-inch diameter tubing, shown as Item 13 - [[]], and Item 12 – [[]], in the Model 2000 Transport Package Licensing Cask Drawings 101E8718 and 105E9520, respectively (Reference 4-2), spiraled through the lead and welded at both ends to the steel flanges that make up the lid. The combined use of these two ports provides means to eliminate water from the cask cavity collected during underwater operations. The third penetration or port is used to test the adequacy of the cask lid closure seal after each loading operation.

A ½ NPT hex socket head pipe plug followed by 1¾-12 UNC cap close each of these penetrations (see Figure 4.1.3-2). The closure of pipe plug is designed for leaktightness as

defined in ANSI N14.5-1997, Section 2.1 (Reference 4-3). Dimensions and components of the port seals are provided in the Model 2000 cask licensing drawings included in Section 1.3.1. Additional information is provided in Section 4.1.3.3.

4.1.3.1. Welds

All cask welds are full penetration groove welds to ensure structural and containment integrity. Each weld is liquid penetrant tested on the root and final passes. In addition, the welds are helium leak tested as required in Chapter 8.

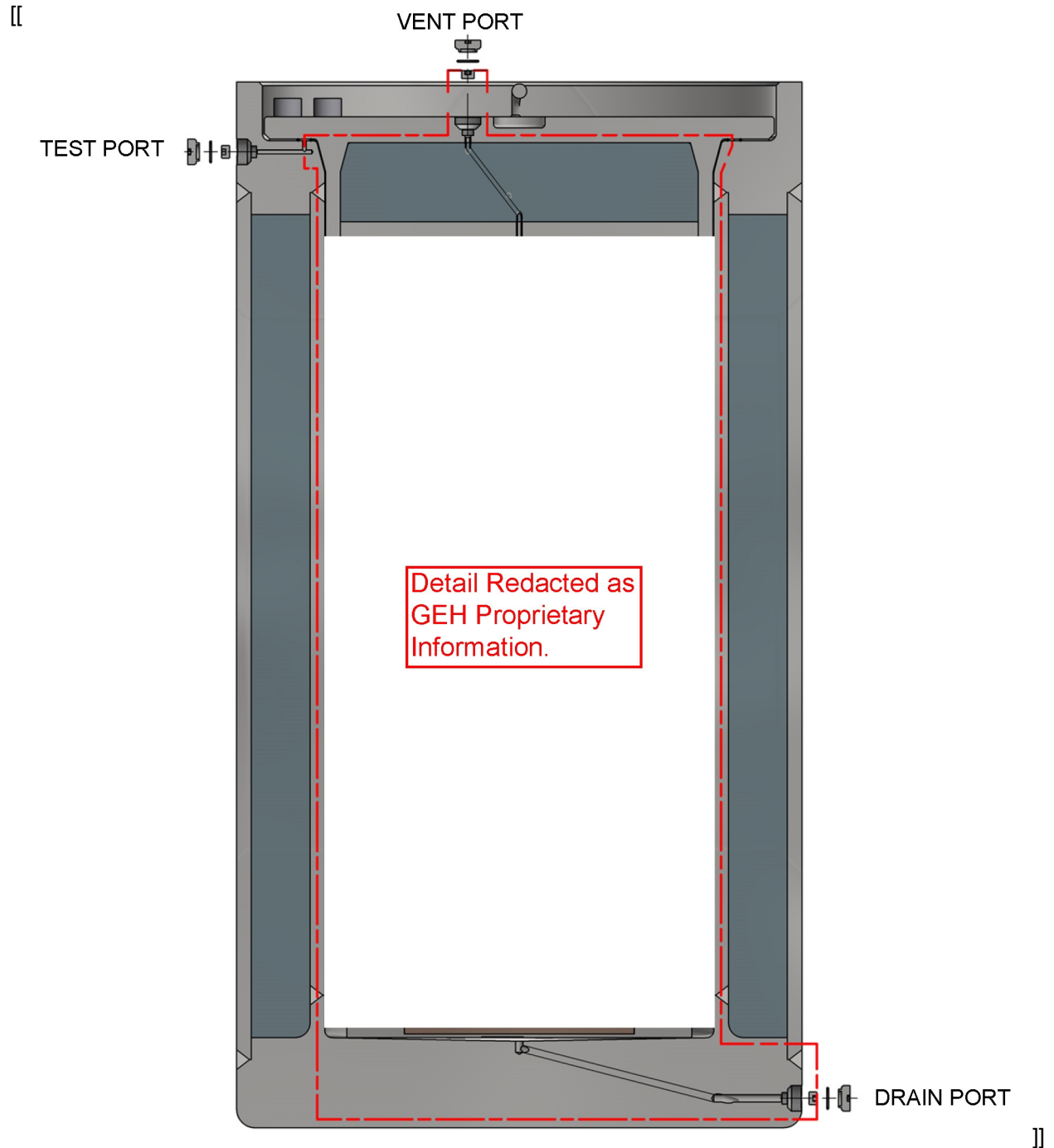


Figure 4.1.3-1. Cask Containment Boundary

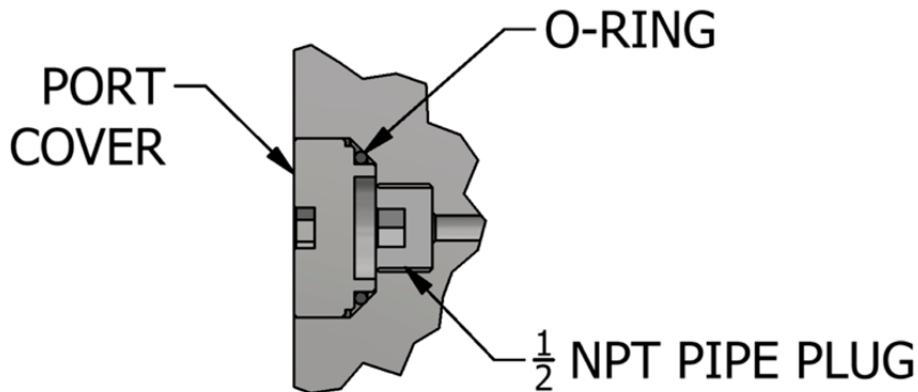


Figure 4.1.3-2. Cask Port Configuration (Assembled View)

4.1.3.2. Cask Lid Closure Seal

The cask lid seal (Parker Gask-O-Seal design) consists of a [[]]-inch thick metal retainer with two concentric [[]] seals on the top and two concentric [[]] seals on the bottom (4 total), as seen in Figure 4.1.3-3. The surfaces of the Model 2000 cask body and the lid flanges have an electropolished finish to ensure that they are clean sealing surfaces for the [[]]. As the load from bolting the lid down is applied, the [[]] seals are compressed between the cask body flange and cask lid flange, and the seals deform to occupy the free volume in the metal retainer. For heat loads between 0 and 1500 W (Configuration 1), a [[]] retainer and the Parker [[]] are used as the seal material. For heat loads between 500 and 3000 W (Configuration 2), a [[]] retainer and the Parker [[]] are used as the seal material.

[[]]

]]

Figure 4.1.3-3. Cask Lid Seal Design

4.1.3.3. Cask Port Seals

The containment boundary for each port is at the respective pipe plug. An exploded view of these components is shown in Figure 4.1.3-4. For the cask port seals, the two O-ring options support the two configurations. Configuration 1 and Configuration 2 offer two O-ring material options, but all other features remain unchanged. For heat loads between 0 and 1500 W (Configuration 1), an [[]] is used as the seal material. For heat loads between 500 and 3000 W (Configuration 2), a high temperature [[]] is used as the seal material. See cask licensing drawings in Section 1.3.1 for more detailed information. For details of the pipe plug installation controls, see Chapter 7.

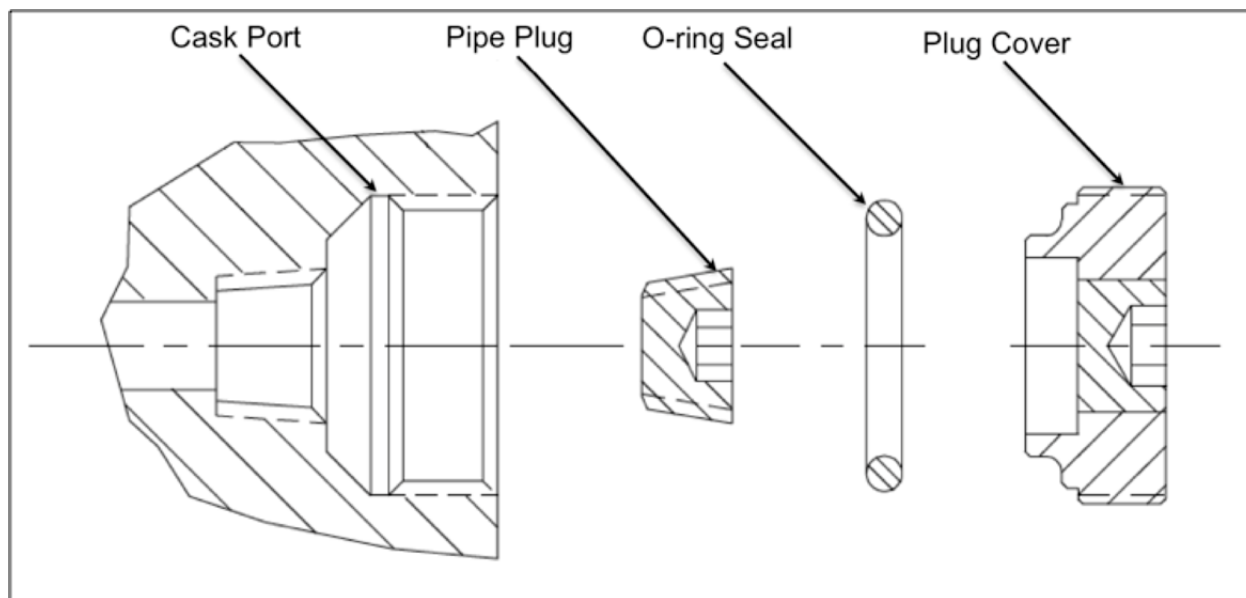


Figure 4.1.3-4. Cask Port Configuration (Exploded View)

4.2 Containment Under Normal Conditions of Transport

The Model 2000 cask containment is designed so that no release of radioactive materials will occur under the NCT, and there will not be any significant increase in external radiation or reduction in package effectiveness. This conclusion is supported by the analyses in Chapters 2 and 3 and the various component qualification tests.

4.2.1. Configuration 1

The cask withstands pressures and temperatures in excess of those encountered in routine transport and normal conditions of transport. The maximum average cask fill gas temperature determined to be 349°F in Section 3.5.1. This temperature value is based on helium occupying the entire cavity volume. The maximum pressure encountered under NCT for 3000 W, 26.8 psia, bounds the 1500 W case. The structural evaluation presented in Chapter 2 shows low stress values throughout the cask structure, especially in the seal area under NCT. The maximum cask lid seal temperatures are bounded by the operational limit of 400°F, which is qualified for the Configuration 1 cask seal, for the 1500 W case (Reference 4-4). Additionally, cask port

temperatures are bounded by the operational limit of 612°F qualified for both configurations, thus containment integrity is maintained (Reference 4-4).

4.2.2. Configuration 2

The cask withstands pressures and temperatures in excess of those encountered in routine transport and normal conditions of transport. The maximum pressure encountered under NCT is 26.8 psia at 3000 W. This pressure corresponds to the maximum average HPI and cask fill gas temperature of 505°F given in Section 3.3.1.1. This pressure value is based on helium occupying the entire cavity volume. The structural evaluation presented in Chapter 2 shows low stress values throughout the cask structure, especially in the seal area under NCT. The maximum cask lid seal temperatures are bounded by the operational limit of 508°F, which is qualified for the Configuration 2 cask lid seal for the 3000 W case (Reference 4-4). Additionally, cask port temperatures are bounded by the operational limit of 612°F qualified for both configurations, thus containment integrity is maintained (Reference 4-4).

4.3 Containment Under Hypothetical Accident Conditions

4.3.1. Configuration 1

As seen in Section 3.5.1.3, the maximum average cask fill gas temperature in the cask cavity for 1500 W, HAC is 421°F. This temperature is based on helium occupying the entire cavity volume. The maximum pressure encountered during HAC for 3000 W bounds the 1500 W case. Temperatures at the cask lid closure seal region for Configuration 1 are bounded by the 400°F design temperature of the seal material (see Table 3.5.1-5 and Reference 4-4). Temperatures at the penetration or port areas for Configuration 1 are bounded by the 612°F design temperature (see Table 3.5.1-5 and Reference 4-4). The analytical evaluations under HAC presented in Chapter 2 show that the stresses throughout the cask structure are below the failure criteria for the material.

4.3.2. Configuration 2

As seen in Sections 3.4.3.1 and 3.4.3.2, the maximum average HPI and cask fill gas temperature in the cask cavity for 3000 W, HAC is 585°F with a corresponding pressure of 29.0 psia. As stated above, this pressure is based on helium occupying the entire cavity volume. This pressure does not exceed the design pressure of 30 psia. Temperatures at the cask lid closure seal region for Configuration 2 are bounded by the 508°F design temperature of the seal material (see Table 3.1.3-1 and Reference 4-4). Temperatures at the penetration or port areas for Configuration 2 are bounded by the 612°F design temperature (see Table 3.1.3-1 and Reference 4-4). The analytical evaluations under HAC presented in Chapter 2 show that the stresses throughout the cask structure are below the failure criteria for the material for modifications related to Configuration 2.

4.4 Leakage Rate Tests for Type B Packages

The maximum temperature at the cask lid seal region is bounded by 508°F for Configuration 2 and the maximum temperature at the penetrations or port areas are bounded by 612°F for both configurations. The internal pressure in the cask cavity may increase to 29.0 psia due to rise in

the temperature. The Model 2000 cask is loaded dry or underwater. If loaded underwater, the cavity must be vacuum dried to remove any residual moisture.

Regardless of how the cask is loaded, a leak test is performed after it is loaded. To perform the leak test, helium is introduced into the cavity to a pressure of 15 psig. The preshipment, fabrication, periodic, and maintenance leakage rate tests are performed in accordance with ANSI N14.5 (Reference 4-3) standards. At the conclusion of the pre-shipment test, the pressure is released. Therefore it can be assumed that helium remains inside the cavity. The peak average fill gas temperature is 585°F under hypothetical accident conditions for the maximum case of 3000 W.

For Configuration 1, full-scale acceptance testing of the cask lid closure seal ([[]]) was performed at maximum pressure with both maximum (400°F) and minimum (-40°F) temperatures in accordance with ANSI N14.5 standards. For Configuration 2, full-scale acceptance testing of the cask lid closure seal ([[]]) was performed at maximum pressure with both maximum (508°F) and minimum (5°F) temperature predictions in accordance with ANSI N14.5 standards (Reference 4-3). Full-scale acceptance testing of the port NPT fittings (same for both configurations) was performed at maximum pressure with both maximum (612°F) and minimum (-40°F) temperature predictions in accordance with ANSI N14.5 standards (Reference 4-3). The pressure of 29.0 psia is less than the design pressure of 30 psia, which is based on Configuration 2. Therefore, the Model 2000 Transport Package design pressure is a conservative design basis for the shipment of the highest decay heat content.

4.5 Appendix

4.5.1. Cask Penetration Leaktightness Test Procedure and Results

A separate report has been generated to compile the results for acceptance testing of Configuration 2 cask lid closure seal and the NPT fittings (same for both configurations), per the American Society for Nondesctructive Testing (ASNT) Level III approved GEH seal acceptance testing procedure (Reference 4-4).

4.6 References

- 4-1 U.S. NRC Code of Federal Regulations, Title 10 Part 71, "Packaging and Transport of Radioactive Material," April 2016.
- 4-2 GE Model 2000 Cask Licensing Drawings: 101E8718 Revision 15, 105E9520 Revision 7.
- 4-3 American National Standards Institute (ANSI), "American National Standard for Radioactive Materials – Leakage Tests on Packages for Shipment," ANSI N14.5, 1997.
- 4-4 GE Hitachi Nuclear Energy, "Model 2000 Cask Containment Boundary Testing," Test Specification 003N1962, Revision 0 (2015), or latest revision.

5 SHIELDING EVALUATION

This chapter outlines the Model 2000 cask shielding analysis, and demonstrates compliance with the external radiation requirements of 10 CFR 71, "Packaging and Transport of Radioactive Material" (Reference 5-1). This shielding evaluation was performed to demonstrate that the Model 2000 Transport Package with the high performance insert (HPI) provides sufficient shielding, such that the external radiation limits are satisfied under Normal Conditions of Transport (NCT) and Hypothetical Accident Conditions (HAC).

5.1 Description of Shielding Design

5.1.1. Design Features

The Model 2000 cask is a cylindrical lead lined cask used for transporting Type B quantities of radioactive materials and solid fissile materials. For any shipments of radioactive material in the Model 2000 cask, the use of the HPI is required, and all contents must be confined inside the HPI cavity. The radiation shielding design features of the Model 2000 with the HPI are the lead and stainless steel (SS) in the Model 2000 cask and the depleted uranium (DU) and stainless steel in the HPI. Narrative descriptions of the HPI, Model 2000 cask, and Model 2000 overpack are provided in Section 1.2. The radiation shielding design features of the Model 2000 with the HPI are provided in Table 5.1-1, including nominal dimensions, materials of construction, and densities of the materials that provide gamma shielding.

Table 5.1-1. Model 2000 Transport Package Shielding Design Features

| Model 2000 Component | Part | Component | Thickness (in) | Thickness (cm) | Material of Construction | Material Density (lb/in ³) | Material Density (g/cm ³) |
|----------------------|--------------------|--------------------------|----------------|----------------|--------------------------|----------------------------------------|---------------------------------------|
| HPI | Top Plug | Inner Shell | [[]] | [[]] | [[]] | 0.29 | 8.000 |
| | | DU | [[]] | [[]] | DU | [[]] | [[]] |
| | | Outer Shell | [[]] | [[]] | [[]] | 0.29 | 8.000 |
| | HPI Body | Inner Shell | [[]] | [[]] | [[]] | 0.29 | 8.000 |
| | | DU | [[]] | [[]] | DU | [[]] | [[]] |
| | | Outer Shell | [[]] | [[]] | [[]] | 0.29 | 8.000 |
| | Bottom [[]] | Inner Shell | [[]] | [[]] | [[]] | 0.29 | 8.000 |
| | | DU | [[]] | [[]] | DU | [[]] | [[]] |
| | | Outer Shell | [[]] | [[]] | [[]] | 0.29 | 8.000 |
| Cask | Cask Lid | Lid Flange | 1.75 | 4.445 | SS304 | 0.29 | 8.000 |
| | | Lead | 5.37 | 13.64 | Lead | 0.41 | 11.34 |
| | | Inner Plate | 1.50 | 3.810 | SS304 | 0.29 | 8.000 |
| | Cask Body (Side) | Cavity Shell | 1.00 | 2.540 | SS304 | 0.29 | 8.000 |
| | | Lead | 4.00 | 10.16 | Lead | 0.41 | 11.34 |
| | | Cask Shell | 1.00 | 2.540 | SS304 | 0.29 | 8.000 |
| | Cask Body (Bottom) | Cask Bottom ¹ | 5.88 | 14.92 | SS304 | 0.29 | 8.000 |

NEDO-33866 Revision 0
Non-Proprietary Information – Class I (Public)

| Model 2000 Component | Part | Component | Thickness (in) | Thickness (cm) | Material of Construction | Material Density (lb/in ³) | Material Density (g/cm ³) |
|-----------------------|-------------------|---------------|----------------|----------------|--------------------------|----------------------------------------|---------------------------------------|
| Overpack ² | Overpack (Top) | Top Plate | 0.50 | 1.27 | SS304 | 0.29 | 8.000 |
| | | End Plate | 0.50 | 1.270 | SS304 | 0.29 | 8.000 |
| | Overpack (Side) | Inner Shell | 0.50 | 1.270 | SS304 | 0.29 | 8.000 |
| | | Outer Shell | 0.50 | 1.270 | SS304 | 0.29 | 8.000 |
| | Overpack (Bottom) | Support Plate | 0.50 | 1.270 | SS304 | 0.29 | 8.000 |
| | | Bottom Plate | 0.50 | 1.270 | SS304 | 0.29 | 8.000 |
| | | End Plate | 0.50 | 1.270 | SS304 | 0.29 | 8.000 |

Notes: ¹ Due to [[]], the minimum thickness is used.

² Credit for shielding provided by the cask overpack is only taken for NCT analyses.

General: All dimensions based on component licensing drawings in Section 1.3.1.

5.1.2. Summary Table of Maximum Radiation Levels

Table 5.1-2 and Table 5.1-3 present the maximum calculated NCT and HAC dose rates, at the appropriate locations for exclusive use shipment of the Model 2000 Transport Package with the HPI. The calculated NCT and HAC dose rates are reported for each of the three content types described in Section 5.2, as well as the overall maximum dose rates from all contents. The 1-meter transportation index dose rate limits are not applicable as the Model 2000 cask will only be shipped exclusive use. The Model 2000 cask will only be shipped in the upright position, thus the 2-meter and occupied position (cab) dose rates are calculated at the appropriate distances from the side of the cask. Dose rates are limited to 90% of the regulatory limit at each location to provide additional assurance that any small uncertainties in the source term or cask modeling will not result in external dose rates exceeding the respective regulatory limit.

Table 5.1-2. Maximum NCT Dose Rates

| Contents | Radiation | Package Surface mSv/hr (mrem/hr) | | | 2-meter mSv/hr (mrem/hr) | Cab mSv/hr (mrem/hr) |
|--------------------------|-----------------|-------------------------------------|---------------|--------------|--------------------------------|----------------------------|
| | | Top | Side | Bottom | Side | Side |
| 1 | Gamma + Neutron | 0.320 (32.0) | 1.800 (180.0) | 0.943 (94.3) | 0.046 (4.6) | 0.009 (0.9) |
| 2 | Gamma | 0.103 (10.3) | 1.800 (180.0) | 0.166 (16.6) | 0.026 (2.6) | 0.005 (0.5) |
| 3 | Gamma | 0.360 (36.0) | 1.716 (171.6) | 0.767 (76.7) | 0.033 (3.3) | 0.006 (0.6) |
| Overall Maximum | | 0.360 (36.0) | 1.800 (180.0) | 0.943 (94.3) | 0.046 (4.6) | 0.009 (0.9) |
| 10 CFR 71.47(b)(2) Limit | | 2 (200) | 2 (200) | 2 (200) | 0.1 (10) | 0.02 (2) |

Contents: 1 – Irradiated fuel

2 – Irradiated hardware and byproducts

3 – Cobalt-60 isotope rods

Table 5.1-3. Maximum HAC Dose Rates

| Contents | HAC | 1 Meter from Package Surface mSv/hr (mrem/hr) | | |
|--------------------------|-----------------|--------------------------------------------------|---------------|--------------|
| | Radiation | Top | Side | Bottom |
| 1 | Gamma + Neutron | 0.512 (51.2) | 0.994 (99.4) | 0.409 (40.9) |
| 2 | Gamma | 0.134 (13.4) | 0.343 (34.3) | 0.085 (8.5) |
| 3 | Gamma | 1.169 (116.9) | 3.391 (339.1) | 0.691 (69.1) |
| Overall Maximum | | 1.169 (116.9) | 3.391 (339.1) | 0.691 (69.1) |
| 10 CFR 71.51(a)(2) Limit | | 10 (1000) | 10 (1000) | 10 (1000) |

Contents: 1 – Irradiated fuel
2 – Irradiated hardware and byproducts
3 – Cobalt-60 Isotope rods

5.2 Source Specification

The four categories of allowable contents for the Model 2000 cask are: 1) irradiated fuel, 2) irradiated hardware and byproducts, 3) cobalt-60 isotope rods, and 4) special nuclear material (SNM). The irradiated fuel contents have photon and neutron source terms for determining package external dose rates. The irradiated hardware and byproduct and cobalt-60 isotope rod contents have photon source terms for determining package external dose rates. The SNM contents have insignificant photon and neutron source terms for determining package external dose rates. Due to the thick layers of shielding provided by the HPI and Model 2000 cask, external dose rate contributions from charged particles (alpha and beta particles) and their secondary particles from interactions (i.e., bremsstrahlung) are negligible. The exception to the above statement is that the neutron source from alpha-n reactions in the irradiated fuel contents is considered, as explained in Section 5.2.2. All content types may be shipped in either Configuration 1 or Configuration 2, as defined in Section 1.2.2.3. The HPI material basket is required for all content types when shipping in Configuration 2. When shipping in Configuration 1, the use of the HPI material basket is optional for all content types.

Irradiated Fuel

The irradiated fuel contents are commercial fuel rods, which are segmented and placed into the HPI. The required parameters for the irradiated fuel that are relevant to the shielding analysis include:

1. Cooling Time: Minimum of 120 days.
2. Length: Minimum active fuel length of 10 inches for each rod segment.
3. Arrangement: Confined, placed into the HPI material basket or additional shoring component that ensures the rods remain upright.
4. Initial enrichment U-235: Maximum of 6 wt%.
5. Fuel exposure: Maximum of 72 GWd/MTU.

Irradiated Hardware and Byproducts

The irradiated hardware and byproduct contents are irradiated components from typical reactor operation. These contents include:

1. Hardware: Irradiated metals composed of materials such as stainless steels, carbon steels, nickel alloys, and zirconium alloys. Examples include:
 - Bundle components: water rods, spacers, and upper/lower tie plates
 - Reactor internals: jet pump beams, core shroud samples
2. Irradiated Byproducts: Irradiated control rod blades with the following neutron poison materials:
 - Hafnium
 - Boron Carbide

Cobalt-60 Isotope Rods

The radioactive material in the isotope rod contents is in the form of pellets or cylindrical solid rods with the source(s) evenly distributed and encapsulated in normal or special form. The isotope rods are loaded into a commercial or research reactor to irradiate the cobalt source pellets. After discharge from the reactor, the isotope rods are loaded into the Model 2000 cask for transport. These rods may be [[]] prior to loading into the HPI. Herein for the cobalt-60 isotope rod contents, the term ‘rod’ refers to a full-length rod, in its form as it is irradiated in a reactor; and the term ‘rod [[]]’ refers to a [[]] rod in its form as it is loaded and shipped in the Model 2000 Transport Package.

Special Nuclear Material

There are no significant gamma or neutron sources in the SNM contents, thus this content type is not applicable for the shielding analysis, as it is not limited by dose rate or thermal calculations.

5.2.1. Gamma Source

5.2.1.1. Irradiated Fuel

To calculate a gamma energy spectrum and source strength for the irradiated fuel contents, the ARP methodology is used, which implements the ORIGEN-S module with the GE 10x10 ARP cross section libraries distributed in the SCALE6.1 code package (Reference 5-2). With the ARP methodology, a problem dependent cross section library is generated by interpolating between cross sections in the SCALE pre-generated libraries. The pre-generated GE 10x10 library covers initial uranium enrichments from 1.5 to 6 wt%, with burnup from 0 to 72 GWd/MTU, and moderator densities from 0.1 to 0.9 g/cm³. Any mention of enrichment refers to the initial U-235 enrichment of the fuel. ORIGEN-ARP has been validated extensively for light water reactor spent fuel, as documented in the Oak Ridge National Lab report ORNL/TM-13584 (Reference 5-3). Details of the parameters used for the ORIGEN-ARP neutron and photon irradiated fuel source term calculations are provided in Section 5.5.1.

The gamma energy spectrum from irradiated fuel contents is based on the radionuclide inventory generated from the irradiation and decay of various nuclides over time. Table 5.2-1 lists the representative gamma energy spectrum from the ORIGEN-ARP source term calculations, in the default 18-group ORIGEN-ARP gamma energy grouping structure. The gamma source strength is dependent on the enrichment (e) band and burnup (b) band. In the ORIGEN-ARP source term analysis, for each initial enrichment band the minimum enrichment is considered, and for each burnup band the maximum burnup is considered. This generates a bounding source strength for each burnup-enrichment pairing. For the calculated source strength for each burnup-enrichment pairing the basis is 1 gram of U-235. Table 5.2-2 lists the total gamma source strength for each burnup-enrichment pairing (in $\gamma/s/gU235$). The source term for irradiated fuel, in γ/s for each energy group, for a given mass of irradiated fuel is calculated by multiplying the values in Table 5.2-1 by the source strength for the respective burnup-enrichment pairing in Table 5.2-2 and the initial mass of U-235 in the rods.

Table 5.2-1. Irradiated Fuel Gamma Source Energy Spectrum

| Energy Group (MeV) | Relative Intensity |
|--------------------|--------------------|
| 5.00E-02 | 2.398E-01 |
| 1.00E-01 | 7.709E-02 |
| 2.00E-01 | 8.045E-02 |
| 3.00E-01 | 1.997E-02 |
| 4.00E-01 | 1.528E-02 |
| 6.00E-01 | 1.632E-01 |
| 8.00E-01 | 3.431E-01 |
| 1.00E+00 | 4.343E-02 |
| 1.33E+00 | 1.024E-02 |
| 1.66E+00 | 5.313E-03 |
| 2.00E+00 | 6.354E-04 |
| 2.50E+00 | 1.406E-03 |
| 3.00E+00 | 5.383E-05 |
| 4.00E+00 | 3.650E-06 |
| 5.00E+00 | 2.743E-09 |
| 6.50E+00 | 1.101E-09 |
| 8.00E+00 | 2.160E-10 |
| 1.00E+01 | 4.585E-11 |

Table 5.2-2. Irradiated Fuel Gamma Source Strengths ($\gamma/s/gU235$)

| Enrichment (wt% U-235) | Burnup (GWd/MTU) | | | | | | |
|-----------------------------|------------------|-------------|-------------|-------------|-------------|-------------|-------------|
| | 0 < b ≤ 10 | 10 < b ≤ 20 | 20 < b ≤ 30 | 30 < b ≤ 40 | 40 < b ≤ 50 | 50 < b ≤ 60 | 60 < b ≤ 72 |
| 0.71 ≤ e < 1.5 ¹ | 1.475E+13 | 1.846E+13 | - | - | - | - | - |
| 1.5 ≤ e < 2.0 | 5.907E+12 | 7.283E+12 | 8.269E+12 | 9.070E+12 | 9.736E+12 | 1.029E+13 | 1.089E+13 |
| 2.0 ≤ e < 2.5 | 4.460E+12 | 5.454E+12 | 6.156E+12 | 6.742E+12 | 7.248E+12 | 7.682E+12 | 8.152E+12 |
| 2.5 ≤ e < 3.0 | 3.586E+12 | 4.362E+12 | 4.898E+12 | 5.350E+12 | 5.751E+12 | 6.107E+12 | 6.499E+12 |
| 3.0 ≤ e < 3.5 | 3.000E+12 | 3.634E+12 | 4.064E+12 | 4.427E+12 | 4.754E+12 | 5.054E+12 | 5.391E+12 |
| 3.5 ≤ e < 4.0 | 2.579E+12 | 3.115E+12 | 3.472E+12 | 3.771E+12 | 4.045E+12 | 4.301E+12 | 4.595E+12 |
| 4.0 ≤ e < 4.5 | 2.263E+12 | 2.726E+12 | 3.030E+12 | 3.282E+12 | 3.515E+12 | 3.736E+12 | 3.994E+12 |

| Enrichment (wt% U-235) | Burnup (GWd/MTU) | | | | | | |
|---------------------------|------------------|-------------|-------------|-------------|-------------|-------------|-------------|
| | 0 < b ≤ 10 | 10 < b ≤ 20 | 20 < b ≤ 30 | 30 < b ≤ 40 | 40 < b ≤ 50 | 50 < b ≤ 60 | 60 < b ≤ 72 |
| 4.5 ≤ e < 5.0 | 2.016E+12 | 2.423E+12 | 2.687E+12 | 2.905E+12 | 3.105E+12 | 3.297E+12 | 3.526E+12 |
| 5.0 ≤ e < 5.5 | 1.818E+12 | 2.181E+12 | 2.414E+12 | 2.604E+12 | 2.779E+12 | 2.948E+12 | 3.150E+12 |
| 5.5 ≤ e < 6.0 | 1.655E+12 | 1.983E+12 | 2.191E+12 | 2.360E+12 | 2.514E+12 | 2.663E+12 | 2.844E+12 |

Note: ¹Determined with a power fit extrapolation of the calculated values, increased by 20%.

5.2.1.2. Irradiated Hardware and Byproducts

For the irradiated hardware and byproduct contents, the gamma source strength and spectra are based on the individual radionuclides in a given shipment. Multiple ORIGEN-S irradiation calculations were used to identify the radionuclides that could be in a shipment of irradiated hardware and byproduct. Table 5.2-3 provides a comprehensive list of all radionuclides that may be present in irradiated hardware and byproduct contents and contribute to external dose rates. Other radionuclides which may be present in irradiated hardware and byproducts but do not emit significant gammas were excluded from Table 5.2-3. However, all radionuclides that may be present in irradiated hardware and byproducts are considered when determining the total decay heat of the payload as described in Section 5.5.4.

External dose rates are calculated individually for 1 Ci of activity with the energy spectrum from each of the listed radionuclides. The energy spectrum for each radionuclide is from the Origen-S Data Library origen.rev04.mpdkgam.data (Reference 5-2). The dose rate contribution from a specific radionuclide at a regulatory dose rate location is calculated by multiplying the total activity for the radionuclide by its respective dose rate per curie multiplier. The total dose rate from a payload of irradiated hardware and byproduct is calculated by summing the dose rate contributions from each radionuclide included in the shipment. Details of the ORIGEN-S irradiated hardware and byproduct source term calculations and the energy spectra for each radionuclide of interest are provided in Section 5.5.2.

Table 5.2-3. Irradiated Hardware and Byproduct - Radionuclides Significant to External Dose Rates

| Radionuclides |
|------------------|
| Sc-46 |
| Cr-51 |
| Mn-54 |
| Co-58 |
| Fe-59 |
| Co-60 |
| Zn-65 |
| Nb-92m |
| Nb-94 |
| Zr/Nb-95 |
| Sb-124 |
| Sb-125 |
| Sb-126 |
| Cs-134 |
| Cs-137 (Ba-137m) |
| Hf-175 |

| Radionuclides |
|---------------|
| Hf-181 |
| Ta-182 |

5.2.1.3. Cobalt-60 Isotope Rods

The primary gamma source in the cobalt-60 isotope rod content is from the cobalt-60 source pellets. Dose rate contributions from the small quantities of radionuclides in crud that has built up on the rods while in the reactor is negligible. The cask external dose rates are dominated by the quantity of cobalt-60 in the isotope rods, and any dose rate contributions from any radionuclides in the rod cladding can be accounted for as irradiated hardware (see Section 5.4.4.4 for further explanation). Table 5.2-4 provides the energy spectrum and gamma source strength for cobalt-60 used for dose rate calculations. The energy spectrum is from the Origen-S data library `origen.rev04.mpdkgam.data` (Reference 5-2). All energy lines less than 0.1 MeV are considered negligible and are thus neglected from the energy spectrum. The source strength is based on the cobalt-60 activity equivalent to the Configuration 2 thermal limit (3000 W). The watt/curie conversion factor is based on the ORIGEN-S decay library `origen.rev03.decay.data` (Reference 5-2). The values from this library and the calculation of a watt/curie conversion factor for multiple radionuclides are presented in Section 5.5.4. Using the watt/curie conversion factor presented in Section 5.5.4, the equivalent activity for 3000 W is 194,500 Ci of cobalt-60.

Table 5.2-4. Isotope Rod Source Term (194,500 Ci Cobalt-60)

| Energy (MeV) | Relative Intensity | Source Strength (γ/sec) |
|--------------|--------------------|-------------------------|
| 0.347 | 7.500E-05 | 5.397E+11 |
| 0.826 | 7.600E-05 | 5.469E+11 |
| 1.173 | 9.985E-01 | 7.186E+15 |
| 1.333 | 9.998E-01 | 7.195E+15 |
| 2.159 | 1.200E-05 | 8.636E+10 |
| 2.506 | 2.000E-08 | 1.439E+08 |
| Total | 1.998E+00 | 1.439E+16 |

5.2.2. Neutron Source

5.2.2.1. Irradiated Fuels

The neutron energy spectrum and source strength for the irradiated fuel contents are calculated with the same method as the gamma energy source term. The ORIGEN-ARP source term calculations detailed in Section 5.5.1 generate both the gamma and neutron source terms for the irradiated fuel contents.

Table 5.2-5 lists the representative neutron energy spectrum calculated in the ORIGEN-ARP source term calculations, in the default 27-group ORIGEN-ARP neutron energy grouping structure. Neutron energies below 2.5E-02 MeV are included in the first group. The representative neutron spectrum is from Case b10e55 as explained in Section 5.5.1. Table 5.2-6 lists the total neutron source strength for each burnup-enrichment pairing (in n/s/gU235).

Table 5.2-5. Irradiated Fuel Neutron Source Energy Spectrum

| E (MeV) | Relative Intensity |
|----------|--------------------|
| 2.50E-02 | 1.311E-03 |
| 1.00E-01 | 8.976E-03 |
| 4.00E-01 | 6.445E-02 |
| 9.00E-01 | 1.390E-01 |
| 1.40E+00 | 1.426E-01 |
| 1.85E+00 | 1.240E-01 |
| 2.35E+00 | 1.337E-01 |
| 2.48E+00 | 3.155E-02 |
| 3.00E+00 | 1.169E-01 |
| 4.80E+00 | 1.862E-01 |
| 6.43E+00 | 3.670E-02 |
| 8.19E+00 | 1.104E-02 |
| 2.00E+01 | 3.637E-03 |

Table 5.2-6. Irradiated Fuel Neutron Source Strengths (n/s/gU235)

| Enrichment (wt% U-235) | Burnup (GWd/MTU) | | | | | | |
|-----------------------------|------------------|-------------|-------------|-------------|-------------|-------------|-------------|
| | 0 < b ≤ 10 | 10 < b ≤ 20 | 20 < b ≤ 30 | 30 < b ≤ 40 | 40 < b ≤ 50 | 50 < b ≤ 60 | 60 < b ≤ 72 |
| 0.71 ≤ e < 1.5 ¹ | 1.827E+04 | 1.699E+05 | - | - | - | - | - |
| 1.5 ≤ e < 2.0 | 1.808E+03 | 1.824E+04 | 6.683E+04 | 1.565E+05 | 2.935E+05 | 5.002E+05 | 9.357E+05 |
| 2.0 ≤ e < 2.5 | 8.949E+02 | 9.447E+03 | 3.675E+04 | 9.110E+04 | 1.773E+05 | 3.061E+05 | 5.692E+05 |
| 2.5 ≤ e < 3.0 | 4.993E+02 | 5.429E+03 | 2.191E+04 | 5.672E+04 | 1.143E+05 | 2.006E+05 | 3.716E+05 |
| 3.0 ≤ e < 3.5 | 3.032E+02 | 3.369E+03 | 1.388E+04 | 3.708E+04 | 7.696E+04 | 1.374E+05 | 2.545E+05 |
| 3.5 ≤ e < 4.0 | 1.963E+02 | 2.217E+03 | 9.217E+03 | 2.518E+04 | 5.354E+04 | 9.729E+04 | 1.806E+05 |
| 4.0 ≤ e < 4.5 | 1.335E+02 | 1.529E+03 | 6.382E+03 | 1.770E+04 | 3.830E+04 | 7.067E+04 | 1.318E+05 |
| 4.5 ≤ e < 5.0 | 9.442E+01 | 1.096E+03 | 4.592E+03 | 1.283E+04 | 2.810E+04 | 5.251E+04 | 9.845E+04 |
| 5.0 ≤ e < 5.5 | 6.903E+01 | 8.098E+02 | 3.406E+03 | 9.549E+03 | 2.108E+04 | 3.978E+04 | 7.504E+04 |
| 5.5 ≤ e < 6.0 | 5.188E+01 | 6.129E+02 | 2.589E+03 | 7.268E+03 | 1.614E+04 | 3.067E+04 | 5.818E+04 |

Note: ¹Determined with a power fit extrapolation of the calculated values, increased by 20%.

The source term, in n/s for each energy group, for a given mass of irradiated fuel is calculated by multiplying the values in Table 5.2-5 by the respective source strength for the respective burnup-enrichment pairing in Table 5.2-6 and the initial mass of U-235 in the rods.

5.2.2.2. Irradiated Hardware and Byproducts / Cobalt-60 Isotope Rods

There is no applicable neutron source term for the irradiated hardware and byproduct, and cobalt-60 isotope rod contents.

5.3 Shielding Model

5.3.1. Configuration of Source and Shielding

The following subsections describe the MCNP6 shielding model geometry and source configuration for the dose rate calculations of each of the described content types of the Model 2000 cask.

5.3.1.1. MCNP Source Distribution

An individual source geometry is used in the MCNP6 shielding model for each of the Model 2000 cask contents. The source geometry for each content type is based on the respective content specifications and the source term calculation.

Irradiated Fuel

For the segmented irradiated fuel rod content, the NCT source geometry is a single 10-inch line source across which the photon and neutron sources are distributed uniformly. The irradiated fuel source specification requires that the fuel rod active fuel length when loaded into the Model 2000 Transport Package is greater than 10 inches. Using the minimum allowable segment length for the MCNP6 model line source ensures a bounding dose rate calculation, as greater distribution of the source activity (a longer line source) results in lower calculated external dose rates.

The axial distribution of activity across an irradiated fuel rod is due to two variables: different initial enrichment across the rod and variations in moderator density during irradiation. The bounding gamma and neutron source strength considered for any given rod segment is based on the minimum enrichment in the rod segment. During the irradiation of the fuel rods, lower moderator densities results in higher source strengths. By calculating all gamma and neutron source strengths at the minimum moderator density (0.1 g/cm³) available in the library, the calculated source strengths are bounding for any expected changes in axial moderator density. Thus, a uniform line source is acceptable despite the variations in the irradiated fuel rod activity profile, because the source term calculation results in bounding gamma and neutron source strengths.

For the HAC MCNP6 shielding model source geometry, it is conservative to assume that the structural components in the cask cavity fail; all activity is concentrated into a single point. The source locations for the NCT model line source and the HAC model point source are in the locations shown in Figure 5.3-1.

Irradiated Hardware and Byproducts

Due to the uncertainty in the form and activity distribution of irradiated hardware or byproduct contents, both the NCT and HAC MCNP6 shielding model conservatively assumes that all the activity is concentrated into a single point. The source locations of the point sources in the MCNP6 shielding models for the irradiated hardware and byproduct dose rate calculations are shown in Figure 5.3-1. Therefore, the use of the HPI material basket is not required. Use of the HPI material basket for shipments of irradiated hardware and byproducts, such as activated SS that may be used as fuel/isotope rod cladding material, is bounded by the shielding results obtained from the point source model, as long as all dose rate and thermal limits are satisfied.

Cobalt-60 Isotope Rods

For the cobalt-60 isotope rod content, the NCT source geometry is a single 12-inch line source, across which the photon source activity is distributed uniformly. There is variation in the distribution of cobalt-60 activity in the HPI cavity with a shipment of cobalt-60 isotope rod

[[]], due to the irradiation history of the rods, [[]] and loading of the rods into the HPI. Section 5.5.3 provides a discussion of the distribution of activity in the HPI cavity for the cobalt-60 isotope rod contents, and the basis for a 12-inch line source for NCT dose rate calculations.

For the HAC MCNP6 shielding model source geometry, it is conservative to assume that the structural components in the cask cavity fail; all activity is concentrated into a single point. The source locations for the NCT model line source and the HAC model point source are in the locations shown in Figure 5.3-1.

5.3.1.2. MCNP Source Locations

The sources for the MCNP6 dose rate calculations are modeled in the HPI cavity in the position that results in the highest dose rate for the respective regulatory dose rate location. This limiting source position changes based on the geometry of the source and the direction of interest. Figure 5.3-1 provides two depictions of the Model 2000 cask with the HPI. This figure shows the positions for any point or line sources in the HPI cavity for all dose rate calculations.

The source positions for side dose rate locations are located at the bottom corner of the HPI cavity, at the interface of the HPI body and the HPI bottom [[]]. This is the most restrictive location for side dose rates because in this area the [[]], due to the step at this interface. For the HAC Side 1-meter dose rate, the calculated dose rate is higher with a point source in the bottom corner than in the top corner of the HPI cavity, despite the slump in the lead column.

The line source positions for top and bottom dose rate locations are centered in the HPI cavity so that particles emitted at any location along the line source can travel at any angle in the direction of interest, unimpeded before entering the respective plug (top or bottom). For a line source pushed to the side against the HPI body, there is a reduction in the calculated dose rates for the top and bottom.

[[

]]

Figure 5.3-1. MCNP Point / Line Source Locations

5.3.1.3. MCNP NCT Shielding Model Geometry

The MCNP NCT model geometry used for the dose rate calculations in this shielding analysis is a detailed three-dimensional model of the HPI, the Model 2000 cask, and the overpack. Table 5.3-1 provides the relevant dimensions of the MCNP shielding model including the modeled thicknesses of each material and the MCNP surface numbers used in the geometry. This table along with Table 5.1-1 allow for a quick review of the most significant dimensions of the shielding model geometry. All HPI shield dimensions are at the minimum, per the respective licensing drawings, with the fabrication tolerances subtracted from the nominal values. The model dimensions for the Model 2000 cask and overpack use predominantly nominal dimensions with some areas of reduced thickness. For example, for the [[]], the cask bottom is considered to be flat at the minimum thickness. The majority of the material thicknesses prescribed by the Model 2000 cask and overpack licensing drawings have tolerances based on ASTM specifications, as the component dimensions are based on ASTM stainless steel stock plate. Per ASTM A480 (Reference 5-4), for plates up to 10 inches in thickness, the tolerance under the specified thickness is 0.01 inches. These plate thicknesses are modeled at the specified nominal plate value.

Table 5.3-1. Relevant MCNP Shielding Model Dimensions

| Model 2000 Component | Part | Dimension | MCNP Surface(s) | Value (cm) | Value (in) |
|----------------------|----------------|------------------------------|-----------------|--------------------|--------------------|
| Cask | Cask Lid | t _{SS1} | 17 / 18 | 3.810 | 1.500 |
| | | t _{Pb} | 18 / 20 | 13.64 | 5.370 |
| | | t _{SS2} | 20 / 23 | 4.445 | 1.750 |
| | Cask Side | r _{cavity} | 3 | 33.66 | 13.25 |
| | | t _{SS1} | 3 / 6 | 2.540 | 1.000 |
| | | t _{Pb} | 6 / 10 | 10.16 | 4.000 |
| | | t _{SS2} | 10 / 11 | 2.540 | 1.000 |
| | | h _{Pb} ³ | 16 / 19 | 141.9 | 55.87 |
| | | t _{SS} | 15 / 115 | 14.94 ¹ | 5.880 ¹ |
| | | h _{cavity} | 115 / 17 | 137.5 | 54.13 |
| HPI | HPI Top Lid | t _{SS1} | 149 / 150 | [[]] | [[]] |
| | | t _{DU} | 150 / 1152 | [[]] | [[]] |
| | | t _{SS2} | 152 / 153 | [[]] | [[]] |
| | HPI Body Side | r _{cavity} | 135 | [[]] | [[]] |
| | | t _{SS1} | 135 / 136 | [[]] | [[]] |
| | | t _{DU} | 136 / 1136 | [[]] | [[]] |
| | | t _{SS2} | 137 / 138 | [[]] | [[]] |
| | HPI Bottom Lid | t _{SS1} | 115 / 140 | [[]] | [[]] |
| | | t _{DU} | 1140 / 145 | [[]] | [[]] |
| | | t _{SS2} | 145 / 146 | [[]] | [[]] |

NEDO-33866 Revision 0
Non-Proprietary Information – Class I (Public)

| Model 2000 Component | Part | Dimension | MCNP Surface(s) | Value (cm) | Value (in) |
|----------------------|--------|------------------|-----------------|------------|------------|
| Overpack | Top | t _{SS1} | 1010 / 1011 | 1.270 | 0.500 |
| | | t _{SS2} | 1012 / 1013 | 1.270 | 0.500 |
| | Side | t _{SS1} | 1001 / 1002 | 1.270 | 0.500 |
| | | t _{SS2} | 1003 / 1004 | 1.270 | 0.500 |
| | Bottom | t _{SS1} | 1005 / 1006 | 1.270 | 0.500 |
| | | t _{SS2} | 1007 / 1008 | 1.270 | 0.500 |
| | | t _{SS3} | 1009 / 15 | 1.270 | 0.500 |

Notes: ¹ Cask Bottom modeled flat, with thickness equal to the 6.13" height minus the [[]].

² Minimum DU thicknesses considered with tolerance gaps explicitly modeled.

³ Lead column height.

There are two different NCT shielding models. One is for photon dose rate calculations and the other is for neutron dose rate calculations. For both of these models the geometry including the tally cells is the same. However, for the photon dose rate model the materials for the HPI, cask, and overpack are defined as prescribed in Section 5.3.2. For the neutron dose rate NCT model, all cells are modeled as void, neglecting any shielding provided by the materials of the packaging. Taking no credit for shielding of neutrons provided by the HPI, the Model 2000 cask, and the Model 2000 overpack results in bounding calculated dose rates. The dose rates calculated considering all shielding materials as void bounds the resulting dose rates crediting the shielding provided by all cask components, any additional neutrons from subcritical multiplication, and the additional photons from neutron interactions in the cask.

[[

]]

Figure 5.3-2. NCT MCNP Shielding Models (Left – Photon / Right – Neutron)

The NCT model conservatively neglects the additional shielding provided by the HPI material basket for irradiated fuel and cobalt-60 isotope rod contents. Due to the use of vertical line sources these contents must be shipped in the upright position. The HPI material basket may be used to position these contents in the upright position.

5.3.1.4. MCNP HAC Shielding Model Geometry

For HAC, the MCNP shielding model only includes the HPI and the Model 2000 cask, with dimensions as prescribed in Table 5.3-1. This model conservatively assumes the removal of the overpack. Additionally, the HAC model also includes the slump in the lead column of the Model 2000 cask body. In Section 2.12.2, the maximum deformation in the lead column is calculated to be 3.56 mm. This value is rounded up to 4 mm for this analysis. It is determined in Chapter 2 that the overpack provides adequate protection from HAC to the cask body. More specifically, in Section 2.12.1 it is stated that the cask dropped 30 feet followed by a drop of 40 inches onto a rigid pin 6 inches in diameter, no gross deformations of the cask are predicted. As with the NCT models, there are two different HAC shielding models, as shown in

Figure 5.3-3. These models have the same geometry but the photon model includes the materials of the HPI and the Model 2000 cask, and the neutron model neglects all materials.

[[

]]

Figure 5.3-3. HAC MCNP Shielding Models (Left – Photons / Right – Neutrons)

5.3.1.5. MCNP Tallies

To calculate the particle flux at the regulatory dose rate locations of interest, multiple arrangements of cell tallies are modeled at each location. The void cells that are added to the model for particle tallying allow for dose rates to be calculated at the multiple locations of interest, without having an effect on the calculated flux. All of the tally cells are modeled as small 1 cm thick volumes, to ensure that the calculated flux is not averaged over too large of a region.

Table 5.3-2 lists the relevant tally locations in the MCNP shielding analysis to demonstrate compliance with each of the regulatory dose rate requirements in 10 CFR 71.47 and 10 CFR 71.51 (Reference 5-1). Table 5.3-3 lists the dimension in the MCNP shielding model from the origin, to the respective dose rate location. The values listed for the top and bottom dose rates refer to the distance along the Y-axis from the origin, and the side dose rate values refer to

the distance along the X-axis from the origin. The origin is specified as the exterior bottom, center point of the Model 2000 cask.

Figures 5.3-4 and 5.3-5 provide depictions of the tally cells used in the MNCP6 shielding analysis models, with the tally cells highlighted in yellow. All tally cells are 1 cm thick and relatively small in size, in order to ensure that the flux calculation is not averaged over a large area, and dose rates are representative of the sampled region.

Table 5.3-2. Regulatory Dose Rate Tally Locations

| Transport Condition | Dose Rate Location | MCNP Tally Number | Tally Location Description |
|---------------------|--------------------|-------------------|------------------------------------------------------------------|
| NCT | Top Surface | 24 | Top surface of the Model 2000 overpack |
| | Side Surface | 24 | Side surface of the Model 2000 overpack |
| | Side 2 meter | 34 | 2 meters from the projected lateral trailer surface ¹ |
| | Cab | 44 | Located 25 feet from the cask centerline ² |
| | Bottom Surface | 24 | Bottom surface of the Model 2000 overpack |
| HAC | Top 1 meter | 34 | 1 Meter from the Model 2000 cask top surface |
| | Side 1 meter | 34 | 1 Meter from the Model 2000 cask side surface |
| | Bottom 1 meter | 34 | 1 Meter from the Model 2000 cask bottom surface |

Notes: ¹ The Model 2000 Trailer is 101.75 inches wide.

² The Model 2000 Trailer provides 28 feet to the cab from the cask centerline (reduced to 25 feet for margin)

Table 5.3-3. Relevant MCNP Tally Dimensions

| Relevant MCNP Dimensions | | Top (Y) | | Side (X) | | Bottom (Y) | |
|--------------------------|----------------------------|---------|--------|----------|---------|------------|---------|
| | | inches | cm | inches | cm | inches | cm |
| Reference Dimensions | Origin ¹ | 0 | 0 | 0 | 0 | 0 | 0 |
| | Cask Surface | 71.00 | 180.34 | 19.25 | 48.895 | 0 | 0 |
| NCT Tallies | Surface Tally ² | 101.5 | 257.81 | 24.25 | 61.595 | -12.750 | -32.385 |
| | 2 meter Tally | - | | 129.6 | 329.22 | - | |
| | Cab Tally | - | | 300.00 | 762.00 | - | |
| HAC Tallies | 1 meter Tally | 110.37 | 280.34 | 58.620 | 148.495 | -39.370 | -100.00 |

Notes: ¹ Model origin is on the cask bottom.

² NCT Package Surface dose rate locations are on Model 2000 overpack surfaces.

II

II

Figure 5.3-4. NCT MCNP Tallies with 10% Margin to the Regulatory Limit

[[

]]

Figure 5.3-5. HAC MCNP Tallies with 10% Margin to the Regulatory Limit

5.3.2. Material Properties

The material compositions used for photon dose rate calculations are listed in Tables 5.3-4 through 5.3-7. There is negligible difference between the two types of stainless steel in terms of shielding effectiveness, however both types are included for accuracy to the actual materials of construction. The densities and material compositions for both stainless steel types are from Pacific Northwest National Lab report PNNL-15870 Revision 1 (Reference 5-5). The densities of the lead and depleted uranium materials are based on the minimum specified densities for these materials in the respective component licensing drawings in Section 1.3.1. All materials are modeled as void for neutron dose rate calculations, so the isotopic composition of materials is not required.

Table 5.3-4. Type 304 Stainless Steel Material Composition

| Elemental Composition | Element | Photon ZA | Mass Fraction |
|------------------------------|---------|-----------|---------------|
| | C | 6000 | 4.00E-04 |
| | Si | 14000 | 5.00E-03 |
| | P | 15000 | 2.30E-04 |
| | S | 16000 | 1.50E-04 |
| | Cr | 24000 | 1.90E-01 |
| | Mn | 25000 | 1.00E-02 |
| | Fe | 26000 | 7.02E-01 |
| | Ni | 28000 | 9.25E-02 |
| Density (g/cm ³) | 8.0 | | |

Table 5.3-5. Type 316 Stainless Steel Material Composition

| Elemental Composition | Element | Photon ZA | Mass Fraction |
|------------------------------|---------|-----------|---------------|
| | C | 6000 | 4.10E-04 |
| | Si | 14000 | 5.07E-03 |
| | P | 15000 | 2.30E-04 |
| | S | 16000 | 1.50E-04 |
| | Cr | 24000 | 1.70E-01 |
| | Mn | 25000 | 1.01E-02 |
| | Fe | 26000 | 6.69E-01 |
| | Ni | 28000 | 1.20E-01 |
| | Mo | 42000 | 2.50E-02 |
| Density (g/cm ³) | 8.0 | | |

Table 5.3-6. Lead Material Composition

| Elemental Composition | Element | Photon ZA | Mass Fraction |
|------------------------------|---------|-----------|---------------|
| | Pb | 82000 | 1.00E+00 |
| Density (g/cm ³) | 11.34 | | |

Table 5.3-7. Depleted Uranium Material Composition

| Elemental Composition | Element | Photon ZA | Mass Fraction |
|------------------------------|---------|-----------|---------------|
| | U | 92000 | 1.00E+00 |
| Density (g/cm ³) | [[]] | | |

5.4 Shielding Evaluation

5.4.1. Methods

5.4.1.1. Computer Codes

The shielding calculations for this analysis were completed using MCNP6 Version 1.0 (Reference 5-6). Photon dose rate calculations used the MCNP photoatomic data library MCPLIB84, which compiles data from the ENDF/B-VI.8 data library (Reference 5-7). Neutron

dose rate calculations used the MCNP continuous energy library ENDF71x, which compiles data from the ENDF/B-VII.1 data library (Reference 5-7). MCNP is a general-purpose, continuous-energy, generalized-geometry, time-dependent, coupled neutron/photon/electron Monte Carlo transport code. MCNP was used in either photon only transport mode or neutron only transport mode to calculate external dose rates for the Model 2000 cask for each of the content types considered.

5.4.1.2. MCNP Variance Reduction

Due to the thick layers of photon shielding provided by the Model 2000 cask and the HPI, multiple variance reduction techniques are used for the MCNP photon dose rate calculations. MCNP variance reduction parameters for weight windows, exponential transform, and source biasing were all used as necessary to aid in the statistical convergence of the MCNP photon dose rate calculations. No variance reduction techniques were required for neutron dose rates.

5.4.1.3. Irradiated Fuel Dose Rate Calculations

The default unit for a particle flux, $\phi(r,p)$, calculated in MCNP is normalized as particles/cm²/emitted particle. By applying the appropriate flux to dose rate conversion factors, $\mathcal{R}(p)$, for the respective particle p , the MCNP dose rate response, $R(r,p)$, and associated standard deviation, $\sigma_R(r,p)$, are calculated following Equations 5-1 and 5-2.

$$R(r,p) \left[\frac{\text{mrem}}{\text{hr}} \cdot \frac{\text{sec}}{\text{emitted } p} \right] = \phi(r,p) \left[\frac{\frac{p}{\text{cm}^2}}{\text{emitted } p} \right] \cdot \mathcal{R}(p) \left[\frac{\frac{\text{mrem}}{\text{hr}}}{\frac{p}{\text{cm}^2 \cdot \text{sec}}} \right] \quad (5-1)$$

$$\sigma_R(r,p) = R(r,p) \cdot \text{fsd}(r,p) \quad (5-2)$$

The quantity $R_\sigma(r,p)$ accounts for the statistical uncertainty. Two standard deviations are added to the calculated MCNP dose rate response in Equation 5-3:

$$R_\sigma(r,p) \left[\frac{\text{mrem}}{\text{hr}} \cdot \frac{\text{sec}}{\text{emitted } p} \right] = (R(r,p) + 2 \cdot \sigma_R(r,p)) \left[\frac{\text{mrem}}{\text{hr}} \cdot \frac{\text{sec}}{\text{emitted } p} \right] \quad (5-3)$$

Equation 5-4 shows that $\ddot{D}R(r,B|E)$ is the dose rate per gU235 at a regulatory dose rate location of interest, r , at the specific burnup and enrichment band, $B|E$, and is calculated by summing the product of the MCNP dose rate response with the calculated source strength, $S(B|E,p)$, for both of the particle types (gammas and neutrons):

$$\ddot{D}R(r,B|E) \left[\frac{\frac{\text{mrem}}{\text{hr}}}{\text{gU235}} \right] = \sum_p R_\sigma(r,p) \left[\frac{\text{mrem}}{\text{hr}} \cdot \frac{\text{sec}}{\text{emitted } p} \right] \cdot S(B|E,p) \left[\frac{\frac{\text{emitted } p}{\text{sec}}}{\text{gU235}} \right] \quad (5-4)$$

The total dose rate, $DR(r)$, at a given burnup and enrichment is determined by multiplying in the mass of U-235, $m(B|E)$, in the contents at the respective burnup and enrichment as shown in Equation 5-5.

$$DR(r) \left[\frac{\text{mrem}}{\text{hr}} \right] = \ddot{D}R(r,B|E) \left[\frac{\frac{\text{mrem}}{\text{hr}}}{\text{gU235}} \right] \cdot m(B|E)[\text{gU235}] \quad (5-5)$$

where

| | | | |
|---------------|-------------------------------------|------------------|-----------------------------------------------|
| R | MCNP calculated dose rate response | R_{σ} | Dose rate response with 2σ uncertainty |
| r | Regulatory dose rate location | $\dot{D}\dot{R}$ | Dose rate per gram U-235 |
| p | Particle (neutron or gamma) | S | Normalized source strength |
| ϕ | MCNP calculated flux | B E | Burnup/Enrichment pairing |
| \mathcal{R} | Flux-to-dose-rate conversion factor | DR | Total dose rate |
| σ | Standard deviation | m | Mass |
| fsd | MCNP fractional standard deviation | | |

5.4.1.4. Irradiated Hardware, Byproduct, and Cobalt-60 Isotope Rod Dose Rate Calculation

To calculate a dose rate response $R(r, X)$ for an individual radionuclide X, the MCNP calculated photon flux $\phi(r, X)$ is multiplied by the dose rate conversion factor \mathcal{R} as well as a per curie multiplier and the total number of gammas per decay of the respective radionuclide $I(X)$.

$$R(r, X) \left[\frac{\text{mrem}}{\text{hr}} \right] = \phi(r, X) \left[\frac{\frac{\gamma}{\text{cm}^2}}{\text{emitted } \gamma} \right] \cdot 3.7 \times 10^{10} \left[\frac{\frac{\text{decays}}{\text{sec}}}{\text{Ci}} \right] \cdot I(X) \left[\frac{\text{emitted } \gamma}{\text{decay}} \right] \cdot \mathcal{R} \left[\frac{\frac{\text{mrem}}{\text{hr}}}{\frac{\gamma}{\text{cm}^2 \cdot \text{sec}}} \right] \quad (5-6)$$

$$\sigma_R(r, X) = R(r, X) \cdot \text{fsd}(r, X) \quad (5-7)$$

To account for statistical uncertainty, the two standard deviations are added to the calculated MCNP dose rate per curie:

$$R_{\sigma}(r, X) \left[\frac{\text{mrem}}{\text{hr}} \right] = (R(r, X) + 2 \cdot \sigma_R(r, X)) \left[\frac{\text{mrem}}{\text{hr}} \right] \quad (5-8)$$

The total dose rate $DR(r)$ is calculated by summing the dose rate from the activity of each radionuclide:

$$DR(r) \left[\frac{\text{mrem}}{\text{hr}} \right] = \sum_X R_{\sigma}(r, X) \left[\frac{\text{mrem}}{\text{hr}} \right] \cdot A(X) [\text{Ci}] \quad (5-9)$$

where

| | | | |
|---------------|-------------------------------------|--------------|------------------------------------------------|
| R | MCNP dose rate per curie | σ | Standard deviation |
| r | Regulatory dose rate location | fsd | MCNP fractional standard deviation |
| X | Radionuclide X | R_{σ} | Dose rate per curie with 2σ uncertainty |
| ϕ | MCNP calculated flux | DR | Total dose rate |
| I | gammas/decay | A | Activity |
| \mathcal{R} | Flux-to-dose-rate conversion factor | | |

5.4.2. Input and Output Data

5.4.2.1. Input Data

Input data will be submitted separately.

5.4.2.2. Output Data

Output data will be submitted separately. The tally fluctuation chart and probability density function plot were studied for each MCNP tally to ensure proper tally bin convergence. This along with a check of the reported fsd for each tally bin and the additional statistical information reported for MCNP tallies ensured the reliability of all MCNP calculated dose rate results.

5.4.3. Flux-to-Dose-Rate Conversion

Consistent with NUREG-1609 Section 5.5.4.3 (Reference 5-8), the ANSI/ANS-6.1.1 1977 flux-to-dose-rate conversion factors (Reference 5-9) are used. The gamma and neutron conversion factors used in the MCNP input files are tabulated in Tables 5.4-1 and 5.4-2, respectively.

Table 5.4-1. Gamma Flux-to-Dose-Rate Conversion Factors (ANSI/ANS-6.1.1 1977)

| Gamma Energy (MeV) | Conversion Factor (mrem/hr)/(gammas/cm ² -s) |
|-----------------------|------------------------------------------------------------|
| 1.00E-02 | 3.96E-03 |
| 3.00E-02 | 5.82E-04 |
| 5.00E-02 | 2.90E-04 |
| 7.00E-02 | 2.58E-04 |
| 1.00E-01 | 2.83E-04 |
| 1.50E-01 | 3.79E-04 |
| 2.00E-01 | 5.01E-04 |
| 2.50E-01 | 6.31E-04 |
| 3.00E-01 | 7.59E-04 |
| 3.50E-01 | 8.78E-04 |
| 4.00E-01 | 9.85E-04 |
| 4.50E-01 | 1.08E-03 |
| 5.00E-01 | 1.17E-03 |
| 5.50E-01 | 1.27E-03 |
| 6.00E-01 | 1.36E-03 |
| 6.50E-01 | 1.44E-03 |
| 7.00E-01 | 1.52E-03 |
| 8.00E-01 | 1.68E-03 |
| 1.00E+00 | 1.98E-03 |
| 1.40E+00 | 2.51E-03 |
| 1.80E+00 | 2.99E-03 |
| 2.20E+00 | 3.42E-03 |
| 2.60E+00 | 3.82E-03 |
| 2.80E+00 | 4.01E-03 |
| 3.25E+00 | 4.41E-03 |
| 3.75E+00 | 4.83E-03 |
| 4.25E+00 | 5.23E-03 |
| 4.75E+00 | 5.60E-03 |
| 5.00E+00 | 5.80E-03 |
| 5.25E+00 | 6.01E-03 |
| 5.75E+00 | 6.37E-03 |

| Gamma Energy (MeV) | Conversion Factor (mrem/hr)/(gammas/cm ² -s) |
|-----------------------|------------------------------------------------------------|
| 6.25E+00 | 6.74E-03 |
| 6.75E+00 | 7.11E-03 |
| 7.50E+00 | 7.66E-03 |
| 9.00E+00 | 8.77E-03 |
| 1.10E+01 | 1.03E-02 |
| 1.30E+01 | 1.18E-02 |
| 1.50E+01 | 1.33E-02 |

Table 5.4-2. Neutron Flux-to-Dose-Rate Conversion Factors (ANSI/ANS-6.1.1 1977)

| Gamma Energy (MeV) | Conversion Factor (mrem/hr)/(neutrons/cm ² -s) |
|-----------------------|--------------------------------------------------------------|
| 2.50E-08 | 3.67E-03 |
| 1.00E-07 | 3.67E-03 |
| 1.00E-06 | 4.46E-03 |
| 1.00E-05 | 4.54E-03 |
| 1.00E-04 | 4.18E-03 |
| 1.00E-03 | 3.76E-03 |
| 1.00E-02 | 3.56E-03 |
| 1.00E-01 | 2.17E-02 |
| 5.00E-01 | 9.26E-02 |
| 1.00E+00 | 1.32E-01 |
| 2.50E+00 | 1.25E-01 |
| 5.00E+00 | 1.56E-01 |
| 7.00E+00 | 1.47E-01 |
| 1.00E+01 | 1.47E-01 |
| 1.40E+01 | 2.08E-01 |
| 2.00E+01 | 2.27E-01 |

5.4.4. External Radiation Levels

The maximum external radiation levels are determined individually for each of the three content types. The limiting dose rate location for all content types is the NCT side package surface. That is, for each of the three contents, the maximum allowable quantity of material is limited by the NCT side surface dose rate. The external radiation levels resulting from each of the three content types are summarized below.

5.4.4.1. Irradiated Fuel

For the irradiated fuel contents, the resulting external dose rates are calculated in two steps. First a dose rate response normalized per emitted particle is calculated in MCNP6 for both neutrons and photons, using the source spectra listed in Tables 5.2-1 and 5.2-5. The associated statistical uncertainty is added on to the calculated dose rate response as shown in Equation 5-3. The resulting values from these calculations are presented in Table 5.4-3.

**Table 5.4-3. Irradiated Fuel Tally Response with 2 σ Statistical Uncertainty
(mrem/hr per particle/s)**

| Tally Location (r) | NCT Top Surface | NCT Side Surface | NCT Bottom Surface | NCT 2-meter | NCT Cab | HAC Top 1-meter | HAC Side 1-meter | HAC Bottom 1-meter |
|--------------------|-----------------|------------------|--------------------|-------------|-----------|-----------------|------------------|--------------------|
| $R_e(n)$ | 6.731E-07 | 4.069E-06 | 2.135E-06 | 1.026E-07 | 1.843E-08 | 5.702E-07 | 5.502E-07 | 6.561E-07 |
| $R_e(\gamma)$ | 7.601E-16 | 3.929E-15 | 1.739E-15 | 7.533E-17 | 1.319E-17 | 1.842E-15 | 4.270E-15 | 1.223E-15 |

With these values, a dose rate per gU235 for each burnup-enrichment pairing is calculated. The dose rates per gU235 are calculated, as shown in Equation 5-4, by summing the neutron and photon dose rate contributions for each dose rate location and each respective burnup-enrichment pairing. The dose rate contribution from each particle type (gamma or neutron) is calculated by multiplying the dose rate for the respective location (in Table 5.4-3) by the particle source strength for the respective burnup-enrichment pairing (in Table 5.2-2 for gammas or Table 5.2-6 for neutrons). The dose rates per gU235 for all burnup-enrichment pairings, at each regulatory dose rate location are provided in Tables 5.4-4 through 5.4-11.

Table 5.4-4. NCT Top Surface Dose Rates per gU235 by Burnup-Enrichment Paring

| Enrichment (wt% U-235) | Top Surface $\dot{D}\dot{R}$ (mrem/hr/gU235) | | | | | | |
|---------------------------|----------------------------------------------|------------------|------------------|------------------|------------------|------------------|------------------|
| | Burnup (GWd/MTU) | | | | | | |
| | 0 < b \leq 10 | 10 < b \leq 20 | 20 < b \leq 30 | 30 < b \leq 40 | 40 < b \leq 50 | 50 < b \leq 60 | 60 < b \leq 72 |
| 0.71 \leq e < 1.5 | 2.351E-02 | 1.284E-01 | - | - | - | - | - |
| 1.5 \leq e < 2.0 | 5.707E-03 | 1.781E-02 | 5.127E-02 | 1.122E-01 | 2.050E-01 | 3.445E-01 | 6.381E-01 |
| 2.0 \leq e < 2.5 | 3.992E-03 | 1.050E-02 | 2.942E-02 | 6.644E-02 | 1.248E-01 | 2.118E-01 | 3.893E-01 |
| 2.5 \leq e < 3.0 | 3.062E-03 | 6.969E-03 | 1.847E-02 | 4.224E-02 | 8.131E-02 | 1.396E-01 | 2.550E-01 |
| 3.0 \leq e < 3.5 | 2.485E-03 | 5.030E-03 | 1.243E-02 | 2.832E-02 | 5.541E-02 | 9.635E-02 | 1.754E-01 |
| 3.5 \leq e < 4.0 | 2.093E-03 | 3.860E-03 | 8.842E-03 | 1.982E-02 | 3.911E-02 | 6.875E-02 | 1.250E-01 |
| 4.0 \leq e < 4.5 | 1.810E-03 | 3.101E-03 | 6.599E-03 | 1.441E-02 | 2.845E-02 | 5.040E-02 | 9.172E-02 |
| 4.5 \leq e < 5.0 | 1.596E-03 | 2.580E-03 | 5.133E-03 | 1.084E-02 | 2.127E-02 | 3.784E-02 | 6.894E-02 |
| 5.0 \leq e < 5.5 | 1.428E-03 | 2.203E-03 | 4.127E-03 | 8.406E-03 | 1.630E-02 | 2.902E-02 | 5.290E-02 |
| 5.5 \leq e < 6.0 | 1.293E-03 | 1.920E-03 | 3.408E-03 | 6.685E-03 | 1.277E-02 | 2.267E-02 | 4.132E-02 |

Table 5.4-5. NCT Side Surface Dose Rates per gU235 by Burnup-Enrichment Paring

| Enrichment (wt% U-235) | Side Surface $\dot{D}\dot{R}$ (mrem/hr/gU235) | | | | | | |
|---------------------------|-----------------------------------------------|------------------|------------------|------------------|------------------|------------------|------------------|
| | Burnup (GWd/MTU) | | | | | | |
| | 0 < b \leq 10 | 10 < b \leq 20 | 20 < b \leq 30 | 30 < b \leq 40 | 40 < b \leq 50 | 50 < b \leq 60 | 60 < b \leq 72 |
| 0.71 \leq e < 1.5 | 1.323E-01 | 7.639E-01 | - | - | - | - | - |
| 1.5 \leq e < 2.0 | 3.057E-02 | 1.028E-01 | 3.044E-01 | 6.724E-01 | 1.233E+00 | 2.076E+00 | 3.850E+00 |
| 2.0 \leq e < 2.5 | 2.116E-02 | 5.987E-02 | 1.737E-01 | 3.972E-01 | 7.498E-01 | 1.276E+00 | 2.348E+00 |
| 2.5 \leq e < 3.0 | 1.612E-02 | 3.922E-02 | 1.084E-01 | 2.518E-01 | 4.877E-01 | 8.401E-01 | 1.537E+00 |
| 3.0 \leq e < 3.5 | 1.302E-02 | 2.799E-02 | 7.246E-02 | 1.683E-01 | 3.318E-01 | 5.791E-01 | 1.057E+00 |
| 3.5 \leq e < 4.0 | 1.093E-02 | 2.126E-02 | 5.114E-02 | 1.173E-01 | 2.337E-01 | 4.127E-01 | 7.528E-01 |
| 4.0 \leq e < 4.5 | 9.433E-03 | 1.693E-02 | 3.787E-02 | 8.492E-02 | 1.696E-01 | 3.022E-01 | 5.518E-01 |
| 4.5 \leq e < 5.0 | 8.306E-03 | 1.398E-02 | 2.924E-02 | 6.362E-02 | 1.265E-01 | 2.266E-01 | 4.144E-01 |
| 5.0 \leq e < 5.5 | 7.423E-03 | 1.186E-02 | 2.334E-02 | 4.908E-02 | 9.671E-02 | 1.735E-01 | 3.177E-01 |
| 5.5 \leq e < 6.0 | 6.713E-03 | 1.028E-02 | 1.914E-02 | 3.884E-02 | 7.553E-02 | 1.353E-01 | 2.479E-01 |

Table 5.4-6. NCT Bottom Surface Dose Rates per gU235 by Burnup-Enrichment Paring

| Enrichment (wt% U-235) | Bottom Surface $\dot{D}\dot{R}$ (mrem/hr/gU235) | | | | | | |
|---------------------------|-------------------------------------------------|-------------|-------------|-------------|-------------|-------------|-------------|
| | Burnup (GWd/MTU) | | | | | | |
| | 0 < b ≤ 10 | 10 < b ≤ 20 | 20 < b ≤ 30 | 30 < b ≤ 40 | 40 < b ≤ 50 | 50 < b ≤ 60 | 60 < b ≤ 72 |
| 0.71 ≤ e < 1.5 | 6.465E-02 | 3.948E-01 | - | - | - | - | - |
| 1.5 ≤ e < 2.0 | 1.413E-02 | 5.160E-02 | 1.570E-01 | 3.498E-01 | 6.435E-01 | 1.086E+00 | 2.016E+00 |
| 2.0 ≤ e < 2.5 | 9.665E-03 | 2.965E-02 | 8.915E-02 | 2.062E-01 | 3.910E-01 | 6.667E-01 | 1.229E+00 |
| 2.5 ≤ e < 3.0 | 7.300E-03 | 1.917E-02 | 5.528E-02 | 1.304E-01 | 2.540E-01 | 4.387E-01 | 8.045E-01 |
| 3.0 ≤ e < 3.5 | 5.864E-03 | 1.351E-02 | 3.670E-02 | 8.685E-02 | 1.725E-01 | 3.022E-01 | 5.526E-01 |
| 3.5 ≤ e < 4.0 | 4.904E-03 | 1.015E-02 | 2.571E-02 | 6.031E-02 | 1.213E-01 | 2.151E-01 | 3.934E-01 |
| 4.0 ≤ e < 4.5 | 4.220E-03 | 8.004E-03 | 1.889E-02 | 4.349E-02 | 8.786E-02 | 1.573E-01 | 2.882E-01 |
| 4.5 ≤ e < 5.0 | 3.707E-03 | 6.553E-03 | 1.447E-02 | 3.244E-02 | 6.537E-02 | 1.178E-01 | 2.163E-01 |
| 5.0 ≤ e < 5.5 | 3.308E-03 | 5.521E-03 | 1.147E-02 | 2.491E-02 | 4.984E-02 | 9.005E-02 | 1.656E-01 |
| 5.5 ≤ e < 6.0 | 2.988E-03 | 4.756E-03 | 9.337E-03 | 1.962E-02 | 3.881E-02 | 7.011E-02 | 1.291E-01 |

Table 5.4-7. NCT 2-meter Dose Rates per gU235 by Burnup-Enrichment Paring

| Enrichment (wt% U-235) | 2 Meter $\dot{D}\dot{R}$ (mrem/hr/gU235) | | | | | | |
|---------------------------|------------------------------------------|-------------|-------------|-------------|-------------|-------------|-------------|
| | Burnup (GWd/MTU) | | | | | | |
| | 0 < b ≤ 10 | 10 < b ≤ 20 | 20 < b ≤ 30 | 30 < b ≤ 40 | 40 < b ≤ 50 | 50 < b ≤ 60 | 60 < b ≤ 72 |
| 0.71 ≤ e < 1.5 | 2.985E-03 | 1.882E-02 | - | - | - | - | - |
| 1.5 ≤ e < 2.0 | 6.304E-04 | 2.419E-03 | 7.477E-03 | 1.673E-02 | 3.084E-02 | 5.208E-02 | 9.679E-02 |
| 2.0 ≤ e < 2.5 | 4.277E-04 | 1.380E-03 | 4.233E-03 | 9.851E-03 | 1.873E-02 | 3.197E-02 | 5.899E-02 |
| 2.5 ≤ e < 3.0 | 3.213E-04 | 8.853E-04 | 2.616E-03 | 6.221E-03 | 1.216E-02 | 2.103E-02 | 3.860E-02 |
| 3.0 ≤ e < 3.5 | 2.571E-04 | 6.193E-04 | 1.730E-03 | 4.137E-03 | 8.252E-03 | 1.448E-02 | 2.651E-02 |
| 3.5 ≤ e < 4.0 | 2.144E-04 | 4.621E-04 | 1.207E-03 | 2.867E-03 | 5.796E-03 | 1.030E-02 | 1.887E-02 |
| 4.0 ≤ e < 4.5 | 1.841E-04 | 3.622E-04 | 8.828E-04 | 2.063E-03 | 4.193E-03 | 7.529E-03 | 1.381E-02 |
| 4.5 ≤ e < 5.0 | 1.616E-04 | 2.950E-04 | 6.734E-04 | 1.535E-03 | 3.116E-03 | 5.634E-03 | 1.036E-02 |
| 5.0 ≤ e < 5.5 | 1.440E-04 | 2.473E-04 | 5.311E-04 | 1.175E-03 | 2.372E-03 | 4.303E-03 | 7.933E-03 |
| 5.5 ≤ e < 6.0 | 1.300E-04 | 2.122E-04 | 4.306E-04 | 9.232E-04 | 1.844E-03 | 3.347E-03 | 6.181E-03 |

Table 5.4-8. NCT Cab Dose Rates per gU235 by Burnup-Enrichment Paring

| Enrichment (wt% U-235) | Cab $\dot{D}\dot{R}$ (mrem/hr/gU235) | | | | | | |
|---------------------------|--------------------------------------|-------------|-------------|-------------|-------------|-------------|-------------|
| | Burnup (GWd/MTU) | | | | | | |
| | 0 < b ≤ 10 | 10 < b ≤ 20 | 20 < b ≤ 30 | 30 < b ≤ 40 | 40 < b ≤ 50 | 50 < b ≤ 60 | 60 < b ≤ 72 |
| 0.71 ≤ e < 1.5 | 5.313E-04 | 3.375E-03 | - | - | - | - | - |
| 1.5 ≤ e < 2.0 | 1.112E-04 | 4.322E-04 | 1.341E-03 | 3.004E-03 | 5.538E-03 | 9.355E-03 | 1.739E-02 |
| 2.0 ≤ e < 2.5 | 7.531E-05 | 2.461E-04 | 7.586E-04 | 1.768E-03 | 3.363E-03 | 5.742E-03 | 1.060E-02 |
| 2.5 ≤ e < 3.0 | 5.650E-05 | 1.576E-04 | 4.683E-04 | 1.116E-03 | 2.183E-03 | 3.777E-03 | 6.934E-03 |
| 3.0 ≤ e < 3.5 | 4.516E-05 | 1.100E-04 | 3.095E-04 | 7.418E-04 | 1.481E-03 | 2.600E-03 | 4.761E-03 |
| 3.5 ≤ e < 4.0 | 3.764E-05 | 8.195E-05 | 2.157E-04 | 5.139E-04 | 1.040E-03 | 1.850E-03 | 3.389E-03 |
| 4.0 ≤ e < 4.5 | 3.231E-05 | 6.414E-05 | 1.576E-04 | 3.695E-04 | 7.522E-04 | 1.352E-03 | 2.481E-03 |
| 4.5 ≤ e < 5.0 | 2.833E-05 | 5.216E-05 | 1.201E-04 | 2.748E-04 | 5.588E-04 | 1.011E-03 | 1.861E-03 |
| 5.0 ≤ e < 5.5 | 2.525E-05 | 4.369E-05 | 9.461E-05 | 2.103E-04 | 4.252E-04 | 7.721E-04 | 1.424E-03 |
| 5.5 ≤ e < 6.0 | 2.278E-05 | 3.745E-05 | 7.662E-05 | 1.651E-04 | 3.306E-04 | 6.005E-04 | 1.110E-03 |

Table 5.4-9. HAC Top 1-meter Dose Rates per gU235 by Burnup-Enrichment Paring

| Enrichment (wt% U-235) | Top 1 Meter $\dot{D}\dot{R}$ (mrem/hr/gU235) | | | | | | |
|---------------------------|----------------------------------------------|-------------|-------------|-------------|-------------|-------------|-------------|
| | Burnup (GWd/MTU) | | | | | | |
| | 0 < b ≤ 10 | 10 < b ≤ 20 | 20 < b ≤ 30 | 30 < b ≤ 40 | 40 < b ≤ 50 | 50 < b ≤ 60 | 60 < b ≤ 72 |
| 0.71 ≤ e < 1.5 | 3.759E-02 | 1.309E-01 | - | - | - | - | - |
| 1.5 ≤ e < 2.0 | 1.191E-02 | 2.381E-02 | 5.334E-02 | 1.059E-01 | 1.853E-01 | 3.042E-01 | 5.536E-01 |
| 2.0 ≤ e < 2.5 | 8.724E-03 | 1.543E-02 | 3.229E-02 | 6.436E-02 | 1.144E-01 | 1.887E-01 | 3.395E-01 |
| 2.5 ≤ e < 3.0 | 6.889E-03 | 1.113E-02 | 2.151E-02 | 4.220E-02 | 7.577E-02 | 1.256E-01 | 2.238E-01 |
| 3.0 ≤ e < 3.5 | 5.699E-03 | 8.614E-03 | 1.540E-02 | 2.930E-02 | 5.264E-02 | 8.768E-02 | 1.550E-01 |
| 3.5 ≤ e < 4.0 | 4.863E-03 | 7.002E-03 | 1.165E-02 | 2.131E-02 | 3.798E-02 | 6.339E-02 | 1.114E-01 |
| 4.0 ≤ e < 4.5 | 4.244E-03 | 5.893E-03 | 9.220E-03 | 1.614E-02 | 2.831E-02 | 4.717E-02 | 8.249E-02 |
| 4.5 ≤ e < 5.0 | 3.768E-03 | 5.089E-03 | 7.567E-03 | 1.267E-02 | 2.174E-02 | 3.601E-02 | 6.263E-02 |
| 5.0 ≤ e < 5.5 | 3.387E-03 | 4.479E-03 | 6.388E-03 | 1.024E-02 | 1.714E-02 | 2.811E-02 | 4.859E-02 |
| 5.5 ≤ e < 6.0 | 3.078E-03 | 4.001E-03 | 5.512E-03 | 8.490E-03 | 1.383E-02 | 2.240E-02 | 3.841E-02 |

Table 5.4-10. HAC Side 1-meter Dose Rates per gU235 by Burnup-Enrichment Paring

| Enrichment (wt% U-235) | Side 1 Meter $\dot{D}\dot{R}$ (mrem/hr/gU235) | | | | | | |
|---------------------------|-----------------------------------------------|-------------|-------------|-------------|-------------|-------------|-------------|
| | Burnup (GWd/MTU) | | | | | | |
| | 0 < b ≤ 10 | 10 < b ≤ 20 | 20 < b ≤ 30 | 30 < b ≤ 40 | 40 < b ≤ 50 | 50 < b ≤ 60 | 60 < b ≤ 72 |
| 0.71 ≤ e < 1.5 | 7.305E-02 | 1.723E-01 | - | - | - | - | - |
| 1.5 ≤ e < 2.0 | 2.622E-02 | 4.113E-02 | 7.208E-02 | 1.248E-01 | 2.031E-01 | 3.191E-01 | 5.613E-01 |
| 2.0 ≤ e < 2.5 | 1.953E-02 | 2.849E-02 | 4.651E-02 | 7.890E-02 | 1.285E-01 | 2.012E-01 | 3.479E-01 |
| 2.5 ≤ e < 3.0 | 1.558E-02 | 2.161E-02 | 3.297E-02 | 5.405E-02 | 8.745E-02 | 1.364E-01 | 2.322E-01 |
| 3.0 ≤ e < 3.5 | 1.298E-02 | 1.737E-02 | 2.499E-02 | 3.930E-02 | 6.264E-02 | 9.719E-02 | 1.630E-01 |
| 3.5 ≤ e < 4.0 | 1.112E-02 | 1.452E-02 | 1.989E-02 | 2.996E-02 | 4.672E-02 | 7.189E-02 | 1.190E-01 |
| 4.0 ≤ e < 4.5 | 9.736E-03 | 1.248E-02 | 1.645E-02 | 2.375E-02 | 3.608E-02 | 5.483E-02 | 8.954E-02 |
| 4.5 ≤ e < 5.0 | 8.661E-03 | 1.095E-02 | 1.400E-02 | 1.946E-02 | 2.871E-02 | 4.296E-02 | 6.922E-02 |
| 5.0 ≤ e < 5.5 | 7.800E-03 | 9.758E-03 | 1.218E-02 | 1.637E-02 | 2.346E-02 | 3.448E-02 | 5.473E-02 |
| 5.5 ≤ e < 6.0 | 7.095E-03 | 8.803E-03 | 1.078E-02 | 1.407E-02 | 1.961E-02 | 2.825E-02 | 4.415E-02 |

Table 5.4-11. HAC Bottom 1-meter Dose Rates per gU235 by Burnup-Enrichment Paring

| Enrichment (wt% U-235) | Bottom 1 Meter $\dot{D}\dot{R}$ (mrem/hr/gU235) | | | | | | |
|---------------------------|-------------------------------------------------|-------------|-------------|-------------|-------------|-------------|-------------|
| | Burnup (GWd/MTU) | | | | | | |
| | 0 < b ≤ 10 | 10 < b ≤ 20 | 20 < b ≤ 30 | 30 < b ≤ 40 | 40 < b ≤ 50 | 50 < b ≤ 60 | 60 < b ≤ 72 |
| 0.71 ≤ e < 1.5 | 3.003E-02 | 1.341E-01 | - | - | - | - | - |
| 1.5 ≤ e < 2.0 | 8.409E-03 | 2.087E-02 | 5.396E-02 | 1.138E-01 | 2.045E-01 | 3.408E-01 | 6.273E-01 |
| 2.0 ≤ e < 2.5 | 6.040E-03 | 1.287E-02 | 3.164E-02 | 6.801E-02 | 1.252E-01 | 2.102E-01 | 3.834E-01 |
| 2.5 ≤ e < 3.0 | 4.712E-03 | 8.895E-03 | 2.036E-02 | 4.376E-02 | 8.204E-02 | 1.391E-01 | 2.518E-01 |
| 3.0 ≤ e < 3.5 | 3.867E-03 | 6.654E-03 | 1.408E-02 | 2.974E-02 | 5.631E-02 | 9.636E-02 | 1.736E-01 |
| 3.5 ≤ e < 4.0 | 3.283E-03 | 5.264E-03 | 1.029E-02 | 2.113E-02 | 4.007E-02 | 6.909E-02 | 1.241E-01 |
| 4.0 ≤ e < 4.5 | 2.854E-03 | 4.336E-03 | 7.892E-03 | 1.563E-02 | 2.943E-02 | 5.093E-02 | 9.134E-02 |
| 4.5 ≤ e < 5.0 | 2.527E-03 | 3.682E-03 | 6.298E-03 | 1.197E-02 | 2.223E-02 | 3.848E-02 | 6.891E-02 |
| 5.0 ≤ e < 5.5 | 2.268E-03 | 3.198E-03 | 5.186E-03 | 9.449E-03 | 1.723E-02 | 2.971E-02 | 5.308E-02 |
| 5.5 ≤ e < 6.0 | 2.057E-03 | 2.826E-03 | 4.378E-03 | 7.654E-03 | 1.366E-02 | 2.338E-02 | 4.165E-02 |

For a defined mass of uranium at a given burnup and initial enrichment, the resulting dose rate at any regulatory dose rate location can be calculated by multiplying the mass of initial fissile material (gU235) by the dose rates per gU235 in the corresponding table, as shown in Equation 5-5. Repeating this dose rate calculation for each loaded fuel rod segment, then summing the resulting dose rates calculates the total external dose rates for each regulatory dose rate location from a load of segmented irradiated fuel rods in the Model 2000 Transport Package.

This process is completed, and recorded in the Irradiated Fuel Loading Table. The use of the Irradiated Fuel Loading Table is described in Section 5.5.5. The maximum possible dose rate for each regulatory location is shown in Table 5.4-12, based on the mass of U-235 resulting in the NCT side surface dose rate equal to 90% of the respective regulatory limit.

Table 5.4-12. Maximum External Dose Rates - Irradiated Fuel

| Location | NCT Top Surface | NCT Side Surface | NCT Bottom Surface | NCT 2-meter | NCT Cab | HAC Top 1-meter | HAC Side 1-meter | HAC Bottom 1-meter |
|----------------------------------|-----------------------|------------------------|--------------------------|----------------|------------|-----------------------|------------------------|--------------------------|
| Dose Rate (mrem/hr) | 31.99 | 180.0 | 94.26 | 4.53 | 0.9 | 51.15 | 99.39 | 40.85 |
| Regulatory Limit (mrem/hr) | 200.0 | 200.0 | 200.0 | 10.0 | 2.0 | 1000 | 1000 | 1000 |

5.4.4.2. Irradiated Hardware and Byproducts

For the irradiated hardware and byproduct contents, the resulting external dose rates are calculated by calculating the dose rate per curie in MCNP6 for each radionuclide individually, using the source spectra listed in Tables 5.5-8 through 5.5-25. The 2σ statistical uncertainty is added on to the calculated dose rate per curie as shown in Equation 5-8. The resulting values from these calculations for NCT and HAC are presented in Tables 5.4-13 and 5.4-14.

Table 5.4-13. Irradiated Hardware and Byproduct Dose Rate per Curie Results - NCT

| Radionuclide | Dose Rate (mrem/hr/Ci) | | | | |
|--------------|---------------------------|-----------------|-------------------|-----------|-----------|
| | Top Surface | Side Surface | Bottom Surface | 2-meter | Cab |
| Co-58 | 1.356E-05 | 2.444E-04 | 2.169E-05 | 3.375E-06 | 5.945E-07 |
| Co-60 | 4.183E-04 | 9.437E-03 | 6.237E-04 | 1.211E-04 | 2.078E-05 |
| Cr-51 | 3.981E-15 | 1.648E-20 | 5.556E-20 | 2.125E-22 | 3.509E-23 |
| Cs-134 | 1.584E-05 | 3.433E-04 | 2.402E-05 | 4.504E-06 | 7.780E-07 |
| Cs-137 | 9.341E-10 | 3.713E-08 | 2.822E-09 | 4.381E-10 | 7.404E-11 |
| Fe-59 | 1.239E-04 | 2.894E-03 | 1.853E-04 | 3.649E-05 | 6.292E-06 |
| Hf-175 | 1.642E-13 | 1.917E-15 | 3.513E-16 | 1.167E-17 | 1.891E-18 |
| Hf-181 | 1.968E-11 | 2.116E-11 | 3.427E-12 | 2.749E-13 | 4.721E-14 |
| Mn-54 | 2.294E-07 | 9.856E-06 | 4.279E-07 | 1.116E-07 | 1.904E-08 |
| Nb-92m | 4.559E-05 | 8.088E-04 | 7.216E-05 | 1.128E-05 | 1.974E-06 |
| Nb-94 | 5.561E-07 | 2.214E-05 | 9.703E-07 | 2.519E-07 | 4.293E-08 |
| Sb-124 | 1.973E-03 | 3.462E-02 | 3.176E-03 | 4.809E-04 | 8.336E-05 |
| Sb-125 | 1.440E-10 | 3.334E-09 | 3.261E-10 | 4.139E-11 | 7.082E-12 |
| Sb-126 | 6.649E-06 | 1.526E-04 | 1.009E-05 | 1.955E-06 | 3.399E-07 |
| Sc-46 | 4.123E-05 | 1.111E-03 | 6.179E-05 | 1.353E-05 | 2.327E-06 |
| Ta-182 | 1.343E-04 | 3.273E-03 | 1.997E-04 | 4.080E-05 | 6.989E-06 |
| Zn-65 | 2.023E-05 | 5.398E-04 | 3.014E-05 | 6.581E-06 | 1.131E-06 |
| Zr-95 | 5.015E-08 | 2.505E-06 | 1.181E-07 | 2.816E-08 | 4.790E-09 |
| Nb-95 | 5.015E-08 | 2.505E-06 | 1.181E-07 | 2.816E-08 | 4.790E-09 |

Table 5.4-14. Irradiated Hardware and Byproduct Dose Rate per Curie Results - HAC

| Radionuclide | Dose Rate (mrem/hr/Ci) | | |
|--------------|---------------------------|--------------|----------------|
| | Top 1-meter | Side 1-meter | Bottom 1-meter |
| Co-58 | 1.795E-05 | 4.460E-05 | 1.155E-05 |
| Co-60 | 6.008E-04 | 1.743E-03 | 3.552E-04 |
| Cr-51 | 1.268E-13 | 5.043E-20 | 9.455E-19 |
| Cs-134 | 2.252E-05 | 6.356E-05 | 1.340E-05 |
| Cs-137 | 3.023E-09 | 9.383E-09 | 3.140E-09 |
| Fe-59 | 1.806E-04 | 5.370E-04 | 1.071E-04 |
| Hf-175 | 1.676E-12 | 4.820E-16 | 7.744E-16 |
| Hf-181 | 1.493E-10 | 6.868E-12 | 5.073E-12 |
| Mn-54 | 4.057E-07 | 2.046E-06 | 3.326E-07 |
| Nb-92m | 5.907E-05 | 1.450E-04 | 3.671E-05 |
| Nb-94 | 9.502E-07 | 4.548E-06 | 7.240E-07 |
| Sb-124 | 2.568E-03 | 6.144E-03 | 1.618E-03 |
| Sb-125 | 6.258E-10 | 9.213E-10 | 4.006E-10 |
| Sb-126 | 9.516E-06 | 2.875E-05 | 5.919E-06 |
| Sc-46 | 6.274E-05 | 2.115E-04 | 3.852E-05 |
| Ta-182 | 1.976E-04 | 6.138E-04 | 1.176E-04 |
| Zn-65 | 3.066E-05 | 1.026E-04 | 1.860E-05 |
| Zr-95 | 9.528E-08 | 5.459E-07 | 1.039E-07 |
| Nb-95 | 9.528E-08 | 5.459E-07 | 1.039E-07 |

The resulting dose rate at any regulatory dose rate location can be calculated, for a cask loading of irradiated hardware or byproducts with a defined radionuclide inventory, by multiplying the activity of each radionuclide by the respective dose rate per curie for the given location and summing the dose rate contributions from each radionuclide, as shown in Equation 5-9. Repeating this dose rate calculation for each regulatory dose rate location determines the total external dose rates for the Model 2000 Transport Package. This process is completed and recorded in the Irradiated Hardware and Byproduct Loading Table. The use of the Irradiated Hardware and Byproduct Loading Table is described in Section 5.5.6.

The maximum activity of each radionuclide, individually, is limited by the minimum of either the activity equivalent to the 3000W (Configuration 2) thermal limit of the cask or the activity resulting in an NCT side surface dose rate equal to 90% of the regulatory limit (180 mrem/hr). The maximum activity limit for each radionuclide individually is presented in Table 5.4-15. These limits are based on the dose rate per curie limits in Tables 5.4-13 and 5.4-14, and the decay heat W/Ci values in Table 5.5-30. The maximum possible dose rates for each regulatory location are summarized in Table 5.4-16. These values are calculated using the activity limits in Table 5-4.15 and the dose rate per curie values in Tables 5.4-13 and 5.4-14, for each radionuclide.

Table 5.4-15. Maximum Activities for Irradiated Hardware and Byproduct Individual Radionuclides

| Radionuclide | Activity Limit (Ci) | Basis ^{1,2} |
|--------------|---------------------|----------------------|
| Co-58 | 5.017E+05 | Thermal |
| Co-60 | 1.907E+04 | Dose Rate |
| Cr-51 | 1.380E+07 | Thermal |
| Cs-134 | 2.945E+05 | Thermal |
| Cs-137 | 2.820E+06 | Thermal |
| Fe-59 | 6.474E+04 | Dose Rate |
| Hf-175 | 1.274E+06 | Thermal |
| Hf-181 | 6.932E+05 | Thermal |
| Mn-54 | 6.023E+05 | Thermal |
| Nb-92m | 2.225E+05 | Dose Rate |
| Nb-94 | 2.876E+05 | Thermal |
| Sb-124 | 5.200E+03 | Dose Rate |
| Sb-125 | 9.486E+05 | Thermal |
| Sb-126 | 1.622E+05 | Thermal |
| Sc-46 | 1.621E+05 | Dose Rate |
| Ta-182 | 8.017E+04 | Dose Rate |
| Zn-65 | 3.335E+05 | Dose Rate |
| Zr-95 | 5.953E+05 | Thermal |
| Nb-95 | 6.256E+05 | Thermal |

Notes: ¹ Thermal – 3000 W thermal limit for Configuration 2.

² Dose Rate – 180 mrem/hr NCT side surface dose rate limit.

Table 5.4-16. Maximum External Dose Rates - Irradiated Hardware and Byproducts

| Location | NCT Top Surface | NCT Side Surface | NCT Bottom Surface | NCT 2-meter | NCT Cab | HAC Top 1-meter | HAC Side 1-meter | HAC Bottom 1-meter |
|----------------------------|-----------------|------------------|--------------------|-------------|---------|-----------------|------------------|--------------------|
| Dose Rate (mrem/hr) | 10.26 | 180.0 | 16.51 | 2.6 | 0.5 | 13.36 | 34.28 | 8.420 |
| Regulatory Limit (mrem/hr) | 200.0 | 200.0 | 200.0 | 10 | 2.0 | 1000 | 1000 | 1000 |

5.4.4.3. Cobalt-60 Isotope Rods

For the cobalt-60 isotope rod contents, the resulting external dose rates are calculated using the dose rate per curie in MCNP6 for cobalt-60, with the cobalt-60 source energy spectrum listed in Table 5.2-4. The 2 σ statistical uncertainty is added on to the calculated dose rate per curie as shown in Equation 5-8. The resulting values from these calculations for NCT and HAC are presented in Tables 5.4-17 and 5.4-18.

Table 5.4-17. Cobalt-60 Isotope Rod Dose Rate per Curie Results – NCT

| Radionuclide | Dose Rate (mrem/hr/Ci) | | | | |
|--------------|------------------------|--------------|----------------|-----------|-----------|
| | Top Surface | Side Surface | Bottom Surface | 2-meter | Cab |
| Co-60 | 1.850E-04 | 8.821E-04 | 3.940E-04 | 1.664E-05 | 2.921E-06 |

Table 5.4-18. Cobalt-60 Isotope Rod Dose Rate per Curie Results - HAC

| Radionuclide | Dose Rate (mrem/hr/Ci) | | |
|--------------|---------------------------|--------------|----------------|
| | Top 1-meter | Side 1-meter | Bottom 1-meter |
| Co-60 | 6.008E-04 | 1.743E-03 | 3.552E-04 |

The resulting dose rate at any regulatory dose rate location can be calculated, for a cask loading of cobalt-60 isotope rod [[]], by filling out the cobalt-60 isotope rod loading table.

To determine the maximum possible dose rate at each regulatory location, the dose rate per curie values in Tables 5.4-17 and 5.4-18 are multiplied by the cobalt-60 activity equivalent to the 3000 W Configuration 2 thermal limit (194,500 Ci). The results of this calculation are presented in Table 5.4-19.

Table 5.4-19. Maximum External Dose Rates – Cobalt-60 Isotope Rods

| Location | NCT Top Surface | NCT Side Surface | NCT Bottom Surface | NCT 2-meter | NCT Cab | HAC Top 1-meter | HAC Side 1-meter | HAC Bottom 1-meter |
|-------------------------------|-----------------------|------------------------|--------------------------|----------------|------------|-----------------------|------------------------|--------------------------|
| Dose Rate (mrem/hr) | 35.99 | 171.6 | 76.63 | 3.3 | 0.6 | 116.9 | 339.1 | 69.09 |
| Regulatory Limit (mrem/hr) | 200.0 | 200.0 | 200.0 | 10 | 2.0 | 1000 | 1000 | 1000 |

5.4.4.4. Combined Contents

There is the possibility of a shipment that includes combined contents. For example, some shipments of irradiated fuel will also include irradiated hardware. This is due to the possibility of being unable to properly remove the segmented fuel rods from bundle hardware and ALARA concerns. For this reason, shipments of irradiated fuel may also include segments of irradiated bundle hardware. In order to demonstrate compliance with the 10 CFR 71 external dose rate limits for a shipment of combined content types, the external dose rate contributions from each content type are calculated separately. In this example, the Irradiated Fuel Loading Table and the Irradiated Hardware Loading Table are completed separately for the two contents, as if they were two separate shipments. The total external dose rates for the shipment of combined contents are calculated as the sum of the dose rate contributions from each content type. This process is completed and recorded in the Combined Contents Loading Table. The use of the Combined Contents Loading Table is described in Section 5.5.7, including an example of a hypothetical shipment with irradiated fuel and bundle hardware.

Another example is a combined content of cobalt-60 isotope rods with irradiated hardware. For this case the Cobalt-60 Isotope Rod Loading Table is filled out for the isotope rod contents and any radionuclide activity in the rod cladding or additional irradiated hardware shipped with the isotope rods is recorded in the Irradiated Hardware and Byproduct Loading Table. The resulting thermal and dose rate contributions from radionuclides in the hardware and cladding are summed with the thermal and dose rate contributions from the cobalt-60 isotope rods in the Combined Contents Loading Table.

5.5 Appendices

5.5.1. ORIGEN-ARP Irradiated Fuel Source Term Calculation

Per the recommendations for spent fuel specifications provided in NUREG/CR-6716 (Reference 5-10), the principal parameters for spent fuel source term generation are burnup, enrichment, and cooling time. To generate a bounding source term, the maximum burnup should be considered, along with the minimum enrichment and cooling time. To provide flexibility for future use of the Model 2000 cask, a wide range of enrichments and burnups are considered. The irradiated fuel source term calculation is performed for several enrichment bands and burnup bands. In the ORIGEN-ARP (Reference 5-2) source term analysis, for each initial enrichment band the minimum enrichment is considered, and for each burnup band the maximum burnup is considered. This generates a bounding source term for each burnup-enrichment pairing. Table 5.5-1 shows the burnup bands and Table 5.5-2 shows the initial enrichment bands for which a separate source term is calculated. The source terms are taken at a cooling time of 120 days. Any irradiated fuel contents are required to have 120 days of cooling time prior to shipment in the Model 2000 cask.

Table 5.5-1. Burnup Bands and Analyzed Values

| Burnup Band (GWd/MTU) | Analyzed Burnup (GWd/MTU) |
|----------------------------------|--------------------------------------|
| $60 < b \leq 72$ | 72 |
| $50 < b \leq 60$ | 60 |
| $40 < b \leq 50$ | 50 |
| $30 < b \leq 40$ | 40 |
| $20 < b \leq 30$ | 30 |
| $10 < b \leq 20$ | 20 |
| $0 < b \leq 10$ | 10 |

Table 5.5-2. Initial Enrichment Bands and Analyzed Values

| Initial Enrichment Band (wt%) | Analyzed Initial Enrichment (wt%) |
|------------------------------------------|----------------------------------------------|
| $1.5 \leq e < 2.0$ | 1.5 |
| $2.0 \leq e < 2.5$ | 2.0 |
| $2.5 \leq e < 3.0$ | 2.5 |
| $3.0 \leq e < 3.5$ | 3.0 |
| $3.5 \leq e < 4.0$ | 3.5 |
| $4.0 \leq e < 4.5$ | 4.0 |
| $4.5 \leq e < 5.0$ | 4.5 |
| $5.0 \leq e < 5.5$ | 5.0 |
| $5.5 \leq e < 6.0$ | 5.5 |

Table 5.5-3 lists the values used for the secondary parameters for the ORIGEN-ARP irradiated fuel source term calculation. While these parameters are not as significant to the irradiated fuel source term calculation as the principal parameters they are selected to generate a bounding source term. The additional parameters include the fuel assembly type analyzed, the presence of burnable poisons, the specific power analyzed, and the moderator density considered. The values used for each parameter are selected to be appropriate, or bounding, for the irradiated fuel rod contents outlined in Section 5.2.

Table 5.5-3. Secondary Source Term Calculation Parameters

| Parameter | Value |
|--------------------|---------------------------------|
| Fuel Assembly Type | GE 10x10 |
| Burnable Poisons | 14 IBAs (5 wt% Gd) ¹ |
| Specific Power | [[]] MW/MTU ² |
| Moderator Density | 0.1 g/cm ³ |

Notes: ¹ IBA – Integral Burnable Absorber rod (UO₂-GdO₃).

² Based on average bundle uranium mass [[]] and power [[]].

The only remaining parameter necessary for the ORIGEN-ARP source term calculation is the mass of uranium. Table 5.5-4 lists the uranium mass used in the ORIGEN-ARP source term calculation for each enrichment analyzed. For a given enrichment, the gamma and neutron source strength calculated in ORIGEN-ARP is proportional to the mass of U-235. The source strengths calculated for each enrichment band are normalized to 1 gU235, so that the total source strength for a shipment of segmented irradiated fuel rods can be calculated by multiplying the source strength for a respective burnup-enrichment pairing by the total mass of U-235.

Table 5.5-4. ORIGEN-ARP Uranium Masses

| Enrichment (wt%) | Mass U ¹ (g) |
|------------------|-------------------------|
| 1.5 | 66.6667 |
| 2.0 | 50.0000 |
| 2.5 | 40.0000 |
| 3.0 | 33.3333 |
| 3.5 | 28.5714 |
| 4.0 | 25.0000 |
| 4.5 | 22.2222 |
| 5.0 | 20.0000 |
| 5.5 | 18.1818 |

Note: ¹ Corresponding to 1 gU235.

The ORIGEN-ARP analysis calculates the source term using the parameters listed above, resulting in the gamma and neutron source strength values for each burnup-enrichment pairing. The gamma source strength values (in γ /s/gU235) are listed in Table 5.2-2 and the neutron source strength values (in n/s/gU235) are listed in Table 5.2-6. The source strength values listed include 120 days of cooling time. Extended cooling times beyond 120 days will only reduce the calculated source strengths. To allow for low enrichment, low burnup irradiated fuel segments, source strengths for burnups below 20 GWd/MTU two values in the enrichment band between 0.71 and 1.5 wt% U-235 were calculated using a power fit extrapolation. This extrapolation is necessary because the ORIGEN-ARP data libraries only include initial enrichments as low as 1.5 wt% U-235. While the power fit through the calculated data points is nearly a perfect fit, to account for uncertainties due to extrapolation outside the available library, the extrapolated values were increased by 20%. The gamma energy spectrum from irradiated fuel contents is based on the radionuclide inventory generated from the irradiation and decay of various nuclides over time. Table 5.2-1 lists the gamma energy spectrum calculated in the ORIGEN-ARP source term calculations, based on the default 18-group ORIGEN-ARP energy grouping structure.

The neutron source term is from radionuclides that emit neutrons through spontaneous fission (SF) and emitted alphas that generate neutrons through alpha-n reactions in the fuel (α -n). The neutron source terms are dominated by Cm-244(SF) and Cm-242(SF), with significant contributions at higher burnups from Cf-252(SF), and at lower burnups from Pu-238(α -n), Pu-239(α -n), Pu-240(SF), and Cm-242(α -n). Table 5.2-5 lists the representative neutron energy spectrum from the ORIGEN-ARP source term calculations, which is based on a burnup of 10 GWd/MTU and initial enrichment of 5.5 wt% U-235. However, specific burnup and enrichment pairing for the neutron source term is irrelevant because the relative neutron spectra does not vary significantly across the bands.

For each burnup-enrichment pairing, the total wattage per gU235 is listed in the outputs from the ORIGEN calculations. The total wattage results from all ORIGEN outputs are listed in Table 5.5-5. These values can be used to ensure that the thermal limit of the cask will not be exceeded from a load of irradiated fuel. The values for natural uranium are calculated with the same method as for the photon and neutron source strengths: using a power extrapolation on a fit curve and increasing by 20%.

Table 5.5-5. Irradiated Fuel Total Radionuclide Decay Heat (W/gU235)

| Enrichment (wt%) | Burnup (GWd/MTU) | | | | | | |
|---------------------|------------------|-----------|-----------|-----------|-----------|-----------|-----------|
| | 0< b ≤10 | 10< b ≤20 | 20< b ≤30 | 30< b ≤40 | 40< b ≤50 | 50< b ≤60 | 60< b ≤72 |
| 0.71 | 2.148E+00 | 2.753E+00 | - | - | - | - | - |
| 1.5 | 8.618E-01 | 1.088E+00 | 1.239E+00 | 1.356E+00 | 1.448E+00 | 1.523E+00 | 1.602E+00 |
| 2.0 | 6.510E-01 | 8.146E-01 | 9.229E-01 | 1.008E+00 | 1.078E+00 | 1.137E+00 | 1.199E+00 |
| 2.5 | 5.238E-01 | 6.516E-01 | 7.345E-01 | 8.000E-01 | 8.559E-01 | 9.042E-01 | 9.564E-01 |
| 3.0 | 4.384E-01 | 5.431E-01 | 6.098E-01 | 6.623E-01 | 7.079E-01 | 7.486E-01 | 7.935E-01 |
| 3.5 | 3.772E-01 | 4.657E-01 | 5.212E-01 | 5.646E-01 | 6.026E-01 | 6.373E-01 | 6.766E-01 |
| 4.0 | 3.310E-01 | 4.076E-01 | 4.551E-01 | 4.918E-01 | 5.241E-01 | 5.540E-01 | 5.885E-01 |
| 4.5 | 2.950E-01 | 3.625E-01 | 4.038E-01 | 4.355E-01 | 4.633E-01 | 4.893E-01 | 5.198E-01 |
| 5.0 | 2.660E-01 | 3.263E-01 | 3.629E-01 | 3.907E-01 | 4.151E-01 | 4.379E-01 | 4.648E-01 |
| 5.5 | 2.423E-01 | 2.967E-01 | 3.296E-01 | 3.543E-01 | 3.758E-01 | 3.960E-01 | 4.200E-01 |

5.5.2. ORIGEN-S Irradiated Hardware and Byproduct Source Term Calculation

The radionuclides that are significant to the irradiated hardware and byproduct dose rate calculations, were determined with multiple ORIGEN-S (Reference 5-2) irradiation calculations. For the irradiation case there are two significant inputs; the composition of the material that is being irradiated and the neutron flux that the material is exposed to. For determining the source term, the quantity of material is irrelevant for the determination of which radionuclides are generated. A generic thermal neutron flux of $1\text{E}+14$ n/s·cm² is assumed for the irradiation cases. For the material compositions of the irradiated hardware/byproducts, there are six materials considered. These materials along with their compositions are listed in Table 5.5-6. The materials selected include multiple stainless steels, a nickel alloy, a zirconium alloy, as well as hafnium and boron carbide. The materials listed in parenthesis in Table 5.5-6, are included as they are similar in composition to the material listed. The materials listed contain all elements expected in any irradiated hardware or byproduct contents, thus the resulting total radionuclide inventory from the ORIGEN-S calculations is comprehensive. The basis for each ORIGEN-S input is 1 kg of the respective material being irradiated. Because elements for each material are entered into the ORIGEN-S input in grams, Table 5.5-6 lists the gram amount of each element

per kilogram of the material. While an increase or decrease in the flux or a variation in the material composition entered for the irradiation case would result in a change to the relative activity of the radionuclides generated, the purpose of the ORIGEN-S source term calculations is not to determine the inventory of each radionuclide, but simply to identify which radionuclides may be present in irradiated hardware/byproduct contents. The quantity of each radionuclide that is significant to dose rate calculations must be entered into the Irradiated Hardware and Byproduct Loading Table to calculate the maximum external dose rates.

The radionuclides calculated from the ORIGEN-S irradiation cases are listed in Table 5.5-7. This table also includes some radionuclides that may be included on the hardware or byproduct contents in the form of surface contamination, as these contents may be exposed to a reactor environment. Radionuclides in cells that are highlighted are considered significant to dose rate calculations. The selection of significant radionuclides is based on the energy of the gamma emissions and half-lives. A radionuclide is considered insignificant to dose rate calculations if it has no gamma emissions greater than 0.3 MeV, or if it has a half-life less than 3 days. All shipments of irradiated hardware and byproducts are required to include a decay time of 30 days prior to shipment. Thus, for any radionuclide with a half-life less than 3 days, there are more than 10 half-lives of decay time prior to shipment.

Tables 5.5-8 through 5.5-25 provide the energy spectra for all radionuclides considered significant to the irradiated hardware and byproduct dose rate calculations. These radionuclide energy spectra are from the ORIGEN-S Data Library `origen.rev04.mpdkgam.data` (Reference 5-2). Any gamma lines under 0.1 MeV are neglected from the listed radionuclide spectra. Though Cs-137 does not emit any significant gammas, the gamma emission of its short-lived daughter Ba-137m is used as its representative spectrum. Also, because Nb-95 is the daughter of Zr-95, the energy spectra of the two radionuclides are combined and only one set of dose rate calculations is performed for both radionuclides. Thus the dose rates calculated for this combined spectrum account for one decay of each radionuclide. This calculates an appropriate dose rate for Zr-95, as it accounts for the decay of its daughter Nb-95. However, this spectrum results in a conservative dose rate for Nb-95, as the calculated dose rate includes the contribution from its parent radionuclide as well. The resulting dose rates from this combined spectrum are used to calculate external dose rates for activities of both Zr-95 and Nb-95, individually.

Table 5.5-6. Irradiated Hardware and Byproduct Irradiation Materials

| Material | Symbol | Element ID No. | wt % | g/kg material | # nuclides |
|--------------------------------|--------|----------------|--------|---------------|------------|
| SS304 (SS302, SS304L) | C | 60000 | 0.0800 | 0.8000 | 10 |
| | N | 70000 | 0.1000 | 1.0000 | |
| | Si | 140000 | 0.7500 | 7.5000 | |
| | P | 150000 | 0.0450 | 0.4500 | |
| | S | 160000 | 0.0300 | 0.3000 | |
| | Cr | 240000 | 19.000 | 190.00 | |
| | Mn | 250000 | 2.0000 | 20.000 | |
| | Fe | 260000 | 67.495 | 674.95 | |
| | Co | 270000 | 0.0800 | 0.8000 | |
| | Ni | 280000 | 10.420 | 104.20 | |
| SS CF3M (SS316) | C | 60000 | 0.0300 | 0.300 | 8 |
| | Si | 140000 | 2.0000 | 20.000 | |
| | Cr | 240000 | 19.000 | 190.00 | |
| | Mn | 250000 | 1.5000 | 15.000 | |
| | Fe | 260000 | 62.970 | 629.70 | |
| | Co | 270000 | 0.0800 | 0.8000 | |
| | Ni | 280000 | 11.920 | 119.20 | |
| | Mo | 420000 | 2.5000 | 25.000 | |
| SS348H | C | 60000 | 0.0700 | 0.7000 | 11 |
| | Si | 140000 | 1.0000 | 10.000 | |
| | P | 150000 | 0.0450 | 0.4500 | |
| | S | 160000 | 0.0300 | 0.3000 | |
| | Cr | 240000 | 18.000 | 180.00 | |
| | Mn | 250000 | 2.0000 | 20.000 | |
| | Fe | 260000 | 64.555 | 645.55 | |
| | Co | 270000 | 0.2000 | 2.0000 | |
| | Ni | 280000 | 13.000 | 130.00 | |
| | Nb | 410000 | 1.0000 | 10.000 | |
| | Ta | 730000 | 0.1000 | 1.0000 | |
| Inconel-718 (Inconel X-750) | B | 50000 | 0.0060 | 0.0600 | 16 |
| | C | 60000 | 0.0800 | 0.8000 | |
| | Al | 130000 | 0.5000 | 5.0000 | |
| | Si | 140000 | 0.3500 | 3.5000 | |
| | P | 150000 | 0.0150 | 0.1500 | |
| | S | 160000 | 0.0150 | 0.1500 | |
| | Ti | 220000 | 0.9000 | 9.0000 | |
| | Cr | 240000 | 19.000 | 190.00 | |
| | Mn | 250000 | 0.3500 | 3.5000 | |
| | Fe | 260000 | 14.934 | 149.34 | |
| | Co | 270000 | 1.0000 | 10.000 | |
| | Ni | 280000 | 54.000 | 540.00 | |
| | Cu | 290000 | 0.3000 | 3.0000 | |
| | Nb | 410000 | 2.7500 | 27.500 | |
| | Mo | 420000 | 3.0500 | 30.500 | |
| | Ta | 730000 | 2.7500 | 27.500 | |

NEDO-33866 Revision 0
Non-Proprietary Information – Class I (Public)

| Material | Symbol | Element ID No. | wt % | g/kg material | # nuclides |
|-------------------------------------|--------|----------------|--------|---------------|------------|
| Zircaloy-2 (Zircaloy-4) | O | 80000 | 0.1200 | 1.2000 | 6 |
| | Cr | 240000 | 0.1000 | 1.0000 | |
| | Fe | 260000 | 0.2000 | 2.0000 | |
| | Ni | 280000 | 0.0800 | 0.8000 | |
| | Zr | 400000 | 97.800 | 978.00 | |
| | Sn | 500000 | 1.7000 | 17.000 | |
| Boron Carbide (B ₄ C) | B | 50000 | 78.261 | 782.61 | 2 |
| | C | 60000 | 21.739 | 217.39 | |
| Hafnium | Hf | 720000 | 100.00 | 1000.0 | 1 |

Table 5.5-7. Irradiated Hardware and Byproduct Radionuclides

| | | | | | |
|--------------------|--------------------|---------------|---------------------|-------------------------------------|---------------------|
| H-3 | Co-58m | Sr-91 | Tc-99 ¹ | Sb-125 | Lu-177m |
| C-14 | Co-60 | Y-89m | Tc-99m | Sb-126 | Yb-175 |
| Na-24 | Co-60m | Y-90 | Tc-101 | Te-125m | Yb-177 |
| Si-31 | Co-61 | Y-90m | Ru-106 ¹ | I-129 ¹ | Ta-180 |
| P-32 | Ni-57 | Y-91 | In-113m | Cs-134¹ | Ta-182 |
| P-33 | Ni-59 | Y-91m | In-114 | Cs-137 (Ba-137m)¹ | Ta-183 |
| S-35 | Ni-63 | Y-92 | In-114m | La-140 ¹ | W-181 |
| Ca-45 | Ni-65 | Nb-91m | In-115m | Ba-140 ¹ | W-183m |
| Sc-46 | Fe-55 | Nb-92m | Sn-113 | Ce-144 ¹ | W-185 |
| Sc-47 | Fe-59 | Nb-94 | Sn-113m | Hf-173 | Re-186 |
| Sc-48 | Cu-64 | Nb-95 | Sn-117m | Hf-175 | Np-237 ¹ |
| V-49 | Cu-66 ¹ | Nb-96 | Sn-119m | Hf-177m | Pu-238 ¹ |
| V-52 ¹ | Zn-65 | Nb-95m | Sn-121 | Hf-180m | Pu-239 ¹ |
| Cr-51 | Zr-89 | Nb-97 | Sn-121m | Hf-181 | Pu-240 ¹ |
| Cr-55 ¹ | Zr-95 | Nb-97m | Sn-123 | Lu-173 | Pu-241 ¹ |
| Mn-54 | Zr-97 | Mo-93 | Sn-123m | Lu-174 | Am-241 ¹ |
| Mn-56 | Sr-87m | Mo-93m | Sn-125 | Lu-174m | Cm-242 ¹ |
| Co-57 | Sr-89 | Mo-99 | Sb-122 | Lu-176m | Cm-243 ¹ |
| Co-58 | Sr-90 ¹ | Mo-101 | Sb-124 | Lu-177 | Cm-244 ¹ |

Notes: ¹ Radionuclides not calculated in ORIGEN-S calculations, but included from previous shipments. Only present in small quantities in surface contamination.

Table 5.5-8. Sc-46 Gamma Emission Energy Spectrum

| Total Photons/Disintegration | |
|------------------------------|-----------|
| 2.000E+00 | |
| Energy | Intensity |
| 0.889 | 1.00E+00 |
| 1.121 | 1.00E+00 |
| 2.010 | 1.30E-07 |

Table 5.5-9. Cr-51 Gamma Emission Energy Spectrum

| Total Photons/Disintegration | |
|------------------------------|-----------|
| 9.910E-02 | |
| Energy | Intensity |
| 0.320 | 9.91E-02 |

Table 5.5-10. Mn-54 Gamma Emission Energy Spectrum

| Total Photons/Disintegration | |
|------------------------------|-----------|
| 9.998E-01 | |
| Energy | Intensity |
| 0.511 | 5.600E-09 |
| 0.835 | 9.998E-01 |

Table 5.5-11. Co-58 Gamma Emission Energy Spectrum

| Total Photons/Disintegration | |
|------------------------------|-----------|
| 1.305E+00 | |
| Energy | Intensity |
| 0.511 | 2.98E-01 |
| 0.811 | 9.95E-01 |
| 0.864 | 6.86E-03 |
| 1.675 | 5.17E-03 |

Table 5.5-12. Fe-59 Gamma Emission Energy Spectrum

| Total Photons/Disintegration | |
|------------------------------|-----------|
| 1.041E+00 | |
| Energy | Intensity |
| 0.143 | 1.02E-02 |
| 0.189 | 9.00E-06 |
| 0.192 | 3.08E-02 |
| 0.335 | 2.70E-03 |
| 0.382 | 1.80E-04 |
| 1.099 | 5.65E-01 |
| 1.292 | 4.32E-01 |
| 1.482 | 5.90E-04 |

Table 5.5-13. Co-60 Gamma Emission Energy Spectrum

| Total Photons/Disintegration | |
|------------------------------|------------|
| 1.998E+00 | |
| Energy | Intensity |
| 0.347 | 7.5000E-05 |
| 0.826 | 7.6000E-05 |
| 1.173 | 9.9850E-01 |
| 1.333 | 9.9983E-01 |
| 2.159 | 1.2000E-05 |
| 2.506 | 2.0000E-08 |

Table 5.5-14. Zn-65 Gamma Emission Energy Spectrum

| Total Photons/Disintegration | |
|------------------------------|-----------|
| 5.289E-01 | |
| Energy | Intensity |
| 0.511 | 2.84E-02 |
| 0.345 | 2.53E-05 |
| 0.771 | 2.68E-05 |
| 1.116 | 5.00E-01 |

Table 5.5-15. Nb-92m Gamma Emission Energy Spectrum

| Total Photons/Disintegration | |
|------------------------------|-----------|
| 1.02E+00 | |
| Energy | Intensity |
| 0.511 | 1.28E-03 |
| 0.449 | 1.63E-05 |
| 0.561 | 2.23E-05 |
| 0.913 | 1.78E-02 |
| 0.934 | 9.91E-01 |
| 1.132 | 5.15E-05 |
| 1.848 | 8.52E-03 |

Table 5.5-16. Nb-94 Gamma Emission Energy Spectrum

| Total Photons/Disintegration | |
|------------------------------|-----------|
| 1.997E+00 | |
| Energy | Intensity |
| 0.703 | 9.98E-01 |
| 0.871 | 9.99E-01 |

Table 5.5-17. Zr/Nb-95 Gamma Emission Energy Spectrum

| Total Photons/Disintegration | |
|------------------------------|-----------|
| 1.99E+00 | |
| Energy | Intensity |
| 0.204 | 2.80E-04 |
| 0.562 | 1.50E-04 |
| 0.724 | 4.43E-01 |
| 0.757 | 5.44E-01 |
| 0.766 | 9.98E-01 |

Table 5.5-18. Sb-124 Gamma Emission Energy Spectrum

| Total Photons/Disintegration | | | | | |
|------------------------------|-----------|--------|-----------|--------|-----------|
| 1.878E+00 | | | | | |
| Energy | Intensity | Energy | Intensity | Energy | Intensity |
| 0.148 | 3.91E-05 | 0.766 | 1.21E-04 | 1.566 | 1.37E-04 |
| 0.190 | 6.36E-05 | 0.775 | 9.39E-05 | 1.580 | 3.81E-03 |
| 0.210 | 5.48E-05 | 0.791 | 7.39E-03 | 1.622 | 4.09E-04 |
| 0.254 | 1.61E-04 | 0.817 | 7.29E-04 | 1.691 | 4.76E-01 |
| 0.292 | 8.70E-05 | 0.857 | 2.38E-04 | 1.721 | 9.51E-04 |
| 0.336 | 7.43E-04 | 0.899 | 1.72E-04 | 1.852 | 6.45E-05 |
| 0.371 | 3.81E-04 | 0.968 | 1.88E-02 | 1.919 | 5.45E-04 |
| 0.400 | 1.39E-03 | 0.977 | 8.32E-04 | 2.016 | 9.49E-04 |
| 0.444 | 1.89E-03 | 1.045 | 1.83E-02 | 2.040 | 6.42E-04 |
| 0.469 | 4.99E-04 | 1.054 | 4.89E-05 | 2.080 | 2.05E-04 |
| 0.481 | 2.37E-04 | 1.087 | 3.78E-04 | 2.091 | 5.49E-02 |
| 0.526 | 1.38E-03 | 1.264 | 4.13E-04 | 2.099 | 4.57E-04 |
| 0.530 | 4.21E-04 | 1.301 | 3.43E-04 | 2.108 | 4.33E-04 |
| 0.572 | 1.90E-04 | 1.326 | 1.58E-02 | 2.172 | 2.05E-05 |
| 0.603 | 9.78E-01 | 1.355 | 1.04E-02 | 2.183 | 4.24E-04 |
| 0.632 | 1.05E-03 | 1.368 | 2.62E-02 | 2.284 | 8.02E-05 |
| 0.646 | 7.42E-02 | 1.376 | 4.83E-03 | 2.294 | 3.20E-04 |
| 0.662 | 2.93E-04 | 1.385 | 6.26E-04 | 2.324 | 2.44E-05 |
| 0.709 | 1.35E-02 | 1.437 | 1.22E-02 | 2.455 | 1.47E-05 |
| 0.714 | 2.28E-02 | 1.445 | 3.30E-03 | 2.682 | 1.65E-05 |
| 0.723 | 1.08E-01 | 1.489 | 6.72E-03 | 2.694 | 3.03E-05 |
| 0.736 | 5.57E-04 | 1.526 | 4.09E-03 | 2.808 | 1.47E-05 |
| 0.736 | 7.14E-04 | | | | |

Table 5.5-19. Sb-125 Gamma Emission Energy Spectrum

| Total Photons/Disintegration | | | |
|------------------------------|-----------|--------|-----------|
| 8.628E-01 | | | |
| Energy | Intensity | Energy | Intensity |
| 0.111 | 1.04E-05 | 0.408 | 1.84E-03 |
| 0.117 | 2.63E-03 | 0.428 | 2.96E-01 |
| 0.133 | 8.58E-06 | 0.444 | 3.06E-03 |
| 0.173 | 1.91E-03 | 0.463 | 1.05E-01 |
| 0.176 | 6.84E-02 | 0.490 | 1.36E-05 |
| 0.179 | 3.37E-04 | 0.491 | 4.74E-05 |
| 0.199 | 1.28E-04 | 0.497 | 3.20E-05 |
| 0.204 | 3.17E-03 | 0.503 | 3.85E-05 |
| 0.208 | 2.48E-03 | 0.539 | 1.39E-05 |
| 0.209 | 4.50E-04 | 0.601 | 1.76E-01 |
| 0.228 | 1.31E-03 | 0.607 | 4.98E-02 |
| 0.315 | 4.03E-05 | 0.617 | 5.33E-05 |
| 0.321 | 4.16E-03 | 0.636 | 1.12E-01 |
| 0.332 | 2.52E-05 | 0.653 | 2.66E-05 |
| 0.367 | 7.99E-05 | 0.671 | 1.79E-02 |
| 0.380 | 1.52E-02 | 0.693 | 4.59E-07 |
| 0.402 | 6.22E-05 | | |

Table 5.5-20. Sb-126 Gamma Emission Energy Spectrum

| Total Photons/Disintegration | | | |
|------------------------------|-----------|--------|-----------|
| 4.304E+00 | | | |
| Energy | Intensity | Energy | Intensity |
| 0.149 | 3.98E-03 | 0.667 | 9.96E-01 |
| 0.209 | 4.98E-03 | 0.675 | 3.69E-02 |
| 0.224 | 1.39E-02 | 0.695 | 9.96E-01 |
| 0.278 | 2.39E-02 | 0.697 | 2.89E-01 |
| 0.297 | 4.48E-02 | 0.721 | 5.38E-01 |
| 0.297 | 4.98E-03 | 0.857 | 1.76E-01 |
| 0.415 | 8.33E-01 | 0.954 | 1.20E-02 |
| 0.415 | 9.96E-03 | 0.958 | 4.98E-03 |
| 0.556 | 1.69E-02 | 0.990 | 6.77E-02 |
| 0.574 | 6.67E-02 | 1.036 | 9.96E-03 |
| 0.593 | 7.47E-02 | 1.061 | 3.98E-03 |
| 0.620 | 8.96E-03 | 1.064 | 8.96E-03 |
| 0.639 | 8.96E-03 | 1.213 | 2.39E-02 |
| 0.656 | 2.19E-02 | 1.477 | 2.79E-03 |

Table 5.5-21. Cs-134 Gamma Emission Energy Spectrum

| Total Photons/Disintegration | |
|------------------------------|-----------|
| 2.228E+00 | |
| Energy | Intensity |
| 0.243 | 2.72E-04 |
| 0.327 | 1.62E-04 |
| 0.475 | 1.48E-02 |
| 0.563 | 8.34E-02 |
| 0.569 | 1.54E-01 |
| 0.605 | 9.76E-01 |
| 0.796 | 8.55E-01 |
| 0.802 | 8.69E-02 |
| 0.847 | 3.00E-06 |
| 1.039 | 9.90E-03 |
| 1.168 | 1.79E-02 |
| 1.365 | 3.02E-02 |

Table 5.5-22. Cs-137 (Ba-137m) Gamma Emission Energy Spectrum

| Total Photons/Disintegration | |
|------------------------------|-----------|
| 8.990E-01 | |
| Energy | Intensity |
| 0.662 | 8.99E-01 |

Table 5.5-23. Hf-175 Gamma Emission Energy Spectrum

| Total Photons/Disintegration | |
|------------------------------|-----------|
| 8.683E-01 | |
| Energy | Intensity |
| 0.114 | 2.94E-03 |
| 0.161 | 2.27E-04 |
| 0.230 | 6.83E-03 |
| 0.319 | 1.68E-03 |
| 0.343 | 8.40E-01 |
| 0.353 | 2.28E-03 |
| 0.433 | 1.44E-02 |

Table 5.5-24. Hf-181 Gamma Emission Energy Spectrum

| Total Photons/Disintegration | |
|------------------------------|-----------|
| 1.466E+00 | |
| Energy | Intensity |
| 0.133 | 4.33E-01 |
| 0.136 | 5.85E-02 |
| 0.137 | 8.61E-03 |
| 0.346 | 1.51E-01 |
| 0.476 | 7.03E-03 |
| 0.482 | 8.05E-01 |
| 0.615 | 2.33E-03 |
| 0.619 | 2.50E-04 |

Table 5.5-25. Ta-182 Gamma Emission Energy Spectrum

| Total Photons/Disintegration | | | | | |
|------------------------------|-----------|--------|-----------|--------|-----------|
| 1.456E+00 | | | | | |
| Energy | Intensity | Energy | Intensity | Energy | Intensity |
| 0.100 | 1.42E-01 | 0.830 | 1.41E-04 | 1.189 | 1.65E-01 |
| 0.110 | 1.07E-03 | 0.892 | 5.74E-04 | 1.221 | 2.72E-01 |
| 0.114 | 1.87E-02 | 0.928 | 6.14E-03 | 1.224 | 2.36E-03 |
| 0.116 | 4.44E-03 | 0.960 | 3.50E-03 | 1.231 | 1.16E-01 |
| 0.122 | 2.36E-05 | 1.002 | 2.09E-02 | 1.257 | 1.51E-02 |
| 0.152 | 7.02E-02 | 1.036 | 6.70E-05 | 1.274 | 6.60E-03 |
| 0.156 | 2.67E-02 | 1.044 | 2.39E-03 | 1.289 | 1.37E-02 |
| 0.179 | 3.12E-02 | 1.113 | 4.45E-03 | 1.343 | 2.57E-03 |
| 0.198 | 1.46E-02 | 1.121 | 3.52E-01 | 1.374 | 2.22E-03 |
| 0.222 | 7.57E-02 | 1.157 | 7.33E-03 | 1.387 | 7.29E-04 |
| 0.229 | 3.64E-02 | 1.158 | 2.89E-03 | 1.410 | 3.96E-04 |
| 0.264 | 3.61E-02 | 1.181 | 8.74E-04 | 1.453 | 3.07E-04 |
| 0.351 | 1.13E-04 | | | | |

5.5.3. Cobalt-60 Isotope Rod Activity Distribution

The cobalt-60 isotope rod shielding analysis utilizes 12-inch long line sources, which distribute the activity of the source uniformly across the line. Distribution of the cobalt-60 activity into a longer line source results in a lower external dose rate, and greater concentration of the cobalt-60 activity into a shorter line source results in a higher external dose rate. Thus, in order to demonstrate compliance with the regulatory dose rate limits for the cobalt-60 isotope rod contents, two requirements must be met. First, it must be shown that the dose rate contribution from all cobalt-60 source activity in a single shipment is less than the regulatory limit. Second, It must also be shown that the distribution of the activity in any single shipment of isotope rod [[]] is distributed axially, such that the uniform line source used in the shielding analysis is bounding of the actual axial distribution of activity.

For the cobalt-60 isotope rod shielding analysis, there are two source geometries considered. The first source geometry is referred to as the ‘bounding’ source geometry, which concentrates all of the cobalt-60 activity into a single 12-inch line source that is located in the most restrictive location for dose rate calculations in the given direction (top, side, or bottom). For side dose rate calculations with the bounding source geometry, dose rates are calculated with the source at both the bottom (Case 1) and top (Case 2) of the HPI cavity to determine the bounding source location.

The second geometry, referred to as the ‘Realistic’ source geometry distributes the cobalt-60 activity into [[]] 12-inch lines, each centered in one of the [[]] of the HPI material basket. This source geometry provides a more realistic radial distribution of the source, as rod [[]] will be distributed throughout the basket during shipment, while still condensing the source axially to 12-inches. The array of line sources for the realistic arrangement is pushed against the top of the HPI for the top dose rate calculations, and is at the bottom of the HPI for bottom and side dose rate calculations. Figure 5.5-1 shows a cross section of the HPI material basket, with locations of the line sources used in the MCNP model.

[[

]]

Figure 5.5-1. HPI Material Basket with ‘Realistic’ Source Geometry Locations

A list of all source geometries analyzed is provided in Table 5.5-26 and a depiction of each source geometry is presented in Figures 5.5-2 through 5.5-8. The ‘realistic’ dose rate calculations are only included to quantify the margin in the bounding dose rates. For the demonstration of compliance with the normal and hypothetical accident condition dose rate limits, the reported dose rates are based on the more restrictive ‘bounding’ source geometries.

Table 5.5-26. Cobalt-60 Isotope Rod Shielding Analysis Case Summary

| NCT Dose Rate Calculation Locations | Source Arrangement | Source Arrangement Figure |
|------------------------------------------------|-------------------------------|------------------------------------------|
| Bottom Surface | Realistic | 5.5-2 |
| | Bounding | 5.5-3 |
| Top Surface | Realistic | 5.5-4 |
| | Bounding | 5.5-5 |
| Side Surface | Realistic | 5.5-6 |
| | Bounding – 1 | 5.5-7 |
| | Bounding – 2 | 5.5-8 |
| 2-meter | Realistic | 5.5-6 |
| | Bounding – 1 | 5.5-7 |
| | Bounding – 2 | 5.5-8 |
| Cab | Realistic | 5.5-6 |
| | Bounding – 1 | 5.5-7 |
| | Bounding – 2 | 5.5-8 |

II

II

Figure 5.5-2. ‘Realistic’ Source Arrangement for Bottom Dose Rates

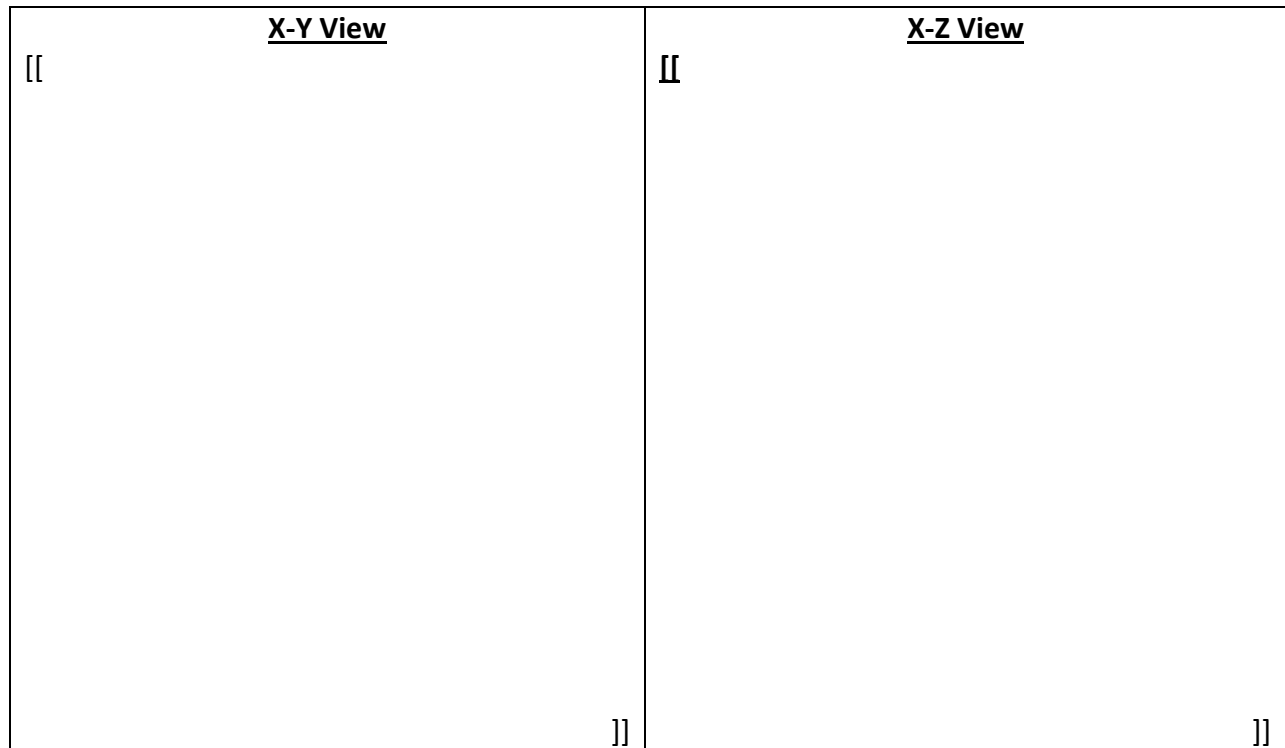


Figure 5.5-3. 'Bounding' Source Arrangement for Bottom Dose Rates

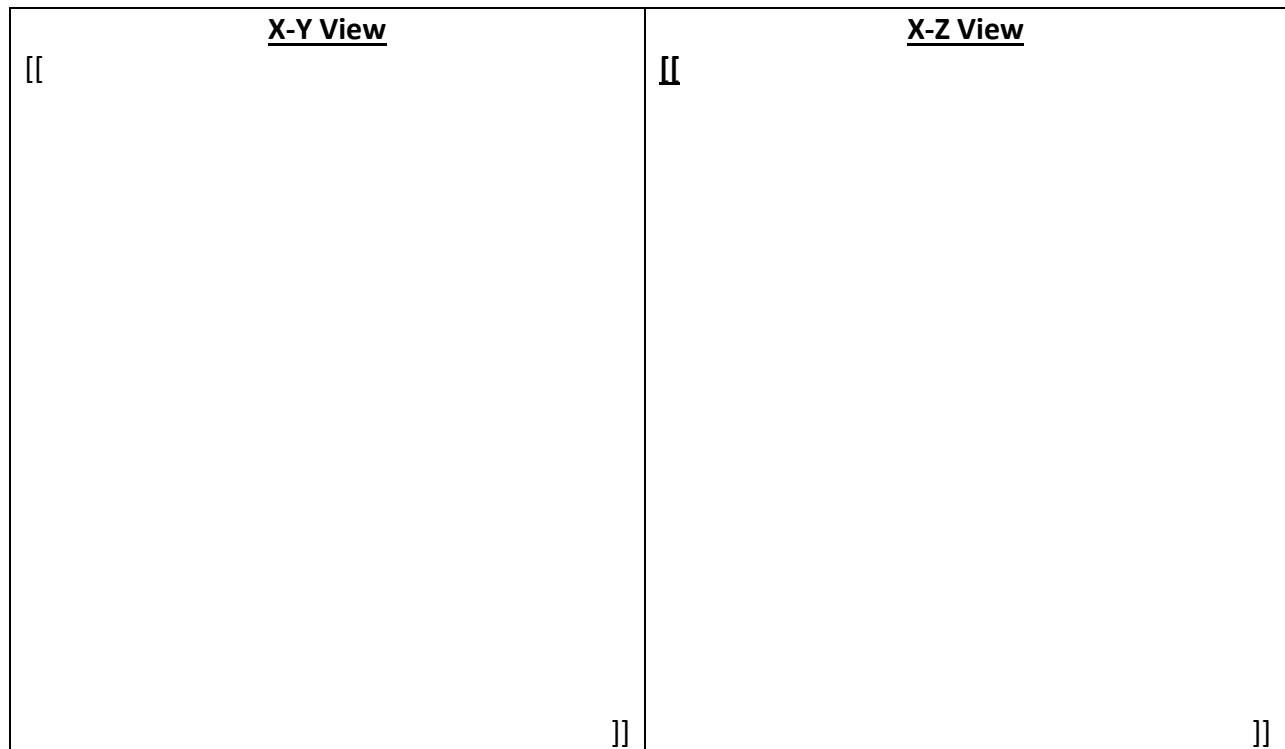


Figure 5.5-4. 'Realistic' Source Arrangement for Top Dose Rates

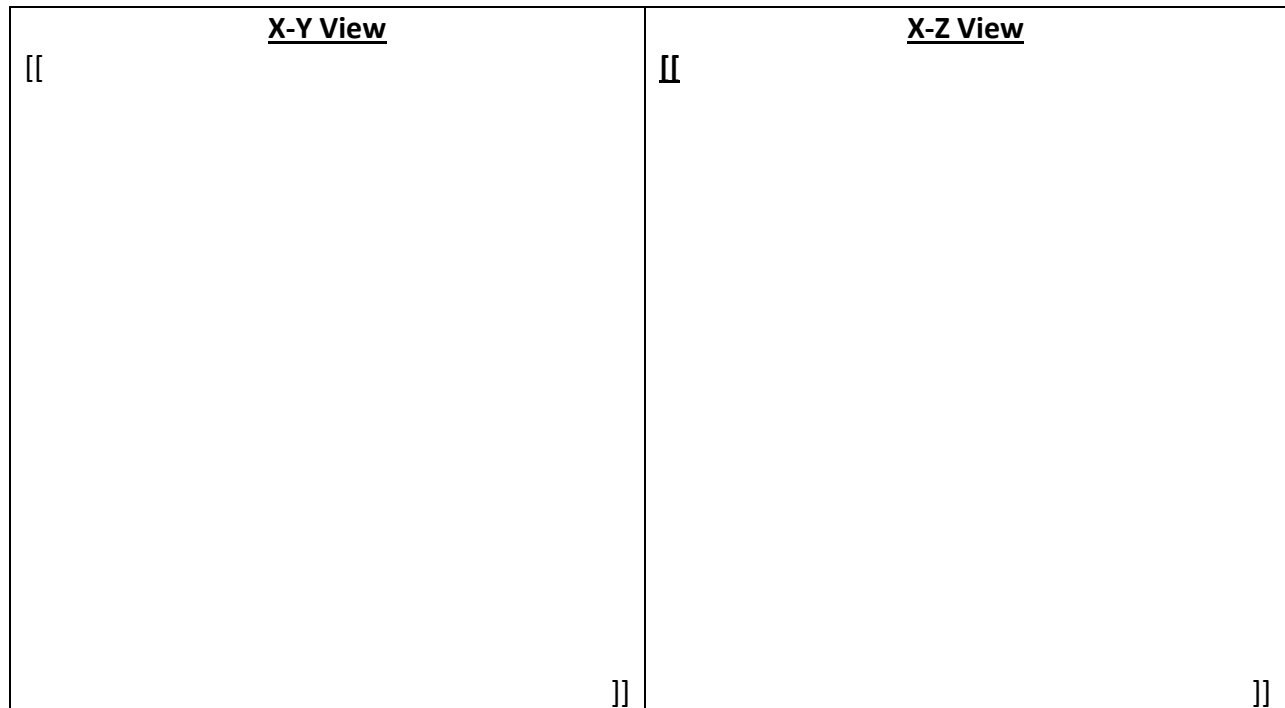


Figure 5.5-5. 'Bounding' Source Arrangement for Top Dose Rates

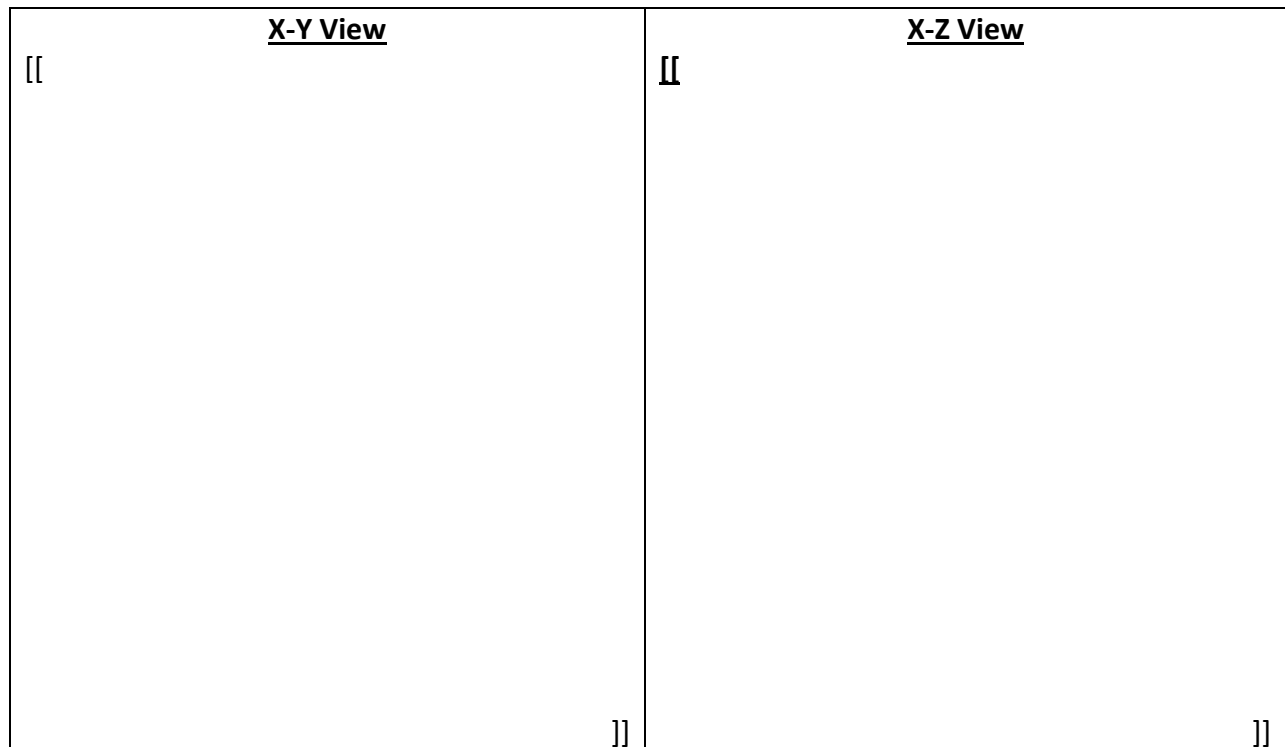


Figure 5.5-6. 'Realistic' Source Arrangement for Side Dose Rates

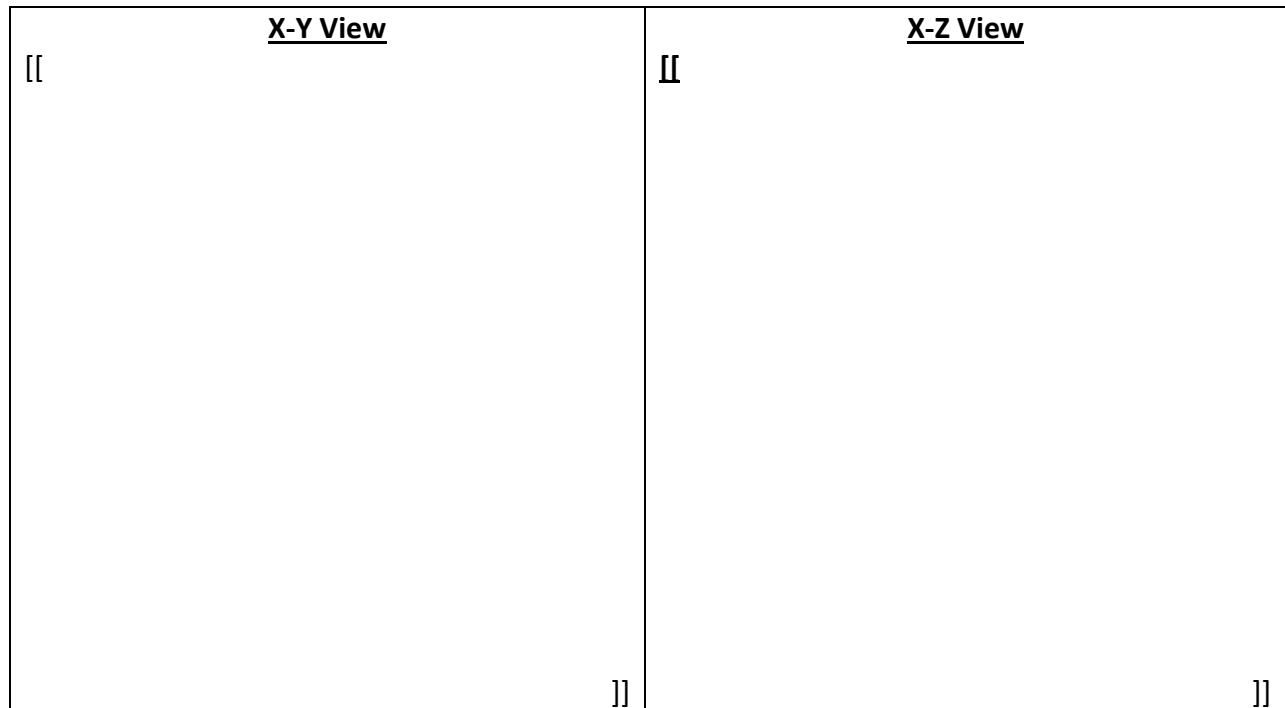


Figure 5.5-7. 'Bounding' Source Arrangement for Side Dose Rates – Case 1

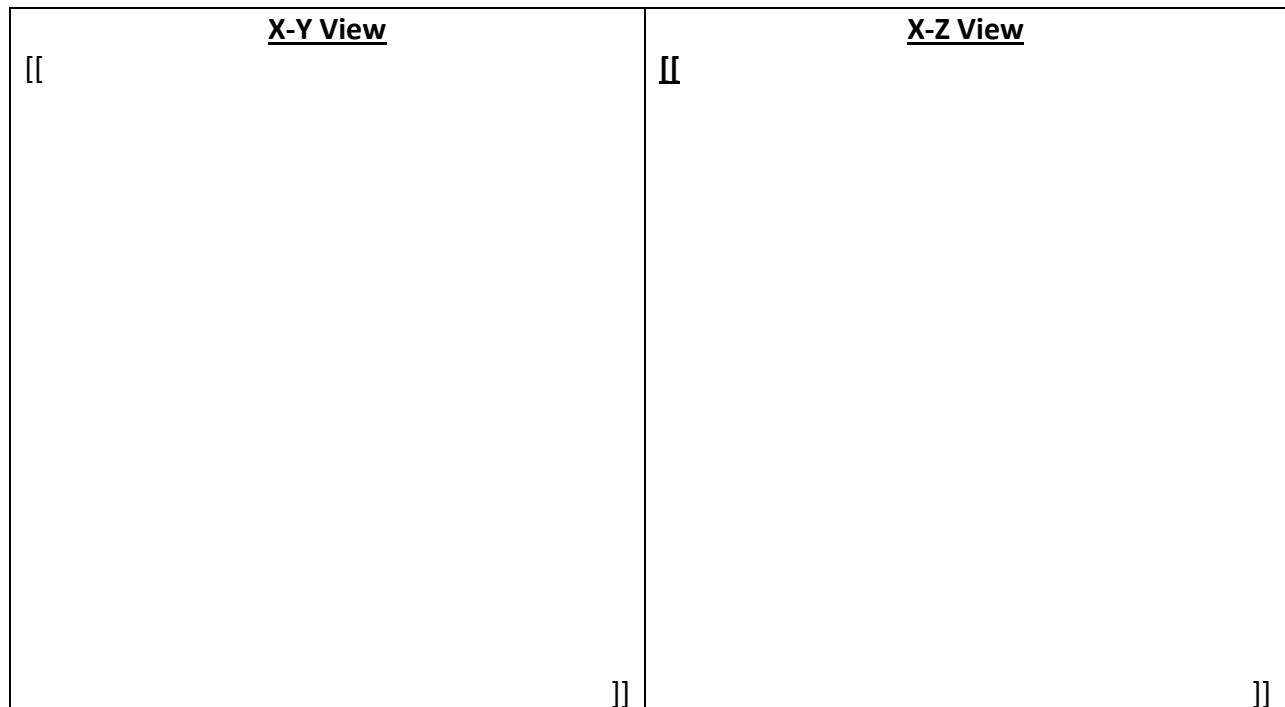


Figure 5.5-8. 'Bounding' Source Arrangement for Side Dose Rates – Case 2

Table 5.5-27 lists the peak dose rate per curie calculated at each NCT regulatory dose rate location for each source geometry included in the cobalt-60 isotope rod shielding analysis, and the overall maximum calculated dose rate for each regulatory dose rate location. All maximum calculated dose rates were calculated with the ‘bounding’ source geometries, where the activity is concentrated into a single line. Also, the line source at the bottom of the HPI cavity calculated higher side dose rates than at the top.

Table 5.5-27. Cobalt-60 Isotope Rod Shielding Analysis NCT Dose Rate Results

| NCT Dose Rate Location | Source Arrangement | Dose Rate (mrem/hr/Ci) | Maximum Location Dose Rate (mrem/hr/Ci) |
|------------------------|--------------------|------------------------|-----------------------------------------|
| Bottom Surface | Realistic | 3.555E-04 | 3.940E-04 |
| | Bounding | 3.940E-04 | |
| Top Surface | Realistic | 1.780E-04 | 1.850E-04 |
| | Bounding | 1.850E-04 | |
| Side Surface | Realistic | 4.422E-04 | 8.821E-04 |
| | Bounding | 8.821E-04 | |
| | Bounding | 8.168E-04 | |
| 2-meter | Realistic | 1.254E-05 | 1.664E-05 |
| | Bounding | 1.664E-05 | |
| | Bounding | 1.348E-05 | |
| Cab | Realistic | 2.277E-06 | 2.921E-06 |
| | Bounding | 2.921E-06 | |
| | Bounding | 2.331E-06 | |

Table 5.5-28 lists the maximum calculated dose rate at each NCT regulatory dose rate location using the dose rate per curie values calculated in Table 5.5-27 and the total cobalt-60 activity resulting in the dose rate equal to the 90% of regulatory limit for the respective location. This activity is 204,000 Ci, which results in an NCT side surface dose rate of 180 mrem/hr. Although a cobalt-60 activity of 204,000 Ci is not permitted in the Model 2000 cask due to the Configuration 2 thermal limit, this table is included to demonstrate at this activity, no regulatory dose rate limits are exceeded.

Table 5.5-28. Cobalt-60 Isotope Rod Shielding Analysis Maximum NCT Dose Rates

| Dose Rate Location | Dose Rate per Curie (mrem/hr/Ci) | Dose Rate ¹ (mrem/hr) |
|--------------------|----------------------------------|----------------------------------|
| Bottom Surface | 3.940E-04 | 80.40 |
| Top Surface | 1.850E-04 | 37.70 |
| Side Surface | 8.821E-04 | 180.0 |
| 2-meter | 1.664E-05 | 3.400 |
| Cab | 2.921E-06 | 0.600 |

Notes: ¹ Based on an activity of 204,000 Ci cobalt-60

In Table 5.5-28 it is demonstrated that external dose rates resulting from any cobalt-60 isotope rod activity up to 204,000 Ci are less than the regulatory dose rate limits. It still must be demonstrated that the activity in any single shipment of isotope rod [[]] is distributed axially, such that the uniform line source used in the shielding analysis is bounding of the actual

axial distribution of activity. The exact axial activity profile of the cobalt-60 isotope rod [] is variable due to differences in the neutron flux profiles when irradiated in a commercial or research reactor. To determine that the uniform source in the MCNP6 shielding analysis is bounding of the distribution of activity in a shipment of rod [], it should first be considered that the source geometry is a single 12-inch line source. Modeling the source in this way assumes that all cobalt-60 activity loaded into the cavity is concentrated into a single line, with a uniform distribution. With all activity in a single line at the most restrictive location of the HPI cavity, any radial distribution of activity is bounded. Thus, the only variation in the source distribution that can cause the external dose rates to increase is in one direction (axially). So, it can be demonstrated that the source distribution of the contents in an actual shipment are bounded, by determining that there is no axial location in the HPI cavity where the concentration of activity is greater than what was analyzed in the MCNP analysis.

With the source arrangement of a single 12-inch line, no external dose rates will exceed the regulatory limits for any activity up to 204,000 Ci. By dividing the activity of 204,000 Ci evenly across the 12-inch uniform MCNP6 source, the result is a source that is concentrated in the axial direction to an activity of 17,000 Ci in each inch of the line source. Thus, it can be demonstrated that the activity distribution in the MCNP shielding model bounds the total activity distribution in the HPI cavity by determining for the package contents, the total activity in any axial 1-inch increment of the HPI cavity is less than 17,000 Ci. If for an actual shipment, there is not more than a total of 17,000 Ci in any axial 1-inch increment of the HPI cavity, there is a greater distribution of the activity in the contents than in the MCNP source and the MCNP source is bounding.

The maximum possible activity in any axial 1-inch increment of the HPI cavity (A_{HPI}) for an actual shipment is calculated by multiplying the peak activity across an inch of the rod [] (A_{rod}) by the total number of rod [] in the shipment (N). Note that, as the neutron flux in any reactor will be essentially constant across any 1-inch axial increment, the cobalt-60 activity across any inch of an isotope rod will be constant.

$$A_{HPI}[Ci] = A_{rod}[Ci] \cdot N \quad (5-10)$$

Alternatively, the maximum allowable activity for an inch of all isotope rod [] can be calculated by dividing the maximum allowable activity in any axial 1-inch increment of the HPI (17,000 Ci) by the number of rod [] in the proposed shipment of cobalt-60 isotope rod [].

$$A_{rod}[Ci] = \frac{17,000[Ci]}{N} \quad (5-11)$$

If the peak activity for any rod [] in a proposed shipment is less than the value calculated in Equation 5-11, it demonstrates that the summed activity in any 1-inch axial increment in the HPI will never exceed the 17,000 Ci limit and the MCNP6 source arrangement is bounding. Table 5.5-29 lists the peak rod activity limit for a few example quantities of rod [].

Table 5.5-29. Cobalt-60 Isotope Rod Peak Activity Limits

| Number of Rod (N) | Peak Rod Activity Limit (Ci) |
|-------------------|------------------------------|
| 10 | 1700 |
| 50 | 340.0 |
| 100 | 170.0 |

The number of rod (N), refers to the total number of rods loaded into the HPI. If any rods are present prior to being loaded into the HPI for shipment each rod counts toward the determination of the number of rod (N) that are loaded.

The values in Table 5.5-29 should be interpreted as follows: for a shipment with up to N rod, the maximum allowable activity in any 1-inch axial increment of a rod is as listed in column 2 of the table. There is no minimum length limit for the rod; as long as each rod counts toward the number of rod segments (N) and the corresponding peak rod activity limit is not exceeded.

To provide a direct example demonstrating compliance with dose rate limits for cobalt-60 isotope rods, data from a previous set of GE14i cobalt-60 rods is used. For this set of GE14i rods, the maximum calculated activity for a whole rod was 192,800 Ci. As an example, a hypothetical shipment of 10 rods with the total activity and activity distribution of this maximum activity (192,800 Ci) GE14i rod is considered. Radionuclide activity in the rod cladding is neglected for this example. With 10 GE14i rods, each with an activity of 19,280 Ci, the total cobalt-60 activity for the shipment is 192,800 Ci. Because this activity is less than 204,000 Ci, the resulting external dose rates are less than the regulatory limits for each location. For this GE14i rod, the maximum activity was calculated for each 1-inch length along the rod; the maximum value was 19,280 Ci. With this activity evenly distributed across the 19.28-inch length, the peak rod activity across a single inch is 1,000 Ci.

1,000 Ci in this hypothetical shipment, or N=50. In Table 5.5-29, the allowable peak rod activity for 50 rod is 340 Ci, which is greater than the peak rod activity for the hypothetical shipment (1,000 Ci). With the calculated peak rod activity of 1,000 Ci for the rod, the maximum possible activity in a 1-inch tall section of the HPI for a load of 50 rod is 1,000 Ci. Thus, the axial distribution of activity from any possible loading of this hypothetical shipment of cobalt-60 isotope rod is bounded by the uniform distribution modeled in the MCNP analysis.

5.5.4. Radionuclide Decay Heat Conversion Factors

In addition to demonstrating compliance with the regulatory dose rate requirements, filling out the Irradiated Hardware and Byproduct Loading Table also demonstrates compliance with the Configuration 1 and Configuration 2 thermal limits of the Model 2000 cask. One characteristic of every radionuclide is a given Q-value, which is the quantity of energy emitted per decay (MeV/Decay). By assuming that all energy emitted is deposited locally in the HPI material basket or the HPI body, the radionuclide decay heat in W/Ci can be calculated. All radionuclides considered in the irradiated hardware and byproduct contents are listed in Table 5.5-7 of

Section 5.5.2, regardless of their significance to dose rate calculations. The Q-values for each of these radionuclides are provided in SCALE6.1 ORIGIN Decay library origen.rev03.decay.data (Reference 5-2). Table 5.5-30 lists all of the irradiated hardware and by-product radionuclides with their ORIGIN library identification number, Q-value, and the calculated decay heat. Radionuclide Q-values are converted to decay heat values as shown in Equation 5-12.

$$\text{Decay Heat} \left[\frac{\text{W}}{\text{Ci}} \right] = Q \left[\frac{\text{MeV}}{\text{disintegration}} \right] \cdot 1.60217 \cdot 10^{-13} \left[\frac{\text{J}}{\text{MeV}} \right] \cdot 3.7 \cdot 10^{10} \left[\frac{\text{disintegrations}}{\text{s}} \right] \left[\frac{\text{s}}{\text{Ci}} \right] \quad (5-12)$$

Table 5.5-30. Isotope Decay Heat Data

| Isotope | ORIGIN Radionuclide ID | Q-Value (MeV/Decay) | Decay Heat (W/Ci) | Isotope | ORIGIN Radionuclide ID | Q-Value (MeV/Decay) | Decay Heat (W/Ci) |
|---------|------------------------|---------------------|------------------------|---------|------------------------|---------------------|------------------------|
| H-3 | 10030 | 5.6900E-03 | 3.373E-05 | Tc-101 | 431010 | 8.1600E-01 | 4.837E-03 |
| C-14 | 60140 | 4.9470E-02 | 2.933E-04 | Ru-106 | 441060 | 1.0030E-02 | 5.946E-05 |
| Na-24 | 110240 | 4.6769E+00 | 2.772E-02 | In-113m | 491131 | 3.9159E-01 | 2.321E-03 |
| Si-31 | 140310 | 5.9645E-01 | 3.536E-03 | In-114 | 491140 | 7.7607E-01 | 4.601E-03 |
| P-32 | 150320 | 6.9490E-01 | 4.119E-03 | In-114m | 491141 | 2.2277E-01 | 1.321E-03 |
| P-33 | 150330 | 7.6430E-02 | 4.531E-04 | in-115m | 491151 | 3.3436E-01 | 1.982E-03 |
| S-35 | 160350 | 4.8758E-02 | 2.890E-04 | Sn-113 | 501130 | 2.9753E-02 | 1.764E-04 |
| Ca-45 | 200450 | 7.6860E-02 | 4.556E-04 | Sn-113m | 501131 | 7.1749E-02 | 4.253E-04 |
| Sc-46 | 210460 | 2.1214E+00 | 1.258E-02 | Sn-117 | 501170 | 0.0000E+00 | 0.000E+00 |
| Sc-47 | 210470 | 2.7132E-01 | 1.608E-03 | Sn-117m | 501171 | 3.1563E-01 | 1.871E-03 |
| Sc-48 | 210480 | 3.5737E+00 | 2.118E-02 | Sn-119 | 501190 | 0.0000E+00 | 0.000E+00 |
| V-49 | 230490 | 4.4514E-03 | 2.639E-05 | Sn-119m | 501191 | 8.7589E-02 | 5.192E-04 |
| V-52 | 230520 | 2.5137E+00 | 1.490E-02 | Sn-121 | 501210 | 1.1582E-01 | 6.866E-04 |
| Cr-51 | 240510 | 3.6680E-02 | 2.174E-04 | Sn-121m | 501211 | 3.7987E-02 | 2.252E-04 |
| Cr-55 | 240550 | 1.1017E+00 | 6.531E-03 | Sn-123 | 501230 | 5.3006E-01 | 3.142E-03 |
| Mn-54 | 250540 | 8.4017E-01 | 4.981E-03 | Sn-123m | 501231 | 6.2147E-01 | 3.684E-03 |
| Mn-56 | 250560 | 2.5226E+00 | 1.495E-02 | Sn-125 | 501250 | 1.1357E+00 | 6.732E-03 |
| Co-57 | 270570 | 1.4380E-01 | 8.525E-04 | Sb-122 | 511220 | 1.0098E+00 | 5.986E-03 |
| Co-58 | 270580 | 1.0088E+00 | 5.980E-03 | Sb-124 | 511240 | 2.2351E+00 | 1.325E-02 |
| Co-58m | 270581 | 2.4744E-02 | 1.467E-04 | Sb-125 | 511250 | 5.3352E-01 | 3.163E-03 |
| Co-60 | 270600 | 2.6006E+00 | 1.542E-02 | Sb-126 | 511260 | 3.1205E+00 | 1.850E-02 |
| Co-60m | 270601 | 6.3045E-02 | 3.737E-04 | Te-125m | 521251 | 1.4546E-01 | 8.623E-04 |
| Co-61 | 270610 | 5.6391E-01 | 3.343E-03 | I-129 | 531290 | 7.4338E-02 | 4.407E-04 |
| Ni-57 | 280570 | 2.0927E+00 | 1.241E-02 | Cs-134 | 551340 | 1.7185E+00 | 1.019E-02 |
| Ni-59 | 280590 | 6.9156E-03 | 4.100E-05 | Cs-137 | 551370 | 1.7945E-01 | 4.985E-03 ¹ |
| Ni-63 | 280630 | 1.7425E-02 | 1.033E-04 | Ba-137m | 561371 | 6.6140E-01 | |
| Ni-65 | 280650 | 1.1863E+00 | 7.032E-03 | La-140 | 571400 | 2.8438E+00 | 1.686E-02 |
| Fe-55 | 260550 | 5.8421E-03 | 3.463E-05 | Ba-140 | 561400 | 5.0041E-01 | 2.966E-03 |
| Fe-59 | 260590 | 1.3060E+00 | 7.742E-03 | Ce-144 | 581440 | 1.1059E-01 | 6.556E-04 |
| Cu-64 | 290640 | 3.1188E-01 | 1.849E-03 | Hf-173 | 721730 | 4.4558E-01 | 2.641E-03 |
| Cu-66 | 290660 | 1.1645E+00 | 6.903E-03 | Hf-175 | 721750 | 3.9728E-01 | 2.355E-03 |
| Zn-65 | 300650 | 5.8284E-01 | 3.455E-03 | Hf-177m | 721771 | 1.5190E+00 | 9.005E-03 |
| Zr-89 | 400890 | 3.5256E-01 | 2.090E-03 | Hf-180m | 721801 | 1.1148E+00 | 6.609E-03 |
| Zr-95 | 400950 | 8.5013E-01 | 9.835E-03 ² | Hf-181 | 721810 | 7.3010E-01 | 4.328E-03 |
| Zr-97 | 400970 | 8.6426E-01 | 5.123E-03 | Lu-173 | 711730 | 2.3057E-01 | 1.367E-03 |
| Sr-87m | 380871 | 3.8798E-01 | 2.300E-03 | Lu-174 | 711740 | 1.5804E-01 | 9.369E-04 |
| Sr-89 | 380890 | 5.8534E-01 | 3.470E-03 | Lu-174m | 711741 | 1.6712E-01 | 9.907E-04 |

| Isotope | ORIGEN Radionuclide ID | Q-Value (MeV/Decay) | Decay Heat (W/Ci) |
|---------|------------------------|---------------------|-------------------|
| Sr-90 | 380900 | 1.9580E-01 | 1.161E-03 |
| Sr-91 | 380910 | 1.3485E+00 | 7.994E-03 |
| Y-89m | 390891 | 9.0902E-01 | 5.389E-03 |
| Y-90 | 390900 | 9.3302E-01 | 5.531E-03 |
| Y-90m | 390901 | 6.8000E-01 | 4.031E-03 |
| Y-91 | 390910 | 6.0617E-01 | 3.593E-03 |
| Y-91m | 390911 | 5.5554E-01 | 3.293E-03 |
| Y-92 | 390920 | 1.7017E+00 | 1.009E-02 |
| Nb-91m | 410911 | 1.2634E-01 | 7.489E-04 |
| Nb-92m | 410921 | 9.7526E-01 | 5.781E-03 |
| Nb-94 | 410940 | 1.7599E+00 | 1.043E-02 |
| Nb-95 | 410950 | 8.0900E-01 | 4.796E-03 |
| Nb-96 | 410960 | 2.7140E+00 | 1.609E-02 |
| Nb-95m | 410951 | 2.4933E-01 | 1.478E-03 |
| Nb-97 | 410970 | 1.1330E+00 | 6.716E-03 |
| Nb-97m | 410971 | 7.4336E-01 | 4.407E-03 |
| Mo-93 | 420930 | 1.6143E-02 | 9.570E-05 |
| Mo-93m | 420931 | 2.4158E+00 | 1.432E-02 |
| Mo-99 | 420990 | 5.4317E-01 | 3.220E-03 |
| Mo-101 | 421010 | 1.9735E+00 | 1.170E-02 |
| Tc-99 | 430990 | 5.5202E-02 | 3.272E-04 |
| Tc-99m | 430991 | 1.4222E-01 | 8.431E-04 |

| Isotope | ORIGEN Radionuclide ID | Q-Value (MeV/Decay) | Decay Heat (W/Ci) |
|---------|------------------------|---------------------|-------------------|
| Lu-176m | 711761 | 4.9032E-01 | 2.907E-03 |
| Lu-177 | 711770 | 1.8133E-01 | 1.075E-03 |
| Lu-177m | 711771 | 2.4764E-01 | 1.468E-03 |
| Yb-175 | 701750 | 2.0070E-01 | 1.190E-03 |
| Yb-177 | 701770 | 6.2579E-01 | 3.710E-03 |
| Ta-180 | 731800 | 1.0251E-01 | 6.077E-04 |
| Ta-182 | 731820 | 1.5156E+00 | 8.985E-03 |
| Ta-183 | 731830 | 6.3433E-01 | 3.760E-03 |
| W-181 | 741810 | 5.1849E-02 | 3.074E-04 |
| W-183m | 741831 | 2.9876E-01 | 1.771E-03 |
| W-185 | 741850 | 1.2690E-01 | 7.523E-04 |
| Re-186 | 751860 | 3.5696E-01 | 2.116E-03 |
| Np-237 | 932370 | 4.9445E+00 | 2.931E-02 |
| Pu-238 | 942380 | 5.5899E+00 | 3.314E-02 |
| Pu-239 | 942390 | 5.2433E+00 | 3.108E-02 |
| Pu-240 | 942400 | 5.2522E+00 | 3.114E-02 |
| Pu-241 | 942410 | 5.3555E-03 | 3.175E-05 |
| Am-241 | 952410 | 5.6280E+00 | 3.336E-02 |
| Cm-242 | 962420 | 6.2153E+00 | 3.684E-02 |
| Cm-243 | 962430 | 6.1779E+00 | 3.662E-02 |
| Cm-244 | 962440 | 5.9011E+00 | 3.498E-02 |

Notes: ¹ Combined decay heat for Cs-137 and Ba-137m

² Decay heat calculated using summed Q-values from Zr-95 and Nb-95.

5.5.5. Irradiated Fuel Loading Table

In order to demonstrate compliance with the 10 CFR 71 (Reference 5-1) regulatory dose rate limits as well as the thermal and criticality limits of the cask, the Irradiated Fuel Loading Table must be filled out for every shipment of irradiated fuel in the Model 2000 cask. An example dose rate calculation for a hypothetical shipment consists of three irradiated fuel rods. The relevant information for each of the example rods is presented in Table 5.5-31.

Table 5.5-31. Hypothetical Irradiated Fuel Rod Shipment Information

| Rod # | Active Length (cm) | Segments (#) | Fuel Rod Radius (cm) | Total Mass (gU) | Minimum Initial Enrichment ³ (wt% U-235) | Total Mass (gU235) | Maximum Burnup ³ (GWd/MTU) |
|-------|--------------------|--------------|----------------------|----------------------|-----------------------------------------------------|----------------------|---------------------------------------|
| 1 | 381 | 10 | 0.438 | 2218.23 ¹ | 3.1 | 68.7651 ² | 46 |
| 2 | 381 | 13 | 0.438 | 2218.23 ¹ | 2.6 | 57.6740 ² | 39 |
| 3 | 381 | 10 | 0.438 | 2218.23 ¹ | 4.2 | 93.1657 ² | 58 |

Notes: ¹ Based on 10.96 g/cm³ UO₂ density and approximation of mU/mUO₂ = 238/(238+2×16)

² Calculated based on initial enrichment

³ Uniform initial enrichment and burnup assumed for each of the hypothetical rods

An example dose rate calculation is completed for the NCT side surface location in Table 5.5-32. The total initial mass (in gU235) is from Table 5.5-31 and the side surface dose rate (in mrem/hr/gU235) for the defined example enrichment and burnup is taken from Table 5.4-5.

The total dose rate from each rod is calculated by multiplying the initial mass of U-235 by the dose rate per gU235.

Table 5.5-32. Irradiated Fuel NCT Side Surface Dose Rate Calculation

| Rod # | m (gU235) | $\dot{D}R$ (mrem/hr/gU235) | DR (mrem/hr) |
|-------|--------------|-------------------------------|-----------------|
| 1 | 68.7651 | 3.318E-01 | 22.816 |
| 2 | 57.6740 | 2.518E-01 | 14.522 |
| 3 | 93.1657 | 3.022E-01 | 28.155 |

By summing the total dose rate contribution from each rod, the total dose rate at the NCT side surface locations is calculated to be 65.5 mrem/hr. By repeating this calculation for each regulatory dose rate location, it can be demonstrated that this hypothetical group of irradiated fuel rods is acceptable for shipment, as the calculated dose rates do not exceed the regulatory limits. Using the hypothetical group of irradiated fuel rods in Table 5.5-31, an example of the complete loading table filled out for these contents is provided in Table 5.5-33. For this loading table example, it is assumed that each of the rods is segmented to even whole lengths, with the mass of the rod being divided evenly as well. It is demonstrated in this table that the criticality, dose rate, and Configuration 2 thermal limit is not exceeded, and the hypothetical fuel rods are acceptable for shipment.

Table 5.5-33. Hypothetical Irradiated Fuel Rod Shipment Irradiated Fuel Loading Table

| Segment # | Segment Length (inches) | Initial Enrichment (wt% U-235) | Burnup (GWd/MTU) | Mass U-235 (g) | Decay Heat (W) | NCT | | | | | HAC | | |
|---------------|-------------------------|--------------------------------|------------------|----------------|----------------|--------------------|-------|--------|------------------|-------------------|------------------|-------|--------|
| | | | | | | DR _{surf} | | | DR _{2m} | DR _{cab} | DR _{1m} | | |
| | | | | | | Top | Side | Bottom | | | Top | Side | Bottom |
| 1 | 15 | 3.0 ≤ e < 3.5 | 40 < b ≤ 50 | 6.877 | 4.868 | 0.381 | 2.282 | 1.187 | 0.057 | 0.010 | 0.362 | 0.431 | 0.387 |
| 2 | 15 | 3.0 ≤ e < 3.5 | 40 < b ≤ 50 | 6.877 | 4.868 | 0.381 | 2.282 | 1.187 | 0.057 | 0.010 | 0.362 | 0.431 | 0.387 |
| 3 | 15 | 3.0 ≤ e < 3.5 | 40 < b ≤ 50 | 6.877 | 4.868 | 0.381 | 2.282 | 1.187 | 0.057 | 0.010 | 0.362 | 0.431 | 0.387 |
| 4 | 15 | 3.0 ≤ e < 3.5 | 40 < b ≤ 50 | 6.877 | 4.868 | 0.381 | 2.282 | 1.187 | 0.057 | 0.010 | 0.362 | 0.431 | 0.387 |
| 5 | 15 | 3.0 ≤ e < 3.5 | 40 < b ≤ 50 | 6.877 | 4.868 | 0.381 | 2.282 | 1.187 | 0.057 | 0.010 | 0.362 | 0.431 | 0.387 |
| 6 | 15 | 3.0 ≤ e < 3.5 | 40 < b ≤ 50 | 6.877 | 4.868 | 0.381 | 2.282 | 1.187 | 0.057 | 0.010 | 0.362 | 0.431 | 0.387 |
| 7 | 15 | 3.0 ≤ e < 3.5 | 40 < b ≤ 50 | 6.877 | 4.868 | 0.381 | 2.282 | 1.187 | 0.057 | 0.010 | 0.362 | 0.431 | 0.387 |
| 8 | 15 | 3.0 ≤ e < 3.5 | 40 < b ≤ 50 | 6.877 | 4.868 | 0.381 | 2.282 | 1.187 | 0.057 | 0.010 | 0.362 | 0.431 | 0.387 |
| 9 | 15 | 3.0 ≤ e < 3.5 | 40 < b ≤ 50 | 6.877 | 4.868 | 0.381 | 2.282 | 1.187 | 0.057 | 0.010 | 0.362 | 0.431 | 0.387 |
| 10 | 15 | 3.0 ≤ e < 3.5 | 40 < b ≤ 50 | 6.877 | 4.868 | 0.381 | 2.282 | 1.187 | 0.057 | 0.010 | 0.362 | 0.431 | 0.387 |
| 11 | 11 | 2.5 ≤ e < 3.0 | 30 < b ≤ 40 | 4.229 | 3.383 | 0.179 | 1.065 | 0.551 | 0.026 | 0.005 | 0.178 | 0.229 | 0.185 |
| 12 | 11 | 2.5 ≤ e < 3.0 | 30 < b ≤ 40 | 4.229 | 3.383 | 0.179 | 1.065 | 0.551 | 0.026 | 0.005 | 0.178 | 0.229 | 0.185 |
| 13 | 11 | 2.5 ≤ e < 3.0 | 30 < b ≤ 40 | 4.229 | 3.383 | 0.179 | 1.065 | 0.551 | 0.026 | 0.005 | 0.178 | 0.229 | 0.185 |
| 14 | 11 | 2.5 ≤ e < 3.0 | 30 < b ≤ 40 | 4.229 | 3.383 | 0.179 | 1.065 | 0.551 | 0.026 | 0.005 | 0.178 | 0.229 | 0.185 |
| 15 | 11 | 2.5 ≤ e < 3.0 | 30 < b ≤ 40 | 4.229 | 3.383 | 0.179 | 1.065 | 0.551 | 0.026 | 0.005 | 0.178 | 0.229 | 0.185 |
| 16 | 11 | 2.5 ≤ e < 3.0 | 30 < b ≤ 40 | 4.229 | 3.383 | 0.179 | 1.065 | 0.551 | 0.026 | 0.005 | 0.178 | 0.229 | 0.185 |
| 17 | 12 | 2.5 ≤ e < 3.0 | 30 < b ≤ 40 | 4.614 | 3.691 | 0.195 | 1.162 | 0.602 | 0.029 | 0.005 | 0.195 | 0.249 | 0.202 |
| 18 | 12 | 2.5 ≤ e < 3.0 | 30 < b ≤ 40 | 4.614 | 3.691 | 0.195 | 1.162 | 0.602 | 0.029 | 0.005 | 0.195 | 0.249 | 0.202 |
| 19 | 12 | 2.5 ≤ e < 3.0 | 30 < b ≤ 40 | 4.614 | 3.691 | 0.195 | 1.162 | 0.602 | 0.029 | 0.005 | 0.195 | 0.249 | 0.202 |
| 20 | 12 | 2.5 ≤ e < 3.0 | 30 < b ≤ 40 | 4.614 | 3.691 | 0.195 | 1.162 | 0.602 | 0.029 | 0.005 | 0.195 | 0.249 | 0.202 |
| 21 | 12 | 2.5 ≤ e < 3.0 | 30 < b ≤ 40 | 4.614 | 3.691 | 0.195 | 1.162 | 0.602 | 0.029 | 0.005 | 0.195 | 0.249 | 0.202 |
| 22 | 12 | 2.5 ≤ e < 3.0 | 30 < b ≤ 40 | 4.614 | 3.691 | 0.195 | 1.162 | 0.602 | 0.029 | 0.005 | 0.195 | 0.249 | 0.202 |
| 23 | 12 | 2.5 ≤ e < 3.0 | 30 < b ≤ 40 | 4.614 | 3.691 | 0.195 | 1.162 | 0.602 | 0.029 | 0.005 | 0.195 | 0.249 | 0.202 |
| 24 | 15 | 4.0 ≤ e < 4.5 | 50 < b ≤ 60 | 9.317 | 5.161 | 0.470 | 2.816 | 1.466 | 0.070 | 0.013 | 0.440 | 0.511 | 0.475 |
| 25 | 15 | 4.0 ≤ e < 4.5 | 50 < b ≤ 60 | 9.317 | 5.161 | 0.470 | 2.816 | 1.466 | 0.070 | 0.013 | 0.440 | 0.511 | 0.475 |
| 26 | 15 | 4.0 ≤ e < 4.5 | 50 < b ≤ 60 | 9.317 | 5.161 | 0.470 | 2.816 | 1.466 | 0.070 | 0.013 | 0.440 | 0.511 | 0.475 |
| 27 | 15 | 4.0 ≤ e < 4.5 | 50 < b ≤ 60 | 9.317 | 5.161 | 0.470 | 2.816 | 1.466 | 0.070 | 0.013 | 0.440 | 0.511 | 0.475 |
| 28 | 15 | 4.0 ≤ e < 4.5 | 50 < b ≤ 60 | 9.317 | 5.161 | 0.470 | 2.816 | 1.466 | 0.070 | 0.013 | 0.440 | 0.511 | 0.475 |
| 29 | 15 | 4.0 ≤ e < 4.5 | 50 < b ≤ 60 | 9.317 | 5.161 | 0.470 | 2.816 | 1.466 | 0.070 | 0.013 | 0.440 | 0.511 | 0.475 |
| 30 | 15 | 4.0 ≤ e < 4.5 | 50 < b ≤ 60 | 9.317 | 5.161 | 0.470 | 2.816 | 1.466 | 0.070 | 0.013 | 0.440 | 0.511 | 0.475 |
| 31 | 15 | 4.0 ≤ e < 4.5 | 50 < b ≤ 60 | 9.317 | 5.161 | 0.470 | 2.816 | 1.466 | 0.070 | 0.013 | 0.440 | 0.511 | 0.475 |
| 32 | 15 | 4.0 ≤ e < 4.5 | 50 < b ≤ 60 | 9.317 | 5.161 | 0.470 | 2.816 | 1.466 | 0.070 | 0.013 | 0.440 | 0.511 | 0.475 |
| 33 | 15 | 4.0 ≤ e < 4.5 | 50 < b ≤ 60 | 9.317 | 5.161 | 0.470 | 2.816 | 1.466 | 0.070 | 0.013 | 0.440 | 0.511 | 0.475 |
| Min? | 11 | | Total | 219.6 | 146.4 | 10.9 | 65.5 | 34.0 | 1.6 | 0.3 | 10.4 | 12.5 | 11.1 |
| Limit | 10 | | Limit | 1750 | 3000 | 180 | 180 | 180 | 9 | 1.8 | 900 | 900 | 900 |
| Criteria Met? | YES | | Criteria Met? | YES | YES | YES | YES | YES | YES | YES | YES | YES | YES |

For every burnup-enrichment pairing, the total allowable mass of U-235 is restricted by either the 1750 gU235 criticality limit, the mass of U-235 corresponding to Configuration 2, thermal limit of 3000 W, or the maximum mass of U-235 corresponding to a dose rate of 180 mrem/hr at the NCT side surface dose location. Tables 5.5-34 and 5.5-35 list the maximum mass of U-235 for each burnup-enrichment pairing corresponding to the NCT side surface dose rate limit and the Configuration 2 3000 W thermal limit, respectively. Table 5.5-36 provides the overall

maximum allowable mass of U-235 for each burnup-enrichment pairing in the Model 2000 cask, by listing the minimum value for each pairing between those in Table 5.5-34, Table 5.5-35, and the 1750 gU235 criticality limit from Section 6.2.

Table 5.5-34. Maximum Allowable Mass of U-235 Based on NCT Side Surface Dose Rate

| Enrichment (wt% U-235) | Burnup (GWd/MTU) | | | | | | |
|---------------------------|------------------|-------------|-------------|-------------|-------------|-------------|-------------|
| | 0 < b ≤ 10 | 10 < b ≤ 20 | 20 < b ≤ 30 | 30 < b ≤ 40 | 40 < b ≤ 50 | 50 < b ≤ 60 | 60 < b ≤ 72 |
| 0.71 ≤ e < 1.5 | 1360.62 | 235.62 | - | - | - | - | - |
| 1.5 ≤ e < 2.0 | 5888.81 | 1750.42 | 591.29 | 267.71 | 146.04 | 86.72 | 46.75 |
| 2.0 ≤ e < 2.5 | 8505.76 | 3006.57 | 1036.12 | 453.23 | 240.06 | 141.12 | 76.66 |
| 2.5 ≤ e < 3.0 | 11167.19 | 4588.99 | 1660.85 | 714.83 | 369.05 | 214.27 | 117.07 |
| 3.0 ≤ e < 3.5 | 13824.12 | 6431.58 | 2484.05 | 1069.68 | 542.45 | 310.83 | 170.35 |
| 3.5 ≤ e < 4.0 | 16463.84 | 8466.48 | 3519.65 | 1534.72 | 770.15 | 436.10 | 239.12 |
| 4.0 ≤ e < 4.5 | 19080.96 | 10631.13 | 4752.88 | 2119.63 | 1061.08 | 595.61 | 326.20 |
| 4.5 ≤ e < 5.0 | 21671.94 | 12874.99 | 6155.86 | 2829.33 | 1422.72 | 794.38 | 434.33 |
| 5.0 ≤ e < 5.5 | 24250.29 | 15172.87 | 7711.82 | 3667.29 | 1861.32 | 1037.68 | 566.59 |
| 5.5 ≤ e < 6.0 | 26813.63 | 17503.72 | 9402.43 | 4633.89 | 2383.09 | 1330.62 | 726.14 |

Table 5.5-35. Maximum Allowable Mass of U-235 Based on Configuration 2 Thermal Limit

| Enrichment (wt% U-235) | Burnup (GWd/MTU) | | | | | | |
|---------------------------|------------------|-------------|-------------|-------------|-------------|-------------|-------------|
| | 0 < b ≤ 10 | 10 < b ≤ 20 | 20 < b ≤ 30 | 30 < b ≤ 40 | 40 < b ≤ 50 | 50 < b ≤ 60 | 60 < b ≤ 72 |
| 0.71 ≤ e < 1.5 | 1396.77 | 1089.89 | - | - | - | - | - |
| 1.5 ≤ e < 2.0 | 3481.13 | 2758.52 | 2420.55 | 2212.91 | 2071.47 | 1969.65 | 1872.33 |
| 2.0 ≤ e < 2.5 | 4608.31 | 3682.80 | 3250.67 | 2976.81 | 2782.57 | 2638.75 | 2501.48 |
| 2.5 ≤ e < 3.0 | 5727.90 | 4604.38 | 4084.38 | 3750.20 | 3505.24 | 3317.75 | 3136.81 |
| 3.0 ≤ e < 3.5 | 6842.55 | 5523.95 | 4919.59 | 4529.82 | 4237.91 | 4007.49 | 3780.60 |
| 3.5 ≤ e < 4.0 | 7953.85 | 6442.11 | 5755.90 | 5313.81 | 4978.35 | 4707.18 | 4434.09 |
| 4.0 ≤ e < 4.5 | 9062.76 | 7359.54 | 6592.65 | 6100.43 | 5724.46 | 5415.54 | 5097.92 |
| 4.5 ≤ e < 5.0 | 10170.15 | 8276.87 | 7429.38 | 6888.57 | 6474.74 | 6130.92 | 5771.53 |
| 5.0 ≤ e < 5.5 | 11276.42 | 9194.11 | 8266.22 | 7677.82 | 7227.98 | 6851.66 | 6453.75 |
| 5.5 ≤ e < 6.0 | 12382.11 | 10111.29 | 9103.32 | 8468.09 | 7983.59 | 7576.60 | 7143.11 |

Table 5.5-36. Overall Maximum Allowable Mass of U-235 Based on All Cask Limits

| Enrichment (wt% U-235) | Burnup (GWd/MTU) | | | | | | |
|---------------------------|------------------|-------------|-------------|-------------|-------------|-------------|-------------|
| | 0 < b ≤ 10 | 10 < b ≤ 20 | 20 < b ≤ 30 | 30 < b ≤ 40 | 40 < b ≤ 50 | 50 < b ≤ 60 | 60 < b ≤ 72 |
| 0.71 ≤ e < 1.5 | 1360.62 | 235.620 | - | - | - | - | - |
| 1.5 ≤ e < 2.0 | 1750.00 | 1750.00 | 591.290 | 267.710 | 146.040 | 86.7200 | 46.7500 |
| 2.0 ≤ e < 2.5 | 1750.00 | 1750.00 | 1036.12 | 453.230 | 240.060 | 141.120 | 76.6600 |
| 2.5 ≤ e < 3.0 | 1750.00 | 1750.00 | 1660.85 | 714.830 | 369.050 | 214.270 | 117.070 |
| 3.0 ≤ e < 3.5 | 1750.00 | 1750.00 | 1750.00 | 1069.68 | 542.450 | 310.830 | 170.350 |
| 3.5 ≤ e < 4.0 | 1750.00 | 1750.00 | 1750.00 | 1534.72 | 770.150 | 436.100 | 239.120 |
| 4.0 ≤ e < 4.5 | 1750.00 | 1750.00 | 1750.00 | 1750.00 | 1061.08 | 595.610 | 326.200 |
| 4.5 ≤ e < 5.0 | 1750.00 | 1750.00 | 1750.00 | 1750.00 | 1422.72 | 794.380 | 434.330 |
| 5.0 ≤ e < 5.5 | 1750.00 | 1750.00 | 1750.00 | 1750.00 | 1750.00 | 1037.68 | 566.590 |
| 5.5 ≤ e < 6.0 | 1750.00 | 1750.00 | 1750.00 | 1750.00 | 1750.00 | 1330.62 | 726.140 |

Notes: ¹ Cells highlighted in green are limited by the NCT side surface dose rate limit
² Cells highlighted in blue are limited by the criticality mass limit

5.5.6. Irradiated Hardware and Byproduct Loading Table

In order to demonstrate compliance with the 10 CFR 71 (Reference 5-1) regulatory dose rate limits and the thermal limit of the cask, the Irradiated Hardware and Byproduct Loading Table must be filled out for every shipment of irradiated hardware or byproducts in the Model 2000 cask. The use of this loading table is simple: for each of the radionuclides included in a shipment, enter the radionuclide into the table, enter the activity of the radionuclide, then calculate the decay heat and dose rate contribution at each regulatory location based on the dose rate per curie and decay heat values presented in Tables 5.4-13, 5.4-14 and 5.5-30.

Tables 5.5-37 through 5.5-39 provide radionuclide inventories for three hypothetical shipments of irradiated hardware, zirconium-95, and hafnium poison rods. The irradiated hardware radionuclide inventory presented in Table 5.5-37 lists the sample activities and percent-activity of the total content for a list of radionuclides based on a previous shipment of a piece of irradiated 304 stainless steel in the Model 2000 cask with all of the radionuclide activities scaled up to higher activities. The zirconium and hafnium poison rod radionuclide inventories in Tables 5.5-38 and 5.5-39 are hypothetical radionuclide inventories, included only to provide additional examples.

Table 5.5-37. Example Irradiated SS304 Radionuclide Inventory

| Nuclide | Ci/sample | % Activity | Total Activity (Ci) |
|---------|-----------|------------|---------------------|
| H-3 | 6.75E-06 | 0.00% | 4.605E-05 |
| P-32 | 3.49E-04 | 0.00% | 2.381E-03 |
| S-35 | 8.26E-04 | 0.00% | 5.635E-03 |
| Cr-51 | 3.73E+00 | 2.12% | 2.545E+01 |
| Mn-54 | 5.60E+00 | 3.18% | 3.821E+01 |
| Fe-55 | 5.69E+01 | 32.35% | 3.882E+02 |
| Fe-59 | 3.32E-01 | 0.19% | 2.265E+00 |
| Co-58 | 2.85E+00 | 1.62% | 1.944E+01 |
| Co-60 | 1.01E+02 | 57.42% | 6.891E+02 |
| Ni-59 | 4.14E-02 | 0.02% | 2.825E-01 |
| Ni-63 | 5.42E+00 | 3.08% | 3.698E+01 |
| Zn-65 | 1.06E-02 | 0.01% | 7.232E-02 |
| Nb-93m | 3.25E-04 | 0.00% | 2.217E-03 |
| Mo-99 | 6.13E-14 | 0.00% | 4.182E-13 |
| Tc-99m | 5.94E-14 | 0.00% | 4.053E-13 |
| Total | 175.89 | 100.00% | 1200 |

Table 5.5-38. Example Zr-95 Radionuclide Inventory

| Nuclide | Total Activity (Ci) |
|---------|---------------------|
| Zr-95 | 80,000 |

Table 5.5-39. Example Hf Poison Rod Radionuclide Inventory

| Nuclide | % Activity | Total Activity (Ci) |
|---------|------------|---------------------|
| Hf-175 | 4.21% | 21,300.0 |
| Hf-181 | 90.09% | 456,000 |
| Ta-182 | 5.70% | 28,844.0 |
| Total | 100.00% | 506,144 |

Tables 5.5-40 through 5.5-42 show the respective Irradiated Hardware and Byproduct Loading Tables for each of the hypothetical shipments outlined in Tables 5.5-37 through 5.5-39. These tables show that all three hypothetical shipments of irradiated hardware and byproduct contents comply with all dose rate and thermal criteria and would be acceptable for shipment. It is assumed that all three hypothetical shipments are made using Configuration 2, with a 3000 W decay heat limit.

Table 5.5-40. Example SS304 Irradiated Hardware and Byproduct Loading Table

| Radionuclide | Activity (Ci) | Decay Heat (W) | NCT | | | | | HAC | | |
|----------------------|---------------|----------------|--------------------|----------|----------|------------------|-------------------|------------------|----------|----------|
| | | | DR _{surf} | | | DR _{2m} | DR _{cab} | DR _{1m} | | |
| | | | Top | Side | Bottom | | | Top | Side | Bottom |
| Cr-51 | 25.40 | 5.53E-03 | 1.01E-13 | 4.19E-19 | 1.41E-18 | 5.41E-21 | 8.93E-22 | 3.23E-12 | 1.28E-18 | 2.41E-17 |
| Mn-54 | 38.20 | 1.90E-01 | 8.77E-06 | 3.77E-04 | 1.63E-05 | 4.26E-06 | 7.27E-07 | 1.55E-05 | 7.82E-05 | 1.27E-05 |
| Fe-55 | 388.2 | 1.34E-02 | 0.00E+00 | 0.00E+00 | 0.00E+00 | 0.00E+00 | 0.00E+00 | 0.00E+00 | 0.00E+00 | 0.00E+00 |
| Fe-59 | 2.300 | 1.75E-02 | 2.81E-04 | 6.56E-03 | 4.20E-04 | 8.27E-05 | 1.43E-05 | 4.09E-04 | 1.22E-03 | 2.43E-04 |
| Co-58 | 19.40 | 1.16E-01 | 2.64E-04 | 4.75E-03 | 4.22E-04 | 6.56E-05 | 1.16E-05 | 3.49E-04 | 8.67E-04 | 2.25E-04 |
| Co-60 | 689.1 | 1.06E+01 | 2.88E-01 | 6.50E+00 | 4.30E-01 | 8.34E-02 | 1.43E-02 | 4.14E-01 | 1.20E+00 | 2.45E-01 |
| Ni-63 | 37.00 | 3.82E-03 | 0.00E+00 | 0.00E+00 | 0.00E+00 | 0.00E+00 | 0.00E+00 | 0.00E+00 | 0.00E+00 | 0.00E+00 |
| Total | - | 10.97 | 0.289 | 6.514 | 0.431 | 0.084 | 0.014 | 0.415 | 1.203 | 0.245 |
| Limit | - | 3000 | 180 | 180 | 180 | 9 | 1.8 | 900 | 900 | 900 |
| Criteria Met? | - | YES | YES | YES | YES | YES | YES | YES | YES | YES |

Table 5.5-41. Example Zr-95 Irradiated Hardware and Byproduct Loading Table

| Radionuclide | Activity (Ci) | Decay Heat (W) | NCT | | | | | HAC | | |
|----------------------|---------------|----------------|--------------------|----------|----------|------------------|-------------------|------------------|----------|----------|
| | | | DR _{surf} | | | DR _{2m} | DR _{cab} | DR _{1m} | | |
| | | | Top | Side | Bottom | | | Top | Side | Bottom |
| Zr-95 | 80,000 | 787.0 | 4.01E-03 | 2.00E-01 | 9.45E-03 | 2.25E-03 | 3.83E-04 | 7.62E-03 | 4.37E-02 | 8.31E-03 |
| Total | - | 787.0 | 4.01E-03 | 2.00E-01 | 9.45E-03 | 2.25E-03 | 3.83E-04 | 7.62E-03 | 4.37E-02 | 8.31E-03 |
| Limit | - | 3000 | 180 | 180 | 180 | 9 | 1.8 | 900 | 900 | 900 |
| Criteria Met? | - | YES | YES | YES | YES | YES | YES | YES | YES | YES |

Table 5.5-42. Example Hf Poison Rod Irradiated Hardware and Byproduct Loading Table

| Radionuclide | Activity (Ci) | Decay Heat (W) | NCT | | | | | HAC | | |
|----------------------|---------------|----------------|--------------------|----------|----------|------------------|-------------------|------------------|----------|----------|
| | | | DR _{surf} | | | DR _{2m} | DR _{cab} | DR _{1m} | | |
| | | | Top | Side | Bottom | | | Top | Side | Bottom |
| Hf-175 | 21,300.0 | 50.200 | 3.46E-09 | 4.04E-11 | 7.40E-12 | 2.46E-13 | 3.98E-14 | 3.53E-08 | 1.01E-11 | 1.63E-11 |
| Hf-181 | 456,000 | 1973.6 | 5.91E-06 | 6.36E-06 | 1.03E-06 | 8.26E-08 | 1.42E-08 | 4.49E-05 | 2.06E-06 | 1.52E-06 |
| Ta-182 | 28,844.0 | 259.10 | 3.88E+00 | 9.44E+01 | 5.76E+00 | 1.18E+00 | 2.02E-01 | 5.70E+00 | 1.77E+01 | 3.39E+00 |
| Total | - | 2282.9 | 3.88 | 94.39 | 5.76 | 1.18 | 0.20 | 5.70 | 17.70 | 3.39 |
| Limit | - | 3000.0 | 180 | 180 | 180 | 9 | 1.8 | 900 | 900 | 900 |
| Criteria Met? | - | YES | YES | YES | YES | YES | YES | YES | YES | YES |

5.5.7. Combined Content Shipments

There is the possibility of a shipment that includes multiple content types. To demonstrate compliance with all regulatory and cask requirements, the total thermal power and dose rate contributions from each content type must be determined. Using the procedure in Section 7.5.4, compliance is demonstrated for shipments of multiple content types. For illustration purposes, a shipment of mixed content that combines both irradiated fuel and hardware and byproduct is used as an example. Both the Irradiated Fuel Loading Table and the Irradiated Hardware and Byproduct Loading Table must be filled out for the respective radioactive contents. Then using the Combined Contents Loading Table in Section 7.5.4, the dose rate and thermal power contributions for each are summed, calculating the total thermal power and external dose rates for the shipment.

An example of this process can be demonstrated by using the hypothetical shipment of fuel rods introduced in Section 5.5.5 (see Table 5.5-31) and the example irradiated SS304 radionuclide inventory in Section 5.5.6 (see Table 5.5-37). For this hypothetical shipment of irradiated fuel and hardware, the Irradiated Fuel Loading Table is filled out (see Table 5.5-33) and the Irradiated Hardware and Byproduct Loading Table (see Table 5.5-40) are filled out for the respective contents. Then by following the procedure in Section 7.5.4, the Combined Contents Loading Table is filled out for this shipment, as shown in Table 5.5-43. Based on the total thermal power and external dose rates calculated in Table 5.5-43, this hypothetical shipment of irradiated fuel and hardware is acceptable for shipment in the Model 2000 cask.

Table 5.5-43. Example Combined Contents Loading Table

| Content | Thermal Power (W) | NCT | | | | | HAC | | |
|------------------------|-------------------|--------------------|-------|--------|------------------|-------------------|------------------|-------|--------|
| | | DR _{surf} | | | DR _{2m} | DR _{cab} | DR _{1m} | | |
| | | Top | Side | Bottom | | | Top | Side | Bottom |
| Fuel | 146.4 | 10.9 | 65.5 | 34.0 | 1.6 | 0.3 | 10.4 | 12.5 | 11.1 |
| Hardware / Byproduct | 10.97 | 0.289 | 6.514 | 0.431 | 0.084 | 0.014 | 0.415 | 1.203 | 0.245 |
| Cobalt-60 Isotope Rods | - | - | - | - | - | - | - | - | - |
| Total | 157.37 | 11.19 | 72.01 | 34.43 | 1.68 | 0.31 | 10.82 | 13.70 | 11.35 |
| Limit | 3000 | 180 | 180 | 180 | 9 | 1.8 | 900 | 900 | 900 |
| Criteria Met? | YES | YES | YES | YES | YES | YES | YES | YES | YES |

For other combinations of contents, the Loading Table of each content type must be completed and the total contribution of the contents to the thermal power and dose rates must be confirmed to be below the limit. Additionally, the requirements for each content type that are defined in Section 1.2.2.3 must be met.

5.6 References

- 5-1 U.S. Code of Federal Regulations, Title 10 Part 71, "Packaging and Transport of Radioactive Material," April 2016.
- 5-2 Oak Ridge National Lab, "SCALE: A Comprehensive Modeling and Simulation Suite for Nuclear Safety Analysis and Design, ORNL/TM-2005/39, Version 6, Vols. I-III," ORNL/TM-2005/39, Version 6.1, June 2011.
- 5-3 L. C. Leal et al., "ARP: Automatic Rapid Process for the Generation of Problem-Dependent SAS2H/ORIGEN-S Cross-Section Libraries," ORNL/TM-13584, April 1998.
- 5-4 American Society for Testing and Materials, "Standard Specification for General Requirements for Flat-Rolled Stainless and Heat-Resisting Steel Plate, Sheet, and Strip," ASTM A480, 2016.
- 5-5 R.J. McConn et al., "Compendium of Material Composition Data for Radiation Transport Modeling," PNNL-15870, Revision 1, March 2011.
- 5-6 T. Goorley, et al., "Initial MCNP Release Overview - MCNP6 Version 1.0," Los Alamos National Laboratory, LA-UR-13-22934, April 2013.
- 5-7 J. Conlin et al., "Listing of Available ACE Data Tables," Los Alamos National Laboratory, LA-UR-13-21822, Revision 4, June 2014.
- 5-8 U.S. Nuclear Regulatory Commission, "Standard Review Plan for Transportation Packages for Radioactive Material," NUREG-1609, March 1999.
- 5-9 ANS 6.1.1 Working Group, M. E. Battat (Chairman), "American National Standard Neutron and Gamma-Ray Flux-to-Dose-Rate Factors," American Nuclear Society, ANSI/ANS-6.1.1-1977, March 1977.
- 5-10 S.M. Bowman et al., "Recommendations on Fuel Parameters for Standard Technical Specifications for Spent Fuel Storage Casks," NUREG/CR-6716, February 2001.

6 CRITICALITY EVALUATION

6.1 Description of Criticality Design

6.1.1. Design Features

This section describes the design features of the Model 2000 Transport Package that are important for maintaining criticality safety.

The Model 2000 cask is a cylindrical lead lined cask used for transporting Type B quantities of radioactive materials and solid fissile materials. For the fissile contents considered in this analysis, the High Performance Insert (HPI) is required to be used along with the Model 2000 cask. The HPI consists of the insert body and two plugs for the top and bottom. Attached to the insert body is a series of [[]] in the Model 2000 cask cavity. Shoring components such as rod holders or the material basket may be present. This analysis is generic by design to allow for the simple loading flexibility of the desired contents into the HPI, then loading of the HPI into the Model 2000 cask. Figure 1.2.3-1 shows the package configuration. The HPI and material basket are described in Section 1.2.2.1 and Section 1.2.2.2, respectively.

The confinement system consists of the Model 2000 cask, HPI, and other components which ensure that the fuel rod content is shipped upright (e.g., material basket and the fuel rod tube).

The Model 2000 cask and HPI retain the contents within a fixed geometry relative to other packages in an array. Fuel rod rearrangement is limited by the HPI cavity. The fuel pellets are confined within the fuel rod tube or other shoring device; however the cladding material of the fuel rod is not credited in the criticality analysis. Shoring components such as rod holders or the material basket may provide additional confinement but are not credited in the criticality analyses.

Transitional states during transport, including variations of flooding, package deformation, and content configuration, affect the normal and hypothetical accident conditions of transport. Packaging structural materials, such as stainless steel (SS), provides neutron absorption. Shielding design features, such as the depleted uranium (DU) shield of the HPI and lead shield of the Model 2000 cask, provide increased reflection and moderation within the package. Additional neutron moderation is provided from external sources consistent with the normal or accident transport conditions, such as full moderator reflector modeled around the array configuration.

6.1.2. Summary Table of Criticality Evaluation

The demonstration of criticality safety meeting 10 CFR 71 (Reference 6-1) provides assurance of the safe transport of the fissile contents with the Model 2000 and the HPI under normal conditions of transport (NCT) and hypothetical accident transport conditions (HAC).

Contents include irradiated fuel rod elements or solid fissile material (i.e., equivalent mass of special nuclear material (SNM)). The configuration of the contents and packaging demonstrate the most reactive configuration for the package.

A summary of most limiting cases is provided in Table 6.1.2-1 for fuel rod content and Table 6.1.2-2 for fissile, free form content. All limiting cases meet the Upper Subcritical Limit (USL), as defined in Section 6.3.4. Fissile mass limits are defined in the summary tables below. The fissile mass limit for fuel rods defined by the criticality safety analyses provide an input to the Irradiated Fuel Rod Loading Table as further discussed in Section 7.5.1. For the fuel rod content, data trends of results in Section 6.4 through Section 6.6 shows that as the fuel rod outer radius increases the overall system reactivity decreases.

Fissile material evaluations and limitations are based on initial, unirradiated fuel, without crediting fuel burnup. Fissile contents are described further in Section 6.2.

The U-235 equivalent mass for SNM is determined by U-235 mass plus 1.63 times Pu-239 mass, plus 2.87 times Pu-241 mass, and 1.37 times U-233 mass. The contents may contain other uranium and plutonium isotopes, as the criticality evaluation conservatively analyzed 100% fissile isotope for each fissile, free form content. The Pu-239 mass limit is converted to an activity limit by multiplying by the specific activity. Per 10 CFR 71 Appendix A, Table A-1, the specific activity for Pu-239 is defined as 6.2E-02 Ci/g. Thus the Pu-239 mass limit is equivalent to an activity of 16.43 Ci. For all contents, shoring components such as rod holders or the HPI material basket may be present.

For the fuel rod content, data trends showed that as the fuel rod outer radius (OR) increases the overall system reactivity decreases, thus the fuel pellet outer radius of 0.2 cm is set as the minimum fuel pellet outer radius. If the equivalent fuel pellet radius is less than 0.2 cm, then the fissile, free form mass limit of 430 gU235 is applied. Fissile material evaluations and limitations are based on initial, unirradiated fuel, without burnup credit.

Shipment of combined contents is allowed except that SNM and irradiated fuel cannot be combined.

Table 6.1.2-1. Fuel Rod Content Summary

| Case Name | Fuel OR (cm) | Half-pitch (cm) | k_{eff} | σ | $k_{eff} \pm 2\sigma$ | Maximum k_{eff} ¹ | H/U-235 | EALF (eV) | M U-235 Limit (g) ² |
|-----------------------|--------------|-----------------|-----------|----------|-----------------------|--------------------------------|---------|-----------|--------------------------------|
| Single Package | | | | | | | | | |
| FRLSmh 1 22 | 0.2 | 0.7 | 0.92307 | 0.00021 | 0.92349 | 0.9328 | 570 | 0.31716 | 1750 |
| NCT, 5N Package Array | | | | | | | | | |
| FRLANmh 1 22 | 0.2 | 0.7 | 0.91810 | 0.00023 | 0.91856 | 0.9278 | 570 | 0.31717 | 1750 |
| HAC, 2N Package Array | | | | | | | | | |
| FRLAHmh 1 22 | 0.2 | 0.7 | 0.92350 | 0.00024 | 0.92398 | 0.9333 | 570 | 0.31681 | 1750 |

NOTES: USL is defined as 0.9387 per Section 6.3.4.

¹ Maximum k_{eff} includes the added 1% uncertainty for pitch geometric modeling –see Section 6.9.1.

² An administratively reduced fissile mass limit is defined –see Section 6.2.1 for further details.

Table 6.1.2-2. Fissile, Free Form Content Summary

| Case Name | Case | Sphere OR (cm) | k_{eff} | σ | $k_{eff} + 2\sigma$ (maximum k_{eff}) | Fissile Mass (g) | H/X | EALF (eV) |
|-------------------|----------------|----------------|-----------|----------|---------------------------------------------|------------------|------|-----------|
| U-235 | | | | | | | | |
| 601HMS12p_430btm | Single Package | [[]] | 0.93873 | 0.00024 | 0.93921 | 430 | 438 | 0.32218 |
| 601HMN115_430btm | NCT, 5N | [[]] | 0.93293 | 0.00028 | 0.93349 | 430 | 385 | 0.31077 |
| 601HMH115_430btm | HAC, 2N | [[]] | 0.93844 | 0.00024 | 0.93892 | 430 | 385 | 0.31967 |
| Pu-239 | | | | | | | | |
| PHMS12pbtm_265 | Single Package | [[]] | 0.93726 | 0.00029 | 0.93784 | 265 | 724 | 0.53326 |
| PHMN115btm_265 | NCT, 5N | [[]] | 0.92964 | 0.00028 | 0.93020 | 265 | 637 | 0.53547 |
| PHMH12pbtm_265 | HAC, 2N | [[]] | 0.93696 | 0.00028 | 0.93752 | 265 | 724 | 0.53763 |
| U-233 | | | | | | | | |
| U233HMS11_315btm | Single Package | [[]] | 0.93949 | 0.00022 | 0.93993 | 315 | 457 | 0.41625 |
| U233HMN115_315btm | NCT, 5N | [[]] | 0.93284 | 0.00026 | 0.93336 | 315 | 522 | 0.40488 |
| U233HMH11_315btm | HAC, 2N | [[]] | 0.93985 | 0.00026 | 0.94037 | 315 | 457 | 0.41720 |
| Pu-241 | | | | | | | | |
| P241HMS115btm_150 | Single Package | [[]] | 0.93188 | 0.00028 | 0.93244 | 150 | 1135 | 0.47000 |
| P241HMN115btm_150 | NCT, 5N | [[]] | 0.92676 | 0.00028 | 0.92732 | 150 | 1135 | 0.46196 |
| P241HMH115btm_150 | HAC, 2N | [[]] | 0.93170 | 0.00027 | 0.93224 | 150 | 1135 | 0.47149 |

NOTE: USL is defined as 0.9406 per Section 6.3.4.

6.1.3. Criticality Safety Index

Per 10 CFR 71.59:

(b) The criticality safety index [(CSI)] must be determined by dividing the number 50 by the value of “N” derived using the procedures specified in paragraph (a) of this section. The value of the CSI may be zero provided that an unlimited number of packages are subcritical, such that the value of “N” is effectively equal to infinity under the procedures specified in paragraph (a) of this section. Any CSI greater than zero must be rounded up to the first decimal place.

As the Model 2000 cask with HPI is shipped exclusive use, a single package defines a conveyance. Thus, the package array criticality evaluation defines the number N of packages as one. Therefore, the CSI equals 50 for the Model 2000 cask with HPI for any fissile contents.

6.2 Fissile Material Contents

The purpose of this analysis is to demonstrate that the desired contents are subcritical for the defined content mass. The criticality analysis demonstrates compliance with 10 CFR 71 of the Model 2000 Transport Package with the HPI containing irradiated fuel rod elements or fissile material, limited to solid fissile, free form material.

6.2.1. Fuel Rods

The fuel rod contents of the package are restricted to low enriched uranium oxide (UO₂) fuel. The fissile material in fuel pellets is assumed to be uranium initially enriched up to a maximum of 6.0 wt% U-235 with the remaining 94 wt% modeled solely as U-238. Any U-232, U-234, or U-236 is assumed to be U-238 because these uranium isotopes are not fissile, are present in small amounts, and have total neutron cross sections that tend to be greater than the total neutron cross section for U-238. Additionally, no pellet dishing fraction or chamfering is modeled, which conservatively increases the number of U-235 atoms. Fissile material in the fuel rod contents is only in the form of uranium oxide, and administratively limited to 1750 grams of U-235. The models use the theoretical density, 10.96 g/cm³, for uranium oxide. For the fuel rod content, sensitivity analyses showed that as the fuel rod OR increases the overall system reactivity decreases, thus the minimum fuel pellet OR of 0.2 cm is used in this analysis. Fissile material evaluations and limitations are based on initial, unirradiated fuel, without credit for burnup.

6.2.2. Fissile, Free Form Mass

The fissile, free form content is limited to solid, free form uranium or plutonium. The fissile material is modeled as a sphere, varying radius based on the amount of water present in the homogeneous mixture. Theoretical density for uranium metal and plutonium metal are analyzed to bound other forms of uranium or plutonium content, respectively. Fissile, free form content is mass limited as follows, based on the single and HAC, package array assessment of Section 6.6 and Section 6.9.4:

- 430 grams of U-235 equivalent mass of special nuclear material
- 265 grams of Pu-239 equivalent mass of special nuclear material
- 315 grams of U-233 equivalent mass of special nuclear material
- 150 grams of Pu-241 equivalent mass of special nuclear material

6.3 General Considerations

6.3.1. Model Configuration

6.3.1.1. Fissile Material Contents Model Configuration

All fissile contents must be in solid form. Theoretical metal density is conservatively evaluated for each content. Fissile material evaluations and limitation are based on initial, unirradiated fuel, without credit for burnup.

6.3.1.1.1. Fuel Rods

The fuel rod contents of the package are restricted to low enriched UO₂ fuel. The fissile material in fuel pellets is assumed to be uranium initially enriched up to a maximum of 6.0 wt% U-235 with the remaining 94 wt% modeled solely as U-238. See Section 6.3.2 for material properties.

The fuel rod is modeled as a long cylinder with an axial length of [[]] cm, which is near equivalent to the interior height of the HPI cavity (i.e., [[]] cm modeled). The modeled

axial length bounds the requirement of minimum 10-inch rod length segments specified by the shielding analysis. The fuel rod OR is varied from 0.2 to 0.5 cm to encompass a variety of fuel designs. Smaller fuel rod OR results in a higher reactivity, see Sections 6.4 through 6.6 for results of each transport assessment. The materials of the fuel rod cladding or structural components are not modeled. Fuel pellets are assumed to be confined within cylindrical components (e.g., fuel rod cladding).

The fuel rods are modeled in a hexagonal array with expanding pitch. The expansion of the lattice is evaluated to determine the optimum H/U-235 ratio. While expansion of the lattice is a condition of HAC, it is also applied to NCT to optimize H/U-235. The fissile mass modeled in the fuel rod array is determined using a mixture of UO₂ and H₂O, with 1,800 grams of U-235 as the basis, which equates to approximately 34,000 grams of UO₂. A circular boundary, which equates to this quantity of U-235, is defined to limit the infinite, heterogeneous lattice to a specific array size. The circular boundary may cut rods radially, thus varying the UO₂ mass represented to less than 1,800 grams of U-235. Therefore, an administratively reduced limit of 1,750 grams of U-235 is defined. The equation below displays how the circular boundary radius is calculated for the varying hexagonal pitch sizes. Additionally, as the pitch is expanded to increase H/U-235, the confinement boundary of the HPI cavity will reduce the fissile mass within the boundary.

$$cavity\ OR = \sqrt{\#rods \frac{2\sqrt{3}P^2}{\pi}}$$

where, P is the hexagonal half-pitch

$$\#rods = M_{UO_2} / (\pi * OR_{fuel}^2 * H * \rho_{UO_2})$$

where,

H is the modeled fuel rod height of [[]] cm

M_{UO₂} is the mass of UO₂ in grams

ρ_{UO₂} is the theoretical density of UO₂

Table 6.3.1-1 defines the variation of fuel outer radii and pitches evaluated for the fuel rod content; the largest pitches for the smallest rods are not modeled as the k_{eff} trend is already shown to be decreasing. Figure 6.3.1-1 shows the fuel rod model geometry, and Figure 6.3.1-2 shows examples of how the circular boundary defines the fissile mass limit by artificially cutting into the lattices.

Structural features of the rods, shoring components such as rod holders, or the HPI material basket may provide additional confinement of the fuel lattice expansion; however, only the HPI cavity is credited for the confinement boundary. Representation of the fuel structural components as water results in an increase in reactivity due to both a decrease in neutron absorption and an increase in fuel rod lattice moderation.

Table 6.3.1-1. Fuel Rod Content Model Parameters

| Parameter | Value (cm) |
|---------------------------|----------------------------------------------------------------------------------------------------------------------------------------------------------|
| Fuel pellet radius (FROR) | 0.2, 0.3, 0.4, 0.5 |
| Half-pitch | FROR[XX]+0.3, FROR[XX]+0.4, FROR[XX]+0.6, FROR[XX]+0.7, FROR[XX]+0.8, FROR[XX]+0.9, FROR[XX]+1.1, FROR[XX]+1.2, FROR[XX]+1.4, FROR[XX]+1.6, FROR[XX]+2.0 |

[[

]]

Figure 6.3.1-1. Fuel Rod Content Model Geometry

[[

]]

Figure 6.3.1-2. Fuel Rod Content Boundary Model Geometry (Not to Scale)

For the transport evaluations of fuel rods, the maximum fuel k_{eff} occurs when the fuel lattice is moderated with full density water. For HAC, when leakage during immersion is possible, moderation in the fuel lattice is assumed present. The full density moderation in the fissile region is conservatively maintained for NCT.

6.3.1.1.2. Fissile, Free Form Mass

The fissile, free form content is limited to a solid, free form, uranium or plutonium. The fissile, free form mass content limits are as follows, based on the HAC, package array assessment of Section 6.6 for 100 wt% U-235 with a mass limit of 430 grams and 100 wt% Pu-239 with a mass limit of 265 grams, and Section 6.9.4 for 100 wt% U-233 with a mass limit of 315 grams and 100 wt% Pu-241 with a mass limit of 150 g. Theoretical density for uranium metal and plutonium metal are analyzed to bound other forms of uranium or plutonium content, respectively. See Section 6.3.2 for material properties.

A parametric study documented in Section 6.9.4 evaluates the fissile, free form material modeled as a sphere, varying radius based on the amount of water present in the homogeneous mixture. By increasing the homogeneous mixture radius while holding the fissile mass constant, the mass of moderation increases, thus increasing H/X. Radii evaluated include [[]], 11, 10, 9, 8, 7, 6, 5, 4, 3, and 2 cm, as well as the sphere radius equivalent to the pure metal mass and density. For each homogeneous mixture of fissile material and water, as the radius of the homogenous sphere increases, the mass fraction of each isotope will vary. For the fissile, free form mass content, a homogenous light water moderator and fissile material mix is maintained for HAC and NCT. However, for NCT the Model 2000 cask cavity region is void, while for HAC all cavity regions are flooded and assessed at varying water densities. This NCT configuration is evaluated for conservatism, and not to imply inleakage of water. Figure 6.3.1-3 displays the fissile mass Monte Carlo N-Particle (MCNP) models.

[[

]]

Figure 6.3.1-3. Package Array HAC, 2N Model Geometry

6.3.1.2. Model 2000 and HPI Model Configuration

The MCNP model geometry used for criticality safety calculations is a detailed three-dimensional model of the HPI and the Model 2000 cask. Some slight simplifications are made to the MCNP geometry to reduce the modeling complexity, such as excluding the [[]]

The design features of the Model 2000 with the HPI are provided in Table 6.3.1-2, including dimensions, materials of construction, and densities of the materials. Table 6.3.1-3 provides the relevant dimensions of the MCNP model including the modeled thicknesses of each material and the MCNP surface numbers used in the geometry. Table 6.3.1-3 along with Table 6.3.1-2 allow for a quick review of the most significant dimensions of the criticality model geometry. It can be noted in Table 6.3.1-3 that all HPI dimensions are minimum, with the fabrication tolerances subtracted from the nominal values. The model dimensions for the Model 2000 cask use both nominal and minimum values where it is appropriate. For example, for the [[]]

]], the cask bottom is considered to be flat at the minimum thickness. However, a number of the dimensions for the cask and overpack are prescribed thicknesses for steel plate that are used for the cask shells (e.g., the 1-inch rolled cask shells). For these instances the prescribed thickness of the steel plate is used for the MCNP geometry.

Table 6.3.1-2. Model 2000 Transport Package/HPI Design Features

| Model 2000 Component | Part | Component | Thickness (in) | Thickness (cm) | Material of Construction | Material Density (lb/in ³) | Material Density (g/cm ³) |
|----------------------|--------------------|--------------------------|----------------|----------------|--------------------------|----------------------------------------|---------------------------------------|
| HPI | Top Plug | Inner Shell | [[]] | [[]] | [[]] | 0.29 | 8.000 |
| | | DU | [[]] | [[]] | DU | 0.67 | [[]] |
| | | Outer Shell | [[]] | [[]] | [[]] | 0.29 | 8.000 |
| | HPI Body | Inner Shell | [[]] | [[]] | [[]] | 0.29 | 8.000 |
| | | DU | [[]] | [[]] | DU | 0.67 | [[]] |
| | | Outer Shell | [[]] | [[]] | [[]] | 0.29 | 8.000 |
| | Bottom [[]] | Inner Shell | [[]] | [[]] | [[]] | 0.29 | 8.000 |
| | | DU | [[]] | [[]] | DU | 0.67 | [[]] |
| | | Outer Shell | [[]] | [[]] | [[]] | 0.29 | 8.000 |
| Cask | Cask Lid | Lid Flange | 1.75 | 4.445 | SS304 | 0.29 | 8.000 |
| | | Lead | 5.37 | 13.64 | Lead | 0.41 | 11.34 |
| | | Inner Plate | 1.50 | 3.810 | SS304 | 0.29 | 8.000 |
| | Cask Body (Side) | Cavity Shell | 1.00 | 2.540 | SS304 | 0.29 | 8.000 |
| | | Lead | 4.00 | 10.16 | Lead | 0.41 | 11.34 |
| | | Cask Shell | 1.00 | 2.540 | SS304 | 0.29 | 8.000 |
| | Cask Body (Bottom) | Cask Bottom ¹ | 5.88 | 14.92 | SS304 | 0.29 | 8.000 |

Notes: ¹ Due to a [[]], the minimum thickness is used.
General: All dimensions based on component licensing drawings in Section 1.3.1.

Table 6.3.1-3. Relevant MCNP Model Dimensions

| Model 2000 Component | Part | Dimension | MCNP Surface(s) | Value (cm) | Value (in) |
|----------------------|----------------|--------------|-----------------|--------------------|--------------------|
| Cask | Cask Lid | t_{SS1} | 17 / 18 | 3.810 | 1.500 |
| | | t_{pb} | 18 / 20 | 13.64 | 5.370 |
| | | t_{SS2} | 20 / 23 | 4.445 | 1.750 |
| | Cask Side | r_{cavity} | 3 | 33.66 | 13.25 |
| | | t_{SS1} | 3 / 6 | 2.540 | 1.000 |
| | | t_{pb} | 6 / 10 | 10.16 | 4.000 |
| | | t_{SS2} | 10 / 11 | 2.540 | 1.000 |
| | | h_{pb}^3 | 16 / 19 | 141.9 | 55.87 |
| | Cask Bottom | t_{SS} | 15 / 115 | 14.94 ¹ | 5.880 ¹ |
| | | h_{cavity} | 115 / 17 | 137.5 | 54.13 |
| HPI | HPI Top Lid | t_{SS1} | 149 / 150 | [[]] | [[]] |
| | | t_{DU} | 150 / 1152 | [[]] | [[]] |
| | | t_{SS2} | 152 / 153 | [[]] | [[]] |
| | HPI Body Side | r_{cavity} | 135 | [[]] | [[]] |
| | | t_{SS1} | 135 / 136 | [[]] | [[]] |
| | | t_{DU} | 136 / 1136 | [[]] | [[]] |
| | | t_{SS2} | 137 / 138 | [[]] | [[]] |
| | HPI Bottom Lid | t_{SS1} | 115 / 140 | [[]] | [[]] |
| | | t_{DU} | 1140 / 145 | [[]] | [[]] |
| | | t_{SS2} | 145 / 146 | [[]] | [[]] |
| | | | | | |

Notes: ¹ Cask bottom modeled flat, with thickness equal to the 6.13" height minus [[]].

² Minimum DU thicknesses considered with tolerance gaps explicitly modeled.

³ Lead column height.

The package has multiple void regions, including within the confinement system. The effect of variations in the package moderation is evaluated by flooding all spaces within the package and varying the light water moderator density from 0.0 to 1.0 g/cm³ (full density). Determining the most reactive package moderation applies to HAC when leakage during immersion is possible. For NCT, the package cavities, unless otherwise noted, are dry with no additional moderation, as this is representative of this transport condition. Varying the H/X ratio optimizes fissile contents, thus a full spectrum of density variation for each cavity region is not necessary to show the trend toward isolation of a package in an array.

Generally for package arrays, moderating only the content fissile region with full density water results in the maximum neutron interaction between packages in an array and bounds any variations in the flooding sequence. The voided space in packaging cavities and between packages in an array allows for increased interaction between the packages. The inclusion of interspersed moderation in these regions would increase the isolation of packages within the array, which leads to a system reactivity approaching that of a single, isolated package. For the single package analysis, the package is fully flooded. Hence, no void regions exist within the model. This generates an increase in reflection, while decreasing particle leakage. However, as the reflection from the DU HPI shields provides the dominant increase in neutron interaction within a package, the variation of moderator density provides little additional neutron moderation to increase the package criticality for the package array and single package.

Additionally, the single package and package array model have a 30.48 cm-thick full density water reflector blanket around the exterior. The specification of 30.48 cm (12 inches) of water reflection is selected as a practical value. SSG-26 (Reference 6-2), Section 6.8.1, specifies 20 cm of water reflection as a practical value, as an additional 10 cm of water reflection would add less than 0.5% in reactivity to an infinite slab of U-235.

Structural evaluations show no damage or deformation to the HPI for NCT or HAC. Model 2000 cask structural evaluations define localized damage for the HAC pin-puncture test and damage to the impact limiters during drop tests, thus, the overpack is conservatively not modeled for HAC. A drop may also allow the content to shift within the HPI cavity. The effect of orientation of the fissile content within the HPI cavity is assessed by positioning the fissile material near the walls of the HPI cavity, increasing the proximity to the HPI DU shields thus increasing neutron interactions in the vicinity. While the fuel rod content is defined as the length of the HPI cavity, the fissile, free form mass content is a sphere allowed to shift within the HPI.

Figure 6.3.1-4 shows the HAC MCNP model geometry.

[[

]]

Figure 6.3.1-4. Package Model Geometry

6.3.1.2.1. NCT Model

For NCT, the MCNP criticality model includes the HPI and the Model 2000 cask, and conservatively neglects the overpack material and spacing to be consistent with the HAC model, even though structural evaluations show that the damage to the overpack is minimal. The materials for the HPI and cask are defined as prescribed in Section 6.3.2 in the appropriate cells of the model. The NCT 5N package array is represented by seven (7) packages in a hexagonal array as to provide maximum reflection and package neutron interaction. Figure 6.3.1-5 shows the top view of the MCNP model, NCT array. For cases where the fissile content size is limited such that it does not occupy the full HPI cavity radius, the contents are positioned within the HPI cavity towards the centroid of the group of packages, see Figure 6.3.1-6 for example of fuel rod case limited by mass.

Light water moderation is used within the fissile material matrix for each content, optimizing the H/X ratio. No leakage of water is evaluated in the various cavity regions of the packaging, for the evaluation of undamaged packages under NCT (per 10 CFR 71.55(d)). The Model 2000 cask cavity region is void and the HPI cavity region is flooded; this NCT configuration is evaluated for conservatism, and not to imply inleakage of water. Full density moderation is maintained between the packages, as k_{eff} result for the single package and package array (NCT and HAC) are very close indicating the shield materials of the HPI and cask provide strong reflection thus neutronically isolating each package within the array.

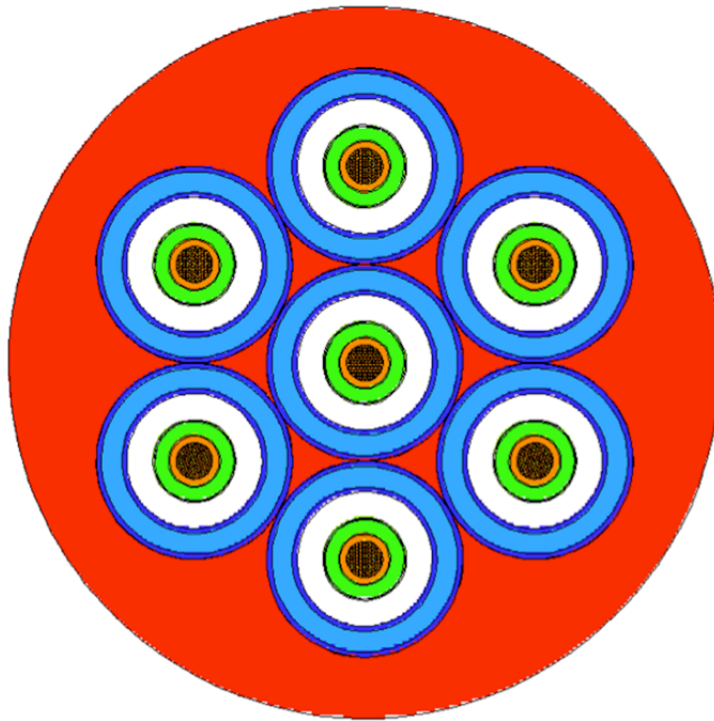


Figure 6.3.1-5. Package Array NCT, 5N Model Geometry

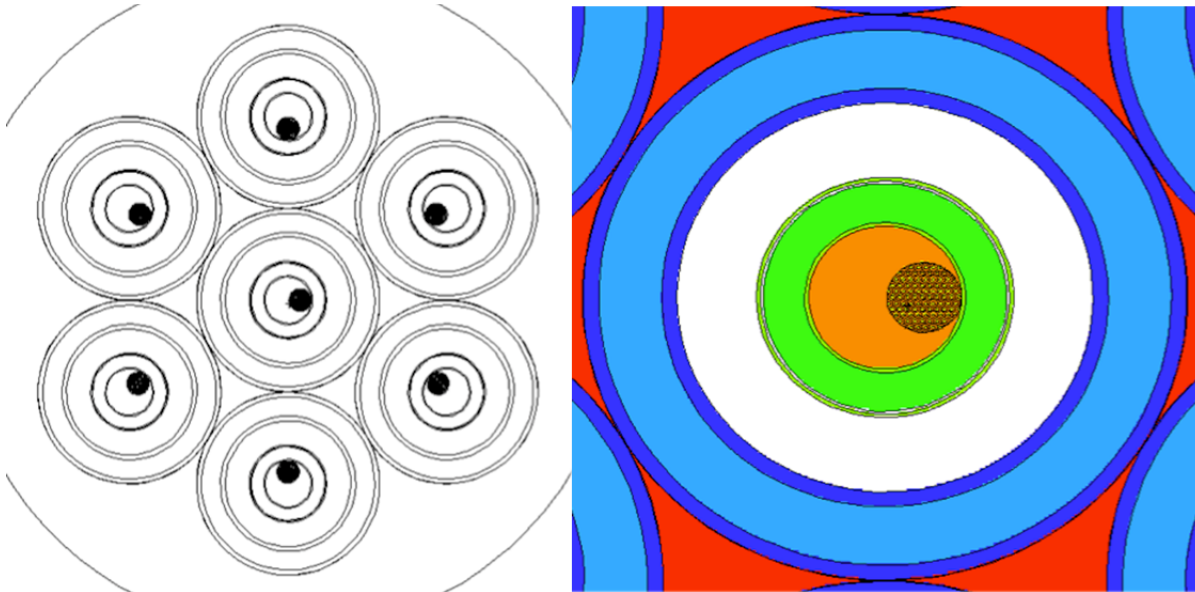


Figure 6.3.1-6. Package Array NCT, 5N Model Geometry, Content Positioning

6.3.1.2.2. HAC Model

For HAC, the MCNP6 criticality model is the same as the shielding model, and only includes the HPI and the Model 2000 cask, neglecting the material and spacing of the overpack. This model conservatively assumes the complete destruction and removal of the overpack. Additionally, to be consistent with shielding analysis, the HAC model includes the lead slump from which the maximum deformation in the lead column is calculated to be 3.56 mm, which is conservatively rounded up to 4 mm for the shielding analysis (Section 2.12.2). Figure 6.3.1-7 shows the MCNP model for the HAC array. For cases where the fissile content size is limited such that it does not occupy the full HPI cavity radius, the contents are positioned within the HPI cavity towards the center package. See Figure 6.3.1-8 for an example of a case limited by fissile mass.

Light water moderation is used within the fissile material matrix for each content, optimizing the H/X ratio. Moderation caused by inleakage is limited to moderators no more effective than water from sources external to the package. Per 10 CFR 71.59(a)(2), the HAC, 2N assessment evaluates the sensitivity of hydrogenous moderation by evaluating water inleakage into all void spaces of the package cavity regions, including those within the containment system. The moderation space is defined as all available space within the packaging cavities, not including any space occupied by the structural and shielding material design. The moderation density is varied from 0 to 1.0 g/cm³ for the HPI cavity region and the Model 2000 cask region. A full spectrum of density variation for each cavity region is not necessary to show the trend toward isolation of the package in an array. The fissile material matrix region is maintained as fully flooded with full density water for both contents.

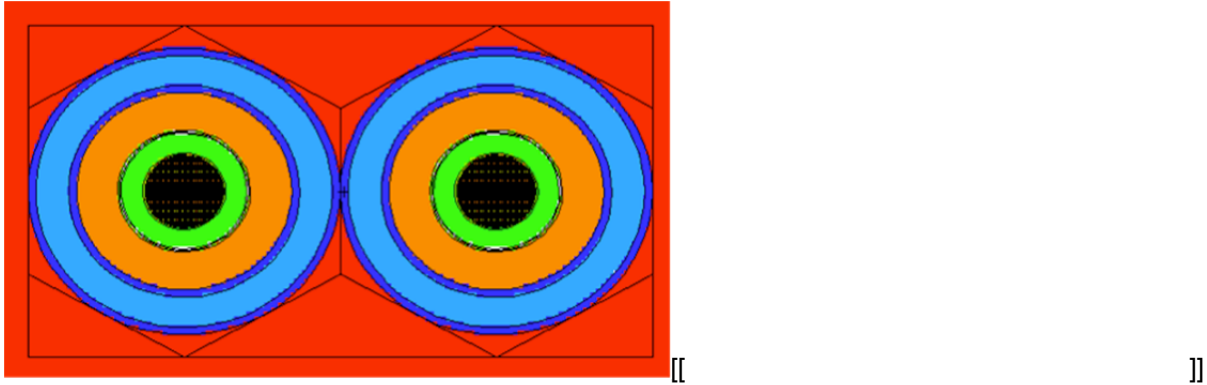


Figure 6.3.1-7. Package Array HAC, 2N Model Geometry

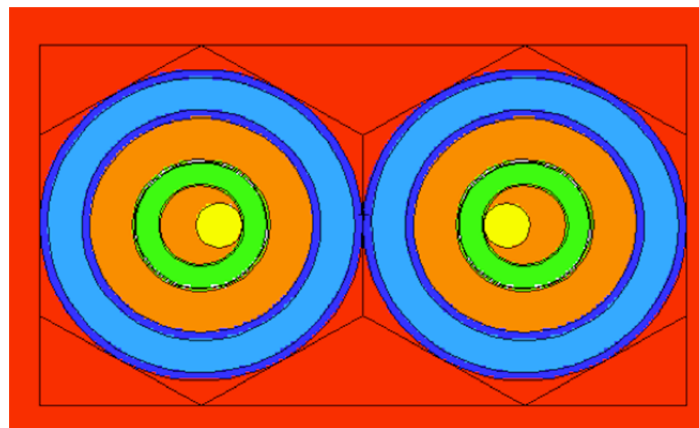


Figure 6.3.1-8. Package Array HAC, 2N Model Geometry, Content Positioning

6.3.2. Material Properties

The material compositions used in the criticality safety analyses are listed in Table 6.3.2-1 through Table 6.3.2-5. The structural components of the Model 2000 cask are constructed of Type 304 stainless steel. The nuclear properties relevant to criticality safety for 304 stainless steel are in Table 6.3.2-1. Type [[]] stainless steel comprises the structural components of the HPI. The nuclear properties relevant to criticality safety for 316 stainless steel are in Table 6.3.2-2. It can be noted that there is negligible difference between the two types of stainless steel in terms of absorption properties. Both types are only included for accuracy of the actual materials of construction. Any slight change in the elemental composition of these steels does not result in any significant increase in calculated reactivity. The densities and material compositions for both stainless steel types are from Pacific Northwest National Lab report PNNL-15870 (Reference 6-3). The shielding material of the Model 2000 cask is solely comprised of lead. The nuclear properties relevant to criticality safety for lead are in Table 6.3.2-3. The shielding material of the HPI is solely comprised of DU. The nuclear properties relevant to criticality safety for DU are in Table 6.3.2-4. The densities of the lead and DU materials are based on the minimum specified densities for these materials in the respective component licensing drawings in Section 1.3.1. Isotopic masses are from SCALE6.1 Manual,

Table M8.2.1 (Reference 6-4). For the modeling of water moderation, the $S(\alpha,\beta)$ thermal kernel treatment for hydrogen in the water is applied. The collision kinematics data includes thermal kinematics kernels to describe thermal scattering in moderating materials such as hydrogen in water. Table 6.3.2-5 defines the fissile material properties.

Table 6.3.2-1. Nuclear Properties of Type 304 Stainless Steel

| Element | Isotope | Neutron ZA | Mass Fraction |
|------------------------------|---------|------------|---------------|
| C | C-12 | 6012 | 3.9537E-04 |
| | C-13 | 6013 | 4.6337E-06 |
| Si | Si-28 | 14028 | 4.5933E-03 |
| | Si-29 | 14029 | 2.4168E-04 |
| | Si-30 | 14030 | 1.6499E-04 |
| P | P-31 | 15031 | 2.3000E-04 |
| S | S-32 | 16032 | 1.4207E-04 |
| | S-33 | 16033 | 1.1568E-06 |
| | S-34 | 16034 | 6.7534E-06 |
| | S-36 | 16036 | 1.6825E-08 |
| Cr | Cr-50 | 24050 | 7.9300E-03 |
| | Cr-52 | 24052 | 1.5903E-01 |
| | Cr-53 | 24053 | 1.8380E-02 |
| | Cr-54 | 24054 | 4.6614E-03 |
| Mn | Mn-55 | 25055 | 1.0000E-02 |
| Fe | Fe-54 | 26054 | 3.9617E-02 |
| | Fe-56 | 26056 | 6.4490E-01 |
| | Fe-57 | 26057 | 1.5160E-02 |
| | Fe-58 | 26058 | 2.0529E-03 |
| Ni | Ni-58 | 28058 | 6.2158E-02 |
| | Ni-60 | 28060 | 2.4768E-02 |
| | Ni-61 | 28061 | 1.0946E-03 |
| | Ni-62 | 28062 | 3.5472E-03 |
| | Ni-64 | 28064 | 9.3254E-04 |
| Density (g/cm ³) | 8.00 | | |

Table 6.3.2-2. Nuclear Properties of Type 316 Stainless Steel

| Element | Isotope | Neutron ZA | Mass Fraction |
|------------------------------|---------|---------------|------------------|
| C | C-12 | 6012 | 4.0525E-04 |
| | C-13 | 6013 | 4.7496E-06 |
| Si | Si-28 | 14028 | 4.6576E-03 |
| | Si-29 | 14029 | 2.4507E-04 |
| | Si-30 | 14030 | 1.6730E-04 |
| P | P-31 | 15031 | 2.3000E-04 |
| S | S-32 | 16032 | 1.4207E-04 |
| | S-33 | 16033 | 1.1568E-06 |
| | S-34 | 16034 | 6.7534E-06 |
| | S-36 | 16036 | 1.6825E-08 |
| Cr | Cr-50 | 24050 | 7.0953E-03 |
| | Cr-52 | 24052 | 1.4229E-01 |
| | Cr-53 | 24053 | 1.6445E-02 |
| | Cr-54 | 24054 | 4.1707E-03 |
| Mn | Mn-55 | 25055 | 1.0140E-02 |
| Fe | Fe-54 | 26054 | 3.7769E-02 |
| | Fe-56 | 26056 | 6.1482E-01 |
| | Fe-57 | 26057 | 1.4453E-02 |
| | Fe-58 | 26058 | 1.9571E-03 |
| Ni | Ni-58 | 28058 | 8.0637E-02 |
| | Ni-60 | 28060 | 3.2131E-02 |
| | Ni-61 | 28061 | 1.4200E-03 |
| | Ni-62 | 28062 | 4.6018E-03 |
| | Ni-64 | 28064 | 1.2098E-03 |
| Mo | Mo-92 | 42092 | 3.5374E-03 |
| | Mo-94 | 42094 | 2.2586E-03 |
| | Mo-95 | 42095 | 3.9322E-03 |
| | Mo-96 | 42096 | 4.1686E-03 |
| | Mo-97 | 42097 | 2.4141E-03 |
| | Mo-98 | 42098 | 6.1715E-03 |
| | Mo-100 | 42100 | 2.5175E-03 |
| Density (g/cm ³) | 8.00 | | |

Table 6.3.2-3. Nuclear Properties of Lead

| Element | Isotope | Neutron ZA | Mass Fraction |
|------------------------------|---------|------------|---------------|
| Pb | Pb-204 | 82204 | 1.3781E-02 |
| | Pb-206 | 82206 | 2.3956E-01 |
| | Pb-207 | 82207 | 2.2074E-01 |
| | Pb-208 | 82208 | 5.2592E-01 |
| Density (g/cm ³) | 11.34 | | |

Table 6.3.2-4. Nuclear Properties of Depleted Uranium

| Element | Isotope | Neutron ZA | Mass Fraction |
|------------------------------|---------|------------|---------------|
| U | U-235 | 92235 | 7.0000E-03 |
| | U-238 | 92238 | 9.9300E-01 |
| Density (g/cm ³) | [[]] | | |

Table 6.3.2-5. Nuclear Properties of Fissile Content

| Element | Isotope | Neutron ZA | Mass Fraction | Density (g/cm ³) |
|-------------------------------|---------|------------|---------------|------------------------------|
| UO ₂ , 6 wt% U-235 | U-235 | 92235 | 5.2257E-02 | 10.96 ¹ |
| | U-238 | 92238 | 8.2917E-01 | |
| | O | 8016 | 1.1857E-01 | |
| U-Metal, 100 wt% U-235 | U-235 | 92235 | 1.0000E+00 | 19.05 ² |
| Pu-Metal, 100 wt% Pu-239 | Pu-239 | 94239 | 1.0000E+00 | 19.84 ³ |

References:

¹ Reference 6-4 Density, Table M8.2.4.

² Reference 6-4 Density, Table M8.2.2.

³ Reference 6-3 Density, Page 235.

6.3.3. Computer Codes and Cross-Section Libraries

The criticality safety analysis was completed using MCNP6 Version 1.0 (Reference 6-5) with the continuous-energy neutron data library ENDF/B-VII.1 (Reference 6-6). MCNP6 is a general-purpose, continuous-energy, generalized-geometry, time-dependent, Monte Carlo radiation-transport code designed to track many particle types over a broad range of energies. The criticality safety assessment is for high-enriched free form uranium, free form plutonium, and low-enriched uranium fuel rods in the Model 2000 cask with the HPI. MCNP6 meets the

recommendations in Section 4, Method of Analysis defined in NUREG/CR-5661 (Reference 6-7).

6.3.3.1. Convergence Criteria

Convergence of the cases in criticality safety analysis was verified through inspection of the Shannon entropy of the fission source distribution. In order to determine the Shannon entropy of the problem, MCNP6 divides the fissionable regions of the problem into several bins, which then tally the fission sources during the random walks of each cycle. As the number of cycles completed increases, the fission source distribution will converge to steady state. In the output, MCNP6 prints which cycle was the first cycle to have a value of Shannon entropy within one standard deviation of the average Shannon entropy of the last half of the cycles analyzed; this is the minimum acceptable source convergence. The proper determination of the source convergence requires inspection of the plot of Shannon entropy versus cycle number, from which it can be determined at which cycle number the Shannon entropy converges. At least that many cycles were discarded, and more than 100 additional cycles are run after source convergence. Additionally, to determine adequacy of k_{eff} convergence, the behavior of k_{eff} with cycle number is evaluated to ensure no upward or downward trends are present.

6.3.4. Demonstration of Maximum Reactivity

A system is considered acceptably subcritical if a calculated k_{eff} plus calculational uncertainties lies at or below the USL (i.e., $k_{\text{system}} + \Delta k_{\text{system}} \leq \text{USL}$). Thus, the USL is the magnitude of the sum of the biases, uncertainties, and administrative and/or statistical margins applied to a set of critical benchmarks, such that a high degree of confidence defines subcriticality of the system (Reference 6-8):

$$\text{USL} = 1 - \Delta k_m + \beta - \Delta\beta$$

where

Δk_m is the additional margin to ensure subcriticality

β is the calculation bias

$\Delta\beta$ is the uncertainty in the bias

Based on a given set of critical experiments, the USL is defined as a function of key system parameters, such as energy of average lethargy causing fission (EALF), fuel enrichment, or H/X ratio. Because both β and $\Delta\beta$ may vary with a given parameter, the USL is typically expressed as a function of the parameter, within an appropriate range of applicability derived from the parameter bounds. Table 6.8.2-1 displays the USL functions for the Model 2000 Transport Package criticality safety analysis.

The low-enriched lattice system USL function is applicable to the fuel rod content. Results of Section 6.4 through 6.6 shows that the limiting cases for the single package and package array have a H/U-235 value of 570. The value of H/U-235 is calculated based on a ratio of volume for the pitch cell and the estimated number of rods modeled (see equation below). Applying this value to the USL equation in Table 6.8.2-1, results in a rounded USL value of 0.9387 for fuel rod contents (e.g., $0.9473 - 1.5031\text{E-}5 \times 570 = 0.93873$ for $X > 214.9$).

$$\frac{H}{X} \text{ Ratio} = \frac{H}{U^{235}} \text{ Ratio} = \text{WTF} \times \frac{H_2O \text{ Density}}{UO_2 \text{ Density}} \times \frac{(1 - \text{Enr. } U^{235})MW_{U^{238}} + \text{Enr. } U^{235}MW_{U^{235}} + 2MW_{O_2}}{MW_{H_2O}} \times \frac{2}{1} \times \frac{1}{\text{Enr. } U^{235}}$$

where

$$\text{Water to Fuel Volume Ratio} = \frac{\text{Water volume in fuel rod cell} \times \# \text{ rods}}{\text{Fuel volume} \times \# \text{ rods}}$$

for FRLA(N/H)_1_22 limiting cases, the #rods is estimated at 203 rods

The highly enriched solution system USL function is applicable to the fissile, free form content. Results of Section 6.4 through Section 6.6 show that the limiting cases for the single package and package array for each material have minimum EALF values of greater than 0.3 eV. The EALF is collected from the MCNP6 output files for the corresponding most limiting cases. Applying this value to the USL equation in Table 6.8.2-1, results in a USL value of 0.9406 for fissile, free form contents.

A fissile mass limit for each content is selected based on a $k_{\text{eff}} + 2 \sigma$ value that allows for an appropriate USL margin that includes uncertainty and an administrative margin.

6.4 Single Package Evaluation

6.4.1. Configuration

This single model represents NCT and HAC for the single package evaluations; models are described in Section 6.3. The reference case for the single package is to fill all cavity regions that are normally void space with full density water. For both contents, the fissile matrix region is moderated with full density water. The fuel rod content is described in Section 6.2.1, and the fissile, free form content is described in Section 6.2.2.

6.4.2. Results

6.4.2.1. Fuel Rod Content

Peak cases for fuel rod content are provided in Table 6.4.2-1; full results are in Section 6.9.5, Table 6.9.5-3. Figure 6.4.2-1 displays the trends for all data. Based on the most limiting case for the single package, FRLSmh_1_22 (OR=0.2 cm, hex, half-pitch=0.7 cm), the $k_{\text{eff}} + 2\sigma$ equals 0.92349. An additional 1% uncertainty is added for the variation of pitch geometric modeling; see Section 6.9.1 for details. Thus the final, maximum k_{eff} for the fuel rod, single package case is 0.9328 (rounded up for conservatism). Data trends show that as the fuel rod OR increase the overall system reactivity decreases, thus the minimum fuel rod OR of 0.2 cm is a limiting parameter. Thus, an equivalent cylindrical fuel radius of ≥ 0.20 cm is required for the 1750-gram mass limit.

Section 6.3.4 defines the USL value as 0.9387 for fuel rod contents.

Table 6.4.2-1. Fuel Rod Content, Single Package, Maximum Cases

| Case Name | Fuel OR (cm) | Half-Pitch (cm) | Estimated No. Rods Modeled | U-235 Mass (g) | k_{eff} | σ | $k_{eff}+2\sigma$ | H/U-235 | EALF (eV) |
|-------------------------|--------------|-----------------|----------------------------|----------------|-----------|----------|-------------------|---------|-----------|
| FRLSmh 1 1 | 0.2 | 0.50 | [[]] | 1766 | 0.85526 | 0.00025 | 0.85576 | -- | -- |
| FRLSmh 1 2 | 0.2 | 0.60 | [[]] | 1766 | 0.90946 | 0.00023 | 0.90992 | -- | -- |
| FRLSmh 1 21 | 0.2 | 0.65 | [[]] | 1766 | 0.92134 | 0.00022 | 0.92178 | -- | -- |
| FRLSmh 1 22 | 0.2 | 0.70 | [[]] | 1766 | 0.92307 | 0.00021 | 0.92349 | 570 | 0.31716 |
| FRLSmh 1 23 | 0.2 | 0.75 | [[]] | 1766 | 0.91659 | 0.00022 | 0.91703 | -- | -- |
| FRLSmh 1 3 | 0.2 | 0.80 | [[]] | 1757 | 0.89990 | 0.00022 | 0.90034 | -- | -- |
| FRLSmh 1 4 ^a | 0.2 | 0.90 | [[]] | 1429 | 0.83653 | 0.00021 | 0.83695 | -- | -- |
| FRLSmh 1 5 ^a | 0.2 | 1.00 | [[]] | 1219 | 0.78051 | 0.00020 | 0.78091 | -- | -- |

NOTE: ^a Number of rod is limited by HPI cavity size, as described in Section 6.3.1.1.1.

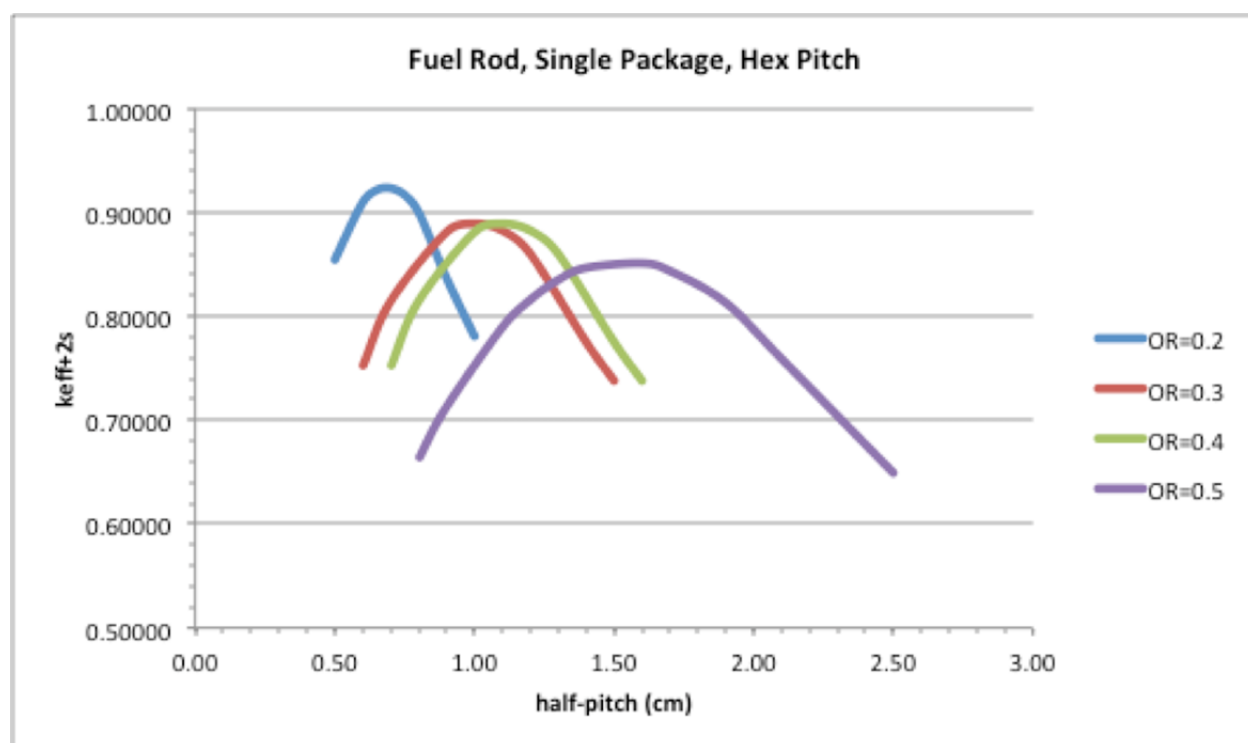


Figure 6.4.2-1. Fuel Rod Content, Single Package, Results

6.4.2.2. Fissile, Free Form Content

Cases for the single package results for fissile, free form content, both U-235 and Pu-239 are provided in Table 6.4.2-2.

Parametric studies were completed to evaluate positioning the content sphere to the bottom of the HPI and varying the radius of the homogeneous, fissile sphere, thus varying the H/X ratio. Parametric study results are shown in Section 6.9.4. The most limiting configurations are a homogeneous sphere with a radius nearly equivalent to the HPI cavity, and positioned at the bottom of the HPI cavity. The fissile mass is varied to define subcriticality under the USL.

When reducing the fissile mass, an optimum H/X ratio is evaluated by also varying the sphere radius for the peak reactivity region.

For single package evaluation, fissile mass limits of 430 grams of 100 wt% U-235 and 265 grams of 100 wt% Pu-239 meet subcriticality under the USL. Section 6.9.3 provides results for the U-233 and Pu-241 content. Limiting cases for each content are highlighted in Table 6.4.2-2, where $k_{\text{eff}} + 2\sigma$ equals 0.93921 for the 430 grams, U-235 content and 0.93784 for the 265 grams, Pu-239 content. The content results for U-233 and Pu-241 are in Section 6.9.3.

Section 6.3.4 defines the USL value as 0.9406 for fissile, free form contents.

Table 6.4.2-2. Fissile, Free Form Content, Single Package, Maximum Cases

| Case Name | Sphere OR (cm) | Fissile Mass (g) | k_{eff} | σ | $k_{\text{eff}}+2\sigma$ | H/X | EALF (eV) |
|------------------|----------------|------------------|------------------|----------|--------------------------|-----|-----------|
| U-235 | | | | | | | |
| 601HMS12 430btm | [[]] | 430 | 0.93475 | 0.00023 | 0.93521 | 481 | -- |
| 601HMS12p 430btm | 12.00 | 430 | 0.93873 | 0.00024 | 0.93921 | 438 | 0.32218 |
| 601HMS115 430btm | 11.50 | 430 | 0.93787 | 0.00023 | 0.93833 | 385 | -- |
| 601HMS11 430btm | 11.00 | 430 | 0.93136 | 0.00023 | 0.93182 | 337 | -- |
| Pu-239 | | | | | | | |
| PHMS12btm 265 | [[]] | 265 | 0.93563 | 0.00026 | 0.93615 | 795 | -- |
| PHMS12pbtm 265 | 12.00 | 265 | 0.93726 | 0.00029 | 0.93784 | 724 | 0.53326 |
| PHMS115btm 265 | 11.50 | 265 | 0.93467 | 0.00026 | 0.93519 | 637 | -- |

6.5 Evaluation of Package Arrays under Normal Conditions of Transport

6.5.1. Configuration

As the Model 2000 cask with HPI is shipped exclusive use, a single package defines a conveyance. Thus, the package array criticality evaluation defines the number N of packages as one. Therefore, for NCT, the package array is modeled as seven (7) packages in a hexagonal array. This evaluation demonstrates that five (5) times N packages is shown to be subcritical with the package arrangement reflected on all sides by 30.48 cm of water. The NCT package array model is described in Section 6.3.1.2.1.

The reference case for the NCT package array is to maintain void in all cavity regions that are normally void space. Full density moderation is maintained between the packages, as k_{eff} results for the single package and package array (NCT and HAC) are very similar, indicating the shield materials of the HPI and cask provide strong reflection, thus neutronically isolating each package within the array. As the reflection from the DU HPI shields provides the dominant increase in neutron interaction within a package, the variation of moderator density provides little additional neutron interaction to increase the package reactivity; see Section 6.9.4.1.3 for comparison. The confinement boundary for NCT and HAC is defined as the HPI cavity. For both contents, the fissile matrix region is moderated with full density water. The fuel rod content is described in Section 6.2.1, and the fissile, free form content is described in Section 6.2.2.

6.5.2. Results

6.5.2.1. Fuel Rod Content

Result of the HAC 2N array show that the combination of the smallest fuel OR and pitch variation produce the highest reactivity in the package array. Therefore only the three smallest fuel OR values (0.2, 0.3, and 0.4 cm) are evaluated for the NCT 5N package array. Peak cases for NCT fuel rod content are provided in Table 6.5.2-1; full results are in Section 6.9.5, Table 6.9.5-4. Figure 6.5.2-1 displays the trends for all evaluated data. For the most limiting case for the NCT package array, FRLANmh_1_22 (OR=0.2 cm, hex, half-pitch=0.7 cm), the $k_{\text{eff}} + 2\sigma$ is 0.91856. An additional 1% uncertainty is added for the variation of pitch geometric modeling; see Section 6.9.1 for details. Thus the final, maximum k_{eff} for the fuel rod, single package case is 0.9278 (rounded up for conservatism). Data trends show that as the fuel rod OR increases the overall system reactivity decreases, thus the minimum fuel rod OR of 0.2 cm is a limiting parameter.

Section 6.3.4 defines the USL value as 0.9387 for fuel rod contents.

Table 6.5.2-1. Fuel Rod Content, NCT 5N, Maximum Cases

| Case Name | Fuel OR (cm) | Half-pitch (cm) | Estimated No. rods modeled | U-235 Mass (g) | k_{eff} | σ | $k_{\text{eff}}+2\sigma$ | H/U-235 | EALF (eV) |
|--------------------------|--------------|-----------------|----------------------------|----------------|------------------|----------|--------------------------|---------|-----------|
| FRLANmh_1_1 | 0.2 | 0.50 | [] | 1766 | 0.83754 | 0.00024 | 0.83802 | -- | -- |
| FRLANmh_1_2 | 0.2 | 0.60 | [] | 1766 | 0.89350 | 0.00023 | 0.89396 | -- | -- |
| FRLANmh_1_21 | 0.2 | 0.65 | [] | 1766 | 0.90893 | 0.00024 | 0.90941 | -- | -- |
| FRLANmh_1_22 | 0.2 | 0.70 | [] | 1766 | 0.91810 | 0.00023 | 0.91856 | 570 | 0.31717 |
| FRLANmh_1_23 | 0.2 | 0.75 | [] | 1766 | 0.91564 | 0.00020 | 0.91604 | -- | -- |
| FRLANmh_1_3 ^a | 0.2 | 0.80 | [] | 1757 | 0.90089 | 0.00020 | 0.90129 | -- | -- |
| FRLANmh_1_4 ^a | 0.2 | 0.90 | [] | 1429 | 0.83616 | 0.00020 | 0.83656 | -- | -- |
| FRLANmh_1_5 ^a | 0.2 | 1.00 | [] | 1219 | 0.77767 | 0.00019 | 0.77805 | -- | -- |

NOTE: ^a Number of rod is limited by HPI cavity size, as described in Section 6.3.1.1.1

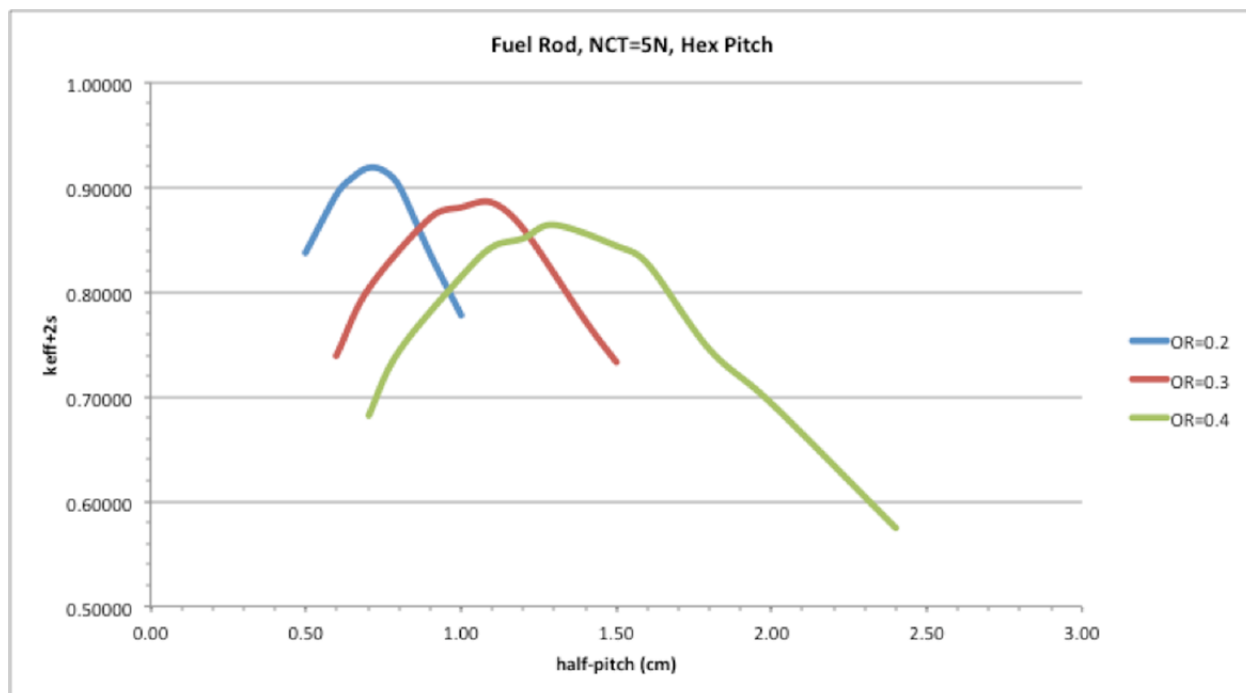


Figure 6.5.2-1. Fuel Rod Content, NCT 5N, Results

6.5.2.2. Fissile, Free Form Content

NCT 5N cases for fissile, free form content, both U-235 and Pu-239, are provided in Table 6.5.2-2. Fissile mass limits are evaluated for NCT package array and the content sphere is positioned in the bottom of the HPI (btm), where the DU shield is thickest. An optimum H/X ratio is evaluated by also varying the sphere radius for the peak reactivity region. The mass variation cases for each content are defined in Table 6.5.2-2; $k_{eff} + 2\sigma$ equals 0.93349 for 430 grams of the U-235 content and 0.93336 for 265 grams of the Pu-239 content.

Section 6.3.4 defines the USL value as 0.9406 for fissile, free form contents.

Table 6.5.2-2. Fissile, Free Form Content, NCT 5N, Maximum Cases

| Case Name | Sphere OR (cm) | k_{eff} | σ | $k_{eff} + 2\sigma$ | H/X | EALF (eV) | Fissile Mass (g) |
|------------------|----------------|-----------|----------|---------------------|-----|-----------|------------------|
| U-235 | | | | | | | |
| 601HMN12_430btm | [[]] | 0.91267 | 0.00028 | 0.91323 | 480 | -- | 430 |
| 601HMN12p_430btm | 12.00 | 0.93284 | 0.00028 | 0.93340 | 438 | -- | 430 |
| 601HMN115_430btm | 11.50 | 0.93293 | 0.00028 | 0.93349 | 385 | 0.31077 | 430 |
| 601HMN11_430btm | 11.00 | 0.92750 | 0.00027 | 0.92804 | 337 | -- | 430 |
| Pu-239 | | | | | | | |
| PHMN12btm_265 | [[]] | 0.91548 | 0.00026 | 0.91600 | 795 | -- | 265 |
| PHMN12pbtm_265 | 12.00 | 0.92600 | 0.00027 | 0.92654 | 724 | -- | 265 |
| PHMN115btm_265 | 11.50 | 0.93284 | 0.00026 | 0.93336 | 637 | 0.53547 | 265 |
| PHMN11btm_265 | 11.00 | 0.92160 | 0.00030 | 0.92220 | 557 | -- | 265 |

6.6 Package Arrays under Hypothetical Accident Conditions

6.6.1. Configuration

As the Model 2000 cask with HPI is shipped exclusive use, a single package defines a conveyance. Thus, the package array criticality evaluation defines the number N of packages as one. Therefore, for HAC, the package array is modeled as two packages side-by-side, evaluating that two times N packages is shown to be subcritical with the package arrangement reflected on all sides by 30.48 cm of water. The HAC, package array model is described in Section 6.3.1.2.2.

The reference case for the HAC package array is to fill all cavity regions that are normally void space with full density water. Full density moderation is maintained between the packages and within the packages. A parametric study assesses varied light water moderator density within the HPI and cask regions. The confinement boundary for HAC is defined as the HPI cavity. For both contents, the fissile matrix region is moderated with full density water. The fuel rod content is described in Section 6.2.1, and the fissile, free form content is described in Section 6.2.2.

6.6.2. Results

6.6.2.1. Fuel Rod Content

Peak cases for HAC package array, fuel rod content are provided in Table 6.6.2-1; full results are in Section 6.9.5, Table 6.9.5-5. Figure 6.6.2-1 displays the trends for all data. For the most limiting case for the HAC package array, FRLAHmh_1_22 (OR=0.2 cm, hex, half-pitch=0.7 cm), the $k_{eff} + 2\sigma$ is 0.92398. An additional 1% uncertainty is added for the variation of pitch geometric modeling, see Section 6.9.1 for details. Thus the final, maximum k_{eff} for the fuel rod, HAC package array case is 0.9333 (rounded up for conservatism). Data trends show that as the fuel rod OR increases the overall system reactivity decreases, thus the minimum fuel rod OR of 0.2 cm is a limiting parameter.

Section 6.3.4 defines the USL value as 0.9387 for fuel rod contents.

Table 6.6.2-1. Fuel Rod Content, HAC 2N, Maximum Cases

| Case Name | Fuel OR (cm) | Half-pitch (cm) | Estimated No. rods modeled | U-235 Mass (g) | k_{eff} | σ | $k_{eff}+2\sigma$ | H/U-235 | EALF (eV) |
|--------------------------|--------------|-----------------|----------------------------|----------------|-----------|----------|-------------------|---------|-----------|
| FRLAHmh_1_1 | 0.2 | 0.50 | [[]] | 1766 | 0.85587 | 0.00026 | 0.85639 | -- | -- |
| FRLAHmh_1_2 | 0.2 | 0.60 | [[]] | 1766 | 0.90895 | 0.00025 | 0.90945 | -- | -- |
| FRLAHmh_1_21 | 0.2 | 0.65 | [[]] | 1766 | 0.92097 | 0.00022 | 0.92141 | -- | -- |
| FRLAHmh_1_22 | 0.2 | 0.70 | [[]] | 1766 | 0.92350 | 0.00024 | 0.92398 | 570 | 0.31681 |
| FRLAHmh_1_23 | 0.2 | 0.75 | [[]] | 1766 | 0.91616 | 0.00025 | 0.91666 | -- | -- |
| FRLAHmh_1_3 ^a | 0.2 | 0.80 | [[]] | 1757 | 0.89981 | 0.00021 | 0.90023 | -- | -- |
| FRLAHmh_1_4 ^a | 0.2 | 0.90 | [[]] | 1429 | 0.83686 | 0.00019 | 0.83724 | -- | -- |
| FRLAHmh_1_5 ^a | 0.2 | 1.00 | [[]] | 1219 | 0.78005 | 0.00019 | 0.78043 | -- | -- |

NOTE: ^a Number of rods is limited by HPI cavity size, as described in Section 6.3.1.1.1.

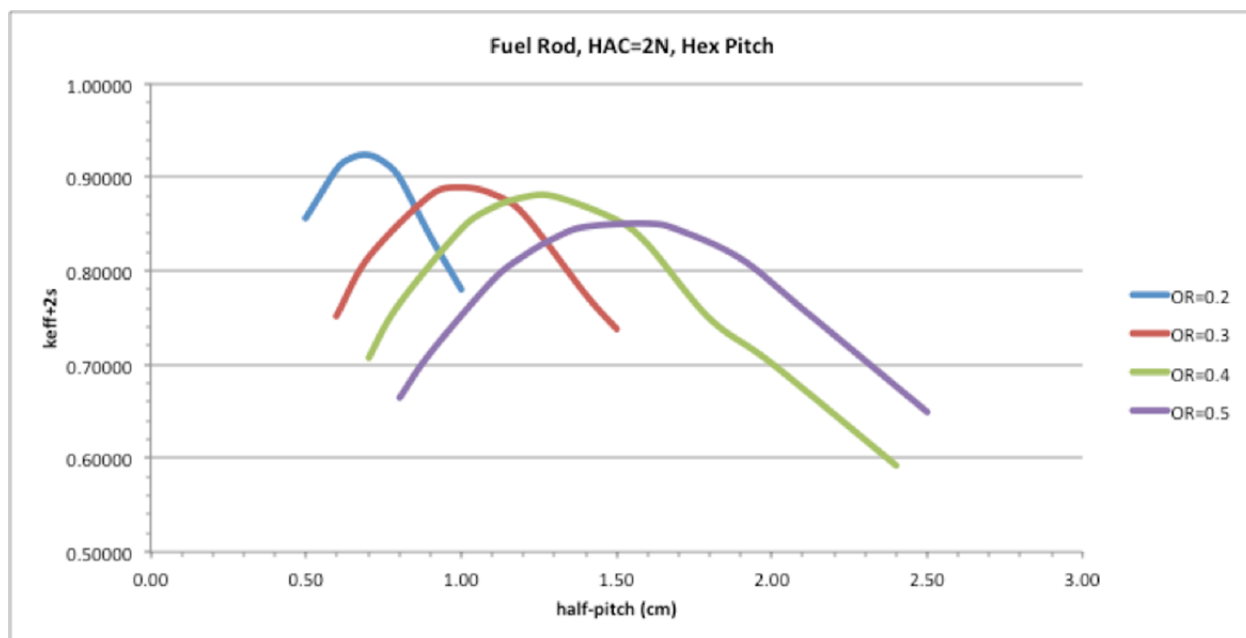


Figure 6.6.2-1. Fuel Rod Content, HAC 2N, Results

6.6.2.2. Fissile, Free Form Content

Cases for the HAC, 2N results for fissile, free form content, both U-235 and Pu-239 are provided in Table 6.6.2-2.

Parametric studies were completed to evaluate positioning the content sphere to the bottom of the HPI and varying the radius of the homogeneous, fissile sphere, thus varying the H/X ratio. Parametric study results are discussed in Section 6.9.4. The most limiting configurations are a homogeneous sphere with a radius nearly equivalent to the HPI cavity, and positioned at the bottom of the HPI cavity. The fissile mass is varied to determine the mass limit for subcriticality under the USL. An optimum H/X ratio is evaluated by also varying the sphere radius for the peak reactivity region.

For HAC 2N package array evaluation, fissile mass limits of 430 grams of 100 wt% U-235 and 265 grams of 100 wt% Pu-239 meet subcriticality under the USL.

Section 6.9.3 provides results for the U-233 and Pu-241 content. The most limiting cases for U-235 and Pu-239 content are highlighted in Table 6.6.2-2, where $k_{eff} + 2\sigma$ equals 0.93892 for the 430 grams, U-235 content and 0.93752 for the 265 grams, Pu-239 content.

Section 6.3.4 defines the USL value as 0.9406 for fissile, free form contents.

Table 6.6.2-2. Fissile, Free Form Content, HAC 2N, Maximum Cases

| Case Name | Sphere OR (cm) | Fissile Mass (g) | k_{eff} | σ | $k_{eff}+2\sigma$ | H/X | EALF (eV) |
|------------------|----------------|------------------|-----------|----------|-------------------|-----|-----------|
| U-235 | | | | | | | |
| 601HMH12_430btm | [[]] | 430 | 0.93484 | 0.00026 | 0.93536 | 481 | -- |
| 601HMH12p_430btm | 12.00 | 430 | 0.93830 | 0.00023 | 0.93876 | 438 | -- |
| 601HMH115_430btm | 11.50 | 430 | 0.93844 | 0.00024 | 0.93892 | 385 | 0.31967 |
| 601HMH11_430btm | 11.00 | 430 | 0.93114 | 0.00024 | 0.93162 | 337 | -- |
| 601HMH10_430btm | 10.00 | 450 | 0.90494 | 0.00023 | 0.90540 | 253 | -- |
| Pu-239 | | | | | | | |
| PHMH12btm_265 | [[]] | 265 | 0.93578 | 0.00023 | 0.93624 | 795 | -- |
| PHMH12pbtm_265 | 12.00 | 265 | 0.93696 | 0.00028 | 0.93752 | 724 | 0.53763 |
| PHMH115btm_265 | 11.50 | 265 | 0.93475 | 0.00029 | 0.93533 | 637 | -- |

6.7 Fissile Material Packages for Air Transport

The Model 2000 Transport Package will not be transported by air.

6.8 Benchmark Evaluations

This section describes the criticality benchmarks for application of MCNP6 (Reference 6-5) with the continuous-energy neutron data library ENDF/B-VII.1 (Reference 6-6) and USLSTATS to the Model 2000 Transport Package criticality safety analysis. The application range is the criticality safety analysis of the proposed contents, consisting of high-enriched free form uranium, free form plutonium, and low-enriched uranium fuel rods in the Model 2000 cask with the HPI.

USLSTATS is used to generate an acceptable USL for the criticality safety analysis. The USLSTATS computer program uses two methods (i.e., (1) confidence band with administrative margin and (2) single-sided uniform-width closed-interval) to calculate and print USL correlations based on a set of user-supplied k_{eff} values and corresponding values of a single associated parameter X (e.g., lattice pitch, fuel enrichment, average energy group causing fission (AEG)), for a set of criticality benchmark calculations.

6.8.1. Applicability of Benchmark Experiments

A total of 69 benchmark experiments were selected to represent the three different content configurations of the Model 2000 Transport Package: high-enriched free form uranium, free form plutonium, and low-enriched uranium fuel rods.

The high-enriched uranium configuration of the Model 2000 Transport Package modeled a homogeneous sphere consisting of 100 wt% U-235 and light water. Experiments that were chosen have U-235 weight percentages of approximately 93% with the uranium in the form of uranyl nitrate or uranium oxyfluoride solutions.

The plutonium configuration of the Model 2000 Transport Package modeled a homogeneous sphere consisting of 100 wt% Pu-239 and water. Experiments that were chosen have high percentages of Pu-239 (on the order of 95%), with other plutonium impurities and small percentages of Pu-241, in the form of plutonium nitrate solutions.

The low-enriched uranium rod lattice configuration of the Model 2000 Transport Package modeled uranium oxide (UO₂) rods with 6 wt% U-235 in hexagonally pitched lattices moderated with light water. No cladding was modeled. Experiments that were chosen have enrichments of either 2.35 wt% or 4.92 wt% U-235 as UO₂ rods in square pitched lattices submerged in light water. Reflectors consisted of steel, lead, or uranium with light water.

6.8.2. Bias Determination

6.8.2.1. Method

Section 4.1 of NUREG/CR-6361, Establishment of an Upper Subcritical Limit (Reference 6-8), explains two methods of determining the USL. The first method applies a statistical calculation of the bias and its uncertainty, plus an administrative margin, to a linear fit of critical experiment benchmark data, also known as Method 1: Confidence Band with Administrative Margin. In the second method, statistical techniques with a rigorous basis are applied in order to determine a combined lower confidence band plus subcritical margin, also known as Method 2: Single-Sided Uniform Width Closed Interval Approach. USLSTATS is a program that calculates USL correlations based on these methods. USLSTATS was used in this analysis in order to calculate the USL.

For this analysis, Method 1 is applied and Method 2 is used as a verification of Method 1 such that the USL function of Method 1 (USL₁) must be less than the USL function of Method 2 (USL₂). If the minimum margin of subcriticality, C*s(p) - W, is less than the administrative margin selected for Method 1, the administrative margin selected is sufficient, as this indicates that the administrative margin is larger than the statistical margin determined by Method 2.

6.8.2.2. Results

NUREG/CR-6361 mentions that the correlation between the trending parameter and the critical data is the primary criterion to select the parameter that will be utilized to determine the USL. The parameter with the highest correlation coefficient was used to develop the USL, which in this calculation was EALF for the highly enriched solution USL function, and H/U-235 for the low-enriched uranium USL function.

For the highly enriched Model 2000 Transport Package contents, the EALF trending parameter correlation coefficient, |r|, is equivalent to 0.2996, as shown in Table 6.8.2-1. For the low-enriched uranium lattice Model 2000 Transport Package contents, the H/U-235 trending parameter correlation coefficient, |r|, is equivalent to 0.3900. Therefore, the USL for highly enriched solution contents is 0.9406 and the USL for low-enriched uranium lattice contents is 0.9387, see Section 6.3.4 for additional details.

The results of the USLSTATS analyses are presented in Table 6.8.2-1. This table includes the USL functions, the applicable trending parameter range, the minimum margin of subcriticality (C*s(p) - W), which is the statistically based subcritical margin from the USL₂ calculation, and the Correlation Coefficient (r) of the trending parameter to the critical data.

Table 6.8.2-1. Model 2000 Transport Package Criticality Safety USL Functions

| Trending Parameter | USL Equation (Method 1) | Trending Parameter Range | C*s(p) – W (Method 2) | Correlation Coefficient (r) |
|-----------------------------------------|---------------------------------------------------------------------------|-----------------------------|-----------------------|-----------------------------|
| HIGHLY ENRICHED SOLUTION SYSTEMS | | | | |
| EALF (eV) | $0.9368 + 7.4863E-2 * X$ ($X < 0.0511$) 0.9406 ($X \geq 0.0511$) | $0.0324 \leq X \leq 0.0807$ | 1.6767E-2 | 0.2996 |
| LOW-ENRICHED LATTICE SYSTEMS | | | | |
| H/U-235 | $0.9473 - 1.5031E-5 * X$ ($X > 214.9$) 0.9441 ($X \leq 214.9$) | $105.5 \leq X \leq 256.3$ | 9.5216E-3 | -0.3900 |

The administrative margin, Δk_m , for these analyses was 0.05, which is greater than C*s(p) – W calculated for each trending parameter. This signifies the selected administrative margin is acceptable.

The following figures plot each trending parameter against k_{norm} . The first line plots the function $k_c(x)$, the line of fit to the critical data. The second line plots the function $k_c(x) - w(x)$, the line of fit of the critical data with a lower band of 95% confidence margin. The third line plots the function $k_c(x) - W$, the line of best fit of the critical data with the largest band of the 95% confidence margin from the second line, $k_c(x) - w(x)$, applied as a conservatism.

The USL₁ and USL₂ plots plateau at a certain constant value to not credit for positive biases in $k_c(x) - W$.

The USL function-defining trending parameter for highly enriched solutions was EALF, as shown in Figure 6.8.2-1. No values were below the lower confidence limit of the calculated critical values, $k_c(x) - W$. As the value of EALF increased, the value of k_{eff} increased. This resulted in a positive correlation between EALF and k_{eff} , with a coefficient of $r = 0.2996$, as shown in Table 6.8.2-1. This is the strongest correlation of the three trending parameters examined for highly enriched solution systems. Therefore, EALF was selected as the USL function-defining trending parameter for highly enriched solution systems.

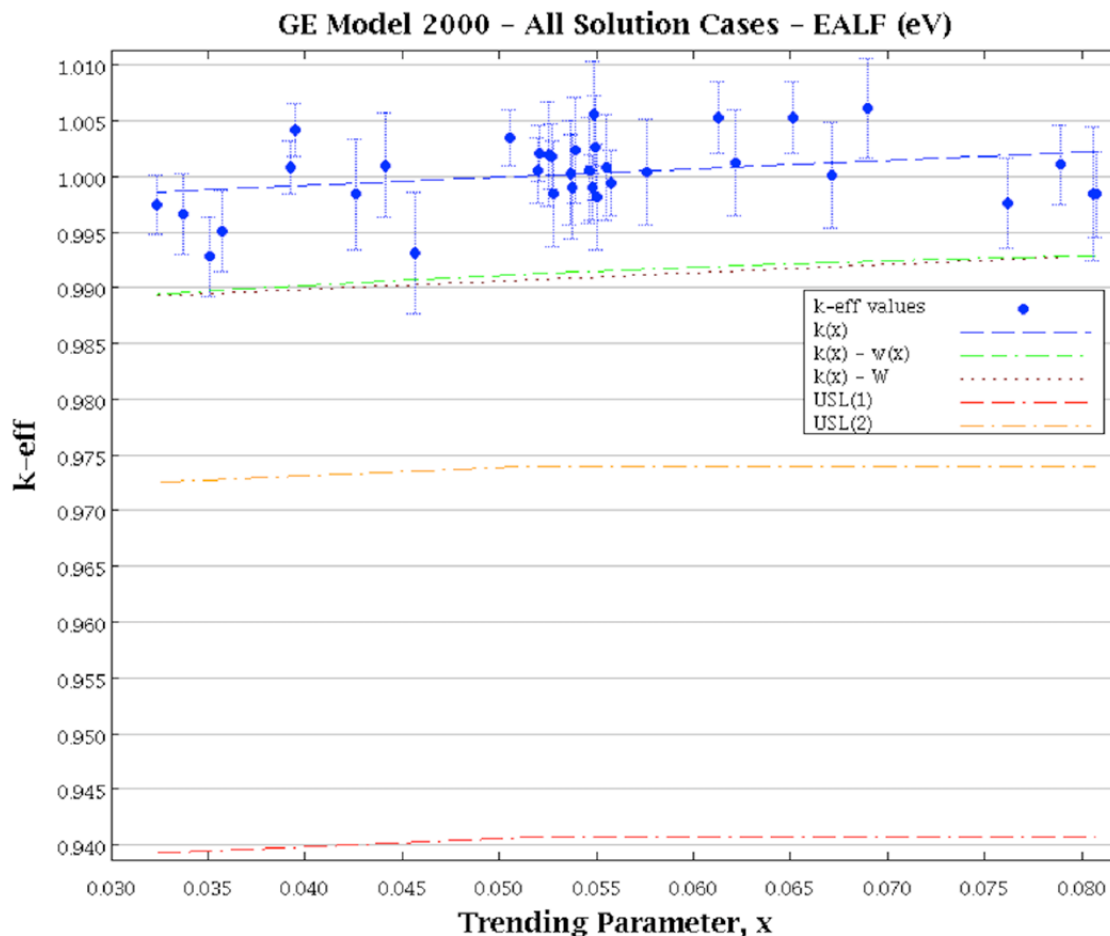


Figure 6.8.2-1. USLSTATS Trend Plot of EALF versus k_{norm} – Solution Systems

The USL function-defining trending parameter for low-enriched uranium lattices was H/U-235, as shown in Figure 6.8.2-2. None of the values were below the lower confidence limit, $k_c(x) - W$, of the calculated critical values. As the value of H/U-235 increased, the value of k_{norm} decreased. This resulted in a negative correlation between H/U-235 and k_{norm} , with a coefficient of $r = -0.3900$, as shown in Table 6.8.2-1. This is the strongest correlation of the three trending parameters examined for low-enriched uranium lattice systems. Therefore, H/U-235 was selected as the USL function-defining trending parameter for low-enriched uranium lattice systems.

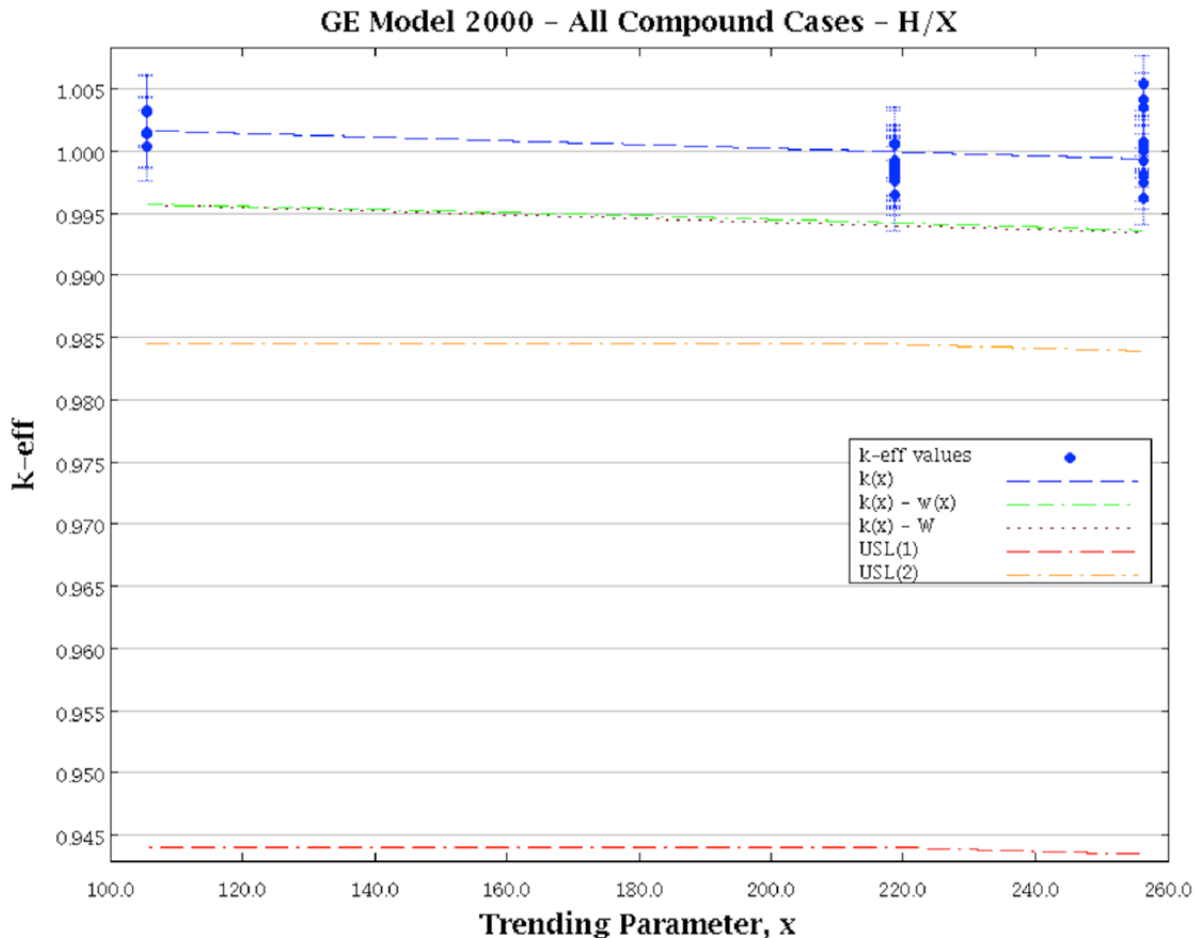


Figure 6.8.2-2. USLSTATS Trend Plot of H/U-235 versus k_{norm} – Lattice Systems

6.9 Appendices

6.9.1. Comparison of Modeled Fuel Rod Pitch

While the fuel rod content is limited by a mass of 1750 grams of U-235 at a maximum of 6 wt% U-235 enrichment, the modeling configuration may vary allowing for a slight variation in the H/U-235 ratio and thus affecting the system criticality. A hexagonal pitch results in tightly packed array of rods, which increases the view factor between rods in the array, while the square pitch results in a slightly higher H/U-235 ratio than a hexagonal pitch. The smallest fuel pellet OR, 0.2 cm, has shown to be the most reactive configuration for fuel rod contents. For a fuel pellet OR of 0.2 cm, the pitch comparison models a square lattice as well as a hexagonal lattice, as shown in Figure 6.9.1-1. Table 6.9.1-1 shows the results of the pitch comparison, and Figure 6.9.1-2 plots the results; full results are in Section 6.9.5, Tables 6.9.5-5 and 6.9.5-6. It can be seen that the optimum H/U-235 ratio that produces the maximum k_{eff} is different for each pitch type, however there are minimal differences between the maximum $k_{\text{eff}} + 2\sigma$ values ($0.92811 - 0.92398 = 0.00413$), and therefore a conservative 1.0% uncertainty is added to the final maximum $k_{\text{eff}} + 2\sigma$ values.

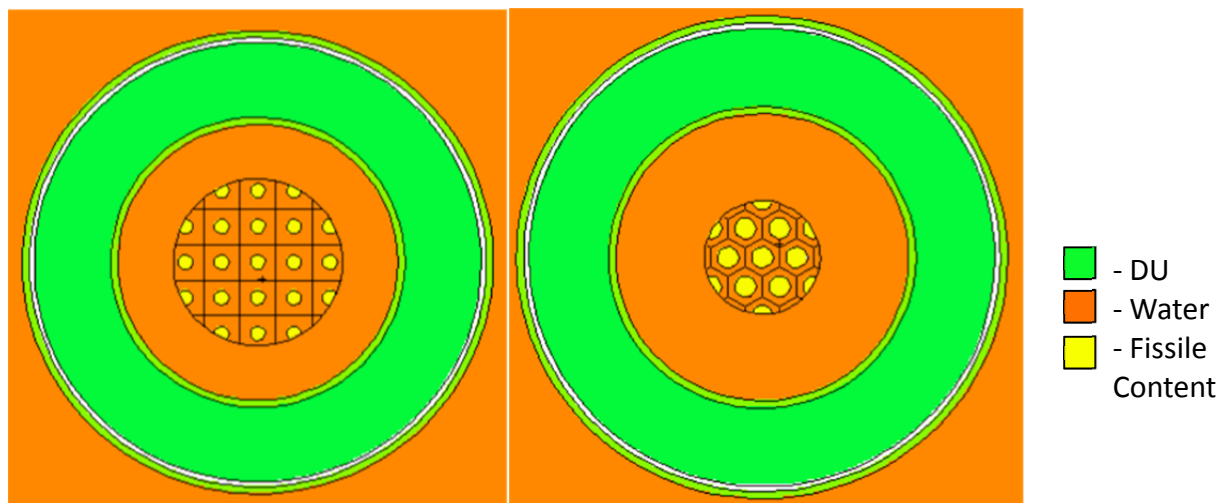


Figure 6.9.1-1. Fuel Rod Content Pitch Modeling Comparison (Not to Scale)

Table 6.9.1-1. Fissile Mass Content, HAC 2N, Maximum Cases

| Fuel OR | Half-pitch | k_{eff} | σ | $k_{eff} + 2\sigma$ | H/U-235 | Mass U-235 (g) | k_{eff} | σ | $k_{eff} + 2\sigma$ | H/U-235 | Mass U-235 (g) |
|---------|------------|----------------------|----------|---------------------|---------|----------------|-------------------------|----------|---------------------|---------|----------------|
| | | HAC 2N, square pitch | | | | | HAC 2N, hexagonal pitch | | | | |
| 0.2 | 0.50 | 0.88665 | 0.00023 | 0.88711 | 317 | 1821.65 | 0.85587 | 0.00026 | 0.85639 | 269 | 1821.65 |
| 0.2 | 0.60 | 0.92539 | 0.00024 | 0.92587 | 477 | 1821.65 | 0.90895 | 0.00025 | 0.90945 | 407 | 1821.65 |
| 0.2 | 0.65 | 0.92769 | 0.00021 | 0.92811 | 568 | 1821.65 | 0.92097 | 0.00022 | 0.92141 | 485 | 1821.65 |
| 0.2 | 0.7 | 0.91849 | 0.0002 | 0.91889 | 665 | 1821.65 | 0.9235 | 0.00024 | 0.92398 | 570 | 1821.65 |
| 0.2 | 0.75 | 0.89758 | 0.00019 | 0.89796 | 771 | 1821.65 | 0.91616 | 0.00025 | 0.91666 | 661 | 1821.65 |
| 0.2 | 0.8 | 0.86402 | 0.00021 | 0.86444 | 883 | 1644.62 | 0.89981 | 0.00021 | 0.90023 | 759 | 1644.62 |
| 0.2 | 0.9 | 0.79759 | 0.0002 | 0.79799 | 1130 | 1299.46 | 0.83686 | 0.00019 | 0.83724 | 972 | 1299.46 |
| 0.2 | 1.0 | 0.74015 | 0.00021 | 0.74057 | 1406 | 1052.56 | 0.78005 | 0.00019 | 0.78043 | 1211 | 1052.56 |

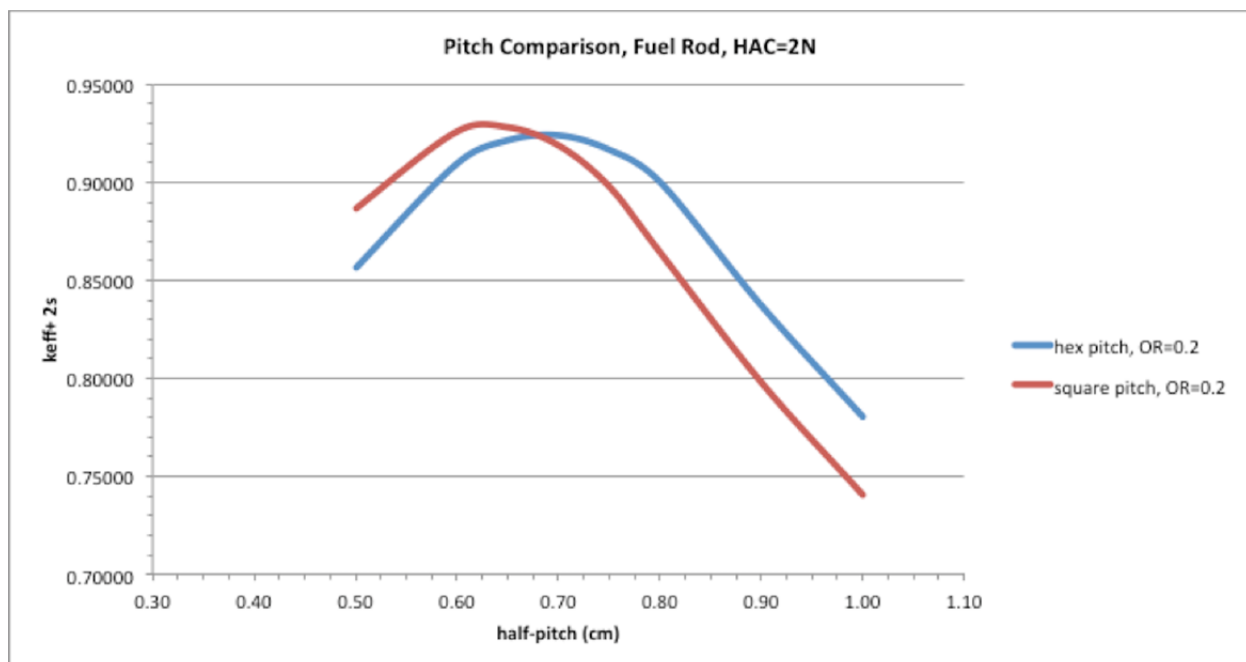


Figure 6.9.1-2. HAC, Fuel Rod Pitch Comparison

6.9.2. Benchmark Critical Experiments

Table 6.9.2-1 and Table 6.9.2-2 list the USLSTATS input data for each critical experiment. The critical benchmark experiments were created for MCNP6 using the benchmark specifications in each critical benchmark experiment report (Reference 6-9). The values of EALF are those determined by MCNP6. The ratio H/X and fuel enrichment were either reported in the critical benchmark experiment reports or were determined with hand calculations.

The values of k_{bench} and σ_{bench} are the reported effective multiplication factors and the 1σ statistical error from the critical benchmark experiment reports, respectively. The values of k_{calc} and σ_{calc} are the effective multiplication factor and the associated Monte Carlo 1σ determined by MCNP6, respectively. The USLSTATS input values of k and σ_{sample} for each critical experiment correspond to k_{norm} and σ_{total} in Table 6.9.2-1 and Table 6.9.2-2. The normalization of k , k_{norm} , is calculated as k_{calc} divided by k_{bench} :

$$k_{\text{norm}} = k_{\text{calc}} / k_{\text{bench}}$$

As the benchmark uncertainty and the calculated uncertainty are independent of each other, the total uncertainty, σ_{total} , was determined by combining the uncertainties using the square root of the sum of the squares:

$$\sigma_{\text{total}} = (\sigma_{\text{bench}}^2 + \sigma_{\text{calc}}^2)^{1/2}$$

Table 6.9.2-1. USLSTATS Input from Critical Benchmark Solution Experiments

| Case | EALF (eV) ¹ | H/X ² | Fissile Enrichment | k _{bench} | σ _{bench} | k _{calc} | σ _{calc} | k _{norm} | σ _{total} |
|--------------------------|------------------------|------------------|--------------------|--------------------|--------------------|-------------------|-------------------|-------------------|--------------------|
| <i>HEU-SOL-THERM-001</i> | | | | | | | | | |
| 1 | 8.0596E-02 | 181.8 | 93.17 | 1.0004 | 0.0060 | 0.99881 | 0.00064 | 0.99841 | 0.00603 |
| 3 | 7.8935E-02 | 185.7 | 93.17 | 1.0003 | 0.0035 | 1.00133 | 0.00059 | 1.00103 | 0.00355 |
| 5 | 4.2600E-02 | 499.4 | 93.17 | 1.0001 | 0.0049 | 0.99849 | 0.00053 | 0.99839 | 0.00493 |
| 6 | 4.4114E-02 | 458.8 | 93.17 | 1.0002 | 0.0046 | 1.00120 | 0.00056 | 1.00100 | 0.00463 |
| 7 | 7.6193E-02 | 193.3 | 93.17 | 1.0008 | 0.0040 | 0.99832 | 0.00064 | 0.99752 | 0.00405 |
| 8 | 8.0725E-02 | 181.8 | 93.17 | 0.9998 | 0.0038 | 0.99819 | 0.00062 | 0.99839 | 0.00385 |
| 10 | 4.5663E-02 | 427.4 | 93.17 | 0.9993 | 0.0054 | 0.99244 | 0.00056 | 0.99314 | 0.00543 |
| <i>HEU-SOL-THERM-010</i> | | | | | | | | | |
| 1 | 5.1975E-02 | 270.0 | 93.12 | 1.0000 | 0.0029 | 1.00048 | 0.00049 | 1.00048 | 0.00294 |
| 2 | 5.2748E-02 | 264.2 | 93.12 | 1.0000 | 0.0029 | 1.00178 | 0.00052 | 1.00178 | 0.00295 |
| 3 | 5.4837E-02 | 245.7 | 93.12 | 1.0000 | 0.0029 | 0.99898 | 0.00055 | 0.99898 | 0.00295 |
| 4 | 5.5775E-02 | 239.0 | 93.12 | 0.9992 | 0.0029 | 0.99861 | 0.00049 | 0.99941 | 0.00294 |
| <i>HEU-SOL-THERM-011</i> | | | | | | | | | |
| 1 | 3.9505E-02 | 523.4 | 93.18 | 1.0000 | 0.0023 | 1.00418 | 0.00048 | 1.00418 | 0.00235 |
| 2 | 3.9253E-02 | 533.1 | 93.18 | 1.0000 | 0.0023 | 1.00079 | 0.00042 | 1.00079 | 0.00234 |
| <i>HEU-SOL-THERM-013</i> | | | | | | | | | |
| 1 | 3.2346E-02 | 1375 | 93.18 | 1.0012 | 0.0036 | 0.99865 | 0.00032 | 0.99745 | 0.00361 |
| 2 | 3.3729E-02 | 1173 | 93.18 | 1.0007 | 0.0036 | 0.99728 | 0.00035 | 0.99658 | 0.00362 |
| 3 | 3.5084E-02 | 1030 | 93.18 | 1.0009 | 0.0036 | 0.99366 | 0.00036 | 0.99277 | 0.00362 |
| 4 | 3.5767E-02 | 971.1 | 93.18 | 1.0003 | 0.0036 | 0.99533 | 0.00035 | 0.99503 | 0.00362 |
| <i>PU-SOL-THERM-004</i> | | | | | | | | | |
| 1 | 5.2529E-02 | 987.0 | 99.46 | 1.0000 | 0.0047 | 1.00197 | 0.00043 | 1.00197 | 0.00472 |
| 2 | 5.2768E-02 | 976.9 | 99.46 | 1.0000 | 0.0047 | 0.99846 | 0.00045 | 0.99846 | 0.00472 |
| 3 | 5.3639E-02 | 934.6 | 99.46 | 1.0000 | 0.0047 | 1.00029 | 0.00044 | 1.00029 | 0.00472 |
| 4 | 5.5003E-02 | 888.9 | 99.46 | 1.0000 | 0.0047 | 0.99818 | 0.00045 | 0.99818 | 0.00472 |
| 5 | 5.3746E-02 | 942.0 | 98.24 | 1.0000 | 0.0047 | 0.99905 | 0.00045 | 0.99905 | 0.00472 |
| 6 | 5.3898E-02 | 927.4 | 96.88 | 1.0000 | 0.0047 | 1.00233 | 0.00046 | 1.00233 | 0.00472 |
| 7 | 5.4894E-02 | 891.7 | 96.88 | 1.0000 | 0.0047 | 1.00560 | 0.00045 | 1.00560 | 0.00472 |
| 8 | 5.5519E-02 | 869.0 | 96.88 | 1.0000 | 0.0047 | 1.00082 | 0.00041 | 1.00082 | 0.00472 |
| 9 | 5.7589E-02 | 805.2 | 96.88 | 1.0000 | 0.0047 | 1.00037 | 0.00046 | 1.00037 | 0.00472 |
| 10 | 6.2163E-02 | 689.4 | 96.88 | 1.0000 | 0.0047 | 1.00119 | 0.00042 | 1.00119 | 0.00472 |
| 11 | 6.7102E-02 | 592.4 | 96.88 | 1.0000 | 0.0047 | 1.00008 | 0.00050 | 1.00008 | 0.00473 |
| 12 | 5.4953E-02 | 892.8 | 96.88 | 1.0000 | 0.0047 | 1.00255 | 0.00046 | 1.00255 | 0.00472 |
| 13 | 5.4640E-02 | 903.1 | 96.57 | 1.0000 | 0.0047 | 1.00049 | 0.00043 | 1.00049 | 0.00472 |
| <i>PU-SOL-THERM-021</i> | | | | | | | | | |
| 1 | 6.5161E-02 | 699.6 | 95.31 | 1.0000 | 0.0032 | 1.00529 | 0.00056 | 1.00529 | 0.00325 |
| 2 | 6.1306E-02 | 795.3 | 95.31 | 1.0000 | 0.0032 | 1.00530 | 0.00052 | 1.00530 | 0.00324 |
| 4 | 5.2063E-02 | 1082 | 95.31 | 1.0000 | 0.0025 | 1.00202 | 0.00043 | 1.00202 | 0.00254 |
| 5 | 5.0550E-02 | 1121 | 95.31 | 1.0000 | 0.0025 | 1.00345 | 0.00046 | 1.00345 | 0.00254 |
| 6 | 6.8967E-02 | 579.4 | 95.31 | 1.0000 | 0.0044 | 1.00608 | 0.00048 | 1.00608 | 0.00443 |

NEDO-33866 Revision 0
Non-Proprietary Information – Class I (Public)

NOTES: ¹ As calculated in MCNP6.

² H/X includes U-235 as X for uranium systems and the sum of Pu-239 and Pu-241 as X for plutonium systems. H/X determined through hand calculations.

Table 6.9.2-2. USLSTATS Input from Critical Benchmark Lattice Experiments

| Case | EALF (eV) ¹ | H/X ² | Fissile Enrichment | M/F Ratio ³ | k _{bench} | σ _{bench} | k _{calc} | σ _{calc} | k _{norm} | σ _{total} |
|---------------------------|------------------------|------------------|--------------------|------------------------|--------------------|--------------------|-------------------|-------------------|-------------------|--------------------|
| <i>LEU-COMP-THERM-010</i> | | | | | | | | | | |
| 1 | 1.2060E-01 | 256.3 | 4.306 | 3.882 | 1.0000 | 0.0021 | 1.00421 | 0.00041 | 1.00421 | 0.00214 |
| 2 | 1.1800E-01 | 256.3 | 4.306 | 3.882 | 1.0000 | 0.0021 | 1.00547 | 0.00043 | 1.00547 | 0.00214 |
| 3 | 1.1616E-01 | 256.3 | 4.306 | 3.882 | 1.0000 | 0.0021 | 1.00347 | 0.00044 | 1.00347 | 0.00215 |
| 4 | 1.1301E-01 | 256.3 | 4.306 | 3.882 | 1.0000 | 0.0021 | 0.99625 | 0.00041 | 0.99625 | 0.00214 |
| 5 | 3.5938E-01 | 256.3 | 4.306 | 3.882 | 1.0000 | 0.0021 | 0.99921 | 0.00039 | 0.99921 | 0.00214 |
| 6 | 2.6608E-01 | 256.3 | 4.306 | 3.882 | 1.0000 | 0.0021 | 1.00040 | 0.00045 | 1.00040 | 0.00215 |
| 7 | 2.1245E-01 | 256.3 | 4.306 | 3.882 | 1.0000 | 0.0021 | 1.00059 | 0.00038 | 1.00059 | 0.00213 |
| 8 | 1.8807E-01 | 256.3 | 4.306 | 3.882 | 1.0000 | 0.0021 | 0.99816 | 0.00041 | 0.99816 | 0.00214 |
| 9 | 1.2527E-01 | 256.3 | 4.306 | 3.882 | 1.0000 | 0.0021 | 0.99928 | 0.00045 | 0.99928 | 0.00215 |
| 10 | 1.2121E-01 | 256.3 | 4.306 | 3.882 | 1.0000 | 0.0021 | 1.00071 | 0.00044 | 1.00071 | 0.00215 |
| 11 | 1.1912E-01 | 256.3 | 4.306 | 3.882 | 1.0000 | 0.0021 | 1.00038 | 0.00043 | 1.00038 | 0.00214 |
| 12 | 1.1533E-01 | 256.3 | 4.306 | 3.882 | 1.0000 | 0.0021 | 1.00002 | 0.00043 | 1.00002 | 0.00214 |
| 13 | 1.1337E-01 | 256.3 | 4.306 | 3.882 | 1.0000 | 0.0021 | 0.99745 | 0.00043 | 0.99745 | 0.00214 |
| 20 | 2.9977E-01 | 105.5 | 4.306 | 1.597 | 1.0000 | 0.0028 | 1.00328 | 0.00045 | 1.00328 | 0.00284 |
| 21 | 2.9155E-01 | 105.5 | 4.306 | 1.597 | 1.0000 | 0.0028 | 1.00326 | 0.00046 | 1.00326 | 0.00284 |
| 22 | 2.7989E-01 | 105.5 | 4.306 | 1.597 | 1.0000 | 0.0028 | 1.00318 | 0.00044 | 1.00318 | 0.00283 |
| 23 | 2.7305E-01 | 105.5 | 4.306 | 1.597 | 1.0000 | 0.0028 | 1.00147 | 0.00047 | 1.00147 | 0.00284 |
| 24 | 6.0531E-01 | 105.5 | 4.306 | 1.597 | 1.0000 | 0.0028 | 1.00041 | 0.00042 | 1.00041 | 0.00283 |
| 25 | 5.5810E-01 | 105.5 | 4.306 | 1.597 | 1.0000 | 0.0028 | 1.00153 | 0.00045 | 1.00153 | 0.00284 |
| 26 | 5.1886E-01 | 105.5 | 4.306 | 1.597 | 1.0000 | 0.0028 | 1.00143 | 0.00042 | 1.00143 | 0.00283 |
| 27 | 4.8592E-01 | 105.5 | 4.306 | 1.597 | 1.0000 | 0.0028 | 1.00315 | 0.00045 | 1.00315 | 0.00284 |
| <i>LEU-COMP-THERM-017</i> | | | | | | | | | | |
| 15 | 1.8165E-01 | 218.7 | 2.35 | 1.600 | 1.0000 | 0.0028 | 0.99830 | 0.00040 | 0.99830 | 0.00283 |
| 16 | 1.7571E-01 | 218.7 | 2.35 | 1.600 | 1.0000 | 0.0028 | 0.99839 | 0.00038 | 0.99839 | 0.00283 |
| 17 | 1.7054E-01 | 218.7 | 2.35 | 1.600 | 1.0000 | 0.0028 | 1.00044 | 0.00041 | 1.00044 | 0.00283 |
| 18 | 1.6926E-01 | 218.7 | 2.35 | 1.600 | 1.0000 | 0.0028 | 0.99894 | 0.00041 | 0.99894 | 0.00283 |
| 19 | 1.6610E-01 | 218.7 | 2.35 | 1.600 | 1.0000 | 0.0028 | 0.99882 | 0.00040 | 0.99882 | 0.00283 |
| 20 | 1.6510E-01 | 218.7 | 2.35 | 1.600 | 1.0000 | 0.0028 | 0.99878 | 0.00039 | 0.99878 | 0.00283 |
| 21 | 1.6365E-01 | 218.7 | 2.35 | 1.600 | 1.0000 | 0.0028 | 0.99811 | 0.00041 | 0.99811 | 0.00283 |
| 22 | 1.6197E-01 | 218.7 | 2.35 | 1.600 | 1.0000 | 0.0028 | 0.99761 | 0.00037 | 0.99761 | 0.00282 |
| 23 | 1.7286E-01 | 218.7 | 2.35 | 1.600 | 1.0000 | 0.0028 | 0.99927 | 0.00041 | 0.99927 | 0.00283 |
| 24 | 1.6843E-01 | 218.7 | 2.35 | 1.600 | 1.0000 | 0.0028 | 1.00066 | 0.00041 | 1.00066 | 0.00283 |
| 25 | 1.6103E-01 | 218.7 | 2.35 | 1.600 | 1.0000 | 0.0028 | 0.99879 | 0.00038 | 0.99879 | 0.00283 |
| 26 | 3.8015E-01 | 218.7 | 2.35 | 1.600 | 1.0000 | 0.0028 | 0.99647 | 0.00039 | 0.99647 | 0.00283 |
| 27 | 3.2488E-01 | 218.7 | 2.35 | 1.600 | 1.0000 | 0.0028 | 0.99816 | 0.00036 | 0.99816 | 0.00282 |
| 28 | 2.8541E-01 | 218.7 | 2.35 | 1.600 | 1.0000 | 0.0028 | 0.99897 | 0.00039 | 0.99897 | 0.00283 |
| 29 | 2.5582E-01 | 218.7 | 2.35 | 1.600 | 1.0000 | 0.0028 | 0.99916 | 0.00037 | 0.99916 | 0.00282 |

NOTES: ¹ As calculated in MCNP6.

² H/X includes U-235 as X for uranium systems. H/X determined through hand calculations.

³ M/F ratio determined through hand calculations.

For all the benchmark experiments, the following key input data for MCNP6 were the minimum values used in order to verify convergence of the cases:

- Neutrons per cycle: 10,000
- Number of skipped cycles: 50
- Total number of cycles: 350

This resulted in a total of 3,000,000 neutron histories analyzed per case. Convergence of the results was verified through inspection of both the Shannon entropy of the fission source distribution and the plot of k_{eff} versus cycle number for each case.

6.9.3. SNM Equivalence Analysis

This section documents the evaluation of fissile isotopes U-233, Pu-239, and Pu-241 for calculating special nuclear material equivalency to U-235 mass.

To assess the mass limit for the U-233 and Pu-241 fissile isotopes, the HAC 2N, single package, NCT 5N package array limiting models for fissile, free form content is used. The model is represented by a homogeneous mixture of fissile material and water in a homogeneous sphere, positioned at the bottom of the HPI cavity. An optimum H/X ratio is evaluated by varying the sphere radius for the peak reactivity region. U-233 and Pu-241 are evaluated for additional contents. Material properties are provided in Table 6.9.3-1. Several fissile masses and sphere radii are evaluated until subcriticality under the USL is met for the limiting case. Results in Tables 6.9.3-2, 6.9.3-3, and 6.9.3-4 show the HAC 2N package array, single package, and NCT 5N package array, respectively, $k_{\text{eff}}+2\sigma$ results are under the USL for a limiting mass of 315 grams of U-233 and 150 grams of Pu-241. The USL for the high enriched systems is defined as 0.9406, per Section 6.3.4.

Table 6.9.3-1. Nuclear Properties of Fissile Content

| Element | Isotope | Neutron ZA | Mass Fraction | Density (g/cm ³) |
|------------------------------|---------|------------|---------------|------------------------------|
| U-233 Metal, 100 wt% U-233 | U-233 | 92233 | 1.0000E0 | 19.05 ¹ |
| Pu-241 Metal, 100 wt% Pu-241 | Pu-241 | 94241 | 1.0000E0 | 19.84 ² |

NOTE: ¹ Reference 6-4 Density, Table M8.2.2; ²Reference 6-3 Density, Page 235.

Table 6.9.3-2. Fissile, Free Form Content Summary, HAC 2N Package Array

| Case Name | Case | Sphere OR (cm) | k_{eff} | σ | $k_{\text{eff}} + 2\sigma$ (maximum k_{eff}) | Fissile Mass (g) | H/X | EALF (eV) |
|-------------------|--------|----------------|------------------|----------|--------------------------------------------------------|------------------|------|-----------|
| U-233 | | | | | | | | |
| U233HMH12_315btm | HAC 2N | [[]] | 0.92108 | 0.00023 | 0.92154 | 315 | 651 | -- |
| U233HMH12p_315btm | | [[]] | 0.93082 | 0.00026 | 0.93134 | 315 | 593 | -- |
| U233HMH115_315tm | | [[]] | 0.93836 | 0.00025 | 0.93886 | 315 | 522 | -- |
| U233HMH11_315btm | | [[]] | 0.93985 | 0.00026 | 0.94037 | 315 | 457 | 0.41720 |
| U233HMH10_315btm | | [[]] | 0.92823 | 0.00025 | 0.92873 | 315 | 343 | -- |
| U233HMH9_315btm | | [[]] | 0.90147 | 0.00027 | 0.90201 | 315 | 249 | -- |
| Pu-241 | | | | | | | | |
| P241HMH12btm_150 | HAC 2N | [[]] | 0.91833 | 0.00023 | 0.91879 | 150 | 1417 | -- |
| P241HMH12pbtm_150 | | [[]] | 0.92675 | 0.00022 | 0.92719 | 150 | 1417 | -- |
| P241HMH115btm_150 | | [[]] | 0.93170 | 0.00027 | 0.93224 | 150 | 1135 | 0.47149 |
| P241HMH11btm_150 | | [[]] | 0.93139 | 0.00025 | 0.93189 | 150 | 993 | -- |
| P241HMH10btm_150 | | [[]] | 0.91574 | 0.00026 | 0.91626 | 150 | 746 | -- |
| P241HMH9btm_150 | | [[]] | 0.8854 | 0.00026 | 0.88592 | 150 | 543 | -- |

Table 6.9.3-3. Fissile, Free Form Content Summary, Single Package

| Case Name | Case | Sphere OR (cm) | k _{eff} | σ | k _{eff} + 2σ (maximum k _{eff}) | Fissile Mass (g) | H/X | EALF (eV) |
|-------------------|-------------------|----------------------|------------------|---------|---------------------------------------------------------|------------------------|------|--------------|
| U-233 | | | | | | | | |
| U233HMS115_315tm | Single Package | [[]] | 0.93825 | 0.00024 | 0.93873 | 315 | 522 | -- |
| U233HMS11_315btm | | [[]] | 0.93949 | 0.00022 | 0.93993 | 315 | 457 | 0.41625 |
| U233HMS10_315btm | | [[]] | 0.92833 | 0.00026 | 0.92885 | 315 | 343 | -- |
| Pu-241 | | | | | | | | |
| P241HMS12pbtm_150 | Single Package | [[]] | 0.92681 | 0.00027 | 0.92735 | 150 | 1417 | -- |
| P241HMS115btm_150 | | [[]] | 0.93188 | 0.00028 | 0.93244 | 150 | 1135 | 0.47000 |
| P241HMS11btm_150 | | [[]] | 0.93065 | 0.00032 | 0.93129 | 150 | 993 | -- |

Table 6.9.3-4. Fissile, Free Form Content Summary, NCT 5N Package Array

| Case Name | Case | Sphere OR (cm) | k _{eff} | σ | k _{eff} + 2σ (maximum k _{eff}) | Fissile Mass (g) | H/X | EALF (eV) |
|-------------------|--------|----------------|------------------|---------|---------------------------------------------------|------------------|------|-----------|
| U-233 | | | | | | | | |
| U233HMN12_315tm | NCT 5N | [[]] | 0.91548 | 0.00026 | 0.91600 | 315 | 651 | -- |
| U233HMN12p_315tm | | [[]] | 0.92600 | 0.00027 | 0.92654 | 315 | 593 | -- |
| U233HMN115_315btm | | [[]] | 0.93284 | 0.00026 | 0.93336 | 315 | 522 | 0.40488 |
| U233HMN11_315btm | | [[]] | 0.93433 | 0.00028 | 0.93489 | 315 | 457 | -- |
| Pu-241 | | | | | | | | |
| P241HMN12pbtm_150 | NCT 5N | [[]] | 0.91267 | 0.00028 | 0.91323 | 150 | 1417 | -- |
| P241HMN12pbtm_150 | | [[]] | 0.92120 | 0.00028 | 0.92176 | 150 | 1290 | -- |
| P241HMN115btm_150 | | [[]] | 0.92676 | 0.00028 | 0.92732 | 150 | 1135 | 0.46196 |
| P241HMN11btm_150 | | [[]] | 0.92639 | 0.00030 | 0.92699 | 150 | 993 | -- |

To express the combined mass of several fissile isotopes as an equivalent amount of U-235, the following equation is used:

$$\text{equivalent U-235 mass} = a_i MR_{235}$$

where,

$$MR_{235} = \frac{A_{235}}{A_i} \text{ is the mass ratio of U-235 to isotope } i$$

A_{235} is the approved mass of 430 grams for U-235 (per Table 6.1.2-2)

a_{235} is the defined content mass for U-235

A_i is the approved mass for isotope i , assured to be subcritical (i.e., U-233, Pu-239, and Pu-241)

a_i is the defined content mass for isotope i

Using the limiting mass values of 265 grams for Pu-239 (see Table 6.1.2-2), 315 grams for U-233 (see Table 6.9.3-2), 150 g for Pu-241 (see Table 6.9.3-2), the special nuclear material U-235 equivalent mass can be calculated. Thus, the U-235 equivalent mass is defined as follows:

- 1.63 times the Pu-239 Content mass, (1.6226 = 430 grams U-235/265 grams Pu-239)
- 1.37 times the U-233 Content mass (1.3651 = 430 grams U-235/315 grams U-233)
- 2.87 times the Pu-241 Content mass (2.8667 = 430 grams U-235/150 grams Pu-241).

6.9.4. Parametric Studies

6.9.4.1. Single Package

6.9.4.1.1. Fissile, Free Form Content, Sphere Radius and Position

Parametric studies were completed to evaluate positioning the content sphere to the bottom of the HPI and varying the radius of the homogeneous, fissile sphere, for the single package assessment of Section 6.4.

The first parametric study evaluates the fissile, free form material modeled as a sphere, varying radius based on the amount of water present in the homogeneous mixture. By increasing the homogeneous mixture radius while holding the fissile mass constant, the mass of moderation

increases, thus increasing H/X. Radii evaluated include [[]], 11, 10, 9, 8, 7, 6, 5, 4, 3, and 2 cm, as well as the sphere radius equivalent to the pure metal mass and density. For the sphere radius parametric study, the fissile mass is modeled 100 wt% U-235 with a mass of 500 grams and 100 wt% Pu-239 with a mass of 300 grams.

Cases for single package, fissile, free form content, both U-235 and Pu-239 results are provided in Table 6.9.4-1. Figure 6.9.4-1 displays the trends for the parametric study of the sphere radius for both U-235 and Pu-239. The sphere radius study shows that as the H/X ratio is decreased the general trend is for decreasing reactivity, with the optimum H/X ratio near the size of the HPI cavity.

The second parametric study evaluated positioning of the content sphere in the center of the HPI cavity and at the bottom of the HPI cavity, where the DU shield is thickest, thus increasing any additional close reflection. For the positioning parametric study, the fissile mass is modeled 100 wt% U-235 with a mass of 425 g. The results are in Table 6.9.4-2, with *btm* identified in the case name, where it is shown positioning the sphere on the bottom of the HPI cavity produces an increase in reactivity.

The limiting configurations, sphere radius near equivalent to the HPI cavity and positioned at the bottom of the HPI cavity, provide the basis for the model evaluated in Section 6.4.

[[

]]

Figure 6.9.4-1. Fissile, Free Form Content, Single Package, Sphere Radius Study

Table 6.9.4-1. Fissile, Free Form Content, Single Package, Sphere Radius Study

| Case Name | Sphere OR (cm) | Fissile Mass (g) | k_{eff} | σ | $k_{eff}+2\sigma$ |
|-----------|----------------|------------------|-----------|----------|-------------------|
| U-235 | | | | | |
| 601HMS_12 | [[]] | 500 | 0.95336 | 0.00025 | 0.95386 |
| 601HMS_11 | 11.00 | 500 | 0.94662 | 0.00024 | 0.94710 |
| 601HMS_10 | 10.00 | 500 | 0.91965 | 0.00023 | 0.92011 |
| 601HMS_9 | 9.00 | 500 | 0.87415 | 0.00025 | 0.87465 |
| 601HMS_8 | 8.00 | 500 | 0.81331 | 0.00059 | 0.81449 |
| 601HMS_7 | 7.00 | 500 | 0.73930 | 0.00026 | 0.73982 |
| 601HMS_6 | 6.00 | 500 | 0.65451 | 0.00026 | 0.65503 |
| 601HMS_5 | 5.00 | 500 | 0.56537 | 0.00024 | 0.56585 |
| 601HMS_4 | 4.00 | 500 | 0.48350 | 0.00018 | 0.48386 |
| 601HMS_3 | 3.00 | 500 | 0.43543 | 0.00015 | 0.43573 |
| 601HMS_2 | 2.00 | 500 | 0.42393 | 0.00013 | 0.42419 |
| 601HMS_1 | 1.8436 | 500 | 0.42371 | 0.00013 | 0.42397 |
| Pu-239 | | | | | |
| PHMS12 | [[]] | 300 | 0.94638 | 0.00026 | 0.94690 |
| PHMS11 | 11.00 | 300 | 0.93440 | 0.00030 | 0.93500 |
| PHMS10 | 10.00 | 300 | 0.90385 | 0.00030 | 0.90445 |
| PHMS9 | 9.00 | 300 | 0.85635 | 0.00030 | 0.85695 |
| PHMS8 | 8.00 | 300 | 0.79283 | 0.00052 | 0.79387 |
| PHMS7 | 7.00 | 300 | 0.71951 | 0.00031 | 0.72013 |
| PHMS6 | 6.00 | 300 | 0.63696 | 0.00024 | 0.63744 |
| PHMS5 | 5.00 | 300 | 0.55179 | 0.00025 | 0.55229 |
| PHMS4 | 4.00 | 300 | 0.47731 | 0.00020 | 0.47771 |
| PHMS3 | 3.00 | 300 | 0.43465 | 0.00016 | 0.43497 |
| PHMS2 | 2.00 | 300 | 0.42469 | 0.00017 | 0.42503 |
| PHMS1 | 1.5340 | 300 | 0.43302 | 0.00016 | 0.43334 |

Table 6.9.4-2. Fissile, Free Form Content, Single Package, Positioning Study

| Case Name | Sphere Position | Sphere OR (cm) | Fissile Mass (g) | k_{eff} | σ | $k_{eff}+2\sigma$ |
|------------------|------------------------|----------------|------------------|-----------|----------|-------------------|
| U-235 | | | | | | |
| 601HMS_12_425 | Centered in HPI cavity | [[]] | 425 | 0.92074 | 0.00025 | 0.92124 |
| 601HMS_12_425btm | Bottom of HPI cavity | [[]] | 425 | 0.93213 | 0.00025 | 0.93263 |

6.9.4.2 HAC, 2N

6.9.4.1.2. Fissile, Free Form Content, Sphere Radius and Position

Parametric studies were completed to evaluate positioning the content sphere to the bottom of the HPI and varying the radius of the homogeneous, fissile sphere, for the HAC package array assessment of Section 6.6.

The first parametric study evaluates the fissile, free form material modeled as a sphere, varying radius based on the amount of water present in the homogeneous mixture. By increasing the homogeneous mixture radius while holding the fissile mass constant, the mass of moderation increases, thus increasing H/X. Radii evaluated include [], 11, 10, 9, 8, 7, 6, 5, 4, 3, and 2 cm, as well as the sphere radius equivalent to the pure metal mass and density. For the sphere radius parametric study, the fissile mass is modeled 100 wt% U-235 with a mass of 500 grams and 100 wt% Pu-239 with a mass of 300 grams.

Cases for HAC package array, fissile, free form content, both U-235 and Pu-239 results are provided in Table 6.9.4-3. Figure 6.9.4-2 displays the trends for the parametric study of the sphere radius for both U-235 and Pu-239. The sphere radius study shows that as the H/X ratio is decreased the general trend is for decreasing reactivity, with the optimum H/X ratio near the size of the HPI cavity.

The second parametric study evaluated positioning of the content sphere in the center of the HPI cavity and at the bottom of the HPI cavity, where the DU shield is thickest, thus increasing any additional close reflection. For the positioning parametric study, the fissile mass is modeled 100 wt% U-235 with a mass of 425 g. The results are in Table 6.9.4-4, with *btm* identified in the case name, where it is shown positioning the sphere on the bottom of the HPI cavity produces an increase in reactivity.

The limiting configurations, sphere radius near equivalent to the HPI cavity and positioned at the bottom of the HPI cavity, provide the basis for the model evaluated in Section 6.6.

[[

]]

Figure 6.9.4-2. Fissile, Free Form Content, HAC 2N, Sphere Radius Study

Table 6.9.4-3. Fissile, Free Form Content, HAC 2N, Sphere Radius Study

| Case Name | Sphere OR (cm) | Fissile Mass (g) | k_{eff} | σ | $k_{eff}+2\sigma$ |
|-----------|----------------|------------------|-----------|----------|-------------------|
| U-235 | | | | | |
| 601HMH12 | [[]] | 500 | 0.95330 | 0.00024 | 0.95378 |
| 601HMH11 | 11.00 | 500 | 0.94279 | 0.00027 | 0.94333 |
| 601HMH10 | 10.00 | 500 | 0.91209 | 0.00026 | 0.91261 |
| 601HMH9 | 9.00 | 500 | 0.86799 | 0.00024 | 0.86847 |
| 601HMH8 | 8.00 | 500 | 0.81044 | 0.00025 | 0.81094 |
| 601HMH7 | 7.00 | 500 | 0.74192 | 0.00025 | 0.74242 |
| 601HMH6 | 6.00 | 500 | 0.66512 | 0.00025 | 0.66562 |
| 601HMH5 | 5.00 | 500 | 0.58333 | 0.00023 | 0.58379 |
| 601HMH4 | 4.00 | 500 | 0.50732 | 0.00019 | 0.50770 |
| 601HMH3 | 3.00 | 500 | 0.45279 | 0.00015 | 0.45309 |
| 601HMH2 | 2.00 | 500 | 0.43031 | 0.00014 | 0.43059 |
| 601HMH1 | 1.8436 | 500 | 0.43030 | 0.00014 | 0.43058 |
| Pu-239 | | | | | |
| PHMH12 | [[]] | 300 | 0.94697 | 0.00030 | 0.94757 |
| PHMH11 | 11.00 | 300 | 0.93038 | 0.00029 | 0.93096 |
| PHMH10 | 10.00 | 300 | 0.89862 | 0.00026 | 0.89914 |
| PHMH9 | 9.00 | 300 | 0.85013 | 0.00028 | 0.85069 |
| PHMH8 | 8.00 | 300 | 0.79146 | 0.00030 | 0.79206 |
| PHMH7 | 7.00 | 300 | 0.72350 | 0.00030 | 0.72410 |
| PHMH6 | 6.00 | 300 | 0.64900 | 0.00028 | 0.64956 |
| PHMH5 | 5.00 | 300 | 0.57132 | 0.00024 | 0.57180 |
| PHMH4 | 4.00 | 300 | 0.50126 | 0.00021 | 0.50168 |
| PHMH3 | 3.00 | 300 | 0.45112 | 0.00018 | 0.45148 |
| PHMH2 | 2.00 | 300 | 0.43209 | 0.00016 | 0.43241 |
| PHMH1 | 1.5340 | 300 | 0.44919 | 0.00017 | 0.44953 |

Table 6.9.4-4. Fissile, Free Form Content, HAC 2N, Positioning Study

| Case Name | Sphere Position | Sphere OR (cm) | Fissile Mass (g) | k_{eff} | σ | $k_{eff}+2\sigma$ |
|-----------------|------------------------|----------------|------------------|-----------|----------|-------------------|
| U-235 | | | | | | |
| 601HMH12_425 | Centered in HPI cavity | [[]] | 425 | 0.92055 | 0.00023 | 0.92101 |
| 601HMH12_425btm | Bottom of HPI cavity | [[]] | 425 | 0.93242 | 0.00021 | 0.93284 |

6.9.4.1.3. Moderation

The moderator density is varied from 0 to 1.0 g/cm³ within the HPI cavity region and the Model 2000 cask region. The moderation space is defined as all available space within the cavities, not including any space with lead or DU shielding. The fissile content region is maintained fully flooded with full density water for both contents. The k_{eff} result for the single package and package array (NCT and HAC) are very similar, indicating the shield materials of the HPI and cask provide strong reflection, thus neutronically isolating each package within the

array. Therefore full density water moderation between the packages is maintained to further increase reflection within the package.

Fuel Rod Content

The moderator density is varied for the peak case of the fuel rod content results in Table 6.6.2-1, FRLAHmh_1_22 (OR=0.2 cm, hex, half-pitch=0.7 cm). The HPI and cask cavity moderator densities are varied independently. Peak cases for fuel rod content are provided in Table 6.9.4-5. Figure 6.9.4-3 displays the trends for all data. Based on the most limiting case, FRLAHmh_1_22w_1_9 (HPI cavity moderator density=1 g/cm³, cask cavity moderator density=0 g/cm³), $k_{\text{eff}} + 2\sigma$ equals 0.92413, as compared to the full density flooded HAC, package array base case of $k_{\text{eff}} + 2\sigma$ equal to 0.92398 (FRLAHmh_1_22w_9_9). The reflection from the DU HPI shields provides the dominant increase in neutron interaction within a package, while varying the water moderation within the HPI and cask cavity provides statistically similar or reduced package system reactivity. Results of the HAC package array base case (FRLAHmh_1_22) and the most limiting case here (FRLAHmh_1_22w_1_9) are statistically indifferent. Therefore, no additional uncertainty is added to the final, maximum k_{eff} for moderation variation.

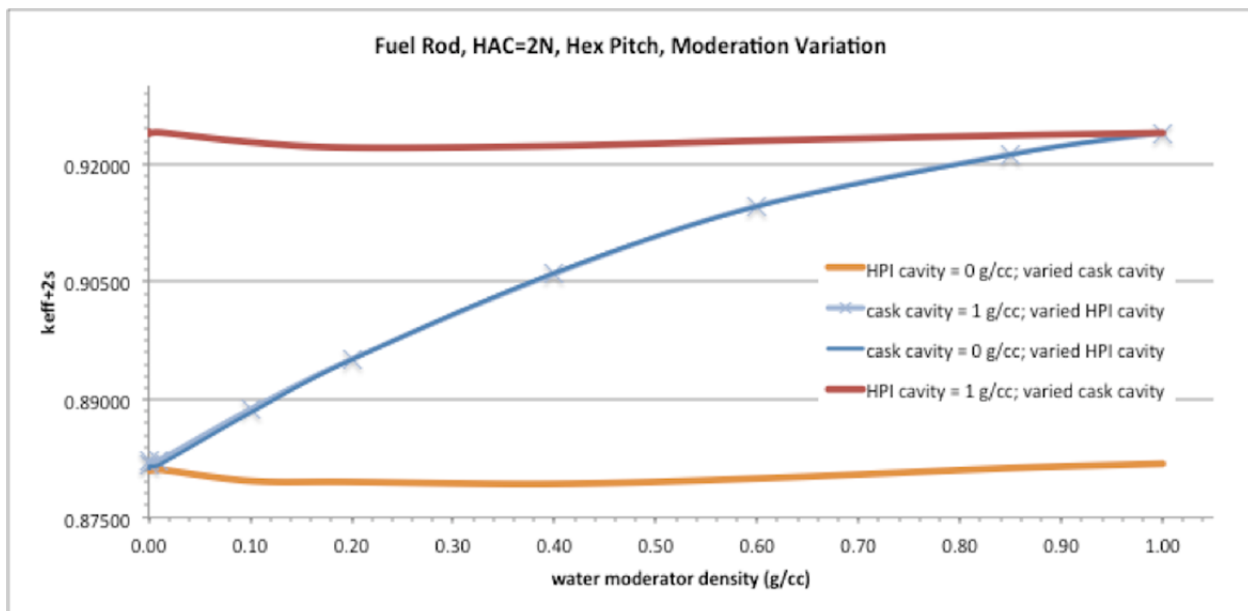


Figure 6.9.4-3. Fuel Rod Content, HAC 2N, Moderator Variation Study

Table 6.9.4-5. Fuel Rod Content, HAC 2N, Moderator Variation Study

| Case Name | HPI cavity water density (g/cm ³) | Cask cavity water density (g/cm ³) | k _{eff} | σ | k _{eff} +2σ |
|------------------------------------------------------|--------------------------------------------------------|------------------------------------------------------|------------------|---------|----------------------|
| Case for HPI cavity at 0 g/cc; cask cavity variation | | | | | |
| FRLAHmh 1 22w 1 1 | 0.000 | 0.000 | 0.88070 | 0.00023 | 0.88116 |
| FRLAHmh 1 22w 2 1 | 0.000 | 0.001 | 0.88048 | 0.00024 | 0.88096 |
| FRLAHmh 1 22w 3 1 | 0.000 | 0.010 | 0.88063 | 0.00024 | 0.88111 |
| FRLAHmh 1 22w 4 1 | 0.000 | 0.100 | 0.87915 | 0.00025 | 0.87965 |
| FRLAHmh 1 22w 5 1 | 0.000 | 0.200 | 0.87906 | 0.00023 | 0.87952 |
| FRLAHmh 1 22w 6 1 | 0.000 | 0.400 | 0.87881 | 0.00023 | 0.87927 |
| FRLAHmh 1 22w 7 1 | 0.000 | 0.600 | 0.87950 | 0.00023 | 0.87996 |
| FRLAHmh 1 22w 8 1 | 0.000 | 0.850 | 0.88086 | 0.00021 | 0.88128 |
| FRLAHmh 1 22w 9 1 | 0.000 | 1.000 | 0.88136 | 0.00024 | 0.88184 |
| Case for cask cavity at 1 g/cc; HPI cavity variation | | | | | |
| FRLAHmh 1 22w 9 1 | 0.000 | 1.000 | 0.88136 | 0.00024 | 0.88184 |
| FRLAHmh 1 22w 9 2 | 0.001 | 1.000 | 0.88181 | 0.00023 | 0.88227 |
| FRLAHmh 1 22w 9 3 | 0.010 | 1.000 | 0.88181 | 0.00024 | 0.88229 |
| FRLAHmh 1 22w 9 4 | 0.100 | 1.000 | 0.88826 | 0.00025 | 0.88876 |
| FRLAHmh 1 22w 9 5 | 0.200 | 1.000 | 0.89467 | 0.00024 | 0.89515 |
| FRLAHmh 1 22w 9 6 | 0.400 | 1.000 | 0.90556 | 0.00024 | 0.90604 |
| FRLAHmh 1 22w 9 7 | 0.600 | 1.000 | 0.91417 | 0.00025 | 0.91467 |
| FRLAHmh 1 22w 9 8 | 0.850 | 1.000 | 0.92079 | 0.00024 | 0.92127 |
| FRLAHmh 1 22w 9 9 | 1.000 | 1.000 | 0.92350 | 0.00024 | 0.92398 |
| Case for cask cavity at 0 g/cc; HPI cavity variation | | | | | |
| FRLAHmh 1 22w 1 1 | 0.000 | 0.000 | 0.88070 | 0.00023 | 0.88116 |
| FRLAHmh 1 22w 1 2 | 0.001 | 0.000 | 0.88111 | 0.00021 | 0.88153 |
| FRLAHmh 1 22w 1 3 | 0.010 | 0.000 | 0.88124 | 0.00022 | 0.88168 |
| FRLAHmh 1 22w 1 4 | 0.100 | 0.000 | 0.88777 | 0.00027 | 0.88831 |
| FRLAHmh 1 22w 1 5 | 0.200 | 0.000 | 0.89460 | 0.00024 | 0.89508 |
| FRLAHmh 1 22w 1 6 | 0.400 | 0.000 | 0.90571 | 0.00022 | 0.90615 |
| FRLAHmh 1 22w 1 7 | 0.600 | 0.000 | 0.91416 | 0.00022 | 0.9146 |
| FRLAHmh 1 22w 1 8 | 0.850 | 0.000 | 0.92073 | 0.00023 | 0.92119 |
| FRLAHmh 1 22w 1 9 | 1.000 | 0.000 | 0.92365 | 0.00024 | 0.92413 |
| Case for HPI cavity at 1 g/cc; cask cavity variation | | | | | |
| FRLAHmh 1 22w 1 9 | 1.000 | 0.000 | 0.92365 | 0.00024 | 0.92413 |
| FRLAHmh 1 22w 2 9 | 1.000 | 0.001 | 0.92353 | 0.00023 | 0.92399 |
| FRLAHmh 1 22w 3 9 | 1.000 | 0.010 | 0.92357 | 0.00024 | 0.92405 |
| FRLAHmh 1 22w 4 9 | 1.000 | 0.100 | 0.92238 | 0.00021 | 0.9228 |
| FRLAHmh 1 22w 5 9 | 1.000 | 0.200 | 0.92162 | 0.00024 | 0.92210 |
| FRLAHmh 1 22w 6 9 | 1.000 | 0.400 | 0.92185 | 0.00023 | 0.92231 |
| FRLAHmh 1 22w 7 9 | 1.000 | 0.600 | 0.92253 | 0.00022 | 0.92297 |
| FRLAHmh 1 22w 8 9 | 1.000 | 0.850 | 0.92320 | 0.00023 | 0.92366 |
| FRLAHmh 1 22w 9 9 | 1.000 | 1.000 | 0.92350 | 0.00024 | 0.92398 |

Fissile, Free Form Content

The moderator density is varied for the 425 grams U-235, fissile, free form content case (601HMH_12_425btm) to evaluate the sensitivity of k_{eff} to package moderation. Table 6.9.4-5 showed the HPI cavity at full flooding was most reactive, therefore only the two extreme cases were evaluated for fissile, free form material (HPI at 1 g/cm³ and 0 g/cm³) where the fissile

content sphere radius is [[]] cm. Results in Table 6.9.4-6 show the peak $k_{\text{eff}} + 2\sigma$ occurs for a fully flooded package with moderator density of 1 g/cm³ (601HMH12w_425btm_9_9), which is the same case from Table 6.9.4-4.

Table 6.9.4-6. Fissile, Free Form (U-235) Content, HAC 2N, Moderator Variation Study

| Case Name | HPI cavity water density (g/cm ³) | Cask cavity water density (g/cm ³) | k_{eff} | σ | $k_{\text{eff}}+2\sigma$ |
|------------------------------------------------------|--------------------------------------------------------|---------------------------------------------------------|------------------|----------|--------------------------|
| Case for cask cavity at 0 g/cc; HPI cavity variation | | | | | |
| 601HMH12w_425btm_1_1 | 0.000 | 0.000 | 0.83354 | 0.00025 | 0.83404 |
| 601HMH12w_425btm_1_2 | 0.001 | 0.000 | 0.83395 | 0.00022 | 0.83439 |
| 601HMH12w_425btm_1_3 | 0.010 | 0.000 | 0.83558 | 0.00022 | 0.83602 |
| 601HMH12w_425btm_1_4 | 0.100 | 0.000 | 0.85348 | 0.00022 | 0.85392 |
| 601HMH12w_425btm_1_5 | 0.200 | 0.000 | 0.87033 | 0.00025 | 0.87083 |
| 601HMH12w_425btm_1_6 | 0.400 | 0.000 | 0.89329 | 0.00024 | 0.89377 |
| 601HMH12w_425btm_1_7 | 0.600 | 0.000 | 0.90876 | 0.00024 | 0.90924 |
| 601HMH12w_425btm_1_8 | 0.850 | 0.000 | 0.92045 | 0.00023 | 0.92091 |
| 601HMH12w_425btm_1_9 | 1.000 | 0.000 | 0.92550 | 0.00021 | 0.92592 |
| Case for cask cavity at 1 g/cc; HPI cavity variation | | | | | |
| 601HMH12w_425btm_9_1 | 0.000 | 1.000 | 0.84088 | 0.00024 | 0.84136 |
| 601HMH12w_425btm_9_2 | 0.001 | 1.000 | 0.84087 | 0.00024 | 0.84135 |
| 601HMH12w_425btm_9_3 | 0.010 | 1.000 | 0.84302 | 0.00023 | 0.84348 |
| 601HMH12w_425btm_9_4 | 0.100 | 1.000 | 0.85975 | 0.00025 | 0.86025 |
| 601HMH12w_425btm_9_5 | 0.200 | 1.000 | 0.87715 | 0.00023 | 0.87761 |
| 601HMH12w_425btm_9_6 | 0.400 | 1.000 | 0.89939 | 0.00022 | 0.89983 |
| 601HMH12w_425btm_9_7 | 0.600 | 1.000 | 0.91439 | 0.00024 | 0.91487 |
| 601HMH12w_425btm_9_8 | 0.850 | 1.000 | 0.92686 | 0.00024 | 0.92734 |
| 601HMH12w_425btm_9_9 | 1.000 | 1.000 | 0.93242 | 0.00021 | 0.93284 |

NOTE: All cases are for 425 grams of U-235.

6.9.5. MCNP Results

This section documents an explanation of the criticality analysis MCNP input/output file structure and naming convention. Representative cases are provided for review (Tables 6.9.5-1 through 6.9.5-6).

Table 6.9.5-1. Fuel Rod Content

| Key | Description | |
|-----------------------------------------------|--------------------------------------|--------------------------------------------------------------------------------------------------------------------------------------------------------------------------------------------------------------------------------------------------------------------------|
| FRLA(H/N)mh_XX_YY | | |
| FRL | Fuel Rod | |
| A | A for package array | |
| H / N | H for HAC N for NCT | |
| mh | mh for mass limited, hexagonal pitch | |
| XX [1-4] | Fuel pellet radius (FROR) | 0.2, 0.3, 0.4, 0.5 (centimeters) |
| YY [1-11] (where applicable) [21-23] | Half-pitch | FROR[XX]+0.3, FROR[XX]+0.4, FROR[XX]+0.6, FROR[XX]+0.7, FROR[XX]+0.8, FROR[XX]+0.9, FROR[XX]+1.1, FROR[XX]+1.2, FROR[XX]+1.4, FROR[XX]+1.6, FROR[XX]+2.0 For XX=1 added cases (Cases 21, 22, and 23, respectively) for FROR[XX]+0.45, FROR[XX]+0.5, FROR[XX]+0.55 |
| FRLAHm_YY | | |
| FRL | Fuel Rod | |
| A | A for package array | |
| H | H for HAC | |
| m | m for mass limited, square pitch | |
| -- | Fuel pellet radius (FROR) | 0.2 (Centimeters) |
| YY [1-8] | Half-pitch | FROR[XX]+0.3, FROR[XX]+0.4, FROR[XX]+0.45, FROR[XX]+0.5, FROR[XX]+0.55, FROR[XX]+0.6, FROR[XX]+0.7, FROR[XX]+0.8 |
| FRLSmh_XX_YY | | |
| FRL | Fuel Rod | |
| S | S for single package | |
| mh | mh for mass limited, hexagonal pitch | |
| XX [1-9] | Fuel pellet radius (FROR) | 0.2, 0.3, 0.4, 0.5 (centimeters) |
| YY [1-11] | Half-pitch | FROR[XX]+0.3, FROR[XX]+0.4, FROR[XX]+0.6, FROR[XX]+0.7, FROR[XX]+0.8, FROR[XX]+0.9, FROR[XX]+1.1, FROR[XX]+1.2, FROR[XX]+1.4, FROR[XX]+1.6, FROR[XX]+2.0 |

Table 6.9.5-2. Fissile, Free Form Mass Content

| Key | | Description |
|--------------------------------------------------|-----------------------------------------------------------|------------------------------------------------------------------------------------------|
| 601HM(S/H/N)XX | | |
| 601HM | 601 is for U-235, free form HM for homogenized mixture | |
| S / H / N | S for single package H is for HAC N is for NCT | |
| XX [[]] | Sphere radius | 1.8436, 2, 3, 4, 5, 6, 7, 8, 9, 10, 11, [[]] (centimeters) [[]] (centimeters) |
| btm | Content located at the bottom of the cavity | |
| 425 | Reduced mass of 425 grams of U-235 | |
| 430 | Reduced mass of 430 grams of U-235 | |
| PHM(S/H/N)XX | | |
| PHM | P for Pu-239, free form HM for homogenized mixture | |
| S / H / N | S for single package H is for HAC N is for NCT | |
| XX [1-12] [[]] | Sphere radius | 1.5340, 2, 3, 4, 5, 6, 7, 8, 9, 10, 11, [[]] (centimeters) [[]] (centimeters) |
| btm | Content located at the bottom of the cavity | |
| 265 | Reduced mass of 265 grams of Pu-239 | |
| U233HM(S/H)XX_YYbtm | | |
| U233 HM | U-233, free form HM for homogenized mixture | |
| S H | S for single package H is for HAC, 2N | |
| XX [9, 10, 11, [[]] (where applicable) | Sphere radius | 9, 10, 11, [[]] (centimeters) |
| btm | Content located at the bottom of the cavity | |
| YY | Mass (grams) | |
| 315 | Reduced mass of 315 grams of U-233 | |
| P241HM(S/H/N)XX_YY | | |
| P241 HM | Pu-241, free form HM for homogenized mixture | |
| S H | S for single package H is for HAC | |
| XX [9, 10, 11, [[]] (where applicable) | Sphere radius | 9, 10, 11, [[]] (centimeters) |
| btm | Content located at the bottom of the cavity | |
| YY | Mass (grams) | |
| 150 | Reduced mass of 150 grams of Pu-241 | |

Table 6.9.5-3. FRLSmh MCNP Results (Section 6.4.2)

| Input File | k_{eff} | σ |
|--------------------|------------------|----------|
| FRLSmh_1_1_in.inp | 0.85526 | 0.00025 |
| FRLSmh_1_2_in.inp | 0.90946 | 0.00023 |
| FRLSmh_1_21.inp | 0.92134 | 0.00022 |
| FRLSmh_1_22.inp | 0.92307 | 0.00021 |
| FRLSmh_1_23.inp | 0.91659 | 0.00022 |
| FRLSmh_1_3_in.inp | 0.89990 | 0.00022 |
| FRLSmh_1_4_in.inp | 0.83653 | 0.00021 |
| FRLSmh_1_5_in.inp | 0.78051 | 0.00020 |
| FRLSmh_2_1_in.inp | 0.75241 | 0.00022 |
| FRLSmh_2_2_in.inp | 0.81435 | 0.00021 |
| FRLSmh_2_3_in.inp | 0.88079 | 0.00024 |
| FRLSmh_2_4_in.inp | 0.88881 | 0.00023 |
| FRLSmh_2_5_in.inp | 0.88239 | 0.00021 |
| FRLSmh_2_6_in.inp | 0.85986 | 0.00022 |
| FRLSmh_2_7_in.inp | 0.77499 | 0.00021 |
| FRLSmh_2_8_in.inp | 0.73769 | 0.00020 |
| FRLSmh_3_1_in.inp | 0.70705 | 0.00026 |
| FRLSmh_3_10_in.inp | 0.70002 | 0.00020 |
| FRLSmh_3_11_in.inp | 0.59209 | 0.00017 |
| FRLSmh_3_2_in.inp | 0.76489 | 0.00024 |
| FRLSmh_3_3_in.inp | 0.84482 | 0.00024 |
| FRLSmh_3_4_in.inp | 0.86684 | 0.00025 |
| FRLSmh_3_5_in.inp | 0.8784 | 0.00021 |
| FRLSmh_3_6_in.inp | 0.87962 | 0.00022 |
| FRLSmh_3_7_in.inp | 0.85379 | 0.00021 |
| FRLSmh_3_8_in.inp | 0.82821 | 0.00023 |
| FRLSmh_3_9_in.inp | 0.74879 | 0.00020 |
| FRLSmh_4_1_in.inp | 0.66359 | 0.00022 |
| FRLSmh_4_10_in.inp | 0.75879 | 0.00020 |
| FRLSmh_4_11_in.inp | 0.64905 | 0.00018 |
| FRLSmh_4_2_in.inp | 0.71248 | 0.00026 |
| FRLSmh_4_3_in.inp | 0.78917 | 0.00023 |
| FRLSmh_4_4_in.inp | 0.81556 | 0.00026 |
| FRLSmh_4_5_in.inp | 0.83477 | 0.00023 |
| FRLSmh_4_6_in.inp | 0.84636 | 0.00025 |
| FRLSmh_4_7_in.inp | 0.85075 | 0.00023 |
| FRLSmh_4_8_in.inp | 0.84337 | 0.00024 |
| FRLSmh_4_9_in.inp | 0.81279 | 0.00023 |

Table 6.9.5-4. FRLANmh MCNP Results (Section 6.5.2)

| Input File | k_{eff} | σ |
|---------------------|------------------|----------|
| FRLANmh_1_1_in.inp | 0.83754 | 0.00024 |
| FRLANmh_1_2_in.inp | 0.89350 | 0.00023 |
| FRLANmh_1_21.inp | 0.90893 | 0.00024 |
| FRLANmh_1_22.inp | 0.91810 | 0.00023 |
| FRLANmh_1_23.inp | 0.91564 | 0.00020 |
| FRLANmh_1_3_in.inp | 0.90089 | 0.00020 |
| FRLANmh_1_4_in.inp | 0.83616 | 0.00020 |
| FRLANmh_1_5_in.inp | 0.77767 | 0.00019 |
| FRLANmh_2_1_in.inp | 0.73940 | 0.00030 |
| FRLANmh_2_2_in.inp | 0.80199 | 0.00027 |
| FRLANmh_2_3_in.inp | 0.87026 | 0.00026 |
| FRLANmh_2_4_in.inp | 0.88039 | 0.00026 |
| FRLANmh_2_5_in.inp | 0.88490 | 0.00023 |
| FRLANmh_2_6_in.inp | 0.86001 | 0.00023 |
| FRLANmh_2_7_in.inp | 0.77229 | 0.00019 |
| FRLANmh_2_8_in.inp | 0.73271 | 0.00021 |
| FRLANmh_3_1_in.inp | 0.68240 | 0.00025 |
| FRLANmh_3_10_in.inp | 0.69325 | 0.00019 |
| FRLANmh_3_11_in.inp | 0.57449 | 0.00018 |
| FRLANmh_3_2_in.inp | 0.74334 | 0.00022 |
| FRLANmh_3_3_in.inp | 0.81419 | 0.00025 |
| FRLANmh_3_4_in.inp | 0.84262 | 0.00023 |
| FRLANmh_3_5_in.inp | 0.85075 | 0.00025 |
| FRLANmh_3_6_in.inp | 0.86365 | 0.00022 |
| FRLANmh_3_7_in.inp | 0.84363 | 0.00024 |
| FRLANmh_3_8_in.inp | 0.82671 | 0.00023 |
| FRLANmh_3_9_in.inp | 0.74479 | 0.00022 |

Table 6.9.5-5. FRLAHmh MCNP Results (Section 6.6.2)

| Input File | k_{eff} | σ |
|---------------------|------------------|----------|
| FRLAHmh_1_1_in.inp | 0.85587 | 0.00026 |
| FRLAHmh_1_2_in.inp | 0.90895 | 0.00025 |
| FRLAHmh_1_21.inp | 0.92097 | 0.00022 |
| FRLAHmh_1_22.inp | 0.92350 | 0.00024 |
| FRLAHmh_1_23.inp | 0.91616 | 0.00025 |
| FRLAHmh_1_3_in.inp | 0.89981 | 0.00021 |
| FRLAHmh_1_4_in.inp | 0.83686 | 0.00019 |
| FRLAHmh_1_5_in.inp | 0.78005 | 0.00019 |
| FRLAHmh_2_1_in.inp | 0.75220 | 0.00025 |
| FRLAHmh_2_2_in.inp | 0.81358 | 0.00026 |
| FRLAHmh_2_3_in.inp | 0.88044 | 0.00022 |
| FRLAHmh_2_4_in.inp | 0.88897 | 0.00020 |
| FRLAHmh_2_5_in.inp | 0.88203 | 0.00022 |
| FRLAHmh_2_6_in.inp | 0.86057 | 0.00022 |
| FRLAHmh_2_7_in.inp | 0.77474 | 0.00021 |
| FRLAHmh_2_8_in.inp | 0.73764 | 0.00021 |
| FRLAHmh_3_1_in.inp | 0.70760 | 0.00023 |
| FRLAHmh_3_10_in.inp | 0.70081 | 0.00020 |
| FRLAHmh_3_11_in.inp | 0.59202 | 0.00018 |
| FRLAHmh_3_2_in.inp | 0.76450 | 0.00023 |
| FRLAHmh_3_3_in.inp | 0.84442 | 0.00023 |
| FRLAHmh_3_4_in.inp | 0.86718 | 0.00025 |
| FRLAHmh_3_5_in.inp | 0.87828 | 0.00023 |
| FRLAHmh_3_6_in.inp | 0.87916 | 0.00024 |
| FRLAHmh_3_7_in.inp | 0.85409 | 0.00022 |
| FRLAHmh_3_8_in.inp | 0.82809 | 0.00020 |
| FRLAHmh_3_9_in.inp | 0.74868 | 0.00020 |
| FRLAHmh_4_1_in.inp | 0.66372 | 0.00022 |
| FRLAHmh_4_10_in.inp | 0.75882 | 0.00021 |
| FRLAHmh_4_11_in.inp | 0.64908 | 0.00020 |
| FRLAHmh_4_2_in.inp | 0.71195 | 0.00024 |
| FRLAHmh_4_3_in.inp | 0.78927 | 0.00025 |
| FRLAHmh_4_4_in.inp | 0.81556 | 0.00024 |
| FRLAHmh_4_5_in.inp | 0.83475 | 0.00026 |
| FRLAHmh_4_6_in.inp | 0.84683 | 0.00023 |
| FRLAHmh_4_7_in.inp | 0.85022 | 0.00024 |
| FRLAHmh_4_8_in.inp | 0.84335 | 0.00023 |
| FRLAHmh_4_9_in.inp | 0.81274 | 0.00020 |

Table 6.9.5-6. FRLAHm MCNP Results (Section 6.9.1)

| Input File | k_{eff} | σ |
|-------------------|------------------|----------|
| FRLAHm_1_1_in.inp | 0.88665 | 0.00023 |
| FRLAHm_1_2_in.inp | 0.92539 | 0.00024 |
| FRLAHm_1_3_in.inp | 0.92769 | 0.00021 |
| FRLAHm_1_4_in.inp | 0.91849 | 0.00020 |
| FRLAHm_1_5_in.inp | 0.89758 | 0.00019 |
| FRLAHm_1_6_in.inp | 0.86402 | 0.00021 |
| FRLAHm_1_7_in.inp | 0.79759 | 0.00020 |
| FRLAHm_1_8_in.inp | 0.74015 | 0.00021 |
| FRLAHm_2_1_in.inp | 0.79426 | 0.00022 |
| FRLAHm_2_2_in.inp | 0.85183 | 0.00026 |
| FRLAHm_2_3_in.inp | 0.87235 | 0.00025 |
| FRLAHm_2_4_in.inp | 0.88724 | 0.00025 |
| FRLAHm_2_5_in.inp | 0.89702 | 0.00022 |
| FRLAHm_2_6_in.inp | 0.90125 | 0.00023 |
| FRLAHm_2_7_in.inp | 0.89588 | 0.00023 |
| FRLAHm_2_8_in.inp | 0.87092 | 0.00020 |

6.10 References

- 6-1 U.S. NRC, "Code of Federal Regulations, Packaging and Transport of Radioactive Material," 10 CFR 71, April 2016.
- 6-2 International Atomic Energy Agency, "Advisory Material for the IAEA Regulations for the Safe Transport of Radioactive Material (2012 Edition)," SSG-26 2012.
- 6-3 R.J. McConn et al., "Compendium of Material Composition Data for Radiation Transport Modeling," PNNL-15870, Revision 1, March 2011.
- 6-4 Oak Ridge National Laboratory (ORNL), "SCALE: A Comprehensive Modeling and Simulation Suite for Nuclear Safety Analysis and Design," ORNL/TM-2005/39, June 2011.
- 6-5 T. Goorley et al., "Initial MCNP 6 Release Overview - MCNP6 Version 1.0," Los Alamos National Laboratory, LA-UR-13-22934, April 2013.
- 6-6 J. Conlin et al., "Listing of Available ACE Data Tables," Los Alamos National Laboratory, LA-UR-13-21822, Revision 4, June 2014.
- 6-7 H. R., Parks, C. V. Dyer, "Recommendations for Preparing the Criticality Safety Evaluation of Transportation Packages," Oak Ridge National Laboratory, NUREG/CR-5661, 1997.
- 6-8 J. J. Lichtenwalter, S. M. Bowman, M. D. DeHart, and C. M. Hopper, "Criticality Benchmark Guide for Light-Water-Reactor Fuel in Transportation and Storage Packages, NUREG/CR-6361, ORNL/TM-13211," Oak Ridge National Laboratory, 1997.
- 6-9 Organization for Economic Cooperation and Development - Nuclear Energy Agency (OECD-NEA), "International Handbook of Evaluated Criticality Safety Benchmark Experiments, NEA/NSC/DOC(95)03," 2014.

7 OPERATING PROCEDURES

Instructions for use of the Model 2000 Transport Package are summarized below, beginning with Section 7.1. A more detailed description of these instructions is included in GE Specification 22A9380, Operations and Maintenance of Model 2000 Transport Package (O&M Manual) (Reference 7-1). The transport package user follows the O&M Manual, but may expand it to include site-specific procedures. A component of the operating procedure is a pre-shipment engineering evaluation to ensure that the packaging, with its proposed contents, satisfies the applicable requirements of the package's license or certificate. This evaluation includes, but is not limited to, the review of:

- Proposed contents' isotopic composition, quantities, and decay heat
- Proposed contents' form, weight, and geometry
- Shielding requirements
- Structural requirements
- Thermal requirements
- Shipping hardware (e.g., material basket and shoring devices)
- Compliance with the respective content requirements listed in Section 7.5.

7.1 Package Loading

Fully trained personnel using approved operating procedures shall carry out all loading operations at the facility. The general sequence is as follows:

- Use respective loading tables and guidance provided in Section 7.5 to ensure compliance of the proposed contents.
- Receive the Model 2000 Transport Package including the HPI.
- Inspect cask and components for damage and prepare for loading.
- For Configuration 1: Load the contents directly into the HPI with additional shoring as required.
- For Configuration 2: Load the contents and any additional required shoring (e.g., rod holders) into the HPI material basket and load the material basket into the HPI.
- Load the HPI with contents into the Model 2000 cask.
- Close the HPI and cask lid.
- If wet loaded, raise and drain the cask, and vacuum dry the cask.
- After vacuum drying is complete, perform pre-shipment leak test.
- Load the cask into the overpack and onto the trailer for transport.

7.1.1. Preparation for Loading

7.1.1.1. Packaging Receipt and Inspection

- a. Position the Model 2000 transport vehicle for packaging inspection upon arrival.
- b. Perform a visual inspection for damage.

7.1.1.2. Removal of the Packaging from the Transport Vehicle

- a. Position the transport vehicle under an overhead crane.
- b. Remove the packaging tie-downs.
- c. Position the spreader bar or strongback and connect the appropriate slings and shackles.
- d. Depending on site-specific issues, either:
 - Lift the overpack top section off the overpack base and place on the overpack stand, or
 - Lift the entire packaging free from the transport vehicle and set it down. Then lift the overpack top section from the overpack base and place on the overpack stand.

7.1.1.3. Preparing To Load the Cask

- a. Perform a visual inspection. Note any damage or unusual conditions. If functionality of the part is impaired, repair or replace as required.
- b. Install the cask ears. Torque the lifting ear screws to 600 ft-lb in four places for each ear. If using a forklift to transport the cask, the standard lifting ears must be used. If lifting the cask by crane, then either the standard or auxiliary ears may be used. If lifted by crane, the lifting slings shall not make an angle of greater than 30° measured from the vertical.
- c. Move the cask to the designated prep area at the site.
- d. With proper radiological protection and monitoring, remove the cask lid and verify presence of the HPI.
- e. If there is a spacer, remove it.
- f. Visually inspect the cask and lid sealing surfaces for damage or foreign material. Note any damage and repair or replace as required.
- g. Visually inspect the cask lid seal for damage, and verify that it is the correct seal for the given contents. Any gouges or cuts in the seal area are cause for replacement. Ensure that the replacement is for the given contents.
 - Configuration 1: [[]] retainer with four Parker Compound No. [[]] rings.
 - Configuration 2: [[]] retainer with four Parker Compound No. [[]] rings.

- h. Place the cask lid seal over the alignment pins on the top of the cask.
- i. Remove vent and drain port plugs and covers, and test port plug and cover, to allow filling and draining of cask as well as to check O-rings to ensure they are correct material for given content.
 - Configuration 1: Parker Compound No. [[]].
 - Configuration 2: Parker Compound No. [[]].

7.1.2. Loading of Contents

7.1.2.1. Cobalt-60 Isotope Rods

The usage of the term ‘rods’ in this section refers to cobalt-60 isotope rods. This content type must be shipped according to the requirements in Section 7.5.3 or Section 7.5.4.

- a. Rods may be shipped using either Configuration 1 or Configuration 2, depending on decay heat load (See Table 1.2-1).
- b. Remove the HPI top plug.
- c. [[]] the rods and load into additional shoring components (e.g., rod holders) as required.
- d. Load the rods with any additional shoring components into the HPI material basket. Depending on site-specific procedures, the HPI material basket may be loaded independently or pre-loaded in the HPI.
- e. If the HPI material basket is loaded independently, load it into the HPI.
- f. If the HPI is loaded independently, load it into the Model 2000 cask.
- g. After the HPI material basket and all contents and required shoring are loaded into the HPI, lower the HPI top plug over the 4 alignment pins with the proper rigging.
- h. If spacer was provided, install over HPI top plug.
- i. Slowly lower the lid onto the cask over the guide pins with proper rigging. Closely watch this operation to ensure that the lid is properly aligned.

7.1.2.2. Irradiated Fuel Rods

The usage of the term ‘rods’ in this section refers to irradiated fuel rods. This content type must be shipped according to the requirements in Section 7.5.1 or Section 7.5.4.

- a. Rods may be shipped using either Configuration 1 or Configuration 2, depending on decay heat load (see Table 1.2-1). The use of the HPI material basket is not required for Configuration 1, although if the HPI material basket is not used, sufficient shoring must be provided such that the rods remain upright.
- b. Remove the HPI top plug.
- c. Segment the rods and load into additional shoring components (e.g., rod holders) as required.

- d. Load the rods with any additional shoring components into the HPI material basket (if necessary). Depending on site-specific procedures, the HPI material basket may be loaded independently or pre-loaded in the HPI.
- e. If the HPI material basket is loaded independently, load it into the HPI. If the HPI material basket is not used, load the contents with any additional required shoring components into the HPI.
- f. If the HPI is loaded independently, load it into the Model 2000 cask.
- g. After the HPI material basket and all contents and required shoring are loaded into the HPI, lower the HPI top plug over the 4 alignment pins with the proper rigging.
- h. If spacer was provided, install over HPI top plug.
- i. Slowly lower the cask lid onto the cask over the guide pins with proper rigging. Closely watch this operation to ensure that the lid is properly aligned.

7.1.2.3. Irradiated Hardware and Byproducts

The usage of the term ‘contents’ in this section refers to Irradiated hardware and byproducts. This content type must be shipped according to the requirements in Section 7.5.2 or Section 7.5.4.

- a. The contents may only be shipped using either Configuration 1 or Configuration 2, depending on decay heat load (see Table 1.2-1). The use of the HPI material basket is not required for Configuration 1, but may be used as a shoring component.
- b. Remove the HPI top plug.
- c. Load the contents with any additional required shoring components into the HPI. Depending on site-specific procedures, the HPI may be loaded independently or pre-loaded in the Model 2000 Transport Package.
- d. If the HPI is loaded independently, load it into the Model 2000 cask.
- e. After the HPI material basket (if used) and all contents and required shoring are loaded into the HPI, lower the HPI top plug over the 4 alignment pins with the proper rigging.
- f. If spacer was provided, install over HPI top plug.
- g. Slowly lower the cask lid onto the cask over the guide pins with proper rigging. Closely watch this operation to ensure that the lid is properly aligned.

7.1.2.4. Special Nuclear Material

The usage of the term ‘contents’ in this section refers to special nuclear material (SNM). For this content type, the equivalent mass of U-235 must be determined based on the mass of any fissile isotopes in the contents using the conversion factors in Section 1.2.2.3. This content type must be shipped according to the requirements in Section 7.5.5.

- a. The contents may only be shipped using either Configuration 1 or Configuration 2, depending on decay heat load (see Table 1.2-1). The use of the HPI material basket is not required for Configuration 1, but may be used as a shoring component.
- b. Remove the HPI top plug.
- c. Load the contents with any additional required shoring components into the HPI. Depending on site-specific procedures, the HPI may be loaded independently or pre-loaded in the Model 2000 Transport Package.
- d. If the HPI is loaded independently, load it into the Model 2000 cask.
- e. After the HPI material basket (if used) and all contents and required shoring are loaded into the HPI, lower the HPI top plug over the 4 alignment pins with the proper rigging.
- f. If spacer was provided, install over HPI top plug.
- g. Slowly lower the cask lid onto the cask over the guide pins with proper rigging. Closely watch this operation to ensure that the lid is properly aligned.

7.1.3. Closing the Cask and Performing Leakage Tests

7.1.3.1. Removing the Cask from the Loading Area

- a. Carefully monitor the cask radiation levels while removing the cask from the loading area.
- b. Tighten the lid bolts so they are hand tight.
- c. If the cask was loaded under water:
 - Raise cask above level of pool to allow for water drainage.
 - After the water has drained, vacuum-dry the cask cavity until 1 torr pressure is attained. Maintain the pressure in the cavity at or below 1 torr for at least 30 minutes.
 - After the 30-minute hold time is reached, isolate the vacuum system from the cask by closing the valve between the vacuum pump and the cask, which is on the vacuum drying system manifold vent port at the top of the Model 2000 cask (refer to O&M Manual (Reference 7-1)). With the vacuum pump valve closed, disconnect the 110 V power cord to the vacuum pump, which shuts off the vacuum pump power.
 - Observe the pressure in the cavity, which must be maintained at or below 1 torr for at least an additional 5 minutes. This ensures that the pressure measurement is reliable and not due to the vacuum pump pulling past a partially open valve.
 - If the pressure rise should exceed 1 torr in the first 30-minute hold or in the second 5-minute hold with the system isolated, turn the vacuum drying system back on and open the cask vent valve to continue the vacuum drying process.
 - Filter the discharged gas of the vacuum pump.

- **NOTE:** Refer to the O&M Manual for a typical vacuum drying set up and its equipment. If the vacuum pump used in this procedure is equipped with a "gas ballast" device, this device must be inoperative during the cask vacuum drying operation. The gas ballast device is used to drive off any moisture that may have been trapped in the vacuum pump oil. If needed to remove water vapor from the pump oil during the vacuum drying operation, the system shall be isolated. Turn on the gas ballast device until the oil is cleared up, turn off the gas ballast, and then place the system back on line.
- d. Decontaminate the cask to a level consistent with 49 CFR 173.443 (Reference 7-2) and 10 CFR 71.87 (Reference 7-3).

7.1.3.2. Securing the Cask Lid

- a. Torque the lid bolts to 500 ft-lb in a crisscross pattern to ensure equal compression of the seal.
- b. Install the drain and vent plugs following the drying operation as applicable. Apply approximately three wraps of high temperature nickel thread tape (poly-temperature, Nickel Anti-Seize Tape #36336, or equivalent). Install using 3 to 3½ revolutions by hand and ¾ to 1 revolution using an Allen wrench or optionally a torque wrench (resulting in approximately 30 ft-lb).

7.1.3.3. Assembly Verification Pre-Shipment Leakage Testing

- a. Perform leakage testing of the cask lid closure seal and vent port and drain port threaded pipe plugs in accordance with the latest edition of the pre-shipment leak test procedure number MSLT-EE-GE Revision 5500-01 (Reference 7-4), or an equivalent procedure, developed by an American Society for Nondestructive Testing (ASNT) Level III examiner, and approved by GEH prior to use.
- b. Upon completion of the vacuum drying procedure, backfill the cask cavity with 2 ± 1 psig helium. For leak testing, pressurize the cask cavity with $15 \pm 1/-0$ psig helium. Introduce helium by using the "quick connect" fitting at the vent port.
- c. Set up and use the helium Mass Spectrometer Leak Detector (MSLD) test instrument according to the written procedure and the manufacturer's instructions.
- d. With the instrument calibrated as indicated in MSLT-EE-GE Revision 5500-01 (Reference 7-4) or latest edition, or an equivalent procedure developed by an ASNT Level III examiner, check the closure seal and the vent and drain threaded pipe plugs for indications of leakage.
- e. If leakage is detected during either of the above checks, repair or replace the offending components and then re-test for leakage.
- f. After leak testing is completed, vent the cask cavity to atmosphere. Assure helium vent hose is exhausted through an approved facility ventilation or HEPA system.

7.1.4. Preparation for Transport

7.1.4.1. Preparing the Cask for Transport

- a. Transport the cask to the overpack base and place the cask on the lower impact limiter base.
- b. Remove the cask lifting ears or redundant ears from the cask and use approved tape to cover the ears' threaded holes for contamination control purposes.
- c. Position the spreader bar over the overpack and connect the slings and shackles.
- d. Slowly lower the overpack over the cask with the locating pins aligned.
- e. Install the overpack bolts, securing the top section to the base section. Torque overpack screws to 100 ft-lb (dry) in 15 places (typ). An adhesive/sealant compound is applied to bolt threads prior to installation to prevent vibration loosening of bolts.
- f. Position the package on the transport vehicle if required.
- g. Remove the shackle and slings and tie down the package to the transport vehicle. The Model 2000 Transport Package does not have any parts or devices that would need to be rendered inoperable pursuant to 10 CFR 71.87(h).
- h. Perform the radiological survey of the package and transport vehicle consistent with 10 CFR 71.47, 71.87 and 49 CFR 173.441, 173.443.
- i. Measure and document the temperature of the overpack paying particular attention to the area around the bolting ring. If any temperature reading exceeds 185°F, install the protective personnel barrier around the package, in accordance with 10 CFR 71.43.
- j. Apply the security seal to the overpack.

7.2 Package Unloading

Operations at the unloading facility are largely the reverse of loading operations. The unloading facility must provide fully trained personnel and shall be supplied with detailed operating procedures to cover all activities as required by 10 CFR 71.89.

7.2.1. Receipt of Package from Carrier

7.2.1.1. Package Receipt and Inspection

Repeat Steps 7.1.1 (a and b) and perform a radiological survey in accordance with the requirements of 10 CFR 20.205 (Reference 7-5) or equivalent agreement state regulations.

7.2.1.2. Removal of the Package from the Transport Vehicle

- a. Position the transport vehicle under an overhead crane.
- b. Remove protective personnel barrier if required.
- c. Remove the packaging tie-downs.
- d. Position the spreader bar and connect the appropriate slings and shackles.

- e. Depending on site-specific issues, either
 - Lift the overpack top section off the overpack base and place on the overpack stand, or
 - Lift the entire packaging free from the transport vehicle and set down. Then lift the overpack top section from the overpack base and place on the overpack stand.

7.2.1.3. Preparing To Unload Contents

- a. Perform a visual inspection. Note any damage or unusual conditions. If functionality of the part is impaired, repair or replace as required.
- b. Perform a radiological survey of the cask.
- c. Install the cask lifting ears or auxiliary ears (if applicable). Torque the cask lifting ear or auxiliary ear screws to 600 ft-lb in four places for each ear. Transport the cask to the unloading area.
- d. With radiological monitoring and controlled ventilation in place, remove the vent plug and drain plugs.
- e. Remove the lid bolts for unloading in either a storage basin or hot cell.
- f. Remove the lid following the placing of the cask within a hot cell or storage basin.
- g. Remove the spacer if present.
- h. Remove the HPI top plug.
- i. If the cask is to be unloaded in air at a waste disposal site, prepare the cask for unloading following a procedure developed by the burial site and reviewed by GEH Nuclear Energy.
- j. If the cask is unloaded in a hot cell or underwater, prepare the cask for unloading following a site-specific procedure, reviewed by GE Hitachi Nuclear Energy.

7.2.2. Removal of Contents

7.2.2.1. Unloading Irradiated Fuel / Co-60 Isotope Rods

The usage of the term 'rods' in this section refers to either irradiated fuel rods or cobalt-60 isotope rods.

- a. Obtain the list identifying the rods to be unloaded.
- b. Verify the identification and location of the rods in the cask.
- c. Transfer the rods, or shoring device such as rod holders if applicable, one at a time in accordance with the site's transfer procedure.

7.2.2.2. Unloading Irradiated Hardware / 500 grams U-235 Equivalent Mass of SNM

The usage of the term 'contents' in this section refers to either irradiated hardware or 500 grams U-235 equivalent mass of SNM.

- a. Unload cask contents in accordance with the site's transfer procedure.

7.2.2.3. Installing the Cask Closure Lid

- a. With proper rigging, slowly lower the HPI top plug over the alignment pins.
- b. Install the spacer, if one came with the packaging.
- c. With proper rigging, slowly lower the lid onto the cask over the guide pins. Closely watch this operation to assure that the lid is properly aligned.

7.2.2.4. Removing the Cask from the Unloading Area

- a. Tighten the lid bolts hand-tight.
- b. Remove the cask to the storage area.

7.2.2.5. Securing the Cask Lid

- a. Repeat Section 7.1.3.2.

7.3 Preparation of Empty Packaging for Transport

The following operations are typically performed after transport of radioactive material.

7.3.1. Cask Cavity Inspection

- a. Remove the lid from the empty cask.
- b. Perform a radiological survey of the cavity to determine extent of any contamination.
- c. Decontaminate the cavity to the limits of 49 CFR 173.428 if the cask is shipped as an empty container as defined in the regulation.
- d. Visually inspect the cask and contents to ensure that moisture has been removed.

7.3.2. Installation of the Cask Closure Lid

- a. With proper rigging, slowly lower the lid onto the cask over the guide pins. Closely watch this operation to assure that the lid is properly aligned.
- b. Install the head bolts and torque to 500 ft-lb in a crisscross pattern to ensure equal compression of the seal.
- c. Inspect the cask to verify that all drain, test, and vent plugs are properly installed.

7.3.3. Assembly Verification Leakage Testing

Leakage testing is not required to be performed on the empty container. As an option, leakage testing may be performed on an empty container prior to shipment for loading operations at a user facility, to assure a new seal performs as required.

7.3.4. Preparing the Empty Cask for Transport

Decontaminate the external surfaces of the cask to a level consistent with 49 CFR 173.427, "Empty Radioactive Materials Packaging".

7.4 Other Operations

There are no provisions required for any special operational controls (e.g., route, weather, mode, shipping time restrictions).

7.5 Appendix

The offeror is responsible for completing the loading table(s) in Sections 7.5.1 through 7.5.5 as necessary, as part of their pre-shipment evaluation review and approval process/system in advance of releasing the shipment in question.

7.5.1. Irradiated Fuel Loading Table

This section is included in order to provide clear instructions for using the Irradiated Fuel Loading Table. Figure 7.5.1-1 shows the Irradiated Fuel Loading Table with cells labeled for clear instruction for data entry. It can be noted in this figure that:

- Columns 1-4 are included to record information on each rod segment that is to be sent in a single Model 2000 Transport Package.
- Column 5 is included to demonstrate compliance with the criticality limits of the cask.
- Column 6 is included to demonstrate compliance with the thermal limits of the cask.
- Columns 7-14 are included to demonstrate compliance with regulatory dose rate limits.
- Row A is filled out individually for each rod segment in the shipment.
- Row B summarizes the information from all rows above.
- Row C provides the respective regulatory/cask limit for each column.
- Row D states whether the proposed shipment meets the respective regulatory/cask requirement. Cells in this row should be filled with either 'YES' or 'NO'. Once the Irradiated Fuel Loading Table is filled out entirely, if all cells in Row D say 'YES', the shipment complies with all necessary criticality, thermal, and dose rate criteria.
- Row E is included to record the personnel who filled out the loading table.

| Column | | | | | | | | | | | | | | | | | |
|--------|---|-----------|-------------------------|-------------------------------|------------------|---------------|-------------------|--------------------|------|--------|------------------|-------------------|------------------|------|--------|----|-----|
| | | 1 | 2 | 3 | 4 | 5 | 6 | 7 | 8 | 9 | 10 | 11 | 12 | 13 | 14 | | |
| A | → | Segment # | Segment Length (Inches) | Initial Enrichment (wt% U235) | Burnup (GWd/MTU) | Mass U235 (g) | Thermal Power (W) | NCT | | | | | | HAC | | | |
| | | | | | | | | DR _{surf} | | | DR _{2m} | DR _{cab} | DR _{2m} | | | | |
| | | | | | | | | Top | Side | Bottom | | | Top | Side | Bottom | | |
| | | | | | | | | A1 | A2 | A3 | A4 | A5 | A6 | A7 | A8 | A9 | A10 |
| | | | | | | | | | | | | | | | | | |
| | | | | | | | | | | | | | | | | | |
| | | | | | | | | | | | | | | | | | |
| Row | | | | | | | | | | | | | | | | | |
| | | | | | | | | | | | | | | | | | |
| | | | | | | | | | | | | | | | | | |
| | | | | | | | | | | | | | | | | | |
| | | | | | | | | | | | | | | | | | |
| | | | | | | | | | | | | | | | | | |
| | | | | | | | | | | | | | | | | | |
| | | | | | | | | | | | | | | | | | |
| | | | | | | | | | | | | | | | | | |
| | | | | | | | | | | | | | | | | | |
| | | | | | | | | | | | | | | | | | |
| | | | | | | | | | | | | | | | | | |
| | | | | | | | | | | | | | | | | | |
| | | | | | | | | | | | | | | | | | |
| | | | | | | | | | | | | | | | | | |
| | | | | | | | | | | | | | | | | | |
| | | | | | | | | | | | | | | | | | |
| | | | | | | | | | | | | | | | | | |
| | | | | | | | | | | | | | | | | | |
| | | | | | | | | | | | | | | | | | |
| | | | | | | | | | | | | | | | | | |
| | | | | | | | | | | | | | | | | | |
| | | | | | | | | | | | | | | | | | |
| | | | | | | | | | | | | | | | | | |
| | | | | | | | | | | | | | | | | | |
| | | | | | | | | | | | | | | | | | |
| | | | | | | | | | | | | | | | | | |
| | | | | | | | | | | | | | | | | | |
| | | | | | | | | | | | | | | | | | |
| | | | | | | | | | | | | | | | | | |
| | | | | | | | | | | | | | | | | | |
| | | | | | | | | | | | | | | | | | |
| | | | | | | | | | | | | | | | | | |
| | | | | | | | | | | | | | | | | | |
| | | | | | | | | | | | | | | | | | |
| | | | | | | | | | | | | | | | | | |
| | | | | | | | | | | | | | | | | | |
| | | | | | | | | | | | | | | | | | |
| | | | | | | | | | | | | | | | | | |
| | | | | | | | | | | | | | | | | | |
| | | | | | | | | | | | | | | | | | |
| | | | | | | | | | | | | | | | | | |
| | | | | | | | | | | | | | | | | | |
| | | | | | | | | | | | | | | | | | |
| | | | | | | | | | | | | | | | | | |
| | | | | | | | | | | | | | | | | | |
| | | | | | | | | | | | | | | | | | |
| | | | | | | | | | | | | | | | | | |
| | | | | | | | | | | | | | | | | | |
| | | | | | | | | | | | | | | | | | |
| | | | | | | | | | | | | | | | | | |
| | | | | | | | | | | | | | | | | | |
| | | | | | | | | | | | | | | | | | |
| | | | | | | | | | | | | | | | | | |
| | | | | | | | | | | | | | | | | | |
| | | | | | | | | | | | | | | | | | |
| | | | | | | | | | | | | | | | | | |
| | | | | | | | | | | | | | | | | | |
| | | | | | | | | | | | | | | | | | |
| | | | | | | | | | | | | | | | | | |
| | | | | | | | | | | | | | | | | | |
| | | | | | | | | | | | | | | | | | |
| | | | | | | | | | | | | | | | | | |
| | | | | | | | | | | | | | | | | | |
| | | | | | | | | | | | | | | | | | |
| | | | | | | | | | | | | | | | | | |
| | | | | | | | | | | | | | | | | | |
| | | | | | | | | | | | | | | | | | |
| | | | | | | | | | | | | | | | | | |
| | | | | | | | | | | | | | | | | | |
| | | | | | | | | | | | | | | | | | |
| | | | | | | | | | | | | | | | | | |
| | | | | | | | | | | | | | | | | | |
| | | | | | | | | | | | | | | | | | |
| | | | | | | | | | | | | | | | | | |
| | | | | | | | | | | | | | | | | | |

Figure 7.5.1-1. Irradiated Fuel Rod Loading Table

The Irradiated Fuel Loading Table is filled out using the following procedure. Cell labels are from Figure 7.5.1-1.

1. Depending on the configuration, enter the thermal limit for the shipment in Cell C6. For a shipment using Configuration 1, enter 1500. For a shipment using Configuration 2, enter 3000.
2. Starting in Cell A1 enter the segment number identifier for the first segment to be entered into the loading table. This number is simply a label for the segment and can be any unique identifying number, or simply start with “1”.
3. In Cell A2 enter the active fuel length of the respective fuel rod segment. Every fuel rod segment loaded into the cask, and entered in this loading table must have an active length of at least 10 inches.
4. In Cell A3 enter the initial enrichment range for the respective segment, considering the minimum initial enrichment (in wt% U-235) for the respective segment. Depending on the minimum initial enrichment of the segment, this cell should be filled according to Table 7.5.1-1 (e.g., if the initial enrichment for the respective segment is 2.7 wt% U-235, the label ‘2.5 ≤ e < 3.0’ should be entered into cell A3).

Table 7.5.1-1. Irradiated Fuel Loading Table Column 3 Labels

| Initial Enrichment Ranges (wt% U-235) |
|------------------------------------------------------|
| $0.71 \leq e < 1.5$ |
| $1.5 \leq e < 2.0$ |
| $2.0 \leq e < 2.5$ |
| $2.5 \leq e < 3.0$ |
| $3.0 \leq e < 3.5$ |
| $3.5 \leq e < 4.0$ |
| $4.0 \leq e < 4.5$ |
| $4.5 \leq e < 5.0$ |
| $5.0 \leq e < 5.5$ |
| $5.5 \leq e < 6.0$ |

5. In Cell A4 enter the burnup range for the respective segment, considering maximum burnup (in GWd/MTU) for the respective segment. Depending on the maximum burnup of the segment, this cell should be filled according to Table 7.5.1-2 (e.g., if the burnup for the respective segment is 45 GWd/MTU, the label ' $40 < b \leq 50$ ' should be entered into cell A4).

Table 7.5.1-2. Irradiated Fuel Loading Table Column 4 Labels

| Burnup Ranges (GWd/MTU) |
|------------------------------------|
| $0 < b \leq 10$ |
| $10 < b \leq 20$ |
| $20 < b \leq 30$ |
| $30 < b \leq 40$ |
| $40 < b \leq 50$ |
| $50 < b \leq 60$ |
| $60 < b \leq 72$ |

6. In Cell A5 enter the initial mass of U-235 for the respective rod segment (in gU-235).
7. In Cell A6, enter the thermal power for the respective rod segment (in W). This value is calculated by multiplying the mass of U-235 for the rod (in Cell A5) by the respective thermal power multiplier in Table 5.5-5. The appropriate thermal power multiplier in Table 5.5-5 is determined based on the initial enrichment range (in Cell A3) and burnup range (in Cell A4) for the respective segment (e.g., if for the respective segment, the initial enrichment range is ' $2.5 \leq e < 3.0$ ' and the burnup range is ' $40 < b \leq 50$ ', the thermal power multiplier from Table 5.5-5 is 8.559E-01 W/gU-235).
8. In Cells A7 through A14, enter the dose rate contribution for the respective rod segment (in mrem/hr) for the dose rate location in the appropriate column. This value is calculated by multiplying the mass of U-235 for the rod (in Cell A5) by the dose rate

multiplier for the respective dose rate location. Table 7.5.1-3 summarizes the information for filling out Cells A7 through A14 and provides an example dose rate contribution multiplier for the example scenario of a rod segment with an initial enrichment range of ' $2.5 \leq e < 3.0$ ' in Cell A3 and a burnup range of ' $40 < b \leq 50$ ' in Cell A4.

Table 7.5.1-3. Irradiated Fuel Loading Table Dose Rate Multipliers

| Irradiated Fuel Loading Table Cell Label | Dose Rate Location | Multiplier Table (in Chapter 5) | Example Multiplier¹ (mrem/hr/gU-235) |
|-----------------------------------------------------|---------------------------|--------------------------------------------|------------------------------------------------------------|
| A7 | NCT Top Surface | 5.4-4 | 8.131E-02 |
| A8 | NCT Side Surface | 5.4-5 | 4.877E-01 |
| A9 | NCT Bottom Surface | 5.4-6 | 2.540E-01 |
| A10 | NCT 2-meter | 5.4-7 | 1.216E-02 |
| A11 | NCT Cab | 5.4-8 | 2.183E-03 |
| A12 | HAC Top 1-meter | 5.4-9 | 7.577E-02 |
| A13 | HAC Side 1-meter | 5.4-10 | 8.745E-02 |
| A14 | HAC Bottom 1-meter | 5.4-11 | 8.204E-02 |

Note: ¹ Multiplier based on example case of segment with initial enrichment range $2.5 \leq e < 3.0$ and initial burnup range $40 < b \leq 50$

9. Repeat Steps 2 through 8 in the following row, filling in Columns 1 through 14, for each fuel rod segment that shall be included in the shipment.
10. With the top portion of the loading table filled out, in Cell B2, enter the minimum value from all segments in Column 2.
11. In Cell B5, sum the masses of U-235 from all segments entered in Column 5 of the top portion of the loading table.
12. In Cell B6, sum the thermal power contributions from all segments entered in Column 6 of the top portion of the loading table.
13. For Cells B7 - B14, sum the dose rate contributions from all segments entered in the top portion of the loading table, for each column (e.g., for Cell B7 sum Column 7, for Cell B8, sum Column 8).
14. For Cell D2, if the value in Cell B2 is greater than or equal to 10 write 'Yes', if not write 'No'.
15. For Cells D5 through D14, if the respective value in Row B is less than or equal to the value in Row C, write 'Yes', if not write 'No'.
16. If all cells in Row D say 'Yes', the proposed load of irradiated fuel rod segments meets all criticality, thermal, and dose rate criteria and is acceptable for shipment. If any cells in Row D say 'No', a limit has been exceeded and the proposed load of irradiated fuel rod segments is not acceptable for shipment.

17. Upon completion of the Irradiated Fuel Table, the name of the personnel responsible for filling out the table is entered in Cell E1.

The following page provides the Irradiated Fuel Loading Table that is to be filled out prior to any shipment of this content type.

7.5.2. Irradiated Hardware and Byproduct Loading Table

This section is included in order to provide clear instructions for using the Irradiated Hardware and Byproduct Loading Table. Figure 7.5.2-1 shows the Irradiated Hardware and Byproduct Loading Table with cells labeled for clear instruction for data entry. It can be noted in this figure that:

- Column 1 is included to record each radionuclide in the Irradiated hardware or byproducts in a single shipment (with activity >1 Ci).
- Column 2 is included to record the activity of each radionuclide listed.
- Column 3 is included to demonstrate compliance with the thermal limits of the cask.
- Columns 4-11 are included to demonstrate compliance with regulatory dose rate limits for each location.
- Row A is filled out individually for each radionuclide in the shipment.
- Row B provides a summed total for each column.
- Row C provides the respective regulatory/cask limit for each column.
- Row D states whether the proposed shipment meets the respective regulatory/cask requirement. Cells in this row should be filled with either 'YES' or 'NO'. Once the Irradiated Hardware and Byproduct Loading Table is filled out entirely, if all cells in Row D say 'YES', the shipment complies with all necessary criticality, thermal, and dose rate criteria.
- Row E is included to record the personnel who filled out the loading table

| Column | | | | | | | | | | | |
|--------|---------------|---------------|-------------------|--------------------|------|-------------------|------------------|-------------------|------------------|------|--------|
| | 1 | 2 | 3 | 4 | 5 | 6 | 7 | 8 | 9 | 10 | 11 |
| A → | Radionuclide | Activity (Ci) | Thermal Power (W) | NCT | | | | | HAC | | |
| | | | | DR _{surf} | | | DR _{2m} | DR _{cab} | DR _{1m} | | |
| | | | | Top | Side | Bottom | | | Top | Side | Bottom |
| | | | | A1 | A2 | A3 | A4 | A5 | A6 | A7 | A8 |
| | | | | | | | | | | | |
| | | | | | | | | | | | |
| | | | | | | | | | | | |
| Row | | ⋮ | | | | ⋮ | | | | ⋮ | |
| | | ⋮ | | | | ⋮ | | | | ⋮ | |
| | | | | | | | | | | | |
| B → | Total | - | B3 | B4 | B5 | B6 | B7 | B8 | B9 | B10 | B11 |
| C → | Limit | - | C3 | 180 | 180 | 180 | 9 | 1.8 | 900 | 900 | 900 |
| D → | Criteria Met? | - | D3 | D4 | D5 | D6 | D7 | D8 | D9 | D10 | D11 |
| E → | | | | | | Filled out by: E1 | | | | | |

Figure 7.5.2-1. Irradiated Hardware and Byproduct Loading Table

NEDO-33866 Revision 0
Non-Proprietary Information – Class I (Public)

The Irradiated Hardware and Byproduct Table is filled out using the following procedure. Cell labels are from Figure 7.5.2-1.

1. Depending on the configuration, enter the thermal limit for the shipment in Cell C3. For a shipment using Configuration 1 enter 1500, and for a shipment using Configuration 2 enter 3000.
2. Starting in Cell A1 enter the first radionuclide into the loading table. This column should simply list the radionuclide name or abbreviation (e.g., enter either 'Cobalt-60' or 'Co-60').
 - Only radionuclides with activity greater than 1 Ci must be entered into the loading table. Any neutron emitting radionuclides are limited to trace amounts, strictly from surface contamination of the hardware or byproducts are permitted for shipment.
 - Any radionuclide with all gamma emissions less than 0.3 MeV or a half-life less than 3 days is irrelevant to dose rate calculations, but should be entered in the table for thermal contributions. If the radionuclide is not included in Table 5.5-30, the thermal power multiplier can be calculated using Equation 5-12 and the Q-value for the radionuclide in the SCALE6.1 ORIGEN decay library `origen.rev03.decay.data` (Reference 7-6).
 - Any contents including radionuclides with an activity greater than 1 Ci that are not listed in Table 5.5-30, that also have gamma emissions greater than 0.3 MeV and a half-life greater than 3 days are not allowable for shipment.
3. In Cell A2 enter the activity in curies of the respective radionuclide.
4. In Cell A3, enter the thermal power for the radionuclide (in W). This value is calculated by multiplying the activity of the radionuclide (in Cell A2) by the thermal power multiplier of the radionuclide listed in Table 5.5-30.
5. In Cells A4 through A11, enter the dose rate contribution for the respective radionuclide (in mrem/hr) for the dose rate location of the appropriate column. This value is calculated by multiplying the activity of the radionuclide (in Cell A2) by the dose rate multiplier of the radionuclide for the respective dose rate location. Dose rate multipliers for all radionuclides that are significant to the shielding analysis are provided in Table 5.4-13 for NCT dose rates and Table 5.4-14 for HAC dose rates. Irradiated hardware and byproduct radionuclides listed in Table 5.5-7, but not in Table 5.4-13 or Table 5.4-14, are not relevant to dose rate calculations, thus cells A4 through A11 may be filled with a '0' for those radionuclides. Table 7.5.2-1 provides the cobalt-60 dose rate multiplier for the NCT side surface and the HAC 1-meter locations, for reference.

Table 7.5.2-1. Irradiated Hardware and Byproduct Loading Table Dose Rate Multipliers

| Irradiated Hardware and Byproduct Loading Table Cell Label | Condition | Multiplier Table (in Chapter 5) | Example Multiplier (mrem/hr/Ci) |
|-------------------------------------------------------------------|------------------|----------------------------------------|----------------------------------------|
| A5 | NCT | 5.4-13 | 9.437E-03 ¹ |
| A10 | HAC | 5.4-14 | 1.743E-03 ² |

Notes: ¹ Multiplier based on cobalt-60 NCT side surface location

² Multiplier based on cobalt-60 HAC side 1-meter location

6. Repeat Steps 2 through 5 in the next row, filling in Columns 1 through 11, for every radionuclide that is included in the irradiated contents.
7. With the top portion of the loading table filled out, in Cell B3, sum the thermal power contributions from all radionuclides entered in Column 3 of the top portion of the loading table.
8. For Cells B4 - B11, sum the dose rate contributions from all radionuclides entered in the top portion of the loading table, for each column (e.g., for Cell B4 sum Column 4, for Cell B5, sum Column 5).
9. For Cells D3 through D11, if the respective value in Row B is less than or equal to the value in Row C, enter 'Yes', if the value in Row B is greater than the value in Row C enter 'No'.
10. If all cells in Row D say 'Yes', the proposed load of irradiated contents meet all thermal and dose rate criteria and are acceptable for shipment. If any cells in Row D say 'No', a limit has been exceeded and the proposed load of irradiated contents is not acceptable for shipment.
11. Upon completion of the Irradiated Hardware and Byproduct Table, the name of the personnel responsible for filling out the table is entered in Cell E1.

The following page provides the Irradiated Hardware and Byproduct Loading Table that is to be filled out prior to any shipment of this content type.

7.5.3. Verification of Compliance for Cobalt-60 Isotope Rods

Compliance with the cask thermal and regulatory dose rate limits for the cobalt-60 isotope rod contents is demonstrated through a check of the peak activity limit across any rod and using the Cobalt-60 Isotope Rod Loading Table. It is determined that a batch of cobalt-60 isotope rods is acceptable for shipment in the Model 2000 Transport Package using the following procedure:

1. Verify that the peak activity of cobalt-60 for any rod is less than the limit calculated as specified in Section 5.5.3, using the following procedure:
 - Determine the number of rod [[]] included in the shipment. This number is N.
 - Determine the allowable peak activity for the isotope rods: calculated as $17,000 \text{ Ci} / N$.
 - Determine the peak activity of any rod included in the shipment. This is the maximum activity across any 1-inch length of the rod.
 - Compare the peak activity across all rods in the shipment to the allowable peak activity. Ensure that the peak activity of the rods is less than the allowable peak activity for the number of rods shipped.
2. Determine if there is any additional significant radionuclide activity in the rod cladding or hardware components shipped with the isotope rods. If there are additional radionuclides in the rod cladding or additional hardware shipped with the isotope rods skip to Step 3. If there are no additional radionuclides other than the cobalt-60 in the isotope rods, check that the total activity of cobalt-60 in the cask is in the range specified for the configuration that the package is shipped in:
 - For Configuration 1: 0 – 97,200 Ci (Thermal equivalent: 0 – 1,500 W)
 - For Configuration 2: 32,500 – 194,500 Ci (Thermal equivalent: 500 – 3,000 W)

If the requirements in Step 1 and 2 are met, the load of cobalt-60 isotope rods meets all cask and regulatory requirements and is acceptable for shipment.

3. Enter the thermal power limit into the 'Limit' row of the Cobalt-60 Isotope Rod Loading Table based on whether the shipment is Configuration 1 (1500 W) or Configuration 2 (3000 W).
4. Enter the total cobalt-60 activity of the cobalt-60 isotope rod contents (in Ci).
5. Enter the thermal power for the cobalt-60 isotope rod contents (in W). This value is calculated by multiplying the activity of the isotope rods by the thermal power multiplier for cobalt-60, $1.542\text{E-}02 \text{ W/Ci}$ (From Table 5.5-30).
6. In Cells A4 through A11, enter the dose rate contribution for the cobalt-60 isotope rod contents (in mrem/hr) for the dose rate location of the appropriate column. This value is calculated by multiplying the total activity of the isotope rods by the dose rate multiplier

for the respective dose rate location. The dose rate multipliers for each dose rate location are provided in Table 5.4-17 for NCT dose rates and Table 5.4-18 for HAC dose rates. Table 7.5.4-1 provides the cobalt-60 dose rate multiplier for the NCT side surface and the HAC 1-meter locations, for reference.

Table 7.5.4-1. Cobalt-60 Isotope Rod Loading Table Dose Rate Multipliers

| Condition | Regulatory Dose Rate Location | Multiplier Table (in Chapter 5) | Example Multiplier (mrem/hr/Ci) |
|-----------|-------------------------------|---------------------------------|---------------------------------|
| NCT | Side Package Surface | 5.4-17 | 8.821E-04 |
| HAC | Side 1-Meter | 5.4-18 | 1.743E-03 |

7. Upon completion of the Cobalt-60 Isotope Rod Loading Table, the name of the personnel responsible for filling out the table is entered into the appropriate cell.
8. If the maximum dose rate is less than or equal to the dose rate limit, enter ‘Yes’ in the ‘Criteria Met?’ row, otherwise enter ‘No’.
9. If all cells in the ‘Criteria Met?’ row of the Cobalt-60 Isotope Rod Loading Table say ‘Yes’, the cobalt-60 isotope rod contents meet all regulatory/cask criteria. Fill out the Irradiated Hardware and Byproduct Table per instructions in Section 7.5.2. This table should be filled out for any significant radionuclide activity in the rod cladding and any irradiated hardware included in the shipment. If there is a measurable thermal or dose rate contribution from the irradiated hardware, also fill out the Combined Contents Loading Table per instructions in Section 7.5.4 to demonstrate that all regulatory/cask requirements are met for the combined contents.

The following page provides the Cobalt-60 Isotope Rod Loading Table that is to be filled out prior to any shipment of this content type.

7.5.4. Combined Contents

For any shipment including multiple content types, compliance with regulatory/cask limits is demonstrated using the following procedure:

1. Fill out the Irradiated Fuel Loading Table per instructions in Section 7.5.1, as applicable.
2. Fill out the Irradiated Hardware and Byproduct Loading Table per instructions in Section 7.5.2, as applicable.
3. Fill out the Cobalt-60 Isotope Rod Loading Table per instructions in Section 7.5.3, as applicable.
4. Enter the thermal power limit into the ‘Limit’ row of the Combined Contents Loading Table based on whether the shipment is Configuration 1 (1500 W) or Configuration 2 (3000 W).
5. Enter the thermal power and dose rate values from the ‘Total’ row of each applicable loading table from Steps 1 through 3 into the respective ‘Fuel’, ‘Hardware/Byproduct’, and ‘Cobalt-60 Isotope Rod’ rows in the Combined Contents Loading Table.
6. Sum the thermal powers and dose rate values from all content types in the ‘Total’ row of the Combined Contents Loading Table.
7. Verify that for each column the value in the ‘Total’ row is less than the value in the ‘Limit’ row. Record this verification by writing ‘Yes’ if the criteria is met, or ‘No’ if the criteria is not met.
8. If all cells in the ‘Criteria Met?’ row of the Irradiated Fuel Loading Table, the Irradiated Hardware and Byproduct Loading Table, and the Combined Contents Loading Table say ‘Yes’, the proposed load of combined contents meets all regulatory/cask criteria and is acceptable for shipment. If any cells in any of the three Tables say ‘No’, a limit has been exceeded and the proposed load of combined contents is not acceptable for shipment.
9. Upon completion of the Combined Contents Loading Table, the name of the personnel responsible for filling out the table is entered into the appropriate cell.

The following page provides the Combined Contents Loading Table that is to be filled out prior to any shipment including multiple content types.

7.5.5. Verification of Compliance for Special Nuclear Material Contents

The SNM contents are limited by the criticality analysis. It is determined that a load of SNM is acceptable for shipment in the Model 2000 Transport Package, using the following procedure:

1. Determine that the U-235 equivalent mass is less than the U-235 mass limit of 430 grams using the following method:

The U-235 equivalent mass is determined by U-235 mass plus 1.63 times Pu-239 mass, plus 2.87 times Pu-241 mass, and 1.39 times U-233 mass. The content may contain other uranium and plutonium isotopes.

2. If the SNM contents are shipped with irradiated hardware, fill out the Irradiated Hardware and Byproduct Loading Table per instructions in Section 7.5.2, and ensure that the Irradiated hardware contents meet all thermal and dose rate requirements.

7.6 References

- 7-1 GE Hitachi Nuclear Energy, "Operations and Maintenance of Model 2000 Transport Package," Specification Number 22A9380 Revision 8, July 2003, or latest revision.
- 7-2 U.S. Department of Transportation Code of Federal Regulations, Title 49 Part 173, "Shippers-General Requirements For Shipments and Packagings," April 2016.
- 7-3 U.S. Nuclear Regulatory Commission Code of Federal Regulations, Title 10 Part 71, "Packaging and Transport of Radioactive Material," April 2016.
- 7-4 Leak Testing Specialists, Inc., "Helium Mass Spectrometer Leak Test Procedure Evacuated Envelope Technique Pre-Shipment Leak Testing of GE 2000 Transport Packging Cask," MSLT-EE-GE, Revision 5500-01, 2014.
- 7-5 U.S. Nuclear Regulatory Commission Code of Federal Regulations, Title 10 Part 20, "Standards for Protection Against Radiation," 2016.
- 7-6 Oak Ridge National Lab, "SCALE: A Comprehensive Modeling and Simulation Suite for Nuclear Safety Analysis and Design, ORNL/TM-2005/39, Version 6, Vols. I-III," ORNL/TM-2005/39, Version 6.1, June 2011.

8 ACCEPTANCE TESTS AND MAINTENANCE PROGRAM

This chapter describes the acceptance tests and maintenance program to be used for the Model 2000 Transport Package, required by 10 CFR 71, Subpart G (Reference 8-1). The acceptance tests are prescribed to verify materials of construction, fabrication processes, and the transport package's design adequately meets the regulations, while the maintenance program outlined in this chapter assures the packaging's performance during its service life, in full compliance with this safety analysis report.

General information related to the Model 2000 Transport Package, including package design details and contents description, is presented in Chapter 1 of this safety analysis report. For package dimensions, refer to the licensing drawings provided in Section 1.3.1. Fabrication and examination of the Model 2000 Transport Package (i.e., cask and overpack), the high performance insert (HPI) assembly, and material basket assembly, conform to the requirements of ASME Section III, as delineated in Section 8.1.

Routine inspection (prior to each loading) consists of visual examination for physical damage of all surfaces and components. Periodic or annual inspection includes visual examination, penetrant inspection of welds, and replacement of damaged or worn components, as necessary.

8.1 Acceptance Test

The inspection and acceptance tests are specified in the fabrication specifications and engineering drawings for the Model 2000 Transport Package and are governed by GEH Quality Assurance Program QAP-1 (Reference 8-2). QAP-1 has been approved by the NRC (Docket Number 71-0170) (Reference 8-3).

8.1.1. Visual Inspections and Measurements

Visual examinations of all dimensions are conducted during fabrication to ensure that the packaging is fabricated and assembled in accordance with manufacturing drawings and specifications. All dimensions and tolerances specified on the drawings are confirmed by measurement. Fabrication deviations are addressed in compliance with QAP-1 for all components important to Safety Category A or B.

8.1.2. Weld Examinations

Visual examinations of all welds, including overpack torodial shells, are conducted during fabrication. In addition, all welds within the cask containment boundary are liquid penetration tested (root and final passes); also, the welds forming the toroidal shell are 100% radiographed. These inspections are performed to ensure no cracks, incomplete fusion, or lack of penetration, exists. Parts that do not meet the established criteria are repaired or replaced in accordance with written procedures. For Model 2000 Transport Package serial number (S/N) 2001, nondestructive examination (NDE) procedures and acceptance standards are based on the ASME Code, Section III, Subsection NG (Reference 8-4). All future fabrication will meet the requirements of the ASME Code, Section III as follows:

Cask assembly including ears (Reference 8-5):

- Materials per NB-2000, Certification NCA-3800
- Fabrication per NB-4000
- NDE per NB-5000
- Pressure testing per NB-6000

The following components of the cask assembly shall be excluded of the above requirements:

- Shielding lead and its installation
- [[]]
- Seals and test port components
- Electro-polishing
- Miscellaneous equipment (e.g., name plate and its screws, honeycomb, and thread inserts).

Overpack assembly per Subsection NF (Reference 8-6):

- Materials per NF-2000
- Fabrication per NF-4000
- NDE per NF-5000

HPI and material basket Importance to Safety Category B components and welds (Reference 8-6):

- Materials per NF-2000
- Forming, fittings, and aligning per NF-4200
- Welding per NF-4400
- Qualification of Weld Procedures and Personnel per NF-4300
- Examination per NF-5000

The shielding materials of the HPI shall be excluded of the above requirements.

8.1.3. Structural and Pressure Tests

The cask cavity is hydrostatically tested to ensure that it is tight, per the requirements of the ASME Boiler and Pressure Vessel Code, Section III, Subsection NB, NB-6200. The test pressure is 45 psia, 50% greater than the design pressure of 30 psia, per the requirement in 10 CFR 71.85(b).

8.1.4. Fabrication Leakage Tests

The fabrication leakage rate tests are performed in accordance with ANSI N14.5-1997, “American National Standard for Radioactive Materials – Leakage Tests on Packages for

Shipment” (Reference 8-7) to ensure leaktightness of the cask welds and seals as follows. All leak testing procedures are developed by an American Society for Nondestructive Testing (ASNT) Level III examiner per ASNT requirements.

During fabrication, maintenance, and periodic inspections, the cask containment boundary is tested to demonstrate whether it is leaktight in accordance with ANSI N14.5-1997. If the cask containment boundary is not demonstrated to be leaktight, the failed component is located, repaired or replaced, and reinspected. This applies to both the cask body and lid, as well as containment boundary components such as cask lid seal or port plugs.

8.1.5. Component and Material Tests

8.1.5.1. Valves, Rupture Discs, and Fluid Transport Devices

Component tests of valves, rupture discs and/or fluid transport devices are not applicable, because these parts do not exist in the Model 2000 Transport Package design.

8.1.5.2. Seal Testing

The procedure for testing the cask containment features is based on ANSI N14.5 and is conducted in accordance with the latest revision of the applicable GEH test specification (Reference 8-8). For Configuration 1 (1500 W), the justification for the [[]] retainer with four Parker Compound No. [[]] rings is as stated in Section 4.1.3. The port penetration containment boundary demonstration is provided in Reference 8-9, which demonstrates leak tightness for the port pipe plug with approved sealant tape. Test temperatures and pressures meet the HAC requirements as defined in Table 3.5.1-4 for Configuration 1 and Table 3.4.3-1 for Configuration 2.

For Configuration 2 (3000 W), an [[]] retainer with four Parker Compound No. [[]] rings is tested under normal, high and low temperature environments; the test temperatures are 70°F, 508°F and 5°F, respectively. For the Parker Compound No. [[]] rings, the minimum allowable internal wattage is set to 500 W. It is determined in the cold case analysis in Section 3.3.1.2, that with an internal wattage of 500 W, the minimum seal temperature at any of the seal regions is 21°F. Testing the Parker Compound No. [[]] rings at 5°F bounds the calculated minimum temperature and the value listed in the vendor specification for this material. The seal material is installed in a test flange and leak tested in accordance with ANSI N14.5. Seal material exceeding the allowable leak rate (leaktight per the ANSI N14.5 definition) is rejected. The test seal/flange joint used for both the Parker Compound No. [[]] ring and No. [[]] ring seal tests is a full-scale model in terms of flange and seal diameter with a representative cask body/lid joint fixture and is conducted in accordance with the latest revision of the applicable GEH test specification (Reference 8-8). The demonstration of the cask lid seal is presented in Reference 8-10.

8.1.5.3. Honeycomb Testing

The honeycomb energy absorber is tested in accordance with MIL-C-7438 latest revision (Reference 8-11), or equivalent. The test procedure determines the compressive properties of the

honeycomb material in the direction normal to the plane of facings. The test produces a load deformation curve, and from this curve the compressive stress at proportional limit load is calculated. If the honeycomb material does not meet the required crush strength, the material is rejected.

8.1.6. Shielding Tests

The shielding material is inspected for integrity. A cobalt source placed inside the lead-shielded cask is surveyed from the outside of the cask with a gamma detection instrument. The cask outside surface is divided by radial lines 12° apart and by equally spaced circumferential lines along the vertical axis. Dose rate readings are taken over each of the 420 rectangular regions (~4 inches square); see Figure 8-1. If an area of void is detected, radiographic film is placed over this area to determine the size and location of the void. The criterion used to evaluate the effect of the void is that the dose rate may not exceed one and one-half times the mean dose rate. Any void area that does not meet the criteria shall be re-poured with lead.

The [[]] is cast and machined to a high precision, to the requirements of the licensing drawings. The shielding integrity of the HPI is determined during manufacturing, where voids in the [[]] are checked for using a visual inspection and the density is verified using the total volume and weight.

8.1.7. Thermal Tests

A thermal test is performed on the first unit built of the Model 2000 Transport Package to determine the thermal performance of the system versus what is predicted by the analysis. This test is only done for the 600 W and 2000 W cases. The 3000 W configuration testing is completed through analysis as described in Section 3.

8.1.7.1. Discussion of Test Setup

Two thermal tests are conducted, one each with a 600 W and a 2000 W heat source. The heat source is installed concentrically within the cask cavity. Thermocouples are strategically placed within the cavity and the external portions of the cask and overpack surfaces as schematically shown in Figure 8-2.

8.1.7.2. Test Procedure

The test is conducted with each of the heat sources in a controlled ambient environment to simulate normal conditions of transport. The temperature data are recorded every 30 minutes with a data acquisition system, permitting easy analysis and plotting of the results. Data are recorded until temperature remains significantly unchanged for a one-hour period.

8.1.7.3. Acceptance Criteria

The results of the thermal test are evaluated against the predicted thermal performances. If the evaluation shows a discrepancy, the analytical thermal model is corrected based on the test results and a new thermal analysis is conducted. If the new analysis results indicate deficiency in

the thermal characteristics of the packaging, thermal barrier coating could be applied to the inner surface of the overpack structure as a corrective measure.

8.1.8. Miscellaneous Tests

No additional tests are required prior to the use of the packaging.

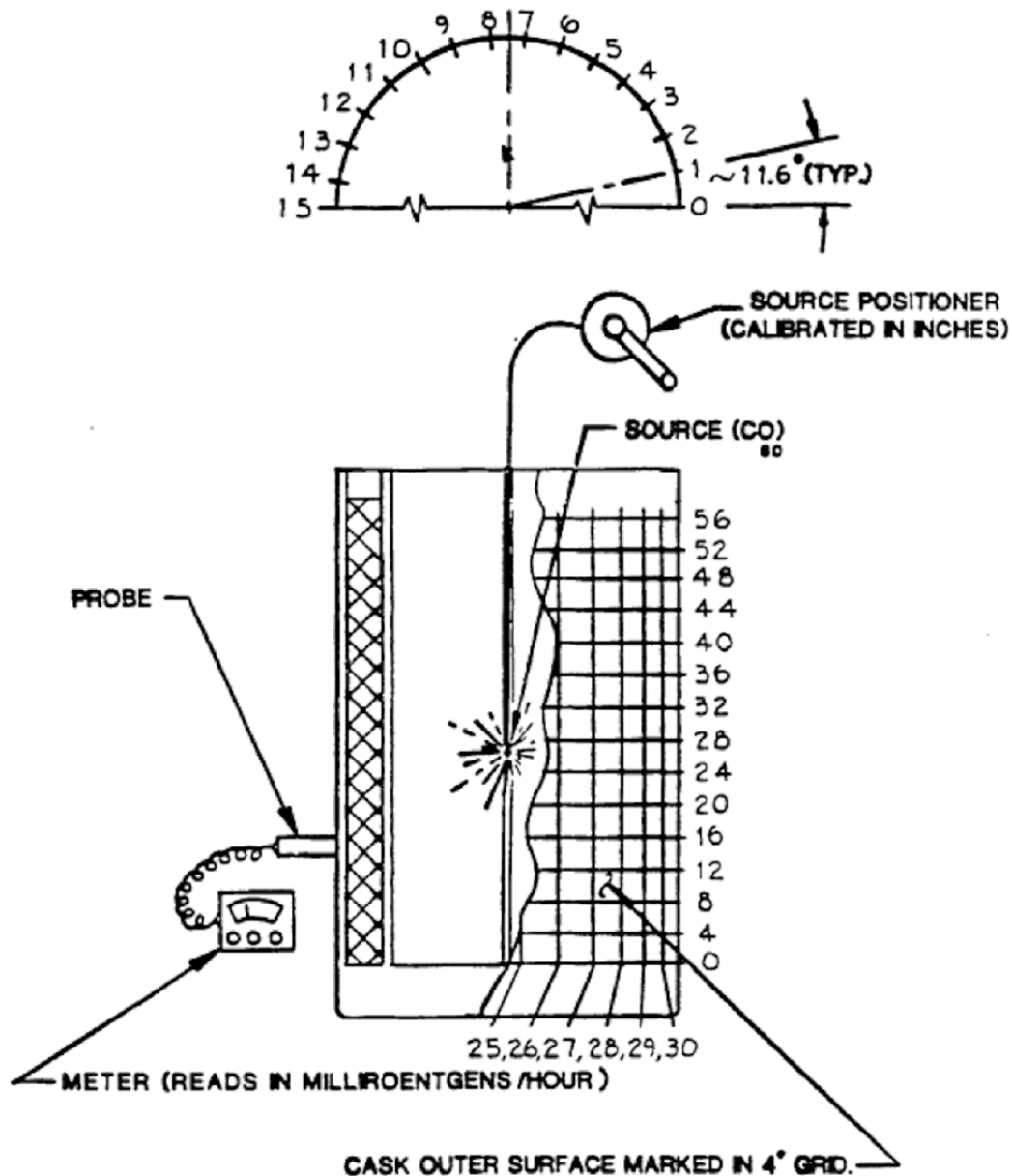


Figure 8-1. Cask Shielding Inspection Points

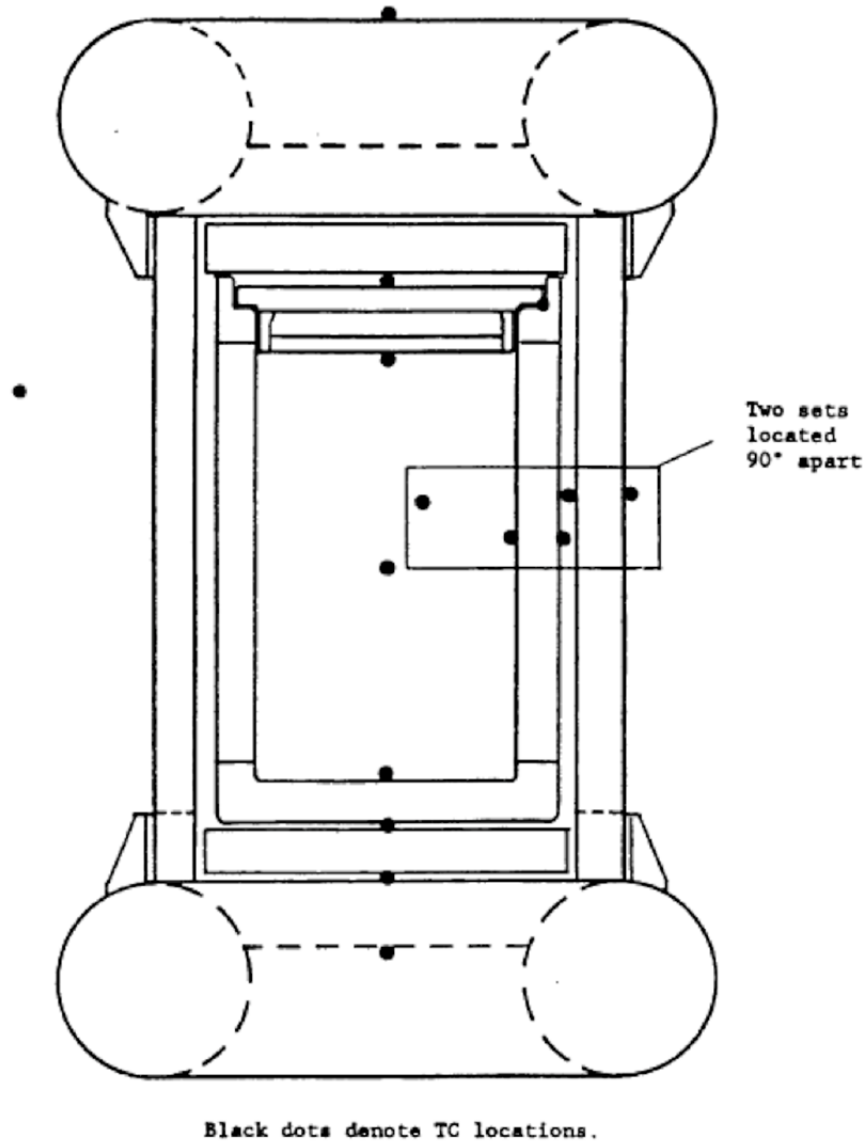


Figure 8-2. Thermocouple Locations

8.2 Maintenance Program

The cask maintenance program is described in detail in GE Specification 22A9380, “Operations and Maintenance of the Model 2000 Transport Package” (Reference 8-12). The specification was developed to implement the requirements established in this chapter. Operators of the Model 2000 Transport Package may develop procedures of their own within the requirements of the GE specification to include site-specific procedures.

Routine inspections are performed prior to each assembly and prior to each shipment. These inspections include visual checks of the packaging and any support structures or devices required to properly assemble the package. It also includes visual inspection of the cask and components and pressurization of the cask cavity. This pressurization is part of the leak check procedure. Additional, more detailed inspections are also performed every twelve (12) usages or at least once within the 12-month period prior to subsequent use, whichever comes first. The cask must be leak tested to 1×10^{-7} ref·cm³/sec prior to its first use, after the third use, and after 12 usages or at least once within the 12-month period prior to each subsequent use, whichever comes first.

8.2.1. Structural and Pressure Tests

8.2.1.1. Routine Inspection

Prior to each loading and assembly operation, the cask and lid are inspected for physical damage, especially the bolt holes, vent ports and sealing surfaces. The cask lid closure bolts, port plugs, O-rings, and lid gasket are all inspected visually and for proper dimensions and identification. In addition, the cask lid closure bolts have a 190-use limit. As part of the leak check, the cask cavity is pressurized to 15 psig with helium and tested per the pre-shipment requirements listed in Section 8.2.2.1. The overpack, HPI assembly, and HPI material basket components are inspected for visible signs of damage.

8.2.1.2. Periodic Inspections

At least once within a 12 month period and after every 12 usages, the following inspections are made. Any maintenance work required is identified on a maintenance checksheet.

The overpack is inspected for:

- Signs of excessive heat or fire.
- Punctures, holes, or other surface failures.
- Crushed sides or ends indicating a drop or severe impact.
- Defects resulting from normal or abnormal wear.
- Compression or damage to the honeycomb absorber material.
- Cracks or other damage to welds.
- Proper identification and damage to the bolts.

The cask is inspected for:

- Wear, corrosion or damage to the vent and drain port plugs, caps, and O-rings.
- Damage to sealing surfaces on the cask and lid.
- Damage or cracks to welds on the cask and lid.
- Proper identification or damage to the lid and ear bolts.

8.2.2. Leak Tests

The pre-shipment, periodic, and maintenance leak tests are all in accordance with ANSI N14.5 standards, with a reference air leakage rate (L_R) criterion of leaktight per the ANSI N14.5 definition of 1×10^{-7} ref·cm³/sec. All leak testing procedures are developed by an ASNT Level III examiner per ASNT requirements.

8.2.2.1. Pre-Shipment

Prior to each shipment, leakage testing of the cask lid closure seal and vent and drain plugs may be performed with a helium Mass Spectrometer Leakage Detector (MSLD). The tests for the cask lid closure seal, vent port, and drain port are performed in accordance with procedure number MSLT-EE-GE (Reference 8-13), or an equivalent procedure approved by GEH, to ensure each containment boundary seal is leaktight, per the ANSI N14.5 definition (1×10^{-7} ref cm³/sec).

8.2.2.2. Periodic

After every 12 months, the cask lid closure seal and vent and drain plugs are tested to ensure each containment boundary seal is leaktight, per the ANSI N14.5 definition (1×10^{-7} ref cm³/sec).

8.2.2.3. Maintenance

After any maintenance on the cask affecting a component of the containment boundary, such as a repair of a containment boundary weld, the affected component is leak tested per ANSI N14.5 standards, ensuring leaktightness ($< 1 \times 10^{-7}$ ref·cm³/sec) of the component.

8.2.3. Component and Material Tests

There are no auxiliary cooling systems or other subsystems requiring maintenance.

8.2.3.1. Valves, Rupture Disks, and Gaskets on Containment Vessel

The cask lid closure seal is used until visual and/or leak test inspections identify the seal as defective. The O-rings on the three penetration caps are replaced when visual or leak test inspections identify them as defective, or during the periodic inspection, whichever comes first. Note that Configuration 2 of the cask lid seal is not qualified for multiple uses.

8.2.3.2. Shielding

The shielding materials are lead and depleted uranium. The initial tests for voids during fabrication and the required radiological surveys following each loading assure shielding integrity. If the results of surveys exceed the regulatory requirements, the contents are reduced or the shipment is not initiated.

8.2.4. Thermal Tests

Thermal testing is only performed following initial fabrication of the cask.

8.2.5. Miscellaneous Tests

No additional periodic tests are required.

8.3 Appendix

The only appendix information for Chapter 8 is provided in Section 8.4, References.

8.4 References

- 8-1 U.S. NRC Code of Federal Regulations, Title 10 Part 71, "Packaging and Transport of Radioactive Material," April 2016.
- 8-2 GE Hitachi Nuclear Energy, "Quality Assurance Program for Transport Packages for Radioactive Material (Docket 71-0170)," QAP-1, latest approved version.
- 8-3 U.S. Nuclear Regulatory Commission (NRC), "Quality Assurance Program Approval for Radioactive Material Packages, Number 0170, Revision 11," May 12, 2014.
- 8-4 American Society of Mechanical Engineers (ASME), Boiler and Pressure Vessel Code, Division I, Section III, Subsection NG, "Core Support Structures," 2010.
- 8-5 American Society of Mechanical Engineers (ASME), Boiler and Pressure Vessel Code, Division I, Section III, Subsection NB, "Class 1 Components," 2010 with addenda.
- 8-6 American Society of Mechanical Engineers (ASME), Boiler & Pressure Vessel Code, Division I, Section III, Subsection NF, "Component Supports," 2010.
- 8-7 American National Standards Institute (ANSI), "American National Standard for Radioactive Materials – Leakage Tests on Packages for Shipment," ANSI N14.5, 1997.
- 8-8 GE Hitachi Nuclear Energy, "Model 2000 Cask Containment Boundary Testing," Test Specification 003N1962 R0, 2015.
- 8-9 GE Hitachi Nuclear Energy, "Summary of Test Results for GE 2000 Pipe Plug," Report 003N2916 R0, 2016.
- 8-10 GE Hitachi Nuclear Energy, "Summary of Test Results for Model 2000 Cask Lid Seals," Report 003N5189 R0, 2016.
- 8-11 Military Specification, "Core Material, Aluminum, for Sandwich Construction," MIL-C-7438, or Equivalent.

NEDO-33866 Revision 0
Non-Proprietary Information – Class I (Public)

- 8-12 GE Hitachi Nuclear Energy, "Operations and Maintenance of Model 2000 Transport Package," Specification Number 22A9380 Revision 8, July 2003.
- 8-13 Leak Testing Specialists, Inc., "Helium Mass Spectrometer Leak Test Procedure, Evacuated Envelope Technique, Pre-Shipment Leak Testing of GE 2000 Transport Packaging Cask," MSLT-EE-GE Revision 5500, 2014, or latest approved revision.